frontiers | Research Topics

Epigenetic regulation of autophagy in inflammatory diseases

Edited by
Kai Wang, Chao Yang, Haiyong Wang,
Bailong Tao and Shicheng Guo

Published in
Frontiers in Immunology

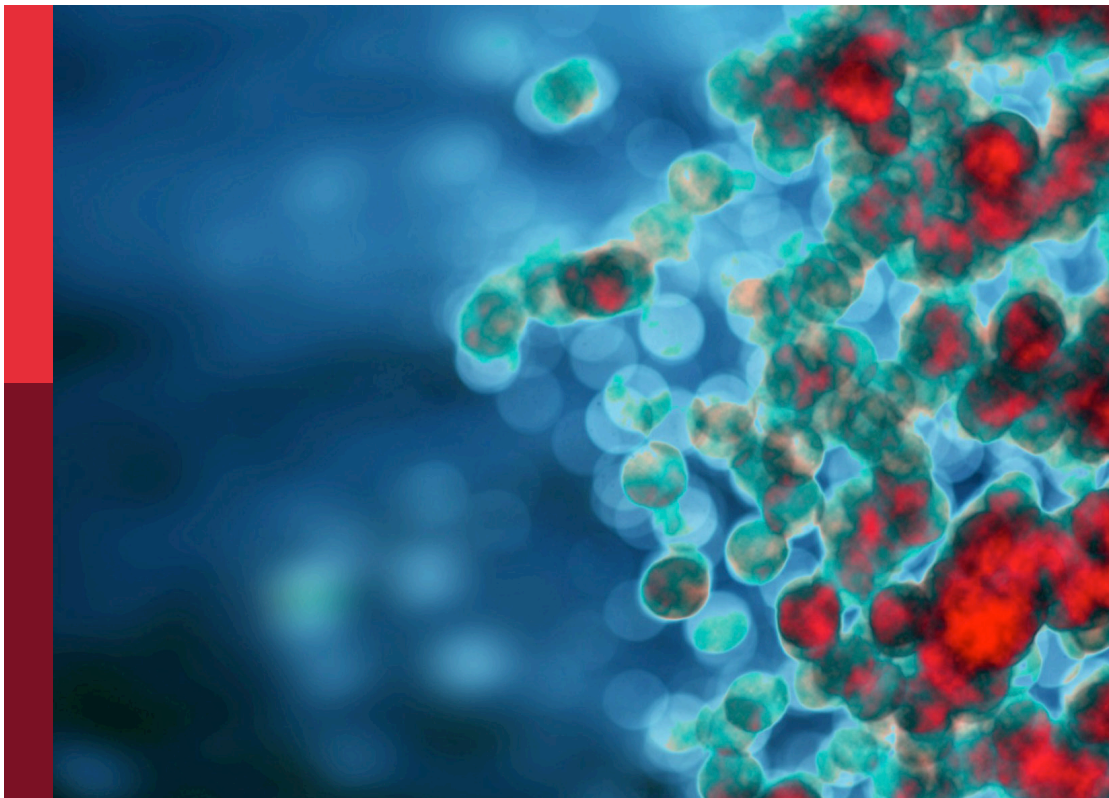

ISSN 1664-8714
ISBN 978-2-8325-4605-5
DOI 10.3389/978-2-8325-4605-5

About Frontiers

Frontiers is more than just an open access publisher of scholarly articles: it is a pioneering approach to the world of academia, radically improving the way scholarly research is managed. The grand vision of Frontiers is a world where all people have an equal opportunity to seek, share and generate knowledge. Frontiers provides immediate and permanent online open access to all its publications, but this alone is not enough to realize our grand goals.

Frontiers journal series

The Frontiers journal series is a multi-tier and interdisciplinary set of open-access, online journals, promising a paradigm shift from the current review, selection and dissemination processes in academic publishing. All Frontiers journals are driven by researchers for researchers; therefore, they constitute a service to the scholarly community. At the same time, the *Frontiers journal series* operates on a revolutionary invention, the tiered publishing system, initially addressing specific communities of scholars, and gradually climbing up to broader public understanding, thus serving the interests of the lay society, too.

Dedication to quality

Each Frontiers article is a landmark of the highest quality, thanks to genuinely collaborative interactions between authors and review editors, who include some of the world's best academicians. Research must be certified by peers before entering a stream of knowledge that may eventually reach the public - and shape society; therefore, Frontiers only applies the most rigorous and unbiased reviews. Frontiers revolutionizes research publishing by freely delivering the most outstanding research, evaluated with no bias from both the academic and social point of view. By applying the most advanced information technologies, Frontiers is catapulting scholarly publishing into a new generation.

What are Frontiers Research Topics?

Frontiers Research Topics are very popular trademarks of the *Frontiers journals series*: they are collections of at least ten articles, all centered on a particular subject. With their unique mix of varied contributions from Original Research to Review Articles, Frontiers Research Topics unify the most influential researchers, the latest key findings and historical advances in a hot research area.

Find out more on how to host your own Frontiers Research Topic or contribute to one as an author by contacting the Frontiers editorial office: frontiersin.org/about/contact

Epigenetic regulation of autophagy in inflammatory diseases

Topic editors

Kai Wang — Southwest Medical University, China
Chao Yang — Zhejiang Ocean University, China
Haiyong Wang — Shandong University, China
Bailong Tao — The First Affiliated Hospital of Chongqing Medical University, China
Shicheng Guo — Arrowhead Pharmaceuticals, United States

Citation

Wang, K., Yang, C., Wang, H., Tao, B., Guo, S., eds. (2024). *Epigenetic regulation of autophagy in inflammatory diseases*. Lausanne: Frontiers Media SA.
doi: 10.3389/978-2-8325-4605-5

Table of contents

frontiers | Frontiers in Immunology

TYPE Editorial
PUBLISHED 05 March 2024
DOI 10.3389/fimmu.2024.1387459

OPEN ACCESS

EDITED AND REVIEWED BY
Pietro Ghezzi,
University of Urbino Carlo Bo, Italy

*CORRESPONDENCE
Kai Wang
wangkai@swmu.edu.cn
Chao Yang
yc52028@hotmail.com
Bailong Tao
taobailong@hospital.cqmu.edu.cn
Shicheng Guo
Shicheng.Guo@wisc.edu
Haiyong Wang
wanghaiyong6688@126.com

†These authors have contributed equally to this work

RECEIVED 17 February 2024
ACCEPTED 26 February 2024
PUBLISHED 05 March 2024

CITATION
Wang K, Yang C, Tao B, Guo S and Wang H (2024) Editorial: Epigenetic regulation of autophagy in inflammatory diseases. *Front. Immunol.* 15:1387459. doi: 10.3389/fimmu.2024.1387459

Editorial: Epigenetic regulation of autophagy in inflammatory diseases

Kai Wang[1*†], Chao Yang[2*†], Bailong Tao[3*†], Shicheng Guo[4*†] and Haiyong Wang[5*†]

[1]Key Laboratory of Epigenetics and Oncology, The Research Center for Preclinical Medicine, Southwest Medical University, Luzhou, China, [2]National Engineering Research Center for Marine Aquaculture, Institute of Innovation & Application, Zhejiang Ocean University, Zhoushan, China, [3]Laboratory Research Center, The First Affiliated Hospital of Chongqing Medical University, Chongqing, China, [4]University of Wisconsin-Madison, Madison, WI, United States, [5]Department of Internal Medicine Oncology, Shandong Cancer Hospital and Institute, Shandong First Medical University and Shandong Academy of Medical Sciences, Jinan, China

KEYWORDS

epigenetic regulation, autophagy, inflammatory diseases, SIRTUIN, M^{6}A modification

Editorial on the Research Topic
Epigenetic regulation of autophagy in inflammatory diseases

Autophagy is a conserved stress response mechanism that occurs in eukaryotes. It involves the degradation of various cargoes (e.g., damaged organelles, misfolded proteins, etc.) within autolysosomes and is regulated by autophagy-related genes (Atgs). Autophagy helps maintain homeostatic balance and regulates physiological functions. Many human diseases are accompanied by inflammation. Autophagy clears pathogens, inhibits the production of inflammatory factors, and regulates the function of immune cells, reducing inflammatory response (1). Dysregulation of autophagy can contribute to the development and progression of various diseases, including inflammatory diseases (ID) (2).

Epigenetic regulation or the regulation of gene expression through chromatin structure alteration and DNA methylation impacts cellular function and physiological states (3). Increasing evidence has revealed the interaction between autophagy, inflammation, and epigenetic regulation (4).

Herein, we aimed to shed light on the role of autophagy and its epigenetic modifications in ID, highlighting the clinical implications of targeting epigenetics and/or autophagy for the prevention and treatment of these pathologies. To this end, this Research Topic includes 11 research articles and reviews.

Using gene enrichment analysis, Cao et al. screened differentially expressed genes (DEGs) from a public RNA-seq dataset and identified four immune- and metabolism-related hub genes (CD40LG, MAPK14, CD28, S100A12), providing new insights into postoperative systemic inflammatory dysregulation. In the past decade, Lin et al. systematically analyzed the regulatory role of autophagy in lung diseases, deepening our understanding of their pathogenesis. Na^+/K^+-ATPase, a major driver of Na^+ transport in alveolar type II epithelial cells, was shown to promote alveolar fluid clearance (5).

Na^+/K^+-ATPase is degraded during autophagy (Wen et al.). Furthermore, using a lipopolysaccharide-induced inflammation mouse model, Wen et al. revealed that insulin upregulated Na^+/K^+-ATPase expression by inhibiting autophagy, leading to a reduction in the inflammatory response. An original study reported by Wang et al. revealed that autophagy-mediated endocytosis of natural killer (NK) group 2D receptors on the surface of NK cells and their lysosomal degradation exacerbates radiation-induced pneumonia.

Autophagy and inflammation studies have identified potential targets for anti-osteoarthritis (OA) therapy. Using relevant datasets derived from Gene Expression Omnibus and autophagy databases, Qin et al. identified four Atgs (MAP1LC3B, CDKN1A, MYC, DDIT3) associated with inflammation/immunity. In addition, Lu et al. reported a heritability study linking OA and spondylitis.

Inflammation and epigenetic regulation mediated through specific factors impact autophagy, affecting the development of inflammation. Yang et al. revealed that the m^6A demethylase, fat mass and obesity-associated protein, regulated autophagy and renal fibrosis by impairing the stability of p62 mRNA. Zhang et al. described how sirtuins, histidine deacetylases, and related co-substrates regulate autophagy and macrophage polarization, impacting glucose metabolism. They also reported that sirtuins regulate autophagy by deacetylating autophagy-related proteins, suggesting the potential use of sirtuin modulators in tuberculosis therapy (Zhang et al.). A review article by Mao et al. described the epigenetic regulation of pulmonary hypertension during autophagy, including acetylation signaling of autophagy, methylation of histones and DNA, and RNA alternative splicing.

These data on targeting autophagy and epigenetic modifications are crucial for understanding how epigenetic modifications influence autophagy mechanisms. They could potentially offer personalized treatment strategies for patients with various diseases, including pulmonary hypertension. Additionally, Jiang et al. discuss how programmed cell death, including autophagy, affected epigenetic regulation in hypoxic-mediated pulmonary hypertension.

Studies on drug regulation of autophagy and epigenetics offer new treatment targets for ID. Canagliflozin, a sodium-glucose cotransporter-2 inhibitor approved by the Food and Drug Administration for the treatment of diabetes, targeted the epigenetic modifiers histone deacetylases 6 and 2, inhibiting the progression of tumors (6, 7) and activated autophagy yielding anti-inflammatory effects (8). Canagliflozin attenuated renal fibrosis *in vitro* and *in vivo* through an autophagy-mediated m^6A modification (Yang et al.).

Obeticholic acid is a specific ligand for farnesoid X receptor (FXR), which is regulated by various epigenetic modifications such as methylation and acetylation (9). It targets the Toll-like receptor 4/transforming growth factor-beta 1/autophagy pathway mitigating non-alcoholic fatty liver disease (10). Using single-cell RNA-seq data, Gou et al. identified CXCL16 as a DEG in NKT cells, exploring the potential of targeting the chemokine (C-X-C motif) ligand (Cxcl)16/CXCR6 pathway. Furthermore, co-treatment with obeticholic acid and 5β-cholanic acid 3 inhibited the malignant progression of hepatocellular carcinoma in an *in situ* carcinoma mouse model (Gou et al.). However, how obeticholic acid-regulated autophagy affects tumor epigenetic modifications still needs to be explored in depth.

This work covers just a fraction of the evolving field of epigenetic regulation of autophagy, which is rapidly advancing. In summary, understanding the interplay between epigenetic regulation and autophagy is crucial for deciphering the pathogenesis of ID and identifying novel treatment targets and strategies.

Author contributions

KW: Funding acquisition, Supervision, Validation, Writing – original draft, Writing – review & editing. CY: Writing – review & editing. BT: Writing – review & editing. SG: Writing – review & editing. HW: Writing – review & editing.

Funding

The author(s) declare that financial support was received for the research, authorship, and/or publication of this article. This work was supported by the Start-Up Grant of Southwest Medical University (41/00040179) and the Sichuan Natural Science Foundation Program from Sichuan Provincial Department of Science and Technology (2023NSFSC0741).

Acknowledgments

We thank all members of the guest editorial team and reviewers who participated in this Research Topic as well as authors who contributed related papers.

Conflict of interest

The authors declare that the research was conducted in the absence of any commercial or financial relationships that could be construed as a potential conflict of interest.

The author(s) declared that they were an editorial board member of Frontiers, at the time of submission. This had no impact on the peer review process and the final decision.

Publisher's note

References

1. Jin M, Zhang Y. Autophagy and inflammatory diseases. *Adv Exp Med Biol*. (2020) 1207:391–400. doi: 10.1007/978-981-15-4272-5_26

2. Klionsky DJ, Petroni G, Amaravadi RK, Baehrecke EH, Ballabio A, Boya P, et al. Autophagy in major human diseases. *EMBO J*. (2021) 40:e108863. doi: 10.15252/embj.2021108863

3. Mishra P, Beura S, Ghosh R, Modak R. Nutritional epigenetics: how metabolism epigenetically controls cellular physiology, gene expression and disease. *Subcell Biochem*. (2022) 100:239–67. doi: 10.1007/978-3-031-07634-3_8

4. Zehender A, Li YN, Lin NY, Stefanica A, Nuchel J, Chen CW, et al. TGFbeta promotes fibrosis by MYST1-dependent epigenetic regulation of autophagy. *Nat Commun*. (2021) 12:4404. doi: 10.1038/s41467-021-24601-y

5. Matthay MA, Zemans RL. The acute respiratory distress syndrome: pathogenesis and treatment. *Annu Rev Pathol*. (2011) 6:147–63. doi: 10.1146/annurev-pathol-011110-130158

6. Jiang D, Ma P. Canagliflozin, characterized as a HDAC6 inhibitor, inhibits gastric cancer metastasis. *Front Oncol*. (2022) 12:1057455. doi: 10.3389/fonc.2022.1057455

7. Biziotis OD, Tsakiridis EE, Ali A, Ahmadi E, Wu J, Wang S, et al. Canagliflozin mediates tumor suppression alone and in combination with radiotherapy in non-small cell lung cancer (NSCLC) through inhibition of HIF-1alpha. *Mol Oncol*. (2023) 17:2235–56. doi: 10.1002/1878-0261.13508

8. Park CH, Lee B, Han M, Rhee WJ, Kwak MS, Yoo TH, et al. Canagliflozin protects against cisplatin-induced acute kidney injury by AMPK-mediated autophagy in renal proximal tubular cells. *Cell Death Discovery*. (2022) 8:12. doi: 10.1038/s41420-021-00801-9

9. Wan YY, Sheng L. Regulation of bile acid receptor activity(☆). *Liver Res*. (2018) 2:180–5. doi: 10.1016/j.livres.2018.09.008

10. Tawfiq RA, Nassar NN, Hammam OA, Allam RM, Elmazar MM, Abdallah DM, et al. Obeticholic acid orchestrates the crosstalk between ileal autophagy and tight junctions in non-alcoholic steatohepatitis: Role of TLR4/TGF-beta1 axis. *Chem Biol Interact*. (2022) 361:109953. doi: 10.1016/j.cbi.2022.109953

frontiers | Frontiers in Immunology

TYPE Original Research
PUBLISHED 16 December 2022
DOI 10.3389/fimmu.2022.1092575

OPEN ACCESS

EDITED BY
Kai Wang,
Southwest Medical University, China

REVIEWED BY
Milad Shirvaliloo,
Tabriz University of Medical Sciences, Iran
Md. Abdul Alim Al-Bari,
Rajshahi University, Bangladesh

*CORRESPONDENCE
Xin Lv
xinlvg@126.com
Sheng Wang
ws2015ma@163.com

†These authors have contributed equally to this work

SPECIALTY SECTION
This article was submitted to Inflammation, a section of the journal Frontiers in Immunology

RECEIVED 08 November 2022
ACCEPTED 28 November 2022
PUBLISHED 16 December 2022

CITATION
Lin F, Chen Y, Mo W, Zhou H, Xiao Z, Hu S, Shi X, Liu M, Wei J, Zhu W, Wang S and Lv X (2022) A bibliometric analysis of autophagy in lung diseases from 2012 to 2021.
Front. Immunol. 13:1092575.
doi: 10.3389/fimmu.2022.1092575

A bibliometric analysis of autophagy in lung diseases from 2012 to 2021

Feihong Lin†, Yong Chen†, Wei Mo†, Huanping Zhou, Zhuoran Xiao, Song Hu, Xuan Shi, Meiyun Liu, Juan Wei, Wanli Zhu, Sheng Wang* and Xin Lv*

Department of Anesthesiology, Shanghai Pulmonary Hospital, School of Medicine, Tongji University, Shanghai, China

Background: Autophagy refers to the process in which cells wrap their damaged organelles or unwanted proteins into a double-membrane structure and direct them to lysosomes for degradation. Autophagy can regulate many lung diseases such as pulmonary hypertension, acute lung injury, and lung cancer. However, few bibliometric studies on autophagy are available. The aim of the present study was to clarify the role of autophagy in lung diseases by bibliometric analysis.

Methods: Publications were retrieved from the 2012–2021 Science Citation Index Expanded of Web of Science Core Collection on 20 September 2022. Bibliometrix package in R software was used for data retrieval. VOSviewer and CiteSpace were used to visualize the research focus and trend regarding the effect of autophagy on lung disease.

Results: A total of 4,522 original articles and reviews on autophagy in lung diseases published between 2012 and 2021 were identified. China had the largest number of published papers and citations, whereas the United States (US) ranked first in the H-index and G-index. Moreover, cooperation network analysis showed close cooperation between the US, China, and some European countries, and the top 10 affiliates were all from these countries and regions. Bibliometric analysis showed that "autophagy" and "apoptosis" were the keywords with the highest frequency. During the past decade, most studies were concerned with basic research on pathways related to the regulatory role of autophagy in the inhibition and attenuation of lung diseases.

Conclusion: The study of autophagy in lung diseases is still in the development stage. The information published in these articles has helped researchers understand further the hot spots and development trends in the field more and learn about the collaboration network information regarding authors, countries, and institutions, as well as the paper citation correlation. More studies have been performed to gain deeper insights into the pathogenesis of autophagy by focusing on the links and effects between various diseases.

More recently, research in this field has paid increasing attention to the function of autophagy in COVID-19–related lung diseases.

KEYWORDS

autophagy, lung, bibliometrics, bibliometrix, VOSviewer, citespace

Introduction

Autophagy ("self-eating" in Greek) refers to the process in which cells wrap their damaged organelles or unwanted proteins into a double-membrane structure and direct them to lysosomes for degradation (1, 2). Autophagy exhibits a strong conservative property in all eukaryotes and is essential for maintaining cellular homeostasis. Hence, nearly all cell types present a basal autophagy level. Normally, autophagy takes charge of regulating the physiological functions, degrading cellular components, and forming building blocks and cell response to stress (RTS) (2). Autophagy can be easily induced by environmental insults, and the autophagic cycle rate (flux) can commonly change in RTS (3). Upon most occasions, induction of autophagy in RTS is a cytoprotective mechanism. Despite this, undue self-degradation results in cell death (4–6). The lung is a complex organ mainly functioning in gas exchange and is composed by many cell types including endothelial, epithelial, inflammatory, and mesenchymal cell types (7). Autophagy is an inducible RTS in lung cells. Agents triggering autophagy present a special association with lung cell biology, including hypoxia, particle and cigarette smoke exposure, pro-inflammatory states, and conditions that promote endoplasmic reticulum (ER) stress or oxidative stress. An increasing number of lung-related diseases are emerging, such as chronic obstructive pulmonary disease (COPD), idiopathic pulmonary fibrosis, pulmonary hypertension, acute lung injury, and lung cancer, which form a crux in the field of malignancy (8), causing high mortality (9, 10). Although some progress has been made in research of the effect of autophagy on lung diseases, many issues need to be further explored.

Bibliometric analysis pays attention to the literature systems and literature characteristics and broadly serves for understanding the knowledge structure as well as exploring the developmental trends by virtue of the qualitative and quantitative scientific literature analysis (11). Bibliometric analysis quantitatively measures the study domain outline distribution as well as the relationship and clustering. It describes and predicts the future development of a certain research field on the one hand and compares the contributions made by different authors, institutions, countries, and journals on the other hand. As bibliometric analysis can help develop guidelines, understand research hot spots, and evaluate the research trends (12), it has been applied to the research of digestive system diseases (13), cancer (14), rheumatic system diseases (15), and nervous system diseases (16). However, there are basically no bibliometric studies investigating the autophagy in lung diseases. Hence, the aim of this study is to make a systematical analysis of the research on the autophagy in lung diseases and to evaluate the related research state and trend.

Materials and methods

Data sources and search strategies

We performed a systematic search for the Science Citation Index Expanded (SCI-Expanded) of Web of Science Core Collection (WoSCC) in 2012–2021 during 1 January 2012 and 31 December 2021, and we downloaded the data on 20 September 2022 for avoiding deviations. The search terms included: TS = (autophagy) AND TS= ("pulmonary" OR "lung"). Two reviewers (FH Lin and JX Yuan) took charge of independently identifying this data search and discussing underlying differences, with the final agreement of 0.90 (17). After excluding the online publication time of 2022 and articles written in non-English and by limiting the publication type to reviews and original articles, we finally obtained 4,522 original articles and reviews that met the criteria for inclusion in the analysis (Figure 1).

Data collection and cleaning

First, the original data were extracted from the SCI-Expanded database of WoSCC. The recorded information included the number of papers and citations, H-index, publication year, countries/regions, affiliations, authors, journals, references, and keywords. Afterward, duplicate authors and misspelled elements were moved artificially. Although inaccurate analysis may not be avoided completely due to multiple versions of cited references, the same abbreviated names of different authors, and different forms of

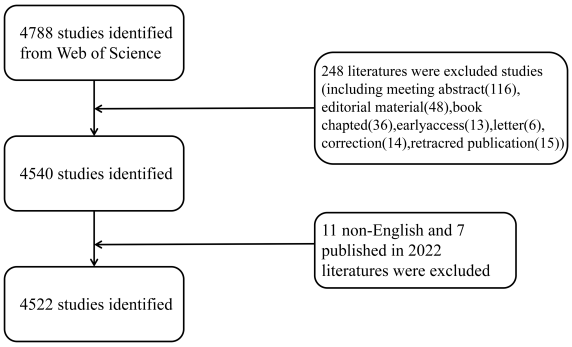

FIGURE 1
Detailed process for literature screening.

cited journals, we pointed out the first extracted original data from the SCI-Expanded database. The recorded information was paper and citation number, H-index, G-index publication year, countries/regions, affiliations, authors, journal, references, and keywords. Then, we removed misspelled elements and duplicate authors. Cited references have different versions, different authors may have the same abbreviated name, and cited journals have different forms, which may lead to inaccurate analysis. Despite this, most raw data were accurate. We removed the misspelled elements and duplicate authors and adopted a thesaurus file for merging duplicates into one word, deleting useless words and correcting the misspelled elements. Later, we imported the cleansed data to VOSviewer (version 1.6.18.0), CiteSpace (version 6.1. R3), and the "bibliometrix package 4.0.1" of R software (version 4.2.1) for the subsequent bibliometric analysis.

Bibliometric analysis

The number of papers and citations is the bibliometric indicator commonly used to represent the bibliographic material. In general, the research level can be evaluated from the perspective of productivity and impact, which, in the paper, were respectively measured *via* the number of publications (NP) and the number of citations without self-citations (NC). Sometimes, H-index is used to evaluate the individual academic achievements or the publication output (18). G-index refers to the highest number of papers that receive H-index or more citations (19). In addition, the article value can also be indicated by the impact factor (IF) from the latest version of Journal Citation Reports (20, 21). We visualized the results for the number of papers per year, country, organization, author, citation, and other relevant aspects. Prior to data analysis, the R4.2.1-based Bibliometrix package was used to store, count, and clean up data. As important indicators of the research, H-index, G-index, and IF were all included in the analysis. Subsequently, the following software was used for bibliometric analysis.

R (version 4.2.1) stands for the language and environment specific to the statistical computing and graphics. It presents a strong extensibility, capable of automating the analyses and creating new functions. The cleansed data received bibliometric analysis under the assistance of bibliometrix package in R (22). To further explain the annual document quantity alternation, we employed the fitting polynomial model for predicting the annual NP. Variable f (x) refers to the annual study number, and x stands for the publication year. Moreover, VOSviewer software assisted in constructing bibliometric maps for obtaining more extensive information regarding the results considering co-citation (CC) and co-occurrence (CO) (23, 24). Co-citation refers to the situation that two items are simultaneously cited by the third one. Keyword co-occurrence takes charge of measuring the keywords appearing in the same documents most frequently (25). Analysis on the keywords serves for demonstrating the autophagy-related research in lung disease.

VOSviewer, CiteSpace, and R (version 4.2.1) were used for the statistical computing and graphics. VOSviewer uses data from WoSCC for establishing the bibliometric maps (23), capable of assisting in comprehensively viewing the bibliometric maps in detail considering the collaborative data. CiteSpace focuses on analyzing the underlying knowledge in the scientific literature and visualizing the collected data (26).

Results

An overview of publications on autophagy in lung disease

The number of retrieved publications was 4,522, including 3,772 original research articles and 750 reviews, with total NC of 114,589, a mean NC/article ratio of 27.91, and a mean H-index of 130.

The annual trend of paper publication quantity

Figure 2A displays the annual NP associated with autophagy in lung diseases. The annual paper number indicates a fast increase from 119 in 2012 to 785 in 2021, and the NP reached the peak in 2021. From 2012, annual NP did not change significantly in the United States (US) and Korea but indicated a fast elevation in China, and there has been a surge since 2015. The annual NP exhibited an obvious relation to the publication year, with the correlation coefficient R^2 of 0.9872 (Figure 2A). The rapidly increasing NP demonstrates the increasing number

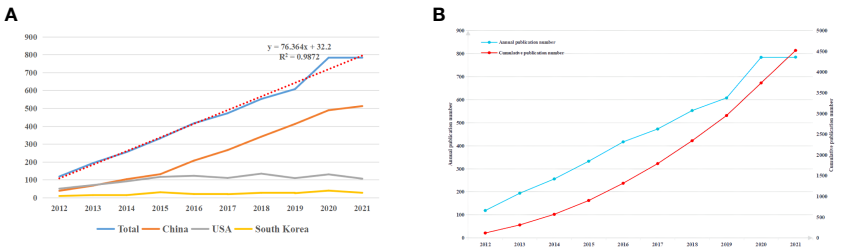

FIGURE 2
(A) The total NP and top three countries by number of published papers during 2012 and 2021. **(B)** The annual NP and accumulation during 2012 and 2021.

of scholars who placed emphasis on this field. There were more than 4,500 publications in 2021, demonstrating the increasing number of scholars who conducted relevant research and the flourish of lung disease-related autophagy research theories (Figure 2B).

Contributions of countries/regions to global publications

The 10 high-output countries/regions with the highest output were ranked according to NP of all authors. China published the most papers (2,564, 56.7%), followed by the US (1,048, 23.18%) and South Korea (234, 5.17%) (Figures 3A, B; Table 1). NC was 23,791 for China, accounting for 38.2% of the total number of citations, followed by the US (47,846) and South Korea (5,449). However, the US enjoyed the highest H-index (181) and G-index (264), about three times that of South Korea (58 of 81).

Figures 3C, D display the publication distribution in various countries and regions. Related cooperation was mainly concentrated upon China and the US, and cooperation with other countries was relatively weak. As shown in Figure 3C, cooperation between countries and regions significantly

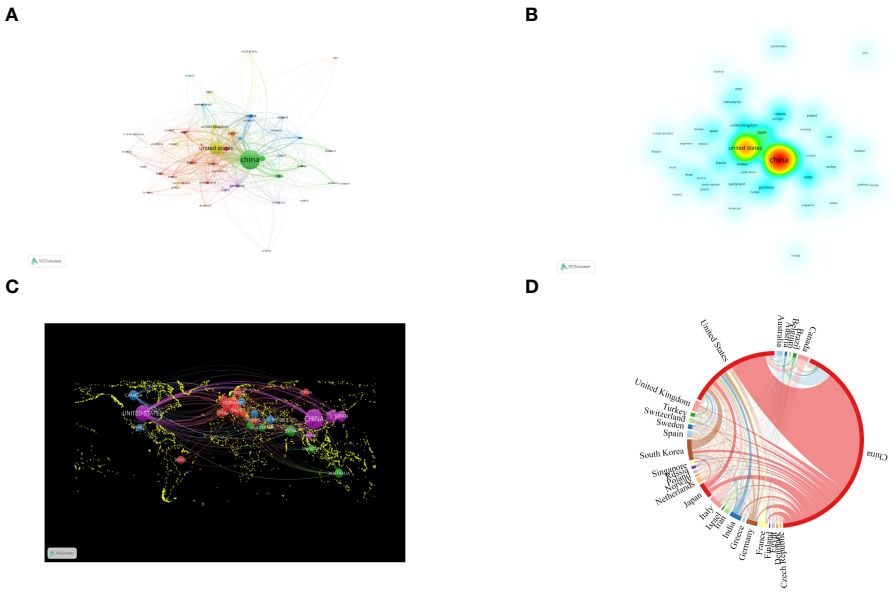

FIGURE 3
Contributions of various countries to the research of autophagy in lung diseases. **(A)** Country collaboration map of autophagy research in lung disease. Circles denote countries, and lines denote their collaborations. **(B)** Countries' density map. **(C)** World map of countries' cooperation density. **(D)** A circle diagram evaluating the international collaboration between clusters.

TABLE 1 Top 10 countries with the most published research on autophagy in lung disease.

Rank	Country/Region	NP	% of (4,522)	NC	H-index	G-index
1	China	2,564	56.70	54,251	118	163
2	United States	1,048	23.18	47,846	181	264
3	South Korea	234	5.17	5,449	58	81
4	Japan	169	3.74	5,943	69	102
5	Italy	148	3 27	6,054	75	105
6	India	132	2.92	3,488	43	72
7	Germany	126	2.79	4,740	62	102
8	United Kingdom	122	2.70	5,042	59	89
9	Canada	121	2 68	5,305	64	100
10	France	92	2.03	4,141	75	134

promoted the development of scientific research. The lines in the figure indicate cooperation: The wider the lines, the stronger the cooperation. Nevertheless, lines cannot be found in most countries, meaning that these countries had no stable communication and cooperation.

Analysis of authors

According to the author visualization chart by VOSviewer, 78 authors performed autophagy-related studies. In terms of the NP, Choi Augustine M. K. (28 publications) ranked first, followed by Ryter Stefan W. (28 publications), Wang Jing (25articles), and Wang Wei (24 articles) (Figure 4A; Table 2). Obviously, there was a relatively low author centrality (≤0.04), demonstrating the necessity to enhance the autophagy impact in lung disease. Co-cited authors refer to those (at least two) who are cited at the same time (Figure 4B). Only six had a frequency of citation of over 400 times amid the 103,587 co-cited authors. The lines between nodes stand for authors' collaboration, and the collaboration graph means that authors' collaboration indeed existed in the field.

Analysis of affiliations

Figure 5 is an institutional co-occurrence map built with CiteSpace, listing the top 10 institutions considering the output and centrality in autophagy-related lung disease studies. Nodes stand for institutions: The larger the node, the more output the institution made. Links between nodes mean institutional collaboration, and the color and thickness denote the collaboration duration and intensity, respectively. China Medical University (n = 190) was in the leading position considering the output, followed by Shandong University (n =180) and Zhejiang University (n = 174). The top three institutions considering the centrality were New York University (0.37), Pittsburgh University (0.30), and Michigan University (0.26) (Table 3). As the data show, institutions were closely collaborated with each other.

Analysis of journals

Table 4 gives the top 10 journals considering the research number of lung disease–related autophagy and the impact

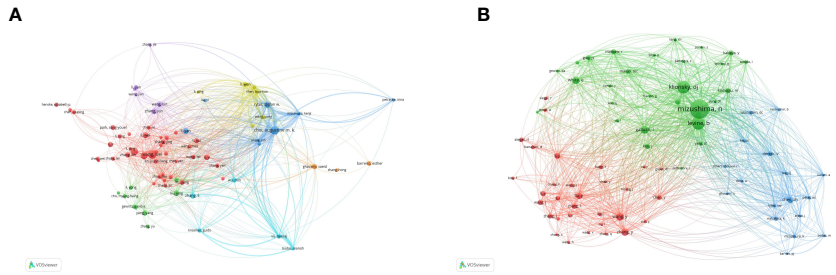

FIGURE 4
Authors related to the research on autophagy in lung disease. **(A)** Author co-occurrence. **(B)** VOSviewer visualization of co-cited authors. Circle size means the number of authors' published articles; the connecting lines stand for authors' mutual communication and interaction.

TABLE 2 Top 10 authors and co-cited authors related to autophagy in lung disease.

Rank	Author	Count (%)	Centrality	Co-cited author	Citation	Centrality
1	Choi Augustine M. K.	28 (0.62%)	0.03	Mizushima N.	1,170	0.02
2	Wang Jing	25 (0.55%)	0.02	Levine B.	696	0.01
3	Wang Wei	24 (0.53%)	0.00	Klionsky D. J.	696	0.01
4	Ryter Stefan W.	21 (0.46%)	0.00	White E.	352	0.01
5	Zhang Wei	19 (0.42%)	0.02	Galluzzi L.	348	0.03
6	Li Yan	18 (0.40%)	0.02	Wang Y.	341	0.02
7	Liu Ying	14 (0.31%)	0.04	Zhang Y.	322	0.01
8	Ghavami Saeid	14 (0.31%)	0.00	Chen Z. H.	311	0.03
9	Li Yi	14 (0.31%)	0.02	Liu Y.	279	0.01
10	Zhang Li	14 (0.31%)	0.02	Kroemer G.	274	0.02

indicators, namely, H-index, G-index, and IF eigenfactor score. These journals had a larger possibility in accepting articles regarding autophagy in lung disease, given their largest NP of relevant topics. Scholars in the autophagy area are suggested to place emphasis on these journals. ONCOTARGET (115 publications, IF = 4.147) had the highest NP, followed by INT J MOL SCI (98 publications, IF = 5.924), PLOS ONE (97 publications, IF = 3.248), CELL DEATH DIS (81 publications, IF = 8.468), and AUTOPHAGY (80 publications, IF = 16.016). Notably, the AUTOPHAGY had higher citations, H-index, and G-index, demonstrating that the quality of many studies was not high. In Figure 6A, the analysis of journals revealed that PLOS ONE (2,677 total citations) presented the highest citation frequency, followed by AUTOPHAGY (2,626 total citations) and J BIOL CHEM (2,440 citations). J BIOL CHEM (0.58) enjoyed the highest centrality, followed by PLOS ONE (0.40) and P NATL ACAD SCI USA (0.39) (Table 5), all of which had a high centrality, demonstrating their stronger impact in this field. In the domain dimension, superposition graph analysis was carried out for the fields involved in the literature (Figure 6B). Among them, the top fields of paper production were oncology, pharmacology and pharmacy, chemistry medicinal, multidisciplinary sciences, and chemistry multidisciplinary. Therefore, in the study of autophagy in lung diseases, oncology and pharmacochemistry are currently the focused areas.

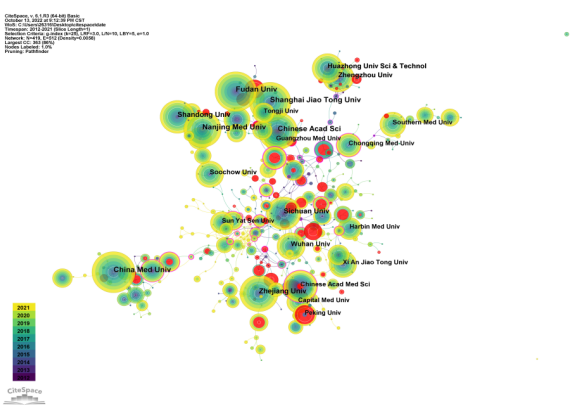

FIGURE 5
Visualization of institutions that performed research on autophagy in lung disease.

CiteSpace assisted in constructing the subject distribution regarding academic journals by virtue of the biplot overlay function (Figure 7). According to the journal biplot overlay, there were mainly two citation paths. Journals publishing articles were basically in medical sciences covering the pharmaceutical, clinical, molecular, biological, and immunological fields, and most cited articles were published in journals in molecular, biological, immunologic, genetic, dermatological, health, nursing, rehabilitation, dental, surgical, sports, neurological, pharmaceutical, and ophthalmological fields.

Co-cited reference clusters analysis

A co-citation network refers to a reference network simultaneously co-cited by at least one paper. Conceptual clusters were created when a set of manuscripts was cited together repeatedly (27). As shown in Figures 8A, B, the most cited article was written by Basant A. Abdulrahman who pointed out that rapamycin, an autophagy stimulator, enhanced the clearance of *C. coronans* by inducing autophagy and significantly reduced the infection of *C. coronans in vitro*.

Rapamycin was found capable of lowering the bacterial burden in the mouse lung *in vitro* and markedly eliminating lung inflammation signs (28). Figure 8C demonstrates a network visualization map regarding cited references, with nodes denoting the cited reference, where the connecting lines stand for the co-citation relationship. The different colors varying from purple to yellow mean different years in the range of 2012 to 2021. Node size denotes the number of co-citation number. Figure 8D displays the 16 relevant clusters

TABLE 3 Top 10 institutions conducting autophagy in lung disease by volume and centrality.

Rank	Affiliations	Count	Rank	Affiliations	Centrality
1	China Med Univ	190	1	New York Univ	0.37
2	Shandong Univ	180	2	Pittsburgh Univ	0.30
3	Zhejiang Univ	174	3	Michigan Univ	0.26
4	Fudan Univ	164	4	Lovelace Resp Res Inst	0.21
5	Nanjing Med Univ	157	5	UIsan Univ	0.21
6	Shang Hai Jiao Tong Univ	157	6	Brigham &Women's Hosp	0.20
7	Sichuan Univ	143	7	Chinese Acad Med Sci	0. 19
8	Chongqing Med Univ	116	8	Seoul Natl Univ	0.19
9	Seoul Natl Univ	111	9	Baylor Coll Med	0.18
10	Huazhong Univ Sci and Technol	109	10	Roma Tor Vergata Univ	0.18

divided by CiteSpace: cancer, lung cancer, signaling pathway, anticancer immunity, ferroptosis, particulate matter (PM2.5), COPD, asthma, ER stress, idiopathic pulmonary, acute lung injury, pulmonary disease, COVID-19, oxidative stress, alveolar type II, respiratory immunity, and autophagy. Citation burst reference refers to the sudden citation increase of specific articles within a certain period, which serves for finding the latest high-profile research topics in relative fields (29). We obtained 674 references with the highest citation burst and selected the top 25 (Figure 8E). The blue line denotes the timeline, and the red sections denote the burst interval, respectively, showing the beginning and end of the year, and the burst duration.

Analysis of keywords

Keywords demonstrate a paper's principal ideas and theme concepts, briefly describing the certain research hot spots. VOSviewer and CiteSpace were used for drawing charts. We identified words that appeared over 13 times in the process of analysis as keywords and finally obtained 155 keywords (Figure 9A; Table 6). As shown in Figure 9C, the closer the keyword was closer to yellow, the more frequently it appeared in the year. According to Figure 9A, clusters 1 and 5 were mainly composed of autophagy, apoptosis, and death, which paid attention to relevant mechanisms in the programmed cell death. Cluster 2 stands for "oxidative stress", "mitochondrial dysfunction", and "lung disease". Oxidative stress, the oxidation-antioxidant imbalance in the body, usually causes mitochondrial dysfunction and lung disease. Cluster 3 emphasizes the function of autophagy in lung diseases caused by COVID-19. Clusters 4 and 5 mainly reflect the cellular mechanism and molecular pathway of lung diseases caused by autophagy. In overlay visualization, the color of keywords depends on the average publication year (APY). As shown in Figure 9B, the VOSviewer colors all keywords on the basis of APY. The most recent keyword was "sars-cov-2" (cluster 3, APY: 2020.53), followed by "COVID-19" (cluster 3, APY: 2020.45), both closely related to COVID-19. The color division confirms that the most recent keywords in the research field were "pyroptosis", "immunity", "COVID-19", and "lung cancer", which are proven to be the recent research hot spots.

TABLE 4 Top 10 journals for co-citation of autophagy research in lung disease.

Rank	Journal	NP	NC	H-index	G-index	IF (2020)
1	ONCOTARGET	115	3,605	35	51	4.147
2	INT J MOL SCI	98	3,351	24	56	5.924
3	PLOS ONE	97	3,491	36	54	3.240
4	CELL DEATH DIS	81	2,487	30	46	8.468
5	AUTOPHAGY	80	4,858	43	69	16.016
6	SCI REP-UK	80	2,013	26	40	4.380
7	BIOCHEM BIOPH RES CO	64	1,025	19	29	3.575
8	BIOMED PHARMACOTHER	55	1,204	20	32	6.529
9	FRONT PHARMACOL	54	903	18	28	5.811
10	ONCOL LETT	53	803	16	26	2.967

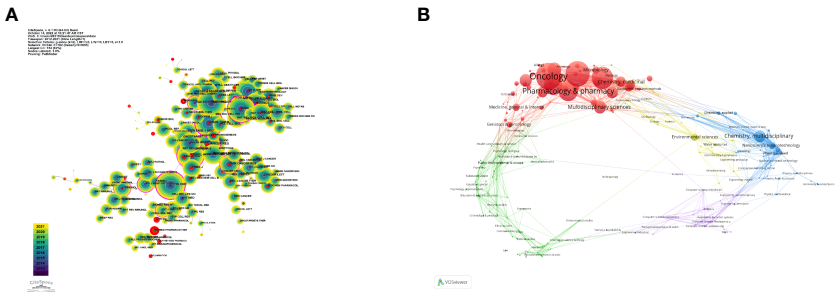

FIGURE 6
Visualization of co-cited journals on lung disease-related autophagy. **(A)** Circles denote co-cited journals; connecting lines stand for journal interaction. **(B)** Superposition analysis of research fields.

Analysis of research for autophagy caused by COVID-19

Following the COVID-19 epidemic outbreak in December 2019, research on lung disease increased markedly in 2020 (Figure 10A). Our study screened out and analyzed 76 papers on lung diseases and autophagy related to COVID-19 from the retrieved literature in an attempt to reveal the research focuses and trends in the association between severe lung diseases and autophagy resulting from COVID-19 (Figure 10B). The terms inflammation, immunology, cytokine storm, oxidative stress, and macrophages all had the highest frequency as revealed in the keyword visualization analysis, in addition to COVID-19, SARS-COV-2, and lung-related diseases, explaining how autophagy exerted its function in severe lung disease caused by the pathogenesis of COVID-19. In addition, the APY-based keyword color classification by VOSviewer confirmed "inflammation" and "oxidative stress" as the top two recent keywords, meeting previous findings on autophagy in lung diseases. In addition, Figure 10 shows the involvement of autophagy in the pathogenesis of COVID-19. We also found that the mechanism of anti-inflammatory treatment and immunomodulation therapy for COVID-19–related lung disease was through inhibiting autophagy activation (Figure 10).

Discussion

In this study, we used VOSviewer, CiteSpace, and R to investigate the research dynamics and hot spots of autophagy in lung diseases in the SCI-Expanded. A total of 4,522 publications were obtained from WoSCC. It was found that there was a substantial increase in the number of annual publications and citations during 2012 and 2021, particularly after 2015. China, which published the most papers, has made greater contributions to the study of autophagy in lung diseases. Moreover, nine of the top 10 productive institutions were from China, including China Medical University, Shandong University, and Zhejiang University, indicating that autophagy has drawn increasing attention from Chinese research institutions in the study of lung diseases recently. However, the H-index and G-index of the US were relatively high compared with that of China. The US ranked first among all countries in both H-index and G-index, demonstrating that the quality of documents from the US is high.

TABLE 5 Top 10 journals for centrality of autophagy research in lung disease.

Rank	Journal	Centrality	JCR	IF (2020)
1	J Biol Chem	0.58	Q2	5.1571
2	Plos One	0.40	Q2	3.204
3	P Natl Acad Sci Usa	0.39	Q1	11.205
4	Cancer Res	0.36	Q1	12.702
5	Am J Resp Crit Care	0.23	Q1	21.404
6	Cell	0.21	Q1	41.584
7	Clin Cancer Res	0.20	Q1	12.531
8	J Immunol	0.16	Q1	5.422
9	Int J Mol Sci	0.14	Q1	5.924
10	Free Radical Bio Med	0.11	Q1	7.376

JCR, Journal Citation Reports.

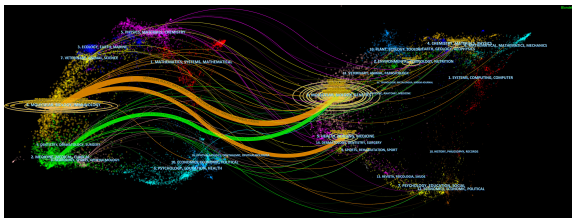

FIGURE 7
A biplot overlay of journals on autophagy research in lung disease (left and right sides refer to the citing journal areas and the cited journal areas, respectively).

Despite China's rapid development and dominant position in the field, it is necessary to improve the collaboration and academic influence in regions. The international distribution of current research in this field is imbalanced.

Choi Augustine M. K. is the most published and cited author in this field. He has long studied the relationship between acute and chronic lung diseases and molecular, cellular, and genetic triggers. He proposed that lung disease may be associated with a pathological accumulation of mutated α1-antitrypsin and that autophagy may be a clearance mechanism for this disease (3). A proper method for monitoring autophagy has been established by Klionsky et al., who suggested that autophagy defects could be induced in favor of lung tumor formation by modulating the tumor microenvironment (28). Noboru Mizushima is also a very influential writer whose works are widely cited. In 1998, Noboru Mizushima reported the homologous gene of Atg12 in human and clarified autophagy (cell self-digestion) as a cellular pathway capable of assisting in degrading proteins and organelles, which is deeply related to human diseases and physiology (30). Yoshinori OhSumi, winner of the 2016 Nobel Prize in Physiology or Medicine, made excellent achievements regarding the function had by autophagy (31). The results of his work have already assisted us in better understanding the function and the effect of autophagy on disease and health (32). The above authors are well respected as they more comprehensively elucidate the mechanism regarding autophagy and contribute to the prevention of lung diseases.

Usually, there is a close relation between the impact of a journal and the impact of its articles (33). Amid the top 10 journals that had the most published papers, AUTOPHAGY exhibited the highest IF (16.016), which was first published in 2005 and is now a leading journal in the field. ONCOTARGET was the most prolific journal, with an IF of 4.147. The journal is sponsored by the US and focuses on articles related to cancer, tumors, autophagy, and cellular immunity. In addition, most active journals are in the professional category. Several multidisciplinary journals, such as CELL DEATH DIS and BIOMED PHARMACOTHER, have also published high-quality studies investigating autophagy in lung disease, which is an emerging and developing research topic and involves molecular biology, cell biology, biochemistry, and medicine. Journals of various disciplines have published advances in such research topic, demonstrating the wide attention paid to lung disease pathogenesis and treatment. In addition, multidisciplinary journals have a wider readership (34), more benefiting interdisciplinary cooperation.

As the research continuously progresses, researchers have revealed the signal pathway that affects different mechanisms. On the basis of keyword mapping, oxidative stress critically impacts the pathogenesis of autophagy, regulating the progression of related lung diseases. The activation of autophagy in response to oxidative stress is mainly for avoiding cell apoptosis (35, 36), In contrast, autophagy inhibition increase oxidative stress damage and even cell death. When ROS is elevated, the HIF-1α transcription factor, p53, FOXO3, and Nrf2 will be activated, which then triggers BNIP3 and NIX, TIGAR, LC3, and p62 (37) to transcribe. The oxidized ATG4 can facilitate LC3 lipidation to initiate autophagy and autophagosome formation. According to a recent report, angiotensin II (Ang II) vasoconstriction can induce autophagy, revealing the ability of Ang II to form autophagic vesicles that contain LC3 and to elevate the ATG12–ATG5, ATG7, and ATG4, thereby simulating the elongation of phagophores (38). As for human glomerular mesangial cells, oxidative stress triggered by Ang II can use mTORC1 signaling for enhancing autophagy, leading to early-stage senescence (39). ROS was found capable of regulating autophagy through pathways dependent of mTOR in the cytoplasm (40, 41). ROS inhibits the PI3K-Akt-mTOR pathway or activates AMPK for suppressing the mTOR signaling pathway, thereby resulting in autophagy activation (42). The increase in ROS oxidizing phosphatase and tensin homolog helps inhibit Akt-mTOR activity (43). Similarly, excess H_2O_2 is capable of triggering autophagy dependent of AMPK, coupled with weakened mTORC1 activity (44). Thioredoxin-interacting protein (TXNIP) takes charge of regulating the autophagy of rats with diabetic nephropathy *via* the mTOR signaling pathway (45). In lung diseases, hypoxia caused by the weakened lung functions primarily stimulates the autophagy induction (45). As for the primary human lung vascular endothelial and smooth muscle-cells, hypoxia could induce BECN1 expression, activate LC3, promote autophagosome formation, and stimulate the autophagic flux, thereby protecting mice from pulmonary vascular disease (46). Therefore, this provides a clear path for us to further explore the autophagy-lung disease relationship.

When we talk about the impact of autophagy on various lung diseases, COVID-19 is an unavoidable topic associated with autophagy-mediated lung disease (Figure 9A). The SARS-CoV-2 virus causing COVID-19 exhibits a strong infectivity and can trigger cytokine-storm, inducing acute respiratory distress syndrome (ARDS)–like lung injury that can develop into pneumonia and severe lung damage, causing high risk of mortality, especially in susceptible populations (47–49). According to recent studies, SARS-CoV-2 is capable of restricting autophagy, which, as anticipated, is an underlying mechanism for serious COVID-19 lung disease as it impairs the viral clearance ability and causes immune dysfunction

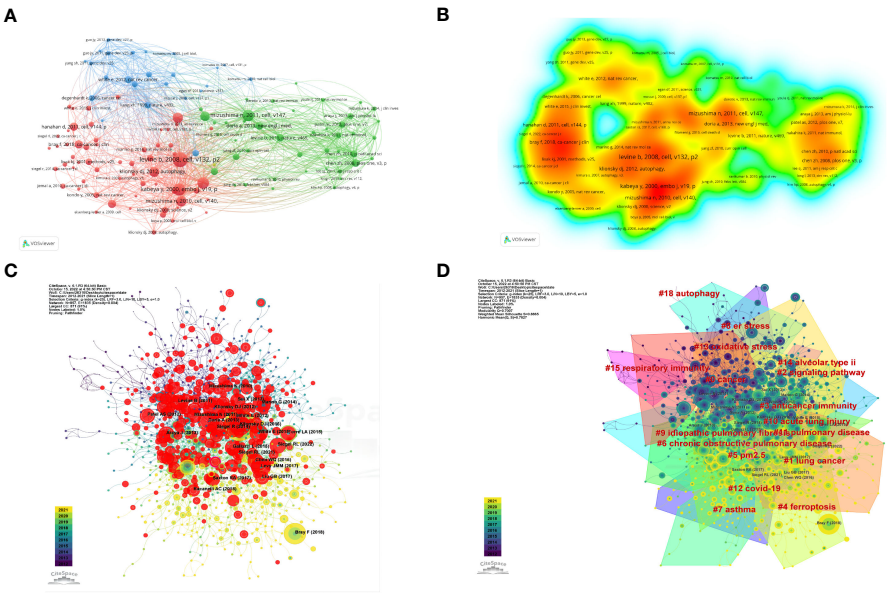

E **Top 45 References with the Strongest Citation Bursts**

References	Year	Strength	Begin	End	2012 - 2022
Mizushima N, 2010, CELL, V140, P313, DOI 10.1016/j.cell.2010.01.028, DOI	2010	22.83	2012	2015	
Klionsky DJ, 2008, AUTOPHAGY, V4, P151, DOI 10.4161/auto.5338, DOI	2008	21.09	2012	2013	
Levine B, 2011, NATURE, V469, P323, DOI 10.1038/nature09782, DOI	2011	19.89	2012	2016	
Kroemer G, 2010, MOL CELL, V40, P280, DOI 10.1016/j.molcel.2010.09.023, DOI	2010	19.49	2012	2015	
Chen ZH, 2010, P NATL ACAD SCI USA, V107, P18880, DOI 10.1073/pnas.1005574107, DOI	2010	17.4	2012	2015	
Mathew R, 2009, CELL, V137, P1062, DOI 10.1016/j.cell.2009.03.048, DOI	2009	16.62	2012	2014	
Nakahira K, 2011, NAT IMMUNOL, V12, P222, DOI 10.1038/ni.1980, DOI	2011	15.04	2012	2016	
Mizushima N, 2008, NATURE, V451, P1069, DOI 10.1038/nature06639, DOI	2008	14.63	2012	2013	
Levine B, 2008, CELL, V132, P27, DOI 10.1016/j.cell.2007.12.018, DOI	2008	13.45	2012	2013	
Chen ZH, 2008, PLOS ONE, V3, P0, DOI 10.1371/journal.pone.0003316, DOI	2008	13.45	2012	2013	
Luciani A, 2010, NAT CELL BIOL, V12, P863, DOI 10.1038/ncb2090, DOI	2010	12.83	2012	2015	
Jemal A, 2010, CA-CANCER J CLIN, V60, P277, DOI 10.3322/caac.20073, DOI	2010	12	2012	2015	
Mizushima N, 2011, CELL, V147, P728, DOI 10.1016/j.cell.2011.10.026, DOI	2011	18.2	2013	2016	
Yang ZNJ, 2011, MOL CANCER THER, V10, P1533, DOI 10.1158/1535-7163.MCT-11-0047, DOI	2011	15.11	2013	2016	
Kim J, 2011, NAT CELL BIOL, V13, P132, DOI 10.1038/ncb2152, DOI	2011	13.73	2013	2016	
Patel AS, 2012, PLOS ONE, V7, P0, DOI 10.1371/journal.pone.0041394, DOI	2012	13.31	2013	2017	
Komatsu M, 2010, NAT CELL BIOL, V12, P213, DOI 10.1038/ncb2021, DOI	2010	12.78	2013	2015	
Amaravadi RK, 2011, CLIN CANCER RES, V17, P654, DOI 10.1158/1078-0432.CCR-10-2634, DOI	2011	12.35	2013	2016	
Guo JY, 2011, GENE DEV, V25, P460, DOI 10.1101/gad.2016311, DOI	2011	12	2013	2016	
Kang R, 2011, CELL DEATH DIFFER, V18, P571, DOI 10.1038/cdd.2010.191, DOI	2011	10.97	2013	2016	
Lee SJ, 2011, AM J RESP CRIT CARE, V183, P649, DOI 10.1164/rccm.201005-0746OC, DOI	2011	10.97	2013	2016	
Klionsky DJ, 2012, AUTOPHAGY, V8, P445, DOI 10.4161/auto.19496, DOI	2012	30.99	2014	2017	
White E, 2012, NAT REV CANCER, V12, P401, DOI 10.1038/nrc3262, DOI	2012	16.64	2014	2017	
Ryter SW, 2015, REDOX BIOL, V4, P215, DOI 10.1016/j.redox.2014.12.010, DOI	2015	11.33	2018	2020	
Saxton RA, 2017, CELL, V168, P960, DOI 10.1016/j.cell.2017.02.004, DOI	2017	11.01	2018	2022	
Siegel RL, 2017, CA-CANCER J CLIN, V67, P7, DOI 10.3322/caac.21387, DOI	2017	10.91	2018	2020	
Levy JMM, 2017, NAT REV CANCER, V17, P528, DOI 10.1038/nrc.2017.53, DOI	2017	19.91	2019	2022	
Racanelli AC, 2018, AUTOPHAGY, V14, P221, DOI 10.1080/15548627.2017.1389823, DOI	2018	15.66	2019	2022	
Siegel RL, 2021, CA-CANCER J CLIN, V71, P7, DOI 10.3322/caac.21654, DOI	2021	13.31	2021	2022	
Dikic I, 2018, NAT REV MOL CELL BIO, V19, P349, DOI 10.1038/s41580-018-0003-4, DOI	2018	13.08	2019	2022	
Liu GB, 2017, INT J MOL SCI, V18, P0, DOI 10.3390/ijms18020367, DOI	2017	12.2	2019	2022	
Bray F, 2018, CA-CANCER J CLIN, V68, P394, DOI 10.3322/caac.21492, DOI	2018	46.2	2020	2022	
Mauthe M, 2018, AUTOPHAGY, V14, P1435, DOI 10.1080/15548627.2018.1474314, DOI	2018	15.22	2020	2022	
Herbst RS, 2018, NATURE, V553, P446, DOI 10.1038/nature25183, DOI	2018	14.4	2020	2022	
Levine B, 2019, CELL, V176, P11, DOI 10.1016/j.cell.2018.09.048, DOI	2019	14.01	2020	2022	
Hirsch FR, 2017, LANCET, V389, P299, DOI 10.1016/S0140-6736(16)30958-8, DOI	2017	10.92	2020	2022	

FIGURE 8
Visualization of co-cited references on autophagy research in lung disease. **(A)** Reference co-citation network. Circles are co-cited literature. **(B)** Co-cited reference density visualization. **(C)** Network visualization diagram of cited references. **(D)** The clustered network map of lung disease autophagy-related co-cited references. **(E)** The 45 references having the highest citation burst.

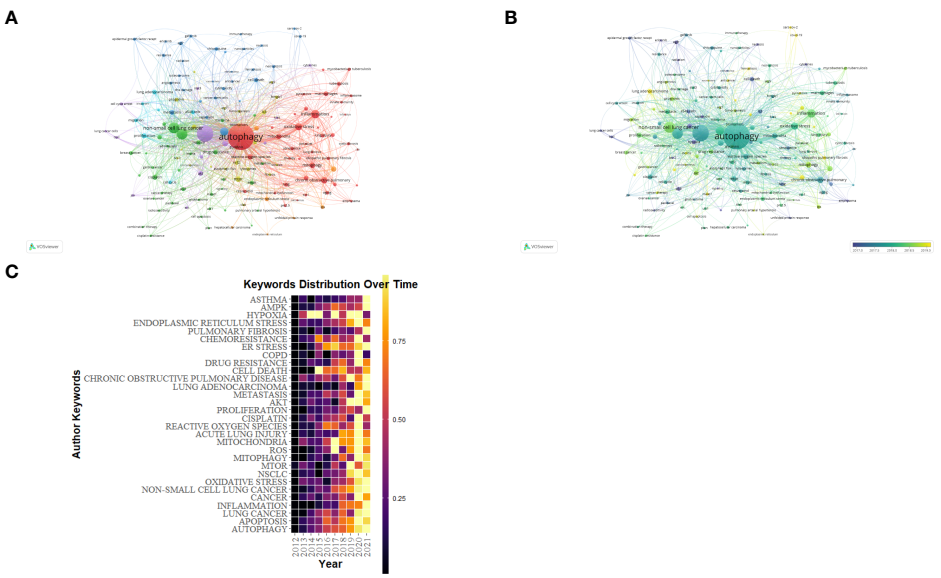

FIGURE 9
The keyword mapping of autophagy research in lung disease. **(A)** The 155 keywords appearing over 13 times fell into five clusters based on colors: Cluster 1, 2, 3, 4, and 5 are, respectively, red, green, blue, yellow, and purple. The node size denotes the occurrence frequency. **(B)** Keywords visualization based on the APY. Keywords in cluster 4 occurred later than those in cluster 3. **(C)** Yearly occurrences of the top keywords.

TABLE 6 Top 20 keywords of publications regarding autophagy research in lung disease based on occurrences.

Rank	Keywords	Occurrences	TLS	Rank	Keywords	Occurrences	TLS
1	Autophagy	1,967	1,734	11	ROS	87	136
2	Apoptosis	757	1,025	12	Mitochondria	85	110
3	Non–small cell lung disease	326	326	13	Reactive Oxygen Species	84	126
4	Lung cancer	309	348	14	Acute lung injury	84	112
5	Inflammation	205	259	15	Cisplatin	75	115
6	Cancer	187	172	16	Proliferation	74	119
7	Oxidative stress	140	203	17	AKT	68	103
8	Chronic obstructive pulmonary disease	117	121	18	Metastasis	67	83
9	MTOR	94	137	19	Macrophages	67	70
10	Mitophagy	89	113	20	Lung adenocarcinoma	64	69

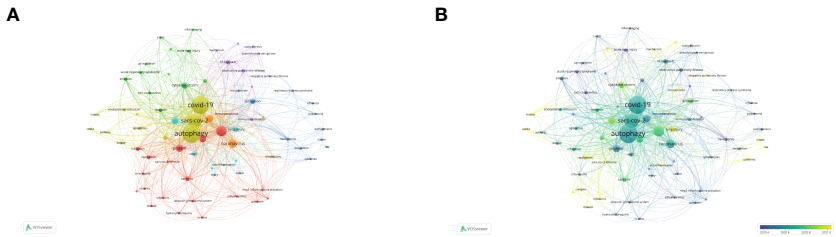

FIGURE 10
Visualization analysis of autophagy research in lung disease resulted from COVID-19. **(A)** Keyword network mapping. A total of 76 keywords appearing for over two times fell into six clusters based on colors. **(B)** APY-based keyword visualization. Keywords in yellow occurred later than those in blue (color version can be found online).

(50, 51). Recently, researchers have revealed the stronger affinity exhibited by NSP6 protein of SARS-CoV-2 in binding with the ER (52). Because of the genetic alternation, virus is capable of restricting autophagy through damaged autophagosome processing, where viral particles can be less degraded by lysosome (52). In addition, relying on PLP2 overexpression in SARS-CoV and MERS-CoV cell lines, the virus is capable of preventing autophagolysosomal formation and suppressing autophagy flux, which may serve for inhibiting autophagy in SARS-CoV-2 (53). These studies reveal the potential ways for SARS-CoV-2 to inhibit autophagy infection or avoid the pathogenic clearance of host cells, meanwhile restricting the sufficient immune response, which is similar to other types of coronaviruses, and need to be further investigated. Eliminating viruses by autophagy (also called virophagy) can well serve for various viral infections (54, 55). Despite the various ways through viruses get access to cells, autophagy augmentation can promote virus clearance, thus reducing the viral load from a strategic perspective (56, 57). To prove this from a conceptual perspective, some recent studies have investigated how the three different drugs (spermidine, MK02206, and niclosamide) induced by autophagy restrict the propagation of SARS-CoV-2 (58). Autophagy induction together with relevant overall immunity upregulation assists in combating the exacerbations, which may prove to be a strategy to enhance immunity and prevent COVID-19 infection (59). Autophagy induction can enhance immunity, restrict viral load, support SARS-CoV-2 clearance, and simultaneously assist in treating COVID-19 infection and preventing negative results, although further investigation is required to confirm these effects.

The pathogenesis regarding severe COVID-19 mediated by SARS-CoV-2 is pointed out to be associated with the activation of many pro-inflammatory cytokines that constitute the cytokine storm, resulting in a hyper-inflammatory state. In addition to destroying the lung and COVID-19–related ARDS, such inflammatory response is also capable of damaging the cardiovascular, nervous, and gastrointestinal systems and bringing into direct and long-term outcomes (60). To support these findings, studies have revealed how autophagy affects the inflammatory response in organ systems including the lung (61, 62). Accordingly, autophagy induction is capable of attenuating lung inflammation in the event of being exposed to pathogens. Hence, except for infection, using autophagy induction for restricting the inflammatory response has huge potentials for treating COVID-19 and decreasing relevant morbidity and mortality.

In this study, we employed the bibliometric approach for visualizing the research on autophagy-mediated lung diseases, thereby gaining a better understanding about the hot spots and trends in this field. Nevertheless, it suffers many limitations (1). The study only included English articles and reviews from the SCI-Expanded. (2) Currently, the limitation of software-based scientific measurement added the difficulty in combining at least two databases for the analysis. Hence, the study only adopted the WoSCC database for the screening and might have missed the other related studies in the literature. Therefore, more databases should be employed for a more rigorous analysis in the future. (3) Open-source journals may have an impact on both citation volume and publication volume. (4) The combination of CiteSpace and VOSviewer for literature analysis may miss information during analysis. Specifically, VOSviewer keyword analysis clustering might not have been able to extract key information, because color was only used to divide the range.

Conclusions

According to bibliometric analysis, the research on autophagy in the field of lung diseases has broad prospects and rapid development. We identified the major contributors, regions, and publications in the research area. China published the largest NP and the US made more huge breakthroughs. The latest studies have been published and new progression regarding the field has been made on AUTOPHAGY and ONCOTARGET. Recently, oxidative stress has been revealed to have significant impact on the pathogenesis of autophagy-mediated lung diseases. In addition, the mechanism of autophagy induction may prove crucial as a treatment strategy for COVID-19 over classical antivirals and provide a tool to end the pandemic. Attenuating the progression of COVID-19–associated lung diseases by inhibiting autophagy may become a new research hotspot in this field.

Data availability statement

The original contributions presented in the study are included in the article/supplementary material. Further inquiries can be directed to the corresponding authors.

Author contributions

FL, YC and WM did the bibliometrics analysis and wrote the manuscript. HZ, ZX, SH, XS, ML, JW and WZ participated in the experimental design and manuscript writing. SW and XL designed this study and organized the manuscript writing. All authors contributed to the article and approved the submitted version.

Funding

This work was supported by the National Natural Science Foundation of China (No. 81871601), the Program of Shanghai Academic Research Leader (No. 21XD1402800), the Shanghai Natural Science Foundation (22ZR1452200), the Development

Fund for the Department of Anesthesiology, Shanghai Pulmonary Hospital.

Conflict of interest

The authors declare that the research was conducted in the absence of any commercial or financial relationships that could be construed as a potential conflict of interest.

Publisher's note

References

1. Klionsky DJ, Emr SD. Autophagy as a regulated pathway of cellular degradation. *Science* (2000) 290(5497):1717–21. doi: 10.1126/science.290.5497.1717

2. Mizushima N, Komatsu M. Autophagy: renovation of cells and tissues. *Cell* (2011) 147(4):728–41. doi: 10.1016/j.cell.2011.10.026

3. Klionsky DJ, Petroni G, Amaravadi RK, Baehrecke EH, Ballabio A, Boya P, et al. Autophagy in major human diseases. *EMBO J* (2021) 40(19):e108863. doi: 10.15252/embj.2021108863

4. Verzella D, Pescatore A, Capece D, Vecchiotti D, Ursini MV, Franzoso G, et al. Life, death, and autophagy in cancer: NF-κB turns up everywhere. *Cell Death Dis* (2020) 11(3):210. doi: 10.1038/s41419-020-2399-y

5. Galluzzi L, Baehrecke EH, Ballabio A, Boya P, Bravo-San Pedro JM, Cecconi F, et al. Molecular definitions of autophagy and related processes. *EMBO J* (2017) 36(13):1811–36. doi: 10.15252/embj.201796697

6. Mizushima N. A brief history of autophagy from cell biology to physiology and disease. *Nat Cell Biol* (2018) 20(5):521–7. doi: 10.1038/s41556-018-0092-5

7. Petersson J, Glenny RW. Gas exchange and ventilation-perfusion relationships in the lung. *Eur Respir J* (2014) 44(4):1023–41. doi: 10.1183/09031936.00037014

8. Nasim F, Sabath BF, Eapen GA. Lung cancer. *Med Clin North Am* (2019) 103 (3):463–73. doi: 10.1016/j.mcna.2018.12.006

9. Ranieri VM, Rubenfeld GD, Thompson BT, Ferguson ND, Caldwell E, Fan E, et al. Acute respiratory distress syndrome: the Berlin definition. *JAMA* (2012) 307 (23):2526–33. doi: 10.1001/jama.2012.5669

10. Beitler JR, Thompson BT, Baron RM, Bastarache JA, Denlinger LC, Esserman L, et al. Advancing precision medicine for acute respiratory distress syndrome. *Lancet Respir Med* (2022) 10(1):107–20. doi: 10.1016/S2213-2600(21)00157-0

11. Ma C, Su H, Li H. Global research trends on prostate diseases and erectile dysfunction: A bibliometric and visualized study. *Front Oncol* (2020) 10:627891. doi: 10.3389/fonc.2020.627891

12. Guler AT, Waaijer CJ, Palmblad M. Scientific workflows for bibliometrics. *Scientometrics* (2016) 107:385–98. doi: 10.1007/s11192-016-1885-6

13. Huang X, Fan X, Ying J, Chen S. Emerging trends and research foci in gastrointestinal microbiome. *J Transl Med* (2019) 17(1):67. doi: 10.1186/s12967-019-1810-x

14. Zhang T, Yin X, Yang X, Man J, He Q, Wu Q, et al. Research trends on the relationship between microbiota and gastric cancer: A bibliometric analysis from 2000 to 2019. *J Cancer* (2020) 11(16):4823–31. doi: 10.7150/jca.44126

15. Liang M, Meng Y, Zhou S, Tao Z, Tao L. Research hotspots and trends analysis of ankylosing spondylitis: a bibliometric and scientometric analysis from 2009 to 2018. *Ann Transl Med* (2020) 8(21):1445. doi: 10.21037/atm-20-1259

16. Martynov I, Klima-Frysch J, Schoenberger J. A scientometric analysis of neuroblastoma research. *BMC Cancer* (2020) 20(1):486. doi: 10.1186/s12885-020-06974-3

17. Landis JR, Koch GG. The measurement of observer agreement for categorical data. *Biometrics* (1977) 33(1):159–74. doi: 10.2307/2529310

18. Hirsch JE. An index to quantify an individual's scientific research output. *Proc Natl Acad Sci U S A.* (2005) 102(46):16569–72. doi: 10.1073/pnas.0507655102

19. Abbas AM. Bounds and inequalities relating h-index, g-index, e-index and generalized impact factor: an improvement over existing models. *PloS One* (2012) 7 (4):e33699. doi: 10.1371/journal.pone.0033699

20. Jones T, Huggett S, Kamalski J. Finding a way through the scientific literature: indexes and measures. *World Neurosurg* (2011) 76(1-2):36–8. doi: 10.1016/j.wneu.2011.01.015

21. Roldan-Valadez E, Salazar-Ruiz SY, Ibarra-Contreras R, Rios C. Current concepts on bibliometrics: a brief review about impact factor, eigenfactor score, CiteScore, SCImago journal rank, source-normalised impact per paper, h-index, and alternative metrics. *Ir J Med Sci* (2019) 188(3):939–51. doi: 10.1007/s11845-018-1936-5

22. Campra M, Riva P, Oricchio G, Brescia V. Bibliometrix analysis of medical tourism. *Health Serv Manage Res* (2022) 35(3):172–88. doi: 10.1177/09514848211011738

23. van Eck NJ, Waltman L. Software survey: VOSviewer, a computer program for bibliometric mapping. *Scientometrics* (2010) 84(2):523–38. doi: 10.1007/s11192-009-0146-3

24. Yao L, Hui L, Yang Z, Chen X, Xiao A. Freshwater microplastics pollution: Detecting and visualizing emerging trends based on citespace II. *Chemosphere* (2020) 245:125627. doi: 10.1016/j.chemosphere.2019.125627

25. Zou X, Vu HL, Huang H. Fifty years of accident analysis & prevention: A bibliometric and scientometric overview. *Accid Anal Prev* (2020) 144:105568. doi: 10.1016/j.aap.2020.105568

26. Chen C. Searching for intellectual turning points: progressive knowledge domain visualization. *Proc Natl Acad Sci U S A.* (2004) 101(Suppl 1):5303–10. doi: 10.1073/pnas.0307513100

27. Shi X, Wang S, Wu Y, Li Q, Zhang T, Min K, et al. A bibliometric analysis of the innate immune DNA sensing cGAS-STING pathway from 2013 to 2021. *Front Immunol* (2022) 13:916383. doi: 10.3389/fimmu.2022.916383

28. Abdulrahman BA, Khweek AA, Akhter A, Caution K, Kotrange S, Abdelaziz DH, et al. Autophagy stimulation by rapamycin suppresses lung inflammation and infection by burkholderia cenocepacia in a model of cystic fibrosis. *Autophagy* (2011) 7(11):1359–70. doi: 10.4161/auto.7.11.17660

29. Miao L, Zhang J, Zhang Z, Wang S, Tang F, Teng M, et al. A bibliometric and knowledge-map analysis of CAR-T cells from 2009 to 2021. *Front Immunol* (2022) 13:840956. doi: 10.3389/fimmu.2022.840956

30. Mizushima N, Levine B, Cuervo AM, Klionsky DJ. Autophagy fights disease through cellular self-digestion. *Nature* (2008) 451(7182):1069–75. doi: 10.1038/nature06639

31. Martinet W, De Meyer GR, Andries L, Herman AG, Kockx MM. *In situ* detection of starvation-induced autophagy. *J Histochem Cytochem* (2006) 54(1):85–96. doi: 10.1369/jhc.5A6743.2005

32. Ohsumi Y. Historical landmarks of autophagy research. *Cell Res* (2014) 24 (1):9–23. doi: 10.1038/cr.2013.169

33. Callaham M, Wears RL, Weber E. Journal prestige, publication bias, and other characteristics associated with citation of published studies in peer-reviewed journals. *JAMA* (2002) 287(21):2847–50. doi: 10.1001/jama.287.21.2847

34. Bolli R. Ten years at the helm of circulation research. *Circ Res* (2019) 124 (12):1707–17. doi: 10.1161/CIRCRESAHA.119.315287

35. Levine B, Kroemer G. Autophagy in the pathogenesis of disease. *Cell* (2008) 132(1):27–42. doi: 10.1016/j.cell.2007.12.018

36. Choi AM, Alam J. Heme oxygenase-1: function, regulation, and implication of a novel stress-inducible protein in oxidant-induced lung injury. *Am J Respir Cell Mol Biol* (1996) 15(1):9–19. doi: 10.1165/ajrcmb.15.1.8679227

37. Lee J, Giordano S, Zhang J. Autophagy, mitochondria and oxidative stress: cross-talk and redox signalling. *Biochem J* (2012) 441(2):523–40.

38. Mondaca-Ruff D, Riquelme JA, Quiroga C, Norambuena-Soto I, Sanhueza-Olivares F, Villar-Fincheira P, et al. Angiotensin II-regulated autophagy is required for vascular smooth muscle cell hypertrophy. *Front Pharmacol* (2018) 9:1553. doi: 10.3389/fphar.2018.01553

39. Yang S, Sun D, Wang L, Wang X, Shi M, Jiang X, et al. The role of STAT3/mTOR-regulated autophagy in angiotensin II-induced senescence of human

glomerular mesangial cells. *Cell Signal* (2019) 53:327–38. doi: 10.1016/j.cellsig.2018.10.021

40. Zhang L, Wang H, Xu J, Zhu J, Ding K. Inhibition of cathepsin s induces autophagy and apoptosis in human glioblastoma cell lines through ROS-mediated PI3K/AKT/mTOR/p70S6K and JNK signaling pathways. *Toxicol Lett* (2014) 228 (3):248–59. doi: 10.1016/j.toxlet.2014.05.015

41. Rahman I, Biswas SK, Kode A. Oxidant and antioxidant balance in the airways and airway diseases. *Eur J Pharmacol* (2006) 533(1-3):222–39. doi: 10.1016/j.ejphar.2005.12.087

42. Zhang J, Kim J, Alexander A, Cai S, Tripathi DN, Dere R, et al. A tuberous sclerosis complex signalling node at the peroxisome regulates mTORC1 and autophagy in response to ROS. *Nat Cell Biol* (2013) 15(10):1186–96. doi: 10.1038/ncb2822

43. Salmeen A, Barford D. Functions and mechanisms of redox regulation of cysteine-based phosphatases. *Antioxid Redox Signal* (2005) 7(5-6):560–77. doi: 10.1089/ars.2005.7.560

44. Koga H, Cuervo AM. Chaperone-mediated autophagy dysfunction in the pathogenesis of neurodegeneration. *Neurobiol Dis* (2011) 43(1):29–37. doi: 10.1016/j.nbd.2010.07.006

45. Bellot G, Garcia-Medina R, Gounon P, Chiche J, Roux D, Pouysségur J, et al. Hypoxia-induced autophagy is mediated through hypoxia-inducible factor induction of BNIP3 and BNIP3L *via* their BH3 domains. *Mol Cell Biol* (2009) 29 (10):2570–81. doi: 10.1128/MCB.00166-09

46. Lee SJ, Smith A, Guo L, Alastalo TP, Li M, Sawada H, et al. Autophagic protein LC3B confers resistance against hypoxia-induced pulmonary hypertension. *Am J Respir Crit Care Med* (2011) 183(5):649–58. doi: 10.1164/rccm.201005-0746OC

47. Li X, Ma X. Acute respiratory failure in COVID-19: is it "typical" ARDS. *Crit Care* (2020) 24(1):198. doi: 10.1186/s13054-020-02911-9

48. Guo T, Fan Y, Chen M, Wu X, Zhang L, He T, et al. Cardiovascular implications of fatal outcomes of patients with coronavirus disease 2019 (COVID-19). *JAMA Cardiol* (2020) 5(7):811–8. doi: 10.1001/jamacardio.2020.1017

49. Chaimayo C, Kaewnaphan B, Tanlieng N, Athipanyasilp N, Sirijatuphat R, Chayakulkeeree M, et al. Rapid SARS-CoV-2 antigen detection assay in comparison with real-time RT-PCR assay for laboratory diagnosis of COVID-19 in Thailand. *Virol J* (2020) 17(1):177. doi: 10.1186/s12985-020-01452-5

50. Mijaljica D, Klionsky DJ. Autophagy/virophagy: a "disposal strategy" to combat COVID-19. *Autophagy* (2020) 16(12):2271–2. doi: 10.1080/15548627.2020.1782022

51. Bonam SR, Muller S, Bayry J, Klionsky DJ. Autophagy as an emerging target for COVID-19: lessons from an old friend, chloroquine. *Autophagy* (2020) 16 (12):2260–6. doi: 10.1080/15548627.2020.1779467

52. Benvenuto D, Angeletti S, Giovanetti M, Bianchi M, Pascarella S, Cauda R, et al. Evolutionary analysis of SARS-CoV-2: how mutation of non-structural protein 6 (NSP6) could affect viral autophagy. *J Infect* (2020) 81(1):e24–7. doi: 10.1016/j.jinf.2020.03.058

53. Chen X, Wang K, Xing Y, Tu J, Yang X, Zhao Q, et al. Coronavirus membrane-associated papain-like proteases induce autophagy through interacting with Beclin1 to negatively regulate antiviral innate immunity. *Protein Cell* (2014) 5 (12):912–27. doi: 10.1007/s13238-014-0104-6

54. Abdoli A, Alirezaei M, Mehrbod P, Forouzanfar F. Autophagy: The multi-purpose bridge in viral infections and host cells. *Rev Med Virol* (2018) 28(4):e1973. doi: 10.1002/rmv.1973

55. Mehrbod P, Ande SR, Alizadeh J, Rahimizadeh S, Shariati A, Malek H, et al. The roles of apoptosis, autophagy and unfolded protein response in arbovirus, influenza virus, and HIV infections. *Virulence* (2019) 10(1):376–413. doi: 10.1080/21505594.2019.1605803

56. Carmona-Gutierrez D, Bauer MA, Zimmermann A, Kainz K, Hofer SJ, Kroemer G, et al. Digesting the crisis: autophagy and coronaviruses. *Microb Cell* (2020) 7(5):119–28. doi: 10.15698/mic2020.05.715

57. Yang N, Shen HM. Targeting the endocytic pathway and autophagy process as a novel therapeutic strategy in COVID-19. *Int J Biol Sci* (2020) 16(10):1724–31. doi: 10.7150/ijbs.45498

58. Woodby B, Arnold MM, Valacchi G. SARS-CoV-2 infection, COVID-19 pathogenesis, and exposure to air pollution: What is the connection. *Ann N Y Acad Sci* (2021) 1486(1):15–38. doi: 10.1111/nyas.14512

59. Hannan MA, Rahman MA, Rahman MS, Sohag AAM, Dash R, Hossain KS, et al. Intermittent fasting, a possible priming tool for host defense against SARS-CoV-2 infection: Crosstalk among calorie restriction, autophagy and immune response. *Immunol Lett* (2020) 226:38–45. doi: 10.1016/j.imlet.2020.07.001

60. Jamwal S, Gautam A, Elsworth J, Kumar M, Chawla R, Kumar P. An updated insight into the molecular pathogenesis, secondary complications and potential therapeutics of COVID-19 pandemic. *Life Sci* (2020) 257:118105. doi: 10.1016/j.lfs.2020.118105

61. Painter JD, Galle-Treger L, Akbari O. Role of autophagy in lung inflammation. *Front Immunol* (2020) 11:1337. doi: 10.3389/fimmu.2020.01337

62. Racanelli AC, Choi A, Choi ME. Autophagy in chronic lung disease. *Prog Mol Biol Transl Sci* (2020) 172:135–56. doi: 10.1016/bs.pmbts.2020.02.001

frontiers | Frontiers in Immunology

TYPE Original Research
PUBLISHED 20 December 2022
DOI 10.3389/fimmu.2022.1095915

OPEN ACCESS

EDITED BY
Kai Wang,
Southwest Medical University, China

REVIEWED BY
Fei Kuang,
University of Duisburg-Essen, Germany
Wenfeng Zhang,
Chongqing Medical University, China
Chi Ma,
National Institutes of Health (NIH), United States

*CORRESPONDENCE
Xiaoli Yang
344920646@qq.com
Kai He
Hekai615@126.com

†These authors have contributed equally to this work

SPECIALTY SECTION
This article was submitted to Inflammation, a section of the journal Frontiers in Immunology

RECEIVED 11 November 2022
ACCEPTED 06 December 2022
PUBLISHED 20 December 2022

CITATION
Gou H, Liu S, Liu L, Luo M, Qin S, He K and Yang X (2022) Obeticholic acid and 5β-cholanic acid 3 exhibit anti-tumor effects on liver cancer through CXCL16/CXCR6 pathway. *Front. Immunol.* 13:1095915. doi: 10.3389/fimmu.2022.1095915

Obeticholic acid and 5β-cholanic acid 3 exhibit anti-tumor effects on liver cancer through CXCL16/CXCR6 pathway

Haoxian Gou[1,2†], Shenglu Liu[2†], Linxin Liu[1], Ming Luo[2], Shu Qin[2], Kai He[1,2*] and Xiaoli Yang[1,2*]

[1]Department of Hepatobiliary Surgery, The Affiliated Hospital of Southwest Medical University, Luzhou, China, [2]Academician Workstation of Sichuan Province, Luzhou, China

Hepatocellular carcinoma (HCC) is the most common type of liver malignancy with a high incidence and mortality rate. Previous *in vitro* and *in vivo* studies have confirmed that liver sinusoidal endothelial cells (LSEC) secrete CXCL16, which acts as a messenger to increase the hepatic accumulation of $CXCR6^+$ natural killer T (NKT) cells and exert potent antitumor effects. However, evidence for this process in humans is lacking and its clinical significance is still unclear. In this study, by dissecting the human HCC single-cell RNA-seq data, we verified this process through cellphoneDB. NKT cells in patients with high expression of CXCL16 exhibited a higher activation state and produced more interferon-γ (IFN-γ) compared with those with low expression. We next investigated the signaling pathways between activated (CD69 high) and unactivated NKT cells (CD69 low) using NKT cell-developmental trajectories and functional enrichment analyses. *In vivo* experiments, we found that farnesoid X receptor agonist (obeticholic acid) combined with the takeda G protein coupled receptor 5 antagonist (5β-cholanic acid 3) exhibited significant tumor suppressive effects in the orthotopic liver tumor model and this result may be related to the CXCL16/CXCR6 axis. In conclusion, our study provides the basis and potential strategies for HCC immunotherapy based on NKT cells.

KEYWORDS

single cell RNA sequencing, hepatocellular carcinoma, immunotherapy, CXCL16, natural killer T cells, bile acids

1 Introduction

Hepatocellular carcinoma (HCC) is one of the most prevalent human cancers associated with a high mortality rate (1). Due to the low resection rate of HCC and the high recurrence risk after hepatectomy or transplantation, comprehensive treatments including surgery, interventional therapy, targeted treatment, and emerging

immunotherapy approaches are necessary (2). Immune checkpoint inhibitors, such as nivolumab and pembrolizumab, which target programmed cell death protein-1 (PD1) mainly enhance the T-cell response to tumors, thus improving the prognoses of patients with HCC (3, 4). However, only approximately 20% of patients with malignancy benefit from this approach (5).

In addition to T cells, the liver is also abundant in natural killer T (NKT) cells which account for 25% of human liver lymphocytes and 40% of mouse liver lymphocytes (6). NKT cells are a heterogeneous subpopulation of T cells coexpressing T-cell receptors and various receptors that are abundantly expressed in NK cells (7). Activated NKT cells exert powerful antitumor function through multiple mechanisms involved in the granzyme and perforin pathway, release immunomodulatory cytokines including interferon (IFN-γ) and tumor necrosis factor (TNF), and form the Fas/FasL and TRAIL/TRAILR complex (8–10). Therefore, immunotherapy based on targeting NKT cells is a promising and novel strategy to improve the outcomes in patients with HCC.

CXCL16, a chemokine mainly secreted by liver sinusoidal endothelial cells (LSEC) in the liver triggers the hepatic recruitment of $CXCR6^+$ NKT cells, thus exerting a potent antitumor effect (11, 12). Ma, et al. found that CXCL16 not only promotes the recruitment of NKT cells to the liver but also promotes the activation of intrahepatic NKT cells, as manifested by the elevation of some activation markers (such as CD69) and the increase of antitumor cytokine (such as IFN-γ) (13). Zhu, et al. also found that CXCR6 deficiency impaired the IFN-γ producing capacity of hepatic NKT cells, and downgraded the accumulation of NKT cells (14). The gut microbiome mediates the conversion of primary bile acids to secondary bile acids. Primary and secondary bile acids have different effects on CXCL16 production in LSEC. Specifically, primary bile acids upregulate CXCL16 secretion in LSEC, enhancing antitumor activity, whereas secondary bile acids exhibit the opposite response (13, 15). Although these findings provide new targets for the treatment of HCC, controlling the gut microbiome or directly altering the composition and ratio of primary and secondary bile acids is complicated.

Abbreviations: AST, aspartate aminotransferase; ALT, alanine aminotransferase; BUN, Blood urea nitrogen; CRE, creatinine; CH, CXCL16 high expression group; CL, CXCL16 low expression group; CNV, copy number variation; DEGs, differentially expressed genes; FXR, farnesoid X receptor; GO, gene ontology; HCC, hepatocellular carcinoma; H&E, hematoxylin and eosin; KM mice, kunming mice; LSEC, liver sinusoidal endothelial cells; NKT cells, natural killer T cells; OCA, obeticholic acid; PD1, programmed cell death protein-1; PCA, principal components analysis; PCs, principal components; PBS, phosphate buffer solution; scRNA-seq, single-cell RNA sequencing; t-SNE, t-distributed stochastic neighbor embedding; TLCA, taurolithocholic acid. TGR5, takeda G protein coupled receptor 5; 5β-CA, 5β-cholanic acid 3.

Primary bile acids are predominantly bound to the farnesoid X receptor (FXR) and secondary bile acids are primarily bound to the takeda G protein coupled receptor 5 (TGR5) in LSEC (16–18). Therefore, we assumed that applying drugs binding to both FXR and TGR5 could directly target CXCL16 production in LSEC, bypassing the bile acids as well as microbiota metabolism, thereby being a promising, feasible immunotherapeutic approach to treat HCC. Given this background, we evaluated the FXR agonist obeticholic acid (OCA) to mimic primary bile acids and 5β-cholanic acid 3 (5β-CA) to block the downstream signaling of secondary bile acids as an approach to treating HCC using an orthotopic HCC mouse model (Figure 1).

Single-cell RNA sequencing (scRNA-seq) is an efficient method for investigating cell heterogeneity, cell-cell interactions, and cell evolution. Given that the interaction of LSEC with NKT cells has not been validated using tissue samples of patients with HCC, we dissected 53,982 human single-cell transcriptomes to explore the feasibility of targeting the LSEC-CXCL16/CXCR6+ NKT cells axis in humans.

2 Materials and methods

2.1 scRNA-seq data collection

The GSE149614 dataset was obtained from the GEO database, which included 71,915 cells from 10 patients with HCC and from 4 relevant sites: primary liver tumor, normal liver, metastatic lymph node, and portal vein tumor thrombus. Among them, 8 patients with HCC having primary tumor tissues and paired normal liver tissues were selected for this study. Two other patients were excluded as only tumor samples were available.

2.2 Data processing

Cell filtering, normalization, dimensionality reduction, clustering, and cell-type annotation were performed using the "Seurat" package (version 4.1.1) in RStudio. The gene-barcode matrix was filtered to exclude low-quality cells (< 600 or > 7000 detected genes, >15% mitochondrial genes) and low-expressed genes (any gene expressed in < 10 cells). Finally, 53,982 cells from primary tumor tissue (26,259 cells) and normal liver tissue (277,23 cells) were selected for subsequent analysis.

Raw counts data were normalized using the "NormalizeData" function with the default parameters (scale.factor = 10000). The top 1500 most variable genes obtained using the "vst" method were used for principal components analysis (PCA). Principal components (PCs) were identified using the "RunPCA" and "Jackstraw" functions. The first 16 PCs were used for cluster identification and t-Distributed Stochastic Neighbor Embedding (t-SNE) dimensionality reduction with the parameter "res = 0.8." The marker genes of the generated clusters were determined by

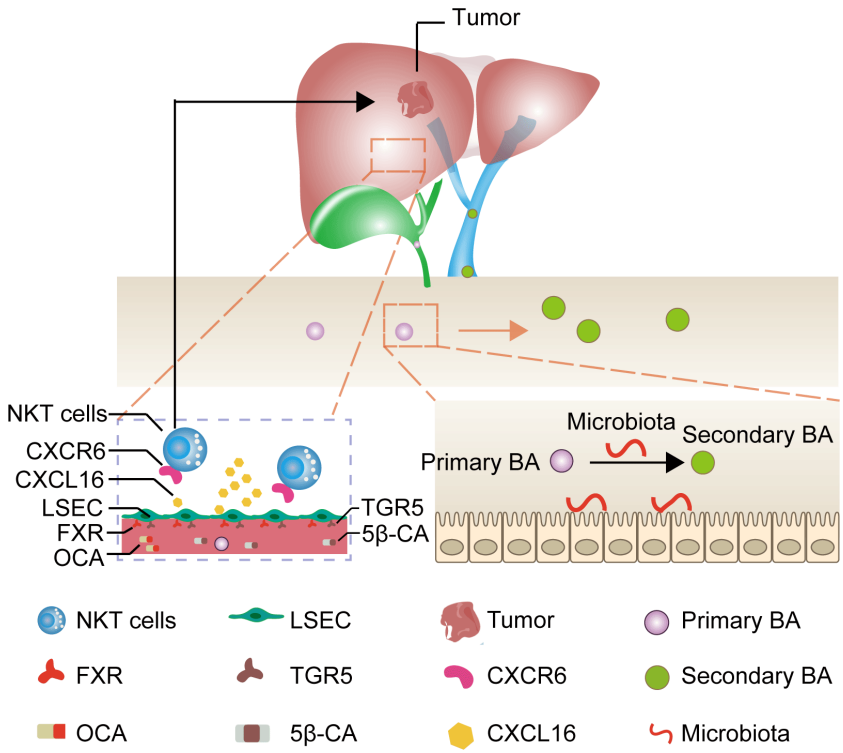

FIGURE 1
Mechanism of liver cancer immunotherapy mediated by OCA and 5β-CA. OCA binds to FXR and 5β-CA binds to TGR5, thus upregulating CXCL16 secretion from LSEC. The increase in CXCL16 promotes NKT cell accumulation in the liver and tumor-suppressive effects.

running the "FindAllMarkers" function with the parameter "only.pos = TRUE, min.pct = 0.25." Next, cell-type annotation was based on the "CellMarker" database and the existing literature.

2.3 Copy number variation inference

Single cells with clonal large-scale chromosome CNV were evaluated using the "inferCNV" R package (version 1.10.1) with the default setting. The setting parameters included "denoise = T," "cutoff = 0.1," and "HMM = F." T cells and B cells from adjacent liver samples were input as the reference group and other cells as the observation group.

2.4 Cell–cell communication analysis

To explore potential receptor–ligand interactions between different cells, the "CellphoneDB" python package (version 3.0.0) was used for cell–cell communication analysis. CellphoneDB is a public repository that includes a known list of ligands, receptors, and their interactions from existing literature.

We investigated the possible presence of ligand–receptor pairs between endothelial cells, myeloid cells, NKT cells, LSEC, hepatocytes, T cells, and B cells in normal liver tissues adjacent to the tumor tissues, and also ligand–receptor pairs between malignant cells, myeloid cells, NKT cells, T cells, and B cells in primary tumor tissues. To quantify the potential communication between these cells, general circos plots and detailed plots for each major cell type were drawn using the igraph package in RStudio. We then selected chemokine ligand–receptor pairs in normal liver tissues and immune-related ligand–receptor couples in primary tumor tissues to draw bubble diagrams.

2.5 Grouping of patients based on scRNA-seq data

We calculated the proportion of LSEC to all cell types in tumor samples and paired normal liver samples separately by the "proportions" function in RStudio. Next, we assigned 8 patients and 4 patients in each group. The adjacent liver tissues in all patients had a cell count ≥ 1940 (Supplementary Figure 4). Thus, to avoid classification errors arising from the varying total number of cells per patient, we randomly selected 1940 cells of each patient from the normal liver tissue using the "sample" function and subsequently calculated the total amount of CXCL16 expressed by all LSEC in the selected cells and used it

as a score for CXCL16 expression in that patient. Lastly, we divided patients into a CXCL16 high-expression group (CH) or a CXCL16 low-expression group (CL) based on their CXCL16 expression scores.

2.6 Cell developmental trajectory

To infer the differentiation trajectory of NKT cells, we used the "Monocle" package (version 2.22.0) to conduct pseudo-temporal analysis on CD69high and CD69low NKT cells. We first used the "FindAllMarkers" function to determine the differentially expressed genes (DEGs) between CD69high and CD69low NKT cells. Next, we ordered each NKT cell along the trajectory for pseudo-temporal analysis, drew a heat map based on the expression changes of characteristic differential genes using the "plot_pseudotime_heatmap" function, and divided these characteristic differential genes into 5 clusters based on their expression patterns. Based on Gene Ontology (GO) analysis for the biological process, we further annotated the critical clusters with different expression patterns to functional categories.

2.7 DEGs identification and GSEA analysis

We first identified the DEGs between CD69high and CD69low NKT cells using the "FindMarkers" function and mapped the volcano plot and heat map. The "clusterProfiler" package (version 4.2.2) was used for GSEA analysis and the gene sets included the Reactome, Kyoto Encyclopedia of Genes and Genomes (KEGG), and GO (biological process) databases. We applied the "sort" function to rank DEGs from large to small and used the "GSEA" function to acquire results from GSEA. Lastly, GSEA enrichment plots were drawn to show significantly activated and suppressed pathways.

2.8 Cell lines and animals

Mouse liver tumor cells (H22) were purchased from PriCells (Wuhan, China). H22 cells were cultured with Roswell Park Memorial Institute-1640 (RPMI-1640) medium containing 1% penicillin-streptomycin and 10% fetal bovine serum (FBS) and incubated at 37°C in an atmosphere of 5% CO2.

The Southwest Medical University Animal Management Committee approved all animal experiments. Seven-week-old male Kunming (KM) mice weighing 18–22 g were purchased from the Experimental Animal Center of Southwest Medical University. All animals were housed in cages with 5 mice/cage and provided access to food and water ad libitum. All cages were maintained at a constant temperature of 20–24°C and relative humidity of 50%.

2.9 Modeling and pharmacologic interventions

KM mice were used to establish the H22 orthotopic liver tumor model. Anesthetized male KM mice were fixed on an operation table. A longitudinal midline incision was made to allow complete liver exposure. H22 cells extracted from the ascites fluid of KM mice were washed with sterile saline and diluted to 4×107 cells/mL with phosphate buffer saline (PBS). Next, 0.01 mL of the H22 cell suspension (4×105 cells) was slowly injected into the left lobe of the liver of each mouse. The puncture made by the syringe needle was immediately pressed using a 75% ethanol-dipped cotton swab to kill the extravasated cancer cells and prevent the leakage of tumor cells into the peritoneal cavity. Mice were randomized into 4 groups after 3 days of surgery and treated with different drugs.

OCA and 5β-CA were purchased from Beijing Jianqiang Weiye Technology Co. Ltd. (Beijing, China). To upregulate CXCL16 secretion in LSEC, mice were gavaged with OCA (20 mg/kg), or 5β-CA (20 mg/kg), or OCA+5β-CA (20 mg/kg+20 mg/kg) every 2 days at 3 days after H22 inoculation. Polysorbate-20 (Tween-20) was added to dissolve OCA or 5β-CA, which was then diluted in PBS. Vehicle (Tween-20 and PBS)-gavaged mice served as the controls. At 17 days after cell inoculation, the liver tissues, tumors, serum, and intestinal contents were collected and the weights of the liver and tumor were recorded.

2.10 Biochemical and cytokine analysis

To assess the adverse effects of the drugs, serum biochemical parameters including aspartate aminotransferase (AST), alanine aminotransferase (ATL), creatinine (CRE), and blood urea nitrogen (BUN) were analyzed according to the instructions in the corresponding assay kits.

The levels of CXCL16, IFN-γ, and TNF-β in the serum, normal liver tissues, and tumor tissues were determined using the corresponding enzyme-linked immunosorbent assay kits (RUIXIN Biotech, Quanzhou, China) in accordance with the manufacturer's instructions. We used "pg/g" as the concentration unit of cytokines in the tumor and adjacent normal liver tissues and "pg/mL" as the concentration unit for the serum.

2.11 Histological analysis

The collected tumors, and liver, kidney, and lung tissues were fixed with 4% paraformaldehyde, paraffin-embedded, and sectioned to a thickness of 5 μm. Subsequently, the sections were stained with hematoxylin and eosin (H&E), and the tumors as well as pharmacological-induced liver, kidney, and

lung damage were visualized using microscopy. Histological photographs were acquired and analyzed using optical microscopy (Leica, Germany).

2.12 Analysis of intrahepatic immune cells

Tumor tissues were mechanically clipped, filtered through a 300-mesh filter, and centrifuged, and the cell concentration was adjusted to 106 cells/mL with PBS. Next, 100 µL of cell suspensions were taken in sterile Eppendorf tubes; 1 µg each of CD8a, CD3, CD49b, CD45, CD4, Live/Dead, CD69, and CXCR6 antibodies were added, thoroughly mixed, and stained at 4°C for 30 min while protecting from light. The cells were detected using a ZE5 flow cytometer (Bio-rad, American) and the data were analyzed using Flowjo software.

2.13 Statistical analysis

Two-tailed unpaired Student's t-test was used to calculate statistical differences between groups. Data analyses were performed using RStudio software. $P < 0.05$ was considered statistically significant (*0.01 ≤ P value < 0.05, **0.001 ≤ P value < 0.01, ***P value < 0.001).

3 Results

3.1 Determination of cell types in the scRNA-seq dataset

Eight tumor specimens and paired adjacent nontumor liver samples were selected from the GSE149614 dataset for subsequent analysis. After the initial quality controls, we retained 53,982 cells for cell annotation (Supplementary Figures 1, 2). Thirty-seven cell clusters from tumor and normal liver tissues were identified and visualized using t-distributed stochastic neighbor embedding (t-SNE) dimensionality reduction (Figures 2A, B and Supplementary Figure 3).

The cells in clusters 3, 4, 6, 7, 10, 15, 23, 25, 26, and 35 originated from tumor specimens and were highly expressed in ALB, KRT18, and CD24; therefore, they were labeled as malignant cells (Figures 2C, F). Furthermore, these malignant HCC cells were also defined by inferred CNV (Supplementary Figure 3). We noticed that AFP, an HCC marker, was lowly expressed in liver cancer cells, this finding was consistent with what was reported by Sun et al. (19), suggesting that it may not be a reliable marker gene for HCC. The possible reason is that AFP is not universally expressed in all liver cancers. Similarly, we observed that the cells in cluster 16 and 30 were all derived from non-tumor liver and highly expressed in GPC3 and CD24; thus, they were annotated as hepatocytes (Figures 2C, F).

The nonimmune cells that were identified mainly included LSEC (CLEC4G and ENG) (20, 21), non-LSEC endothelial cells (endothelial, CDH5, and ENG), and hepatocytes (ALB and KRT18). The immune cells that were identified consisted of T cells (CD3E and CD7), B cells (CD79A and IGKC), NKT cells (NCAM1 and CD3D), and myeloid cells (CD68 and CD163) (Figures 2C, D). Next, we performed differential gene expression analysis among 9 cell types to verify the accuracy of cell annotation (Figure 2E and Supplementary Table 1). The identified immune cell types were co-present in the tumors and adjacent liver sections but at different proportions, revealing the heterogeneity of the HCC microenvironment. Despite this variation, tumors and adjacent liver specimens had similar proportions of B cells (Supplementary Figure 4).

3.2 Cell-cell communication in human HCC

To gain insight into cell–cell interactions in HCC, we calculated the number of ligand–receptor pairs among tumor tissues and paired nontumor liver tissues using the CellphoneDB. The heat map shows the level of interactions between each cell type and others (Supplementary Figure 5), and the number of ligand–receptor pairs is presented by color variation. Myeloid cells were notably active and interacted with all cell types in the liver tissues adjacent to the tumor (Figures 3A, B).

Previous animal experiments have found that LSEC recruits CXCR6+ NKT cells by secreting CXCL16. However, whether this mechanism also exists in humans remains unclear. We have widely identified chemokine ligand–receptor complexes between LSEC and other cell types. The bubble diagram revealed that the extent of CXCL16/CXCR6 signaling was the highest between LSEC and NKT cells, suggesting that the mechanism of LSEC using CXCL16 as a messenger to recruit NKT cells may similarly present in human HCC (Figure 3C). In addition to NKT cells, LSEC may also recruit T cells *via* the CXCL16/CXCR6 complex. Interestingly, several rarely reported cell–cell interactions (CXCL2/DPP4, CCR1/CCL23, CCR1/CCL14, CCL3L3/DPP4) between LSEC and myeloid cells were identified, suggesting that LSEC may recruit myeloid cells by multiple ways. In addition to LSEC, NKT cells may also recruit myeloid cells through receptor–ligand singling including CCL5/CCR1, CCL3/CCR1, and CCL4L2/PGRMC2 (Figure 3C).

In the tumor samples, we noticed that B cells had the weakest interaction with tumor cells, indicating that B cells may have relatively weak antitumor effects (Figures 3D, E). We further analyzed cell–cell interaction in tumor tissues and an interesting finding was that TNFRSF14, a co-stimulatory molecule (22), interacted with MIF widely existing in all major immune cell types and malignant cells of the liver, indicating that TNFRSF14/MIF signaling may be a promising target of immunotherapy in HCC (Figure 3F).

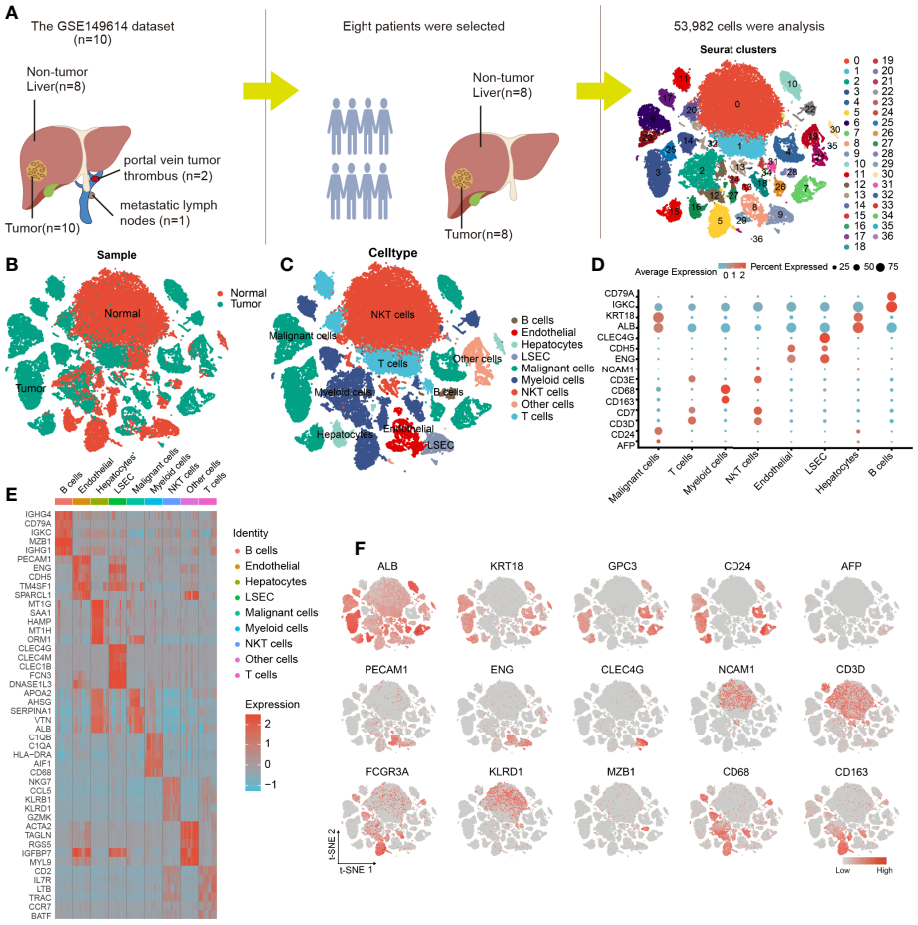

FIGURE 2
Cellular annotation of scRNA-seq data for tumor and adjacent liver tissue samples from 8 patients. **(A)** Processing procedure of GSE149614 scRNA-seq dataset and t-SNE distribution of 53,982 cells. **(B)** The cluster map illustrates the cell origins by color (non-tumor liver and HCC samples). **(C)** The t-SNE plot shows the 8 identified cell types and 1 undefined cell type (annotated as other cells) from 10× Genomics. **(D)** The bubble plot displaying the normalized expression levels of selected marker genes across the 9 clusters, the variation from high to low expression is represented by the colors from orange to blue. **(E)** Heatmap of top 5 DEGs in the identified cell types. **(F)** Feature t-SNE plots showing the expression levels of 15 well-known marker genes.

3.3 Patient grouping

We investigated the proportion of LSEC in adjacent liver and tumor tissues and found that LSEC were almost absent in the tumor regions and exclusively restricted to the adjacent liver sections (Figure 3G and Supplementary Figure 4). In the liver, it is known that CXCL16 is mainly secreted by LSEC. Therefore, based on the total amount of CXCL16 expressed by LSEC in each patient, the 8 patients in our study were categorized into either a CXCL16 high-expression (CH) group or CXCL16 low-expression (CL) group, with 4 patients in each group (Figure 3H).

To explore the differences in immune function between both groups, we performed differential gene expression analysis. We noticed that the activation marker CD69, antitumoral cytokine IFN-γ, and chemokines CCL3 and CCL4 were notably highly expressed in NKT cells in the CH group (Figure 3I). In addition, samples in the CH group contained a much higher proportion of CD69high NKT cells (Figure 3J). These findings suggested that higher expression of CXCL16 is associated with a stronger function of NKT cells. Furthermore, the histograms indicate that the CH group has a higher proportion of NKT cells and LSEC (Figures 3K, L). Therefore, in human HCC, CXCL16 may also trigger the hepatic accumulation of NKT cells. This phenomenon was previously identified only in animal models of liver cancer.

3.4 Pseudotime trajectory analysis of NKT cells

CD69 is an activation marker of NKT cells. We found that the level of CD69 normalized expression was substantially higher in the CH group compared with that in the CL group;

10.3389/fimmu.2022.1095915

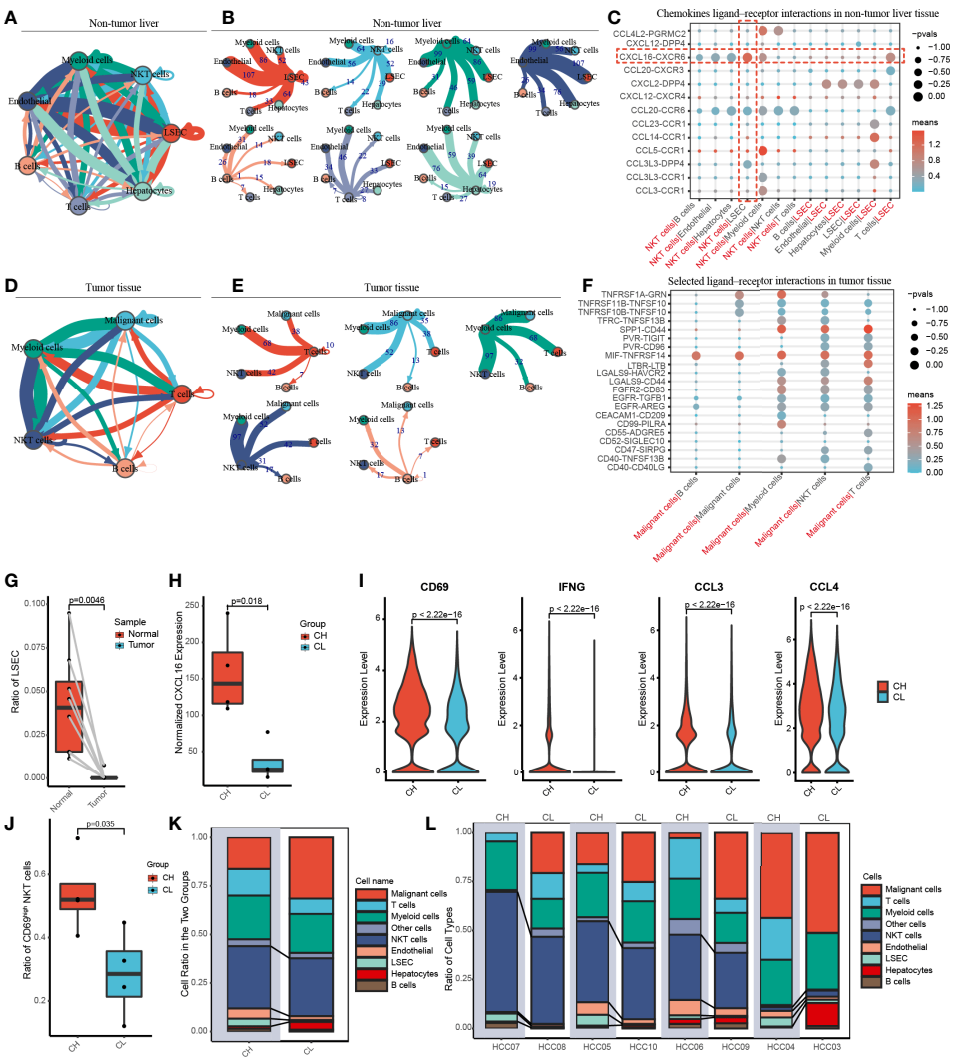

FIGURE 3
Cell-cell communication networks and patient grouping. **(A, B)** The map showing in detail the number of putative ligand–receptor interactions between each cell type and others in the non-tumor liver. The width of the connecting lines is proportional to the imputed events, which are also labelled with numbers. **(C)** Summary of selected chemokines ligand-receptor interactions that may exist between LSEC and other cells in the noncancerous tissue. The size of the circles is inversely proportional to the p-value, and the color variation represent the level of interaction. **(D, E)** The graph quantifies potential communication between various immune cells and malignant cells in tumor tissue. **(F)** Detailed view of the selected ligand-receptor interactions between major immune cells and cancer cells. **(G)** The ratio of LSEC in tumor and adjacent normal liver samples. **(H)** According to the level of CXCL16 expressed by LSEC, eight patients were divided into the CXCL16 high group (CH) and the CXCL16 low group (CL). **(I)** Violin plots indicating CD69, IFNG (IFN-γ), CCL3 and CCL4 were highly expressed in NKT cells from the CH sample. **(J)** The boxplot displaying the ratio of $CD69^{high}$ NKT cells in CH and CL. **(K)** Overview of the proportion of each cell type in CH and CL. **(L)** The histograms showing the proportion of cell types in each patient.

moreover, the CH group had a higher percentage of $CD69^{high}$ NKT cells (Figures 3I, J). To determine the correlation between CD69 expression and NKT cell function, we investigated the alterations in gene expression and associated functional variations during the differentiation of $CD69^{low}$ to $CD69^{high}$ NKT cells using pseudotime trajectory analysis.

$CD69^{low}$ NKT cells were predominantly distributed at the beginning of the differentiation trajectory, whereas $CD69^{high}$ NKT cells were primarily found at end of the trajectory (Figures 4A, B). Next, we analyzed normalized CD69 expression along the trajectory in samples from the CH and CL groups separately. At end of the trajectory, the normalized CD69 expression of NKT cells obtained from patient samples in the CH group was significantly higher compared with that in the CL group (Figure 4C). All cells were divided into 7 states along the differentiation process (Figure 4D). As the cell state transitioned along the differentiation trajectory, the ratio of $CD69^{high}$ NKT cells increased gradually (Figure 4E).

We studied the variation in gene expression patterns associated with NKT cell state transition and determined 149 dynamic genes with notable alterations in expression; these genes were divided into 5 clusters (Supplementary Table 2). Next, we extracted these dynamic genes from different clusters for GO analysis. Cluster 1 was characterized by the downregulated expression of metabolism-related genes such as PCNA, HMGB2, PKM, and ENO1. GO analysis revealed that signaling pathways such as the carbohydrate catabolic process, glucose metabolic process, and ATP generation were enriched in cells at the beginning of the trajectory ($CD69^{low}$ NKT cells) (Figure 4F and Supplementary Figure 6A). Interestingly, clusters 3 and 4 were characterized by the upregulated expression of immune cell differentiation–related genes such as IL7R, IRF1, RORA, and NCR3, and chemokines including CCL4, CCL5, XCL1, and XCL2. Moreover, enrichment analysis indicated that the pathways involved in the differentiation of lymphocytes, mononuclear cells, and T cells; positive regulation of cytokine production; regulation of innate immune response; and cellular response to chemokines and IFN-γ were enriched in cells at end of the trajectory ($CD69^{high}$ NKT cells) (Figure 4F, Supplementary Figure 6B, C). Additionally, we found that cytotoxicity-related genes including GZMH, GZMK, KLRD1, and NKG7; chemokines including CCL4, CCL5, XCL1, XCL2, and CCL4L2; and the anti-tumoral cytokine IFN-γ were gradually upregulated as differentiation progressed (Figures 4G-I). These findings collectively suggested that $CD69^{high}$ NKT cells had stronger immune function compared with $CD69^{low}$ NKT cells but may be at a disadvantage with respect to substance metabolism.

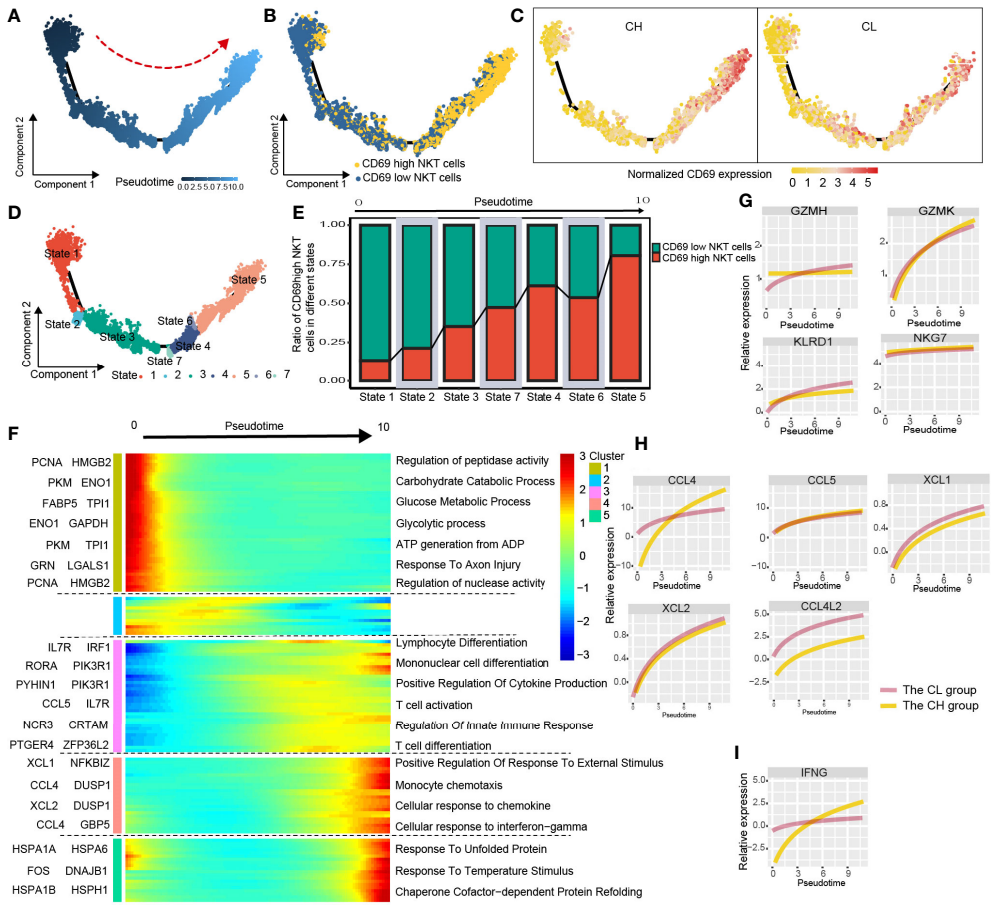

FIGURE 4
Simulation of NKT-cell differentiation trajectory in HCC. **(A)** The red arrow represents the simulated development direction of NKT cells. **(B)** 2D trajectory chart showing the distribution of $CD69^{high}$ NKT cells and $CD69^{low}$ NKT cells along with the trajectory. **(C)** 2D graph showing the dynamics of normalized expression of CD69, from CH and CL samples. **(D)** All cells are divided into 7 states and labeled with different colors. **(E)** The graph showing the proportion of $CD69^{high}$ NKT cells in different states, along the developmental trajectory. **(F)** Heatmap displaying the dynamic variation of differentiation-related gene expression. The dynamic expression of cytotoxic-related genes **(G)**, chemokines **(H)** and anti-tumoral cytokine IFNG (IFN-γ) **(I)**.

3.5 Identification of DEGs and GSEA

To further investigate the functional differences between CD69high NKT cells and CD69low NKT cells, we identified their DEGs and performed GSEA. Volcano plots and heat maps displaying the most significant DEGs are depicted in Figures 5A, B and Supplementary Table 3. We performed GSEA using genes ranked by the absolute value of log2 (fold change). We observed that the pathways associated with the T-cell receptor signaling pathway, response to TNF, and leukocyte differentiation were mainly enriched in CD69high NKT cells, whereas pathways related to the cell cycle such as cell cycle checkpoints were primarily enriched in CD69low NKT cells (Figures 5C, D).

3.6 OCA combined with 5β-CA suppresses orthotopic H22 liver cancer development

We constructed an H22 orthotopic liver cancer mouse model to better mimic the immune microenvironment of human HCC. First, mice were inoculated with H22 cells inoculation on day 0 and were then treated with various drugs (Tween-20 and PBS, OCA, 5β-CA, OCA+5β-CA) (Figure 6A). At the end of the experiment, representative macroscopy images of livers from the 4 groups are shown in Figure 6B. H&E staining was used to evaluate the microscopic features of H22 orthotopic liver tumors. The cancer cells varied

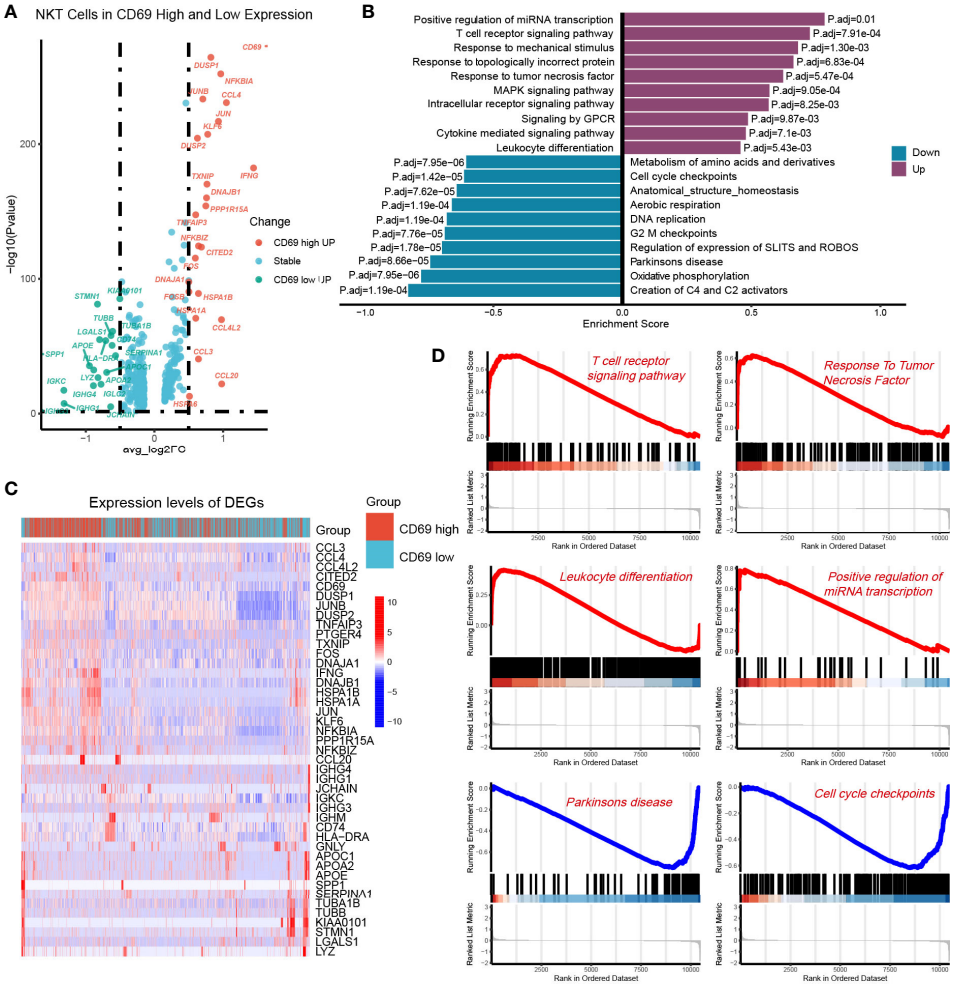

FIGURE 5
Identification of DEGs between the CD69^{high} NKT cells and CD69^{low} NKT cells. **(A)** Volcano plot showing the DEGs between CD69^{high} NKT cells and CD69^{low} NKT cells. Red and green colors represented high expression genes within CD69^{high} and CD69^{low} NKT cells, respectively. The blue color represented the genes with no significant changes. **(B)** Heatmap displaying the top 43 significant DEGs between CD69^{high} NKT cells and CD69^{low} NKT cells. Red and blue colors represented upregulated and downregulated genes, respectively. **(C, D)** GSEA functional enrichment analysis of the ranked DEGs. The numbers marked on the chart represent the adjusted P-values. The purple and blue colors represented upregulated and downregulated pathways in the CD69^{high} NKT cells, separately. The gene sets included Reactome, KEGG and GO (Biological process) databases.

in size and exhibited large nuclei and increased mitotic figures, suggesting the successful establishment of the orthotopic model of liver cancer (Figure 6C).

Tumors and livers were collected on day 17 to compare the tumor burden between different groups. The tumor and liver weights of the OCA and 5β-CA treatment groups were lower than those of samples obtained from the control group, indicating a partial tumor-suppression effect. Samples from the OCA+5β-CA group had the lowest tumor and liver weights, revealing a more pronounced therapeutic effect. Additionally, the OCA+5β-CA group exhibited the smallest tumor/liver ratio (Figure 6D). The body weights were recorded every 2 days to evaluate tumor-induced cachexia. No apparent body weight loss was observed in any group except during the first 3 days after tumor inoculation, indicating that all mice were in the early disease stage (Figure 6E). No significant differences in serum ALT and AST levels were determined between mice treated with different drugs, suggesting that OCA and 5β-CA did not exert obvious hepatoprotective effect or hepatotoxicity. OCA and 5β-CA were not associated with nephrotoxicity or pulmonary toxicity as serum BUN and CRE levels were similar among all 4 groups (Figure 6F and Supplementary Figure 6).

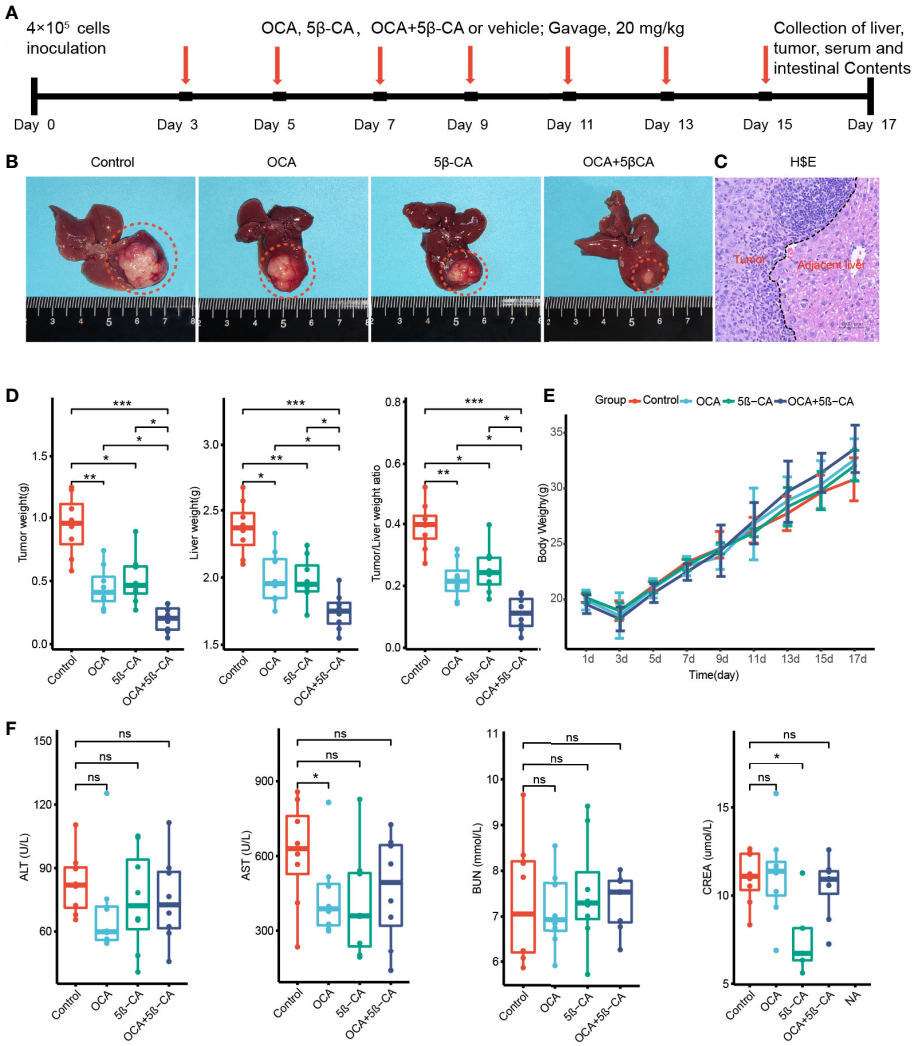

FIGURE 6
OCA combined with 5β-CA significantly inhibited orthotopic H22 liver tumor. **(A)** The experimental flow chart. **(B)** Representative liver images in the 4 groups are shown. The tumors were outlined with an orange dashed curve. **(C)** The orthotopic H22 mice model was assessed by H&E images. A black dashed line outlines the border between the tumor and the non-tumor liver. **(D)** The liver weight, tumor weight and the ratios of tumor/liver weight from 4 groups were recorded while mice were executed. **(E)** The body weight variation. **(F)** Tumor-induced liver injury, drug-induced hepatotoxicity or drug-induced liver protective effect was assessed by serum levels of ALT and AST. Drug-induced nephrotoxicity was assessed by BUN and CREA (ns, no significance; *0.01 ≤ P value < 0.05; **0.001 ≤ P value < 0.01; ***P value < 0.001).

3.7 *In vivo* immunity analysis after various treatments

In vivo immunity analysis was conducted to further explore the molecular mechanism of OCA+5β-CA-mediated significant tumor growth inhibition. On day 17, orthotopic tumors were digested into single-cell suspensions for flow cytometry. OCA +5β-CA treatment led to a remarkable increase in NKT cells, whereas $CD4^+$ T, $CD8^+$ T, and NK cells did not exhibit much change. A slight increase in the number of NKT cells was observed in the OCA and 5β-CA groups (Figures 7A, B). To provide mechanistic insight into the increase in NKT cell numbers and to investigate whether OCA+5β-CA treatment affected NKT cell activation, we analyzed the NKT cell phenotype of CXCR6 and CD69 (a marker of NKT cell activation). Notably elevated proportions of $CD69^+$ NKT cells and $CXCR6^+$ NKT cells were observed after treatment with OCA+5β-CA (Figures 7A, B).

INF-γ and TNF-β derived from NKT cells are beneficial for NKT-initiated antitumor immunity. Higher IFN-γ levels in the serum, tumors, and livers were found in NKT cells obtained from OCA+5β-CA-treated mice; however, TNF-β levels did not change obviously (Figures 7C-E). CXCL16, a ligand for CXCR6, is mainly secreted by LSEC and recruits $CXCR6^+$ NKT cells to the liver. Elevated CXCL16 levels in the tumors, serum, and livers of OCA +5β-CA-treated mice explained the accumulation of intratumoral NKT cells (Figures 7C-E). Importantly, OCA+5β-CA exhibited superior effects in enhancing NKT cell infiltration, promoting their activation and, hence, increasing the antitumor function of NKT cells compared with OCA and 5β-CA monotherapy (Figure 7A-E).

4 Discussion

So far, only immune checkpoint inhibitors targeting the PD1/PDL1 axis are available to clinicians for HCC immunotherapy, and their response rates are still limited (23, 24). NKT cells, with robust antitumor activity, store thousands of fold higher levels of antitumor cytokines than NK cells and $CD8^+$ T cells (25–27). Previous *in vitro* and *in vivo* experiments have confirmed that LSEC use CXCL16 as a messenger to control the accumulation of CXCR6+ NKT cells in the liver (11, 13, 14, 28). However, this evidence in human samples is lacking. Based on human scRNA-seq data, we found that high CXCL16 expression in LSEC was associated with an increased number and activated phenotype of NKT cells. Further animal experiments determined that OCA combined with 5β-CA was highly effective in upregulating CXCL16 production, thereby increasing the hepatic number of NKT cells and exerting a significant tumor growth–inhibition effect.

By forming ligand–receptor complexes, cell–cell communication plays a crucial role in coordinating diverse biological processes in the tumor immune microenvironment (29, 30). CellphoneDB is an open database where ligands, receptors, and their interactions are stored, enabling users to achieve a systematic and comprehensive analysis of intercellular communication. Notably, the CellphoneDB takes into account the ligand and receptor subunits and, therefore, allows an accurate representation of the heteromeric complexes (31). We used the CellphoneDB and found that LSEC express relatively high levels of CXCL16, and that CXCR6 (the receptor of CXCL16) is overexpressed in NKT cells, revealing the potential interactions in biological processes between LSEC and NKT cells.

CD69 is a classic activation marker of NKT cells (32). NKT cells exhibit potent antitumor effects upon activation by rapidly releasing multiple cytokines such as IFN-γ, TNF-β, and chemokines (33, 34). Differential analysis suggested that compared with NKT cells from the CL group, those from the CH group were characterized by the overexpression of CD69, IFN-γ, CCL3, and CCL4, suggesting an activated phenotype. In addition, samples from the CH group had a higher proportion of NKT cells. Therefore, hepatic CXCL16 levels correlated with the accumulated number and immune function of NKT cells.

Cells constantly switch from one differentiated state to another throughout the growth cycle. This process has also been described as cell differentiation. Cells in different differentiation states have distinct gene expression patterns, resulting in dynamic cell function changes (35). During cell differentiation, the expression of some genes was gradually reduced while that of others was activated (36). The purification and extraction of cells in different differentiation states are complex, leading to difficulties in describing the gene expression transients in animal or cellular experiments. Pseudotime trajectory is a method that enables the determination of dynamic gene expression patterns and functional status alterations without having to purify cells (37). Results from the analysis indicated that during the differentiation of $CD69^{low}$ NKT to $CD69^{high}$ NKT cells, cytotoxic-related genes such as GZMH, GZMK, KLRD1, and NKG7; chemokines such as CCL4, CCL5, XCL1, XCL2, and CCL4L2; and the classic antitumoral cytokine IFN-γ were gradually upregulated. For GO analysis, we extracted the significantly dynamic genes during the differentiation process of $CD69^{low}$ NKT to $CD69^{high}$ NKT cells. The results suggested that the signaling pathways involved in the differentiation of lymphocytes, mononuclear cells, and T cells; positive regulation of cytokine production; regulation of innate immune responses; and cellular response to chemokines and IFN-γ were significantly enriched. We further determined the DEGs between $CD69^{high}$ and $CD69^{low}$ NKT cells and conducted GSEA. The pathways associated with the T-cell receptor–signaling pathway and the response to TNF and leukocyte differentiation were mainly enriched in $CD69^{high}$ NKT cells. These findings demonstrated that $CD69^{high}$ NKT cells exerted more cytotoxicity and had higher antitumor immune functions compared with $CD69^{low}$ NKT cells.

Pathak et al. (38) reported that the FXR agonists alter the abundance of bile acid–producing bacteria, thus increasing the levels of the secondary bile acid taurolithocholic acid (TLCA) by

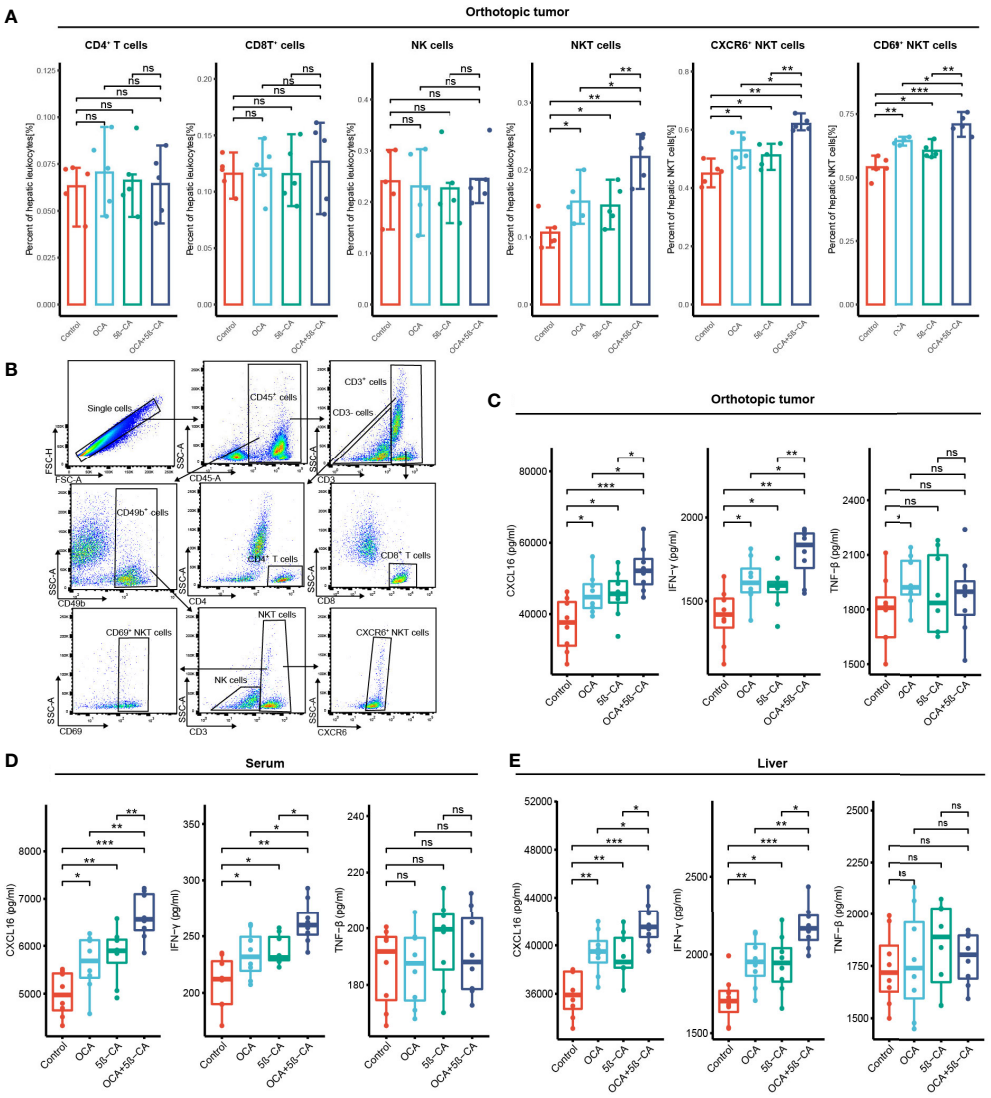

FIGURE 7
OCA plus 5β-CA improving the number and enhancing the function of NKT cells. **(A)** Proportions of tumor-infiltrating $CD4^+$ T cells, $CD8^+$ T cells, NK cells, NKT cells, $CXCR6^+$ NKT cells and $CD69^+$ NKT cells after various treatments. **(B)** Flow cytometry diagrams showing the gating strategy of $CD4^+$ T cells ($CD3^+$ $CD4^+$), $CD8^+$ T cells ($CD3^+$ $CD8^+$), NK cells ($CD49b^+$ $CD3^+$), NKT cells ($CD49b^+$ $CD3^+$), $CXCR6^+$ NKT cells, $CD69^+$ NKT cells. **(C-E)** CXCL16, INF-γ and TNF-β concentrations in the orthotopic tumor, serum and normal liver adjacent to the tumor after various drug treatments (ns, no significance; *0.01 ≤ P value < 0.05; **0.001 ≤ P value < 0.01; ***P value < 0.001).

thousands of times. Based on this finding, we speculated that when OCA was used alone, the increase in TLCA may reduce CXCL16 secreted from LSEC by binding to TGR5, and the TGR5 antagonist may offset this TLCA-induced adverse event. Therefore, we tested the combination of OCA and 5β-CA for the treatment of HCC using an orthotopic HCC mouse model. OCA+5β-CA treatment led to the highest proportion of NKT, $CXCR6^+$ NKT, and $CD69^+$ NKT cells. NKT cells that accumulated after OCA+5β-CA treatment produced more IFN-γ. In addition, OCA+5β-CA treatment led to the lowest tumor and liver weights compared with that using the vehicle or using OCA or 5β-CA monotherapy, suggesting that the combination treatment may be a promising immunotherapeutic approach in the management of HCC.

5 Conclusion

Our study presents the important targets and potential immunotherapeutic strategies for the treatment of HCC. By dissecting the scRNA-seq data, we verified that in the human HCC microenvironment, CXCL16 secreted from LSEC could also increase

the accumulated number of hepatic NKT cells. The accumulated NKT cells in the liver in turn exhibited a higher activation state and produced more IFN-γ. We also investigated the differences in gene expression patterns and signaling pathways between activated CD69high NKT cells and unactivated CD69low NKT cells using NKT cell-developmental trajectories, differential analysis, and functional enrichment analysis. *In vivo* experiments in an orthotopic liver tumor mouse model were conducted to confirm the enhanced antitumor efficacy of the combination of OCA with 5β-CA.

Data availability statement

Publicly available datasets were analyzed in this study. This data can be found here: GSE149614.

Ethics statement

The animal study was reviewed and approved by Southwest Medical University Animal Ethics Committee.

Author contributions

HG and SL wrote the original draft. HG, SL and LL performed the animal experiments. ML performed the flow cytometry. SQ prepared the packages on RStudio. KH designed this study. XY supervised the whole experiments and reviewed the original draft. In addition, HG and SL contributed equally for this work. All authors contributed to the article and approved the submitted version.

Funding

This work was supported by the Key Research and Development Project of the Science & Technology Department of Sichuan Province (Nos.2021YFS0231) and Luzhou Administration of Science and Technology Nos.2022-SYF-55 and 2021-SYF29.

Acknowledgments

We would like to thank Zhenhua Hu and Zeyu Zhang (Chinese Academy of Sciences) for providing free high-performance server.

Conflict of interest

The authors declare that the research was conducted in the absence of any commercial or financial relationships that could be construed as a potential conflict of interest.

The handling editor KW declared a shared parent affiliation with the authors at the time of review.

Publisher's note

Supplementary material

The Supplementary Material for this article can be found online at: https://www.frontiersin.org/articles/10.3389/fimmu.2022.1095915/full#supplementary-material

References

1. Bertuccio P, Turati F, Carioli G, Rodriguez T, La Vecchia C, Malvezzi M, et al. Global trends and predictions in hepatocellular carcinoma mortality. *J Hepatol* (2017) 67:302–9. doi: 10.1016/j.jhep.2017.03.011

2. Llovet JM, Kelley RK, Villanueva A, Singal AG, Pikarsky E, Roayaie S, et al. Hepatocellular carcinoma. *Nat Rev Dis Primers* (2021) 7:6. doi: 10.1038/s41572-020-00240-3

3. Yau T, Park JW, Finn RS, Cheng AL, Mathurin P, Edeline J, et al. Nivolumab versus sorafenib in advanced hepatocellular carcinoma (CheckMate 459): a randomised, multicentre, open-label, phase 3 trial. *Lancet Oncol* (2022) 23:77–90. doi: 10.1016/S1470-2045(21)00604-5

4. Finn RS, Ryoo BY, Merle P, Kudo M, Bouattour M, Lim HY, et al. Pembrolizumab as second-line therapy in patients with advanced hepatocellular carcinoma in KEYNOTE-240: A randomized, double-blind, phase III trial. *J Clin Oncol* (2020) 38:193–202. doi: 10.1200/JCO.19.01307

5. Braun DA, Burke KP, Van Allen EM. Genomic approaches to understanding response and resistance to immunotherapy. *Clin Cancer Res* (2016) 22:5642–50. doi: 10.1158/1078-0432.CCR-16-0066

6. Gao B, Radaeva S, Park O. Liver natural killer and natural killer T cells: immunobiology and emerging roles in liver diseases. *J Leukoc Biol* (2009) 86:513–28. doi: 10.1189/JLB.0309135

7. Bendelac A, Savage PB, Teyton L. The biology of NKT cells. *Annu Rev Immunol* (2007) 25:297–336. doi: 10.1146/annurev.immunol.25.022106.141711

8. Bandyopadhyay K, Marrero I, Kumar V. NKT cell subsets as key participants in liver physiology and pathology. *Cell Mol Immunol* (2016) 13:337–46. doi: 10.1038/cmi.2015.115

9. Liu X, Li L, Si F, Huang L, Zhao Y, Zhang C, et al. NK and NKT cells have distinct properties and functions in cancer. *Oncogene* (2021) 40:4521–37. doi: 10.1038/s41388-021-01880-9

10. Nelson A, Lukacs JD, Johnston B. The current landscape of NKT cell immunotherapy and the hills ahead. *Cancers* (2021) 13:5174. doi: 10.3390/cancers13205174

11. Mossanen JC, Kohlhepp M, Wehr A, Krenkel O, Liepelt A, Roeth AA, et al. CXCR6 inhibits hepatocarcinogenesis by promoting natural killer T- and CD4(+) T-Cell-Dependent control of senescence. *Gastroenterology* (2019) 156:1877–89. doi: 10.1053/j.gastro.2019.01.247

12. Geissmann F, Cameron TO, Sidobre S, Manlongat N, Kronenberg M, Briskin MJ, et al. Intravascular immune surveillance by CXCR6+ NKT cells patrolling liver sinusoids. *PloS Biol* (2005) 3:e113. doi: 10.1371/journal.pbio.0030113

13. Ma C, Han M, Heinrich B, Fu Q, Zhang Q, Sandhu M, et al. Gut microbiome-mediated bile acid metabolism regulates liver cancer *via* NKT cells. *Science* (2018) 360:eaan5931. doi: 10.1126/science.aan5931

14. Zhu H, Zhang Q, Chen G. CXCR6 deficiency ameliorates ischemia-reperfusion injury by reducing the recruitment and cytokine production of hepatic NKT cells in a mouse model of non-alcoholic fatty liver disease. *Int Immunopharmacol* (2019) 72:224–34. doi: 10.1016/j.intimp.2019.04.021

15. Yamada S, Takashina Y, Watanabe M, Nagamine R, Saito Y, Kamada N, et al. Bile acid metabolism regulated by the gut microbiota promotes non-alcoholic steatohepatitis-associated hepatocellular carcinoma in mice. *Oncotarget* (2018) 9:9925–39. doi: 10.18632/oncotarget.24066

16. Arab JP, Karpen SJ, Dawson PA, Arrese M, Trauner M. Bile acids and nonalcoholic fatty liver disease: Molecular insights and therapeutic perspectives. *Hepatology* (2017) 65:350–62. doi: 10.1002/hep.28709

17. Wahlstrom A, Kovatcheva-Datchary P, Stahlman M, Khan MT, Backhed F, Marschall HU. Induction of farnesoid X receptor signaling in germ-free mice colonized with a human microbiota. *J Lipid Res* (2017) 58:412–9. doi: 10.1194/jlr.M072819

18. Thomas C, Auwerx J, Schoonjans K. Bile acids and the membrane bile acid receptor TGR5–connecting nutrition and metabolism. *Thyroid* (2008) 18:167–74. doi: 10.1089/thy.2007.0255

19. Sun Y, Wu L, Zhong Y, Zhou K, Hou Y, Wang Z, et al. Single-cell landscape of the ecosystem in early-relapse hepatocellular carcinoma. *Cell* (2021) 184:404–21. doi: 10.1016/j.cell.2020.11.041

20. Ramachandran P, Dobie R, Wilson-Kanamori JR, Dora EF, Henderson B, Luu NT, et al. Resolving the fibrotic niche of human liver cirrhosis at single-cell level. *Nature* (2019) 575:512–8. doi: 10.1038/s41586-019-1631-3

21. Aizarani N, Saviano A, Sagar, Mailly L, Durand S, Herman JS, et al. A human liver cell atlas reveals heterogeneity and epithelial progenitors. *Nature* (2019) 572:199–204. doi: 10.1038/s41586-019-1373-2

22. Chen L, Flies DB. Molecular mechanisms of T cell co-stimulation and co-inhibition. *Nat Rev Immunol* (2013) 13:227–42. doi: 10.1038/nri3405

23. Sangro B, Sarobe P, Hervas-Stubbs S, Melero I. Advances in immunotherapy for hepatocellular carcinoma. *Nat Rev Gastroenterol Hepatol* (2021) 18:525–43. doi: 10.1038/s41575-021-00438-0

24. Llovet JM, Castet F, Heikenwalder M, Maini MK, Mazzaferro V, Pinato DJ, et al. Immunotherapies for hepatocellular carcinoma. *Nat Rev Clin Oncol* (2022) 19:151–72. doi: 10.1038/s41571-021-00573-2

25. Swain MG. Hepatic NKT cells: friend or foe? *Clin Sci (Lond)* (2008) 114:457–66. doi: 10.1042/CS20070328

26. Swain MG. Natural killer T cells within the liver: conductors of the hepatic immune orchestra. *Dig Dis* (2010) 28:7–13. doi: 10.1159/000282059

27. Wang H, Yin S. Natural killer T cells in liver injury, inflammation and cancer. *Expert Rev Gastroenterol Hepatol* (2015) 9:1077–85. doi: 10.1586/17474124.2015.1056738

28. Yu Z, Guo J, Liu Y, Wang M, Liu Z, Gao Y, et al. Nano delivery of simvastatin targets liver sinusoidal endothelial cells to remodel tumor microenvironment for hepatocellular carcinoma. *J Nanobiotechnol* (2022) 20:9. doi: 10.1186/s12951-021-01205-8

29. Peng L, Wang F, Wang Z, Tan J, Huang L, Tian X, et al. Cell-cell communication inference and analysis in the tumour microenvironments from single-cell transcriptomics: data resources and computational strategies. *Brief Bioinform* (2022) 23:bbac234. doi: 10.1093/bib/bbac234

30. Dimitrov D, Turei D, Garrido-Rodriguez M, Burmedi PL, Nagai JS, Boys C, et al. Comparison of methods and resources for cell-cell communication inference from single-cell RNA-seq data. *Nat Commun* (2022) 13:3224. doi: 10.1038/s41467-022-30755-0

31. Efremova M, Vento-Tormo M, Teichmann SA, Vento-Tormo R. CellPhoneDB: inferring cell-cell communication from combined expression of multi-subunit ligand-receptor complexes. *Nat Protoc* (2020) 15:1484–506. doi: 10.1038/s41596-020-0292-x

32. Nemeth E, Baird AW, O'Farrelly C. Microanatomy of the liver immune system. *Semin Immunopathol* (2009) 31:333–43. doi: 10.1007/s00281-009-0173-4

33. Riese P, Trittel S, May T, Cicin-Sain L, Chambers BJ, Guzman CA. Activated NKT cells imprint NK-cell differentiation, functionality and education. *Eur J Immunol* (2015) 45:1794–807. doi: 10.1002/eji.201445209

34. Fujii S, Shimizu K, Okamoto Y, Kunii N, Nakayama T, Motohashi S, et al. NKT cells as an ideal anti-tumor immunotherapeutic. *Front Immunol* (2013) 4:409. doi: 10.3389/fimmu.2013.00409

35. Trapnell C, Cacchiarelli D, Grimsby J, Pokharel P, Li S, Morse M, et al. The dynamics and regulators of cell fate decisions are revealed by pseudotemporal ordering of single cells. *Nat Biotechnol* (2014) 32:381–6. doi: 10.1038/nbt.2859

36. Qiu X, Hill A, Packer J, Lin D, Ma YA, Trapnell C. Single-cell mRNA quantification and differential analysis with census. *Nat Methods* (2017) 14:309–15. doi: 10.1038/nmeth.4150

37. Zheng Z, Qiu X, Wu H, Chang L, Tang X, Zou L, et al. TIPS: trajectory inference of pathway significance through pseudotime comparison for functional assessment of single-cell RNAseq data. *Brief Bioinform* (2021) 22:bbab124. doi: 10.1093/bib/bbab124

38. Pathak P, Xie C, Nichols RG, Ferrell JM, Boehme S, Krausz KW, et al. Intestine farnesoid X receptor agonist and the gut microbiota activate G-protein bile acid receptor-1 signaling to improve metabolism. *Hepatology* (2018) 68:1574–88. doi: 10.1002/hep.29857

frontiers | Frontiers in Immunology

TYPE Original Research
PUBLISHED 04 January 2023
DOI 10.3389/fimmu.2022.1094556

OPEN ACCESS

EDITED BY
Kai Wang,
Southwest Medical University, China

REVIEWED BY
Zixue Xuan,
Hangzhou Medical College, China
Yuan Gui,
University of Connecticut,
United States

*CORRESPONDENCE
Jianzhong Li
ljzsnk@hotmail.com
Shasha Tao
taoqishu619@126.com

†These authors have contributed equally to this work

SPECIALTY SECTION
This article was submitted to Inflammation, a section of the journal Frontiers in Immunology

RECEIVED 10 November 2022
ACCEPTED 09 December 2022
PUBLISHED 04 January 2023

CITATION
Yang Y, Li Q, Ling Y, Leng L, Ma Y, Xue L, Lu G, Ding Y, Li J and Tao S (2023) m6A eraser FTO modulates autophagy by targeting SQSTM1/P62 in the prevention of canagliflozin against renal fibrosis.
Front. Immunol. 13:1094556.
doi: 10.3389/fimmu.2022.1094556

m6A eraser FTO modulates autophagy by targeting SQSTM1/P62 in the prevention of canagliflozin against renal fibrosis

Youjing Yang[1†], Qianmin Li[2†], Yi Ling[2], Linxin Leng[2], Yu Ma[1], Lian Xue[2], Guoyuan Lu[3], Yue Ding[3], Jianzhong Li[3*] and Shasha Tao[1,2*]

[1]Chongqing University Central Hospital and Chongqing Emergency Medical Center, Chongqing, China, [2]School of Public Health, Medical College of Soochow University, Suzhou, China, [3]Department of Nephrology, The First Affiliated Hospital of Soochow University, Suzhou, Jiangsu, China

The dysregulation of autophagy contributes to renal fibrosis. N6-Methyladenosine (m6A) RNA modification is a critical mediator of autophagy. Our previous studies have reported that the disorder of the PPARα/fatty acid oxidation (FAO) axis in renal tubular cells is suppressed by STAT6, which is involved in the regulation of renal fibrotic processes. Here, we found that canagliflozin significantly upregulates SQSTM1/P62, promoting PPARα-mediated FAO by inducing autophagy-dependent STAT6 degradation both in TGF-β1-treated HK2 cells and in unilateral ureteral occlusion (UUO) and ischemia–reperfusion (I/R) renal fibrosis mouse models. Knockdown of P62/SQSTM1 led to the impairment autophagic flux and the dysregulation of the STAT6/PPARα axis, which was confirmed by SQSTM1/P62^{cKO} mice with UUO treatment along with bioinformatics analysis. Furthermore, SQSTM1/P62 deficiency in renal tubular cells inhibited canagliflozin's effects that prevent FAO disorder in renal tubular cells and renal fibrosis. Mechanistically, the level of m6A eraser FTO, which interacted with SQSTM1 mRNA, decreased in the renal tubular cells both *in vitro* and *in vivo* after canagliflozin administration. Decrease in FTO stabilized SQSTM1 mRNA, which induced autophagosome formation. Collectively, this study uncovered a previously unrecognized function of canagliflozin in FTO in the autophagy modulation through the regulation of SQSTM1 mRNA stability in the renal tubular STAT6/PPARα/FAO axis and renal fibrosis.

KEYWORDS

autophagy, canagliflozin, N6-methyladenosine, renal fibrosis, SQSTM1, STAT6

1 Introduction

Renal fibrosis is considered the final common pathogenic process for all kidney diseases. It is characterized by the deposition of the extracellular matrix, tubular atrophy, and loss of peritubular microvasculature (1, 2). When histopathological damage is consistent, structural destruction and functional impairment occur, leading to the poor prognoses of patients with chronic kidney diseases (3). Thus, effective strategies that alleviate renal fibrosis are urgently needed.

Renal tubular cells require high levels of adenosine triphosphate (ATP) through fatty acid oxidation (FAO), and impairment in FAO in these cells causes ATP deficiency, intracellular lipid accumulation, partial epithelial–mesenchymal transition, inflammation, and eventually interstitial fibrosis (4). Our previous study has reported that STAT6, which is activated in the process of kidney fibrosis, negatively regulates PPARα signals. STAT6 inhibition promotes a shift to FAO for energy utilization by inducing PPARα activation in tubular cells, thereby attenuating the lipid accumulation and alleviating renal fibrosis (5). Moreover, STAT6 can be degraded by autophagy-dependent pathways (6). Autophagy is an evolutionarily conserved catabolic pathway that degrades cytoplasmic components, moves organelles, and recycles cytoplasmic contents in eukaryotic cells, contributing to the maintenance of kidney homeostasis and function (7, 8). As one of the most important self-protection mechanisms, basal autophagy in the kidney is critical for maintaining renal homeostasis, structure, and function (9). In acute kidney injury, autophagy is activated as an intrinsic protective mechanism in renal tubular cells (10). However, the role of autophagy in the development of interstitial fibrosis remains a highly controversial issue. On the one hand, autophagy is regarded as an inducer of tubular cell injury and tubular atrophy, leading to fibrosis progression in the kidney. On the other hand, autophagy plays a protective role in renal fibrosis by mediating extracellular matrix protein expression, cell cycle G2/M arrest, or inflammation (11–13). Thus, autophagy is a potential therapeutic target for kidney fibrosis. Moreover, whether autophagy-involved protein degradation is a potential strategy that alleviates renal fibrosis is largely unknown.

Sodium-glucose cotransporter 2 inhibitor (SGLT2i), as a class of anti-hyperglycemic medication, has attracted considerable interest. Canagliflozin (Cana) is the first SGLT2 inhibitor approved by the Food and Drug Administration (FDA). As reported, Cana has been implicated in several biological processes that are independent of SGLT2-involved glucose-lowering effects, including lipid metabolism. Osataphan et al. showed that Cana can promote fatty acid oxidation and ketogenesis in livers (14). Moreover, autophagy can be induced by Cana treatment as reported, but the underlying regulatory mechanisms remain unknown. The most abundant chemical modification of eukaryotic messenger RNA, N6-methyladenosine (m6A) regulates a number of fundamental bioprocesses by targeting the gene expression (15–17). In general, m6A is composed of three kinds of protein, the "Writers," the "Readers," and the "Erasers." Accumulated evidence has shown that m6A modification mediates autophagy (18, 19). However, no evidence of the role of m6A modification in SGLT2i-induced autophagy activation has been obtained.

The aim of this study was to explore the role and modulation of m6A in autophagy regulation toward Cana-mediated renoprotective effects. *In vivo* and *in vitro* evidence has demonstrated that Cana is efficient in providing protection against unilateral ureteral occlusion (UUO)- or ischemia–reperfusion (I/R)-caused renal fibrosis by normalizing the FAO gene program dependent on autophagy. Precisely, the m6A eraser FTO modulates Cana/autophagy by regulating SQSTM1 mRNA stability.

2 Materials and methods

2.1 Animals and treatments

C57BL/6 mice were purchased from SLAC Laboratory Animal Co., Ltd. $Atg7^{flox/flox}$ mice were gifts from Dr. Jianrong Wang, Medical College of Soochow University (20). $SQSTM1^{flox/flox}$ mice were gifts from Dr. Hongting Zheng, Xinqiao Hospital, Army Medical University (21). All mice were housed with a standard 12-h light/dark cycle, climate-controlled, and pathogen-free facility. All experiments were conducted in accordance with the Guide for the Care and Use of Laboratory Animals, and the study protocols were approved by the Laboratory Animal Welfare and Ethics Committee of Chongqing University. To generate tubular-specific Atg7-deficient and SQSTM1-deficient mice, $Atg7^{flox/flox}$ and $SQSTM1^{flox/flox}$ mice were crossed with γGTcre mice (Cyagen Biosciences). Gender-matched wild-type and specific knockout mice (6–8 weeks old) from the same litter were selected randomly to indicated groups. Two animal studies were performed as follows: a) mice were divided into four groups (n = 8 per group): (i) Ctrl with sham operation, (ii) canagliflozin (Cana) (Selleck S2760; 20 mg/kg in PBS, daily intragastric administration till the mice were harvested), (iii) UUO (sacrificed 7 days after the performance), and (iv) Cana + UUO, and b) mice were divided into four groups (n = 8 per group): (i) Ctrl with sham operation, (ii) canagliflozin (Cana) (Selleck S2760; 20 mg/kg in PBS, daily intragastric administration for consecutive 21 days), (iii) I/R (sacrificed 21 days after the performance), and (iv) Cana + I/R. I/R and UUO operation was performed according to our previous study (5).

2.2 Cell culture and treatments

Human proximal renal tubular cell line HK2 was purchased from the Cell Bank of the Chinese Academy of Sciences. HK2 cells were cultured in Dulbecco's Modified Eagle's Medium (DMEM, Corning) containing 10% FBS (HyClone) in a 5% CO_2 incubator at 37°C. TGF-β1 (5 ng/ml) was added to the medium to induce the fibrotic protein expression and lipid accumulation.

2.3 Hematoxylin and eosin, immunohistochemical, Oil Red O, and Sirius Red staining

The kidney of each mouse was removed and fixed with 4% paraformaldehyde before embedding. H&E staining was performed for pathological analysis. For IHC staining, kidney sections were incubated with primary antibody LC3 or FTO overnight and then a horseradish peroxidase (HRP) polymer secondary antibody was used. Oil Red O staining and Sirius Red staining were performed using a corresponding kit based on the manufacturer's instructions (Solarbio, Chondrex). Images were collected and analyzed with a fluorescence microscope (Leica DM 2500).

2.4 Assay of serum blood urea nitrogen and lipid parameters

Levels of blood urea nitrogen (BUN) and total cholesterol (TC), low-density lipoprotein cholesterol (LDL), and high-density lipoprotein cholesterol (HDL) in serum were assayed by a corresponding kit (BioAssay Systems, USA, DIUR-500, Nanjing Jiancheng, China, TC: A111-1-1, LDL: A113-1-1, A112-1-1) according to the manufacturer's construction.

2.5 Assay of kidney TG levels

Levels of TG in kidney tissue were measured by using a commercial kit (Nanjing Jiancheng, A:110-1-1). Tissues were weighted and added with PBS (1:9) for homogenization, and the supernatant was obtained. Then, the supernatant and the working solution of the kit were mixed and subjected to measurement of the absorbance at 546 nm. Cellular TG levels were measured using a commercial TG Quantification Colorimetric Kit (BioVision; USA, K622) according to the manufacturer's protocol. In brief, cells were homogenized in solution containing 5% NP-40 in water and then heated to 100°C. Then, 20 μl cell lysate was adjusted to the volume of 50 μl/well with a triglyceride assay buffer. Finally, the absorbance at 570 nm was measured.

2.6 Nucleus and cytoplasm protein isolation

The nucleus and cytoplasm protein of HK2 cells were isolated by using a Nucleus/Cytosolic Extraction Kit (Fude Biological Technology, China, FD0199) based on the manufacturer's instructions. Briefly, cells were incubated with Nc-Buffer A for 10 min on ice and then added with Nc-Buffer B. After centrifugation, the supernatant was collected to obtain the cytoplasm protein. Nc-Buffer C was added to the deposit to collect the nuclear protein. All the Nc-Buffer should be added with 1% protease inhibitor before use. Nuclear and cytoplasmic proteins were subjected to immunoblot analyses.

2.7 Immunoblot analyses

Proteins of cells and tissues were isolated using a RIPA buffer containing protease and phosphatase inhibitor cocktail. Total protein was quantified using the BCA method (Fude Biological Technology, China, FD2001). Equal amounts of protein from each group were separated through an SDS-polyacrylamide gel. The following antibodies were used: STAT6 (sc-374021), p-STAT6 (sc-136019), Arg-1 (sc-166920), TGF-β1 (sc-146), α-SMA (sc-53142), FN (sc-18827), LC3I/II (sc-398822), SQSTM1 (sc-28359), CPT-1α (sc-393070), PPARα (sc-398394), and GAPDH (sc-32233) from Santa Cruz Biotechnology. FTO (AF6936) and N6-Methyladenosine (m6A) Rabbit Polyclonal Antibody (AF7407) were from Beyotime. Protein half-life assays were performed according to our previous protocol (22). Briefly, cell lysates from the control or Cana group were collected at different time points after cycloheximide (CHX) administration and subjected to immunoblot analyses with the anti-STAT6 and anti-GAPDH antibodies. The prestained protein marker (Vazyme Biotech Co., Ltd., MP102-01) was used to identify the specific bands.

2.8 Indirect immunofluorescence

For indirect immunofluorescence, cells were fixed on round glass coverslips (Fisher Scientific) with chilled methanol. After incubation with the primary antibodies and the respective secondary antibodies for 50 min each, coverslips were washed with PBS and mounted with antifade mounting solution (Invitrogen). A fluorescence microscope (Leica DM 2500) was used to obtain representative images.

2.9 Cell viability assay

Cell viability assay was performed according to the previously described method. Briefly, the potential cytotoxicity of Cana in HK2 cells was assessed by the functional impairment of the mitochondria with 3-(4,5-dimethylthiazol-2-yl)-2,5-diphenyltetrazolium bromide (MTT, Sigma). Approximately 1 × 10^4 cells per well were plated in a 96-well plate and incubated overnight. The cells were treated with different doses of Cana for 48 h. Then, MTT was added into the cells followed by incubation at 37°C for 2 h. The medium was removed, and 100 µl isopropanol/HCl was added into each well. Absorbance at 570 nm was measured by a synergy 2 multimode microplate reader (BioTek, Seattle, USA).

2.10 Actinomycin D treatment

HK2 cells were treated with 5 µg/ml actinomycin D (GC16866, GLPBIO, USA) to inhibit mRNA transcription. Cells were collected at 0, 3, and 6 h. RNA was extracted as below described and used for quantitative polymerase chain reaction (qPCR).

2.11 RNA extraction and real-time qPCR

Total RNA was isolated from cells and kidney tissues using TRIzol reagent (CWBiotech, China, CW0580S). Equal amounts of mRNA were synthesized using a iScript cDNA Synthesis Kit based on the manufacturer's instructions (Vazyme Biotech, China, R333-01) with a 0.2-ml PCR tube (Nest, China, 401001). Real-time PCR was performed using a qPCR SYBR Green Master Mix (Yeasen, 11184). Primer sequences were listed in the supplementary.

2.12 RNA immunoprecipitation qPCR

HK2 cells were harvested and lysed in an IP lysis buffer (Beyotime Biotechnology, P0013) containing a protease inhibitor cocktail and RNase inhibitor (Beyotime Biotechnology, R0102-2KU). After centrifugation, the supernatant was collected and 10% of the lysate was taken out for input. The remaining lysate was added to anti-FTO antibody incubated with protein A/G agarose beads at 4°C for 24 h. IgG was used for negative control RNA immunoprecipitation (RIP) reaction. 10% of the complex was collected to test the efficiency of immunoprecipitation after resuspending with a lysis buffer. The remaining lysate was subjected to centrifugation, and RNA was extracted as described above. RNA enrichment was normalized to the input control.

2.13 Methylated RNA immunoprecipitation qPCR

Total RNA was extracted as described above. An EpiQuik™ CUT&RUN m6A Enrichment kit (EpiGentek, USA, P-9018) was used to monitor the status of m6A in RNA. 200 ng of RNA was collected and stored at -80°C after cleavage. Anti-m6A antibody or IgG was incubated with affinity beads for 90 min and then washed with a wash buffer. A protein digestion buffer containing proteinase K was added and incubated with an antibody–RNA complex for 15 min at 55°C. Next, the RNA binding beads were resuspended and added to the complex and then the RNA was eluted with an elution buffer. The input of RNA and eluted RNA was subjected to qPCR as described above.

2.14 m6A dot blot

Total RNA was isolated as described above and spotted onto nylon membranes. Then, the membranes were crosslinked by ultraviolet (UV) and subjected to methylene blue and then blocked for 1 h with a blocking buffer (5% milk in phosphate-buffered saline with 1% Tween 20). Corresponding secondary antibodies were added and incubated for 1 h.

2.15 m6A quantification

The levels of global m6A in mRNA were measured by using an EpiQuik m6A RNA Methylation Quantification kit (Colorimetric) (EpiGentek, Germany) based on the manufacturer's instruction.

2.16 Live-cell imaging

HK2 cells were transfected with mRFP-GFP-LC3 for 24 h and then either left untreated or separately treated with rapamycin, CQ, or Cana. Finally, cells were gently washed with PBS and images were captured with a fluorescence microscope (Leica DM2500, USA).

2.17 Microarray data processing

The expression profile and corresponding annotation platform of GSE118337 were downloaded from the National Center for Biotechnology Information (https://www.ncbi.nlm.nih.gov/) (23). The profile was then normalized by function *normalizeBetweenArrays()*. The normalized microarray series matrix was processed by the limma R package (24) to calculate the log fold change, p value, and adjusted p value of gene

expression for further analysis, and genes that meet |log2FC| >1 and p < 0.05 were considered differentially expressed. A volcano plot and heatmap created by R were graphed to show the overall condition of the data.

2.18 Protein–protein interaction analysis

Genes in GSE118337 regulated by TGF-β1 and restored by Cana (p < 0.05, |log2FC| >1) were used to create a protein–protein interaction (PPI) network on String and visualized by Cytoscape (25, 26). Retrieved from functional enrichment results, the genes related to fibrosis and fatty acid oxidation were highlighted.

2.19 Enrichment analysis

The upregulated and downregulated genes in GSE118337 were respectively used for biological process functional enrichment on Metascape (27), the results of which were used to create bar plots showing functions related to the present investigation by R. Gene sets used for functional enrichment analysis and gene set enrichment analysis (GSEA) were downloaded from GSEA (http://www.gsea-msigdb.org/gsea/index.jsp) (28, 29). Then, software GSEA 4.2.2 and R package "ClusterProfiler" were employed for GSEA and visualization (30).

2.20 Correlation analysis

Correlation between the expression level of genes was calculated by Pearson correlation analysis. The p-value of the correlation coefficient was analyzed with package "hmisc," and p-value <0.05 was considered statistically significant. An absolute value of Pearson correlation coefficients between 0.6 and 1 indicated a strong correlation, and that between 0.4 and 0.6 indicated a moderate one. The correlation was finally visualized by software Cytoscape and R package "corrplot" (31).

2.21 Construction of the autophagy gene signature

We applied a methodology to quantify the autophagy level (autophagy score) of samples. First, we chose 19 genes with frequent existence in pathways related to autophagy or reported in previous studies (32). Next, principal component analysis (PCA) was performed to establish the autophagy gene signature of genes selected above. Finally, we selected principal components 1 as signature scores.

2.22 Statistical analysis

The investigators were blinded to group allocation. Data were presented as mean ± SD. GraphPad Prism 8.0 and R statistical software were performed for graphics and statistical analyses. Unpaired Student's t tests were applied for comparison between two groups. For multiple comparison analyses, one-way ANOVA with Bonferroni's correction were performed. The differences with $^*p < 0.05$ was considered statistically significant.

3 Results

3.1 Cana showed tight regulation both on renal fibrosis and fatty acid metabolism

To verify the effects of Cana on renal fibrosis and lipid metabolism, the microarray expression dataset GSE118337 retrieved from the GEO database was analyzed. As shown in Figure 1A, there were 541 genes regulated by TGF-β1 and 589 genes regulated by Cana ($p < 0.05$, |log2FC| >1), with 332 genes at their intersection. 61.3% of the genes changed by TGF-β1 were further restored by Cana, revealing the potential therapeutic effect of Cana on renal fibrosis (Figure 1B). Among them, 193 genes and 139 genes were separately upregulated and downregulated by TGF-β1 and restored by Cana. Enrichment functions of all genes regulated by both TGF-β1 and Cana ($p < 0.05$) were conducted by Metascape (https://metascape.org/). As shown in Figures 1C–E, gene ontology terms associated with fibrosis and fatty acid metabolism were significantly mediated and the PPI network was graphed, suggesting that fatty acid metabolism and fibrosis-related genes are closely interacted with each other. These data showed that Cana exhibited the significant modulation both on renal fibrosis and fatty acid metabolism.

3.2 Cana improved aberrant lipid metabolism and renal fibrosis induced by UUO and I/R

Based on the bioinformatic analysis above, we next conducted an *in vivo* study *via* establishing UUO and I/R models to confirm the protection of Cana on renal fibrosis. H&E staining showed that the histological injury caused by UUO and I/R was attenuated by Cana, so did the lipid accumulation as shown by Oil Red O staining and triglyceride (TG) content in the kidney, without damage on renal function (Figures 2A, B, F, G, S1A). In addition, Sirius Red staining exhibited the alleviated collagen deposition by Cana (Figures 2C, H). Our previous study showed that STAT6, a key nuclear

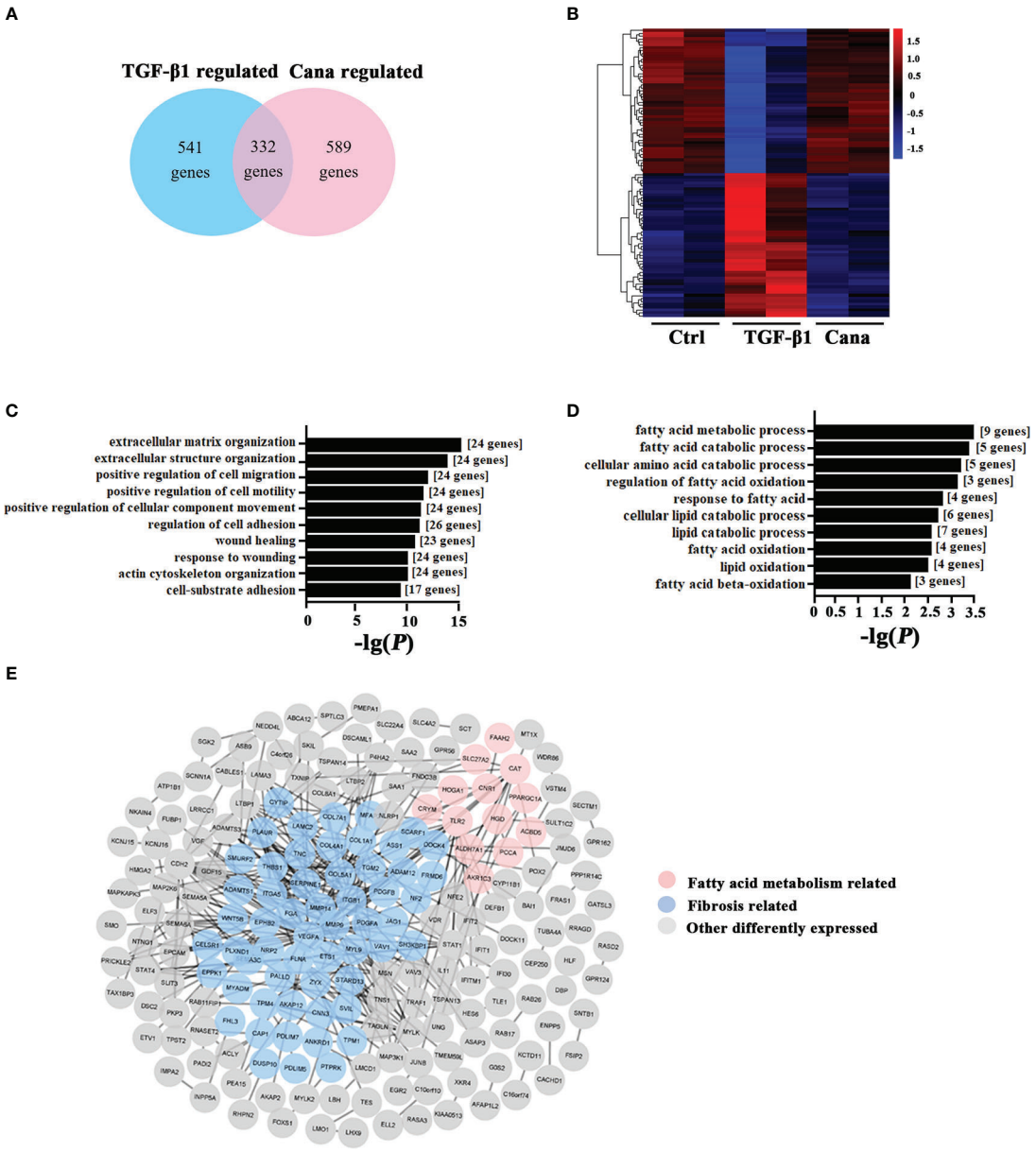

FIGURE 1
Cana positively regulated the abnormality of lipid metabolism and tubulointerstitial fibrosis. **(A–E)** The microarray expression dataset GSE118337 was retrieved from the GEO database. **(A)** A total of 541 genes were regulated by TGF-β1, and 589 genes were by Cana ($p < 0.05$, |log2FC| >1), with 332 genes at their intersection. **(B)** The heatmap displayed the top 50 upregulated and downregulated genes of two samples in the TGF-β1 group and two samples in the Cana group by z-score, in comparison with the Ctrl group. GO analysis was separately conducted with genes upregulated by TGF-β1 and downregulated by Cana **(C)** and genes downregulated by TGF-β1 and upregulated by Cana **(D)**, and the 10 highest-ranking biological process terms are shown. **(E)** The interaction network of above 332 genes both regulated by TGF-β1 and Cana, in which fibrosis-related genes and fatty acid metabolism-related genes according to enrichment results are highlighted.

transcription factor, is activated in fibrosis-associated tissue disorder and it could negatively regulate PPARα related-lipid metabolism, which contributes to lipid accumulation in renal tubular cells and kidney fibrosis (5). To explore the potential mechanism of Cana on the regulation of FAO and renal fibrosis, the expressions of STAT6 signal-related protein (STAT6, p-STAT6, Arg-1) and fibrosis-related protein (α-SMA, FN) were detected by immunoblot analyses (Figures 2D, I). Interestingly, here we found that STAT6 was suppressed in the kidney of UUO or I/R mice with Cana treatment. The deactivation of the STAT6 pathway was accompanied by reduced expressions of fibrosis-related protein α-SMA and FN

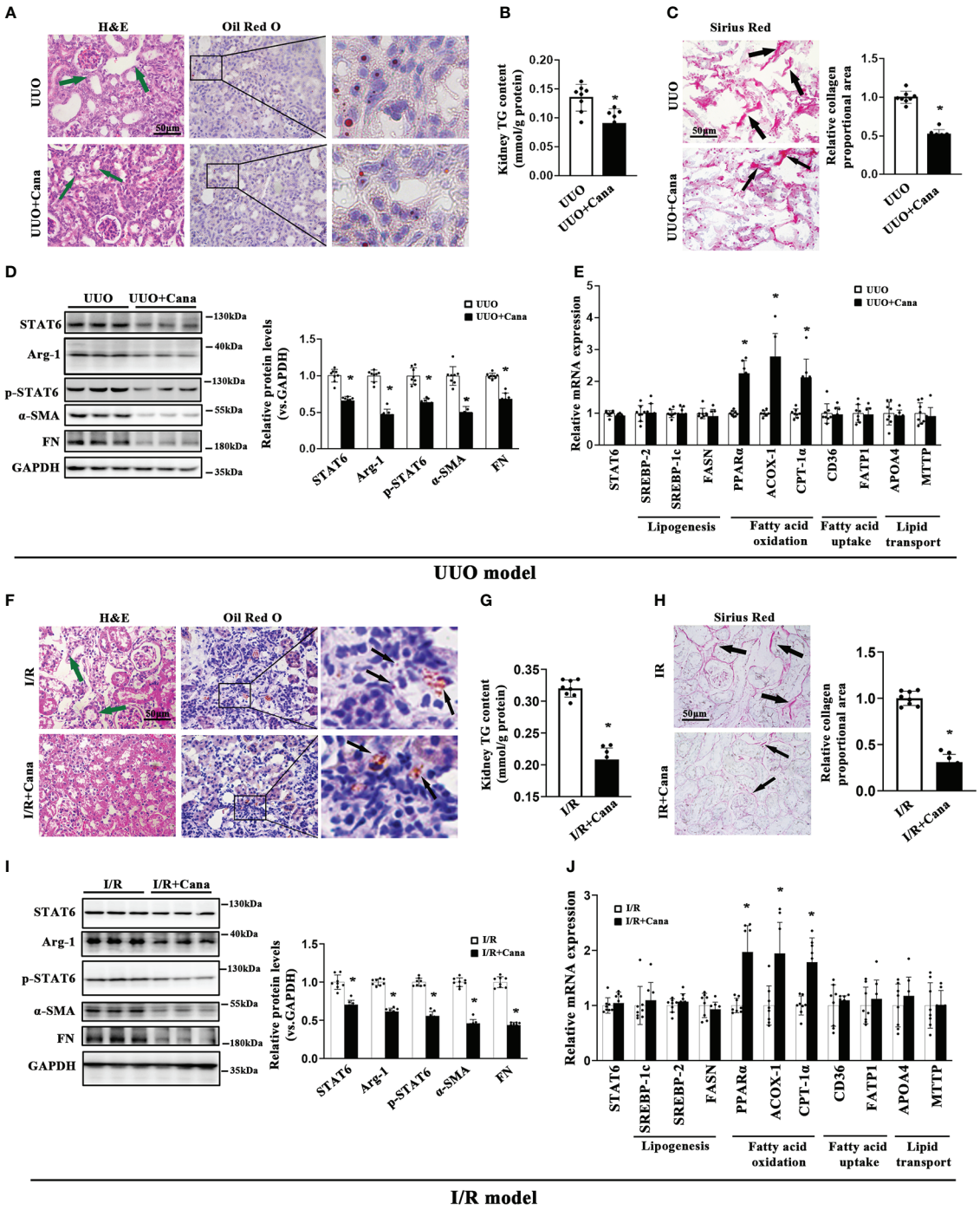

FIGURE 2
Cana intervention attenuated aberrant lipid metabolism and tubulointerstitial fibrosis in UUO or I/R mice. A tubulointerstitial fibrosis model was conducted by UUO or I/R operation. The mice of UUO or UUO+Cana were sacrificed at day 7, and mice of I/R or I/R+Cana were sacrificed at day 21. **(A)** Representative micrographs for H&E and Oil Red O staining in the kidney sections from the indicated groups. **(B)** TG content was determined in the kidneys from the indicated groups. **(C)** Representative micrographs for Sirius Red staining and quantification of relative collagen proportion in the kidneys from the indicated groups. **(D)** Kidney tissue lysates from each group were subjected to immunoblot analyses with the indicated antibodies. Representative blots of three independent samples in each group were shown, and quantification of relative protein expression was determined. **(E)** The mRNA levels of genes related to lipid metabolism in the kidneys from the indicated groups. Mice received intragastric administration of saline or Cana intervention after IR operation. **(F)** H&E and Oil Red O staining, **(G)** TG content, **(H)** Sirius Red staining, **(I)** immunoblot analyses, and **(J)** qPCR. Results were expressed as the mean ± SD (n = 8, $*p < 0.05$, UUO *vs.* UUO + Cana or IR *vs.* IR + Cana).

in UUO and I/R kidney. Consistently, Cana mainly upregulated the FAO in the kidney with UUO and I/R performance (Figures 2E, J). These data suggested that Cana may attenuate UUO- and I/R-induced renal fibrosis through STAT6 inhibition and FAO activation.

3.3 Cana alleviated TGF-β1-induced HK2 cell aberrant lipid metabolism and fibrosis-related protein expression through suppressing STAT6 expression

Next, we conducted *in vitro* studies using HK2 cells to further confirm Cana's protection effects observed in animal studies above. MTT assay was employed to select the dose range (0–40 μM) in the following *in vitro* experiments (Figure 3A). Consistently, Western blot showed that Cana decreased the expression and activation of STAT6 signals (STAT6, p-STAT6, and Arg-1) in a dose-dependent manner along with the increased expressions of SQSTM1 and LC3II and less effect on LC3I (Figure 3B). Since STAT6 could be degraded by autophagy according to others' and our previous studies, the stability of STAT6 was next detected. Cana shortened STAT6 half-life from 7.38 to 5.11 h (Figure 3C). Consistent with Figure 3B, immunofluorescence (IF) staining showed that Cana increased LC3 expression in a dose-dependent manner (Figure 3D). Moreover, a tandem mouse red fluorescent protein (mRFP)-GFP-LC3 construct was employed. Two positive controls were conducted to differentiate increased formation of autophagosomes (rapamycin) from blockage of autophagosome degradation (bafilomycin A1, BafA1). As shown in Figure 3E, cells treated with Cana contained red puncta but less yellow puncta, which was the same as rapamycin, indicating that Cana may act as an inducer of autophagy. Moreover, qPCR and Western blot assays indicated that Cana alleviated TGF-β1-induced abnormal lipid metabolism and fibrotic protein expression (Figures 3F, G). Then, the effects of downregulated STAT6 by Cana were further explored. Overexpression of STAT6 exacerbated TGF-β1-induced aberrant lipid metabolism and fibrotic protein expression and impaired the protective effect of Cana, which further confirmed that Cana improved FAO and fibrosis *via* autophagy degradation of STAT6 (Figures 3G–I). These data suggested that Cana suppressed STAT6 through activation of autophagy to alleviate TGF-β1-induced aberrant lipid metabolism and fibrotic protein expression.

3.4 Autophagy mediated Cana's protection effects for renal fibrosis *via* inducing STAT6 degradation in tubular cells

Since we found that Cana decreased STAT6, HK2 cells treated with different doses of Cana were separated to detect STAT6 expression in the cytoplasm and nucleus, respectively. The results showed that the expression of STAT6 in both cytoplasm and nucleus was decreased after Cana treatment (Figure 4A). To further determine the method of STAT6 degradation, cells were treated with Cana along with proteasome inhibitor (MG132) or autophagy inhibitor (BafA1). Results showed that the expressions of SQSTM1 and LC3II were both increased after Cana treatment. Higher levels of LC3II and SQSTM1 were found in the Cana and BafA1 combined treatment group (Figure 4B), which was consistent with Figure 3E that Cana induced the autophagosome formation. Moreover, only BafA1 treatment reversed the decrease in STAT6 signaling.

Whether autophagy is involved in the protective effect of Cana against tubulointerstitial fibrosis *in vivo* was further confirmed. There was no obvious different histological change and collagen deposition (Figure S2A). Interestingly, remarkable tubular atrophy and interstitial collagen deposition were observed in the WT group with UUO performance, which was significantly ameliorated by Cana administration. These protective effects of Cana were inhibited in the tubular-Atg7$^{-/-}$ (Atg7^{cKO}) group (Figures 4C, D). Consistently, Western blot showed that Atg7 deficiency in tubular cells vanished Cana's effect of suppressing STAT6 signaling, inhibiting fibrotic protein expression, and increasing FAO-related protein expression (Figure 4E). These data suggested that Cana improved renal tubular cells' FAO and kidney fibrosis through degradation of STAT6 in an autophagy-dependent manner.

3.5 Cana-induced autophagy was significantly associated with SQSTM1

SQSTM1 is well known as the receptor of autophagy-related degradation. In the above experiments, we found that SQSTM1 was induced after Cana treatment (Figures 3B, 4B). To elucidate the functional role of SQSTM1, a siRNA-based strategy was used to interfere HK2 cells' SQSTM1 expression and then detected the change of STAT6 and autophagy levels. The efficiency of siSQSTM1 was confirmed at the protein level. During knockdown of SQSTM1, the suppressed expression of STAT6 was alleviated while the increased expression of LC3II caused by Cana was inhibited (Figure 5B). In line with the results from Western blot, IF staining also showed that Cana barely induced LC3 expression with siSQSTM1 transfection (Figure 5A).

In order to further identify that Cana and SQSTM1 were related to autophagy, we systematically searched publicly available renal gene-expression data sets and chose GSE118337 for the next analysis. The Cana group and control group were selected as the object (33). Differentially expressed genes (DEGs) between the two groups were determined using the R package limma. The results represented by volcano plot showed that many DEGs were related to autophagy (Figure 5C). Moreover,

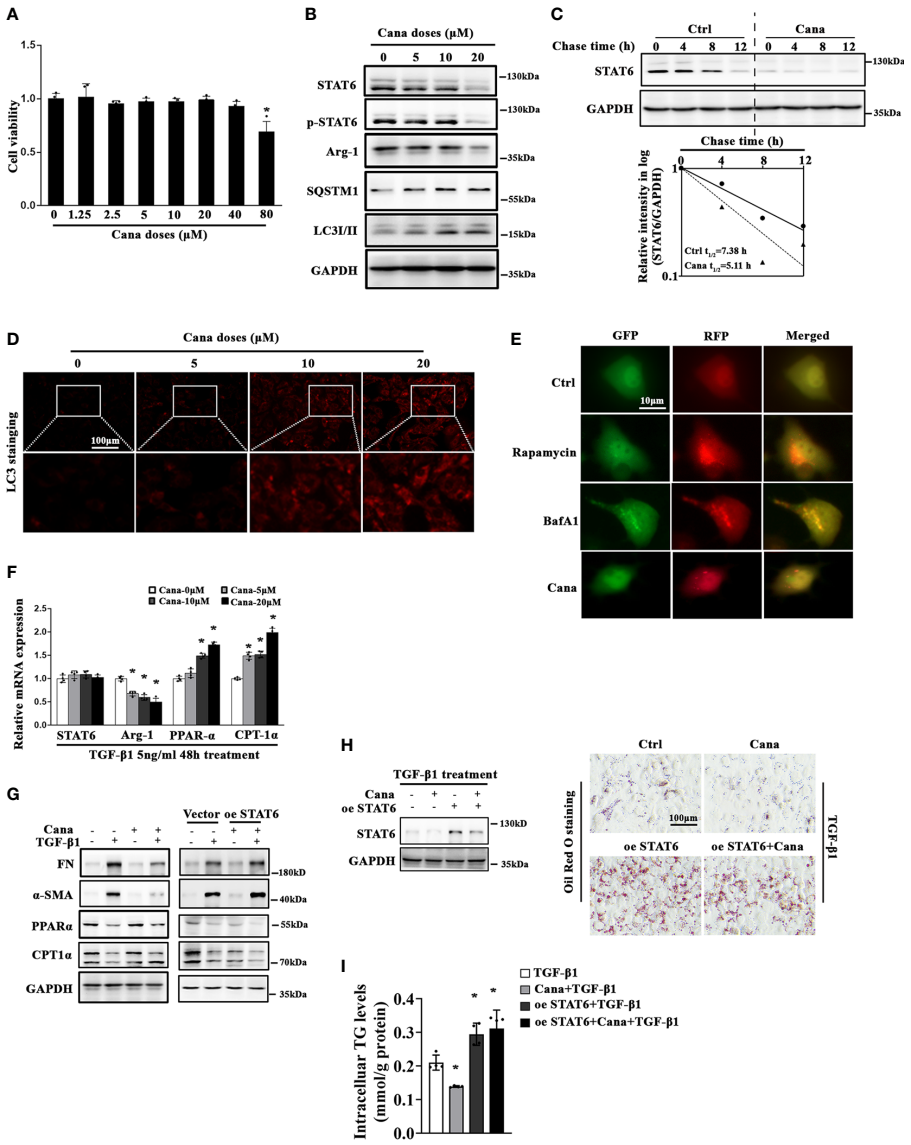

FIGURE 3
Cana causes STAT6 degradation through inducing autophagy. **(A)** HK2 cells were treated with the indicated doses of Cana for 48 h serum-free medium culture and cell viability was determined using MTT assay. (n = 4, *$p < 0.05$, Cana 0 μM *vs.* other doses of Cana). **(B)** HK2 cells were treated with Cana (0–20 μM) for 24 h, and then cell lysates were harvested and subjected to immunoblot analyses with the indicated antibodies. **(C)** To test its protein stability, the half-life of STAT6 was determined. HK2 cells were left untreated or treated with Cana (20 μM) for 24 h, and CHX (50 μM) was added at different time points. The intensity of STAT6 and GAPDH bands was quantified and plotted against the time after CHX addition. **(D)** HK2 cells were treated with Cana (0–20 μM) for 24 h and subjected to immunofluorescence staining of LC3. **(E)** HK2 cells were transfected with a tandem mRFP-GFP-LC3 construct for 24 h and then either left untreated or separately treated with rapamycin (1 μM), BafA1 (100 nM), or Cana (40 μM) for 24 h. Representative micrographs of the indicated cells are shown. **(F)** The mRNA levels of STAT6, Arg-1, PPARα, and CPT-1α in HK2 cells treated with Cana (0–20 μM) for 24 h were measured by qPCR. (*$p < 0.05$, Cana 0 μM *vs.* other doses of Cana). **(G–I)** HK2 cells were transfected with vector or plasmid of STAT6 overexpression. Followed by 24 h serum-free medium culture, cells were treated with TGF-β1 (5 ng/ml) for another 24 h and cotreated with or without Cana (20 μM). **(G)** Immunoblot analysis was conducted with the indicated antibodies. **(H)** Immunoblot analyses were employed to confirm the efficiency of overexpressing STAT6. Representative microphages showed the Oil Red O staining in HK2 cells with the indicated treatments. **(I)** TG content was determined enzymatically. (n = 4, *$p < 0.05$, TGF-β1 *vs.* TGF-β1 with other treatments).

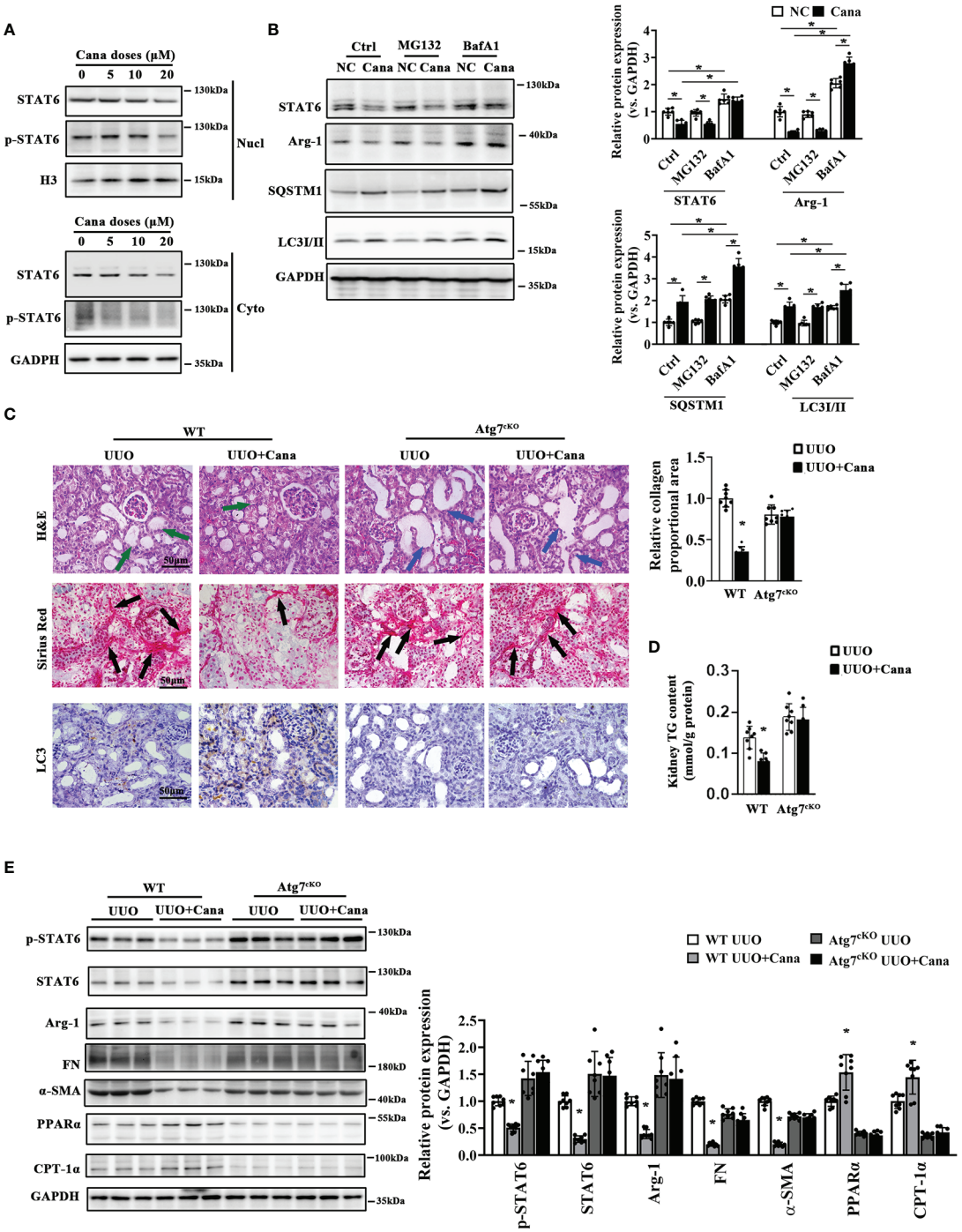

FIGURE 4
Atg7 deficiency vanished the protection of Cana in tubulointerstitial fibrosis. **(A)** HK2 cells were treated with Cana (0–20 μM) for 24 h. The protein expression of STAT6 and p-STAT6 in nucleus and cytoplasm was separated and determined by immunoblot analyses. **(B)** HK2 cells were pretreated with MG132 (10 μM) or BafA1 (100 nM) for 4 h and cotreated with or without Cana after being cultured with serum-free medium for 24 h. The cell lysates were subjected to immunoblot analyses with the indicated antibodies. **(C–E)** WT and Atg7^{cKO} mice received intragastric administration of saline or Cana (20 mg/kg) after UUO operation. **(C)** Representative images of H&E, Sirius Red, and IHC staining of kidney sections from the indicated group of mice. Quantification of the relative collagen proportional area from each group of mice was performed. **(D)** TG content in kidney tissue was measured by a commercial kit. **(E)** Immunoblot analyses for the protein levels of p-STAT6, STAT6, Arg-1, FN, α-SMA, PPARα, CPT-1α, and GAPDH in kidney from the indicated group with quantification on the right panel (n = 8, *$p < 0.05$, UUO *vs.* UUO + Cana).

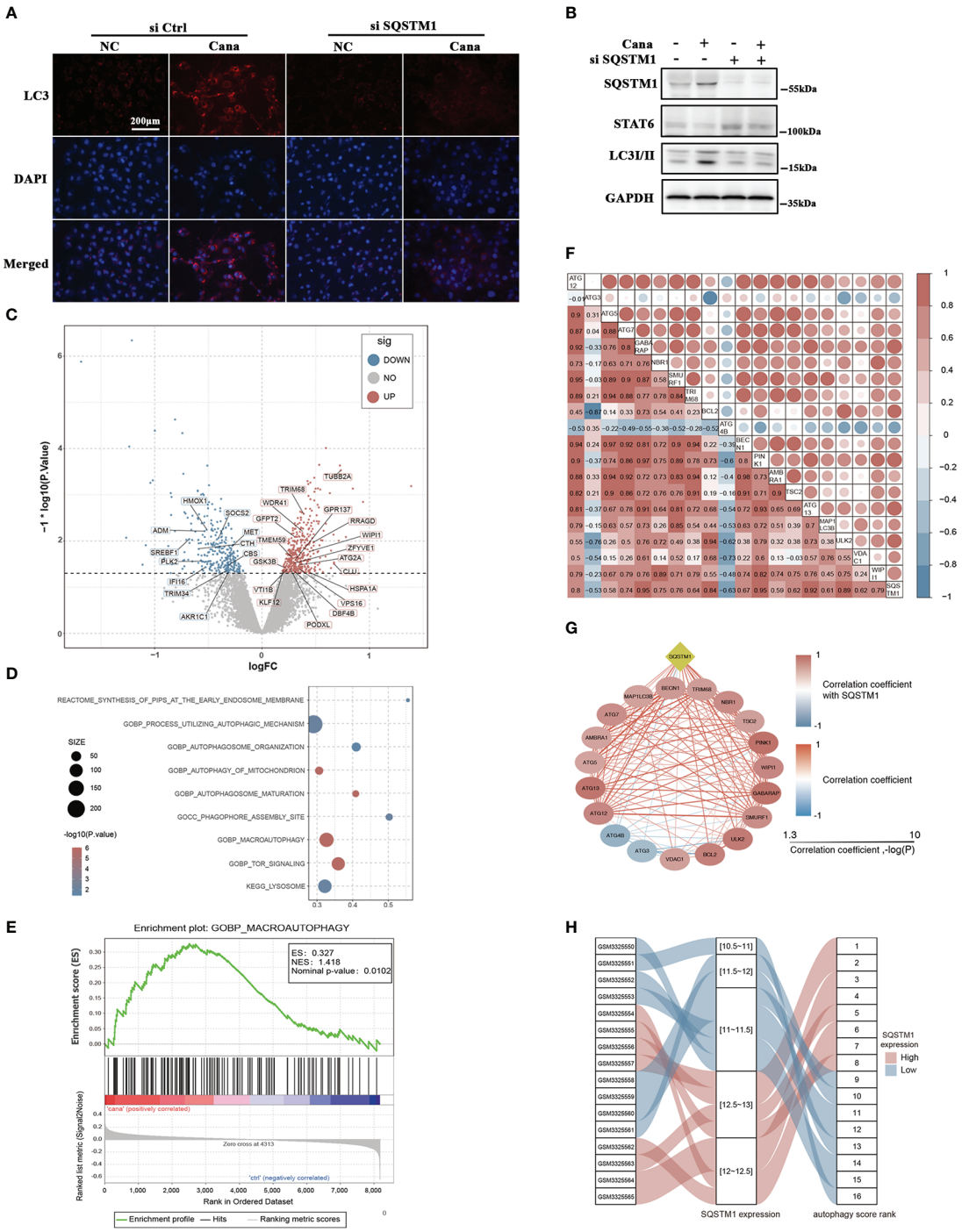

FIGURE 5
Autophagy was significantly associated with SQSTM1/P62 and Cana. **(A, B)** HK2 cells were transfected with or without SQSTM1 siRNA. Followed by 24 h serum-free medium culture, cells were treated with or without Cana (20 μM) for another 24 h. **(A)** Representative microphages of immunofluorescence from the indicated group are shown. **(B)** Immunoblot analyses was performed. **(C)** Volcano map showing that DEGs between Cana treated and control samples with autophagy-related genes were labeled. **(D)** Functional enrichment analysis of DEGs. **(E)** Gene set enrichment analysis result. **(F, G)** Correlation between SQSTM1 and genes related to autophagy. **(H)** The variation of SQSTM1 expression level and its corresponding autophagy score rank shown by alluvial diagram.

functional enrichment analysis revealed that DEGs were significantly enriched in pathways related to autophagy (Figure 5D). To further explore the changes of autophagy, gene set enrichment analysis (GSEA) was used to observe the enrichment of gene signatures in different phenotypes. The results showed that autophagy-related genes were significantly enriched in the Cana-treated group (Figure 5E). It was concluded that Cana treatment was closely related to autophagy of renal proximal convoluted tubule epithelial cells and might upregulate the level of autophagy. Additionally, the correlation between SQSTM1 and 19 feature genes related to autophagy was calculated. The results indicated that autophagy-related genes were mostly positively correlated with SQSTM1 (Figures 5F, G). Then, 19 feature genes were extracted for further PCA to establish the autophagy score and rank. Samples were ranked based on gene expression of SQSTM1, and its relationship with PCA score was visualized with an alluvial diagram which showed that a high SQSTM1 expression got a high autophagy score rank and vice versa (Figure 5H). The above results indicated that there was a close relationship among autophagy, Cana treatment, and SQSTM1.

3.6 Cana enhanced the stability of SQSTM1 mRNA through inhibiting FTO

In the above results, we found that SQSTM1 is a key factor in the protection of Cana on renal fibrosis; we next sought to analyze its potential mechanism. To confirm Cana's function from the perspective of m6A modification, we firstly identified whether m6A participates in the process of Cana administration. It was found that m6A levels were significantly increased in HK2 cells following Cana administration (Figures 6A, B). Consistently, the kidney of mice treated with Cana exhibited the same trend (Figure 6C). It was reported that the m6A level was mainly modified by methyltransferase or demethylase. Thus, we examined related gene expression to verify whether Cana regulates through mediating RNA methyltransferases or demethylases. As shown in Figure 6D, the expression of SQSTM1 was consistently upregulated and Arg-1 (a typical STAT6 downstream gene) expression was decreased. Notably, Cana significantly inhibited FTO expression, with no obvious change of other methyltransferase- or demethylase-related genes. In accordance with the results of qPCR, we validated that Cana deceased FTO at the protein level both *in vitro* and *in vivo* (Figures 6E, F). Next, the transcriptional downregulation manner of FTO by Cana was further confirmed in the cells with either proteasome inhibitor (MG132) or autophagy blocker (BafA1) treatment. Interestingly, the levels of FTO in the BafA1-treated group were dramatically increased compared with the Ctrl group. However, BafA1 treatment could not recover the decrease of FTO caused by Cana, as well as MG132, which indicated that the downregulation of FTO by Cana is not caused by increased protein degradation through either proteasome or autophagy (Figure 6G). Next, IF staining and Western blot were employed to further investigate the effect of FTO on autophagy. The results showed that the increased LC3II and SQSTM1 was inversed with FTO overexpression (Figures 6H, I). Also, a tandem mouse red fluorescent protein (mRFP)-GFP-LC3 construct was employed. As shown in Figure S3A, HK2 cells treated with Cana contained red puncta but less yellow puncta, indicating its induction of autophagy. However, overexpression of FTO attenuated Cana's effect on autophagy induction. Moreover, we found that Cana treatment increased the stability of SQSTM1 mRNA, whereas overexpressing FTO resulted in decreased stability of SQSTM1 mRNA. These data suggested that Cana decreased FTO transcription, which negatively regulated autophagy through modulation of the SQSTM1 mRNA stability (Figure 6J).

Then, we profiled that SQSTM1 mRNA contained the potential m6A modification region (position: 1906) with an FTO-binding motif as shown in Figure S4. Next, the RNA immunoprecipitation (RIP)-qPCR experiment was conducted and the results confirmed that FTO protein interacted with SQSTM1 mRNA (Figure 6K). Moreover, the methylated RNA immunoprecipitation (MeRIP) assay showed that Cana increased the m6A modification of SQSTM1 mRNA, whereas overexpression of FTO attenuated Cana's effect of increasing SQSTM1 mRNA m6A modification (Figure 6L). With the vital role of SQSTM1 in the modulation of autophagy, we then downregulated SQSTM1 to observe the effect of Cana. As shown in Figure 6M, the knockdown efficiency was confirmed using immunoblot analysis. Cana significantly alleviated TGF-β1-induced lipid accumulation. Oppositely, siSQSTM1 exacerbated TGF-β1-induced lipid accumulation and impaired the protective effect of Cana. Collectively, these data suggested that Cana showed negative regulation on FTO and enhanced SQSTM1 mRNA stability.

3.7 SQSTM1 deficiency eliminated the protection effect of Cana against renal fibrosis

To further provide evidence for the *in vivo* role of SQSTM1, renal tubular-specific SQSTM1 deficiency mice were generated using $SQSTM1^{flox/flox}$ and γGT^{Cre} mice. There were no obvious differences in histological change and collagen deposition, while there were comparisons between WT and $SQSTM1^{cKO}$ mice at 2 months after birth (Figure S5A). As shown in Figure 7A, obvious

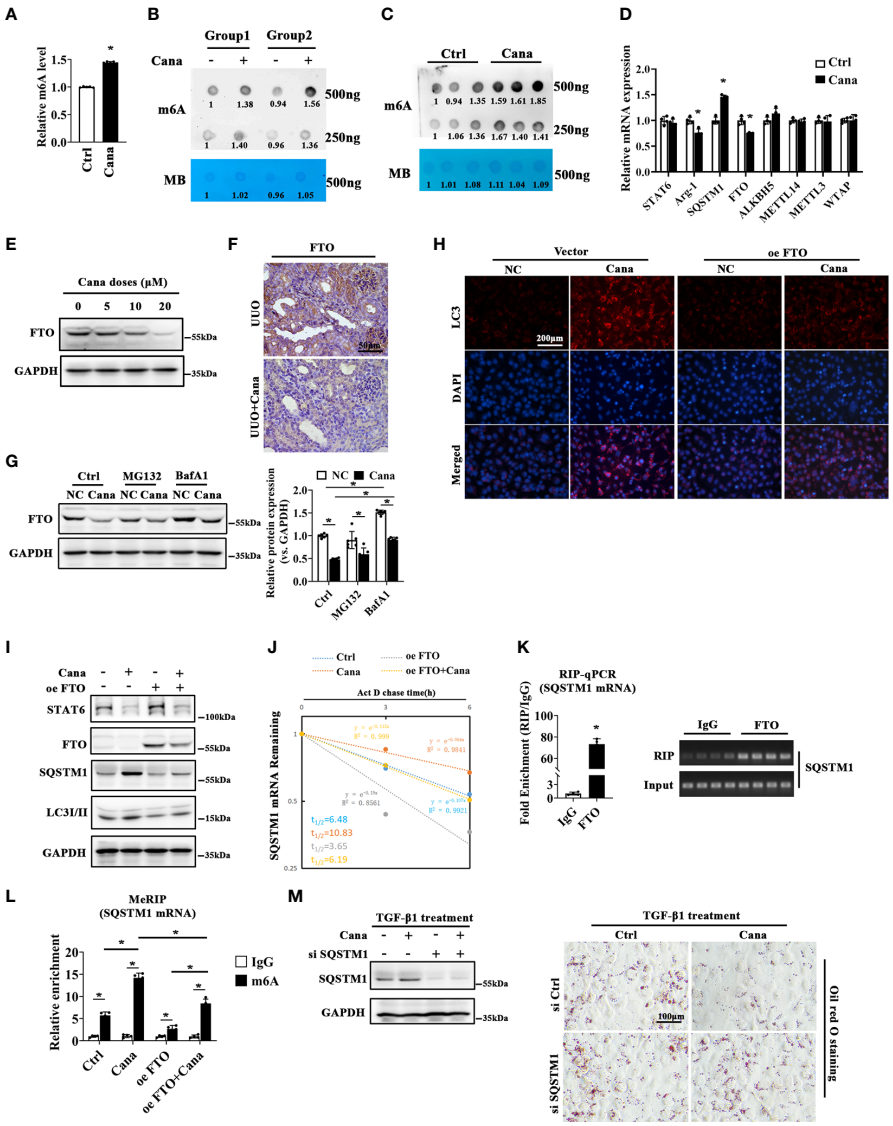

FIGURE 6
FTO was downregulated by Cana to enhance the stability of SQSTM1 mRNA through installing m6A modification of its mRNA. m6A levels of HK2 cells treated with or without Cana (20 μM) were detected by using the EpiQuik^{TM} m6A RNA methylation quantification kit **(A)** and RNA dot blot analyses **(B)**. Methylation blue (MB) staining served as a loading control. **(C)** RNA dot blot analyses of m6A levels in mice from the indicated group. **(D)** HK2 cells treated with or without Cana (20 μM) were harvested and subjected to qPCR to determined STAT6, Arg-1, SQSTM1, FTO, ALKBH5, METTL14, METTL3, and WTAP mRNA levels. (n = 4, *$p < 0.05$, Ctrl *vs.* Cana). **(E)** HK2 cells treated with Cana (0–20 μM) for 24 h were subjected to detected the protein levels of FTO by immunoblot analyses. **(F)** Mice received intragastric administration of saline or Cana (20 mg/kg) after UUO treatment. The expression of FTO was determined through IHC staining. **(G)** HK2 cells were pretreated with MG132 (10 μM) or BafA1 (100 nM) for 4 h and cultured with serum-free medium for 24 h. Then, the cells were left and treated with or without Cana (20 μM) for another 24 h. Immunoblot analyses was performed to detect the protein level of FTO. **(H–J, L)** HK2 cells were transfected with or without plasmid of FTO overexpression 48 h. Then, cells were treated with or without Cana (20 μM) for another 24 h. **(H)** The levels of LC3 in HK2 cells from the indicated group were detected through immunofluorescence staining. **(I)** Immunoblot analysis was performed to determine the protein levels of STAT6, FTO, SQSTM1, LC3I/II, and GAPDH. **(J)** qPCR analyses of SQSTM1 mRNA stability in HK2 cells from the indicated group (*$p < 0.05$). **(K)** RNA immunoprecipitation (RIP)-qPCR analyses revealed the SQSTM1 mRNA level enriched by the FTO antibody. The agarose gel electrophoresis analyses of qPCR products are shown on the panel (*$p < 0.05$). **(L)** MeRIP-qPCR assay indicated the m6A modification level of HK2 cells from the indicated group (*$p < 0.05$). **(M)** HK2 cells transfected with or without SQSTM1 siRNA for 24 h and then treated with Cana (20 μM) along with TGF-β1 (5 ng/ml) for another 48 h. The efficiency of knockdown SQSTM1 in HK2 cells was confirmed by immunoblot analyses. Representative microphages showed the Oil Red O staining in HK2 cells with indicated treatments.

tubular atrophy and interstitial collagen deposition were presented in the WT group with UUO treatment, which was ameliorated with Cana administration. These protective effects were dampened in the SQSTM1^{cKO} group. Additionally, SQSTM1^{cKO} mice exhibited more aggravated renal morphological damage and fibrosis in comparison with the indicated WT mice. Also, Cana was found to decrease the TG content in WT mice, whereas there was no change in

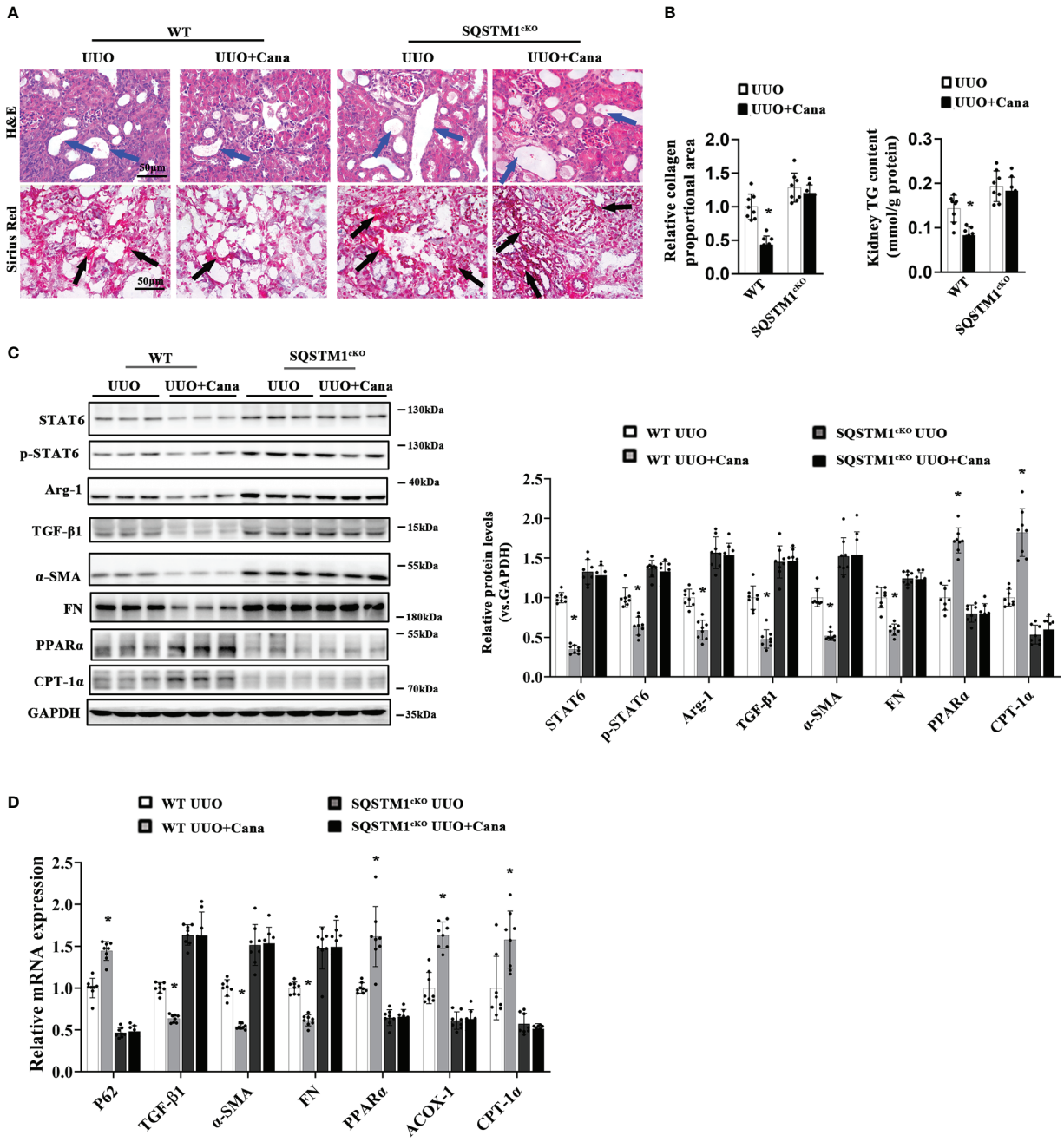

FIGURE 7
SQSTM1 deletion eliminated the protection effect of Cana against tubulointerstitial fibrosis. **(A)** Representative micrographs for H&E and Sirius Red staining of kidney sections from the indicated groups of mice. Quantification of the relative collagen proportional area from each group of mice was performed. **(B)** TG content was determined in the kidneys from each group of mice. **(C)** Immunoblot analyses in the kidneys from each indicated group with quantification. **(D)** The mRNA levels were measured by qPCR assay in the kidneys from each indicated group. Results are expressed as mean ± SD (n = 8 *$p < 0.05$, UUO *vs.* UUO+ Cana).

SQSTM1^{cKO} mice. Furthermore, TG content in SQSTM1^{cKO} mice was even higher than that in WT mice (Figure 7B). Consistently, immunoblot and qPCR analyses also showed that suppression of the STAT6 signaling pathway by Cana only in WT mice and the SQSTM1^{cKO} group showed higher levels of STAT6 and p-STAT6 expression compared with the WT group. Consistently, Cana eliminated the alteration of UUO-induced fibrosis-related protein and PPARα-related FAO gene expression, whereas SQSTM1^{cKO} mice exhibited more fibrosis-related gene expression and less FAO-related gene expression in comparison with WT mice (Figures 7C, D). These data suggested that SQSTM1 was essential for the function of Cana on renal fibrosis and SQSTM1 deletion eliminated the protection of Cana against renal fibrosis.

4 Discussion

Here, our study firstly revealed that Cana ameliorated UUO- or I/R-induced renal lipid metabolism disorder and fibrosis based on the degradation of STAT6 in a SQSTM1/autophagy-dependent manner. Specifically, after Cana administration, relative m6A levels increased *in vivo* and *in vitro*. Cana decreased the expression of m6A eraser FTO and recovered SQSTM1 mRNA stability. Deficiency in endogenous SQSTM1 in mice deteriorated the protective effect of Cana. Overall, our study presented a novel mechanism by which Cana (a commercial antidiabetic drug based on the inhibition of SGLT2) acts to counter to abnormal renal fatty acid metabolism and interstitial fibrosis through the m6A-modified SQSTM1/autophagy/STAT6 axis.

Renal fibrosis is a complex and coordinated process, which involves multiple cell types and cytokines (34–36). Tubular cells are highly specialized cells that use high amounts of ATP to maintain intense reabsorption and excretion processes (37). In tubular cells, FAO impaired by a specific inhibitor or endogenic gene knockdown can induce aberrant lipid accumulation, resulting in the progression of kidney fibrosis (38). STAT6 is a major regulatory transcription factor for type II-related gene expression (involving TGF-β), and our previous study revealed the crucial role of STAT6 in regulating PPARα-mediated FAO in tubular cells and kidney interstitial fibrosis (5, 39, 40). Substantial evidence indicates that SGLT2 inhibitors elicit unanticipated renoprotective effects in non-diabetic and diabetic kidney disease (41, 42). Thus, improving improper lipid metabolism reprogramming represents a pivotal target by which SGLT2i mitigates kidney fibrosis after renal damage, but the mechanism by which they improve lipid metabolism is elusive. In our study, the potential roles of Cana in regulating fibrosis and FAO were firstly verified and evaluated by relative bioinformatics analysis (Figure 1). *In vivo* studies were also carried out to demonstrate that Cana can improve UUO- or I/R-induced renal fibrosis and FAO dysregulation. The induction of STAT6 in fibrotic kidneys was blunted by Cana treatment (Figure 2). Glycolysis is critical for energy metabolism, and SGLT2 inhibition can suppress fibrogenesis in diabetic kidneys by suppressing aberrant glycolysis (43). Moreover, Dufort et al. found that STAT6 mediated glycolysis in B cells (44). Therefore, STAT6/glycolysis may be one of the mechanisms underlying the protective effects of Cana and warrants further investigation.

Next, the mechanisms about Cana-suppressed STAT6 induction were explored, which is important for intracellular homeostasis. Autophagy is a well-known major intracellular degradation system where cytoplasmic materials are delivered and degraded by lysosome, and the process can be activated by many stimuli including starvation, genotoxicity, and inflammatory stress (45–48). As we previously reported, STAT6 can be degraded *via* the autophagosomal pathway (22). Moreover, autophagy can be induced by SGLT2i through several signaling pathways, such as AMPK/mTOR and SIRT1 or SIRT3 signaling (49–52). Consistently, the results of our bioinformatic analysis here also indicated the close association between autophagy and Cana treatment (Figure 4). Thus, the renoprotective effect exerted by Cana treatment was speculated through autophagy-mediated STAT6 degradation, and this prediction was confirmed by the obtained results. First, both *in vivo* and *vitro* results showed the induction of autophagy following Cana treatment, and STAT6 protein degradation was mostly affected by the autophagolysosomal pathway, rather than the ubiquitin–proteasomal pathway. Second, the inhibition of autophagy impaired the protection of Cana on lipid metabolism disorder and renal fibrosis by Atg7 knockout in tubular cells.

In the current study, SQSTM1 was upregulated dose-dependently by Cana treatment in HK-2 cells, hinting that SQSTM1 is a potential target gene of Cana. During the process of autophagy, SQSTM1/P62 acts as a vital and multifunction protein. In general, SQSTM1 is a robust indicator of dynamic autophagic flux, given that it is an autophagy receptor that directly interacts with selected cargoes for degradation. Primarily, the inhibition of autophagy leads to intracellular SQSTM1 accumulation (53). Moreover, SQSTM1 is an upstream regulator of autophagy and binds to arginylated substrates. Deficiency in SQSTM1 inhibits the formation of autophagosome and impaired autophagy (54). In Hela cells, SQSTM1 deficiency inhibited the recruitment of MAP1/LC3, resulting in autophagosome formation inhibition (55). Consistently, in our study, we found a close association between SQSTM1 and autophagy through bioinformatic analysis and showed that SQSTM1 knockdown inhibited autophagy induced by Cana in HK2 cells. Therefore, SQSTM1/autophagy may be an important target for Cana treatment.

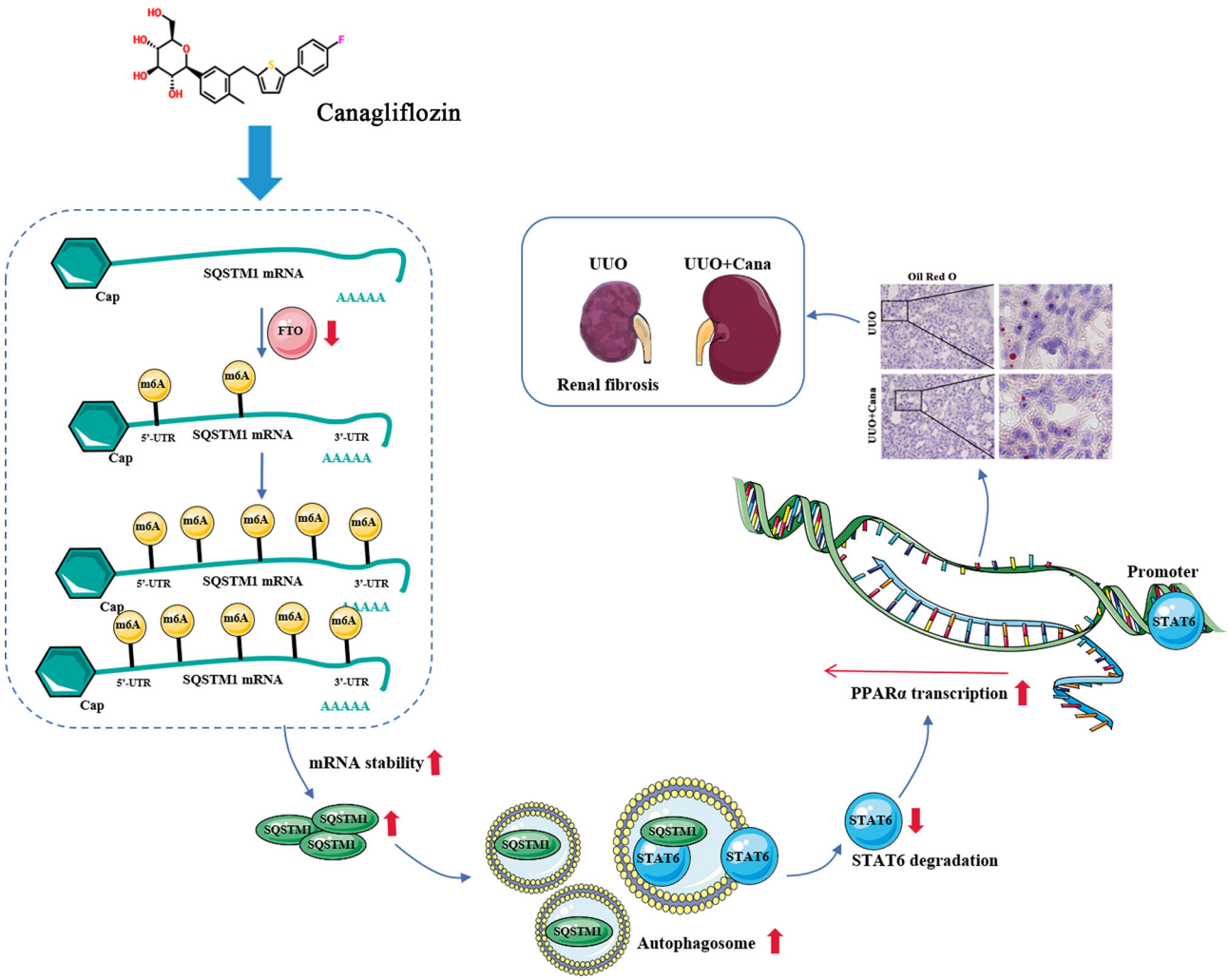

FIGURE 8
Proposed model for the therapeutic action of Cana against renal fibrosis. Cana attenuates renal tubular cells' FAO disorder and renal fibrosis by SQSTM1/autophagy-mediated STAT6 degradation in an m6A-dependent manner.

10.3389/fimmu.2022.1094556

Furthermore, we explored the mechanism underlying this mode of Cana-mediated SQSTM1/autophagy. m6A is the most prevalent form of posttranscriptional modification in RNA molecules and involved in diverse key biological processes, including alternative splicing, stability, mRNA translation, and miRNA maturation (56–58). Emerging evidence suggests that m6A modification plays a remarkable role in autophagy regulation (59, 60). Herein, Cana treatment markedly increased the m6A level in HK2 cells and mouse kidneys. qPCR analysis further identified that FTO, the first identified m6A demethylase, is the only methyltransferase- or demethylase-related gene with a significant difference. It was reported that FTO plays a role in regulating renal fibrosis, and the m6A modification of lncRNA GAS5 may participate in the process (61, 62). In addition, some studies that have explored the relationship between FTO and autophagy and the results showed that FTO deficiency inhibits mTORC1 signaling and activates autophagy in MEFs (19). Another study has shown that the forced expression of FTO augments the activation of autophagy in 3T3-L1 and porcine primary preadipocytes, suggesting that the role of FTO in autophagy induction is controversial (19). In arsenic-associated human skin lesions, FTO is degraded upon autophagy (63). These results indicate the existence of a probable feedback loop between FTO and autophagy. Our data showed that FTO overexpression resulted in the inhibition of autophagy induced by Cana. Meanwhile, after BafA1 (autophagy inhibitor) treatment, FTO expression increased but failed to restore the downregulation caused by Cana. Thus, FTO may be the upstream of Cana-induced autophagy activation. Overall, a feedback loop may be involved in the FTO and autophagy regulation in tubular cells.

We then explored how FTO regulates autophagy with Cana stimulation. SQSTM1 nuclear mRNA can be modified by m6A reader protein YTHDC1 through methylation in diabetic keratinocytes, and m6A modification may be involved in SQSTM1 expression (64). Consistently, we predicted that SQSTM1 mRNA contained an m6A modification region (position: 1906) with an FTO-binding motif. The results of the RIP-qPCR assay confirmed that FTO interacted with SQSTM1 mRNA. Cana treatment decreased the transcription of FTO, and the m6A methylation of SQSTM1 mRNA increased after Cana treatment. However, FTO overexpression reduced SQSTM1 m6A methylation and suppressed its mRNA stability. These results indicated that Cana increased SQSTM1 mRNA expression *via* FTO. Furthermore, the *in vivo* study employed with SQSTM1 cKO mice confirmed that SQSTM1 in tubular cells played a critical role in the protective effect of Cana on renal fibrosis. Notably, SQSTM1 can contribute to the regulation of fibrotic process *via* the vitamin D receptor or NRF2 pathway, which are independent autophagy programs (65, 66). Thus, the role of SQSTM1 in regulating the protective effects of Cana in renal fibrosis may be either dependent or independent of the autophagy pathways.

Followed by our previous study that STAT6 activation negatively regulates PPARα signaling and causes FAO disorder and aggravates renal fibrosis (5), here we found that Cana attenuates renal tubular cells' FAO disorder and renal fibrosis by SQSTM1/autophagy-mediated STAT6 degradation in an m6A-dependent manner. We further clarified that Cana functioned mainly by inhibiting FTO, increasing the stability of SQSTM1 mRNA, and immediately increasing autophagy, which is essential to the degradation of STAT6 (Figure 8). Overall, our study will provide valuable insights of Cana into the treatment of chronic kidney disease.

Data availability statement

The original contributions presented in the study are included in the article/Supplementary Material. Further inquiries can be directed to the corresponding authors.

Ethics statement

The animal study was reviewed and approved by Laboratory Animal Welfare and Ethics Committee of Chongqing University.

Author contributions

YY and QL designed the experiments and performed part of the experiments. YL and LL performed software, investigation. YM and LX provided technical and material support. GL and YD performed and analyzed the result of mouse model. ST and JL performed conceptualization, visualization, writing—review and editing, supervision, and project administration. All authors contributed to the article and approved the submitted version.

Funding

This work was supported by the National Natural Science Foundation of China (Grant ref: 81703205); a project funded by the Priority Academic Program Development of Jiangsu Higher Education Institutions (PAPD); Foundation from Chongqing Yuzhong District Science and Technology Bureau (201930) and the Natural Science Foundation of Chongqing Science and Technology Bureau (cstc2020jcyj-msxmX0529); special funds of Clinical Science and Technology of Suzhou (LCZX2020003); and Chongqing Key Laboratory of Emergency Medicine (2022KFKT08).

Conflict of interest

The authors declare that the research was conducted in the absence of any commercial or financial relationships that could be construed as a potential conflict of interest.

Publisher's note

All claims expressed in this article are solely those of the authors and do not necessarily represent those of their affiliated organizations, or those of the publisher, the editors and the reviewers. Any product that may be evaluated in this article, or claim that may be made by its manufacturer, is not guaranteed or endorsed by the publisher.

Supplementary material

The Supplementary Material for this article can be found online at: https://www.frontiersin.org/articles/10.3389/fimmu.2022.1094556/full#supplementary-material

References

1. Humphreys BD. Mechanisms of renal fibrosis. *Annu Rev Physiol* (2018) 80:309–26. doi: 10.1146/annurev-physiol-022516-034227

2. Liu Y. Cellular and molecular mechanisms of renal fibrosis. *Nat Rev Nephrology* (2011) 7(12):684–96. doi: 10.1038/nrneph.2011.149

3. Ruggenenti P, Cravedi P, Remuzzi G. Mechanisms and treatment of CKD. *J Am Soc Nephrol JASN.* (2012) 23(12):1917–28. doi: 10.1681/asn.2012040390

4. Liu L, Ning X, Wei L, Zhou Y, Zhao L, Ma F, et al. Twist1 downregulation of PGC-1α decreases fatty acid oxidation in tubular epithelial cells, leading to kidney fibrosis. *Theranostics.* (2022) 12(8):3758–75. doi: 10.7150/thno.71722

5. Li J, Yang Y, Li Q, Wei S, Zhou Y, Yu W, et al. STAT6 contributes to renal fibrosis by modulating PPARα-mediated tubular fatty acid oxidation. *Cell Death dis* (2022) 13(1):66. doi: 10.1038/s41419-022-04515-3

6. Cadwell K. Crosstalk between autophagy and inflammatory signalling pathways: balancing defence and homeostasis. *Nat Rev Immunol* (2016) 16 (11):661–75. doi: 10.1038/nri.2016.100

7. Parzych KR, Klionsky DJ. An overview of autophagy: morphology, mechanism, and regulation. *Antioxidants Redox Signaling* (2014) 20(3):460–73. doi: 10.1089/ars.2013.5371

8. Kaushal GP, Chandrashekar K, Juncos LA, Shah SV. Autophagy function and regulation in kidney disease. *Biomolecules.* (2020) 10(1). doi: 10.3390/biom10010100

9. Ren C, Bao X, Lu X, Du W, Wang X, Wei J, et al. Complanatoside a targeting NOX4 blocks renal fibrosis in diabetic mice by suppressing NLRP3 inflammasome activation and autophagy. *Phytomed Int J phytother phytopharmacol* (2022) 104:154310. doi: 10.1016/j.phymed.2022.154310

10. Xu T, Guo J, Wei M, Wang J, Yang K, Pan C, et al. Aldehyde dehydrogenase 2 protects against acute kidney injury by regulating autophagy via the beclin-1 pathway. *JCI Insight* (2021) 6(15):e138183. doi: 10.1172/jci.insight.138183

11. Lovisa S, Zeisberg M, Kalluri R. Partial epithelial-to-Mesenchymal transition and other new mechanisms of kidney fibrosis. *Trends Endocrinol metabolism: TEM* (2016) 27(10):681–95. doi: 10.1016/j.tem.2016.06.004

12. Yang C, Wu HL, Li ZH, Chen XC, Su HY, Guo XY, et al. Autophagy inhibition sensitizes renal tubular epithelial cell to G1 arrest induced by transforming growth factor beta (TGF-β). *Med Sci monitor Int Med J Exp Clin Res* (2020) 26:e922673. doi: 10.12659/msm.922673

13. Liu BC, Tang TT, Lv LL, Lan HY. Renal tubule injury: a driving force toward chronic kidney disease. *Kidney Int* (2018) 93(3):568–79. doi: 10.1016/j.kint.2017.09.033

14. Osataphan S, Macchi C, Singhal G, Chimene-Weiss J, Sales V, Kozuka C, et al. SGLT2 inhibition reprograms systemic metabolism *via* FGF21-dependent and -independent mechanisms. *JCI Insight* (2019) 4(5):e123130. doi: 10.1172/jci.insight.123130

15. Zhu ZM, Huo FC, Pei DS. Function and evolution of RNA N6-methyladenosine modification. *Int J Biol Sci* (2020) 16(11):1929–40. doi: 10.7150/ijbs.45231

16. Jiang X, Liu B, Nie Z, Duan L, Xiong Q, Jin Z, et al. The role of m6A modification in the biological functions and diseases. *Signal transduction targeted Ther* (2021) 6(1):74. doi: 10.1038/s41392-020-00450-x

17. Liu N, Zhou KI, Parisien M, Dai Q, Diatchenko L, Pan T. N6-methyladenosine alters RNA structure to regulate binding of a low-complexity protein. *Nucleic Acids Res* (2017) 45(10):6051–63. doi: 10.1093/nar/gkx141

18. Li Q, Ni Y, Zhang L, Jiang R, Xu J, Yang H, et al. HIF-1α-induced expression of m6A reader YTHDF1 drives hypoxia-induced autophagy and malignancy of hepatocellular carcinoma by promoting ATG2A and ATG14 translation. *Signal transduction targeted Ther* (2021) 6(1):76. doi: 10.1038/s41392-020-00453-8

19. Wang X, Wu R, Liu Y, Zhao Y, Bi Z, Yao Y, et al. m(6)A mRNA methylation controls autophagy and adipogenesis by targeting Atg5 and Atg7. *Autophagy.* (2020) 16(7):1221–35. doi: 10.1080/15548627.2019.1659617

20. Yuan Y, Fang Y, Zhu L, Gu Y, Li L, Qian J, et al. Deterioration of hematopoietic autophagy is linked to osteoporosis. *Aging Cell* (2020) 19(5): e13114. doi: 10.1111/acel.13114

21. Li X, Zhou L, Peng G, Liao M, Zhang L, Hu H, et al. Pituitary P62 deficiency leads to female infertility by impairing luteinizing hormone production. *Exp Mol Med* (2021) 53(8):1238–49. doi: 10.1038/s12276-021-00661-4

22. Li J, Yang Y, Wei S, Chen L, Xue L, Tian H, et al. Bixin protects against kidney interstitial fibrosis through promoting STAT6 degradation. *Front Cell Dev Biol* (2020) 8:576988. doi: 10.3389/fcell.2020.576988

23. Barrett T, Wilhite SE, Ledoux P, Evangelista C, Kim IF, Tomashevsky M, et al. NCBI GEO: Archive for functional genomics data sets–update. *Nucleic Acids Res* (2013) 41(Database issue):D991–5. doi: 10.1093/nar/gks1193

24. Ritchie ME, Phipson B, Wu D, Hu Y, Law CW, Shi W, et al. Limma powers differential expression analyses for RNA-sequencing and microarray studies. *Nucleic Acids Res* (2015) 43(7):e47. doi: 10.1093/nar/gkv007

25. Szklarczyk D, Gable AL, Lyon D, Junge A, Wyder S, Huerta-Cepas J, et al. STRING v11: Protein-protein association networks with increased coverage, supporting functional discovery in genome-wide experimental datasets. *Nucleic Acids Res* (2019) 47(D1):D607–D13. doi: 10.1093/nar/gky1131

26. Shannon P, Markiel A, Ozier O, Baliga NS, Wang JT, Ramage D, et al. Cytoscape: A software environment for integrated models of biomolecular interaction networks. *Genome Res* (2003) 13(11):2498–504. doi: 10.1101/gr.1239303

27. Zhou Y, Zhou B, Pache L, Chang M, Khodabakhshi AH, Tanaseichuk O, et al. Metascape provides a biologist-oriented resource for the analysis of systems-level datasets. *Nat Commun* (2019) 10(1):1523. doi: 10.1038/s41467-019-09234-6

28. Liberzon A, Birger C, Thorvaldsdóttir H, Ghandi M, Mesirov JP, Tamayo P. The molecular signatures database (MSigDB) hallmark gene set collection. *Cell systems* (2015) 1(6):417–25. doi: 10.1016/j.cels.2015.12.004

29. Subramanian A, Tamayo P, Mootha VK, Mukherjee S, Ebert BL, Gillette MA, et al. Gene set enrichment analysis: A knowledge-based approach for interpreting genome-wide expression profiles. *Proc Natl Acad Sci United States America* (2005) 102(43):15545–50. doi: 10.1073/pnas.0506580102

30. Yu G, Wang LG, Han Y, He QY. clusterProfiler: an r package for comparing biological themes among gene clusters. *Omics J Integr Biol* (2012) 16(5):284–7. doi: 10.1089/omi.2011.0118

31. Shannon P, Markiel A, Ozier O, Baliga NS, Wang JT, Ramage D, et al. Cytoscape: A software environment for integrated models of biomolecular interaction networks. *Genome Res* (2003) 13(11):2498–504. doi: 10.1101/gr.1239303

32. Levine B, Kroemer G. Biological functions of autophagy genes: A disease perspective. *Cell* (2019) 176(1-2):11–42. doi: 10.1016/j.cell.2018.09.048

33. Pirklbauer M, Schupart R, Fuchs L, Staudinger P, Corazza U, Sallaberger S, et al. Unraveling reno-protective effects of SGLT2 inhibition in human proximal

tubular cells. *Am J Physiol Renal Physiol* (2019) 316(3):F449–f62. doi: 10.1152/ajprenal.00431.2018

34. Sun YB, Qu X, Caruana G, Li J. The origin of renal fibroblasts/myofibroblasts and the signals that trigger fibrosis. *Differentiation Res Biol diversity.* (2016) 92(3):102–7. doi: 10.1016/j.diff.2016.05.008

35. Brennan EP, Cacace A, Godson C. Specialized pro-resolving mediators in renal fibrosis. *Mol aspects Med* (2017) 58:102–13. doi: 10.1016/j.mam.2017.05.001

36. Wu R, Li J, Tu G, Su Y, Zhang X, Luo Z, et al. Comprehensive molecular and cellular characterization of acute kidney injury progression to renal fibrosis. *Front Immunol* (2021) 12:699192. doi: 10.3389/fimmu.2021.699192

37. Liu BC, Tang TT, Lv LL. How tubular epithelial cell injury contributes to renal fibrosis. *Adv Exp Med Biol* (2019) 1165:233–52. doi: 10.1007/978-981-13-8871-2_11

38. Kang HM, Ahn SH, Choi P, Ko YA, Han SH, Chinga F, et al. Defective fatty acid oxidation in renal tubular epithelial cells has a key role in kidney fibrosis development. *Nat Med* (2015) 21(1):37–46. doi: 10.1038/nm.3762

39. Rahal OM, Wolfe AR, Mandal PK, Larson R, Tin S, Jimenez C, et al. Blocking interleukin (IL)4- and IL13-mediated phosphorylation of STAT6 (Tyr641) decreases M2 polarization of macrophages and protects against macrophage-mediated radioresistance of inflammatory breast cancer. *Int J Radiat oncology biology physics.* (2018) 100(4):1034–43. doi: 10.1016/j.ijrobp.2017.11.043

40. Yu T, Gan S, Zhu Q, Dai D, Li N, Wang H, et al. Modulation of M2 macrophage polarization by the crosstalk between Stat6 and Trim24. *Nat Commun* (2019) 10(1):4353. doi: 10.1038/s41467-019-12384-2

41. Abbas NAT, El Salem A, Awad MM. Empagliflozin, SGLT(2) inhibitor, attenuates renal fibrosis in rats exposed to unilateral ureteric obstruction: potential role of klotho expression. *Naunyn-Schmiedeberg's Arch Pharmacol* (2018) 391(12):1347–60. doi: 10.1007/s00210-018-1544-y

42. Fathi A, Vickneson K, Singh JS. SGLT2-inhibitors; more than just glycosuria and diuresis. *Heart failure Rev* (2021) 26(3):623–42. doi: 10.1007/s10741-020-10038-w

43. Li J, Liu H, Takagi S, Nitta K, Kitada M, Srivastava SP, et al. Renal protective effects of empagliflozin via inhibition of EMT and aberrant glycolysis in proximal tubules. *JCI Insight* (2020) 5(6):e129034. doi: 10.1172/jci.insight.129034

44. Dufort FJ, Bleiman BF, Gumina MR, Blair D, Wagner DJ, Roberts MF, et al. Cutting edge: IL-4-mediated protection of primary b lymphocytes from apoptosis *via* Stat6-dependent regulation of glycolytic metabolism. *J Immunol (Baltimore Md 1950).* (2007) 179(8):4953–7. doi: 10.4049/jimmunol.179.8.4953

45. Levine B, Deretic V. Unveiling the roles of autophagy in innate and adaptive immunity. *Nat Rev Immunol* (2007) 7(10):767–77. doi: 10.1038/nri2161

46. Rosenfeldt MT, Ryan KM. The multiple roles of autophagy in cancer. *Carcinogenesis.* (2011) 32(7):955–63. doi: 10.1093/carcin/bgr031

47. Bhattacharya A, Eissa NT. Autophagy as a stress response pathway in the immune system. *Int Rev Immunol* (2015) 34(5):382–402. doi: 10.3109/08830185.2014.999156

48. Murrow L, Debnath J. Autophagy as a stress-response and quality-control mechanism: Implications for cell injury and human disease. *Annu Rev pathol* (2013) 8:105–37. doi: 10.1146/annurev-pathol-020712-163918

49. Packer M. Role of impaired nutrient and oxygen deprivation signaling and deficient autophagic flux in diabetic CKD development: Implications for understanding the effects of sodium-glucose cotransporter 2-inhibitors. *J Am Soc Nephrol JASN.* (2020) 31(5):907–19. doi: 10.1681/asn.2020010010

50. Ren C, Sun K, Zhang Y, Hu Y, Hu B, Zhao J, et al. Sodium-glucose CoTransporter-2 inhibitor empagliflozin ameliorates sunitinib-induced cardiac dysfunction *via* regulation of AMPK-mTOR signaling pathway-mediated autophagy. *Front Pharmacol* (2021) 12:664181. doi: 10.3389/fphar.2021.664181

51. Packer M. Mitigation of the adverse consequences of nutrient excess on the kidney: A unified hypothesis to explain the renoprotective effects of sodium-glucose cotransporter 2 inhibitors. *Am J nephrology* (2020) 51(4):289–93. doi: 10.1159/000506534

52. Wang CY, Chen CC, Lin MH, Su HT, Ho MY, Yeh JK, et al. TLR9 binding to beclin 1 and mitochondrial SIRT3 by a sodium-glucose Co-transporter 2 inhibitor protects the heart from doxorubicin toxicity. *Biology* (2020) 9(11):369. doi: 10.3390/biology9110369

53. Liu WJ, Ye L, Huang WF, Guo LJ, Xu ZG, Wu HL, et al. p62 links the autophagy pathway and the ubiqutin-proteasome system upon ubiquitinated protein degradation. *Cell Mol Biol letters* (2016) 21:29. doi: 10.1186/s11658-016-0031-z

54. Rubio N, Verrax J, Dewaele M, Verfaillie T, Johansen T, Piette J, et al. p38 (MAPK)-regulated induction of p62 and NBR1 after photodynamic therapy promotes autophagic clearance of ubiquitin aggregates and reduces reactive oxygen species levels by supporting Nrf2-antioxidant signaling. *Free Radical Biol Med* (2014) 67:292–303. doi: 10.1016/j.freeradbiomed.2013.11.010

55. Bjørkøy G, Lamark T, Brech A, Outzen H, Perander M, Overvatn A, et al. p62/SQSTM1 forms protein aggregates degraded by autophagy and has a protective effect on huntingtin-induced cell death. *J Cell Biol* (2005) 171(4):603–14. doi: 10.1083/jcb.200507002

56. Kasowitz SD, Ma J, Anderson SJ, Leu NA, Xu Y, Gregory BD, et al. Nuclear m6A reader YTHDC1 regulates alternative polyadenylation and splicing during mouse oocyte development. *PLoS Genet* (2018) 14(5):e1007412. doi: 10.1371/journal.pgen.1007412

57. Oerum S, Meynier V, Catala M, Tisné C. A comprehensive review of m6A/m6Am RNA methyltransferase structures. *Nucleic Acids Res* (2021) 49(13):7239–55. doi: 10.1093/nar/gkab378

58. van den Homberg DAL, van der Kwast R, Quax PHA, Nossent AY. N-6-Methyladenosine in vasoactive microRNAs during hypoxia; a novel role for METTL4. *Int J Mol Sci* (2022) 23(3):1057. doi: 10.3390/ijms23031057

59. Lin Z, Niu Y, Wan A, Chen D, Liang H, Chen X, et al. RNA m(6) a methylation regulates sorafenib resistance in liver cancer through FOXO3-mediated autophagy. *EMBO J* (2020) 39(12):e103181. doi: 10.15252/embj.2019103181

60. Chen X, Gong W, Shao X, Shi T, Zhang L, Dong J, et al. METTL3-mediated m(6)A modification of ATG7 regulates autophagy-GATA4 axis to promote cellular senescence and osteoarthritis progression. *Ann rheumatic diseases* (2022) 81(1):87–99. doi: 10.1136/annrheumdis-2021-221091

61. Wang CY, Shie SS, Tsai ML, Yang CH, Hung KC, Wang CC, et al. FTO modulates fibrogenic responses in obstructive nephropathy. *Sci Rep* (2016) 6:18874. doi: 10.1038/srep18874

62. Li X, Li Y, Wang Y, He X. The m(6)A demethylase FTO promotes renal epithelial-mesenchymal transition by reducing the m(6)A modification of lncRNA GAS5. *Cytokine.* (2022) 159:156000. doi: 10.1016/j.cyto.2022.156000

63. Cui YH, Yang S, Wei J, Shea CR, Zhong W, Wang F, et al. Autophagy of the m(6)A mRNA demethylase FTO is impaired by low-level arsenic exposure to promote tumorigenesis. *Nat Commun* (2021) 12(1):2183. doi: 10.1038/s41467-021-22469-6

64. Liang D, Lin WJ, Ren M, Qiu J, Yang C, Wang X, et al. m(6)A reader YTHDC1 modulates autophagy by targeting SQSTM1 in diabetic skin. *Autophagy.* (2022) 18(6):1318–37. doi: 10.1080/15548627.2021.1974175

65. Duran A, Hernandez ED, Reina-Campos M, Castilla EA, Subramaniam S, Raghunandan S, et al. p62/SQSTM1 by binding to vitamin d receptor inhibits hepatic stellate cell activity, fibrosis, and liver cancer. *Cancer Cell* (2016) 30(4):595–609. doi: 10.1016/j.ccell.2016.09.004

66. Zeng Q, Zhou T, Zhao F, Xiong D, He B, Hua Q, et al. p62-Nrf2 regulatory loop mediates the anti-pulmonary fibrosis effect of bergenin. *Antioxidants (Basel)* (2022) 11(2):307. doi: 10.3390/antiox11020307

frontiers | Frontiers in Immunology

TYPE Review
PUBLISHED 13 March 2023
DOI 10.3389/fimmu.2023.1121495

OPEN ACCESS

EDITED BY
Kai Wang,
Southwest Medical University, China

REVIEWED BY
Tie Fu Liu,
Fudan University, China
Dimin Wang,
Zhejiang University, China

*CORRESPONDENCE
Kangling Zhang
kazhang@utmb.edu
Chinnaswamy Jagannath
cjagannah@houstonmethodist.org

SPECIALTY SECTION
This article was submitted to Inflammation, a section of the journal Frontiers in Immunology

RECEIVED 11 December 2022
ACCEPTED 01 February 2023
PUBLISHED 13 March 2023

CITATION
Zhang K, Sowers ML, Cherryhomes EI, Singh VK, Mishra A, Restrepo BI, Khan A and Jagannath C (2023) Sirtuin-dependent metabolic and epigenetic regulation of macrophages during tuberculosis. *Front. Immunol.* 14:1121495. doi: 10.3389/fimmu.2023.1121495

Sirtuin-dependent metabolic and epigenetic regulation of macrophages during tuberculosis

Kangling Zhang[1*], Mark L. Sowers[1], Ellie I. Cherryhomes[1], Vipul K. Singh[2], Abhishek Mishra[2], Blanca I. Restrepo[3], Arshad Khan[2] and Chinnaswamy Jagannath[2*]

[1]Department of Pharmacology and Toxicology, University of Texas Medical Branch, Galveston, TX, United States, [2]Department of Pathology and Genomic Medicine, Houston Methodist Research Institute, Weill-Cornell Medicine, Houston, TX, United States, [3]University of Texas Health Houston, School of Public Health, Brownsville, TX, United States

Macrophages are the preeminent phagocytic cells which control multiple infections. Tuberculosis a leading cause of death in mankind and the causative organism *Mycobacterium tuberculosis* (MTB) infects and persists in macrophages. Macrophages use reactive oxygen and nitrogen species (ROS/RNS) and autophagy to kill and degrade microbes including MTB. Glucose metabolism regulates the macrophage-mediated antimicrobial mechanisms. Whereas glucose is essential for the growth of cells in immune cells, glucose metabolism and its downsteam metabolic pathways generate key mediators which are essential co-substrates for post-translational modifications of histone proteins, which in turn, epigenetically regulate gene expression. Herein, we describe the role of sirtuins which are NAD^+-dependent histone histone/protein deacetylases during the epigenetic regulation of autophagy, the production of ROS/RNS, acetyl-CoA, NAD^+, and S-adenosine methionine (SAM), and illustrate the cross-talk between immunometabolism and epigenetics on macrophage activation. We highlight sirtuins as emerging therapeutic targets for modifying immunometabolism to alter macrophage phenotype and antimicrobial function.

KEYWORDS

human macrophages, autophagy, glycolysis, metabolism, histone modifications, SIRTUIN

Introduction

Macrophages are the preeminent phagocytic cells which respond to pathogen invasion using a variety of anti-microbial mechanisms. Circulating monocytes originating in bone marrow become macrophages (MΦs) at tissue sites of infection after getting exposed to cytokines and microbial stimuli. During tuberculosis, the causative organism *Mycobacterium tuberculosis* (MTB) infects and grows in naive MΦs. That tuberculosis continues to kill more than a million people each year indicates that MTB has evasion mechanisms to survive and

grow in MΦs. Indeed, MTB evades antimicrobial mechanisms of MΦs using multiple strategies including epigenetic modifications (1, 2). For example, MTB encodes for dozens of methyltransferases of which, products from *Rv1988* and *Rv2966c* methylate DNA (2, 3); DNA hypermethylation of MΦs was reported to decrease immunity in TB patients (4). MTB derived *Rv3423.1* acetylates histones affecting gene expression, whereas Enhanced intracellular survival (Eis) protein acetylates histone H3 at K9 and K14 and increases IL-10 (5). Together, these observations suggest that 'acetylation and methylation' are important for controlling antimicrobial mechanisms within MΦs during intracellular infections like tuberculosis.

Intriguingly, T cell derived cytokines like IFN-γ drive naïve MΦs into an M1-MΦ phenotype whereas, IL-4, IL-10 and IL-13 differentiate them into M2-MΦs. We recently reported that MTB infected human M1- and M2-MΦs show unique transcriptional responses and M1-MΦs were able to inhibit the growth of MTB using a nitric oxide- and autophagy-dependent mechanism, whereas M2-MΦs were permissive for growth (6). During these studies, we noted that M1- and M2-MΦs expressed differing levels of sirtuin (SIRT) histone/protein deacetylases and significantly, SIRT2 blockade increased the ability of MΦs to kill MTB suggesting a pivotal role.

Recent studies demonstrate that the activity of MΦ derived histone acetyltransferases is regulated by their co-substrate, acetyl-CoA (ac-CoA), whereas the activity of sirtuin proteins which are nicotinamide adenine dinucleotide (NAD^+)-dependent histone deacetylases, is dependent on NAD^+. It is also known that the activity of histone methyltransferases and DNA methyltransferases is regulated by their specific co-substrate, s-adenosylmethionine (SAM) (7). Therefore, chromatin-modifying enzymes can sense the metabolic status and translate this information into gene expression. In MΦs, this would determine their polarization state as either pro-inflammatory IFN-γ/LPS inducible M1-MΦs or alternatively activated and anti-inflammatory, IL-4/IL-10 and IL-13 driven M2-MΦs. Interestingly, Glucose metabolism differs between M1- and M2-MΦs and glycolysis and its associated pentose-phosphate-pathway (PPP), serine biosynthesis, and one-carbon metabolism are major sources for the co-substrates for methylation and acetylation. In M1-MΦs, glucose uptake is elevated by up-regulated glucose transporter GLUT1, followed by up-regulated glycolysis (8, 9). High glucose intake and metabolism is essential for phagocytosis, production of reactive-oxygen-species (ROS) and reactive-nitrogen-species (RNS), and secretion of pro-inflammatory cytokines (10).

Emerging evidence also links glycolysis to epigenetics. Locasale's and Schultz's groups have demonstrated that histone acetylation is enhanced by glucose flux in a variety of cell types (11, 12). Acetylation is strongly associated with ac-CoA levels but inversely correlated with the ratio of ac-CoA to free CoA (11). Inhibition of glycolysis results in the reduced production of ac-CoA and reduction of histone acetylation leading to differentiation of embryonic stem cells (13). In bacteria, two-thirds of glycolytic and TCA cycle enzymes are acetylated, with acetylation inhibiting their catalytic activity and promoting degradation (14). Glycolysis also regulates histone deacetylation because NAD^+-dependent srtuin proteins regulate the expression of glycolytic enzymes and the ratio of NAD^+/NADH is controlled by the glycolytic flux, and vice versa (15–18). In addition to acetylation, glycolysis also indirectly affects methylation through serine biosynthesis that utilizes 3-phospho-glycerate (3-P-G) as the starting material (19). Through one-carbon metabolism, serine is used for the *de novo* synthesis of methionine and SAM which is the co-substrate of methyltransferases (19, 20).

In this review, we summarize the recent research on the regulation of glucose metabolism and its associated metabolism by sirtuin proteins and their co-substrate NAD^+ and their impact on epigenetic regulation of MΦ activation, polarization, and autophagy activity. We also discuss the NAD^+-dependent sirtuin histone deacetylases as emerging drug targets for the treatment of infectious diseases, specifically for tuberculosis. Since we wish to focus on metabolism-derived co-substrates of histone acetylation/methylation enzymes and the NAD^+-dependent histone deacetylase-sirtuin proteins, epigenetic regulation of autophagy by other histone modification enzymes or modification states is beyond the scope of this review and are covered elsewhere (21, 22).

Glucose metabolism and immune responses

Glucose metabolism exerts a strong impact on immune cell function (Figure 1) (23). For example, hexokinase (HK) binds to bacterium-produced N-acetylglucosamine and causes its deactivation as well as its dissociation from mitochondrial voltage-dependent anion channels (VDACs), which in turn, leads to NOD-Like Receptor family Pyrin domain containing 3 (NLRP3) inflammasome activation in MΦs (24, 25). Phosphoglucose isomerase (PGI) is identical to the protein known as Autocrine Motility Factor (AMF) which is upregulated in cancer cells together with other glycolysis enzymes and thought to play a key role in cancer metastasis by activating Epithelial-Mesenchymal Transition (EMT) and the MAPK/ERK or PI3K/AKT pathways (26, 27). These pathways are also upregulated in glucose deprived MΦs (28–30). Fructose-bisphosphate aldolase (FBA) is immuno-responsive during pathogen infection and is a potential vaccination target (31). Triosephosphate isomerase (TPI) catalyzes the interconversion of dihydroxyacetone phosphate (DHAP) and glyceraldehyde-3-phosphate (G3P). TPI has been predicted to be essential for growth of MTB (32). Phosphoglycerate kinase (PGK) enhances the immunity to *Streptococcus agalactiae* in tilapia (33). Immunization of phosphoglyceromutase (PGM) induces Th1- and Th2-related immune responses in mice infected with Brucella (34). Deficiency of enolase (ENO1) causes the reduction of pyruvate which then contributes to a dysfunction in mitochondrial homeostasis and affects dendritic cell survival, maturation and antigen presentation (35). Pyruvate kinase 2 (PKM2) is required for the expression of PD-L1 in immune cells and tumors. Loss of PKM2 impairs endothelial cell proliferation and migration and triggers innate immune signaling (36). Glyceraldehyde-3-phosphate dehydrogenase (GAPDH) binds to 3'-UTR of inflammatory mRNAs and inhibits the translation of tumor necrosis factor alpha (TNF-α) and interferon gamma (IFN-γ) (37). PDK2/4 serves as a metabolic checkpoint for polarization of macrophages into the pro-inflammatory M1 phenotype (38). Though not generally characterized as a glycolytic enzyme involved in the 10

10.3389/fimmu.2023.1121495

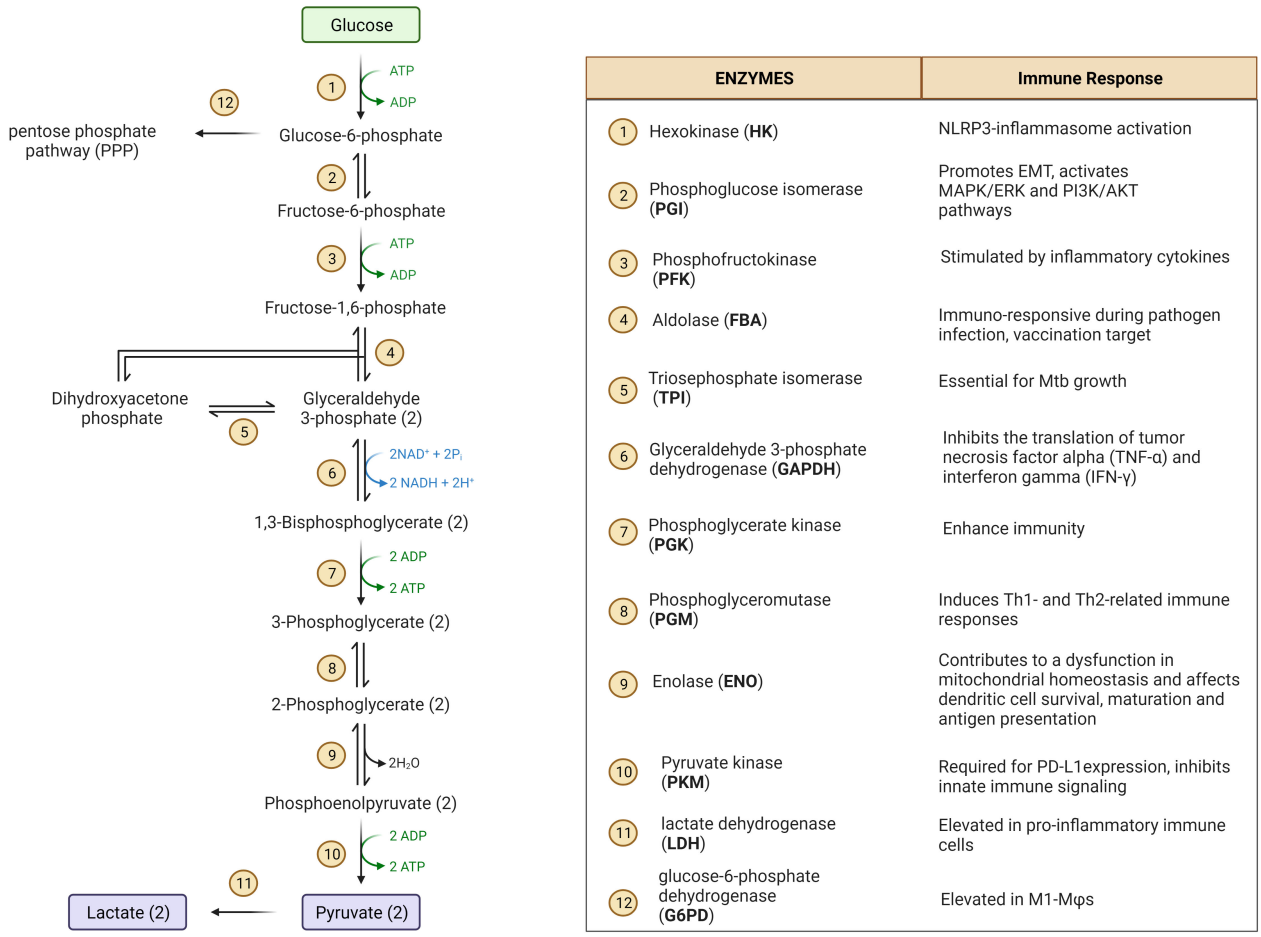

FIGURE 1
A diagram of glycolysis and glycolic enzymes involved in the regulation of immune responses.

steps of glycolysis, lactate dehydrogenase (LDH) is elevated in pro-inflammatory immune cells to produce surplus lactate. Another glycolysis-related enzyme is glucose-6-phosphate dehydrogenase (G6PD) which acts at the first and the rate-limiting step of the pentose phosphate pathway (PPP). G6PD level is elevated in M1-MΦs and cells deficient in G6PD have a reduced ability to induce the innate immune response, thereby increasing host susceptibility to infection with pathogens (39). In addition to glycolytic enzymes, the glycolytic intermediates also play a significant role in the activation of the immune system. Pyruvate is reduced by LDH to form lactate that regulates immune response in macrophages and dendritic cells (40). Importantly, phosphoenolpyruvate (PEP), the precursor of pyruvate, is an immune signaling molecule; it promotes pro-inflammatory functions and activates T cells by regulating Ca^{2+}-transportation and translocation of nuclear factor of activated T cells (NFAT) (41). Other metabolic enzymes and their products associated with glucose and immunometabolism have been reviewed elsewhere. These pathways include PPP (42), TCA cycle (43, 44), serine biosynthesis and one-carbon metabolism (45, 46), glutamine metabolism (47), and arginine metabolism (48).

Glucose metabolism, reactive oxygen (ROS) and reactive nitrogen species (RNS) production in macrophages, and their action on bactericidal function

Reduction-oxidation (redox) reactions occur in various metabolic processes including glycolysis, TCA cycle, but predominantly in the electron-transport chain (ETC) of mitochondria, which is essential for the generation of energy (ATP) for living cells. Oxidants, typically reactive oxygen species (ROS), are produced as the byproducts of redox reactions in ETC (49, 50). The major cellular redox reactions are conversions between NAD^+ and NADH, $NADP^+$ and NADPH, and FAD and FADH2. NAD^+ is reduced/converted into NADH during glycolysis (two molecules) and in TCA cycle (three molecules) (51). NADH is re-oxidized to NAD^+ by either lactate dehydrogenation (LDH) which catalyze the conversion of pyruvate into lactate, or by the ETC complex I through which, one proton and two electrons are released and ROS (O_2^-) is formed when the electrons are added to O_2 (51, 52). Paralleling the glycolysis

initiating at glucose-6-phosphate, the pentose-phosphate-pathway (PPP) generates NADPH (from $NADP^+$) from pentose as well as ribose 5-phosphate, a precursor for the synthesis of nucleotides. Similar to NAD^+/NADH, NADPH is oxidized by NADPH oxidase (NOX) to be converted back to $NADP^+$ and ROS is formed when the released electrons are added to O_2 (53). NOX is a membrane-bound flavocytochrome, containing two molecules of heme and one molecule of flavin adenine dinucleotide (FAD) with a spectroscopic absorbance^{max} of 558 nm. For this reason, NOX is also referred to as flavocytochrome b558 which contains $p22^{phox}$ (α-subunit, the production of the CYBA gene) and $NOX2/gp91^{phox}$ (β-subunit, CYBB gene) (54). NOX is found in functional phagocytes including neutrophils, eosinophils, monocytes, dendritic cells, and macrophages (55). The third pair of redox reaction is FAD and FADH2, which are bound to succinate dehydrogenase complex (SDH). The substrate of SDH is succinate, an intermediate of TCA cycle, which is synthesized directly from succinyl-CoA. Succinate synthesis is enhanced in M1-MΦs due to the inhibition of TCA cycle (9). In addition, succinate can also be synthesized *via* glutamine-dependent anaplerosis or the γ-aminobutyric acid (GABA) shunt, which promotes and maintains polarization of M1-MΦs (56). SDH is a part of ETC Complex II, and mediates oxidation of succinate into fumarate. This reaction is coupled with the reduction of ubiquinone (UQ) to ubiquinol (UQH2) coupling with the oxidation of FADH2 to FAD. When high amounts of succinate are oxidized to fumarate under low oxidative phosphorylation conditions, electron flux moves in the opposite direction of ETC, from complex II toward complex I, leading to reverse electron transport (RET) and generating ROS (9, 57, 58) (Figure 2). The production of mitochondrial ROS is also mediated by immunoresponsive gene 1 (IRG1), which utilizes β-oxidation of fatty acids to generate ROS and improved activity of ETC increases ROS production in phagosomes thereby augmenting bactericidal activity (59). On the other hand, IRG1 is also called Aconitate Decarboxylase 1 (ACOD1), an important enzyme in the

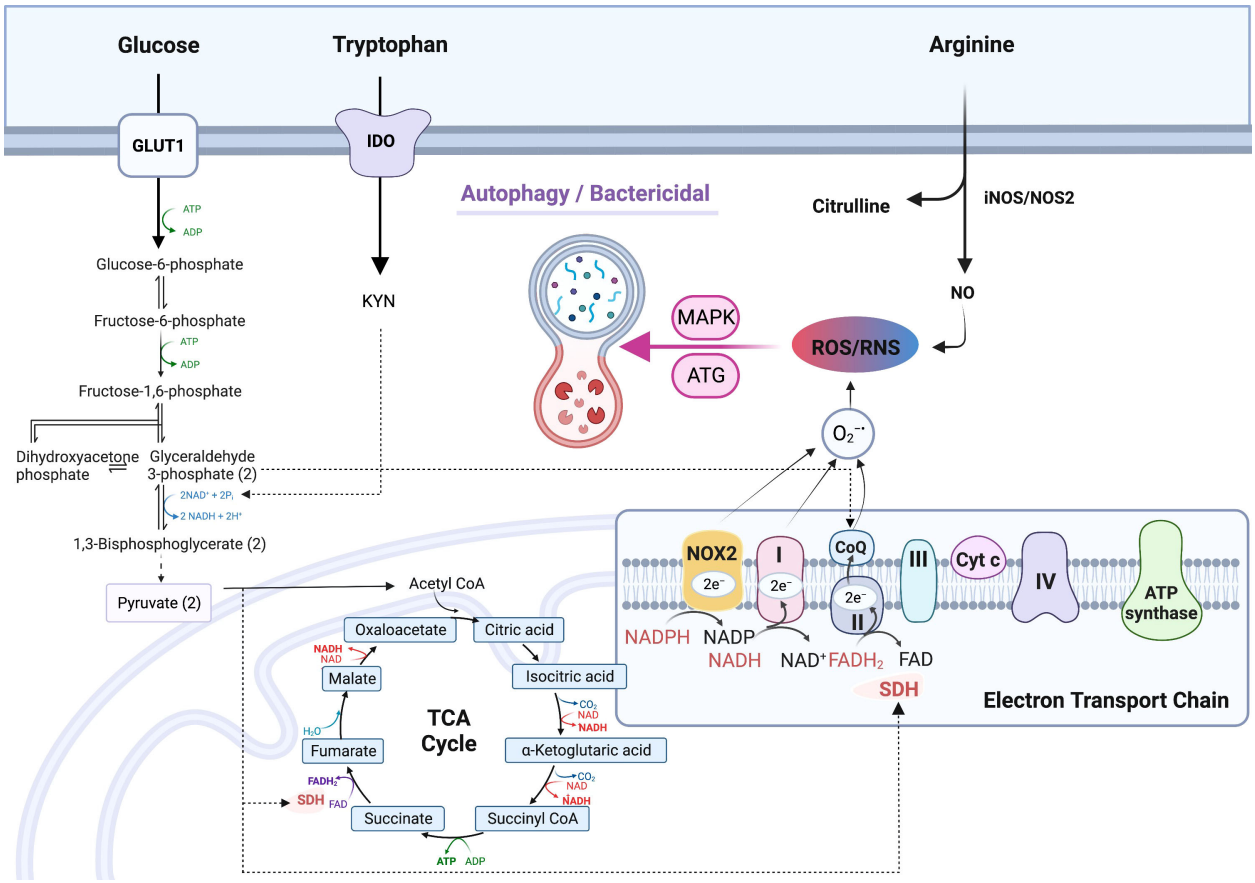

FIGURE 2
Up-regulated production of reactive oxygen species (ROS) and reactive nitrogen species (RNS) in M1- macrophages. Increased production of NADH from reduction of NAD^+ *via* glycolysis fuels the electron transport chain (ETC) complex 1 to generate $O_2^{\cdot-}$; NAD^+ is continuously replenished by upregulated NAD^+ *de novo* synthesis from tryptophan metabolism. Increased production of NADPH *via* the pentose-phosphate-pathway (PPP), which is also up-regulated in M1- type macrophages (MΦs), fuels the ETC to produce $O_2^{\cdot-}$. $O_2^{\cdot-}$ is also generated *via* succinate dehydrogenase (SDH) which is coupled with FADH2/FAD redox reaction in complex II of ETC. In M1-MΦs, RNS is derived from nitric oxide (NO) which is produced by arginine metabolism through iNOS/NOS2. Mitochondrial ROS/RNS regulates phagocytosis, bacterial killing, and polarization towards M1-MΦs *via* ATG and MAPK activation. *Additional symbols:* 1,3-BPG, 1,3-bisphosphoglyceric acid; α-KG, alpha-ketoglutarate; ATG, Autophagy regulating gene; CIT, citrate; DHAP, dihydroxyacetone phosphate; F-1, 6-P, Fructose-1, 6-biphosphate; F-6-P, Fructose-6-phosphate; FUM, fumarate; G-3-P, glycerol-3-phosphate; G-6-P, glucose-6-phosphate; GABA, γ-aminobutyrate; GA, glutaminase; GABA-T, GABA transferase; GAD, glutamate decarboxylase; GDH, Glutamate dehydrogenase; Gln, glutamine; Glu, glutamate; GLUT1, glucose transporter protein type 1; iCIT, isocitrate; IDO, Indoleamine-pyrrole 2,3-dioxygenase; Kyn, kynurenine; Lac, lactate; MAL, malate; OAA, oxaloacetic acid Pyr, pyruvate; SSA, succinate semialdehyde; SSADH, succinate semialdehyde dehydrogenase; SUC-CoA, succinyl-CoA; SUC, succinate.

TCA cycle, which converts aconitate to itaconic acid that has a canonical antibacterial role through isocitrate lyase inhibition (60, 61). IRG1 is specifically up-regulated in LPS induced pro-inflammatory murine M1-MΦs (62, 63). ROS are essential for macrophages to fight against invasive pathogens through the M1-MΦ-dependent innate immune defense system, but they also play a critical role in signal transduction, differentiation, and gene expression (64, 65). In addition to ROS, cells generate oxidants through reactive nitrogen species (RNS). RNS are produced from the reaction of nitric oxide (•NO) with superoxide ($O_2^{\bullet-}$) to form highly reactive peroxynitrite ($ONOO^-$) (66) (Figure 2). NO is synthesized from arginine by NO synthase (NOS2/iNOS) (67, 68). Macrophages produce both ROS and RNS in response to phagocytosis and are required for killing of pathogens (69). The antimicrobial function of macrophages mainly depends on NOS2 and NOX2 genes which are upregulated in both murine and human M1-MΦs to generate abundant ROS and RNS (70–74). Therefore, M1-MΦs exhibit a high bactericidal function to defend against many intracellular pathogens including MTB (75). It has been noted that M1-MΦs have lower acidification rate and reduced proton pumping activity and thereby increased proton moving force compared to M2-MΦs; this facilitates M1-MΦs to generate ROS and efficiently control pathogens (76). Interestingly, NO also enhances the accumulation of itaconic acid in inflammatory cells increasing anti-bacterial activity (77); consequently, gene disruption of IRG1 reduces itaconic acid increasing the susceptibility to MTB infection and lung immunopathology (78). Paradoxically, for some pathogens, excess ROS can hijack host immune system and become favorable to pathogen survival (79). The mechanisms of ROS dependent hijack are not clear but inhibition of ETC complex I and regulation of TCA intermediates by NO may provide a plausible explanation (77, 80).

Metabolic profiles of mouse and human M1- versus M2-MΦs during tuberculosis infection

Metabolic gene expression profiling has revealed a biphasic metabolic behavior of MTB infection using an animal model (81). In the early phase post infection (up to 8 hr), the innate immune system is activated to generate proinflammatory cytokines including interleukin-1β (IL-1β), IL-6, IL-12, and TNF-α, predominantly in the M1-MΦs. In this early phase, glucose uptake aided by upregulated GLUT1 is accelerated and the genes of glycolysis are activated to increase the production of ATP and glycolytic intermediates and increase the consumption of NAD^+. Concurrently, oxidative metabolism is down regulated indicated by a decrease in key enzymes of the TCA cycle and mitochondrial ETC complexes in mice exposed to MTB (82–84). However, as the infection progresses to 24 and 48 hr, post-infection, the M1- metabolic state of macrophages is reversed and an increase in TCA cycle and oxidative phosphorylation with dampened glycolysis are observed suggesting a switch towards M2-MΦs (9, 81, 85). These data are consistent with increased glycolysis and reduced TCA proteins in human M1-MΦs and switch towards M2-MΦs observed using proteomics analysis in our lab (86). Whereas most proteins of the ETC complexes II-IV were down-regulated, majority of proteins in complex I were up-regulated in human M1-MΦs (86).

Although many metabolic profiling studies have been done using mouse macrophages, recent studies are focusing on human macrophages (86–92). For example, mice are more susceptible to tuberculosis whereas nearly 90% of humans exposed to tuberculosis develop latent infection indicating a better control by their macrophages. In this direction, Gleeson, et al. identified that lactate derived from glycolysis-generated pyruvate, is increased in M1-MΦs when activity of TCA cycle is down-regulated, suggesting it as a key player during metabolic remodeling in MTB-infected human macrophages (93). Treatment of resting human macrophages with exogenous lactate caused a decrease in extracellular acidification rate while an increase of oxygen consumption rate (analogous to oxidative phosphorylation), resulted in an increased capacity to kill MTB possibly through autophagy (94). The same study also found that tuberculosis antimicrobial drugs, such as clofazimine, reshaped the immunometabolic profiles of MTB infected human macrophages towards oxidative phosphorylation similar to the effects of lactate (95).

On the other hand, Cumming, et al. found that in MTB-infected human monocyte-derived macrophages (nondifferentiated/resting state) both glycolysis and oxidative phosphorylation were suppressed leading to a state of metabolic quiescence resulting in a decrease of ATP production in mitochondria and a switch from dependency on glucose to fatty acids (88). This study suggested that MTB promoted polarization of macrophages towards M2-MΦs. We suggest that this discrepancy could arise when the starting monocyte-macrophage populations are different. Nonetheless, there seems to be a consensus that MTB infected human macrophages undergo a transition from M1-MΦs during early phase of infection to M2-MΦs during late phase similar to the mouse data (81).

Interestingly, pharmaceutical modulation with histone deacetylase inhibitor, suberanilohydroxamic acid (SAHA) promoted the glycolysis rate of human macrophages with increased production of pro-inflammatory cytokine IL-1β (a marker of M1-MΦs) and decreased production of anti-inflammatory cytokine IL-10 (a marker of M2-MΦs) during the early stage of MTB infection associated with enhanced T helper cell responses *ex vivo* (87). In this direction, we recently reported RNA-seq based transcriptomic data supporting metabolic profiling; genes of glycolysis, TCA cycle, and ETC complexes were all up-regulated that MTB infected in M1-MΦs at 24 hr post infection (6). We further demonstrated that human M1-MΦs expressed unique innate immune response genes to defend against tuberculosis through increased production of NO, accelerated autophagy- dependent killing of MTB and increased antigen presentation to T cells through an *ATG-RAB7*-cathepsin pathway (6). Taken together, these data indicate that MTB infection promotes naïve macrophage polarization progressively from M1-MΦ to M2-MΦ phenotype. The biphasic metabolic switch observed using *ex-vivo* MTB-infected human macrophages is similar to that of mouse macrophages infected with MTB. However, mice still develop progressive tuberculosis after aerosol infection with MTB unlike humans suggesting that differences in metabolic regulation of M1-*vs.* M2-MΦs may exist. For example, we found that sirtuins were differentially expressed by MTB infected M1 and M2-MΦs unlike similarly infected in mouse MΦs (96). The metabolic basis for the

differences in the antimicrobial function of M1 *vs.* M2-MΦs is discussed below.

Glucose has a profound impact on immunometabolism and autophagy in human MΦs

Glucose metabolism and glycolysis are key players in inflammatory response (10). In mouse M1-MΦs exposed to pathogens, both glycolysis and GLUT1 expression are upregulated in the early phase of infection to facilitate rapid glucose uptake and consumption, resulting in eventual depletion of glucose, increased acidification of the microenvironment, both of which can be detrimental to proliferating pathogens (8, 9, 97). In addition to ROS/RNS discussed above, another bactericidal mechanism of macrophages is autophagy which is regulated by nutritional and metabolic states (98). Autophagy is generally induced by decreased availability of glucose or other nutrients such as amino acids (Figure 3A). In contrast, it can be stimulated by metabolites such as fatty acids and ammonia. Under nutrition-restricted conditions, glucose, acetyl-CoA, and amino acids are depleted, and NAD^+

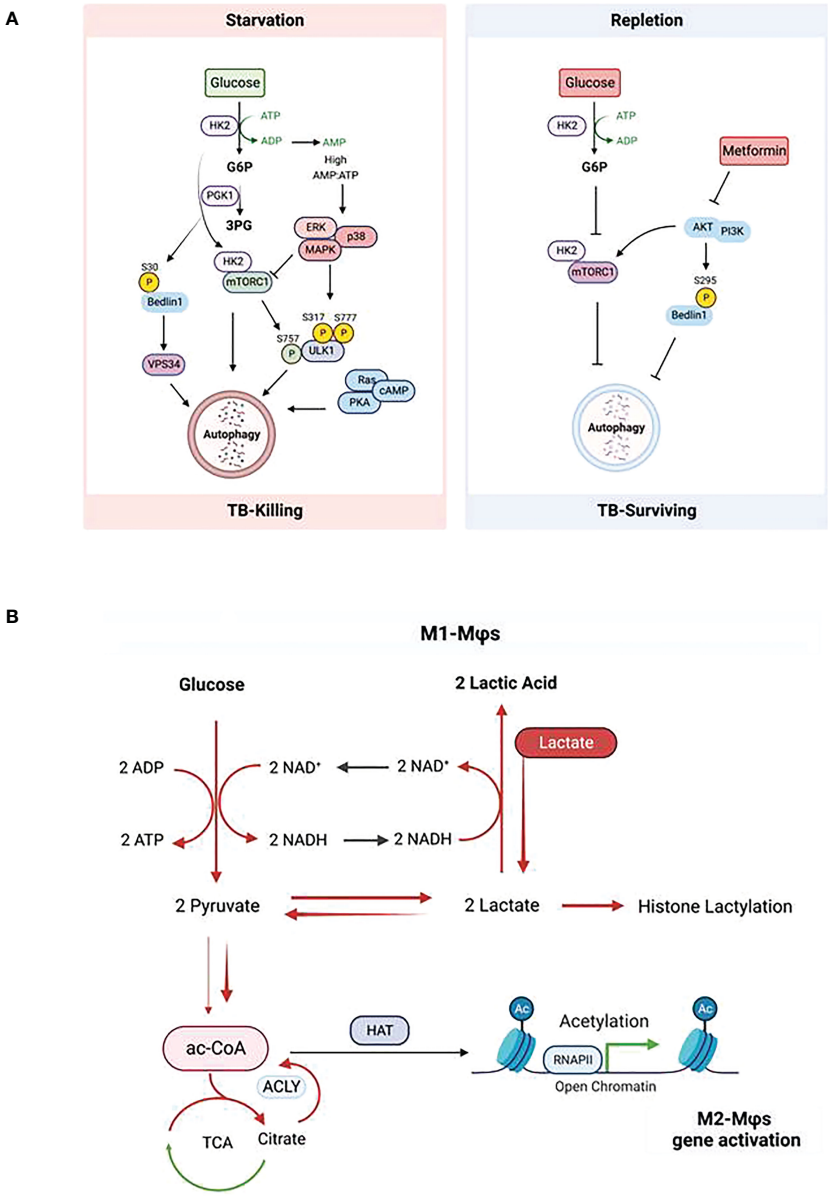

FIGURE 3
Impact of glucose metabolism on autophagy in macrophages during tuberculosis. **(A)** Regulation of autophagy by glucose homeostasis (*Left*: glucose starvation; *Right*: glucose repletion) dependent metabolic sensor kinases. Description of the scheme is referred to the text. **(B)** Glycolysis-promoted histone lactylation and acetylation during macrophage polarization. Upregulation of glycolysis in M1-Mφs increases lactate production from pyruvate; however, excess of lactate provided exogenously pushes the equilibrium of the conversion between pyruvate and lactate further to the synthesis of citrate from pyruvate and the former is broken up to acetyl -CoA by ACLY; this results in the elevation of both global histone acetylation and acetylation of chromatins associated with the promoters of genes which promote polarization towards M2-Mφs.

accumulates leading to an increase in the NAD^+/NADH ratio (51) which in turn, regulates autophagy (99, 100). Several metabolic-sensor kinases also regulate this process (Figure 3A).

The target of rapamycin complex 1 (mTORC1) of the mTOR complex is a positive regulator of glycolysis and is activated in M1-MΦs. Whereas mTORC1 inhibits autophagy, inhibition of mTORC2 activates the process. Roberts et al. demonstrated that during glucose-limiting conditions, HK2 binds and inhibits mTORC1 thereby activating autophagy, whereas in glucose-repletion condition, glucose-6-phosphate (G6P) inhibits the binding of HK2 to mTORC1 to suppress autophagy (101, 102). Therefore, HK2 and G6P are pharmaceutical targets to induce autophagy in glucose-rich condition. Indeed, Metformin, a biguanide antidiabetic drug, lowers G6P in hepatocytes by activation of glucose phosphorylation, which is downstream of glycolysis and triggers autophagy (103, 104). This means that during early phase of infection of macrophages, high glucose intake produces excess ATP that activates ROS-dependent oxidative stress response and thereby up-regulated pro-inflammatory cytokines but this process also reduces autophagy without pharmacological intervention (102, 105). However, during the later phase of infection of macrophages, glucose and other nutrients are depleted, resulting in activation of autophagy and ROS level.

The second class of kinases is the AMP-activated kinases (AMPKs) which activate autophagy. Under glucose starvation, AMPK promotes autophagy by directly activating ULK1 through phosphorylation of Ser317 and Ser777 (106, 107), which can be prevented by mTORC1 that phosphorylates Ulk1 at Ser757 (106, 107). Glycolysis provides most of ATP in M1-MΦs which is hydrolyzed into ADP and further into AMP, generating energy needed by cells. During glucose starvation, the AMP/ATP ratio increases leading to the activation of AMPK (108). Activation of AMPK inhibits mTOR resulting in an increase of autophagy (109, 110). Seemingly redundant to mTORC1, the RAS/cAMP-dependent protein kinase A (PKA) signaling pathway also regulates the induction of autophagy in yeast and mammals (111, 112). In addition to mTORC1 and PKA, Akt in the PI3K/Akt signaling pathway also regulates autophagy. Akt inhibits autophagy through phosphorylating the C-terminal Ser279 of Beclin-1 in the core autophagy machinery independent of mTORC1 (113, 114). Interestingly, during glutamine deprivation or hypoxia, a glycolytic enzyme – phosphoglycerate (PGK1), also directly phosphorylates the N-terminal Ser30 of Beclin-1 leading to enhanced VPS34 activity and subsequent autophagy (115). Of note, phosphorylation of Beclin-1 at N-terminus or C-terminus has different effects on autophagy; phosphorylation at the N-terminus enhances autophagy while at the C-terminus inhibits. Akt is a major mediator of insulin signaling and has been reported to be involved in mediating obesity and type 2 diabetes-related inflammatory disease (116). Metformin inhibits Akt activating autophagy, which is consistent with its activation of autophagy by lowering G6P as a result of inhibition of glucose flux and glycolysis (117). Deletion of Akt promotes macrophage polarization towards to M1-MΦs and increased NO synthesis from arginine (118, 119). These observations suggest that, besides its antidiabetic effect, metformin can significantly reduce the risk of TB in patients with diabetes mellitus (120). Contradictory findings on the relationship between glucose metabolism and autophagy have been also revealed. Collins and coworkers reported that loss of mTORC1 in macrophages enhanced pro-inflammatory functions which are normally related to M1-MΦs with upregulated glycolysis and activation of mTORC1 (121). These results were evaluated using rapamycin to polarize mouse and human macrophage models (122). The discrepancy can be explained by the differential localization of mTOR in lysosomes under M1- and M2-conditions (119). Mechanistically, it is known that, under starvation of glucose, a p38 MAPK-dependent pathway can trigger autophagy independent of the AMPK-mTOR pathway (123). We illustrate a diagram of Mtb-killing or survival during autophagy or nitric oxide (NO) through metabolite-sensing kinases corresponding to glucose homeostasis (Figure 3A).

During MTB infection of macrophages, glucose metabolism plays a significant role centered around autophagy. Glucose is a major metabolic source producing ac-CoA through glycolysis and SAM through serine biosynthesis and one-carbon metabolism. Ac-CoA and SAM are the necessary cofactors of histone acetyltransferases and methyltransferases (including DNA methyltransferases); further, glycolysis consumes NAD^+ that is an essential cofactor of histone deacetylases. It is evident that glucose metabolism controls the level of cofactors and thereby, the epigenetic regulation through histone acetylation and methylation (and DNA methylation) which is further reviewed below. IFN-γ which drives M1-MΦs promotes a metabolic switch from oxidative phosphorylation to glycolysis, a process similar to the Warburg effect of hypoxia in cancer cells. Increased glycolysis causes the production and enrichment of copious lactate. Interestingly, Zhang et al. identified that histones can be modified by lactylation, and increased lactate promoted histone lactylation and polarization towards M2-MΦs (124). These data suggest that M1-MΦs can self-differentiate into M2-MΦs after prolonged glycolysis culminating in excess lactate. Noe et al. also show that glucose is still required for M2-MΦ polarization; under glucose starvation, exogenously added lactate matching the measured concentration of lactate produced by IL-4 primed M2-MΦs rescued the loss of lactate endogenously produced from glucose metabolism. This process enriched citrate from pyruvate by the half-blocked TCA cycle, and subsequently increased ac-CoA after ACLY cleavage resulting in global histone acetylation and M2 gene promoter-specific acetylation (Figure 3B) (125). Together, these observations indicate that lactate is a driver of M2 polarization from either M0- or M1-MΦs. Interestingly, the lactate-treated M2-MΦs had increased capacity to kill MTB possibly through autophagy (94). However, it remains unclear how histone lactylation is regulated and whether it causes histone acetylation to promote autophagy during TB.

Acetyl-CoA production from glycolysis is regulated by protein acetylation and sirtuins

Proteins acetylation dictates how cells choose glycolytic versus oxidative metabolism as a function of energy availability and then determine storage or utilization of carbon source (126, 127). Being a fundamental building block for fatty acid synthesis, ac-CoA is a necessary co-substrate of protein acetyltransferases to provide acetyl groups for acetylation of proteins, mostly on the ϵ-amino group of

lysine, but also on the hydroxyl groups of serine, threonine, and tyrosine specifically among bacteria (128). Though it can be formed by fatty acid β-oxidation, amino acid catabolism, and break-up of citrate, ac-CoA is mainly produced by glycolysis (129, 130). Many enzymes in glycolysis, TCA cycle and proteins in mitochondria are the substrates of histone acetyltransferases whose acetylation sites have been identified by proteomics; nearly two-thirds of glycolic and TCA cycle enzymes show acetylation sites (14). Acetylation promotes or inhibits the activities of these enzymes, thereby increasing or decreasing the production of metabolites (129, 131). For instance, the enzymatic activity of phosphoglycerate mutase-1 (PGAM1), a protein critical for glycolysis, is regulated by glucose availability and SIRT1-dependent reversible deacetylation (15). When glucose is available, acetylation of PGAM1 stimulates catalysis. When glucose is restricted, SIRT1 levels increase, leading to deacetylation of PGAM1 and decrease in its enzymatic activity (15). Another positive correlation between acetylation and enzymatic activity is SIRT2 expression during iPSC reprogramming when OCT4 induces miR-200c-5p to suppress the expression of SIRT2 *via* microRNA binding sites in its coding sequence. As a result of downregulation of SIRT2, the activities of glycolytic enzymes (ALDOA, GAPDH, PGK1, ENO1 and PKM1/2) are increased due to elevated acetylation levels of these proteins (132). In contrast, acetylation of some glycolic enzymes can reduce their activity. It was reported that PKM2, a pyruvate kinase which is involved in the last step of glycolysis to produce pyruvate and ac-CoA, is acetylated at K305 by p300/(CREB binding protein) associated factor (PCAF) resulting in a decrease of its enzymatic activity (133). Moreover, acetylation of PKM2 enhanced its interaction with HSC70 and promoted its lysosome-dependent degradation *via* chaperone mediated autophagy under high glucose intake (133). Deacetylation at K305 by SIRT2 inhibits the pyruvate kinase of PKM2 by promoting its tetramerization (134), whereas deacetylation at K433 by SIRT6 inhibited the pyruvate kinase of PKM2 by suppressing its nuclear localization (135). The decrease of both enzymatic activity and protein level resulted in the accumulation of glycolytic metabolites upstream of PKM2, including FBP (fructose-1, 6-bisphophate) and G6P (glucose-6-phosphate). FBP was then found to couple with glycolytic flux to activate Ras and its downstream targets MEK and ERK driving autophagy (136); in contrast, G6P inhibited autophagy during glucose depletion (101, 102, 137). Interestingly, desuccinylation at K311 by SIRT5 counters acetylation at K355 and K433 to activate the pyruvate kinase of PKM2 by promoting its tetramer-to-dimer transition and nuclear localization, thereby blocking macrophage IL-1β production and preventing dextran sulfate sodium (DSS)-induced colitis in mice (138). These observations suggest that glucose metabolism and ac-CoA production are regulated by the acetylation states of glycolytic enzymes and sirtuin proteins play a major regulatory role.

Histone acetylation is responsive to metabolite levels and regulates autophagy

Acetylation of histones is a critical epigenetic modification that changes chromatin architecture and regulates gene expression. Many studies show that metabolism regulates acetylation, and, the changes in glucose metabolism can regulate histone acetylation (12, 13, 139). Using multiplexed stable isotopic labeling by amino acids in cell culture (SILAC)-based proteomics, Locasale's lab found that the acetylation levels of half of identified histone acetylation sites and lysine acylation modifications at these sites were modulated by the rate of glycolysis and that histone acetylation levels were strongly correlated with ac-CoA levels and inversely associated with the ratio of ac-CoA to free CoA (11). However, glycolysis-generated, ac-CoA-dependent histone acetylation was competitively regulated by citrate-generated ac-CoA by ATP-citrate lyase (ACLY) (140–142). Moreover, the production of ac-CoA seems to be counter-balanced by utilization of ac-CoA to form lactate from pyruvate *via* LDH, reaction with OAA to form citrate entering the TCA cycle, acetylation of amino acids, and synthesis of fatty acids and other molecules in various metabolic pathways. Therefore, histone acetylation regulates metabolism and macrophage activation, whereas acetylation is fine-tuned by metabolism in polarized macrophages (143, 144). LPS/IFN-γ promotes polarization towards M1-MΦs characterized by up-regulated glycolysis and production of pro-inflammatory cytokines, such as IL-1β whose expression is enhanced by histone acetylation (145). The acetylation was thought to be due to the increased production of ac-CoA from elevated glucose metabolism and upregulated ACLY that reciprocally up-regulates glycolytic gene expression (146, 147). Higher levels of histone acetyltransferase MOF expression and acetylation at histone H4K16 were detected in inflammatory macrophages at the wound sites of diet-induced-obese mice compared to the anti-inflammatory macrophages in the healing phase (148). In addition, ACLY-mediated citrate metabolism in the TCA cycle contributes to the production of ROS and RNS in inflammatory cells (149). In contrast, Noe and co-workers reported that ACLY activation also promoted naive M0 to M2 polarization through the lactate-citrate-ac-CoA route for histone acetylation in tumor microenvironments (TME) (125). It remains unclear whether data from animal studies can be translated to humans although, some studies do reveal a positive correlation. For example, Vlad et al. found that histone acetylation, the expression of histone acetyltransferases p300, and the expression of NADPH oxidase-5 (Nox5) were all elevated in human atherosclerotic specimens. They were co-localized in the area of $CD45^+/CD68^+$ immune cells and lipid-rich deposits within atherosclerotic plaques (150); in these microenvironments, increased glucose intake and enhanced glycolysis were proposed (151). Consistently, ACLY was activated in inflammatory macrophages and human atherosclerotic plaques (152). In contrast, inhibition or silencing of Slc25a1, a transporter of citrate, resulted in decreased production of NO, ROS, and PGE_2 in U937 cells (153) and inhibition of ACLY had the same effects (154). However, the role of ACLY in macrophage polarization was challenged by Namgaladze et al. who found that silencing ACLY expression using CRISPR/Cas9 in human THP-1 cells did not attenuate IL-4 induced gene expression as ACLY inhibitors did and concluded that ACLY might not be the major regulator of nucleocytoplasmic ac-CoA contributing to IL-4-induced M2-MΦ polarization of human macrophages (155). Erika Palmier and coworkers performed ^{13}C tracing experiments using [U-^{13}C]-glucose and glutamine and found that NO inhibited mitochondrial aconitase (ACO2) resulting in blockade of TCA, and that inflammatory macrophages rerouted pyruvate away from pyruvate

dehydrogenase (PDH) in an NO-dependent but hypoxia-inducible factor 1α (HIF1α)-independent manner. This process promoted glutamine-based anaplerosis which sustained the TCA cycle using the glutamine generated αKG and OAA from pyruvate carboxylation (80). This suggested that ac-CoA generated from glycolysis would be reduced resulting in decreased histone acetylation in M1-MΦs due to NO-mediated inhibition of PDH. This is an intriguing cross regulation by NO in M1-MΦs that needs additional investigation. Besides production of ac-CoA from metabolism, histone acetyltransferases themselves also determine the acetylation level of histones and expression of autophagy genes. Fullgrabe et al. demonstrated that induction of autophagy by starvation or rapamycin inhibition of mTOX was coupled to reduction of histone H4 lysine 16 acetylation (H4K16ac) through downregulation of the histone acetyltransferase hMOF/KAT8/MYST1 in both mouse embryonic fibroblasts (MEF) and human transfected cells (156). However, downregulation of histone acetylation and hMOF also led to a transcriptional repression of autophagy genes based on a feedback mechanism, preventing chronic autophagy that could lead to cell apoptosis (156).

Sirtuins and NAD^+ regulate protein/histone deacetylation and autophagy-mediated killing of bacteria

Sirtuins and antimicrobial mechanisms

Sirtuins, the class III histone deacetylases (HDAC), are crucial regulators of inflammation and immune cell metabolism and function (157–159). Metabolism is controlled not only by histone acetylation but also deacetylation. Activities of sirtuins are dependent of NAD^+, NADH, or their ratio as NAD^+ is their essential co-substrate (160). There are seven currently known sirtuins (SIRT1-7). Each sirtuin isoform is located at a specific compartment of the cell and has its specific preferred substrate. SIRT1, SIRT6, and SIRT7 are predominantly located in the cell nucleus (161). SIRT1 also exists in cytosol and is a master metabolic regulator and the most studied sirtuin protein so far; it is downregulated in cells with high insulin resistance and its overexpression increases insulin sensitivity (162–164). High concentration of glucose significantly downregulates SIRT1 expression at both mRNA and protein levels, which is related to upregulation of pro-inflammatory cytokines, IL-1β and TNF-α in RAW264.7 macrophages (165). On the other hand, SIRT1 is up-regulated under calorie-restrict conditions known to extend life-span (166, 167). SIRT1 also stimulates autophagy by deacetylating autophagy-related proteins (*ATG*) including *ATG5, ATG7*, and *LC3* which are required for autophagy in cultured cells, embryonic and neonatal tissues (168, 169). SIRT1-dependent mechanism of autophagy induction is not clear; it may stabilize *ATG* proteins by forming a complex with them to prevent from degradation or prevent deacetylation at the promoters of *ATG5* and *ATG7* genes by other sirtuins due to its usage of NAD^+ thereby activating expression of *ATG5* and *ATG7* (170). SIRT1 can also promote autophagy by activating AMPK to improve mitochondrial function (171), inhibiting the mTORC1 signaling pathway (172), and enhancing transcriptional activities of FOXO1 and FOXO3 through their deacetylation (169). Cheng and co-workers reported that MTB infection down-regulated SIRT1 in animal models and patients with active TB. Activation of SIRT1 by its activators, such as Resveratrol, not only induced autophagy but also dampened MTB-mediated chronic inflammation *via* deacetylation of RelA/p65 and impaired binding of RelA to the promoter of inflammatory genes (173). Similar results were obtained by others using mouse models (174). Another mechanism of the anti-TB property of SIRT1 was revealed by Yang, et al. who found that activation of SIRT1 prevented cell death in MTB-infected macrophages through BAX and GSK-3β (175, 176). In addition, SIRT1 activators also enhanced anti-TB drug efficacy (173). Interestingly, SIRT1 inhibition by sirtinol has also been reported to induce autophagy and autophagic cell death in MCF-7 cells (177). The mechanism is not known. Off target effects on NAD^+ biosynthesis and/or salvage pathways is possible, since an enhanced activation of these pathways increases autophagy (178). SIRT6 is essentially a deacetylase of histones H3 and H4, which changes chromatin density and regulates gene expression and is required for normal base excision repair and double-strand break repair of DNA damage in mammalian cells (179). SIRT6, together with histone H3K9 methyltransferase G9a, participate in inflammatory response in macrophages, contribute to the IFN-sterol antiviral activity, and play an active role in inflammation-mediated glucose intolerance during obesity (180, 181). SIRT6 seems to facilitate MTB survival in macrophages by epigenetically modulating host cholesterol accumulation (182). SIRT7 was originally found to facilitate the transcription of DNA by DNA polymerase I, DNA polymerase II, and DNA polymerase III (183, 184). It has recently been found as a nutrient sensor similar to SIRT1 during glucose starvation or calorie-restricted diet and its depletion causes impaired activation of autophagy (185). The effects of SIRT7 on tuberculosis remain unclear.

SIRT2 is mainly cytoplasmic and also exists in nuclei where it can deacetylate histones. SIRT2 suppresses T cell metabolism by targeting key enzymes involved in glycolysis, TCA cycle, fatty acid oxidation, and glutaminolysis. SIRT2-deficient murine T cells and SIRT2 blockaded human tumor-infiltrating lymphocytes showed increased glycolysis and oxidative phosphorylation, enhanced proliferation and effector functions and thereby superior antitumor activity (186). SIRT2 dysregulated autophagy in high-fat-exposed mouse immune-tolerant and hypo-inflammatory macrophages (187). We found that the expression of SIRT2 was higher in MTB-infected human peripheral blood derived M2-MΦs which had lower autophagy activity than M1-MΦs infected with MTB (6). Pharmaceutical inhibition of SIRT2 increased autophagy and killing of MTB by M2-MΦs; morover, SIRT2 blockade combined with anti-TB drug dramatically increased MTB clearance in macrophages (6) (our unpublished data). Although Cardoso, et al. claimed that SIRT2 blockade only had a transient effect on MTB infection of mice (188), it is likely that human and mouse macrophages differ in sirtuin dependent regulation.

SIRT3, SIRT4, and SIRT5 are all found in the mitochondrial compartment and therefore implicated in regulating metabolic processes by deacetylating mitochondrial proteins. SIRT3 showed anti-inflammation property and mitigated endotoxin-induced acute lung injury (189). In MTB-infected macrophages, SIRT3 is down-

regulated resulting in reduced expression of SIRT3-target genes including IDH2 and ETC complex I subunits and consequent accumulation of isocitrate, reduction of ETC complex I and II activity, lower GSH/GSSG ratio, and increase mtROS, promoting cell death (190). Paradoxically, activation of SIRT3 is necessary for autophagy and can provide protection for mitochondria in MTB-infected macrophages (191). However, anti-TB activity of SIRT3 is dependent on its genetic variants; for example, the minor allele genotype (A carriers) of rs3782118 shows a decreased risk of TB susceptibility, whereas the haptotype AGAAG (containing the major allete G of rs3782118) is associated with an increased risk of TB (192). SIRT4 is a mitochondrial ADP-ribosyltransferase that inhibits mitochondrial glutamate dehydrogenase 1 (GLUD1) activity, thereby downregulating insulin secretion in response to amino acids (193). SIRT4 shows opposite activity of SIRT1 and SIRT3 (194) and it counters SIRT1 and SIRT3 activity by suppressing their expression by rebalancing glycolysis and glucose oxidation during recovery of acute inflammatory response in monocytes (195).

SIRT5 exhibits multiple enzymatic activities, as it is a deacetylase, desuccinylase, and demalonylase, and capable of removing acetyl, succinyl, and malonyl groups from the lysine residues of proteins (196, 197). SIRT5 has dual functions of increasing ammonia production *via* promoting glutaminolysis and removing it by activating urea cycle. SIRT5 deacetylates and regulates carbamoyl phosphate synthetase (CPS1), the rate-limiting and initiating step of the urea cycle in liver mitochondria and therefore plays a critical role in ammonia detoxification (14, 197). On the other hand, SIRT5 stabilizes glutaminase (GLS) by desuccinylation, the enzyme transforming glutamine into glutamate generating ammonia (198). As ammonia is a diffusible regulator of autophagy (199), the regulation of autophagy by SIRT5 may be dependent on net ammonia concentration produced and consumed from glutaminolysis and urea cycle. Indeed, Polletta et al. demonstrated that in human breast cancer MDA-MB-231 and mouse myoblast C2C12 cell lines, ammonia production was increased when SIRT5 was silenced and decreased in SIRT5-overexpression cells (200). Morover, when GLS was activated by SIRT5, production of ammonia was increased and consequently autophagy activity was increased, whereas inhibition of SIRT5 decreased both ammonia production and autophagy (200). SIRT5 is therefore appears to be a potential regulator of autophagy and has additional, tangential effects like desuccinylation of mitochondrial proteins (201). Desuccinylation of ETC complex I and II occurs upon the binding of SIRT5 to the mitochondria-exclusive phospholipid-cardiolipin, which maintains the integrity of ETC residing on the inner mitochondrial membrane hence promoting the oxidation of NADH into NAD^+ and the production of ROS and ATP (202, 203). Further, SIRT5 can desuccinylate glycolytic enzyme PKM2 causing its deactivation; in LPS activated but SIRT5 knock-out macrophages, IL-1β production was boosted due to an increase in succinylation of PKM2, demonstrating that SIRT5 is related to anti-inflammation (138). In our studies, we found that SIRT5 was up-regulated in MTB-infected and -uninfected human M1-MΦs in contrast to SIRT2 which was up-regulated in M2-MΦs (6). We found that both inflammatory IL-1β production and autophagy were up-regulated in MTB infected M1-MΦs unlike mouse macrophages (6, 96), and in contrast with Wang, et al. (138), we found that SIRT5 was related to a pro-inflammatory response. These issues underscore sirtuin- dependent differences between human and mouse macrophages. In cancer studies, SIRT5 was found to be downregulated in gastric cancer tissues and it enhanced autophagy *via* the AMP-activated protein kinase-mTOR signaling pathway (204). From these observations, we propose a tentative conclusion, though debatable, that of the seven sirtuin proteins, SIRT1, 3, 5, and 7 perform a protective function against infections with MTB whereas, SIRT2, SIRT4 and SIRT6 interfere with macrophage pathways facilitating pathogen survival. However, it is also likely that sirtuins are interdependent and compete with the shared resource of NAD^+; for example, activity of one sirtuin protein may be enhanced by inhibition of another one. An example is that SIRT5 counters the inhibitory effects of SIRT2 and enhances the innate immune responses in macrophages by blocking SIRT2-dependent deacetylation of RelA/p65 activating NF-γB and increased production of downstream cytokines (205).

Sirtuins and arginine metabolism

An intriguing effect of SIRT5 is its ability to regulate arginine metabolism and NO production. As discussed above, SIRT5 deacetylates, desuccinates, and deglutarylates CPS1 to promote the formation of carbamoyl phosphate from ammonia in the urea cycle (196, 197). This process potentially increases the synthesis of citrulline because of interaction between carbmoyl phosphate and ornithine (Figure 4). Interestingly, acetylated glutamate (NAG) additively activates CPS1 (206). With the aid of catalytic enzyme arginosuccinate synthetase (ASS1), citrulline reacts with aspartate to form arginosuccinate which is then converted into arginine and fumarate by argininosuccinate lyase (ASL). Both ornithine and aspartate can be acetylated in macrophages. Therefore, it appears that acetylation of amino acids (glutamate, aspartate, and ornithine) and SIRT5 are involved in the conjugated urea cycle and arginine metabolism cycle. Nitric oxide, the RNS (reactive-nitrogen-species) precursor, is produced by arginine oxidation with the help of iNOS/NOS2. Increased citrulline can replenish arginine consumption for oxidation (207). We propose that an identification of the targets and functions of SIRT5 using mouse liver and human kidney cells can shed a light on the role of SIRT5 during macrophage activation and polarization.

In this direction, we measured mRNA expression of SIRT5 which was significantly higher in MTB-infected and uninfected M1-MΦs than in M2-MΦs cultured under identical conditions (6). Because we had detected that a majority of the proteins in the ETC complex I in M1-MΦs was up-regulated (86), we suspected that not only desuccinylation by SIRT5 but also protein expression of ETC complex I promote NADH oxidation into NAD^+ and ROS in M1-MΦs. We also found an inverse relationship between acetylated amino acids and acetylated histones (86). Therefore, we speculated that acetylation of amino acids and acetylation of histones might compete for ac-CoA to fulfill acetylation; in M1-MΦs, glycolysis generated acetyl-CoA cannot enter the partially blocked TCA cycle but is consumed by acetylation of amino acids as a consequence of which, the supply of ac-CoA for acetylation of histones is diminished. Another possibility is that histone acetylation was reduced by deacetylation with increased production of NAD^+ by ETC complex

10.3389/fimmu.2023.1121495

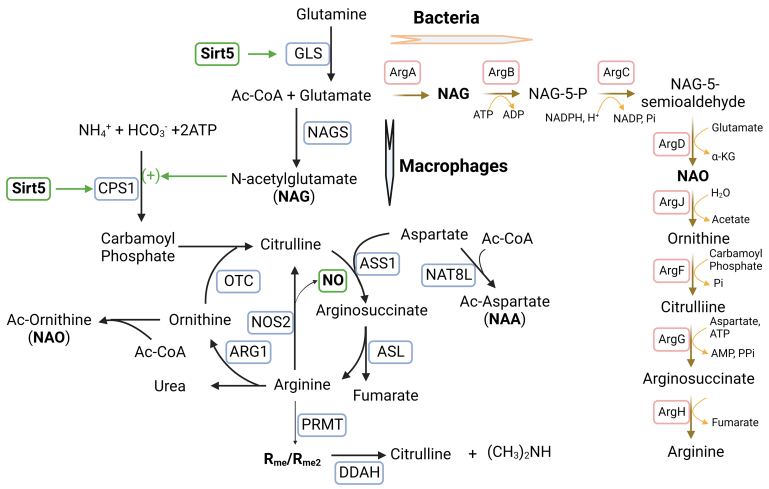

FIGURE 4
Sirtuin5 plays a vital role in arginine metabolism during macrophage activation and polarization. Arginine is converted into citrulline to release NO in M1-MΦs where iNOS/NOS2 is up-regulated, whereas arginine is converted into ornithine in M2-MΦs where ARG1 is up-regulated. In addition, arginine metabolism is regulated by glutamine metabolism which is involved in the urea cycle by N-acetylglutamate (NAG). NAG which is an allosteric activator and is required for the initial and rate-limiting enzyme of the urea cycle, carbamoyl phosphate synthetase 1 (CPS1). The formation of this unique co-substrate from glutamate and acetyl Coenzyme-A is catalyzed by NAG synthase (NAGS). Sirtuin-5 (SIRT5) desuccinates and activates CPS1 to promote the formation of carbamoyl phosphate from ammonia. Carbamoyl phosphate can modify ornithine to form citrulline through the enzyme ornithine transcarbomoylase (OTC). Citrulline can react with aspartate facilitated by the catalytic enzyme arginosuccinate synthetase (ASS1) to form arginosuccinate, which can return to arginine and fumarate through argininosuccinate lyase (ASL). Both aspartate and ornithine can be acetylated to form acetylated aspartate (NAA) and acetylated ornithine (NAO). Asymmetric di-methylated arginine (ADMA/R_{me2}) can be hydrolyzed by enzyme dimethylarginine dimethylaminohydrolase (DDAH) into citrulline and dimethylamine. In bacteria, arginine biosynthesis can start with glutamate acetylation and a set of bacterium-specific catalytic enzymes (ArgA-H) are involved. *Additional Symbols*: NAT8L, N-acetyltransferase 8 like; PRMT, Protein arginine methyltransferase.

I (86). Interestingly, acetylated aspartate (NAA), glutamate (NAG) and ornithine (NAO) were not only enriched in M1-MΦs but were also connected with arginine metabolism (Figure 4). Both NAO and methylated arginine inhibit iNOS/NOS2 required for the production of NO (208–211). In addition, arginine is metabolized into citrulline releasing NO to form RNS that is upregulated in M1-MΦs. These intriguing data led us to the tantalizing questions: how does SIRT5 regulate acetylation of amino acids and histones to leverage arginine metabolism and further, how is RNS production regulated by SIRT5 *via* arginine metabolism?

We note here that, bacteria including Mtb can synthesize arginine from glutamate by acetylation. NAG which is synthesized from glutamate by ArgA and NAO which is synthesized from NAG-5-semialdehyde by ArgD, are the important intermediates. Because mutation dependent loss of function for ArgA or ArgD led to antibiotic resistance in bacteria (212), it appears important to determine, how amino acid acetylation in macrophages is regulated by SIRT5 to replenish NAG and NAO during urea and arginine cycles in relation to drug resistance. Additional studies are warranted in this area.

Sirtuins and tryptophan metabolism

Deacetylation activities of sirtuins are regulated by the availability of NAD^+. Two and three molecules of NAD^+ are respectively consumed in glycolysis and TCA cycle. NAD^+ can be recovered from NADH oxidation, pyruvate reduction to lactate, and the redox reaction in ETC complex I. NAD^+ can also be *de novo* synthesized from tryptophan metabolism and synthesized *via* the nicotinamide salvage pathway (Figure 5). Thus, the overall level of NAD^+ is well regulated under physiologic conditions to maintain optimal metabolism, appropriate energy production, and proliferation. Isotope tracing studies performed by Minhas et al. revealed that macrophage NAD^+ was derived substantially from kynurenine pathway of tryptophan metabolism to maintain normal innate immune functions, whereas breakdown of this *de novo* NAD^+ synthesis pathway could occur after LPS stimulation. They also demonstrated that inhibiting the expression of quinolinate phosphoribosytransferase (QPRT) decreased NAD^+ level and caused innate immune dysfunction during aging and age-related diseases (213). Another study by Cameron et al. indicated that synthesis of NAD^+ by the salvage pathway drove an immediate macrophage inflammatory response to LPS (214). The mechanistic insight was that LPS-induced ROS caused DNA damage through heightened expression of CD38 and increased PARP activity, a process which consumes NAD^+ to trigger the salvage pathway for repletion of NAD^+ (214, 215).

Using triomics to analyze IFN-γ activated but rested and uninfected human donor derived M1-MΦs, we found significantly increased expression of QRPT and the production of Niacin (aka, nicotinic acid or vitamin B_3) which is the precursor of NAD^+; this indicated up-regulated *de novo* NAD^+ synthesis through tryptophan metabolism. We proposed that elevated NAD^+ level would result in an increased deacetylation by sirtuins and thereby decreased histone acetylation. Indeed, we found decreased histone acetylation in uninfected M1-MΦs using mass spectrometric measurements (86). However, during MTB infection, we propose that NAD^+ level could

10.3389/fimmu.2023.1121495

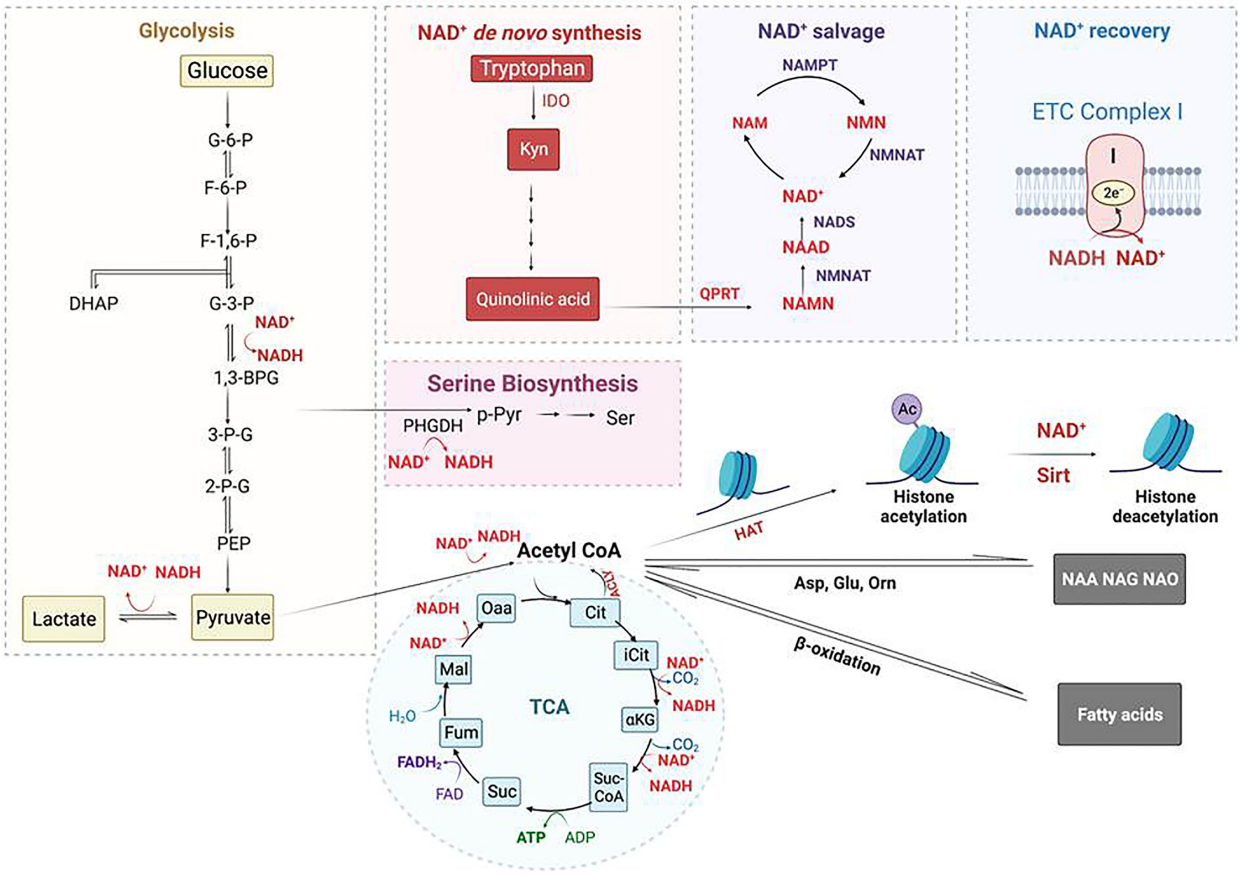

FIGURE 5
Regulation of Histone acetylation and deacetylation by metabolism-generated acetyl-CoA and NAD$^+$. Acetyl-CoA is an essential co-substrate of histone acetyltransferase (HAT) that is mainly generated from glycolysis and fatty-aid β-oxidation; it is required for histone acetylation, amino acid acetylation including forming n-acetyl-aspartate (NAA), n-acetyl-glutamate (NAG), and n-acetyl-ornithine (NAO), and fatty-acid synthesis. NAD$^+$ is an essential co-substrate of NAD$^+$-dependent histone deacetylases that includes Sirtuin proteins. NAD$^+$ is consumed by glycolysis (2 molecules) and TCA cycle (3 molecules), whereas it is regenerated from NADH oxidation *via* conversion of pyruvate into lactate and through ETC complex I. NAD$^+$ is biosynthesized from quinolinic acid, the end product of tryptophan metabolism, catalyzed by the rate-limiting enzyme quinolinate phosphoribosyl transferase (QPRT). The NAD$^+$ *de novo* biosynthesis pathway is coupled with and regulated by the NAD$^+$ salvage pathway. Regulation of NAD$^+$ usage and production in MΦs controls Sirt deacetylase activity, and hence, histone acetylation level. *Additional Symbols*: ACLY, ATP-citrate lyase; NAM, niacinamide; NAMPT, nicotinamide phosphoribosylransferase; NMN, nicotinamide mononucleotide; NMNAT, nicotinamide nucleotide adenylyltransferase; Orn, ornithine; PHGDH, phosphoglycerate dehydrogenase; p-Pyr, phosphopyruvate.

be depleted by glycolysis or the inhibition of NAD$^+$ salvage pathway by tuberculosis necrotizing toxin (TNT) resulting in the death of macrophages (216, 217). Further, NAD$^+$ replenishment alone or its combination with resveratrol (RSV) or cyclosporin A (CsA) can counter the toxicity of TNT and protect macrophages from MTB-induced cell death (173, 216, 218). Others found that NAD$^+$ levels can also be raised by treatment with fatty acid oxidation inhibitors such as Trimetazidine (TMZ) which induced NADPH oxisase and autophagy mediated control of tuberculosis (219). Together, these data suggest that cellular NAD$^+$ concentration controls both sirtuin deaceylase activity and antimycobacterial function of macrophages.

Pharmacological modulation of sirtuins to increase antimicrobial mechanisms

Sirtuins have been found as potential immunotherapeutic targets against tuberculosis because of their regulation of central energy metabolism *via* NAD$^+$-dependent deacetylation. It has been reported that MTB infection depleted NAD$^+$ level and perturbed sirtuin activity in MΦs (173, 190, 191, 217). Others reported that inhibition of SIRT2 with AGK2 restricted the growth of both dug-sensitive and -resistant strains of MTB and enhanced the efficacy of anti-TB drug Isoniazid in the mouse model of infection (220). In contrast, SIRT1 activators, such as resveratrol (RES), achieved a similar outcome by reducing lung pathology, chronic inflammation, and enhanced the efficacy of anti-TB drugs (173). As previously noted, hMOF is a specific histone H4K16 acetyltransferase; low activity of hMOF and low H4K16 acetylation is related to starvation-induced autophagy, which causes chronic repression of autophagic genes (156). SIRT1 is a H4K16 specific deacetylase. Mechanistically, activation of SIRT1 may keep the global H4K16 acetylation at low levels but on the other hand, it may deacetylate and activate ac-coA synthetase 1 (AceCS1) accumulating ac-CoA from acetate (221). Moreover, SIRT1 can also deacetylate hMOF to facilitate its binding to the chromatin at the promoters of autophagic genes promoting H4K16 acetylation due to increase in AceCS1 derived ac-Co-A (222). In murine J2-macrophages, the

mRNA expression levels of SIRT1, SIRT3, SIRT5, and SIRT7 were all decreased at 24 hr post-infection of TB, which was also validated using mouse bone marrow derived macrophages (BMDM) (190). A detailed study of SIRT3 demonstrated that, over-expression of SIRT3 or treatment with SIRT3 activator Honokiol prevented MTB from inducing mitochondrial ROS accumulation in murine BMDM and cell death, whereas reduced expression of SIRT3 in $Sirt3^{-/-}$ mice increased bacterial burden (190). A similar report revealed that SIRT3 enhanced anti-TB defense through coordinated mitochondrial and autophagic functions (191). SIRT7 has protective effects against TB-infection through regulation of NO production and apoptosis demonstrated using an *in-vitro* model (223). Prakhar et al. observed restricted growth of TB and development of granulomatous lesion in the lungs and spleen of SIRT6 heterozygous mice infected with TB (182). Together these data suggest that the activators of SIRT3, SIRT5 and SIRT7 are potential anti-TB drugs in addition to the SIRT1 activator-Resveratrol. In contrast, we found that SIRT2 blockade increases autophagy-mediated killing of MTB. Of note, there are no data on whether SIRT4 contributes to anti-tuberculosis immunity.

Prospects for sirtuin modulators as drugs against tuberculosis

Despite reports that sirtuin inhibitors or activators in combination with the FDA-approved frontline anti-TB drugs enhance killing of drug resistant and dormant TB (173, 220, 224), none has been approved by FDA. Metformin is a direct SIRT1 activator based on computational modeling and experimental validation (225). Although it is not a TB-specific drug, it shows therapeutic efficacy for patients who have comorbidity of TB and diabetes and can be used as a pure adjunctive therapy for TB (226). Because, small chemical compounds that modulate sirtuin function have been pursued as anticancer agents (227), we propose that efforts should be made to use a combination of sirtuin activators and inhibitors to treat tuberculosis in combination with existing therapies.

Beside sirtuin proteins, the NAD^+ biosynthesis pathway may also be a promising target for tuberculosis therapy. Recent elucidation of the mechanism of isoniazid (INH), a frontline anti-TB drug, indicated that INH couples with NADH catalyzed by KatG to form the active INH-NAD adduct, which in turn, binds tightly to the enoyl-acyl carrier protein reductase InhA so that the synthesis of mycolic acid for mycobacterial cell wall formation is inhibited (228). As MTB depends solely on its own *de novo* pathway to meet its NAD^+ demand (229), MTB-QPRT provides an attractive target for designing novel anti-TB drugs (230). Coincidentally, NAD^+ in the host M1-MΦ is significantly higher than M2-MΦs to maintain autophagy and bactericidal activity. Because of QPRT occurs in both host macrophages and MTB, its non-specific inhibition would decrease autophagy mediated killing capacity of macrophages. As crystal structures of both human and MTB derived QPRT have been elucidated (229, 231), to avoid toxicity, a drug to selectively target MTB-QPRT but not human-QPRT based on their structural difference at the substrate binding sites would be crucial. Quinolinic acid (QA) is the first intermediate in the *de novo* pathway of NAD^+ biosynthesis that is common to all organisms and is mainly produced by the degradation of tryptophan in most eukaryotes. In contrast, in prokaryotes, including MTB, it is mainly produced from L-aspartate and dihydroxyacetone phosphate by the enzymes encoded by *nadA* (quinolinic acid synthetase) and *nadB* (L-aspartate oxidase) (232). Therefore, we propose that a drug to target nadA/B may be an alternative to QPRT inhibitors to control tuberculosis (233).

Sirtuins intersect the serine biosynthesis, one-carbon metabolism, and methylation of DNA and histones

The biosynthesis of serine starts with the oxidation of 3-phosphoglycerate (an intermediate from glycolysis) by NAD^+ to 3-phosphohydroxypyruvate and NADH catalyzed by phosphoglycerate dehydrogenase (PHGDH), which is a rate-limiting enzyme (Figures 5, 6); the other two are Phosphoserine aminotransferase (PSAT) and Phosphoserine Phosphatase (PSPH). Since NAD^+ is required for facilitating the functions of both PHGDH in serine biosynthesis and GAPDH in glycolysis, serine biosynthesis competes with the glycolysis pathway. Supporting this concept, serine deprivation in LPS-Simulated macrophages caused a reduction of pyruvate, decreased NAD^+/NADH ratio, and decreased ROS level, partially resembling M2-MΦ phenotype but still maintaining a pro-inflammatory cytokine profile of M1-MΦs (234). However, Rodrigues et al. reported that serine is required for LPS induction of IL-1β mRNA expression but not inflammasome activation, because serine is used for conversion to glycine that is needed for macrophage GSH synthesis to support IL-1β production (235). Serine is required for the growth of MTB (236). Serine is converted to glycine by SHMT1 in the cytosol and SHMT2 in the mitochondria, which then donates one carbon to the folate cycle adjacent to the methionine cycle through methionine synthase (MTR) that in turn, requires vitamin B_{12} as a co-substrate. In the methionine cycle, SAM is synthesized from S-Adenosyl Homocysteine (SAH) with the donation of a methyl group from methionine. SAM is an essential co-substrate of methyltransferases, and provides the methyl group for methylation of histone, DNA and other biological compounds in the cells. In M1-MΦs, up-regulated glycolysis would increase the supply of 3-phosphohydroxypyruvate for serine biosynthesis. Because nitric oxide in M1-MΦs is toxic to vitamin B_{12}, the transportation of B_{12} crossing the cell membrane is inhibited by hypoxia, and the mitochondrial citramalyl-CoA lyase (CLYBL) appears to be indirectly involved in the inhibition of vitamin B_{12} metabolism, depletion of B_{12} and as expected, subsequent inactivation of methionine synthase (MTR). As a result, one-carbon metabolism is hindered resulting in reduced formation of SAM and consequently, decreased methylation of histones or DNA (Figure 6). However, increased extracellular methionine uptake can still be triggered *via* the feedback mechanism to restore the loss. Excess methionine increases the production of SAM and DNA methylation attenuating LPS-induced inflammation (237). Because hypermethylation in macrophages reduces pro-inflammatory responses, we propose that a similar mechanism may favor the survival of MTB (238). Notably, MTB synthesizes its own methionine and SAM from homoserine which is produced through aspartate pathway (239, 240). Dinardo et al. performed methylation-sensitive enzyme-quantitative PCR (MSRE-PCR) and observed that in the PBMCs of TB-infected patients, pro-inflammatory genes including

10.3389/fimmu.2023.1121495

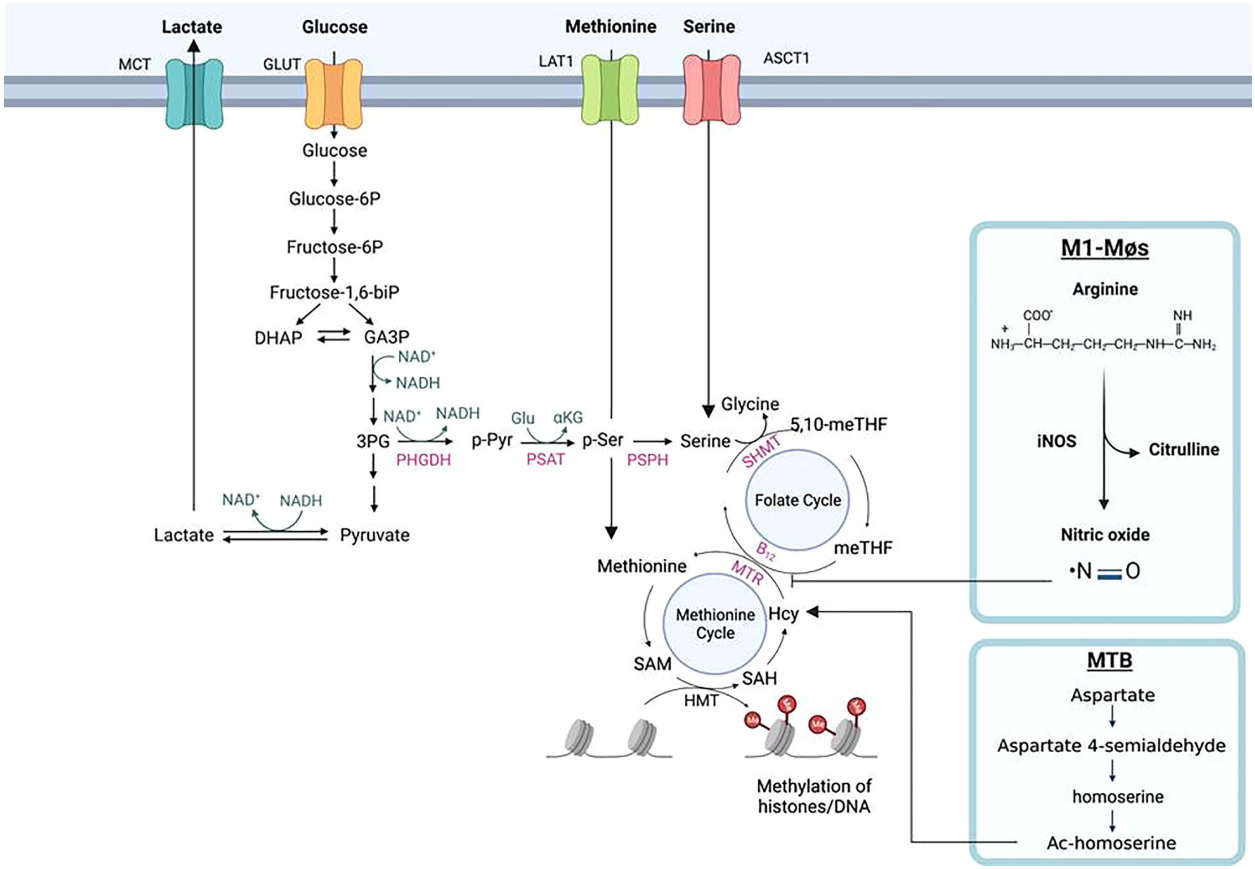

FIGURE 6
Histone methylation through one-carbon metabolism and serine biosynthesis in macrophages. Serine is biosynthesized from 3-phophoglycerol (3PG), an intermediate of glycolysis, by phosphoglycerol dehydrogenase (PHGDH) to form phosphopyruvate (p-Pyr) and catalyzed by phosphoserine aminotransferase (PSAT) to form phosphoserine (p-Ser) and then phosphoserine phosphate (PSPH) to form serine. With the aid of catalytic enzyme serine hydroxymethyltransferase (SHMT), serine is further converted into glycine donating one-carbon (a methyl group) to the tetrahydrofolate (THF) in the folate cycle to form sequentially 5, 10-methylenetetrahydrofolate (5,10-meTHF) and 5-methyl-tetrahydrofolate (meTHF); the methyl group of the latter is transferred to homocysteine (Hcy) to form methionine (Met) and S-adenosyl-methionine (SAM). SAM is the co-substrate of methyltransferases for DNA and histone methylation. Methionine and serine can also be respectively delivered from extracellular environment to the cells by their transporters, L-type amino acid transporter/solute carrier family member 5 (LAT1/SLC7A5) and alanine/serine/cysteine/threonine transporter 1 (ASCT1). The methyl transfer from meTHF to Hcy needs methionine synthesis (MS/MTR) and its co-substrate vitamin B_{12}. In M1-MΦs, elevated nitric oxide (NO) poisons vitamin B_{12} causing deactivation of MTR and the disruption of one-carbon metabolism, resulting in reduced Met and SAM for histones/DNA methylation. In *Mycobacterium tuberculosis* MTB) infected MΦs, independent of vitamin B_{12}, the pathogen can bypass the one-carbon metabolic pathway to synthesize methionine and SAM through homoserine, a product of aspartate metabolic pathway.

IL-1β and IFN-γ were DNA-hypermethylated resulting in dampened host immune responsiveness (4). MTB mediated hypermethylation of inflammatory genes is therefore a pathogen evasion strategy.

Proteomics has identified that the one-carbon enzyme, MTHFD1L (methylenetetrahydrofolate dehydrogenase [$NADP^+$ dependent 1-like]) in the folate cycle, is a substrate for SIRT5 mediated desuccinylation/malonylation and SIRT5 also interacts with SHMT2 (241–244). In SIRT5 knock-down (KD) melanoma cells, reduced H3K4me3 and H3K9me3 were observed, indicating that reduced SAM production from impaired one-carbon metabolism of H3K4me3 and H3K9me3 sense the SAM levels in the cells (243, 245). SIRT5 also desuccinylates and activates SHMT2 to promote one-carbon metabolism and potential histone methylation in cancer cells (244). If this is true in immune cells, one-carbon metabolism and histone methylation would be enhanced in M1-MΦs as SIRT5 is up-regulated based on our RNA-seq data (6), which is opposite to what we proposed: that one-carbon metabolism would be down-regulated due to B_{12} depletion/MTR inactivation discussed above. In contrast, in breast cancer, SIRT2 regulates the reversible acetylation of PHGDH through TIP60 and promotes the binding of PHGDH and RNF5 to induce PHGDH degradation and reducing serine and glycine derived from glucose metabolism *via* the serine biosynthesis pathway in (246). If this information is also true in immune cells, in M2-MΦs upregulated SIRT2 would reduce serine synthesis from glucose metabolism potentially resulting in histone hypomethylation. Therefore, we propose that the methylation state in M1-MΦs versus M2-MΦ depends on which metabolic pathway is dominant- glycolysis and glucose intake, serine biosynthesis and intake, one-carbon metabolism and methionine intake, depending upon specific tissue microenvironments.

In order to understand how MTB regulates lysine and arginine methylation or other free amino acids and histones differently in M1- versus M2-MΦs, we will need to use isotope tracers and mass spectrometry. This will allow us to monitor how methyl migration to lysine and arginine residues from methionine/SAM produced by glucose derived serine occurs, and to determine whether serine is synthesized from intracellular source or directly taken up from extracellular nutrients

in naïve versus polarized macrophages. Additionally, using isotope-labeled aspartate, we may be able to trace the methyl group migrating through the aspartate-homoserine-homocysteine route to lysine and arginine in MTB infected macrophages (Figure 6). We will then have a clear picture of methylation and epigenetic profiles differentially affected by metabolism in naïve or polarized macrophages infected with MTB.

Conclusion and perspectives

Glycolysis not only generates energy (ATP) to meet the demand of cells for their surviving but also controls the homeostasis of NAD^+ which prevents cells from death and is an essential co-substrate of sirtuin proteins, the type-III histone deacetylases. Importantly, glycolysis is also a source of directly or indirectly producing ac-CoA and SAM, the co-substrates of histone acetyltransferases and methyltransferases respectively. Upregulated glycolysis in M1-MΦs generates increased ac-CoA from pyruvate and thereby increased histones acetylation which is counter-regulated by NAD^+. NAD^+ is consumed in glycolysis and TCA cycle and other redox processes. It is also reproduced by oxidation in metabolic pathways such as lactate synthesis from pyruvate and ETC. Increased NAD^+ from *de novo* synthesis and the NAD^+ salvage pathway would tip the balance towards hypoacetylation. Glycolysis also links to serine biosynthesis, a fuel for one-carbon metabolism, and the synthesis of SAM for histone/DNA methylation. Metabolic switch between M1- and M2-MΦs therefore causes an imbalance of co-substrates (ac-CoA and SAM) of histone acetyltransferases and methyltransferases thereby changing the landscapes of acetylation and methylation of histones and proteins in the metabolic pathways. Consequently, metabolism controls macrophage gene expression, the production of anti-mycobacterial oxidants, and autophagy during pathogen infection. Since the co-substrates produced by metabolites from glucose are regulated by other metabolic pathways, future work needs to be focused on the dynamic correlation between metabolism and histone modifications through measurement of the levels of co-substrates produced in polarized macrophages and the states of histone modifications on a time scale. For example, we can use stable isotope labeled glucose as the major probe during early and late phase of infection. It is also important to seek an insight into the impact of glucose metabolism on the expression of cytokines and autophagy genes regulated by co-substrates. Moreover, we can use stable-isotope labeled glutamine and arginine, to probe the mechanism of how sirtuin proteins control glutaminolysis and NO production through conjunction of the urea cycle and arginine metabolism cycle. Sirtuin proteins and their substrates are therefore promising targets for treatment of tuberculosis and likely other intracellular infections.

Author contributions

KZ wrote the manuscript. MS, EC, VS, BR, AK: contributed to supporting data and made graphics. CJ: Proposed the contents and edited the manuscript. All authors contributed to the article and approved the submitted version.

Acknowledgments

The authors wish to acknowledge funding support from NIH RO1 AI161015 (CJ, Janice Endsley, AK), AI138587 (CJ and Deepak Kaushal).

Conflict of interest

The authors declare that the research was conducted in the absence of any commercial or financial relationships that could be construed as a potential conflict of interest.

Publisher's note

References

1. Rahlwes KC, Dias BRS, Campos PC, Alvarez-Arguedas S, Shiloh MU. Pathogenicity and virulence of mycobacterium tuberculosis. *Virulence* (2023) 14:2150449. doi: 10.1080/21505594.2022.2150449

2. Pal R, Bisht MK, Mukhopadhyay S. Secretory proteins of mycobacterium tuberculosis and their roles in modulation of host immune responses: Focus on therapeutic targets. *FEBS J* (2022) 289:4146–71. doi: 10.1111/febs.16369

3. Rahman A, Srivastava SS, Sneh A, Ahmed N, Krishnasastry MV. Molecular characterization of tlyA gene product, Rv1694 of mycobacterium tuberculosis: A non-conventional hemolysin and a ribosomal RNA methyl transferase. *BMC Biochem* (2010) 11:35. doi: 10.1186/1471-2091-11-35

4. DiNardo AR, Rajapakshe K, Nishiguchi T, Grimm SL, Mtetwa G, Dlamini Q, et al. DNA Hypermethylation during tuberculosis dampens host immune responsiveness. *J Clin Invest* (2020) 130:3113–23. doi: 10.1172/JCI134622

5. Duan L, Yi M, Chen J, Li S, Chen W. Mycobacterium tuberculosis EIS gene inhibits macrophage autophagy through up-regulation of IL-10 by increasing the acetylation of histone H3. *Biochem Biophys Res Commun* (2016) 473:1229–34. doi: 10.1016/j.bbrc.2016.04.045

6. Khan A, Zhang K, Singh VK, Mishra A, Kachroo P, Bing T, et al. Human M1 macrophages express unique innate immune response genes after mycobacterial infection to defend against tuberculosis. *Commun Biol* (2022) 5:480. doi: 10.1038/s42003-022-03387-9

7. Katada S, Imhof A, Sassone-Corsi P. Connecting threads: Epigenetics and metabolism. *Cell* (2012) 148:24–8. doi: 10.1016/j.cell.2012.01.001

8. Freemerman AJ, Johnson AR, Sacks GN, Milner JJ, Kirk EL, Troester MA, et al. Metabolic reprogramming of macrophages: Glucose transporter 1 (GLUT1)-mediated glucose metabolism drives a proinflammatory phenotype. *J Biol Chem* (2014) 289:7884–96. doi: 10.1074/jbc.M113.522037

9. Viola A, Munari F, Sanchez-Rodriguez R, Scolaro T, Castegna A. The metabolic signature of macrophage responses. *Front Immunol* (2019) 10:1462. doi: 10.3389/fimmu.2019.01462

10. Soto-Heredero G, Gomez de Las Heras MM, Gabande-Rodriguez E, Oller J, Mittelbrunn M. Glycolysis - a key player in the inflammatory response. *FEBS J* (2020) 287:3350–69. doi: 10.1111/febs.15327

11. Cluntun AA, Huang H, Dai L, Liu X, Zhao Y, Locasale JW. The rate of glycolysis quantitatively mediates specific histone acetylation sites. *Cancer Metab* (2015) 3:10. doi: 10.1186/s40170-015-0135-3

12. Friis RM, Wu BP, Reinke SN, Hockman DJ, Sykes BD, Schultz MC. A glycolytic burst drives glucose induction of global histone acetylation by picNuA4 and SAGA. *Nucleic Acids Res* (2009) 37:3969–80. doi: 10.1093/nar/gkp270

13. Moussaieff A, Rouleau M, Kitsberg D, Cohen M, Levy G, Barasch D, et al. Glycolysis-mediated changes in acetyl-CoA and histone acetylation control the early differentiation of embryonic stem cells. *Cell Metab* (2015) 21:392–402. doi: 10.1016/j.cmet.2015.02.002

14. Nakayasu ES, Burnet MC, Walukiewicz HE, Wilkins CS, Shukla AK, Brooks S, et al. Ancient regulatory role of lysine acetylation in central metabolism. *mBio* (2017) 8. doi: 10.1128/mBio.01894-17

15. Hallows WC, Yu W, Denu JM. Regulation of glycolytic enzyme phosphoglycerate mutase-1 by Sirt1 protein-mediated deacetylation. *J Biol Chem* (2012) 287:3850–8. doi: 10.1074/jbc.M111.317404

16. Gaal Z, Csernoch L. Impact of sirtuin enzymes on the altered metabolic phenotype of malignantly transformed cells. *Front Oncol* (2020) 10:45. doi: 10.3389/fonc.2020.00045

17. Barron JT, Gu L, Parrillo JE. NADH/NAD redox state of cytoplasmic glycolytic compartments in vascular smooth muscle. *Am J Physiol Heart Circ Physiol* (2000) 279:H2872–2878. doi: 10.1152/ajpheart.2000.279.6.H2872

18. Luengo A, Li Z, Gui DY, Sullivan LB, Zagorulya M, Do BT, et al. Increased demand for NAD(+) relative to ATP drives aerobic glycolysis. *Mol Cell* (2021) 81:691–707 e696. doi: 10.1016/j.molcel.2020.12.012

19. Locasale JW. Serine, glycine and one-carbon units: Cancer metabolism in full circle. *Nat Rev Cancer* (2013) 13:572–83. doi: 10.1038/nrc3557

20. Maddocks OD, Labuschagne CF, Adams PD, Vousden KH. Serine metabolism supports the methionine cycle and DNA/RNA methylation through *De novo* ATP synthesis in cancer cells. *Mol Cell* (2016) 61:210–21. doi: 10.1016/j.molcel.2015.12.014

21. Baek SH, Kim KI. Epigenetic control of autophagy: Nuclear events gain more attention. *Mol Cell* (2017) 65:781–5. doi: 10.1016/j.molcel.2016.12.027

22. Shi Y, Shen HM, Gopalakrishnan V, Gordon N. Epigenetic regulation of autophagy beyond the cytoplasm: A review. *Front Cell Dev Biol* (2021) 9:675599. doi: 10.3389/fcell.2021.675599

23. Pearce EL. Metabolism as a driver of immunity. *Nat Rev Immunol* (2021) 21:618–9. doi: 10.1038/s41577-021-00601-3

24. Wolf AJ, Reyes CN, Liang W, Becker C, Shimada K, Wheeler ML, et al. Hexokinase is an innate immune receptor for the detection of bacterial peptidoglycan. *Cell* (2016) 166:624–36. doi: 10.1016/j.cell.2016.05.076

25. O'Sullivan D, Kelly B, Pearce EL. When hexokinase gets that NAG-ing feeling. *Cell Metab* (2016) 24:198–200. doi: 10.1016/j.cmet.2016.07.021

26. Ahmad A, Aboukameel A, Kong D, Wang Z, Sethi S, Chen W, et al. Phosphoglucose isomerase/autocrine motility factor mediates epithelial-mesenchymal transition regulated by miR-200 in breast cancer cells. *Cancer Res* (2011) 71:3400–9. doi: 10.1158/0008-5472.CAN-10-0965

27. Schultze SM, Hemmings BA, Niessen M, Tschopp O. PI3K/AKT, MAPK and AMPK signalling: Protein kinases in glucose homeostasis. *Expert Rev Mol Med* (2012) 14:e1. doi: 10.1017/S1462399411002109

28. Papa S, Choy PM, Bubici C. The ERK and JNK pathways in the regulation of metabolic reprogramming. *Oncogene* (2019) 38:2223–40. doi: 10.1038/s41388-018-0582-8

29. Sharif O, Brunner JS, Vogel A, Schabbauer G. Macrophage rewiring by nutrient associated PI3K dependent pathways. *Front Immunol* (2019) 10:2002. doi: 10.3389/fimmu.2019.02002

30. Bednarczyk RB, Tuli NY, Hanly EK, Rahoma GB, Maniyar R, Mittelman A, et al. Macrophage inflammatory factors promote epithelial-mesenchymal transition in breast cancer. *Oncotarget* (2018) 9:24272–82. doi: 10.18632/oncotarget.24917

31. McCarthy JS, Wieseman M, Tropea J, Kaslow D, Abraham D, Lustigman S, et al. Onchocerca volvulus glycolytic enzyme fructose-1,6-bisphosphate aldolase as a target for a protective immune response in humans. *Infect Immun* (2002) 70:851–8. doi: 10.1128/IAI.70.2.851-858.2002

32. Trujillo C, Blumenthal A, Marrero J, Rhee KY, Schnappinger D, Ehrt S. Triosephosphate isomerase is dispensable *in vitro* yet essential for mycobacterium tuberculosis to establish infection. *mBio* (2014) 5:e00085. doi: 10.1128/mBio.00085-14

33. Wang YT, Huang HY, Tsai MA, Wang PC, Jiang BH, Chen SC. Phosphoglycerate kinase enhanced immunity of the whole cell of streptococcus agalactiae in tilapia, oreochromis niloticus. *Fish Shellfish Immunol* (2014) 41:250–9. doi: 10.1016/j.fsi.2014.09.008

34. Li Z, Zhang H, Zhang J, Xi L, Yang G, Wang S, et al. Brucella abortus phosphoglyceromutase and dihydrodipicolinate reductase induce Th1 and Th2-related immune responses. *World J Microbiol Biotechnol* (2018) 34:22. doi: 10.1007/s11274-017-2405-4

35. Ryans K, Omosun Y, McKeithen DN, Simoneaux T, Mills CC, Bowen N, et al. The immunoregulatory role of alpha enolase in dendritic cell function during chlamydia infection. *BMC Immunol* (2017) 18:27. doi: 10.1186/s12865-017-0212-1

36. Stone OA, El-Brolosy M, Wilhelm K, Liu X, Romao AM, Grillo E, et al. Loss of pyruvate kinase M2 limits growth and triggers innate immune signaling in endothelial cells. *Nat Commun* (2018) 9:4077. doi: 10.1038/s41467-018-06406-8

37. Millet P, Vachharajani V, McPhail L, Yoza B, McCall CE. GAPDH binding to TNF-alpha mRNA contributes to posttranscriptional repression in monocytes: A novel mechanism of communication between inflammation and metabolism. *J Immunol* (2016) 196:2541–51. doi: 10.4049/jimmunol.1501345

38. Min BK, Park S, Kang HJ, Kim DW, Ham HJ, Ha CM, et al. Pyruvate dehydrogenase kinase is a metabolic checkpoint for polarization of macrophages to the M1 phenotype. *Front Immunol* (2019) 10:944. doi: 10.3389/fimmu.2019.00944

39. Ge T, Yang J, Zhou S, Wang Y, Li Y, Tong X. The role of the pentose phosphate pathway in diabetes and cancer. *Front Endocrinol (Lausanne)* (2020) 11:365. doi: 10.3389/fendo.2020.00365

40. Manoharan I, Prasad PD, Thangaraju M, Manicassamy S. Lactate-dependent regulation of immune responses by dendritic cells and macrophages. *Front Immunol* (2021) 12:691134. doi: 10.3389/fimmu.2021.691134

41. Ho PC, Bihuniak JD, Macintyre AN, Staron M, Liu X, Amezquita R, et al. Phosphoenolpyruvate is a metabolic checkpoint of anti-tumor T cell responses. *Cell* (2015) 162:1217–28. doi: 10.1016/j.cell.2015.08.012

42. Stincone A, Prigione A, Cramer T, Wamelink MM, Campbell K, Cheung E, et al. The return of metabolism: Biochemistry and physiology of the pentose phosphate pathway. *Biol Rev Camb Philos Soc* (2015) 90:927–63. doi: 10.1111/brv.12140

43. Choi I, Son H, Baek JH. Tricarboxylic acid (TCA) cycle intermediates: Regulators of immune responses. *Life (Basel)* (2021) 11. doi: 10.3390/life11010069

44. Williams NC, O'Neill LAJ. A role for the Krebs cycle intermediate citrate in metabolic reprogramming in innate immunity and inflammation. *Front Immunol* (2018) 9:141. doi: 10.3389/fimmu.2018.00141

45. Kurniawan H, Kobayashi T, Brenner D. The emerging role of one-carbon metabolism in T cells. *Curr Opin Biotechnol* (2021) 68:193–201. doi: 10.1016/j.copbio.2020.12.001

46. Richter FC, Clarke AJ. One carbon (metabolism) to rule T cell identity. *Nat Rev Immunol* (2021) 21:206. doi: 10.1038/s41577-021-00530-1

47. Cruzat V, Macedo Rogero M, Noel Keane K, Curi R, Newsholme P. Glutamine: Metabolism and immune function, supplementation and clinical translation. *Nutrients* (2018) 10. doi: 10.3390/nu10111564

48. Bronte V, Zanovello P. Regulation of immune responses by l-arginine metabolism. *Nat Rev Immunol* (2005) 5:641–54. doi: 10.1038/nri1668

49. Schieber M, Chandel NS. ROS function in redox signaling and oxidative stress. *Curr Biol* (2014) 24:R453–462. doi: 10.1016/j.cub.2014.03.034

50. Zhao RZ, Jiang S, Zhang L, Yu ZB. Mitochondrial electron transport chain, ROS generation and uncoupling (Review). *Int J Mol Med* (2019) 44:3–15. doi: 10.3892/ijmm.2019.4188

51. Canto C, Menzies KJ, Auwerx J. NAD(+) metabolism and the control of energy homeostasis: A balancing act between mitochondria and the nucleus. *Cell Metab* (2015) 22:31–53. doi: 10.1016/j.cmet.2015.05.023

52. Chenault HK, Whitesides GM. Lactate dehydrogenase-catalyzed regenertion of NAD from NADH for use in enzyme-catalyzed synthesis. *Biooganic Chem* (1989) 17:400–9. doi: 10.1016/0045-2068(89)90041-2

53. Vermot A, Petit-Hartlein I, Smith SME, Fieschi F. NADPH oxidases (NOX): An overview from discovery, molecular mechanisms to physiology and pathology. *Antioxidants (Basel)* (2021) 10. doi: 10.3390/antiox10060890

54. Bedard K, Krause KH. The NOX family of ROS-generating NADPH oxidases: physiology and pathophysiology. *Physiol Rev* (2007) 87:245–313. doi: 10.1152/physrev.00044.2005

55. Cross AR, Segal AW. The NADPH oxidase of professional phagocytes–prototype of the NOX electron transport chain systems. *Biochim Biophys Acta* (2004) 1657:1–22. doi: 10.1016/j.bbabio.2004.03.008

56. Tannahill GM, Curtis AM, Adamik J, Palsson-McDermott EM, McGettrick AF, Goel G, et al. Succinate is an inflammatory signal that induces IL-1beta through HIF-1alpha. *Nature* (2013) 496:238–42. doi: 10.1038/nature11986

57. Hadrava Vanova K, Kraus M, Neuzil J, Rohlena J. Mitochondrial complex II and reactive oxygen species in disease and therapy. *Redox Rep* (2020) 25:26–32. doi: 10.1080/13510002.2020.1752002

58. Speijer D. Can all major ROS forming sites of the respiratory chain be activated by high FADH2/NADH ratios?: ancient evolutionary constraints determine mitochondrial ROS formation. *Bioessays* (2019) 41:e1800180. doi: 10.1002/bies.201800180

59. Hall CJ, Boyle RH, Astin JW, Flores MV, Oehlers SH, Sanderson LE, et al. Immunoresponsive gene 1 augments bactericidal activity of macrophage-lineage cells by regulating beta-oxidation-dependent mitochondrial ROS production. *Cell Metab* (2013) 18:265–78. doi: 10.1016/j.cmet.2013.06.018

60. Jaiswal AK, Yadav J, Makhija S, Mazumder S, Mitra AK, Suryawanshi A, et al. Irg1/itaconate metabolic pathway is a crucial determinant of dendritic cells immune-priming function and contributes to resolute allergen-induced airway inflammation. *Mucosal Immunol* (2022) 15:301–13. doi: 10.1038/s41385-021-00462-y

61. Sasikaran J, Ziemski M, Zadora PK, Fleig A, Berg IA. Bacterial itaconate degradation promotes pathogenicity. *Nat Chem Biol* (2014) 10:371–7. doi: 10.1038/nchembio.1482

62. Michelucci A, Cordes T, Ghelfi J, Pailot A, Reiling N, Goldmann O, et al. Immune-responsive gene 1 protein links metabolism to immunity by catalyzing itaconic acid production. *Proc Natl Acad Sci U.S.A.* (2013) 110:7820–5.

63. O'Neill LAJ, Artyomov MN. Itaconate: the poster child of metabolic reprogramming in macrophage function. *Nat Rev Immunol* (2019) 19:273–81. doi: 10.1038/s41577-019-0128-5

64. Canton M, Sanchez-Rodriguez R, Spera I, Venegas FC, Favia M, Viola A, et al. Reactive oxygen species in macrophages: Sources and targets. *Front Immunol* (2021) 12:734229. doi: 10.3389/fimmu.2021.734229

65. Tan HY, Wang N, Li S, Hong M, Wang X, Feng Y. The reactive oxygen species in macrophage polarization: Reflecting its dual role in progression and treatment of human diseases. *Oxid Med Cell Longev* (2016) 2016:2795090. doi: 10.1155/2016/2795090

66. Radi R. Oxygen radicals, nitric oxide, and peroxynitrite: Redox pathways in molecular medicine. *Proc Natl Acad Sci U.S.A.* (2018) 115:5839–48.

67. Weinberg JB. Nitric oxide production and nitric oxide synthase type 2 expression by human mononuclear phagocytes: A review. *Mol Med* (1998) 4:557–91. doi: 10.1007/BF03401758

68. Mori M, Gotoh T. Regulation of nitric oxide production by arginine metabolic enzymes. *Biochem Biophys Res Commun* (2000) 275:715–9. doi: 10.1006/bbrc.2000.3169

69. Herb M, Schramm M. Functions of ROS in macrophages and antimicrobial immunity. *Antioxidants (Basel)* (2021). doi: 10.3390/antiox10020313

70. Ding AH, Nathan CF, Stuehr DJ. Release of reactive nitrogen intermediates and reactive oxygen intermediates from mouse peritoneal macrophages. *Comparison Activating Cytokines Evidence Independent Production J Immunol* (1988) 141:2407–12.

71. Drapier JC, Wietzerbin J, Hibbs JBJr. Interferon-gamma and tumor necrosis factor induce the l-arginine-dependent cytotoxic effector mechanism in murine macrophages. *Eur J Immunol* (1988) 18:1587–92. doi: 10.1002/eji.1830181018

72. Lyons CR, Orloff GJ, Cunningham JM. Molecular cloning and functional expression of an inducible nitric oxide synthase from a murine macrophage cell line. *J Biol Chem* (1992) 267:6370–4. doi: 10.1016/S0021-9258(18)42704-4

73. Zhong J, Scholz T, Yau ACY, Guerard S, Huffmeier U, Burkhardt H, et al. Mannan-induced Nos2 in macrophages enhances IL-17-driven psoriatic arthritis by innate lymphocytes. *Sci Adv* (2018) 4:eaas9864. doi: 10.1126/sciadv.aas9864

74. Baran CP, Zeigler MM, Tridandapani S, Marsh CB. The role of ROS and RNS in regulating life and death of blood monocytes. *Curr Pharm Des* (2004) 10:855–66. doi: 10.2174/1381612043452866

75. Iovine NM, Pursnani S, Voldman A, Wasserman G, Blaser MJ, Weinrauch Y. Reactive nitrogen species contribute to innate host defense against campylobacter jejuni. *Infect Immun* (2008) 76:986–93. doi: 10.1128/IAI.01063-07

76. Canton J, Khezri R, Glogauer M, Grinstein S. Contrasting phagosome pH regulation and maturation in human M1 and M2 macrophages. *Mol Biol Cell* (2014) 25:3330–41. doi: 10.1091/mbc.e14-05-0967

77. Bailey JD, Diotallevi M, Nicol T, McNeill E, Shaw A, Chuaiphichai S, et al. Nitric oxide modulates metabolic remodeling in inflammatory macrophages through TCA cycle regulation and itaconate accumulation. *Cell Rep* (2019) 28:218–230 e217. doi: 10.1016/j.celrep.2019.06.018

78. Nair S, Huynh JP, Lampropoulou V, Loginicheva E, Esaulova E, Gounder AP, et al. Irg1 expression in myeloid cells prevents immunopathology during m. tuberculosis infection. *J Exp Med* (2018) 215:1035–45. doi: 10.1084/jem.20180118

79. Paiva CN, Bozza MT. Are reactive oxygen species always detrimental to pathogens? *Antioxid Redox Signal* (2014) 20:1000–37. doi: 10.1089/ars.2013.5447

80. Palmieri EM, Gonzalez-Cotto M, Baseler WA, Davies LC, Ghesquiere B, Maio N, et al. Nitric oxide orchestrates metabolic rewiring in M1 macrophages by targeting aconitase 2 and pyruvate dehydrogenase. *Nat Commun* (2020) 11:698. doi: 10.1038/s41467-020-14433-7

81. Shi L, Jiang Q, Bushkin Y, Subbian S, Tyagi S. Biphasic dynamics of macrophage immunometabolism during mycobacterium tuberculosis infection. *mBio* (2019) 10. doi: 10.1128/mBio.02550-18

82. Howard NC, Khader SA. Immunometabolism during mycobacterium tuberculosis infection. *Trends Microbiol* (2020) 28:832–50. doi: 10.1016/j.tim.2020.04.010

83. Park JH, Shim D, Kim KES, Lee W, Shin SJ. Understanding metabolic regulation between host and pathogens: New opportunities for the development of improved therapeutic strategies against mycobacterium tuberculosis infection. *Front Cell Infect Microbiol* (2021) 11:635335. doi: 10.3389/fcimb.2021.635335

84. Shi L, Salamon H, Eugenin EA, Pine R, Cooper A, Gennaro ML. Infection with mycobacterium tuberculosis induces the warburg effect in mouse lungs. *Sci Rep* (2015) 5:18176. doi: 10.1038/srep18176

85. Diskin C, Palsson-McDermott EM. Metabolic modulation in macrophage effector function. *Front Immunol* (2018) 9:270. doi: 10.3389/fimmu.2018.00270

86. Sowers ML, Tang H, Singh VK, Khan A, Mishra A, Restrepo BI, et al. Multi-OMICs analysis reveals metabolic and epigenetic changes associated with macrophage polarization. *J Biol Chem* (2022) 298:102418. doi: 10.1016/j.jbc.2022.102418

87. Cox DJ, Coleman AM, Gogan KM, Phelan JJ, Dunne PJ, Basdeo SA, et al. Inhibiting histone deacetylases in human macrophages promotes glycolysis, IL-1beta, and T helper cell responses to mycobacterium tuberculosis. *Front Immunol* (2020) 11:1609. doi: 10.3389/fimmu.2020.01609

88. Cumming BM, Addicott KW, Adamson JH, Steyn AJ. Mycobacterium tuberculosis induces decelerated bioenergetic metabolism in human macrophages. *Elife* (2018) 7. doi: 10.7554/eLife.39169

89. Mishra A, Singh VK, Jagannath C, Subbian S, Restrepo BI, Gauduin MC, et al. Human macrophages exhibit GM-CSF dependent restriction of mycobacterium tuberculosis infection *via* regulating their self-survival, differentiation and metabolism. *Front Immunol* (2022) 13:859116. doi: 10.3389/fimmu.2022.859116

90. Phelan JJ, McQuaid K, Kenny C, Gogan KM, Cox DJ, Basdeo SA, et al. Desferrioxamine supports metabolic function in primary human macrophages infected with mycobacterium tuberculosis. *Front Immunol* (2020) 11:836. doi: 10.3389/fimmu.2020.00836

91. van Doorn CLR, Steenbergen SAM, Walburg KV, Ottenhoff THM. Pharmacological poly (ADP-ribose) polymerase inhibitors decrease mycobacterium tuberculosis survival in human macrophages. *Front Immunol* (2021) 12:712021. doi: 10.3389/fimmu.2021.712021

92. Pu W, Zhao C, Wazir J, Su Z, Niu M, Song S, et al. Comparative transcriptomic analysis of THP-1-derived macrophages infected with mycobacterium tuberculosis H37Rv, H37Ra and BCG. *J Cell Mol Med* (2021) 25:10504–20. doi: 10.1111/jcmm.16980

93. Gleeson LE, Sheedy FJ, Palsson-McDermott EM, Triglia D, O'Leary SM, O'Sullivan MP, et al. Cutting edge: Mycobacterium tuberculosis induces aerobic glycolysis in human alveolar macrophages that is required for control of intracellular bacillary replication. *J Immunol* (2016) 196:2444–9. doi: 10.4049/jimmunol.1501612

94. Cox DJ, Phelan JJ, Mitermite M, Murphy DM, Leisching G, Thong L, et al. Lactate alters metabolism in human macrophages and improves their ability to kill mycobacterium tuberculosis. *Front Immunol* (2021) 12:663695. doi: 10.3389/fimmu.2021.663695

95. Cahill C, Cox DJ, O'Connell F, Basdeo SA, Gogan KM, O'Maoldomhnaigh C, et al. The effect of tuberculosis antimicrobials on the immunometabolic profiles of primary human macrophages stimulated with mycobacterium tuberculosis. *Int J Mol Sci* (2021) 22. doi: 10.3390/ijms222212189

96. Roy S, Schmeier S, Kaczkowski B, Arner E, Alam T, Ozturk M, et al. Transcriptional landscape of mycobacterium tuberculosis infection in macrophages. *Sci Rep* (2018) 8:6758. doi: 10.1038/s41598-018-24509-6

97. Martinez J, Verbist K, Wang R, Green DR. The relationship between metabolism and the autophagy machinery during the innate immune response. *Cell Metab* (2013) 17:895–900. doi: 10.1016/j.cmet.2013.05.012

98. Galluzzi L, Pietrocola F, Levine B, Kroemer G. Metabolic control of autophagy. *Cell* (2014) 159:1263–76. doi: 10.1016/j.cell.2014.11.006

99. Marino G, Pietrocola F, Eisenberg T, Kong Y, Malik SA, Andryushkova A, et al. Regulation of autophagy by cytosolic acetyl-coenzyme a. *Mol Cell* (2014) 53:710–25. doi: 10.1016/j.molcel.2014.01.016

100. Ye J, Kumanova M, Hart LS, Sloane K, Zhang H, De Panis DN, et al. The GCN2-ATF4 pathway is critical for tumour cell survival and proliferation in response to nutrient deprivation. *EMBO J* (2010) 29:2082–96. doi: 10.1038/emboj.2010.81

101. Roberts DJ, Tan-Sah VP, Ding EY, Smith JM, Miyamoto S. Hexokinase-II positively regulates glucose starvation-induced autophagy through TORC1 inhibition. *Mol Cell* (2014) 53:521–33. doi: 10.1016/j.molcel.2013.12.019

102. Kundu M. Too sweet for autophagy: Hexokinase inhibition of mTORC1 activates autophagy. *Mol Cell* (2014) 53:517–8. doi: 10.1016/j.molcel.2014.02.009

103. Moonira T, Chachra SS, Ford BE, Marin S, Alshawi A, Adam-Primus NS, et al. Metformin lowers glucose 6-phosphate in hepatocytes by activation of glycolysis downstream of glucose phosphorylation. *J Biol Chem* (2020) 295:3330–46. doi: 10.1074/jbc.RA120.012533

104. De Santi M, Baldelli G, Diotallevi A, Galluzzi L, Schiavano GF, Brandi G. Metformin prevents cell tumorigenesis through autophagy-related cell death. *Sci Rep* (2019) 9:66. doi: 10.1038/s41598-018-37247-6

105. Cruz CM, Rinna A, Forman HJ, Ventura AL, Persechini PM, Ojcius DM. ATP activates a reactive oxygen species-dependent oxidative stress response and secretion of proinflammatory cytokines in macrophages. *J Biol Chem* (2007) 282:2871–9. doi: 10.1074/jbc.M608083200

106. Egan D, Kim J, Shaw RJ, Guan KL. The autophagy initiating kinase ULK1 is regulated *via* opposing phosphorylation by AMPK and mTOR. *Autophagy* (2011) 7:643–4. doi: 10.4161/auto.7.6.15123

107. Kim J, Kundu M, Viollet B, Guan KL. AMPK and mTOR regulate autophagy through direct phosphorylation of Ulk1. *Nat Cell Biol* (2011) 13:132–41. doi: 10.1038/ncb2152

108. Hardie DG. Minireview: The AMP-activated protein kinase cascade: The key sensor of cellular energy status. *Endocrinology* (2003) 144:5179–83. doi: 10.1210/en.2003-0982

109. Gwinn DM, Shackelford DB, Egan DF, Mihaylova MM, Mery A, Vasquez DS, et al. AMPK phosphorylation of raptor mediates a metabolic checkpoint. *Mol Cell* (2008) 30:214–26. doi: 10.1016/j.molcel.2008.03.003

110. Inoki K, Li Y, Xu T, Guan KL. Rheb GTPase is a direct target of TSC2 GAP activity and regulates mTOR signaling. *Genes Dev* (2003) 17:1829–34. doi: 10.1101/gad.1110003

111. Yorimitsu T, Zaman S, Broach JR, Klionsky DJ. Protein kinase a and Sch9 cooperatively regulate induction of autophagy in saccharomyces cerevisiae. *Mol Biol Cell* (2007) 18:4180–9. doi: 10.1091/mbc.e07-05-0485

112. Stephan JS, Yeh YY, Ramachandran V, Deminoff SJ, Herman PK. The tor and PKA signaling pathways independently target the Atg1/Atg13 protein kinase complex to control autophagy. *Proc Natl Acad Sci U.S.A.* (2009) 106:17049–54.

113. Menon MB, Dhamija S. Beclin 1 phosphorylation - at the center of autophagy regulation. *Front Cell Dev Biol* (2018) 6:137. doi: 10.3389/fcell.2018.00137

114. Wang RC, Wei Y, An Z, Zou Z, Xiao G, Bhagat G, et al. Akt-mediated regulation of autophagy and tumorigenesis through beclin 1 phosphorylation. *Science* (2012) 338:956–9. doi: 10.1126/science.1225967

115. Qian X, Li X, Cai Q, Zhang C, Yu Q, Jiang Y, et al. Phosphoglycerate kinase 1 phosphorylates Beclin1 to induce autophagy. *Mol Cell* (2017) 65:917–931 e916. doi: 10.1016/j.molcel.2017.01.027

116. Huang X, Liu G, Guo J, Su Z. The PI3K/AKT pathway in obesity and type 2 diabetes. *Int J Biol Sci* (2018) 14:1483–96. doi: 10.7150/ijbs.27173

117. Hoxhaj G, Manning BD. The PI3K-AKT network at the interface of oncogenic signalling and cancer metabolism. *Nat Rev Cancer* (2020) 20:74–88. doi: 10.1038/s41568-019-0216-7

118. Vergadi E, Ieronymaki E, Lyroni K, Vaporidi K, Tsatsanis C. Akt signaling pathway in macrophage activation and M1/M2 polarization. *J Immunol* (2017) 198:1006–14. doi: 10.4049/jimmunol.1601515

119. Zubova SG, Suvorova II, Karpenko MN. Macrophage and microglia polarization: Focus on autophagy-dependent reprogramming. *Front Biosci (Schol Ed)* (2022) 14:3. doi: 10.31083/j.fbs1401003

120. Yu X, Li L, Xia L, Feng X, Chen F, Cao S, et al. Impact of metformin on the risk and treatment outcomes of tuberculosis in diabetics: a systematic review. *BMC Infect Dis* (2019) 19:859. doi: 10.1186/s12879-019-4548-4

121. Collins SL, Oh MH, Sun IH, Chan-Li Y, Zhao L, Powell JD, et al. mTORC1 signaling regulates proinflammatory macrophage function and metabolism. *J Immunol* (2021) 207:913–22. doi: 10.4049/jimmunol.2100230

122. Mercalli A, Calavita I, Dugnani E, Citro A, Cantarelli E, Nano R, et al. Rapamycin unbalances the polarization of human macrophages to M1. *Immunology* (2013) 140:179–90. doi: 10.1111/imm.12126

123. Moruno-Manchon JF, Perez-Jimenez E, Knecht E. Glucose induces autophagy under starvation conditions by a p38 MAPK-dependent pathway. *Biochem J* (2013) 449:497–506. doi: 10.1042/BJ20121122

124. Zhang D, Tang Z, Huang H, Zhou G, Cui C, Weng Y, et al. Metabolic regulation of gene expression by histone lactylation. *Nature* (2019) 574:575–80. doi: 10.1038/s41586-019-1678-1

125. Noe JT, Rendon BE, Geller AE, Conroy LR, Morrissey SM, Young LEA, et al. Lactate supports a metabolic-epigenetic link in macrophage polarization. *Sci Adv* (2021) 7:eabi8602. doi: 10.1126/sciadv.abi8602

126. Guarente L. The logic linking protein acetylation and metabolism. *Cell Metab* (2011) 14:151–3. doi: 10.1016/j.cmet.2011.07.007

127. Anderson KA, Hirschey MD. Mitochondrial protein acetylation regulates metabolism. *Essays Biochem* (2012) 52:23–35. doi: 10.1042/bse0520023

128. Mukherjee S, Hao YH, Orth K. A newly discovered post-translational modification–the acetylation of serine and threonine residues. *Trends Biochem Sci* (2007) 32:210–6. doi: 10.1016/j.tibs.2007.03.007

129. Shi L, Tu BP. Acetyl-CoA and the regulation of metabolism: Mechanisms and consequences. *Curr Opin Cell Biol* (2015) 33:125–31. doi: 10.1016/j.ceb.2015.02.003

130. Watson JA, Fang M, Lowenstein JM. Tricarballylate and hydroxycitrate: Substrate and inhibitor of ATP: Citrate oxaloacetate lyase. *Arch Biochem Biophys* (1969) 135:209–17. doi: 10.1016/0003-9861(69)90532-3

131. Huang W, Wang Z, Lei QY. Acetylation control of metabolic enzymes in cancer: an updated version. *Acta Biochim Biophys Sin (Shanghai)* (2014) 46:204–13. doi: 10.1093/abbs/gmt154

132. Kwon OS, Han MJ, Cha HJ. Suppression of SIRT2 and altered acetylation status of human pluripotent stem cells: Possible link to metabolic switch during reprogramming. *BMB Rep* (2017) 50:435–6. doi: 10.5483/BMBRep.2017.50.9.119

133. Lv L, Li D, Zhao D, Lin R, Chu Y, Zhang H, et al. Acetylation targets the M2 isoform of pyruvate kinase for degradation through chaperone-mediated autophagy and promotes tumor growth. *Mol Cell* (2011) 42:719–30. doi: 10.1016/j.molcel.2011.04.025

134. Park SH, Ozden O, Liu G, Song HY, Zhu Y, Yan Y, et al. SIRT2-mediated deacetylation and tetramerization of pyruvate kinase directs glycolysis and tumor growth. *Cancer Res* (2016) 76:3802–12. doi: 10.1158/0008-5472.CAN-15-2498

135. Bhardwaj A, Das S. SIRT6 deacetylates PKM2 to suppress its nuclear localization and oncogenic functions. *Proc Natl Acad Sci U.S.A.* (2016) 113:E538–547. doi: 10.1073/pnas.1520045113

136. Peeters K, Van Leemputte F, Fischer B, Bonini BM, Quezada H, Tsytlonok M, et al. Fructose-1,6-bisphosphate couples glycolytic flux to activation of ras. *Nat Commun* (2017) 8:922. doi: 10.1038/s41467-017-01019-z

137. Tan VP, Miyamoto S. HK2/hexokinase-II integrates glycolysis and autophagy to confer cellular protection. *Autophagy* (2015) 11:963–4. doi: 10.1080/15548627.2015.1042195

138. Wang F, Wang K, Xu W, Zhao S, Ye D, Wang Y, et al. SIRT5 desuccinylates and activates pyruvate kinase M2 to block macrophage IL-1beta production and to prevent DSS-induced colitis in mice. *Cell Rep* (2017) 19:2331–44. doi: 10.1016/j.celrep.2017.05.065

139. Yucel N, Wang YX, Mai T, Porpiglia E, Lund PJ, Markov G, et al. Glucose metabolism drives histone acetylation landscape transitions that dictate muscle stem cell function. *Cell Rep* (2019) 27:3939–3955 e3936. doi: 10.1016/j.celrep.2019.05.092

140. Zhao S, Torres A, Henry RA, Trefely S, Wallace M, Lee JV, et al. ATP-citrate lyase controls a glucose-to-Acetate metabolic switch. *Cell Rep* (2016) 17:1037–52. doi: 10.1016/j.celrep.2016.09.069

141. Deb DK, Chen Y, Sun J, Wang Y, Li YC. ATP-citrate lyase is essential for high glucose-induced histone hyperacetylation and fibrogenic gene upregulation in mesangial cells. *Am J Physiol Renal Physiol* (2017) 313:F423–9. doi: 10.1152/ajprenal.00029.2017

142. Wellen KE, Hatzivassiliou G, Sachdeva UM, Bui TV, Cross JR, Thompson CB. ATP-citrate lyase links cellular metabolism to histone acetylation. *Science* (2009) 324:1076–80. doi: 10.1126/science.1164097

143. Ivashkiv LB. Epigenetic regulation of macrophage polarization and function. *Trends Immunol* (2013) 34:216–23. doi: 10.1016/j.it.2012.11.001

144. Torres A, Makowski L, Wellen KE. Immunometabolism: Metabolism fine-tunes macrophage activation. *Elife* (2016) 5. doi: 10.7554/eLife.14354

145. Dong Z, Li R, Xu L, Xin K, Xu Y, Shi H, et al. Histone hyperacetylation mediates enhanced IL-1beta production in LPS/IFN-gamma-stimulated macrophages. *Immunology* (2020) 160:183–97. doi: 10.1111/imm.13183

146. Dominguez M, Brune B, Namgaladze D. Exploring the role of ATP-citrate lyase in the immune system. *Front Immunol* (2021) 12:632526. doi: 10.3389/fimmu.2021.632526

147. Lauterbach MA, Hanke JE, Serefidou M, Mangan MSJ, Kolbe CC, Hess T, et al. Toll-like receptor signaling rewires macrophage metabolism and promotes histone acetylation *via* ATP-citrate lyase. *Immunity* (2019) 51:997–1011 e1017. doi: 10.1016/j.immuni.2019.11.009

148. denDekker AD, Davis FM, Joshi AD, Wolf SJ, Allen R, Lipinski J, et al. TNF-alpha regulates diabetic macrophage function through the histone acetyltransferase MOF. *JCI Insight* (2020) 5. doi: 10.1172/jci.insight.132306

149. Kelly B, O'Neill LA. Metabolic reprogramming in macrophages and dendritic cells in innate immunity. *Cell Res* (2015) 25:771–84. doi: 10.1038/cr.2015.68

150. Vlad ML, Manea SA, Lazar AG, Raicu M, Muresian H, Simionescu M, et al. Histone acetyltransferase-dependent pathways mediate upregulation of NADPH oxidase 5 in human macrophages under inflammatory conditions: A potential mechanism of reactive oxygen species overproduction in atherosclerosis. *Oxid Med Cell Longev* (2019) 20193201062. doi: 10.1155/2019/3201062

151. Bories GFP, Leitinger N. Macrophage metabolism in atherosclerosis. *FEBS Lett* (2017) 591:3042–60. doi: 10.1002/1873-3468.12786

152. Baardman J, Verberk SGS, van der Velden S, Gijbels MJJ, van Roomen C, Sluimer JC, et al. Macrophage ATP citrate lyase deficiency stabilizes atherosclerotic plaques. *Nat Commun* (2020) 11:6296. doi: 10.1038/s41467-020-20141-z

153. Infantino V, Convertini P, Cucci L, Panaro MA, Di Noia MA, Calvello R, et al. The mitochondrial citrate carrier: A new player in inflammation. *Biochem J* (2011) 438:433–6. doi: 10.1042/BJ20111275

154. Infantino V, Iacobazzi V, Palmieri F, Menga A. ATP-citrate lyase is essential for macrophage inflammatory response. *Biochem Biophys Res Commun* (2013) 440:105–11. doi: 10.1016/j.bbrc.2013.09.037

155. Namgaladze D, Zukunft S, Schnutgen F, Kurrle N, Fleming I, Fuhrmann D, et al. Polarization of human macrophages by interleukin-4 does not require ATP-citrate lyase. *Front Immunol* (2018) 9:2858. doi: 10.3389/fimmu.2018.02858

156. Fullgrabe J, Lynch-Day MA, Heldring N, Li W, Struijk RB, Ma Q, et al. The histone H4 lysine 16 acetyltransferase hMOF regulates the outcome of autophagy. *Nature* (2013) 500:468–71. doi: 10.1038/nature12313

157. Hamaidi I, Kim S. Sirtuins are crucial regulators of T cell metabolism and functions. *Exp Mol Med* (2022) 54:207–15. doi: 10.1038/s12276-022-00739-7

158. Vachharajani VT, Liu T, Wang X, Hoth JJ, Yoza BK, McCall CE. Sirtuins link inflammation and metabolism. *J Immunol Res* (2016) 2016:8167273. doi: 10.1155/2016/8167273

159. Warren JL, MacIver NJ. Regulation of adaptive immune cells by sirtuins. *Front Endocrinol (Lausanne)* (2019) 10:466. doi: 10.3389/fendo.2019.00466

160. Anderson KA, Madsen AS, Olsen CA, Hirschey MD. Metabolic control by sirtuins and other enzymes that sense NAD(+), NADH, or their ratio. *Biochim Biophys Acta Bioenerg* (2017) 1858:991–8. doi: 10.1016/j.bbabio.2017.09.005

161. Aguilar-Arnal L, Ranjit S, Stringari C, Orozco-Solis R, Gratton E, Sassone-Corsi P. Spatial dynamics of SIRT1 and the subnuclear distribution of NADH species. *Proc Natl Acad Sci U.S.A.* (2016) 113:12715–20.

162. Liang F, Kume S, Koya D. SIRT1 and insulin resistance. *Nat Rev Endocrinol* (2009) 5:367–73. doi: 10.1038/nrendo.2009.101

163. Moynihan KA, Grimm AA, Plueger MM, Bernal-Mizrachi E, Ford E, Cras-Meneur C, et al. Increased dosage of mammalian Sir2 in pancreatic beta cells enhances glucose-stimulated insulin secretion in mice. *Cell Metab* (2005) 2:105–17. doi: 10.1016/j.cmet.2005.07.001

164. Bordone L, Motta MC, Picard F, Robinson A, Jhala US, Apfeld J, et al. Sirt1 regulates insulin secretion by repressing UCP2 in pancreatic beta cells. *PloS Biol* (2006) 4:e31.

165. Jia Y, Zheng Z, Wang Y, Zhou Q, Cai W, Jia W, et al. SIRT1 is a regulator in high glucose-induced inflammatory response in RAW264.7 cells. *PloS One* (2015) 10:e0120849.

166. Civitarese AE, Carling S, Heilbronn LK, Hulver MH, Ukropcova B, Deutsch WA, et al. Calorie restriction increases muscle mitochondrial biogenesis in healthy humans. *PloS Med* (2007) 4:e76. doi: 10.1371/journal.pmed.0040076

167. Bordone L, Guarente L. Calorie restriction, SIRT1 and metabolism: Understanding longevity. *Nat Rev Mol Cell Biol* (2005) 6:298–305. doi: 10.1038/nrm1616

168. Latifkar A, Ling L, Hingorani A, Johansen E, Clement A, Zhang X, et al. Loss of sirtuin 1 alters the secretome of breast cancer cells by impairing lysosomal integrity. *Dev Cell* (2019) 49:393–408 e397. doi: 10.1016/j.devcel.2019.03.011

169. Di Malta C, Cinque L, Settembre C. Transcriptional regulation of autophagy: Mechanisms and diseases. *Front Cell Dev Biol* (2019) 7:114. doi: 10.3389/fcell.2019.00114

170. Lee IH, Cao L, Mostoslavsky R, Lombard DB, Liu J, Bruns NE, et al. A role for the NAD-dependent deacetylase Sirt1 in the regulation of autophagy. *Proc Natl Acad Sci U.S.A.* (2008) 105:3374–9.

171. Price NL, Gomes AP, Ling AJ, Duarte FV, Martin-Montalvo A, North BJ, et al. SIRT1 is required for AMPK activation and the beneficial effects of resveratrol on mitochondrial function. *Cell Metab* (2012) 15:675–90. doi: 10.1016/j.cmet.2012.04.003

172. Ghosh HS, McBurney M, Robbins PD. SIRT1 negatively regulates the mammalian target of rapamycin. *PloS One* (2010) 5:e9199. doi: 10.1371/journal.pone.0009199

173. Cheng CY, Gutierrez NM, Marzuki MB, Lu X, Foreman TW, Paleja B, et al. Host sirtuin 1 regulates mycobacterial immunopathogenesis and represents a therapeutic target against tuberculosis. *Sci Immunol* (2017) 2. doi: 10.1126/sciimmunol.aaj1789

174. Yang H, Hu J, Chen YJ, Ge B. Role of Sirt1 in innate immune mechanisms against mycobacterium tuberculosis *via* the inhibition of TAK1 activation. *Arch Biochem Biophys* (2019) 667:49–58. doi: 10.1016/j.abb.2019.04.006

175. Yang H, Chen J, Chen Y, Jiang Y, Ge B, Hong L. Sirtuin inhibits m. tuberculosis -induced apoptosis in macrophage through glycogen synthase kinase-3beta. *Arch Biochem Biophys* (2020) 694:108612. doi: 10.1016/j.abb.2020.108612

176. Yang H, Chen J, Chen Y, Jiang Y, Ge B, Hong L. Sirt1 activation negatively regulates overt apoptosis in mtb-infected macrophage through bax. *Int Immunopharmacol* (2021) 91:107283. doi: 10.1016/j.intimp.2020.107283

177. Wang J, Kim TH, Ahn MY, Lee J, Jung JH, Choi WS, et al. Sirtinol, a class III HDAC inhibitor, induces apoptotic and autophagic cell death in MCF-7 human breast cancer cells. *Int J Oncol* (2012) 41:1101–9. doi: 10.3892/ijo.2012.1534

178. Ng F, Tang BL. Sirtuins' modulation of autophagy. *J Cell Physiol* (2013) 228:2262–70. doi: 10.1002/jcp.24399

179. Klein MA, Denu JM. Biological and catalytic functions of sirtuin 6 as targets for small-molecule modulators. *J Biol Chem* (2020) 295:11021–41. doi: 10.1074/jbc.REV120.011438

180. Bresque M, Cal K, Perez-Torrado V, Colman L, Rodriguez-Duarte J, Vilaseca C, et al. SIRT6 stabilization and cytoplasmic localization in macrophages regulates acute and chronic inflammation in mice. *J Biol Chem* (2022) 298:101711. doi: 10.1016/j.jbc.2022.101711

181. Dantoft W, Robertson KA, Watkins WJ, Strobl B, Ghazal P. Metabolic regulators nampt and Sirt6 serially participate in the macrophage interferon antiviral cascade. *Front Microbiol* (2019) 10:355. doi: 10.3389/fmicb.2019.00355

182. Praveen Prakhar BB, Mukherjee T, Kolthur-Seetharam U, Sundaresan NR, Rajmani RS, Balaji KN. G9a and Sirtuin6 epigenetically modulate host cholesterol accumulation to facilitate mycobacterial survival. *bioRxiv* (2021). doi: 10.1101/2021.02.27.433201

183. Blank MF, Chen S, Poetz F, Schnolzer M, Voit R, Grummt I. SIRT7-dependent deacetylation of CDK9 activates RNA polymerase II transcription. *Nucleic Acids Res* (2017) 45:2675–86. doi: 10.1093/nar/gkx053

184. Blank MF, Grummt I. The seven faces of SIRT7. *Transcription* (2017) 8:67–74. doi: 10.1080/21541264.2016.1276658

185. Simonet NG, Thackray JK, Vazquez BN, Ianni A, Espinosa-Alcantud M, Morales-Sanfrutos J, et al. SirT7 auto-ADP-ribosylation regulates glucose starvation response through mH2A1. *Sci Adv* (2020) 6:eaaz2590. doi: 10.1126/sciadv.aaz2590

186. Hamaidi I, Zhang L, Kim N, Wang MH, Iclozan C, Fang B, et al. Sirt2 inhibition enhances metabolic fitness and effector functions of tumor-reactive T cells. *Cell Metab* (2020) 32:420–436 e412. doi: 10.1016/j.cmet.2020.07.008

187. Roychowdhury S, Gandhirajan A, Kibler C, Wang X, Vachharajani V. Sirtuin 2 dysregulates autophagy in high-Fat-Exposed immune-tolerant macrophages. *Cells* (2021) 10. doi: 10.3390/cells10040731

188. Cardoso F, Castro F, Moreira-Teixeira L, Sousa J, Torrado E, Silvestre R, et al. Myeloid sirtuin 2 expression does not impact long-term mycobacterium tuberculosis control. *PloS One* (2015) 10:e0131904. doi: 10.1371/journal.pone.0131904

189. Kurundkar D, Kurundkar AR, Bone NB, Becker EJJr., Liu W, Chacko B, et al. SIRT3 diminishes inflammation and mitigates endotoxin-induced acute lung injury. *JCI Insight* (2019) 4. doi: 10.1172/jci.insight.120722

190. Smulan LJ, Martinez N, Kiritsy MC, Kativhu C, Cavallo K, Sassetti CM, et al. Sirtuin 3 downregulation in mycobacterium tuberculosis-infected macrophages reprograms mitochondrial metabolism and promotes cell death. *mBio* (2021) 12. doi: 10.1128/mBio.03140-20

191. Kim TS, Jin YB, Kim YS, Kim S, Kim JK, Lee HM, et al. SIRT3 promotes antimycobacterial defenses by coordinating mitochondrial and autophagic functions. *Autophagy* (2019) 15:1356–75. doi: 10.1080/15548627.2019.1582743

192. Wu T, Jiao L, Bai H, Hu X, Wang M, Zhao Z, et al. The dominant model analysis of Sirt3 genetic variants is associated with susceptibility to tuberculosis in a Chinese han population. *Mol Genet Genomics* (2020) 295:1155–62. doi: 10.1007/s00438-020-01685-7

193. Haigis MC, Mostoslavsky R, Haigis KM, Fahie K, Christodoulou DC, Murphy AJ, et al. SIRT4 inhibits glutamate dehydrogenase and opposes the effects of calorie restriction in pancreatic beta cells. *Cell* (2006) 126:941–54. doi: 10.1016/j.cell.2006.06.057

194. Chang HC, Guarente L. SIRT1 and other sirtuins in metabolism. *Trends Endocrinol Metab* (2014) 25:138–45. doi: 10.1016/j.tem.2013.12.001

195. Tao J, Zhang J, Ling Y, McCall CE, Liu TF. Mitochondrial sirtuin 4 resolves immune tolerance in monocytes by rebalancing glycolysis and glucose oxidation homeostasis. *Front Immunol* (2018) 9:419. doi: 10.3389/fimmu.2018.00419

196. Du J, Zhou Y, Su X, Yu JJ, Khan S, Jiang H, et al. Sirt5 is a NAD-dependent protein lysine demalonylase and desuccinylase. *Science* (2011) 334:806–9. doi: 10.1126/science.1207861

197. Nakagawa T, Lomb DJ, Haigis MC, Guarente L. SIRT5 deacetylates carbamoyl phosphate synthetase 1 and regulates the urea cycle. *Cell* (2009) 137:560–70. doi: 10.1016/j.cell.2009.02.026

198. Lukey MJ, Greene KS, Cerione RA. Lysine succinylation and SIRT5 couple nutritional status to glutamine catabolism. *Mol Cell Oncol* (2020) 7:1735284. doi: 10.1080/23723556.2020.1735284

199. Eng CH, Yu K, Lucas J, White E, Abraham RT. Ammonia derived from glutaminolysis is a diffusible regulator of autophagy. *Sci Signal* (2010) 3:ra31. doi: 10.1126/scisignal.2000911

200. Polletta L, Vernucci E, Carnevale I, Arcangeli T, Rotili D, Palmerio S, et al. SIRT5 regulation of ammonia-induced autophagy and mitophagy. *Autophagy* (2015) 11:253–70. doi: 10.1080/15548627.2015.1009778

201. Rardin MJ, He W, Nishida Y, Newman JC, Carrico C, Danielson SR, et al. SIRT5 regulates the mitochondrial lysine succinylome and metabolic networks. *Cell Metab* (2013) 18:920–33. doi: 10.1016/j.cmet.2013.11.013

202. Zhang M, Wu J, Sun R, Tao X, Wang X, Kang Q, et al. SIRT5 deficiency suppresses mitochondrial ATP production and promotes AMPK activation in response to energy stress. *PloS One* (2019) 14:e0211796. doi: 10.1371/journal.pone.0211796

203. Zhang Y, Bharathi SS, Rardin MJ, Lu J, Maringer KV, Sims-Lucas S, et al. Lysine desuccinylase SIRT5 binds to cardiolipin and regulates the electron transport chain. *J Biol Chem* (2017) 292:10239–49. doi: 10.1074/jbc.M117.785022

204. Gu W, Qian Q, Xu Y, Xu X, Zhang L, He S, et al. SIRT5 regulates autophagy and apoptosis in gastric cancer cells. *J Int Med Res* (2021) 49:300060520986355. doi: 10.1177/0300060520986355

205. Qin K, Han C, Zhang H, Li T, Li N, Cao X. NAD(+) dependent deacetylase sirtuin 5 rescues the innate inflammatory response of endotoxin tolerant macrophages by promoting acetylation of p65. *J Autoimmun* (2017) 81:120–9. doi: 10.1016/j.jaut.2017.04.006

206. McCudden CR, Powers-Lee SG. Required allosteric effector site for n-acetylglutamate on carbamoyl-phosphate synthetase I. *J Biol Chem* (1996) 271:18285–94. doi: 10.1074/jbc.271.30.18285

207. Valaei K, Mehrabani J, Wong A. Effects of l-citrulline supplementation on nitric oxide and antioxidant markers after high-intensity interval exercise in young men: A randomized controlled trial. *Br J Nutr* (2021), 1–23.

208. Fast W, Nikolic D, Van Breemen RB, Silverman RB. Mechanistic studies of the inactivation of inducible nitric oxide synthase by N^5-(1-iminoethyl)-L-ornithine (L-NIO). *J Am Chrm. Soc* (1999) 121:903–16.

209. Vitecek J, Lojek A, Valacchi G, Kubala L. Arginine-based inhibitors of nitric oxide synthase: therapeutic potential and challenges. *Mediators Inflammation* (2012) 2012:318087. doi: 10.1155/2012/318087

210. Leiper J, Vallance P. Biological significance of endogenous methylarginines that inhibit nitric oxide synthases. *Cardiovasc Res* (1999) 43:542–8. doi: 10.1016/S0008-6363(99)00162-5

211. Vallance P, Leone A, Calver A, Collier J, Moncada S. Accumulation of an endogenous inhibitor of nitric oxide synthesis in chronic renal failure. *Lancet* (1992) 339:572–5. doi: 10.1016/0140-6736(92)90865-Z

212. Schrader SM, Botella H, Jansen R, Ehrt S, Rhee K, Nathan C, et al. Multiform antimicrobial resistance from a metabolic mutation. *Sci Adv* (2021) 7. doi: 10.1126/sciadv.abh2037

213. Minhas PS, Liu L, Moon PK, Joshi AU, Dove C, Mhatre S, et al. Macrophage *de novo* NAD(+) synthesis specifies immune function in aging and inflammation. *Nat Immunol* (2019) 20:50–63. doi: 10.1038/s41590-018-0255-3

214. Cameron AM, Castoldi A, Sanin DE, Flachsmann LJ, Field CS, Puleston DJ, et al. Inflammatory macrophage dependence on NAD(+) salvage is a consequence of reactive oxygen species-mediated DNA damage. *Nat Immunol* (2019) 20:420–32. doi: 10.1038/s41590-019-0336-y

215. Billingham LK, Chandel NS. NAD-biosynthetic pathways regulate innate immunity. *Nat Immunol* (2019) 20:380–2. doi: 10.1038/s41590-019-0353-x

216. Pajuelo D, Gonzalez-Juarbe N, Tak U, Sun J, Orihuela CJ, Niederweis M. NAD(+) depletion triggers macrophage necroptosis, a cell death pathway exploited by mycobacterium tuberculosis. *Cell Rep* (2018) 24:429–40. doi: 10.1016/j.celrep.2018.06.042

217. Sun J, Siroy A, Lokareddy RK, Speer A, Doornbos KS, Cingolani G, et al. The tuberculosis necrotizing toxin kills macrophages by hydrolyzing NAD. *Nat Struct Mol Biol* (2015) 22:672–8. doi: 10.1038/nsmb.3064

218. Gan H, He X, Duan L, Mirabile-Levens E, Kornfeld H, Remold HG. Enhancement of antimycobacterial activity of macrophages by stabilization of inner mitochondrial membrane potential. *J Infect Dis* (2005) 191:1292–300. doi: 10.1086/428906

219. Chandra P, He L, Zimmerman M, Yang G, Koster S, Ouimet M, et al. Inhibition of fatty acid oxidation promotes macrophage control of mycobacterium tuberculosis. *mBio* (2020) 11. doi: 10.1128/mBio.01139-20

220. Bhaskar A, Kumar S, Khan MZ, Singh A, Dwivedi VP, Nandicoori VK. Host sirtuin 2 as an immunotherapeutic target against tuberculosis. *Elife* (2020) 9. doi: 10.7554/eLife.55415

221. Hallows WC, Lee S, Denu JM. Sirtuins deacetylate and activate mammalian acetyl-CoA synthetases. *Proc Natl Acad Sci U.S.A.* (2006) 103:10230–5.

222. Bosch-Presegue L, Vaquero A. Sirtuin-dependent epigenetic regulation in the maintenance of genome integrity. *FEBS J* (2015) 282:1745–67. doi: 10.1111/febs.13053

223. Zhang S, Liu Y, Zhou X, Ou M, Xiao G, Li F, et al. Sirtuin 7 regulates nitric oxide production and apoptosis to promote mycobacterial clearance in macrophages. *Front Immunol* (2021) 12:779235. doi: 10.3389/fimmu.2021.779235

224. Smulan L, Kornfeld H, Singhal A. Sirtuin deacetylases: Linking mycobacterial infection and host metabolism (2021) sirtuin deacetylases: Linking mycobacterial infection and host metabolism. In: Karakousis PC, Hafner R, Gennaro ML, editors. *Advances in host-directed therapies against tuberculosis*. Cham: Springer (2021). doi: 10.1007/978-3-030-56905-1_2

225. Cuyas E, Verdura S, Llorach-Pares L, Fernandez-Arroyo S, Joven J, Martin-Castillo B, et al. Metformin is a direct SIRT1-activating compound: Computational modeling and experimental validation. *Front Endocrinol (Lausanne)* (2018) 9:657. doi: 10.3389/fendo.2018.00657

226. Naicker N, Sigal A, Naidoo K. Metformin as host-directed therapy for TB treatment: Scoping review. *Front Microbiol* (2020) 11:435. doi: 10.3389/fmicb.2020.00435

227. Kozako T, Suzuki T, Yoshimitsu M, Arima N, Honda S, Soeda S. Anticancer agents targeted to sirtuins. *Molecules* (2014) 19:20295–313. doi: 10.3390/molecules191220295

228. Rozwarski DA, Grant GA, Barton DH, Jacobs WRJr., Sacchettini JC. Modification of the NADH of the isoniazid target (InhA) from mycobacterium tuberculosis. *Science* (1998) 279:98–102. doi: 10.1126/science.279.5347.98

229. Sharma V, Grubmeyer C, Sacchettini JC. Crystal structure of quinolinic acid phosphoribosyltransferase from mmycobacterium tuberculosis: a potential TB drug target. *Structure* (1998) 6:1587–99. doi: 10.1016/S0969-2126(98)00156-7

230. Kim H, Shibayama K, Rimbara E, Mori S. Biochemical characterization of quinolinic acid phosphoribosyltransferase from mycobacterium tuberculosis H37Rv and inhibition of its activity by pyrazinamide. *PloS One* (2014) 9:e100062. doi: 10.1371/journal.pone.0100062

231. Malik SS, Patterson DN, Ncube Z, Toth EA. The crystal structure of human quinolinic acid phosphoribosyltransferase in complex with its inhibitor phthalic acid. *Proteins* (2014) 82:405–14. doi: 10.1002/prot.24406

232. Begley TP, Kinsland C, Mehl RA, Osterman A, Dorrestein P. The biosynthesis of nicotinamide adenine dinucleotides in bacteria. *Vitam Horm* (2001) 61:103–19. doi: 10.1016/S0083-6729(01)61003-3

233. Jansen RS, Mandyoli L, Hughes R, Wakabayashi S, Pinkham JT, Selbach B, et al. Aspartate aminotransferase Rv3722c governs aspartate-dependent nitrogen metabolism in mycobacterium tuberculosis. *Nat Commun* (2020) 11:1960. doi: 10.1038/s41467-020-15876-8

234. Kurita K, Ohta H, Shirakawa I, Tanaka M, Kitaura Y, Iwasaki Y, et al. Macrophages rely on extracellular serine to suppress aberrant cytokine production. *Sci Rep* (2021) 11:11137. doi: 10.1038/s41598-021-90086-w

235. Rodriguez AE, Ducker GS, Billingham LK, Martinez CA, Mainolfi N, Suri V, et al. Serine metabolism supports macrophage IL-1beta production. *Cell Metab* (2019) 29:1003–1011 e1004.

236. Borah K, Beyss M, Theorell A, Wu H, Basu P, Mendum TA, et al. Intracellular mycobacterium tuberculosis exploits multiple host nitrogen sources during growth in human macrophages. *Cell Rep* (2019) 29:3580–3591 e3584. doi: 10.1016/j.celrep.2019.11.037

237. Ji J, Xu Y, Zheng M, Luo C, Lei H, Qu H, et al. Methionine attenuates lipopolysaccharide-induced inflammatory responses *via* DNA methylation in macrophages. *ACS Omega* (2019) 4:2331–6. doi: 10.1021/acsomega.8b03571

238. Berney M, Berney-Meyer L, Wong KW, Chen B, Chen M, Kim J, et al. Essential roles of methionine and s-adenosylmethionine in the autarkic lifestyle of mycobacterium tuberculosis. *Proc Natl Acad Sci U.S.A.* (2015) 112:10008–13.

239. Chaton CT, Rodriguez ES, Reed RW, Li J, Kenner CW, Korotkov KV. Structural analysis of mycobacterial homoserine transacetylases central to methionine biosynthesis reveals druggable active site. *Sci Rep* (2019) 9:20267. doi: 10.1038/s41598-019-56722-2

240. Hasenoehrl EJ, Rae Sajorda D, Berney-Meyer L, Johnson S, Tufariello JM, Fuhrer T, et al. Derailing the aspartate pathway of mycobacterium tuberculosis to eradicate persistent infection. *Nat Commun* (2019) 10:4215. doi: 10.1038/s41467-019-12224-3

241. Colak G, Pougovkina O, Dai L, Tan M, Te Brinke H, Huang H, et al. Proteomic and biochemical studies of lysine malonylation suggest its malonic aciduria-associated regulatory role in mitochondrial function and fatty acid oxidation. *Mol Cell Proteomics* (2015) 14:3056–71. doi: 10.1074/mcp.M115.048850

242. Park J, Chen Y, Tishkoff DX, Peng C, Tan M, Dai L, et al. SIRT5-mediated lysine desuccinylation impacts diverse metabolic pathways. *Mol Cell* (2013) 50:919–30. doi: 10.1016/j.molcel.2013.06.001

243. Giblin W, Bringman-Rodenbarger L, Guo AH, Kumar S, Monovich AC, Mostafa AM, et al. The deacylase SIRT5 supports melanoma viability by influencing chromatin dynamics. *J Clin Invest* (2021) 131. doi: 10.1172/JCI138926

244. Yang X, Wang Z, Li X, Liu B, Liu M, Liu L, et al. SHMT2 desuccinylation by SIRT5 drives cancer cell proliferation. *Cancer Res* (2018) 78:372–86. doi: 10.1158/0008-5472.CAN-17-1912

245. Gao X, Reid MA, Kong M, Locasale JW. Metabolic interactions with cancer epigenetics. *Mol Aspects Med* (2017) 54:50–7. doi: 10.1016/j.mam.2016.09.001

246. Wang C, Wan X, Yu T, Huang Z, Shen C, Qi Q, et al. Acetylation stabilizes phosphoglycerate dehydrogenase by disrupting the interaction of E3 ligase RNF5 to promote breast tumorigenesis. *Cell Rep* (2020) 32:108021. doi: 10.1016/j.celrep.2020.108021

frontiers | Frontiers in Immunology

TYPE Review
PUBLISHED 16 June 2023
DOI 10.3389/fimmu.2023.1206406

OPEN ACCESS

EDITED BY
Shicheng Guo,
University of Wisconsin-Madison,
United States

REVIEWED BY
Hai-Jian Sun,
National University of Singapore, Singapore
Lin Deng,
Southern University of Science and Technology, China
Yu Wang,
University of Virginia, United States
Lingjie Sang,
University of Texas Southwestern Medical Center, United States

*CORRESPONDENCE
Hanmin Liu
liuhm@scu.edu.cn
Jingxin Liu
liujingxin@sztu.edu.cn
Bin Zeng
zengbin@sztu.edu.cn

†These authors have contributed equally to this work

RECEIVED 15 April 2023
ACCEPTED 30 May 2023
PUBLISHED 16 June 2023

CITATION
Mao M, Song S, Li X, Lu J, Li J, Zhao W, Liu H, Liu J and Zeng B (2023) Advances in epigenetic modifications of autophagic process in pulmonary hypertension. *Front. Immunol.* 14:1206406. doi: 10.3389/fimmu.2023.1206406

Advances in epigenetic modifications of autophagic process in pulmonary hypertension

Min Mao[1,2,3,4,5†], Shasha Song[6†], Xin Li[1,2,3,4,5], Jiayao Lu[6], Jie Li[7,8], Weifang Zhao[9], Hanmin Liu[1,2,3,4,5*], Jingxin Liu[2*] and Bin Zeng[2*]

[1]Department of Pediatric Pulmonology and Immunology, West China Second University Hospital, Sichuan University, Chengdu, China, [2]Key Laboratory of Birth Defects and Related Diseases of Women and Children (Sichuan University), Ministry of Education, Chengdu, China, [3]National Health Commission (NHC) Key Laboratory of Chronobiology (Sichuan University), Chengdu, China, [4]The Joint Laboratory for Lung Development and Related Diseases of West China Second University Hospital, Sichuan University and School of Life Sciences of Fudan University, West China Institute of Women and Children's Health, West China Second University Hospital, Sichuan University, Chengdu, China, [5]Sichuan Birth Defects Clinical Research Center, West China Second University Hospital, Sichuan University, Chengdu, China, [6]College of Pharmacy, Shenzhen Technology University, Shenzhen, China, [7]Marketing Department, Shenzhen Reyson Biotechnology Co., Ltd, Shenzhen, China, [8]Nanjing Evertop Electronics Ltd., Nanjing, China, [9]Quality Management Department International Registration, North China Pharmaceutical Co., Ltd. (NCPC), Hebei Huamin Pharmaceutical Co., Ltd., Shijiazhuang, China

Pulmonary hypertension is characterized by pulmonary arterial remodeling that results in increased pulmonary vascular resistance, right ventricular failure, and premature death. It is a threat to public health globally. Autophagy, as a highly conserved self-digestion process, plays crucial roles with autophagy-related (ATG) proteins in various diseases. The components of autophagy in the cytoplasm have been studied for decades and multiple studies have provided evidence of the importance of autophagic dysfunction in pulmonary hypertension. The status of autophagy plays a dynamic suppressive or promotive role in different contexts and stages of pulmonary hypertension development. Although the components of autophagy have been well studied, the molecular basis for the epigenetic regulation of autophagy is less understood and has drawn increasing attention in recent years. Epigenetic mechanisms include histone modifications, chromatin modifications, DNA methylation, RNA alternative splicing, and non-coding RNAs, which control gene activity and the development of an organism. In this review, we summarize the current research progress on epigenetic modifications in the autophagic process, which have the potential to be crucial and powerful therapeutic targets against the autophagic process in pulmonary hypertension development.

KEYWORDS

pulmonary hypertension, autophagy, epigenetic modifications, histone modifications, DNA methylation, alternative RNA splicing

1 Introduction

Autophagy has been implicated in multiple physiological processes that are important for human health and disease (1, 2). It is an adaptive process that occurs in response to different forms of stress, including hypoxia, infection, and nutrition deprivation. The damaged organelles, pathogen, aggregated proteins, or long-lived proteins are collected, delivered to lysosomes, digested by lysosomal hydrolases, and recycled to produce amino acids and fatty acids necessary for ATP production and cellular response (3). Multiple signaling pathways and autophagy-related proteins (ATG proteins) have been implicated in completing the autophagic process. So far, according to the human autophagy database developed by the Laboratory of Experimental Cancer Research headed by Dr. Guy Berchem, more than 200 different autophagic genes directly or indirectly modulating the autophagic process have been discovered. More than 40 genes encoding ATG proteins have been identified in yeast, and most of the genes (ATG1-ATG10, ATG12-ATG14, ATG16-ATG18) are conserved between yeast and mammals, which indicates the autophagic process as an intracellular evolutionarily conserved degradation process (4). The so-called core ATG proteins essential for autophagic process completion undergo different modifications, including epigenetic modifications, acetylation, phosphorylation, and ubiquitylation, which affect the role of autophagy-related proteins in the autophagic process. Numerous signaling pathways serve as upstream regulators of autophagy, including the NF-κB, STAT3, p53, FOXO, Sirt1, and HDAC signaling pathways. These signaling pathways also have significant influences on angiogenesis, endothelial-to-mesenchymal transition, and programed cell death, resulting in vascular remodeling and vascular resistance. Epigenetics refers to the regulation of epigenomic gene expression by epigenetic alterations (DNA methylation, histone modifications, and alternative RNA splicing) that are independent of changes in gene sequences and are heritable. Factors such as DNA methylation, histone modifications, and alternative RNA spliced isoforms are responses to changes in environmental stimuli that interact to regulate gene expression and control cellular phenotypes, all of which are necessary to maintain environmental stability in the body and contribute to normal physiological functioning. The epigenetic modifications of these signaling pathways affect the expression, stability, and function of autophagy-related proteins.

Direct links exist between autophagy and pulmonary hypertension (PH) according to various research. Pulmonary hypertension is a fatal and heterogeneous disease characterized by elevated pulmonary vascular resistance and pulmonary artery pressure, resulting in the remodeling of the pulmonary vasculature (5). PH is divided into five categories according to inherited or unknown causes, heart disease, lung disease, the blockage of blood vessels, or other medical conditions such as some blood disorders (Figure 1) (6). The pathologic process of PH begins with vasoconstriction and remodeling of the small pulmonary arteries, leading to an increase in pulmonary vascular resistance (PVR). This can be caused by a variety of factors including genetic mutations, viral infections, and exposure to toxins such as cigarette smoke. As PVR increases, the right ventricle must work harder to pump blood through the lungs into the left side of the heart, leading to right ventricular hypertrophy and eventually right heart failure (7). The primary cellular mechanism underlying the pathologic progression of PH is abnormal smooth muscle cell and endothelial cell proliferation. As the disease progresses, these cells proliferate excessively and invade the surrounding extracellular matrix, leading to a narrowing of the lumen of the pulmonary artery and increasing the resistance to blood flow. Additionally, there is also a shift towards a pro-inflammatory and thrombotic state, further contributing to disease progression. The histopathological changes in PH include intimal fibrosis, medial hypertrophy, and adventitial remodeling. Intimal fibrosis refers to the thickening of the intima, or innermost layer, of the pulmonary artery due to a buildup of collagen and other

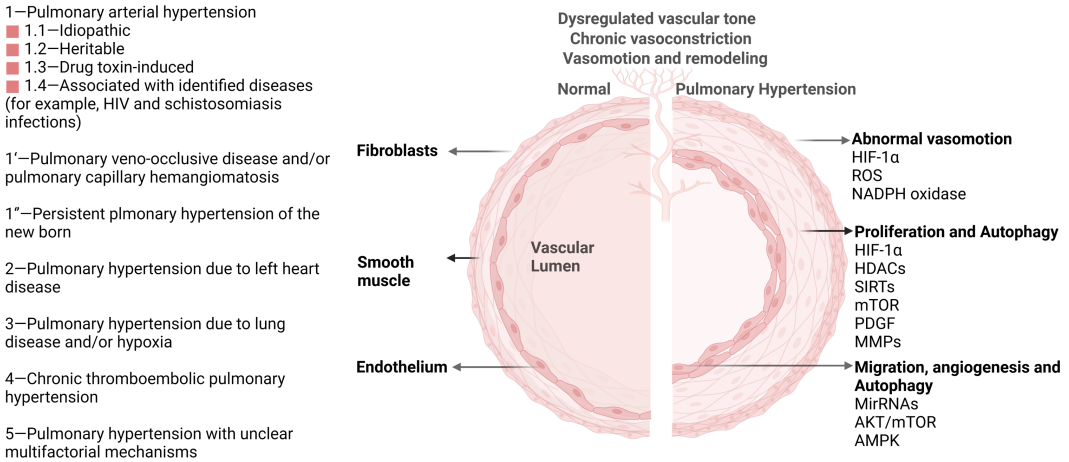

FIGURE 1
Pulmonary hypertension classification and vascular pathological progression in pulmonary hypertension. As agreed at the 6th World Symposium on Pulmonary Hypertension in 2018, pulmonary hypertension is now classified into five groups (Left) (6). Multiple signaling pathways (HIF-1α, HDACs, AKT/mTOR, et. al) participate in the pathological progression and phenotype in PH (Right). These important pathways also activate autophagy and impact PH progression through the autophagy process.

extracellular matrix proteins. Medial hypertrophy refers to the thickening of the media, or middle layer, of the pulmonary artery due to an increase in smooth muscle cell mass. Adventitial remodeling involves changes in the outermost layer of the pulmonary artery, including inflammation and fibrosis (8). Autophagy has been discovered to be upregulated in PH patients compared with healthy controls. Administration of an autophagy antagonist prevents the progression of experimental pulmonary hypertension (9). This phenomenon provides a clue about the importance of discovering the underlying key regulatory mechanism of autophagy in PH. As a homeostatic mechanism essential for cell survival, autophagy activation under stress affects various pathological processes of pulmonary hypertension, including disrupted redox balance, blocked apoptosis, inflammation, angiogenesis, vascular calcification, and remodeling (10, 11). Understanding these mechanisms of autophagy will provide novel therapeutic targets for PH. Despite the great advances in the investigation of the autophagic process in PH, the mechanism of autophagy remains elusive. In this review, we focus on epigenetic modification in autophagic process of PH.

2 The autophagic process in PH

Autophagy is a conserved adaptive process that has played an important role in human disease. During the development of PH, the cellular autophagy mechanism, which removes useless materials such as aging, damaged, and abnormal cells, plays different roles at different stages of progression. In the early stage of PH, autophagy plays a protective role. Studies have shown that the expression levels of autophagy-related proteins are low in the lung tissues of patients with PH, but an increase in autophagy levels through drug or genetic intervention can alleviate the pathological damage of PH (12). Autophagy can clear harmful molecules such as excess proteins, organelles, and oxidative products that cause cell death, promote cell survival, and function maintenance. In addition, in the early stage of PH, autophagy can also regulate the reactive oxygen species (ROS) level of endothelial cells, inhibit pulmonary vascular contraction, and maintain normal blood flow. In the mid-to-late stages of PH, autophagy plays a dual role. On the one hand, autophagy activation can protect pulmonary artery endothelial cells (PAECs) from apoptosis (13). Endothelial dysfunction and apoptosis are key features of PH, and autophagy activation can maintain endothelial cell survival by clearing damaged organelles and proteins. On the other hand, excessive autophagy activation in the mid-to-late stages of PH can lead to abnormal cellular metabolism and inflammation, which may contribute to the progression of PH (14, 15). Studies have shown that the levels of autophagy-related proteins increase significantly in the lungs of patients with PH, suggesting a potential link between autophagy dysregulation and disease progression. Therefore, it is important to strike a balance between autophagy activation and inhibition to achieve optimal therapeutic effects in PH (Figure 2, left).

Autophagy refers to macroautophagy, mitophagy, and chaperone-mediated autophagy (Figure 2, right). The autophagic process involves five core complexes: (i) the ULK kinase complex, consisting of ULK1/2, ATG13, RB1CC1/FIP200, and ATG101; (ii) the ATG9A/ATG2-WIPI1/2 trafficking system; (iii) the class III PI3K complex, which includes VPS34, Beclin 1, p115, and either ATG14 in PI3KC3 complex I or UVRAG in complex II; (iv) WIPI proteins and their interaction partner ATG2; and (v) two ubiquitin-like proteins and their conjugation machinery. Autophagy acts as a

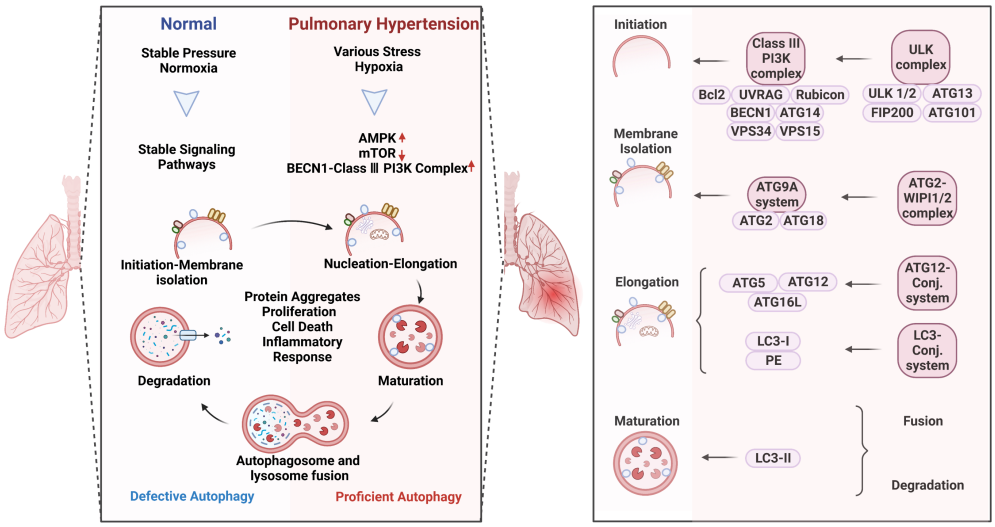

FIGURE 2
Autophagy activation in pulmonary hypertension (Left) and the specific role of the complexes in the process of autophagy (Right). Autophagy is a process of intracellular waste degradation and reuse in response to different microenvironment stresses. Its activation promotes the survival and proliferation of pulmonary vascular endothelial cells while also regulating different cell types such as alveolar macrophages, smooth muscle cells, and fibroblasts, thereby participating in the occurrence and development of pulmonary hypertension. In addition, autophagy can also promote cellular metabolic balance, reduce oxidative stress, and inflammatory response, and is expected to become a new target for the treatment of pulmonary hypertension.

double-edged sword in human diseases which can promote cell survival or apoptosis under different stresses (16). These opposite effects could possibly be attributed to the different modifications of ATG-related proteins in a context-dependent manner. In response to different pathological stimulus, autophagy is abnormally activated in PH patients (9). The research surrounding the altered autophagy phenotypes has bloomed since work on autophagy won the Nobel Prize in 2016, making great progress in the understanding of the underlying mechanisms in PH.

The key autophagy-related genes (LC3B-II, Beclin1) and upper signaling molecules (AMPK, mTOR, ·BMP, ROS, NF-κB) have been discovered activated and playing important roles in regulating autophagy in PH. Activated autophagy promotes the proliferation of PASMC (pulmonary arterial smooth muscle cells) and PAEC (pulmonary arterial endothelial cells), inhibits ROS production, and regulates mitochondrial function in PH (11). Autophagy plays a dual role in endothelial cells. On the one hand, it promotes the survival and adaptation of these cells under stress conditions by removing damaged organelles and recycling nutrients to provide energy for the cell. On the other hand, excessive autophagy can result in endothelial dysfunction and apoptosis, leading to impaired vascular homeostasis and contributing to PH progression (13). The underlying mechanism involves modulation of key signaling pathways such as AKT/mTOR, AMPK, and ERK1/2. In smooth muscle cells, autophagy has been shown to regulate the proliferation and migration of these cells (14). Specifically, inhibition of autophagy leads to reduced smooth muscle cell proliferation and increased apoptosis. This effect is mediated through the modulation of RhoA and mTOR pathways. In addition, autophagy also plays a role in the regulation of immune cells during PH development. Autophagy promotes antigen presentation by dendritic cells, enhances T-cell survival, and regulates macrophage polarization towards an anti-inflammatory phenotype (17). Dysregulation of autophagy in immune cells can lead to inflammation, promoting progression of PH. The exact molecular mechanisms behind autophagy-mediated immune cell regulation in PH are still being investigated. Overall, autophagy is a complex process that plays a multifaceted role in PH pathogenesis, affecting multiple cell types and signaling pathways. Increasing our understanding of the specific molecular mechanisms underlying autophagy in PH may enable development of new therapies targeting this process to improve patient outcomes.

Multiple signaling genes are important in human diseases through affecting various downstream pathways. Various modifications play key roles in regulating the expression or functions of the signaling molecules themselves or downstream molecules. These modifications include post-transcriptional, post-translation, and pre-transcriptional modifications. Epigenetics refers to histone modification and chromatin remodeling, which means reversible and hereditary changes in gene expression without alterations in DNA sequences. Post-translational modification of histones, including acetylation, methylation, phosphorylation, SUMOylation, ubiquitination, and ADP-ribosylation, occur mainly in the N-terminal tails and have profound effects on chromatin structure. Epigenetic modification affects autophagosome formation, autophagy-related protein expression, and signaling pathway activation and potentially functions as the PTM switch to regulate autophagy (18). As histone acetylation or methylation modifying enzymes, HDACs, SIRT1, SIRT3, and BRD4 proteins are confirmed with significant alternation in expression levels and play important roles in the proliferation, inflammatory and fibrotic phenotypes of vascular cells (19). Additionally, these signal molecular genes regulating autophagy are also reported to be impacted by epigenetic modifications such as acetylation (Ac) and methylation (Me), which affect the chromatin state, thus altering expression of specific genes (20, 21).

3 Acetylation signaling of autophagy relevant to pulmonary hypertension

Acetylation refers to the process of transferring and adding acetyl groups to protein lysine residues or protein N-terminus under the catalysis of acetyltransferases (or non-enzymes). Histone acetylation affects the pathological progression of PH through repressing ATG genes transcriptionally. Research has shown that the acetylation of autophagy-related proteins plays an important role in the regulation of autophagy in PH. Specifically, increased levels of acetylated proteins such as LC3B and ATG7 have been observed in animal models of PH and in human patients with the disease. These proteins are key components of the autophagy machinery and their acetylation has been shown to impair autophagic function (22). We summarize recent research which has shown that histone-modifying enzymes occupy an important position in regulating autophagic process of PH (Figure 3).

Histone lysine acetyltransferases (HATs) and deacetylases (HDACs) gene families are the main regulators of histone acetylation (19). Acetylation of histone tails neutralizes positively charged lysine, which is thought to disrupt the interaction between the tail and negatively charged nucleosome DNA, thereby promoting the opening of chromatin and thus positive transcription. At present, 18 HDACs have been found in humans belonging to four categories (I, II, III, and IV). Among them, 11 subtypes, such as class I, II, and IV, were Zn2+-dependent proteins. Seven subtypes of the class III subgroup, Sirt1~7, use NAD+ as the catalytic active site. Acetylation of lysine at histone tails is highly dynamic and important for the regulation of chromatin structure, transcription, and DNA repair. Acetylation of non-histones, including tumor suppressors and oncogenes (i.e., p53, Rb, and Myc), regulates protein stability, DNA binding, protein interactions, enzyme activity, or protein localization.

HDAC1, HDAC2, and HDAC3 are elevated in PH fibro6blasts (23). Additionally, HDAC1 and HDAC5 have also been reported as being activated in human idiopathic PAH (IPAH) lung homogenates (24). HDACs play crucial roles in the control of pathological hypertrophy, inflammation, fibrosis, restenosis, and left ventricular (LV) cardiac remodeling in various preclinical models of LV failure (25). The prototypical HDAC inhibitor (HDACi), trichostatin A (TSA), attenuates both load- and

10.3389/fimmu.2023.1206406

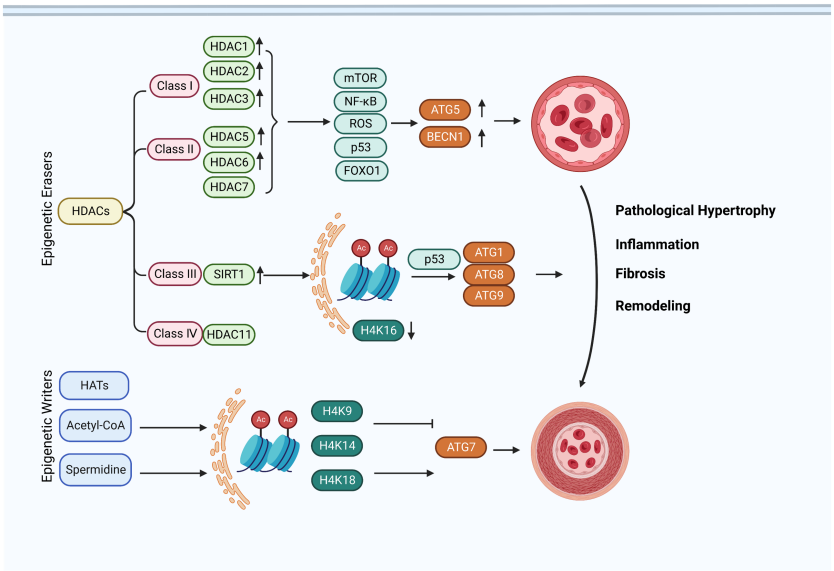

FIGURE 3
Acetylation signaling pathway in regulating autophagy activation of pulmonary hypertension. Acetylation modifications can modulate the activity of autophagy, thereby exerting a protective effect against pulmonary hypertension. In addition, various drugs can also be used to treat pulmonary hypertension by modifying acetylation modifications. However, further research is needed on the specific mechanism and effect of acetylation modification in pulmonary hypertension.

agonist-induced hypertrophic growth and abolishes the associated activation of autophagy through affecting ATG5 or BECN 1, two essential autophagy effectors (26). HDAC6 is essential for autophagosome-lysosome fusion through binding to polyubiquitinated proteins (27). On the contrary, HDAC7 deactivates autophagy through depressed ERK signaling (28). These pieces of evidence show the importance of HDACs in the pathological progression of PH through autophagy.

The mechanisms underlying the HDAC-related autophagy embrace multiple signaling pathways. In most cases, mTOR inhibition, NF-κB hyperacetylation, ROS accumulation, and the p53 pathway are observed in HDAC-related autophagy signaling (29). Deacetylation of p53 by HDAC enable the accessibility of p53 to its target genes. Additionally, the nuclear export, proteasomal degradation, and co-activator recruitment of p53 are also regulated by HDAC (30). Distinct acetylated residues of p53 are attached by several HATs, increasing the stability and transcriptional activity of p53 binding to sequence-specific target DNA (31). Furthermore, the balance between autophagy and apoptosis is also regulated by p53, providing new insights into the role of p53 in the development of therapeutic drugs of PH.

Multiple inhibitors of HDACs have been developed recently and autophagy activation are frequently observed in the effects of HDAC inhibitor (HDACi) administration. Forkhead box protein O1 (FoxO1) is another important transcript factor in regulating the proliferation and inflammatory signaling of pulmonary artery smooth muscle cells (PASMCs) of PH (32). Inhibiting HDAC with SAHA and TSA activates FoxO1, resulting in mTOR-suppression and ATG-upregulation (33). Acetylation of FoxO1 by SIRT2 prevents its interaction with ATG7, thereby inhibiting autophagy induction (34).

Death-associated protein kinase (DAPK) is a calcium/calmodulin modulated cytoskeleton-associated enzyme, which is closely associated with different MAPKs such as ERK in response to inflammatory apoptotic stimuli (35). Nuclear translocation of DAPK expression is also involved in HDACi-related autophagy activation (36). Additionally, dephosphorylation of DAPK1 at serine 308 by HDAC inhibitor LBH589 promotes autophagy in HCT116 colon cancer cells (37). Studies have shown that DAPK can regulate vascular smooth muscle cell proliferation and migration, promoting vascular inflammation and the development of hypertension diseases (38). Furthermore, vascular calcification is also alleviated by DAPK deficiency (39), which provides a clue regarding the importance of DAPK in PH progression and needs further research.

Sirtuins belong to class III of HDACs. The distinguishing feature of this class of HDACs is that the catalytic activity of the enzyme depends on NAD+ and is regulated by dynamic changes in the NAD+/NADH ratio, suggesting that sirtuins may have evolved into a sensor of energy and redox states in cells. Among the histone-modifying enzymes, the NAD-dependent deacetylase SIRT1 (sirtuin 1) is a particularly well-known modulator of pulmonary hypertension (19). Studies have shown that SIRT1 can regulate the occurrence and process of autophagy and promote the treatment of PH diseases by enhancing the activity of autophagy (40). Specifically, SIRT can promote autophagy by activating key molecules in the autophagy pathway, such as LC3, Beclin-1, and ATG7, or by inhibiting the expression of mTOR, an inhibitor of

autophagy. In PH diseases, the expression level of SIRT1 is also regulated. Under hypoxic stress, SIRT1 expression increases, promoting the occurrence of autophagy, which inhibits excessive cell proliferation and hypertrophy of lung vascular wall cells (41). The deacetylase-inactive mutant of SIRT1 disables the induction of autophagy under starvation in mouse embryonic fibroblasts compared with the SIRT1 wild-type gene (34). Histone mark H4K16 is deacetylated by SIRT1 and has great influence on transcriptionally repressing various ATG genes (ULK1/ATG1, ULK3/ATG1, ATG9A/ATG9, LC3/ATG8), leading to the decreased turnover of LC3/ATG8 and autophagic flux (42). Additionally, ATG5, ATG7, and ATG8 bind directly with SIRT1 and can be deacetylated by this binding (43). The stability and function of p53 are also impacted by the enzymatic activity of SIRT1. The degradation of p53 by MDM2 ubiquitination is reversed by SIRT1 expression, which acetylates p53 at lysine 382 and leads to autophagy activation in MCF-7 breast cancer cells (44). Meanwhile, the apoptosis and autophagic cell death of Ishikawa cells are inhibited by SIRT1 through p53 regulation. The subcellular localization of SIRT1 is another influencing factor in autophagy regulation. While SIRT1 limits autophagy in a nucleus under starvation or rapamycin treatment, deacetylation of cytoplasmic proteins by SIRT1 is responsible for autophagy induction (34). These pieces of evidence show that SIRT1 regulates autophagy by both epigenetic and post-translational mechanisms.

Starvation or rapamycin treatment is the well-recognized autophagy-inducing pathway. This canonical process is accompanied by the downregulation of KAT8 and deacetylation of H4K16. Histone acetyltransferase TIP60 activates the acetylation of ULK-1 during starvation-induced autophagy (45). Acetyl coenzyme A (acetyl-CoA), which serves as the donor for acetylation reactions, unavoidably plays an important role in regulating autophagy. High levels of acetyl-CoA inhibit the transcription of ATG7 by hyperacetylation of histone 3 (on K9, K14, and K18) (46). As another well-known autophagy inducer, spermidine is a naturally endogenous polyamine synthesized by diamine putrescine, leading to the inhibition of histone acetyltransferase activity and hypoacetylation of histone 3 (K9, K14, K18) (47). Acetylation of ATG7 promoter is activated and the autophagy-related genes (ATG7, ATG11, ATG15) are increased during spermidine treatment (48).

Generally, acetylation is a common modification and the acetylating regulators have been discovered with abnormal expression in PH. Specifically, acetylation affects autophagy-related genes and proteins such as BECN 1, ATG5, and ATG7, thereby affecting autophagy initiation, autophagosome formation, and the subsequent steps of autophagy. By regulating the expression and function of these key factors, acetylation ultimately affects the role of autophagy in PH. Furthermore, acetylation can also participate in the occurrence and development of pulmonary hypertension through pathways such as regulating endothelial dysfunction, inflammation, mitochondrial energy, and oxidative stress. Therefore, targeting acetylation signaling pathways may represent a promising therapeutic strategy for the treatment of PH.

4 Methylation of DNA and histones in the autophagy process of pulmonary hypertension

Methylation refers to the catalytic transfer of methyl groups from active methyl compounds to other compounds. Various methyl compounds can be formed, or certain proteins or nucleic acids can be chemically modified to form methylation products. Within biological systems, methylation is enzymatically catalyzed, involving regulation of gene expression, regulation of protein function, and RNA processing.

4.1 DNA methylation

DNA methylation involved in autophagy is regulated by both methyltransferase and demethylase, affecting protein–protein interactions, protein activity, and the interplay with other modifications. There are five members of the DNA methyltransferases (DNMT) family: DNMT1, DNMT2, DNMT3A, DNMT3B, and DNMT3L. DNMT1 catalyzes the methylation of mir-152-3p promoter region and inhibits its expression, which reduces cell viability and inhibits mitophagy progression (49). Additionally, the acetylation of DNMT1 KG-linker is linked to the stability of DNMT1 through USP77 with its UBL1-2 region. The fifth carbon of a cytosine ring in cytosineguanine dinucleotide (CpG) dinucleotides generating 5-methylcytosine (5mC) is transferred with a methyl group by DNMT3A (50), which leads to a stable and heritable DNA methylation mode on target ATGs. Meanwhile, autophagy activation promotes DNMT3A expression, resulting in its combination and transcriptional repression with LC3A, LC3B, and LC3BII genes (51). lncRNA MEG3 promoter methylation is also mediated by DNMT1, which in turn inhibits the ERK/p38/autophagy signaling pathway in bleomycin-induced pulmonary fibrosis (52). DNA methylation of ULK2, ATG5 gene promoter, nitro domain-containing protein 1 (NOR1), death-associated protein kinase (DAPK), and SOX1 also impact the autophagic process (20, 53, 54).

In PH, DNMT1 and DNMT3B are reported with elevated expression in experimental models induced by Sugen 5416 and hypoxia (55). The DNMT1-HIF-1α- pyruvate dehydrogenase kinase pathway also has an effect on right ventricular fibrosis in MCT-PAH (56). Additionally, bone morphogenetic protein receptor type 2 (BMPR2) promoter is also hypermethylated by switch-independent 3a in human pulmonary arterial smooth muscle cells (57). Furthermore, of therapeutic significance, the present study opens a new avenue for PH treatment by targeting the DNA methylation pathway in pulmonary vessel cells that can modulate the epigenetic landscape of pulmonary vascular genes, and therefore pulmonary vascular and RV remodeling. Given the widespread occurrence of DNA methylation regulation, the direct contact between DNA methylation and autophagy is relatively incomplete and more effort is needed to understand the pathological progression of PH (Figure 4).

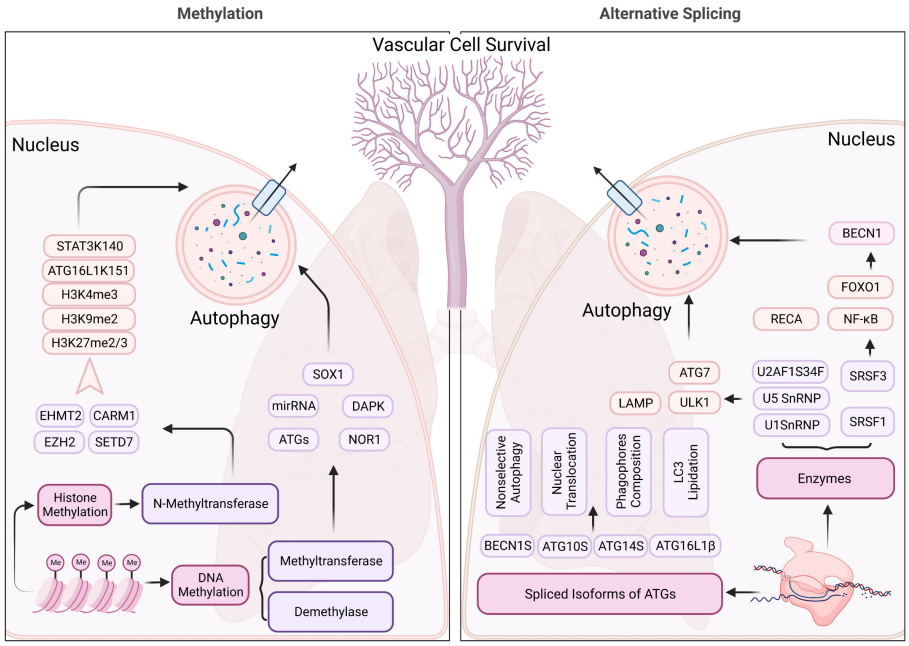

FIGURE 4
Methylation and alternative splicing located in nucleus regulating the autophagy process of pulmonary hypertension. N-methyltransferase (includes EHMT2, CARM1, EZH2, and SETD7) modulate the autophagy process through methylating histone 3, ATG16L1, and STAT3, contributing to the changes in the structure, function, and expression levels of certain genes, which impact the autophagy process in pulmonary hypertension. Alternative splicing, on the other hand, SnRNPs, and SRSFs regulate the RNA splicing process and can generate different isoforms of proteins involved in autophagy, which may have distinct structures and functions. These mechanisms may contribute to the dysregulation of autophagy in pulmonary hypertension, which is a pathological condition characterized by abnormal cellular remodeling in the lungs.

4.2 Histone methylation

Histone methylation mainly occurs on lysine and arginine. Lysine can be monomethylated (me1), dimethylated (me2), or trimethylated (me3), while arginine can be monomethylated (me1), symmetrically dimethylated (me2s), or asymmetrically dimethylated (me2a) on its guanidine group (58). Histone methylation is regulated by protein lysine methyltransferases (PKMTs or PLMTs) and protein arginine methyltransferases (PRMTs), including members of the PRMT family, SET gene family, and non-SET gene family (59, 60). Meanwhile, demethylases mediate the removal of methyl groups from different residues on histones (61). Histone methylation serves as a specific binding site for transcription factors and coregulators. Differential methylation on lysines is able to guide differential activation, causing it to bind to specific promoters. Thus, histone methylation sites form intermediate stations on chromatin that link specific transcription factors or cofactors to downstream gene expression.

Accumulating evidence indicates that histone methylation contributes to the control of cell fate and to the maintenance or suppression of autophagy. Enhancer of zeste homolog 2 (EZH2) gene encodes a histone lysine N-methyltransferase, which methylates histone H3 at position 27 lysine and induces transcriptional repression of the mTOR pathway under serum starvation conditions (62). Metastasis-associated 1 family member 2 (MTA2) recruits EZH2 at specific target gene promoters and catalyzes H3K27me3. In a transverse aortic constriction (TAC)-induced PH mouse model, EZH2 was overexpressed (63). EZH2 promotes vascular smooth muscle cell (VSMC) survival through catalyzing H3K27me2/3, suppressing autophagic cell death by inhibiting the ERK1/2 signaling pathway (64). By inhibiting the expression of EZH2, the proliferation and cell hypertrophy of pulmonary vascular smooth muscle cells can be weakened, and the occurrence of autophagy can be promoted to achieve the effect of treating PH diseases (65, 66). Furthermore, EZH2 methylates STAT3 at Lys180 to activate the STAT3 signaling pathway, which promotes the expression of BCL2 and BCL2L1 and directly inhibits autophagic functions (67). Inhibiting EZH2 with GSK343 or UNC1999 upregulates LC3B and autophagic progression, leading to VSMC loss, enhanced drug sensitivity, and cell death (68, 69). Meanwhile, endogenous knocking-down of EZH2 with RNA interference technology activates cellular senescence-signaling proteins (p16, p53, p14) and inhibits autophagy, which also leads to cell death (70).

H3K9 and H3K4 methylation levels are mainly catalyzed by histone methyltransferases (HMTs) such as euchromatic histone lysine methyltransferase 2 (EHMT2) (71). The dimethylation of H3K9 by EHMT2 represses autophagy gene transcription, which is achieved by the enrichment of EHMT2 on the promoters of ATGs (21). Inhibition of EHMT2 reverses the H3K9me2, resulting in the dissociation of EHMT2 and H3K9me2 from the promoter of ATG6 (72). Autophagy activation also promotes the dissociates EHMT2 from histone H3K9, further decreasing H3K9 dimethylation (73). Additionally, H3K4me3 is also recruited at the promoter region of the damage-regulated autophagy modulator (DRAM) gene upon

serum deprivation conditions. DRAM expression is increased by H3K4me3 in serum deprivation-induced autophagy activation. EHMT2 inhibition displays reduced H3K4 methylation and ATGs' expression in VSMC and various tumors (74). In addition, EHMT2 can also be assembled in the appropriate DNA region, regulating the expression level of autophagy-related nuclear factor transcription factors (75). The methylation levels of H3K4 likely serve as an upstream regulator of autophagy in PH. Specifically, lower methylation levels of EHMT2 are found in hypertensive patients as compared with normotensive subjects (76). Furthermore, emerging evidence suggests a role of DNA methylation in blood physiology, providing a clue regarding the direct link between EHMT2 expression and PH pathology. Overall, in-depth study of the specific mechanism of EHMT2 regulating autophagy will help to further reveal the pathogenesis of PH disease and open up new therapeutic pathways for the treatment of this disease (76).

Coactivator associated arginine methyltransferase 1(CARM1) belongs to PRMTs and increases H3R17me2 levels under glucose deprivation. CARM1 regulates autophagy through transcriptionally coactivating ATGs and lysosomal genes with transcription factor EB (TFEB) (77). Stem cell factor (SCF) E3 ubiquitin ligase is responsible for degrading and destabilizing CARM1 when autophagy is depressed by AMPK inhibition. CARM1-mediated histone arginine methylation seems to be a critical nuclear event in the regulation of autophagy and targeting the AMPK-CARM1 signaling pathway may abrogate the pathological progression in autophagy-related diseases. In addition, CARM1 can also regulate the expression levels of ATGs and nuclear factors by assembling in the appropriate DNA region, playing a regulatory role in multiple cellular responses such as nuclear factors, transcription factors, and cell signaling pathways (78). The homocysteine metabolism pathway is also reported to be regulated by CARM1, which is a risk factor for vascular disease (79). This evidence provides a clue regarding the importance of CARM1 in autophagy regulation of PH disease.

SET domain containing 7 (SETD7) belongs to the SET gene family, which is histone lysine methyltransferase containing highly conserved SET domains. SETD7 methylates ATG16L1 at lysine 151, impairing the ATG16L1-ATG12-ATG5 complex and autophagy progression. This methylation of ATG16L1 is reversed by lysine demethylase 1A (LSD1/KDM1A), inhibiting hypoxia/reoxygenation-induced cardiomyocyte apoptosis (80). Furthermore, methylated ATG16L1 at lysine 151 prevents its phosphorylation at S139, which is critical for autophagy maintenance (81). Moreover, SETD7 also dimethylates STAT3 at Lys 140, which prevents its phosphorylation at Tyr705 and inhibits STAT3 activity (82). STAT3 is critical for transcriptionally upregulating HIF1a, which is stabilized and induces autophagy under hypoxic conditions in PH (83). Located at 4q28.3-31.23, SETD7 deletion may impact lung vascular malformation leading to PH (84). The direct link between SETD7 regulation in the autophagy process of PH still needs more investigation and may play a significant role in the development of PH therapeutic drugs. Above all, histone methylation has been discovered with widespread existence in numerous human diseases. Many methylation regulators exhibit abnormal phenotype expression and have effects on PH progression. Studies of G9a and EZH2 in PH indicate that histone methylation plays an essential role in PASMC proliferation of PH. Specifically, increased levels of H3K9me2 and H3K9me3 contribute to impaired autophagic flux and the exacerbation of PH pathogenesis, while targeting these histone modifications has shown promise as a therapeutic strategy for PH.

5 RNA alternative splicing is another important regulatory machinery affecting autophagy

5.1 RNA alternative splicing regulatory enzymes

Transcription and translation make up the entire process of gene expression, and RNA splicing is a crucial step in this process. Due to the complexity and diversity of RNA splicing, alternative splicing is an important contributor to proteome richness. Small nuclear ribonucleoproteins (SnRNPs) and splicing regulatory factors (SRSF proteins, hnRNPs, RBPs) play important roles in finishing the transcription, and are involved in numerous human diseases including PH through ATGs regulation (Figure 4).

U1 snRNP overexpression induced by presenilin 1 affects autophagy by impairment of lysosomal biogenesis and autophagosome-lysosome fusion, which in turn affects the turnover of these peptides and accelerates neuronal cell death (85). Knocking-down the pre-mRNA splicing factor (PRPF8), which is a component of U5 snRNP and central module of the spliceosome, leads to enhanced skipped splicing of exon 22 and exon 23 of ULK1 at the mRNA level. This splicing process abrogates mitophagosome formation and the clearance of mitochondria (86, 87). U2AF1S34F mutant protein of the pre-mRNA splicing factor U2AF alters the 3′end formation of mRNAs through distal cleavage and polyadenylation sites, which results in ATG7' depression (88).

SRSF1 and SRSF3 belong to the splicing regulatory factor family and inhibit autophagosome formation through their effect on the transcription factor (RELA proto-oncogene, NF-κB subunit, forkhead box O1)-BECN1 pathway in lung adenocarcinoma cells (89). The splicing of the long isoform of Bcl-x that interacts with Beclin1 is also promoted by SRSF1, thereby dissociating the Beclin1-PIK3C3 complex (89). Similarly, the 3′UTR of BECN1 is also regulated by binding with hnRNPA1, the effects of which remain to be established in PH (90).

Alternative splicing of the autophagy gene ATG5 has been shown to regulate apoptosis of pulmonary artery smooth muscle cells (PASMCs) in PH. The inclusion of a specific exon in the ATG5 mRNA, which is promoted by the splicing factor SRSF1, results in increased autophagy activity and decreased PASMC apoptosis (91).

SRSF3 has been shown to promote PH by regulating the expression of the autophagy gene ATG16L1. Specifically, SRSF3 promotes the inclusion of a specific exon in the ATG16L1 mRNA, resulting in increased autophagy activity and enhanced vascular remodeling (92). Conversely, other splicing factors such as RBM4 (RNA binding motif protein 4) can inhibit PH by promoting the exclusion of the same exon

from the ATG16L1 mRNA, leading to decreased autophagy activity and attenuated vascular remodeling (93).

Muscleblind like splicing regulators (MBNLs) modulate alternative splicing through exon skipping. MBNL1 and MBNL2 interact directly with the rubicon autophagy regulator (RUBCN) through RNA binding, leading to the exon skipping of RUBCN and increases of autophagy (94, 95). Additionally, utilizing the antiautophagic drug chloroquine is sufficient to upregulate MBNL1 and 2 proteins (96). Chloroquine has been proven to be efficient in experimental mouse PH models, but the expression and function of MBNLs deserve a deeper study.

Alternative splicing regulation is an emerging mechanism of gene expression control, which affects protein translation and function by altering the splicing patterns of RNA. Alternative splicing of BMPR2 by SRSF2 has a role in PH penetration and makes developing PH more likely (97). Specifically, this regulatory mechanism can affect the transcription and alternative splicing of genes related to autophagy, thereby influencing the progression and efficiency of autophagy. These studies suggest that alternative splicing regulation plays a crucial role in autophagy in pulmonary hypertension. Therefore, a deeper understanding of the mechanisms underlying the alternative splicing regulation of autophagy in pulmonary hypertension is crucial for drug development and treatment.

5.2 Alternative spliced isoforms of ATGs affect the autophagic process differentially

Alternative splicing creates multiple isoforms of ATGs which may differ from the primary subunit in structure and function. An additional splice variant of BECN1 called BECN1 short isoform (BECN1S) that lacks both exon 10 and 11 has been reported in multiple cell types. This different BECN1 variant exhibits distinct functions in controlling autophagy compared to BECN1. Overexpression of BECN1S abrogates starvation-induced autophagy in AML cells as a negative regulator (98). Whereas BECN1S is useless in macroautophagy, it could on the other hand support mitophagy (99). These phenomena point out its effect in non-selective autophagy and selective mitophagy. Studies have shown that the ratio of BECN-1S to BECN-1 is altered in PH, with a shift towards the production of BECN-1. This shift has been shown to impair autophagy flux and lead to endothelial cell dysfunction. In addition to BECN-1, other autophagy-related genes have also been shown to undergo alternative splicing in PH (100). For example, the splicing of ATG5, another key autophagy regulator, has been shown to be altered in PH. This altered splicing leads to the production of a truncated isoform of ATG5, which has been shown to impair autophagy flux and lead to endothelial cell dysfunction (101).

Likewise, ATG10S, which is distinct from ATG10 at 36 amino acids at the N terminus promotes autophagy completion that degrades HCV subgenomic and genomic replicons. Meanwhile, the absence at Cys44 of ATG10S makes it possible for its nuclear translocation and combination with interferon lambda 2 (IL28A), which mediate the clearance of viral infections through autophagy (102).

ATG14 is another essential core component in the early steps of autophagy (103). ATG14S is a short variant of ATG14 which lacks the cysteine repeats-containing domain required for autophagosome-endolysosome fusion. Moreover, this oligomerization domain is not functional in the PtdIns3K nucleation complex formation, which retains the function of ATG14L and ATG14S in phagophores composition (104).

ATG7 is required for LC3 lipidation for its E1-like enzyme activity. ATG7(2) is distinct from ATG7(1) at a deprived exon of 27 amino acids. Additionally, ATG7(2) lacks the region required for homodimerization and the binding between ATG7 and LC3, thus inhibiting the lipidation of LC3 (105).

ATG16L1 participates in autophagy regulation in multiple aspects, like binding with ATG5 through its N-terminal region and engaging in LC3 lipidation (106). Three slicing variants of ATG16L1 have been discovered so far and ATG16L1β (absence of exon 9) contains a unique β-isoform lipid-binding region, which is indispensable for LC3 lipidation under endosomal stress (107).

Lysosomal-associated membrane protein 2B (LAMP2B) is abundant in lysosomes and is indispensable in autophagosome fusion with late endosomes/lysosomes. The differences between LAMP2C and LAMP2B are located at the lysosomal carboxyl-terminal transmembrane region and the cytoplasmic short tail. Meanwhile, LAMP2C affects DNautophagy and RNautophagy through interacting with RBPs (108). LAMP2C is reported to interact with RBPs and nucleic acid proteins such as histone 1, suggesting a role in the uptake and degradation of RNA and DNA molecules within the lysosome, processes known as DNautophagy and RNautophagy (108).

To summarize, studies have shown that alternative splicing variants of ATGs may be associated with the occurrence and development of PH. Specifically, some alternative splicing variants of autophagy genes increase the expression levels in pulmonary vascular smooth muscle cells, leading to enhanced intracellular autophagy processes and promoting the development of PH. In addition, certain alternative splicing variants may also affect PH through pathways such as cell apoptosis, proliferation, and metabolism. However, the research on the relationship between alternative splicing variants of ATGs and PH is still in its early stages and requires further investigation.

5.3 MirRNAs

MirRNAs are small (21–25 nucleotides) single stranded RNAs that bind to complementary nascent mRNAs and render them susceptible to degradation prior to translation, thereby inhibiting the expression of specific target genes. RNA interference is an epigenetic mechanism of gene regulation that occurs post-transcriptionally. MirRNAs plays an important role in autophagy regulation. For example, some microRNAs can inhibit the expression of autophagy-related genes, thus inhibiting the autophagy process, while some long non-coding RNAs can participate in the induction and execution process of autophagy. For example, MirRNA-10a, MirRNA-20a, and MirRNA-885-3p target RB1CC1, ULK1, and ULK2, respectively, and impact the

induction of autophagy (109–111). MirRNA-34a, MirRNA-195, MirRNA-30a, and MirRNA-30a bind ATG9, ATG14, BECN1, and UVRAG, respectively, in the nucleation process of autophagy (112–114). The elongation of autophagy phospholipid membrane is regulated by ATG4, ATG5, ATG7, ATG10, ATG12, ATG16, LC3, and SQSTM1, which are also affected by MirRNA-101, MirRNA-30a, MirRNA-17, MirRNA-519a, MirRNA-30d, MirRNA-519a, MirRNA-204, and MirRNA-17 (111, 115–119). This evidence elucidates that MirRNA participates in regulating the whole process of autophagy and has an effect on the completion of autophagy.

In recent years, small RNAs have gained more and more attention and numerous studies have made progress in the regulation of small RNAs in PH. CircSIRT1 impacts the biological behavior of hypoxia-stimulated PASMC *via* modulating the Mir-145-5p/Akt3 pathway (120). The circ-calm4/Purb/BECN1 signal axis is involved in the occurrence of hypoxia-induced PASMCs autophagy, and the novel regulatory mechanisms and signals transduction pathways in PASMC autophagy are induced by hypoxia (121). LncRNA-GAS5/Mir-382-3p axis promotes autophagy and inhibits pulmonary artery remodeling. MirRNA-874-5P regulates autophagy and proliferation in PASMCs by targeting Sirtuin3 (41). Mir204 enhances autophagy and promotes endothelial-mesenchymal in hypoxia PH (122). Targeting this MirRNA has been shown to restore autophagy and improve disease symptoms in animal models of PH. These non-coding RNAs modulate the ATGs with relatively simple and direct mechanisms through binding and inhibiting the target genes. These molecules have emerged as attractive targets for PH therapy due to their ability to modulate various signaling pathways involved in disease progression, including autophagy.

Targeting MirRNAs that regulate autophagy is a potential personalized therapy. Currently, research on the mechanism of MirRNA regulating autophagy mainly focuses on the following aspects: identifying and describing new regulatory factors, exploring the molecular mechanisms of regulatory factors, and studying the role of regulatory factors in PH. These studies are of great significance for us to deepen our understanding of autophagy regulation mechanisms, develop treatment methods for autophagy-related diseases, and so on. However, it should be noted that there are still many unknowns about the mechanism of MirRNA regulating autophagy which require further research and exploration.

6 Conclusions and future perspectives

PH is a type of chronic life-threatening cardiovascular disease that is difficult to cure clinically, the pathogenesis of which is complex and not yet fully understood. Epigenetic regulation affects the expression, stability, and function of ATGs and plays important roles in the development of PH. Certain epigenetic modification patterns (such as DNA methylation and histone modification) are reported with abnormal dysfunction in patients with pulmonary hypertension, leading to dysregulated gene expression and promoting pathological processes such as pulmonary vessel tension and cell proliferation. In this review, mounting evidence has demonstrated that crosstalk between epigenetic modifications and autophagy is related to the initiation and progression of PH. Acetylation regulated by HDACs and HATs occurs in multiple signaling pathways which directly or indirectly act on ATGs, which can either promote or inhibit autophagic activity depending on the specific lysine residues targeted and the acetyltransferase/deacetylase enzymes involved. In preclinical studies, HDAC inhibition has been shown to attenuate PH by enhancing autophagy in both endothelial cells and smooth muscle cells. This effect is mediated by the acetylation of histones upstream of autophagy-related genes such as BECN-1 and LC3 (123). A HDAC inhibitor is one potential approach for personalized treatment strategies targeting epigenetic regulation of autophagy. However, more research is needed to determine whether HDACi are a viable therapeutic option for human PH (124). Understanding the precise mechanisms by which acetylation regulates autophagy is an active area of research, with potential therapeutic implications for diseases associated with autophagy in PH. Targeting acetylation and deacetylation pathways may offer new strategies for enhancing or inhibiting autophagy in disease states, although further preclinical and clinical studies are needed to evaluate their efficacy and safety.

Additionally, the aberrant methylation of histones and DNA in nucleus serves as another important pattern contributing to autophagy dysfunction in various diseases, such as cancer, neurodegenerative disorders, metabolic disorders, and PH. Hypermethylation of ATGs leads to decreased autophagic activity and increased growth. However, the relationship between methylation and autophagy is complex and context-dependent, and more research is needed to fully understand the underlying mechanisms. Furthermore, it remains unclear whether targeting DNA methylation could be a viable therapeutic approach for modulating autophagy in PH. Overall, the study of methylation regulation of autophagy presents an exciting avenue for future research, with potential implications for the development of novel therapeutic strategies.

Alternative splicing has effects on autophagy in PH through producing multiple protein isoforms with distinct structures. It can generate both pro-autophagic and anti-autophagic isoforms with opposing functions. Considering the complexity of alternative splicing, more research is needed to elucidate the exact molecular pathways involved. Overall, the study of alternative splicing regulation of autophagy presents a promising area for future research. With a better understanding of the complex interplay between alternative splicing and autophagy, researchers may be able to uncover new targets for drug development and improve our ability to treat PH involving autophagy dysfunction.

As for now, the clinical treatment of autophagy in PH has progressed rapidly, which will be elaborated in depth below. First, cytokine inhibitors (125): currently, research has found that one of the therapeutic strategies for autophagy is to regulate autophagy by regulating cytokine levels. Specifically, the evaluation and regulation of cytokines such as TGF-β, BMP, and PDGF in PH diseases has become a research hotspot. Treatments that target these cytokines, such as the use of specific inhibitors, play an important role in restorative enhancement therapy for autophagy (126). Second, the

development of agonists and inhibitors (127): studies have found that treatment targeting specific autophagy modulators can promote cardiovascular recovery and reduce symptoms of PH. There are currently many autophagy regulators being developed, including autophagy agonists and inhibitors. Studies of autophagy agonists in the treatment of PH have shown that some autophagy agonists can reduce symptoms in patients with PH by enhancing the activity of autophagy (128). For example, according to one study, Sirt1 agonists reduce symptoms in rats with PH, reducing the pulmonary vascular resistance and right ventricular weight index by promoting autophagy. Similarly, another study showed that a drug called RapaLink-1 that utilizes autophagy pathway drug delivery can reduce pathological damage and thymus peptide secretion in mice. These findings suggest that autophagy agonists may become a novel drug for the treatment of PH. Acting as an autophagy inhibitor, chloroquine has a significant therapeutic effect in patients with PH. A randomized, double-blind, placebo-controlled trial of chloroquine in the treatment of PH showed that chloroquine significantly reduced clinical symptoms and blood biochemical parameters and increased exercise tolerance and lung function (129). These data suggest that chloroquine, as a drug regulating autophagy, may be a good prospect in the treatment of PH. In general, chloroquine will become a major trend in the development of autophagy agonists in the treatment of PH. Its complex mechanism of action and definite efficacy provides a new treatment option for patients with PH. However, chloroquine needs further clinical studies to support it as the first-line drug for the treatment of PH (9). As such, personalized treatment strategies targeting these pathways may be effective in improving outcomes for patients with PH.

Above all, epigenetic regulation of autophagy plays an important role in the pathogenesis of PH. Researchers are currently exploring how to use epigenetic regulation and autophagy to treat PH. Inhibiting autophagy through drug intervention can successfully alleviate the severity of PH. In addition, some epigenetic modification repair technologies are also under development to restore damaged gene expression patterns. Further clinical and translational research is needed to optimize screening, diagnostics (including genetic testing), establish therapies, and tailor therapy to treat the underlying pathological processes in PH patients. With the advancement of technology and knowledge, we can expect more effective and personalized treatment options to emerge focusing on epigenetic regulation and autophagy.

Author contributions

MM and SS designed and wrote the manuscript. XL and JYL sourced the relevant literature. JiL and WZ helped write the manuscript with constructive discussions. HL, JXL, and BZ developed the concepts, design, definition of intellectual content, and undertook the literature search. All authors read and approved the final version of the manuscript.

Funding

This work was supported by grants from the National Natural Science Foundation of China (No.81802508, No. 81700056), (Grant No: 20211063010052), the Natural Science Foundation Project of Chongqing (CSTB2022NSCQ-MSX0206), the Key Special Projects of National Key Research and Development Plan (2021YFA1301302), the Belt and Road Initiative and China-Africa Science and Technology Cooperation Project of the Department of Science and Technology of Jiangxi Province (20202BDH80007), the National Natural Science Foundation of China (32200606), the Natural Science Foundation of Top Talent of SZTU (GDRC202118), and the Self-developed Experimental Instrument and Equipment Project of SZTU (JSZZ202301022).

Conflict of interest

Author JiL was employed by companies Shenzhen Reyson Biotechnology Co., Ltd. and Nanjing Evertop Electronics Ltd. Author WZ was employed by company NCPC Hebei Huamin Pharmaceutical Co., Ltd.

The remaining authors declare that the research was conducted in the absence of any commercial or financial relationships that could be construed as a potential conflict of interest.

Publisher's note

References

1. Li X, He S, Ma B. Autophagy and autophagy-related proteins in cancer. *Mol Cancer.* (2020) 19(1):12. doi: 10.1186/s12943-020-1138-4

2. Dikic I, Elazar Z. Mechanism and medical implications of mammalian autophagy. *Nat Rev Mol Cell Biol* (2018) 19(6):349–64. doi: 10.1038/s41580-018-0003-4

3. Fraidenburg DR, Yuan JX. Hungry for more: autophagy in the pathogenesis of pulmonary arterial hypertension. *Circ Res* (2013) 112(8):1091–3. doi: 10.1161/CIRCRESAHA.113.301247

4. Klionsky DJ, Cregg JM, Dunn WAJr., Emr SD, Sakai Y, Sandoval IV, et al. A unified nomenclature for yeast autophagy-related genes. *Dev Cell* (2003) 5(4):539–45. doi: 10.1016/s1534-5807(03)00296-x

5. Daniell H, Mangu V, Yakubov B, Park J, Habibi P, Shi Y, et al. Investigational new drug enabling angiotensin oral-delivery studies to attenuate pulmonary hypertension. *Biomaterials* (2020) 233:119750. doi: 10.1016/j.biomaterials.2019.119750

6. Simonneau G, Montani D, Celermajer DS, Denton CP, Gatzoulis MA, Krowka M, et al. Haemodynamic definitions and updated clinical classification of pulmonary hypertension. *Eur Respir J* (2019) 53(1):1801913. doi: 10.1183/13993003.01913-2018

7. Hoeper MM, Humbert M, Souza R, Idrees M, Kawut SM, Sliwa-Hahnle K, et al. A global view of pulmonary hypertension. *Lancet Respir Med* (2016) 4(4):306–22. doi: 10.1016/S2213-2600(15)00543-3

8. Humbert M, Guignabert C, Bonnet S, Dorfmuller P, Klinger JR, Nicolls MR, et al. Pathology and pathobiology of pulmonary hypertension: state of the art and research perspectives. *Eur Respir J* (2019) 53(1):1801887. doi: 10.1183/13993003.01887-2018

9. Long L, Yang X, Southwood M, Lu J, Marciniak SJ, Dunmore BJ, et al. Chloroquine prevents progression of experimental pulmonary hypertension *via* inhibition of autophagy and lysosomal bone morphogenetic protein type II receptor degradation. *Circ Res* (2013) 112(8):1159–70. doi: 10.1161/CIRCRESAHA.111.300483

10. Nakahira K, Cloonan SM, Mizumura K, Choi AM, Ryter SW. Autophagy: a crucial moderator of redox balance, inflammation, and apoptosis in lung disease. *Antioxid Redox Signal* (2014) 20(3):474–94. doi: 10.1089/ars.2013.5373

11. Ornatowski W, Lu Q, Yegambaram M, Garcia AE, Zemskov EA, Maltepe E, et al. Complex interplay between autophagy and oxidative stress in the development of pulmonary disease. *Redox Biol* (2020) 36:101679. doi: 10.1016/j.redox.2020.101679

12. Zhang CF, Zhao FY, Xu SL, Liu J, Xing XQ, Yang J. Autophagy in pulmonary hypertension: emerging roles and therapeutic implications. *J Cell Physiol* (2019) 234 (10):16755–67. doi: 10.1002/jcp.28531

13. Chichger H, Rounds S, Harrington EO. Endosomes and autophagy: regulators of pulmonary endothelial cell homeostasis in health and disease. *Antioxid Redox Signal* (2019) 31(13):994–1008. doi: 10.1089/ars.2019.7817

14. Mao J, Ma L. Research progress on the mechanism of phenotypic transformation of pulmonary artery smooth muscle cells induced by hypoxia. *Zhejiang Da Xue Xue Bao Yi Xue Ban.* (2023) 51(6):750–7. doi: 10.3724/zdxbyxb-2022-0282

15. Chen R, Jiang M, Li B, Zhong W, Wang Z, Yuan W, et al. The role of autophagy in pulmonary hypertension: a double-edge sword. *Apoptosis* (2018) 23(9-10):459–69. doi: 10.1007/s10495-018-1477-4

16. Bu S, Singh KK. Epigenetic regulation of autophagy in cardiovascular pathobiology. *Int J Mol Sci* (2021) 22(12):6544. doi: 10.3390/ijms22126544

17. Wang K, Chen Y, Zhang P, Lin P, Xie N, Wu M. Protective features of autophagy in pulmonary infection and inflammatory diseases. *Cells* (2019) 8(2):123. doi: 10.3390/cells8020123

18. Baek SH, Kim KI. Epigenetic control of autophagy: nuclear events gain more attention. *Mol Cell* (2017) 65(5):781–5. doi: 10.1016/j.molcel.2016.12.027

19. Chelladurai P, Boucherat O, Stenmark K, Kracht M, Seeger W, Bauer UM, et al. Targeting histone acetylation in pulmonary hypertension and right ventricular hypertrophy. *Br J Pharmacol* (2021) 178(1):54–71. doi: 10.1111/bph.14932

20. Hu LF. Epigenetic regulation of autophagy. *Adv Exp Med Biol* (2019) 1206:221–36. doi: 10.1007/978-981-15-0602-4_11

21. Lapierre LR, Kumsta C, Sandri M, Ballabio A, Hansen M. Transcriptional and epigenetic regulation of autophagy in aging. *Autophagy* (2015) 11(6):867–80. doi: 10.1080/15548627.2015.1034410

22. Feng W, Wang J, Yan X, Zhang Q, Chai L, Wang Q, et al. ERK/Drp1-dependent mitochondrial fission contributes to HMGB1-induced autophagy in pulmonary arterial hypertension. *Cell Prolif.* (2021) 54(6):e13048. doi: 10.1111/cpr.13048

23. Pratt R, Dufrenoy J. Practical three-hour and two-hour cylinder-plate assays for penicillin. *Nature* (1947) 159(4043):576. doi: 10.1038/159576a0

24. Zhao L, Chen CN, Hajji N, Oliver E, Cotroneo E, Wharton J, et al. Histone deacetylation inhibition in pulmonary hypertension: therapeutic potential of valproic acid and suberoylanilide hydroxamic acid. *Circulation* (2012) 126(4):455–67. doi: 10.1161/CIRCULATIONAHA.112.103176

25. Cavasin MA, Stenmark KR, McKinsey TA. Emerging roles for histone deacetylases in pulmonary hypertension and right ventricular remodeling (2013 grover conference series). *Pulm Circ* (2015) 5(1):63–72. doi: 10.1086/679700

26. Cao DJ, Wang ZV, Battiprolu PK, Jiang N, Morales CR, Kong Y, et al. Histone deacetylase (HDAC) inhibitors attenuate cardiac hypertrophy by suppressing autophagy. *Proc Natl Acad Sci U S A.* (2011) 108(10):4123–8. doi: 10.1073/pnas.1015081108

27. Zhang J, Zhong Q. Histone deacetylase inhibitors and cell death. *Cell Mol Life Sci* (2014) 71(20):3885–901. doi: 10.1007/s00018-014-1656-6

28. Ahn MY, Yoon JH. Histone deacetylase 7 silencing induces apoptosis and autophagy in salivary mucoepidermoid carcinoma cells. *J Oral Pathol Med* (2017) 46 (4):276–83. doi: 10.1111/jop.12560

29. Mrakovcic M, Bohner L, Hanisch M, Frohlich LF. Epigenetic targeting of autophagy *via* HDAC inhibition in tumor cells: role of p53. *Int J Mol Sci* (2018) 19 (12):3952. doi: 10.3390/ijms19123952

30. Sykes SM, Stanek TJ, Frank A, Murphy ME, McMahon SB. Acetylation of the DNA binding domain regulates transcription-independent apoptosis by p53. *J Biol Chem* (2009) 284(30):20197–205. doi: 10.1074/jbc.M109.026096

31. Gu W, Roeder RG. Activation of p53 sequence-specific DNA binding by acetylation of the p53 c-terminal domain. *Cell* (1997) 90(4):595–606. doi: 10.1016/s0092-8674(00)80521-8

32. Savai R, Al-Tamari HM, Sedding D, Kojonazarov B, Muecke C, Teske R, et al. Pro-proliferative and inflammatory signaling converge on FoxO1 transcription factor in pulmonary hypertension. *Nat Med* (2014) 20(11):1289–300. doi: 10.1038/nm.3695

33. Ellis L, Bots M, Lindemann RK, Bolden JE, Newbold A, Cluse LA, et al. The histone deacetylase inhibitors LAQ824 and LBH589 do not require death receptor signaling or a functional apoptosome to mediate tumor cell death or therapeutic efficacy. *Blood* (2009) 114(2):380–93. doi: 10.1182/blood-2008-10-182758

34. Lee IH, Cao L, Mostoslavsky R, Lombard DB, Liu J, Bruns NE, et al. A role for the NAD-dependent deacetylase Sirt1 in the regulation of autophagy. *Proc Natl Acad Sci U S A.* (2008) 105(9):3374–9. doi: 10.1073/pnas.0712145105

35. Gandesiri M, Chakilam S, Ivanovska J, Benderska N, Ocker M, Di Fazio P, et al. DAPK plays an important role in panobinostat-induced autophagy and commits cells to apoptosis under autophagy deficient conditions. *Apoptosis* (2012) 17(12):1300–15. doi: 10.1007/s10495-012-0757-7

36. Zhang J, Ng S, Wang J, Zhou J, Tan SH, Yang N, et al. Histone deacetylase inhibitors induce autophagy through FOXO1-dependent pathways. *Autophagy* (2015) 11(4):629–42. doi: 10.1080/15548627.2015.1023981

37. Fulda S, Kufer MU, Meyer E, van Valen F, Dockhorn-Dworniczak B, Debatin KM. Sensitization for death receptor- or drug-induced apoptosis by re-expression of caspase-8 through demethylation or gene transfer. *Oncogene* (2001) 20(41):5865–77. doi: 10.1038/sj.onc.1204750

38. Usui T, Sakatsume T, Nijima R, Otani K, Kazama K, Morita T, et al. Death-associated protein kinase 3 mediates vascular structural remodelling *via* stimulating smooth muscle cell proliferation and migration. *Clin Sci (Lond).* (2014) 127(8):539–48. doi: 10.1042/CS20130591

39. Li KX, Du Q, Wang HP, Sun HJ. Death-associated protein kinase 3 deficiency alleviates vascular calcification *via* AMPK-mediated inhibition of endoplasmic reticulum stress. *Eur J Pharmacol* (2019) 852:90–8. doi: 10.1016/j.ejphar.2019.03.007

40. Lai YC, Tabima DM, Dube JJ, Hughan KS, Vanderpool RR, Goncharov DA, et al. SIRT3-AMP-Activated protein kinase activation by nitrite and metformin improves hyperglycemia and normalizes pulmonary hypertension associated with heart failure with preserved ejection fraction. *Circulation* (2016) 133(8):717–31. doi: 10.1161/CIRCULATIONAHA.115.018935

41. Zhang L, Ma C, Wang X, Bai J, He S, Zhang J, et al. MicroRNA-874-5p regulates autophagy and proliferation in pulmonary artery smooth muscle cells by targeting sirtuin 3. *Eur J Pharmacol* (2020) 888:173485. doi: 10.1016/j.ejphar.2020.173485

42. Fullgrabe J, Klionsky DJ, Joseph B. The return of the nucleus: transcriptional and epigenetic control of autophagy. *Nat Rev Mol Cell Biol* (2014) 15(1):65–74. doi: 10.1038/nrm3716

43. Morselli E, Marino G, Bennetzen MV, Eisenberg T, Megalou E, Schroeder S, et al. Spermidine and resveratrol induce autophagy by distinct pathways converging on the acetylproteome. *J Cell Biol* (2011) 192(4):615–29. doi: 10.1083/jcb.201008167

44. Wang J, Kim TH, Ahn MY, Lee J, Jung JH, Choi WS, et al. Sirtinol, a class III HDAC inhibitor, induces apoptotic and autophagic cell death in MCF-7 human breast cancer cells. *Int J Oncol* (2012) 41(3):1101–9. doi: 10.3892/ijo.2012.1534

45. Lin SY, Li TY, Liu Q, Zhang C, Li X, Chen Y, et al. Protein phosphorylation-acetylation cascade connects growth factor deprivation to autophagy. *Autophagy* (2012) 8(9):1385–6. doi: 10.4161/auto.20959

46. Eisenberg T, Schroeder S, Andryushkova A, Pendl T, Kuttner V, Bhukel A, et al. Nucleocytosolic depletion of the energy metabolite acetyl-coenzyme a stimulates autophagy and prolongs lifespan. *Cell Metab* (2014) 19(3):431–44. doi: 10.1016/j.cmet.2014.02.010

47. Ghosh I, Sankhe R, Mudgal J, Arora D, Nampoothiri M. Spermidine, an autophagy inducer, as a therapeutic strategy in neurological disorders. *Neuropeptides* (2020) 83:102083. doi: 10.1016/j.npep.2020.102083

48. Eisenberg T, Knauer H, Schauer A, Buttner S, Ruckenstuhl C, Carmona-Gutierrez D, et al. Induction of autophagy by spermidine promotes longevity. *Nat Cell Biol* (2009) 11(11):1305–14. doi: 10.1038/ncb1975

49. Deng Z, Yao J, Xiao N, Han Y, Wu X, Ci C, et al. DNA Methyltransferase 1 (DNMT1) suppresses mitophagy and aggravates heart failure *via* the microRNA-152-3p/ETS1/RhoH axis. *Lab Invest.* (2022) 102(8):782–93. doi: 10.1038/s41374-022-00740-8

50. Ehrlich M, Wang RY. 5-methylcytosine in eukaryotic DNA. *Science* (1981) 212 (4501):1350–7. doi: 10.1126/science.6262918

51. Gonzalez-Rodriguez P, Cheray M, Fullgrabe J, Salli M, Engskog-Vlachos P, Keane L, et al. The DNA methyltransferase DNMT3A contributes to autophagy long-term memory. *Autophagy* (2021) 17(5):1259–77. doi: 10.1080/15548627.2020.1816664

52. Ting L, Feng Y, Zhou Y, Tong Z, Dong Z. IL-27 induces autophagy through regulation of the DNMT1/lncRNA MEG3/ERK/p38 axis to reduce pulmonary fibrosis. *Respir Res* (2023) 24(1):67. doi: 10.1186/s12931-023-02373-x

53. Motoo I, Nanjo S, Ando T, Yamashita S, Ushijima T, Yasuda I. Methylation silencing of ULK2 *via* epithelial-mesenchymal transition causes transformation to poorly differentiated gastric cancers. *Gastric Cancer.* (2022) 25(2):325–35. doi: 10.1007/s10120-021-01250-0

54. Chen YC, Lin IC, Su MC, Hsu PY, Hsiao CC, Hsu TY, et al. Autophagy impairment in patients with obstructive sleep apnea modulates intermittent hypoxia-induced oxidative stress and cell apoptosis *via* hypermethylation of the ATG5 gene promoter region. *Eur J Med Res* (2023) 28(1):82. doi: 10.1186/s40001-023-01051-4

55. Jacob C, Kitagawa A, Signoretti C, Dzieciatkowska M, D'Alessandro A, Gupte A, et al. Mediterranean G6PD variant mitigates expression of DNA methyltransferases and right heart pressure in experimental model of pulmonary hypertension. *J Biol Chem* (2022) 298(12):102691. doi: 10.1016/j.jbc.2022.102691

56. Tian L, Wu D, Dasgupta A, Chen KH, Mewburn J, Potus F, et al. Epigenetic metabolic reprogramming of right ventricular fibroblasts in pulmonary arterial hypertension: a pyruvate dehydrogenase kinase-dependent shift in mitochondrial

metabolism promotes right ventricular fibrosis. *Circ Res* (2020) 126(12):1723–45. doi: 10.1161/CIRCRESAHA.120.316443

57. Bisserier M, Mathiyalagan P, Zhang S, Elmastour F, Dorfmuller P, Humbert M, et al. Regulation of the methylation and expression levels of the BMPR2 gene by SIN3a as a novel therapeutic mechanism in pulmonary arterial hypertension. *Circulation* (2021) 144(1):52–73. doi: 10.1161/CIRCULATIONAHA.120.047978

58. Greer EL, Shi Y. Histone methylation: a dynamic mark in health, disease and inheritance. *Nat Rev Genet* (2012) 13(5):343–57. doi: 10.1038/nrg3173

59. Murray K. The occurrence of epsilon-N-Methyl lysine in histones. *Biochemistry* (1964) 3:10–5. doi: 10.1021/bi00889a003

60. Byvoet P, Shepherd GR, Hardin JM, Noland BJ. The distribution and turnover of labeled methyl groups in histone fractions of cultured mammalian cells. *Arch Biochem Biophys* (1972) 148(2):558–67. doi: 10.1016/0003-9861(72)90174-9

61. Mosammaparast N, Shi Y. Reversal of histone methylation: biochemical and molecular mechanisms of histone demethylases. *Annu Rev Biochem* (2010) 79:155–79. doi: 10.1146/annurev.biochem.78.070907.103946

62. Wei FZ, Cao Z, Wang X, Wang H, Cai MY, Li T, et al. Epigenetic regulation of autophagy by the methyltransferase EZH2 through an MTOR-dependent pathway. *Autophagy* (2015) 11(12):2309–22. doi: 10.1080/15548627.2015.1117734

63. Aljubran SA, Cox RJr., Tamarapu Parthasarathy P, Kollongod Ramanathan G, Rajanbabu V, Bao H, et al. Enhancer of zeste homolog 2 induces pulmonary artery smooth muscle cell proliferation. *PloS One* (2012) 7(5):e37712. doi: 10.1371/journal.pone.0037712

64. Li R, Yi X, Wei X, Huo B, Guo X, Cheng C, et al. EZH2 inhibits autophagic cell death of aortic vascular smooth muscle cells to affect aortic dissection. *Cell Death Dis* (2018) 9(2):180. doi: 10.1038/s41419-017-0213-2

65. Wang Y, Huang XX, Leng D, Li JF, Liang Y, Jiang T. Effect of EZH2 on pulmonary artery smooth muscle cell migration in pulmonary hypertension. *Mol Med Rep* (2021) 23(2):129. doi: 10.3892/mmr.2020.11768

66. Shi ZL, Fang K, Li ZH, Ren DH, Zhang JY, Sun J. EZH2 inhibition ameliorates transverse aortic constriction-induced pulmonary arterial hypertension in mice. *Can Respir J* (2018) 2018:9174926. doi: 10.1155/2018/9174926

67. Kim E, Kim M, Woo DH, Shin Y, Shin J, Chang N, et al. Phosphorylation of EZH2 activates STAT3 signaling *via* STAT3 methylation and promotes tumorigenicity of glioblastoma stem-like cells. *Cancer Cell* (2013) 23(6):839–52. doi: 10.1016/j.ccr.2013.04.008

68. Hsieh YY, Lo HL, Yang PM. EZH2 inhibitors transcriptionally upregulate cytotoxic autophagy and cytoprotective unfolded protein response in human colorectal cancer cells. *Am J Cancer Res* (2016) 6(8):1661–80.

69. Qian C, Yang C, Tang Y, Zheng W, Zhou Y, Song M, et al. Pharmacological manipulation of Ezh2 with salvianolic acid B results in tumor vascular normalization and synergizes with cisplatin and T cell-mediated immunotherapy. *Pharmacol Res* (2022) 182:106333. doi: 10.1016/j.phrs.2022.106333

70. Sun Y, Jin L, Liu JH, Sui YX, Han LL, Shen XL. Interfering EZH2 expression reverses the cisplatin resistance in human ovarian cancer by inhibiting autophagy. *Cancer Biother Radiopharm.* (2016) 31(7):246–52. doi: 10.1089/cbr.2016.2034

71. Jin Q, Yu LR, Wang L, Zhang Z, Kasper LH, Lee JE, et al. Distinct roles of GCN5/PCAF-mediated H3K9ac and CBP/p300-mediated H3K18/27ac in nuclear receptor transactivation. *EMBO J* (2011) 30(2):249–62. doi: 10.1038/emboj.2010.318

72. Park SE, Yi HJ, Suh N, Park YY, Koh JY, Jeong SY, et al. Inhibition of EHMT2/G9a epigenetically increases the transcription of beclin-1 *via* an increase in ROS and activation of NF-kappaB. *Oncotarget* (2016) 7(26):39796–808. doi: 10.18632/oncotarget.9290

73. Artal-Martinez de Narvajas A, Gomez TS, Zhang JS, Mann AO, Taoda Y, Gorman JA, et al. Epigenetic regulation of autophagy by the methyltransferase G9a. *Mol Cell Biol* (2013) 33(20):3983–93. doi: 10.1128/MCB.00813-13

74. Greer EL, Maures TJ, Hauswirth AG, Green EM, Leeman DS, Maro GS, et al. Members of the H3K4 trimethylation complex regulate lifespan in a germline-dependent manner in c. *elegans. Nature.* (2010) 466(7304):383–7. doi: 10.1038/nature09195

75. Fang R, Barbera AJ, Xu Y, Rutenberg M, Leonor T, Bi Q, et al. Human LSD2/KDM1b/AOF1 regulates gene transcription by modulating intragenic H3K4me2 methylation. *Mol Cell* (2010) 39(2):222–33. doi: 10.1016/j.molcel.2010.07.008

76. Gonzalez-Jaramillo V, Portilla-Fernandez E, Glisic M, Voortman T, Bramer W, Chowdhury R, et al. The role of DNA methylation and histone modifications in blood pressure: a systematic review. *J Hum Hypertens* (2019) 33(10):703–15. doi: 10.1038/s41371-019-0218-7

77. Shin HJ, Kim H, Oh S, Lee JG, Kee M, Ko HJ, et al. AMPK-SKP2-CARM1 signalling cascade in transcriptional regulation of autophagy. *Nature* (2016) 534 (7608):553–7. doi: 10.1038/nature18014

78. Suresh S, Huard S, Dubois T. CARM1/PRMT4: making its mark beyond its function as a transcriptional coactivator. *Trends Cell Biol* (2021) 31(5):402–17. doi: 10.1016/j.tcb.2020.12.010

79. Kullo IJ, Ding K, Boerwinkle E, Turner ST, Mosley THJr., Kardia SL, et al. Novel genomic loci influencing plasma homocysteine levels. *Stroke* (2006) 37(7):1703–9. doi: 10.1161/01.STR.0000225929.96190.b3

80. Song H, Feng X, Zhang M, Jin X, Xu X, Wang L, et al. Crosstalk between lysine methylation and phosphorylation of ATG16L1 dictates the apoptosis of hypoxia/reoxygenation-induced cardiomyocytes. *Autophagy* (2018) 14(5):825–44. doi: 10.1080/15548627.2017.1389357

81. Yin Z, Chen C, Yang J, Feng W, Liu X, Zuo R, et al. Histone acetyltransferase MoHat1 acetylates autophagy-related proteins MoAtg3 and MoAtg9 to orchestrate functional appressorium formation and pathogenicity in magnaporthe oryzae. *Autophagy* (2019) 15(7):1234–57. doi: 10.1080/15548627.2019.1580104

82. Kong J, Kong F, Gao J, Zhang Q, Dong S, Gu F, et al. YC-1 enhances the anti-tumor activity of sorafenib through inhibition of signal transducer and activator of transcription 3 (STAT3) in hepatocellular carcinoma. *Mol Cancer.* (2014) 13:7. doi: 10.1186/1476-4598-13-7

83. Mazure NM, Pouyssegur J. Hypoxia-induced autophagy: cell death or cell survival? *Curr Opin Cell Biol* (2010) 22(2):177–80. doi: 10.1016/j.ceb.2009.11.015

84. Duga B, Czako M, Komlosi K, Hadzsiev K, Torok K, Sumegi K, et al. Deletion of 4q28.3-31.23 in the background of multiple malformations with pulmonary hypertension. *Mol Cytogenet* (2014) 7:36. doi: 10.1186/1755-8166-7-36

85. Cheng Z, Du Z, Zhai B, Yang Z, Zhang T. U1 small nuclear RNA overexpression implicates autophagic-lysosomal system associated with AD. *Neurosci Res* (2018) 136:48–55. doi: 10.1016/j.neures.2018.01.006

86. Luo HR, Moreau GA, Levin N, Moore MJ. The human Prp8 protein is a component of both U2- and U12-dependent spliceosomes. *RNA* (1999) 5(7):893–908. doi: 10.1017/s1355838299990520

87. Xu G, Li T, Chen J, Li C, Zhao H, Yao C, et al. Autosomal dominant retinitis pigmentosa-associated gene PRPF8 is essential for hypoxia-induced mitophagy through regulating ULK1 mRNA splicing. *Autophagy* (2018) 14(10):1818–30. doi: 10.1080/15548627.2018.1501251

88. Yoshida K, Sanada M, Shiraishi Y, Nowak D, Nagata Y, Yamamoto R, et al. Frequent pathway mutations of splicing machinery in myelodysplasia. *Nature* (2011) 478(7367):64–9. doi: 10.1038/nature10496

89. Lv Y, Zhang W, Zhao J, Sun B, Qi Y, Ji H, et al. SRSF1 inhibits autophagy through regulating bcl-x splicing and interacting with PIK3C3 in lung cancer. *Signal Transduct Target Ther* (2021) 6(1):108. doi: 10.1038/s41392-021-00495-6

90. Ji E, Lee H, Ahn S, Jung M, Lee SH, Lee JH, et al. Heterogeneous nuclear ribonucleoprotein A1 promotes the expression of autophagy-related protein 6 in human colorectal cancer. *Biochem Biophys Res Commun* (2019) 513(1):255–60. doi: 10.1016/j.bbrc.2019.03.179

91. Woodcock CC, Hafeez N, Handen A, Tang Y, Harvey LD, Estephan LE, et al. Matrix stiffening induces a pathogenic QKI-miR-7-SRSF1 signaling axis in pulmonary arterial endothelial cells. *Am J Physiol Lung Cell Mol Physiol* (2021) 320(5):L726–38. doi: 10.1152/ajplung.00407.2020

92. Wei R, Chen L, Li P, Lin C, Zeng Q. IL-13 alleviates idiopathic pulmonary hypertension by inhibiting the proliferation of pulmonary artery smooth muscle cells and regulating macrophage infiltration. *Am J Transl Res* (2022) 14(7):4573–90.

93. Tang Y, Zha L, Zeng X, Yu Z. Identification of biomarkers related to systemic sclerosis with or without pulmonary hypertension using Co-expression analysis. *J Comput Biol* (2020) 27(10):1519–31. doi: 10.1089/cmb.2019.0492

94. Isakson P, Holland P, Simonsen A. The role of ALFY in selective autophagy. *Cell Death Differ* (2013) 20(1):12–20. doi: 10.1038/cdd.2012.66

95. Tranchevent LC, Aube F, Dulaurier L, Benoit-Pilven C, Rey A, Poret A, et al. Identification of protein features encoded by alternative exons using exon ontology. *Genome Res* (2017) 27(6):1087–97. doi: 10.1101/gr.212696.116

96. Bargiela A, Sabater-Arcis M, Espinosa-Espinosa J, Zulaica M, Lopez de Munain A, Artero R. Increased muscleblind levels by chloroquine treatment improve myotonic dystrophy type 1 phenotypes in *in vitro* and *in vivo* models. *Proc Natl Acad Sci U S A.* (2019) 116(50):25203–13. doi: 10.1073/pnas.1820297116

97. Cogan J, Austin E, Hedges L, Womack B, West J, Loyd J, et al. Role of BMPR2 alternative splicing in heritable pulmonary arterial hypertension penetrance. *Circulation* (2012) 126(15):1907–16. doi: 10.1161/CIRCULATIONAHA.112.106245

98. Niu YN, Liu QQ, Zhang SP, Yuan N, Cao Y, Cai JY, et al. Alternative messenger RNA splicing of autophagic gene beclin 1 in human b-cell acute lymphoblastic leukemia cells. *Asian Pac J Cancer Prev* (2014) 15(5):2153–8. doi: 10.7314/apjcp.2014.15.5.2153

99. Cheng B, Xu A, Qiao M, Wu Q, Wang W, Mei Y, et al. BECN1s, a short splice variant of BECN1, functions in mitophagy. *Autophagy* (2015) 11(11):2048–56. doi: 10.1080/15548627.2015.1100785

100. Jin Y, Choi AM. Cross talk between autophagy and apoptosis in pulmonary hypertension. *Pulm Circ* (2012) 2(4):407–14. doi: 10.4103/2045-8932.105029

101. Ivanovska J, Shah S, Wong MJ, Kantores C, Jain A, Post M, et al. mTOR-Notch3 signaling mediates pulmonary hypertension in hypoxia-exposed neonatal rats independent of changes in autophagy. *Pediatr Pulmonol.* (2017) 52(11):1443–54. doi: 10.1002/ppul.23777

102. Zhang MQ, Li JR, Peng ZG, Zhang JP. Differential effects of autophagy-related 10 protein on HCV replication and autophagy flux are mediated by its Cysteine(44) and Cysteine(135). *Front Immunol* (2018) 9:2176. doi: 10.3389/fimmu.2018.02176

103. Sun Q, Fan W, Chen K, Ding X, Chen S, Zhong Q. Identification of barkor as a mammalian autophagy-specific factor for beclin 1 and class III phosphatidylinositol 3-kinase. *Proc Natl Acad Sci U S A.* (2008) 105(49):19211–6. doi: 10.1073/pnas.0810452105

104. Diao J, Liu R, Rong Y, Zhao M, Zhang J, Lai Y, et al. ATG14 promotes membrane tethering and fusion of autophagosomes to endolysosomes. *Nature* (2015) 520(7548):563–6. doi: 10.1038/nature14147

105. Greer SU, Chen J, Ogmundsdottir MH, Ayala C, Lau BT, Delacruz RGC, et al. Germline variants of ATG7 in familial cholangiocarcinoma alter autophagy and p62. *Sci Rep* (2022) 12(1):10333. doi: 10.1038/s41598-022-13569-4

106. Gammoh N. The multifaceted functions of ATG16L1 in autophagy and related processes. *J Cell Sci* (2020) 133(20):jcs249227. doi: 10.1242/jcs.249227

107. Lystad AH, Carlsson SR, de la Ballina LR, Kauffman KJ, Nag S, Yoshimori T, et al. Distinct functions of ATG16L1 isoforms in membrane binding and LC3B lipidation in autophagy-related processes. *Nat Cell Biol* (2019) 21(3):372–83. doi: 10.1038/s41556-019-0274-9

108. Fujiwara Y, Furuta A, Kikuchi H, Aizawa S, Hatanaka Y, Konya C, et al. Discovery of a novel type of autophagy targeting RNA. *Autophagy* (2013) 9(3):403–9. doi: 10.4161/auto.23002

109. Bryant A, Palma CA, Jayaswal V, Yang YW, Lutherborrow M, Ma DD. miR-10a is aberrantly overexpressed in Nucleophosmin1 mutated acute myeloid leukaemia and its suppression induces cell death. *Mol Cancer*. (2012) 11:8. doi: 10.1186/1476-4598-11-8

110. Wu H, Wang F, Hu S, Yin C, Li X, Zhao S, et al. MiR-20a and miR-106b negatively regulate autophagy induced by leucine deprivation *via* suppression of ULK1 expression in C2C12 myoblasts. *Cell Signal* (2012) 24(11):2179–86. doi: 10.1016/j.cellsig.2012.07.001

111. Huang Y, Chuang AY, Ratovitski EA. Phospho-DeltaNp63alpha/miR-885-3p axis in tumor cell life and cell death upon cisplatin exposure. *Cell Cycle* (2011) 10 (22):3938–47. doi: 10.4161/cc.10.22.18107

112. Yang J, Chen D, He Y, Melendez A, Feng Z, Hong Q, et al. MiR-34 modulates caenorhabditis elegans lifespan *via* repressing the autophagy gene atg9. *Age (Dordr)*. (2013) 35(1):11–22. doi: 10.1007/s11357-011-9324-3

113. Shi G, Shi J, Liu K, Liu N, Wang Y, Fu Z, et al. Increased miR-195 aggravates neuropathic pain by inhibiting autophagy following peripheral nerve injury. *Glia* (2013) 61(4):504–12. doi: 10.1002/glia.22451

114. Huang Y, Guerrero-Preston R, Ratovitski EA. Phospho-DeltaNp63alpha-dependent regulation of autophagic signaling through transcription and micro-RNA modulation. *Cell Cycle* (2012) 11(6):1247–59. doi: 10.4161/cc.11.6.19670

115. Korkmaz G, le Sage C, Tekirdag KA, Agami R, Gozuacik D. miR-376b controls starvation and mTOR inhibition-related autophagy by targeting ATG4C and BECN1. *Autophagy* (2012) 8(2):165–76. doi: 10.4161/auto.8.2.18351

116. Yu Y, Yang L, Zhao M, Zhu S, Kang R, Vernon P, et al. Targeting microRNA-30a-mediated autophagy enhances imatinib activity against human chronic myeloid leukemia cells. *Leukemia* (2012) 26(8):1752–60. doi: 10.1038/leu.2012.65

117. Comincini S, Allavena G, Palumbo S, Morini M, Durando F, Angeletti F, et al. microRNA-17 regulates the expression of ATG7 and modulates the autophagy process, improving the sensitivity to temozolomide and low-dose ionizing radiation treatments in human glioblastoma cells. *Cancer Biol Ther* (2013) 14(7):574–86. doi: 10.4161/cbt.24597

118. Atala A. Re: VHL-regulated miR-204 suppresses tumor growth through inhibition of LC3B-mediated autophagy in renal clear cell carcinoma. *J Urol.* (2012) 188(6):2434. doi: 10.1016/j.juro.2012.08.067

119. Meenhuis A, van Veelen PA, de Looper H, van Boxtel N, van den Berge IJ, Sun SM, et al. MiR-17/20/93/106 promote hematopoietic cell expansion by targeting sequestosome 1-regulated pathways in mice. *Blood* (2011) 118(4):916–25. doi: 10.1182/blood-2011-02-336487

120. Jing X, Wu S, Liu Y, Wang H, Huang Q. Circular RNA Sirtuin1 represses pulmonary artery smooth muscle cell proliferation, migration and autophagy to ameliorate pulmonary hypertension *via* targeting microRNA-145-5p/protein kinase-B3 axis. *Bioengineered* (2022) 13(4):8759–71. doi: 10.1080/21655979.2022.2036302

121. Zhang J, Li Y, Chen Y, Yu X, Wang S, Sun H, et al. Circ-calm4 regulates hypoxia-induced pulmonary artery smooth muscle autophagy by binding purb. *J Mol Cell Cardiol* (2023) 176:41–54. doi: 10.1016/j.yjmcc.2023.01.009

122. Liu T, Zou XZ, Huang N, Ge XY, Yao MZ, Liu H, et al. Down-regulation of miR-204 attenuates endothelial-mesenchymal transition by enhancing autophagy in hypoxia-induced pulmonary hypertension. *Eur J Pharmacol* (2019) 863:172673. doi: 10.1016/j.ejphar.2019.172673

123. Travers JG, Wennersten SA, Pena B, Bagchi RA, Smith HE, Hirsch RA, et al. And blocks covert extracellular matrix remodeling. *Circulation* (2021) 143(19):1874–90. doi: 10.1161/CIRCULATIONAHA.120.046462

124. Wang J, Saren G, Jiang H. HDAC inhibition: a novel therapeutic target for attenuating pulmonary hypertension by regulating tregs. *Int J Cardiol* (2015) 198:176–7. doi: 10.1016/j.ijcard.2015.06.172

125. Humbert M, McLaughlin V, Gibbs JSR, Gomberg-Maitland M, Hoeper MM, Preston IR, et al. Sotatercept for the treatment of pulmonary arterial hypertension. *N Engl J Med* (2021) 384(13):1204–15. doi: 10.1056/NEJMoa2024277

126. Thenappan T, Ormiston ML, Ryan JJ, Archer SL. Pulmonary arterial hypertension: pathogenesis and clinical management. *BMJ* (2018) 360:j5492. doi: 10.1136/bmj.j5492

127. Wu YC, Wang WT, Lee SS, Kuo YR, Wang YC, Yen SJ, et al. Glucagon-like peptide-1 receptor agonist attenuates autophagy to ameliorate pulmonary arterial hypertension through Drp1/NOX- and atg-5/Atg-7/Beclin-1/LC3beta pathways. *Int J Mol Sci* (2019) 20(14):3435. doi: 10.3390/ijms20143435

128. Zhou Y, Wang Y, Wang X, Tian X, Zhang S, Yang F, et al. The protective effects of kappa-opioid receptor stimulation in hypoxic pulmonary hypertension involve inhibition of autophagy through the AMPK-MTOR pathway. *Cell Physiol Biochem* (2017) 44(5):1965–79. doi: 10.1159/000485886

129. Wu K, Zhang Q, Wu X, Lu W, Tang H, Liang Z, et al. Chloroquine is a potent pulmonary vasodilator that attenuates hypoxia-induced pulmonary hypertension. *Br J Pharmacol* (2017) 174(22):4155–72. doi: 10.1111/bph.13990

frontiers | Frontiers in Immunology

TYPE Original Research
PUBLISHED 15 August 2023
DOI 10.3389/fimmu.2023.1162159

OPEN ACCESS

EDITED BY
Chao Yang,
Zhejiang Ocean University, China

REVIEWED BY
Qiao Shi,
Renmin Hospital of Wuhan University, China
Adriana R. Silva,
Oswaldo Cruz Foundation (Fiocruz), Brazil

*CORRESPONDENCE
Qi-quan Wan
13548685542@163.com

RECEIVED 09 February 2023
ACCEPTED 24 July 2023
PUBLISHED 15 August 2023

CITATION
Wen X-p, Li M, Zhang R-q and Wan Q-q (2023) Insulin reverses impaired alveolar fluid clearance in ARDS by inhibiting LPS-induced autophagy and inflammatory. *Front. Immunol.* 14:1162159. doi: 10.3389/fimmu.2023.1162159

Insulin reverses impaired alveolar fluid clearance in ARDS by inhibiting LPS-induced autophagy and inflammatory

Xu-peng Wen[1,2], Min Li[3], Ru-qi Zhang[3] and Qi-quan Wan[1]*

[1]Transplantation Center, the Third Xiangya Hospital, Central South University, Changsha, Hunan, China, [2]Department of Critical Care Medicine, Zhongshan Hospital, Fudan University, Shanghai, China, [3]Department of Anatomy and Neurobiology, School of Basic Medical Sciences, Central South University, Changsha, Hunan, China

Until now, acute respiratory distress syndrome (ARDS) has been a difficult clinical condition with a high mortality and morbidity rate, and is characterized by a build-up of alveolar fluid and impaired clearance. The underlying mechanism is not yet fully understood and no effective medications available. Autophagy activation is associated with ARDS caused by different pathogenic factors. It represents a new direction of prevention and treatment of ARDS to restrain autophagy to a reasonable level through pharmacological and molecular genetic methods. Na, K-ATPase is the main gradient driver of pulmonary water clearance in ARDS and could be degraded by the autophagy-lysosome pathway to affect its abundance and enzyme activity. As a normal growth hormone in human body, insulin has been widely used in clinical for a long time. To investigate the association of insulin with Na, K-ATPase, autophagy and inflammatory markers in LPS-treated C57BL/6 mice by survival assessment, proteomic analysis, histologic examination, inflammatory cell counting, myeloperoxidase, TNF-α and IL-1β activity analysis etc. This was also verified on mouse alveolar epithelial type II (AT II) and A549 cells by transmission electron microscopy. We found that insulin restored the expression of Na, K-ATPase, inhibited the activation of autophagy and reduced the release of inflammatory factors caused by alveolar epithelial damage. The regulation mechanism of insulin on Na, K-ATPase by inhibiting autophagy function may provide new drug targets for the treatment of ARDS.

KEYWORDS

ARDS, insulin, Na, K-ATPase, autophagy, inflammatory response

Abbreviations: ARDS, Acute respiratory distress syndrome; LPS, Lipopolysaccharide; BALF, Bronchoalveolar lavage fluid; AT II, Alveolar type II epithelial; W/D, Wet/dry; ENaC, Epithelial Na+ channel; A549, Human non-small cell lung cancer cell line/Human AT II cell line; AFC, Alveolar fluid clearance; GO, Gene Ontology; MPO, Myeloperoxidase; TEM, Transmission electron microscopy; ATP1A1, Na, K-ATPase α1; ATP1B1, Na, K-ATPase β1; HE, Hematoxylin-eosin; BCA, Bicinchoninic acid; ELISA, Enzyme-linked immunosorbent assay; TNF-α, Tumor necrosis factor α; AMPK, Adenosine 5'-monophosphate (AMP)-activated protein kinase; AP, Autophagosomes; ASS, Autolysosomes; SP-C, Surfactant-associated protein C.

1 Introduction

Acute respiratory distress syndrome (ARDS) is a clinically life-threatening disease with poor prognosis and high treatment cost, characterized by intractable hypoxemia due to the accumulation of alveolar fluid. Severe pulmonary inflammation, damaged alveolar epithelium and impaired gas exchange with pulmonary edema are one of the main pathological features of ARDS (1, 2). The mechanisms of ARDS are intricately related to each other, which makes it extremely difficult to treat, and the mortality rate is as high as 35-55% (3, 4). For most patients with ARDS, effective removal of excess edema fluid from the alveoli and maintenance of a dry environment in the alveolar space are the main ways to relieve ARDS. In the past few years, researches on pulmonary water removal in ARDS have been in full swing, but no breakthroughs have been achieved so far.

Na, K-ATPase -mediated Na^+ transport at the basolateral of alveolar type II epithelial (AT II) cells is the main driving force for alveolar fluid clearance (AFC) (5). The dysregulation of Na, K-ATPase in the ARDS state subsequently exacerbates pulmonary edema production mostly due to the restriction of Na^+ transport and disruption of alveolar barrier function (6). Na, K-ATPase is a trimeric structure consisting of α, β and γ subunits. Among them, the α subunit plays a key role in edema fluid transporting (7). The α1, which carries several binding and functional domains, is not only most common in AT II cells and the main driver of intrapulmonary Na^+ - K^+ exchange but also facilitates AFC (8, 9). Intriguingly, Na, K-ATPase could be degraded via the autophagy-lysosome pathway, and it has been shown that the connection between the Na, K-ATPase and autophagy requires the involvement of the Na, K-ATPase α1 (10).

Pulmonary autophagy is a response of alveolar epithelial cells to long-term and sustained stimulation of external and internal factors. It maintains the balance of structure, metabolism and function of alveolar epithelial cells by phagocytosis of its cytoplasm or organelles and degradation in lysosomes (11). Several studies have shown that excessive autophagy exacerbates cellular injury. In contrast, inhibiting autophagy to a moderate level is beneficial in reducing lung injury in ARDS (12, 13). Studies have shown that Na, K-ATPase α1 and AMPK may serve as the "on" and "off" states of the autophagy pathway (10). Taken together, autophagy appears to contribute to endothelial barrier disruption caused by edema-inducing mediators, and inhibition of autophagy can protect against endothelial barrier function caused by ARDS.

Insulin has been reported to prevent or attenuate the occurrence of lipopolysaccharides (LPS)-induced acute lung injury in rats (14). Insulin upregulated the relative abundance of Na, K-ATPase on cell membranes and restored the efficiency of transporting (15). Therefore, insulin may act as a potential co-promoter of the Na, K-ATPase, suggesting that insulin may be promising as a therapeutic agent for ARDS. In our study, we found that LPS induced autophagy in ARDS mice, A549 cells and AT II cells, inhibited Na, K-ATPase α1 activity, and promoted the inflammatory response. Meanwhile, insulin inhibited their autophagy and inflammation levels and upregulated Na, K-ATPase function. Our study reveals that insulin is likely to regulate Na, K-ATPase α1 expression by inhibiting autophagy and thus reversing the impaired AFC in ARDS caused by LPS, and the effect of insulin on inflammatory response may also improve the prognosis of ARDS by targeting various key factors which promote AFC.

2 Materials and methods

2.1 Animal experiment

All experimental animal treatment procedures were approved by the Department of Laboratory Animals of Xiangya School of Medicine, Central South University, and are carried out under the Guide for the Use of Laboratory Animals by the National Institutes of Health. The male C57BL/6 mice from 6 to 8 weeks old were purchased from the Department of Laboratory Animals of Xiangya School of Medicine, Central South University (Changsha, China). All mice were housed in specific pathogen-free conditions at 22°C environment under 12 h light/dark cycle.

2.2 *In vivo* model of ARDS

A total of 120 mice were randomly divided into different groups according to different experimental requirements. To assess mortality, mice are treated with different doses (0.5, 1.0 and 1.5 IU/kg) of insulin 0.5 h after injection of 10 mg/kg LPS intratracheally. Different doses of insulin were dissolved in different concentrations of glucose solution (1%, 5%, 10%) to avoid hypoglycemia and to keep the blood glucose concentration in the appropriate range. The mortality of the mice was recorded every 12 h for 3 days after LPS injection. The experiments were performed using mice from the same litter, with 10 mice in each group.

To further investigate the effect of insulin on ARDS, mice were randomly divided into four groups: 1) control group (n=6): mice received normal saline (NS) instilled intratracheally; 2) LPS group (n=6): mice were administered LPS (10 mg/kg) instilled intratracheally; 3) Insulin group (n=6): mice were given insulin (1.0 IU/kg) under subcervical skin 0.5 h after saline administration (n=6); 4) LPS+insulin group(n=6) mice received insulin (1.0 IU/kg) 0.5 h after LPS (10 mg/kg) administration (n=6).

Mice were anesthetized by using sodium pentobarbital (30 mg/kg, i.p.) throughout modeling. LPS and saline were administered via a tracheal tube connected to the animal's ventilator, which allows the LPS and saline to be evenly distributed in the lungs of the mice. Insulin and saline were administered by subcutaneous injection under the neck. A blood glucose meter detected blood glucose level during drug administration (Figure 1).

2.3 Pulmonary histopathology

The lung tissues were fixed in 4% formaldehyde, embedded in paraffin and cut into 5 μm thick sections. Next, the sections were

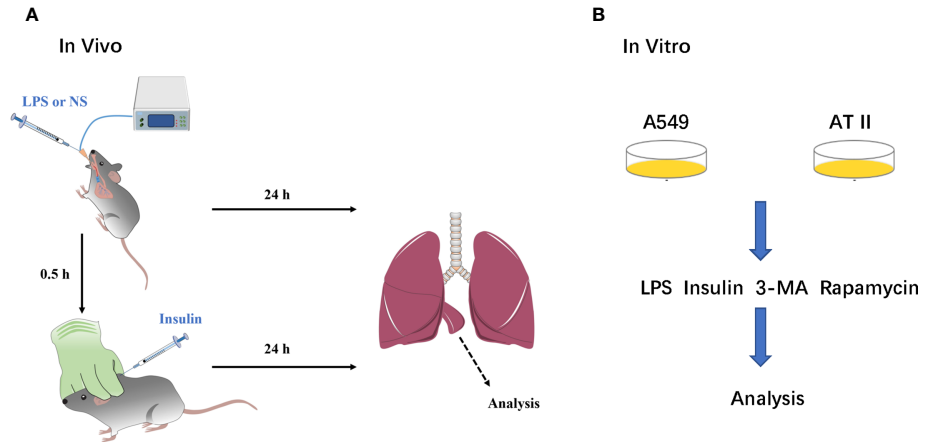

FIGURE 1
A simple flow chart of animals and cells experiments. **(A)** ARDS animals model and insulin intervention; **(B)** ARDS cells model and insulin intervention.

stained with hematoxylin-eosin (HE). Changes in lung histopathology were observed under the microscope and a pathology score was obtained. Depending on the degree of lung injury, hemorrhage, edema, exudation, necrosis, congestion, neutrophil infiltration, and pulmonary atelectasis, the score is based on a scale of 0 to 4 (16): no injury = 0, lesion field <25% = 1, lesion field 25-50% = 2, lesion field 50-70% = 3, full field of vision = 4. Scores were calculated for statistical analysis.

2.4 Inflammatory cell counting and protein concentration determination in the BALF

The collected bronchoalveolar lavage fluid (BALF) was centrifuged at 1000×g for 15 minutes at 4°C, the supernatant was collected and frozen at -80°C for subsequent assays. The total number of inflammatory cells in the BALF was determined by counting cells with a blood cell counter (Beckman Coulter, Inc.) after resuspension of the cell precipitate in PBS and exclusion of dead cells by Tissue Blue staining. For analysis of cell numbers, 100 µl of BALF was centrifuged onto slides by Cytospin (Thermo Fisher Scientific, Waltham, USA). After the slides were dried, the cells were fixed and stained using Wright's staining solution (32857, Sigma, USA) according to the manufacturer's instructions. The number of neutrophils was sorted to determine the percentage of neutrophils by a laboratory technician who was unaware of the experimental design. The frozen BALF supernatant was thawed and mixed thoroughly and the total protein concentration was determined by the BCA (bicinchoninic acid) method.

2.5 Lung wet/dry ratios

Mice were sacrificed and the lung was removed and aspirated. Wet weights were obtained immediately. The lungs were then dried in an oven at 80°C for 48 hours to obtain a dry weight. Lung tissue edema was assessed by calculating the ratio of wet to dry lungs.

2.6 Enzyme-linked immunosorbent assay

Collect BALF as described above. Myeloperoxidase (MPO) was measured in BALF using MPO ELISA kits (Cusabio, China) per the manufacturer's instructions. And the levels of TNF-α and IL-1β in serum were determined using ELISA kits according to the manufacturer's instructions.

2.7 Cell culture and treatment

We performed the isolation, culture and purification of mouse primary AT II cells: According to the Elise M method (17).A549 cell line was purchased from ATCC. AT II and A549 cells were cultured in DMEM (Gibco, USA) supplemented with 10% FBS (Gibco, USA) and 1% penicillin/streptomycin (Cytiva, USA). LPS was administered to AT II and A549 cells at 1µg/ml for 12h and insulin (100nM) was administered at the eighth hour (Figure 1).

2.8 Cell viability assay

Cell viability was assessed by using the CCK-8 kit (APE Bio, USA). CCK-8 solution (20 µl) was added to 200 µl of a complete medium in each well of the 96 wells and incubated for 30 minutes. The absorbance value at 450 nm was measured using a microplate reader.

2.9 Transmission electron microscopy

A549 cells were collected, washed 3 times with 0.1 M PBS and prefixed with a 3% glutaraldehyde, then postfixed in 1% osmium tetroxide, dehydrated in series acetone, infiltrated in Epox 812 for a longer, and embedded, fixed overnight at 4°C in 2.5% glutaraldehyde, then dehydrated using an acetone gradient, embedded, sectioned and routinely stained. Semi-thin sections were stained with methylene blue, ultra-thin sections were cut with a diamond knife and stained

with uranyl acetate and lead citrate sections were examined with HT7800 transmission electron microscope from HITACHI to visualize autophagosomes and autolysosomes.

2.10 Proteomic analysis

We used the label-free quantification for proteomic analysis, with each sample prepared and detected by LC-MS/MS independently, as described in the Supplementary Material. Data are available via ProteomeXchange with identifier PXD040288.

2.11 Western blot

Protein preparation and western blot detection as previously described (18). The lung tissues, A549 cells and AT II cells were lysed with RIPA lysis buffer (Beyotime, China) on ice for 1h. Then, electrophoresed on 10-12% SDS-PAGE gels before being transferred to PVDF membranes (millipore). After blocking with 5% nonfat dry milk for 1 h, the membrane was left overnight at 4°C with the primary antibody against Beclin1, light chain 3 (LC3), P62/SQSTM1, ATG5, Na, K-ATPase α1(ATP1A1), Na, K-ATPase β1(ATP1B1), GAPDH and β-actin followed by 2 h incubation with an appropriate peroxidase-conjugated rabbit or mouse secondary antibody. The immune-reactive bands were visualized by enhanced chemiluminescence and exposed to the gel imaging system. Immunoreactive bands were analysed using image analysis software with the ECL system. The gel images were analyzed with the Image J software.

2.12 Statistical analysis

Distributed data are presented as means ± standard deviation (SD). Experimental data were compared between two independent groups by unpaired Student's t-test. The difference across multiple groups was assessed by one-way analysis of variance (ANOVA), followed by a Tukey test for multiple comparisons. Survival data was presented by the Kaplane-Meier method and comparisons were made by the log rank test All data processing using the GraphPad 8.0 software. Statistical significance was established at $P < 0.05$.

3 Results

3.1 Insulin reduces cumulative mortality in LPS-induced ARDS mice

To verify whether insulin has a therapeutic effect on the ARDS model and determine the concentration of insulin to be used in subsequent experiments, we used insulin (0.5/1.0/1.5 IU/kg) which were administered 0.5 h after LPS (10 mg/kg) administration, and found that (as shown in Figure 2) insulin significantly improved the survival of LPS-induced ARDS mice, with cumulative survival rates of 60% and 40% during 3 days in the 1.0 IU/kg and 1.5 IU/kg insulin groups, respectively, significantly higher than that in the LPS group (10%, $P < 0.01$), and the cumulative survival rate was higher at 1.0 IU/kg (60%) than at 1.5 IU/kg (40%) ($P < 0.05$) insulin group. No preventive effect of 0.5 IU/kg insulin on death (30%, $P > 0.05$). Therefore, we chose 1.0 IU/kg insulin to go for the subsequent series of experiments.

3.2 Proteomics found that autophagy-lysosome pathway plays an indispensable role in the treatment of ARDS mice with insulin

To understand the specific regulatory mechanism of insulin in the process of ARDS and reveal the differential expression of related proteins after ARDS, we established the interaction group of insulin and LPS at the protein expression level by label-free quantification (Figure 3). C57 mice were treated with LPS to simulate inflammatory injury and additionally intervened with insulin. For group comparisons, we used volcano plots to display (Figures 4A–C) up- and down-regulated proteins for each group. To test the rationality and accuracy of the selected differentially expressed proteins, we used the screened proteins to perform hierarchical clustering on each group of samples. Compared with the control group (Control), the interacting proteins of the experimental group (LPS, LPS + Insulin) were significantly enriched, which indicates that the differentially expressed proteins have higher specificity (Figure 4D). Notably, we ranked the proteins in the LPS and LPS+Insulin groups according to Fold Change (FC) values and listed the top 10 candidate proteins that were significantly up- or down-regulated as following Table 1.

After that, we tried to use GO enrichment analysis to study the biological processes that differentially expressed proteins participated in. Interestingly, we found that many proteins are all related to autophagy-lysosomal degradation in the normal group (Control), ARDS group (LPS), and treatment group (LPS + Insulin) (Figure 5). These MS-based GO analysis data provide us with a clue that insulin may regulate the occurrence and development of ARDS through the autophagy-lysosomal degradation system.

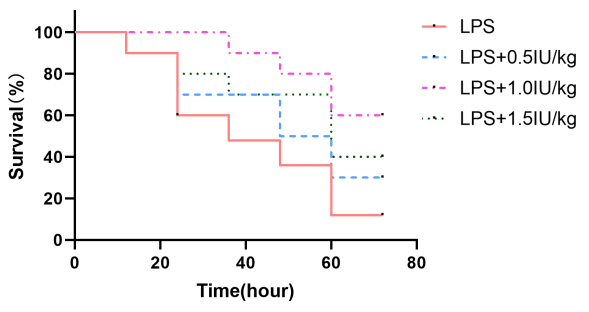

FIGURE 2
Effect of different concentrations of insulin on survival in ARDS mice. Mice were challenged with LPS (10 mg/kg) with or without different doses of insulin treatment (0.5, 1.0 and 1.5 IU/kg). Survival was observed for 12, 24, 36, 48, 60 and 72 h. Experiments were performed using mice from the same litter, each group contains 10 mice.

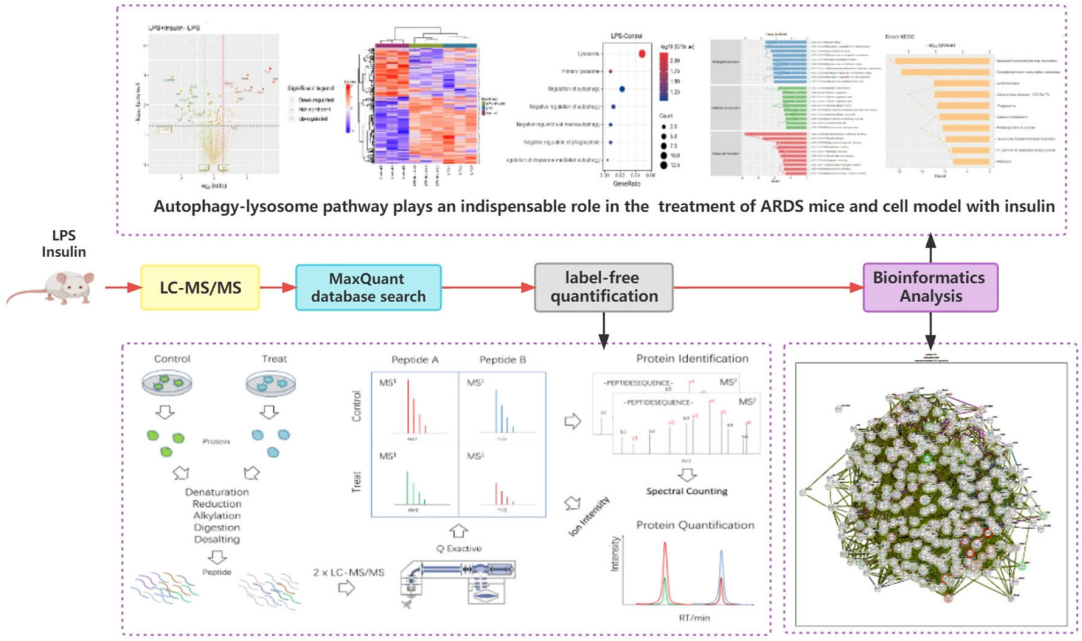

FIGURE 3
Proteomics Graphical Abstracts.

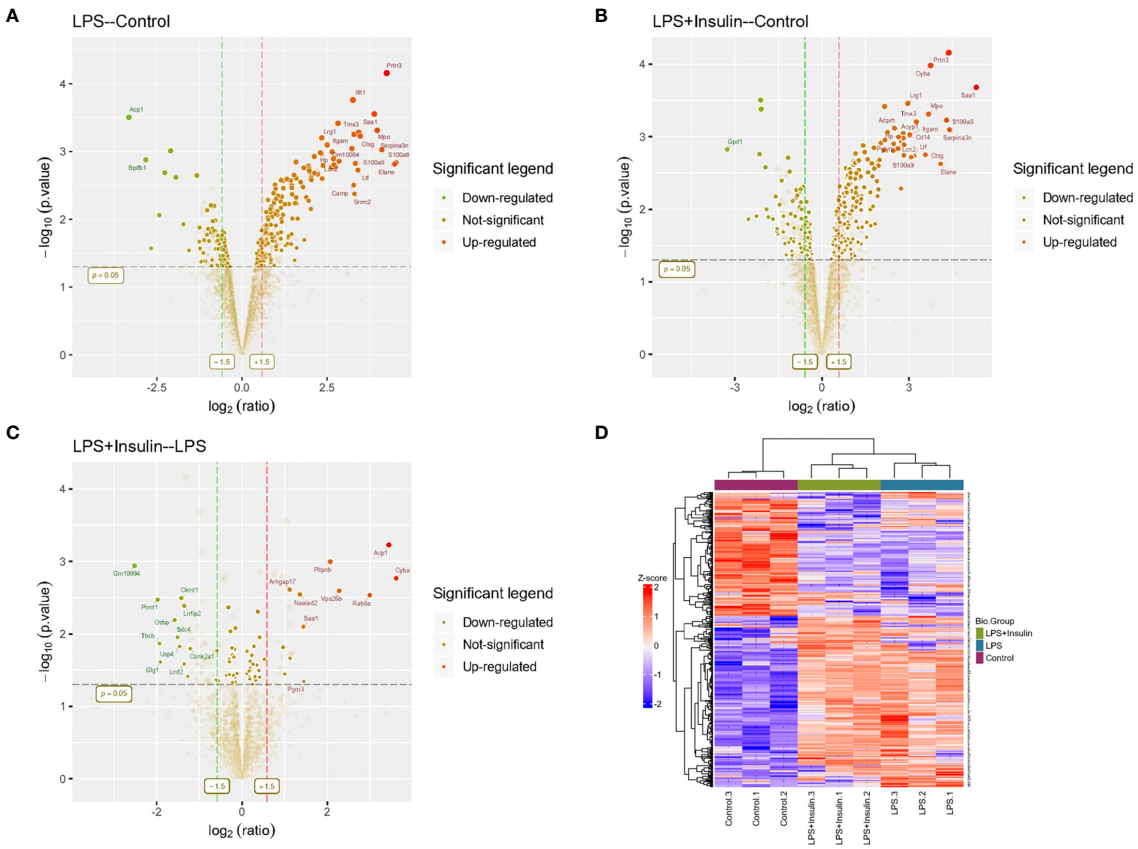

FIGURE 4
Linkage of insulin and LPS-induced ARDS by proteomics. **(A–C)** Volcano plots for LPS-Control, LPS+Insulin-Control and LPS+Insulin-LPS. Proteins with significant differences between the two groups are indicated in dark green (down-regulated) and orange-red (up-regulated), respectively. Proteins with no statistical difference are shown in brown. **(D)** Differential protein hierarchical clustering analysis, the top color bar represents the grouping of samples; the bottom is the corresponding sample name; the protein name on the right corresponds to the symbol column in the differential protein list (Supplemental Material.csv).

10.3389/fimmu.2023.1162159

TABLE 1 Up- or down-regulated proteins in the top 10 FC rankings in LPS+Insulin group vs LPS group.

Rank	LPS-A549 vs Control-A549		
	Annotation	Alias	FC*
1	keratin 17	KRT17	3.20673671
2	dihydrolipoamide dehydrogenase	DLD	2.619500792
3	nicalin	NCLN	2.355100614
4	mutS homolog 2	MSH2	2.355100614
5	heterogeneous nuclear ribonucleoprotein H3 (2H9)	HNRNPH3	1.619500792
6	stearoyl-CoA desaturase (delta-9-desaturase)	SCD	1.619500792
7	LIM and SH3 protein 1	LASP1	1.451281189
8	coatomer protein complex, subunit beta 2 (beta prime)	COPB2	1.451281189
9	coiled-coil domain containing 86	CCDC86	1.355100614
10	solute carrier family 1 (neutral amino acid transporter), member 5	SLC1A5	1.355100614
Down-regulated Proteins			
1	ribosomal RNA processing 1 homolog B	RRP1B	-3.459431619
2	dolichyl-phosphate mannosyltransferase polypeptide 1	DPM1	-2.584962501
3	GDP dissociation inhibitor 2	GDI2	-2.321928095
4	nucleoporin 107kDa	NUP107	-2.321928095
5	talin 1	TLN1	-2.321928095
6	WD repeat domain 36	WDR36	-2.321928095
7	WD repeat domain 46	WDR46	-2.149102965
8	DEAH (Asp-Glu-Ala-Asp/His) box polypeptide 57	DHX57	-2.000000000
9	G1 to S phase transition 2	GSPT2	-2.000000000
10	nuclear factor of kappa light polypeptide gene enhancer in B-cells 2	NFKB2	-2.000000000

3.3 Insulin alleviates symptoms of LPS-induced ARDS mice and exerts anti-inflammatory effect.

To explain whether insulin alleviated inflammation of ARDS induced by LPS *in vivo*, we developed the ARDS mouse model induced by LPS administration, and evaluated the changes of pulmonary histopathological features by HE staining, lung W/D ratio and lung injury score. It was indicated that the lung tissues accompanied with inflammatory cell infiltration, edema, vascular congestion and alveolar wall thickening in ARDS model induced by LPS (Figures 6A–D). However, insulin significantly attenuated LPS-induced histopathological changes. Importantly, a scoring system was used to assess the degree of lung injury. As shown in (Figure 6E), the quantitative scoring of histological lung injury in the ARDS mice was markedly increased compared with that in the control group 24 h after LPS challenge. However, insulin markedly decreased the pathological scores compared with those in the LPS group.

Lung W/D ratio and BALF total protein concentration, two commonly used indicators of pulmonary vascular permeability, are important features of ARDS. Importantly, the lung W/D ratio and BALF total protein concentration dramatically increased after LPS administration, and the phenomena were reversed with insulin treatment ($P < 0.05$) (Figures 7A, B). Meanwhile, compared with those in the LPS group, insulin significantly inhibited the increase of MPO activity and the number of neutrophil cells induced by LPS (Figures 7C, D). Besides, to investigate the anti-inflammatory effect of insulin, the levels of TNF-α and IL-1β in BALF were detected in this study. As shown in Figures 7E, F, compared with the normal control group, the levels of TNF-α and IL-1β in the BALF of the LPS group were significantly increased. Compared with the LPS group, the levels of TNF-α and IL-1β in the BALF of the LPS+insulin group were significantly decreased. These results suggest that insulin attenuates pulmonary edema and inflammation in LPS-challenged mice.

3.4 Insulin regulates the expression of the Na, K-ATPase by inhibiting autophagy in LPS-induced ARDS mouse model

Na, K-ATPase participates in the autophagy-lysosome pathway through its α1 subunit, and ATP1A1 may act as a shutdown factor of

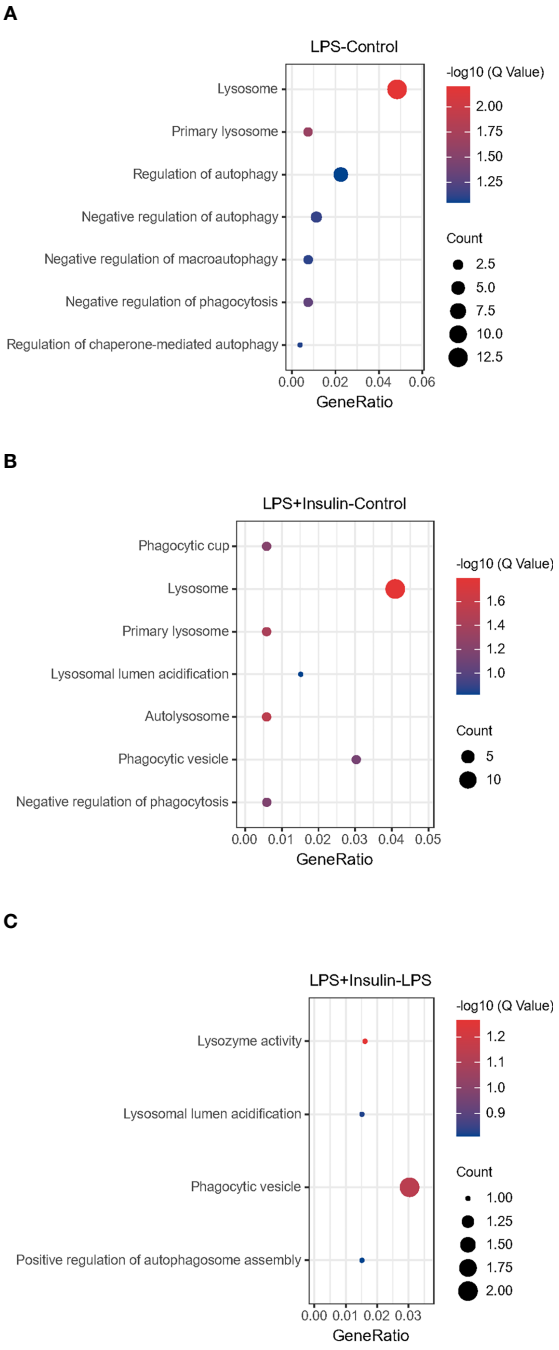

FIGURE 5
Gene Ontology analysis **(A–C)** Gene Ontology analysis revealing enrichment of biological process terms of differentially expressed proteins under LPS-Control, LPS+Insulin-Control and LPS+Insulin-LPS.

the autophagy pathway (10). To explain whether insulin reduces LPS-induced ARDS inflammation and improves Na, K-ATPase by inhibiting autophagy *in vivo*, we examined autophagy levels in an LPS-induced ARDS mouse model. We first assessed the protein levels of LC3-II/I, Beclin-1, ATG5 and P62 by western blotting. As shown in Figures 8A–E, LC3-II/I, Beclin-1 and ATG5 expression were significantly elevated and P62 expression was decreased in the LPS group. In particular, the treatment of insulin resulted in remarkably decreased LC3-II/I, Beclin-1 and ATG5 expression, while p62 accumulation was effectively enhanced in the LPS-induced ARDS mouse model. Our results suggest that LPS-induced autophagy activation was reversed by insulin *in vivo*. Furthermore, the reduce in ATP1A1 accumulation following exposure to LPS was attenuated considerably by insulin (Figures 8F, G). It can be seen that inhibiting autophagy may be crucial for regulating the expression of Na, K-ATPase in the lung tissue, improving the inflammatory response, and inhibiting the generation of pulmonary edema fluid.

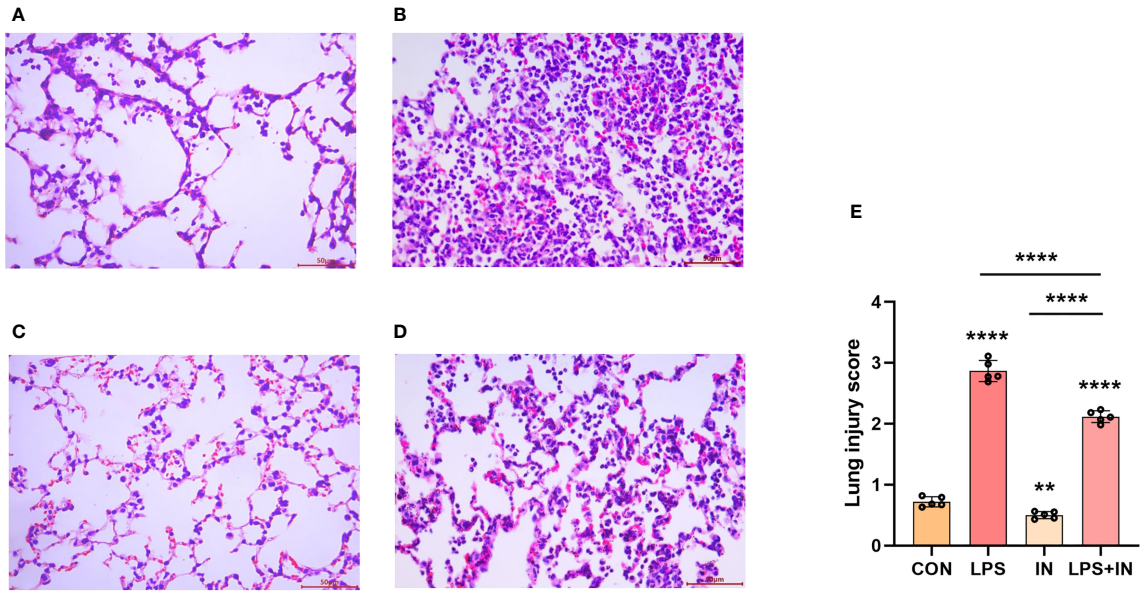

FIGURE 6
Effects of insulin on lung histopathological changes in LPS-induced ARDS mice. Mice were challenged by LPS (10 mg/kg) with or without insulin treatment (1.0 IU/kg). Representative histological changes of lung obtained from mice of different groups. **(A)** Control group, **(B)** LPS group, **(C)** Insulin group, **(D)** LPS + insulin group, (Hematoxylin and eosin staining, Scale bar, 50μm). **(E)** Lung histologic injury score. The data are presented as mean ± SD. n = 5, the horizontal line represents the comparison between each two groups, $^{**}p < 0.01$.$^{****}p < 0.0001$.

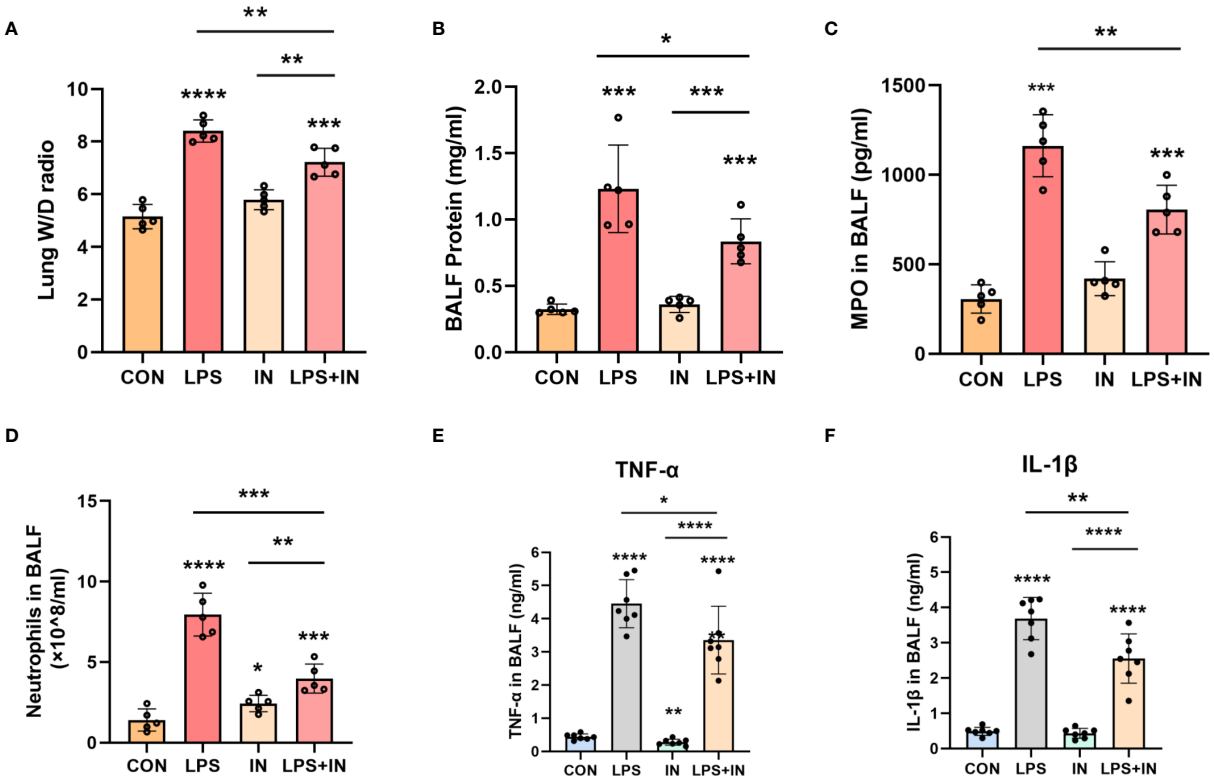

FIGURE 7
Effects of insulin on pulmonary edema and inflammation in LPS-induced ARDS mice. Treat the mice as described in Materials and Methods. **(A)** Lung W/D ratio. **(B)** BALF protein concentration. **(C)** MPO in BALF. **(D)** Neutrophils in BALF. **(E, F)** Effects of insulin on TNF-α and IL-1β production in the BALF. The data are presented as mean ± SD. n = 5, the horizontal line represents the comparison between each two groups, $^{*}p<0.05$. $^{**}p < 0.01$. $^{***}p < 0.001$. $^{****}p < 0.0001$.

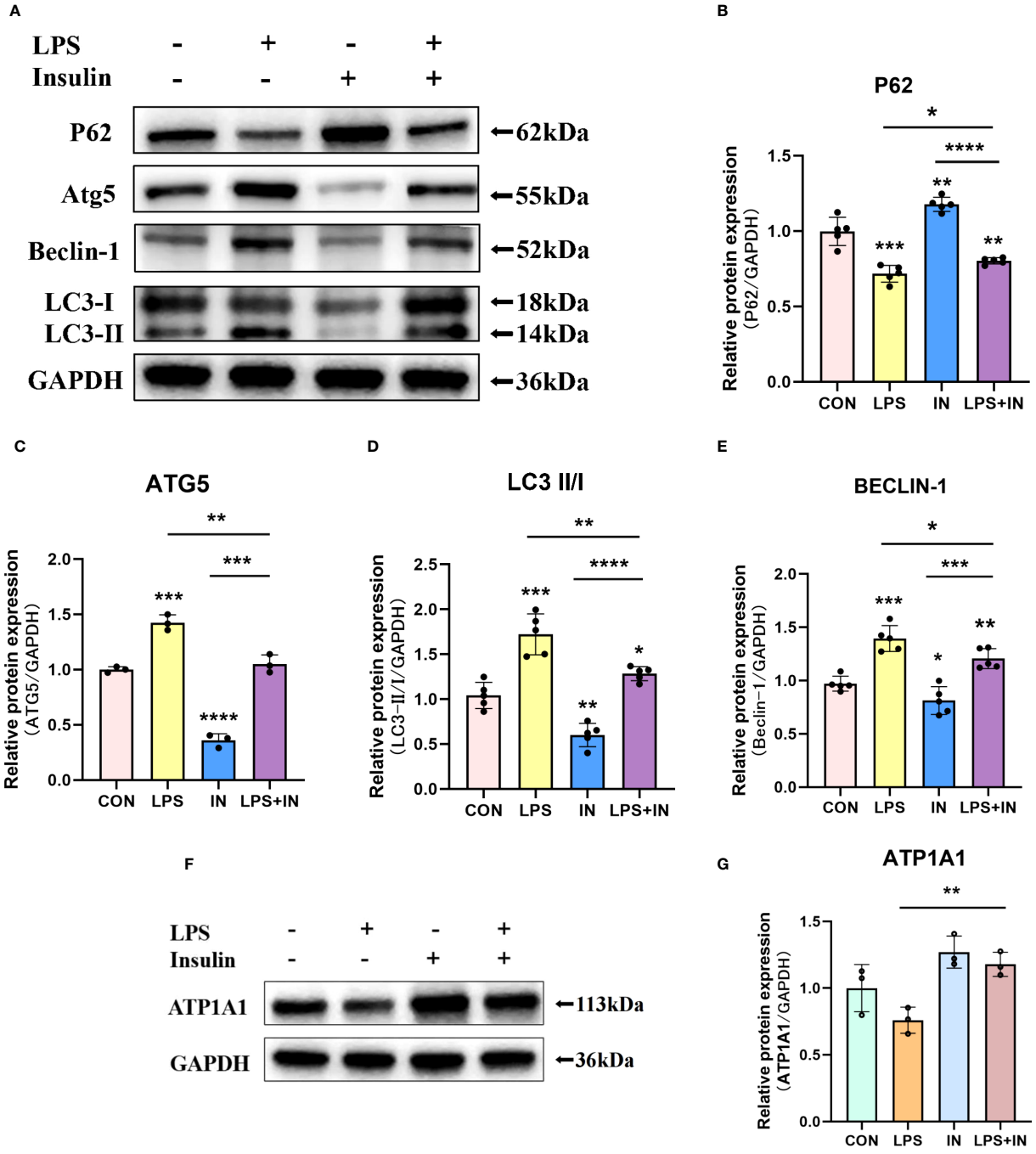

FIGURE 8
Effects of insulin on autophagy-related proteins and ATP1A1 expression in LPS-induced ARDS mice. Treat the mice as described in Materials and Methods. **(A, F)** Representative western blotting detected the levels of LC3-II/I, Beclin-1, ATG5, P62 and ATP1A1 in lung tissues **(B–E, G)** Quantitative analysis of LC3-II/I, Beclin-1, ATG5, P62 and ATP1A1 were shown in bar graphs, respectively. The data are presented as mean ± SD. n = 3, the horizontal line represented the comparison between each two groups, *p<0.05. **p < 0.01. ***p < 0.001. ****p < 0.0001.

3.5 Insulin attenuates autophagy levels and improves Na, K-ATPase expression in LPS-induced A549 cells

To directly investigate the role of LPS and insulin in the development of ARDS *in vitro*, we utilized LPS-induced human AT II cell line (A549) as a model of ARDS. To determine the optimal concentration and duration of action of LPS and insulin affecting ATP1A1 expression in A549 cells, we first utilized western blotting to detect ATP1A1 expression levels, and the results showed that ATP1A1 was significantly inhibited at LPS concentration of 1.0μg/ml after using separately LPS at 0μg/ml, 0.1μg/ml, 0.5μg/ml, 1.0μg/ml, 5.0μg/ml, and 10.0μg/ml(Figures 9A, C). Subsequently, after using 1.0μg/ml to act on A549 cells for 0h, 3h, 6h, 12h, 24h,

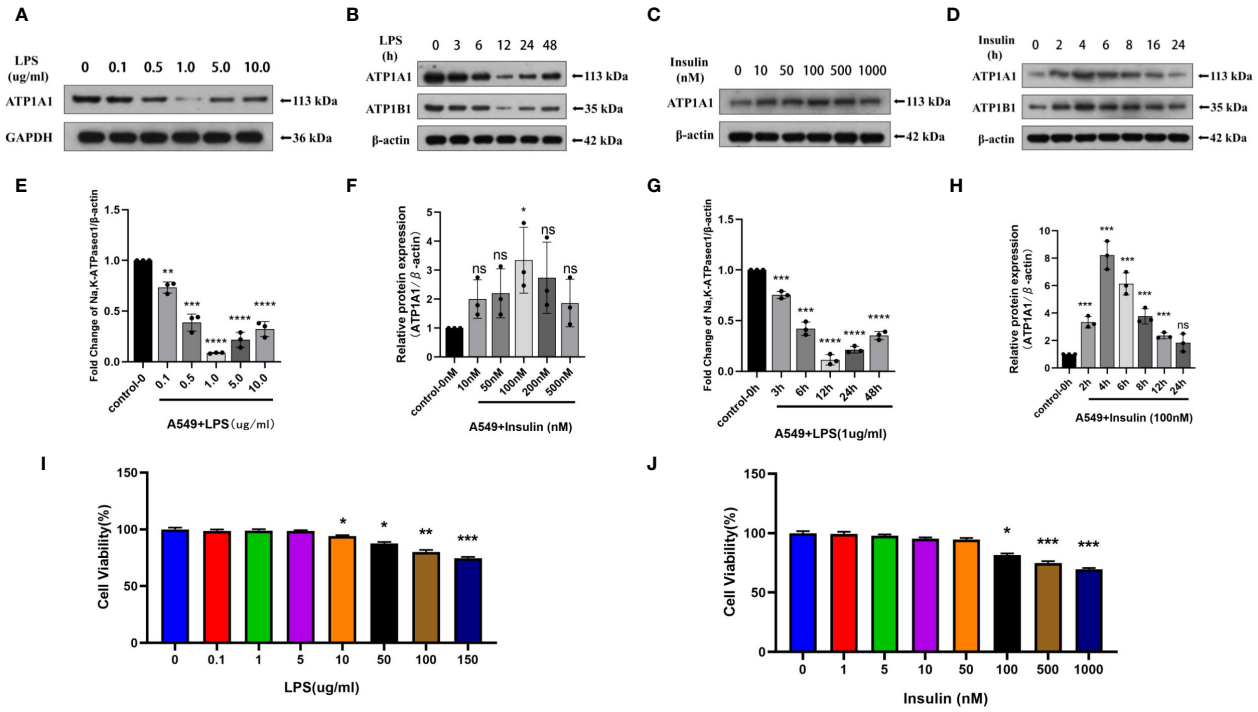

FIGURE 9
Effects of LPS and insulin on Na, K-ATPase expression and cellular activity in A549 cells. **(A, B, E, F)** Representative western blotting detected the levels of ATP1A1 in A549 cells by different LPS and insulin concentrations and duration **(C, D, G, H)** Quantitative analysis of ATP1A1 was shown in bar graphs, respectively. **(I, J)** Effects of different doses of LPS and insulin on the survival rate of A549 cells using CCK-8 assay. The data are presented as mean ± SD. n = 3, the horizontal line represented the comparison between each two groups, *p<0.05. **p < 0.01. ***p < 0.001. ****p < 0.0001.

and 48 h, respectively, it was found that 12 h was the suitable time period when ATP1A1 was significantly inhibited (Figures 9B, D). Similarly, we puzzled over a range of insulin concentrations and times. We found that the expression of ATP1A1 increased significantly when the insulin concentration was 100 nM and acted for 4h (Figures 9E–H).

To ensure the accuracy and stability of subsequent experiments, we also examined the effects of concentration gradients of LPS and insulin on cell viability using CCK-8 assay. Which showed that after 12h and 4h of LPS and insulin acting on A549 cells, respectively the viability of A549 cells decreased with increasing doses of LPS and insulin in a concentration-dependent manner (Figures 9I, J). Combining the above data, we chose 1 μg/ml LPS and 100 nM insulin to act on A549 cells for 12h and 4h, respectively, for subsequent cell-modeling doses of ARDS.

Intriguingly, to investigate whether the protective effect of insulin on LPS-induced Na, K-ATPase in A549 cells is related to autophagy, we detected the levels of several key autophagy-related proteins using western blotting. A549 cells were treated with LPS for 12 hours, and insulin was administrated at the eighth hour. As shown in the Figures 10A–E, LPS treatment significantly up-regulated LC3-II/LC3-I, ATG5 and Beclin-1 levels, while P62 decreased, suggesting autophagy activation (P < 0.01). On the contrary, insulin can reverse the activation of autophagy and play an inhibitory role (P < 0.05). Subsequently, insulin treatment significantly up-regulated the expression of ATP1A1, which was inhibited by LPS (Figure 10F), which indicated that insulin increased the expression of Na, K-ATPase in LPS-treated cells, which may be related to the inhibition of autophagy. The above results indicate that insulin inhibited autophagy and improved Na, K-ATPase expression in ARDS *in vitro*, which may play an important role in limiting pulmonary edema.

3.6 Insulin improves Na, K-ATPase expression by inhibiting autophagy in ARDS which was confirmed by autophagy inhibitors and promoters

To make our results more robust and accurate, we administered the autophagy inhibitor 3-methyladenine (3-MA, 3mM) and the autophagy promoter rapamycin (1nM) 30min before LPS induction and then intervened with insulin in A549 cells after LPS administration.

Notably, we obtained better results. It was found that in the LPS+3-MA group compared with the LPS group, the expression level of ATP1A1 increased, suggesting that inhibition of autophagy could restore the level of ATP1A1 inhibited by LPS to some extent. And the same effect was exerted in the LPS+insulin group. In addition, the administration of Rapamycin on top of LPS and insulin revealed that the expression level of ATP1A1 decreased, suggesting that the effect of insulin could be attenuated after promoting autophagy (Figures 11A–C). The above results further demonstrate that insulin inhibits autophagy and improves the expression of Na, K-ATPase in ARDS *in vitro*, which may play an important role in limiting pulmonary edema.

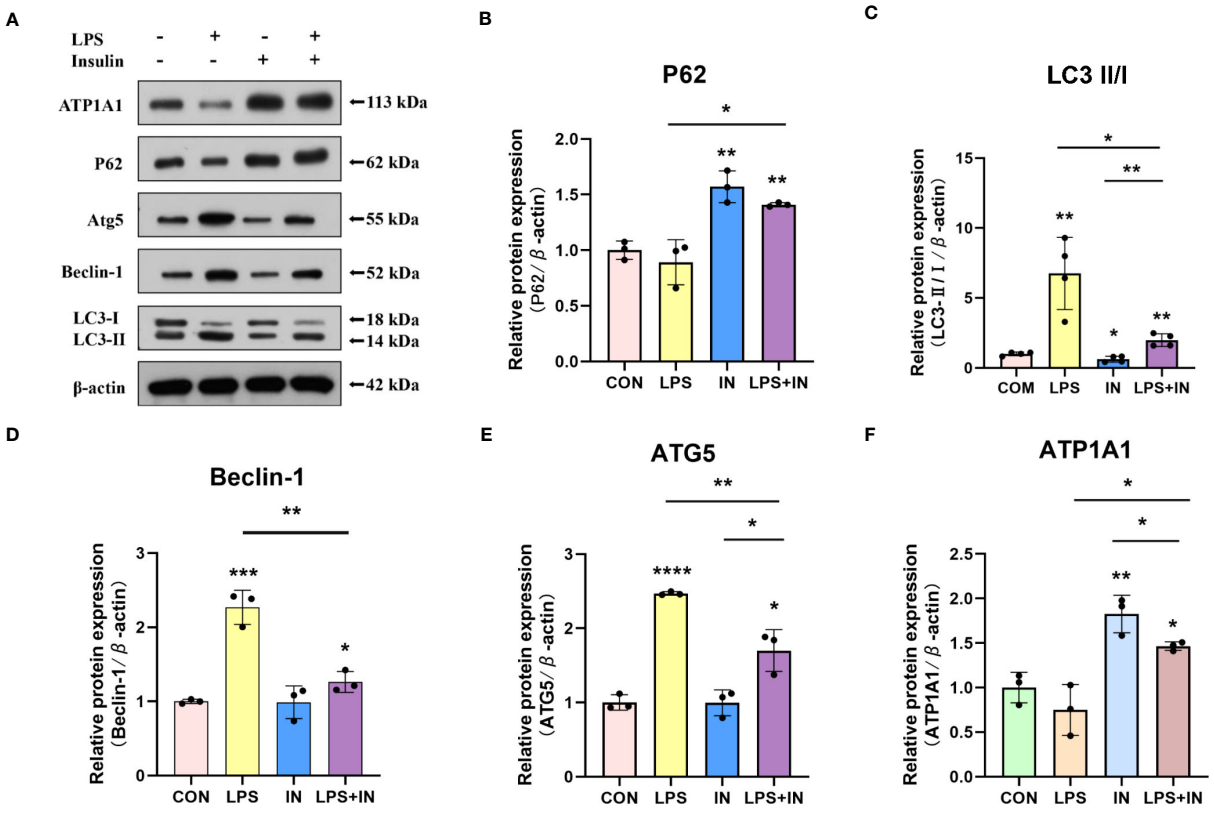

FIGURE 10
Effects of insulin on autophagy-related proteins and ATP1A1 expression in LPS-induced A549 cells. **(A)** Representative western blotting detected the levels of LC3-II/I, ATG5, Beclin-1, P62 and ATP1A1 **(B–F)** Quantitative analysis of LC3-II/I, Beclin-1, ATG5, P62 and ATP1A1 were shown in bar graphs, respectively. The data are presented as mean ± SD. n = 3, the horizontal line represented the comparison between each two groups, *p<0.05. **p < 0.01. ***P < 0.001. ****P < 0.0001.

3.7 Ultrastructure of A549 cells induced by LPS after insulin administration observed by TEM

Using transmission electron microscopy (TEM) to observe cell autophagy and its morphological structure is currently a highly recommended and more accurate method for autophagy detection. To further study the effect of insulin on the number of autophagosomes (AP) and autolysosomes (ASS) induced by LPS in A549 cells, we used TEM to observe them compared with the control group. It revealed that the number of AP and ASS increased after LPS treatment, and decreased in the insulin group. Compared with the LPS group, The number of AP and ASS decreased significantly in the LPS+insulin group (Figures 12A, B). Therefore, insulin may inhibit the autophagy activated by LPS in cells.

3.8 Insulin attenuates autophagy levels and improves Na, K-ATPase expression in LPS-induced mouse primary AT II cells

To ensure the accuracy, credibility, practicality and stability of our results, we also repeated and verified the above experiments on AT II cells, and to our delight is that the results are almost the same. First, we isolated AT II cells from C57 mice, purified and cultured them, and then detected pulmonary surfactant-associated protein C (SP-C) by immunofluorescence (Figure 13A). AT II cells grew in an island shape under an inverted phase-contrast microscope, and the cells were short spindle-shaped, polygonal or cuboidal (Figure 13B). Last but not least, we also induced AT II cells with LPS and intervened with insulin. The results showed that the expressions of LC3-II/I and ATG5 increased and P62 decreased after LPS administration, which suggested that LPS activated autophagy in AT II cells, while insulin played an inhibitory role on the contrary (Figures 13C–F). Interestingly, we detected Na, K-ATPase β1 (ATP1B1) at the same time as ATP1A1 detection, and surprisingly found that the expression trend of ATP1B1 was consistent with that of ATP1A1, both of which were inhibited by LPS and increased by insulin (Figures 13G–I). The above results are sufficient to prove that insulin inhibited LPS-induced autophagy activation and improved the expression of Na, K-ATPase in lung tissue, thereby limiting the generation of pulmonary edema.

4 Discussion

Pulmonary infection is the main cause of ARDS, especially LPS induced alveolar epithelial cell injury and increased vascular

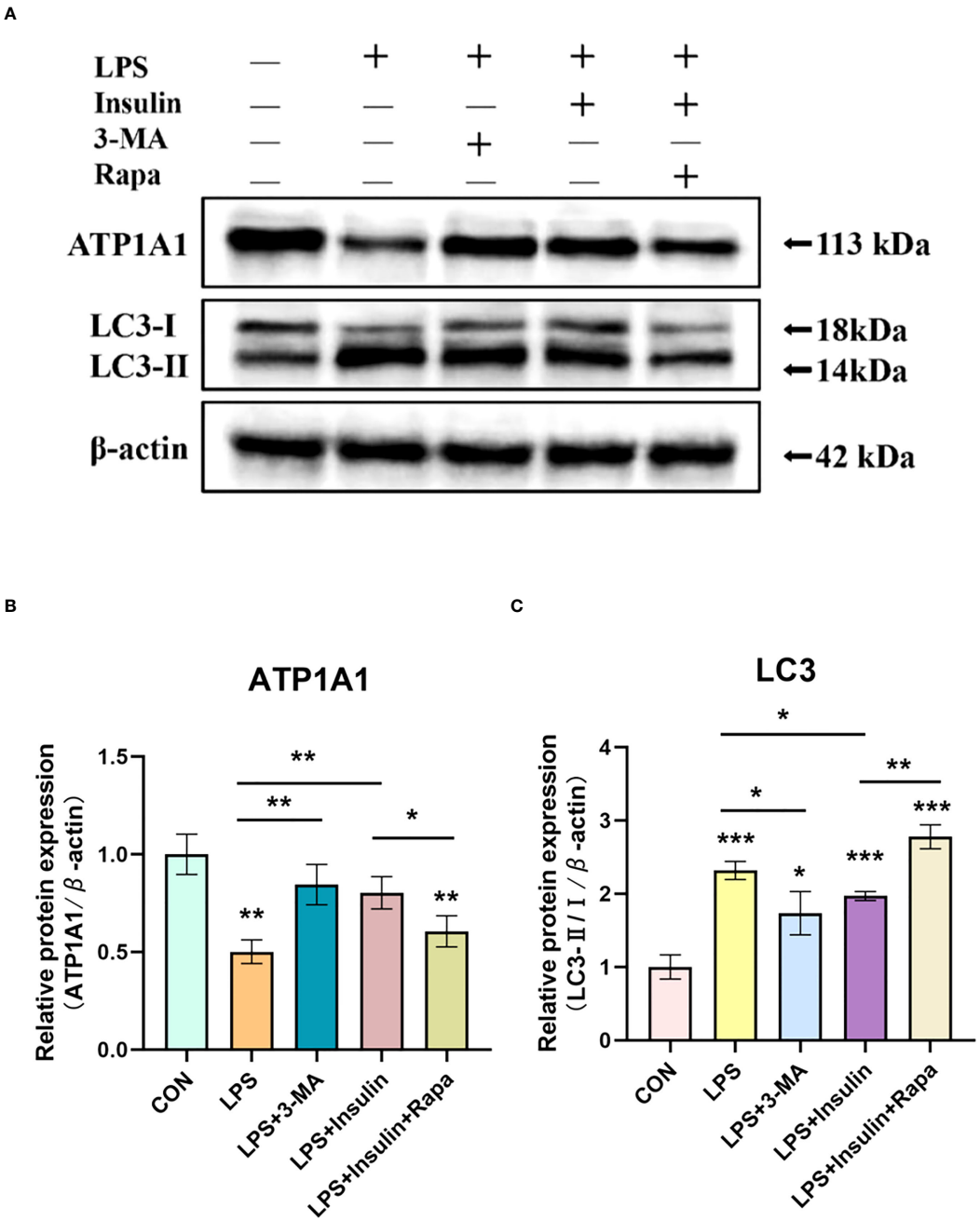

FIGURE 11
Effect of 3-MA and Rapamycin on the role of insulin in LPS-induced autophagy in A549 cells. **(A)** Western blot assay for LC3-II/I and ATP1A1. **(B, C)** Quantitative analysis. The data are presented as mean ± SD. n = 3, the horizontal line represented the comparison between each two groups, $^{*}P < 0.05$, $^{**}P < 0.01$, $^{***}P < 0.001$.

endothelial cell permeability that leading to pulmonary edema fluid leakage and thus resulting in severe hypoxemia (19). ARDS is often accompanied by abnormal Na, K-ATPase function. Upregulating Na, K-ATPase expression or increasing the amount of Na,K-ATPase may enhance trans-epithelial sodium transport in alveolar cells, thereby promoting intra-alveolar edema fluid reabsorption and limiting the development of pulmonary edema (20). The current researches focus on the mechanism of Na, K-ATPase regulatng in the alveolar epithelium during lung injury, and the dysregulation of Na, K-ATPase subsequently exacerbates the development of pulmonary edema, thus regulating alveolar epithelial Na, K-ATPase is important for limiting pulmonary edema.

Autophagy occurs in the lung is a response of alveolar epithelial cells to long-term and continuous stimuli from intrapulmonary and extrapulmonary factors (21). Liu Y et al. found that Na, K-ATPase participates in autophagy-lysomytosterios through its α1 subunit,

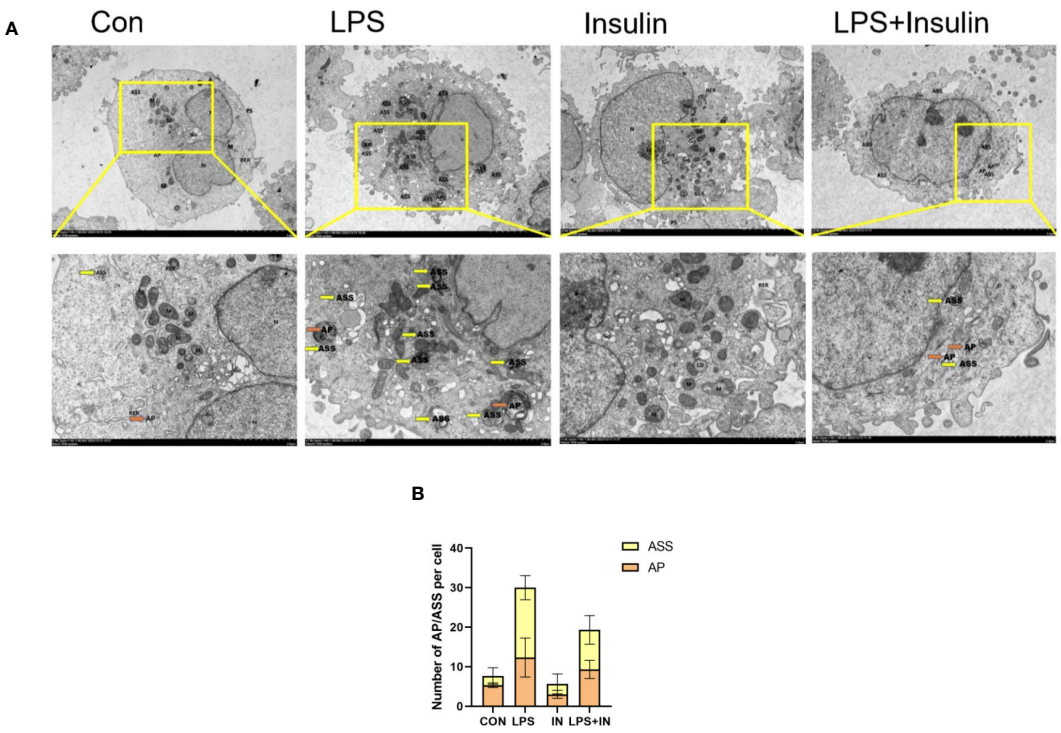

FIGURE 12
The remarkable images of autophagosomes ultrastructure by TEM in A549 cells **(A)** Representative photographs of TEM showed autophagosomes and autolysosomes. **(B)** Quantitative analysis of autophagosomes (orange dots) and autolysosomes (yellow dots), bars represented as mean ± SD.

and AMPK (one of the most important positive regulators of autophagy) and ATP1A1 may act as the "on" and "off" states of the autophagic pathways (10). In addition, the novel mechanism of ATP1A1 as a mediator of signal transduction and autophagy during ischemia-reperfusion provides new ideas for the intervention of ischemic stroke (22, 23). Our previous study revealed that the ATP1A1 regulatory mechanism may be related to the autophagy-lysosome pathway (24). Few studies have been conducted on the degradation of Na, K-ATPase via the autophagy-lysosome pathway, However, the relationship between them is worthy of extensive attention and discussions to affect the abundance and enzyme activity of ATP1A1, enhance the lung water clearance ability, and improve the prognosis of ARDS in the future.

Insulin is a normal growth hormone in human body, which has been widely used in clinical practice for a long time without any toxic side effects. It is only necessary to inject concentrated sugar to prevent the occurrence of hypoglycemia, and the dose of 6 IU/h of continuous intravenous pumped insulin is approximately the same as that of 1.0 IU/kg intraperitoneal injection in mice and 100 nM conversion in A549 and ATII cells, so the clinical results are highly consistent with the results of animal and cellular experiments. Our study was conducted to use these characteristics of insulin as described above, and validated on LPS-induced animal and cell ARDS models. We found that LPS activates autophagy and promotes inflammatory responses, leading to Na, K-ATPase degradation and alveolar epithelial damage thus exacerbating intra-alveolar fluid accumulation. In contrast, insulin inhibited both autophagy and inflammatory response, allowing Na, K-ATPase activity to be improved, thus reversing the impaired lung water clearance caused by LPS in ARDS. It is highly likely that there are many close links between the key factors of autophagy, inflammation and Na, K-ATPase, and insulin plays a crucial role in this regard. The specific mechanisms deserve to be explored in depth.

Several key autophagy proteins were well validated in our experiments. P62/SQSTM1, is a multifunctional autophagy protein. It is involved in ubiquitin-proteasome and autophagy-lysosome degradation processes and is an important regulatory molecule linking ubiquitinated proteins to the autophagic machinery (13). It is now known that insulin activates mTORC1 through upregulation of AKT to elevate P62, which binds to Keap1 and transports it to the lysosome for degradation, where Keap1-bound transcription factor NRF2 dissociates from Keap1 into the nucleus and initiates transcription for anti-inflammatory effects (25). We found that insulin also inhibited autophagy and upregulated P62 levels in ARDS mice and A549 cells as well as ATII cells. The above evidence suggests that insulin is likely to upregulate P62 levels, inhibit the release of inflammatory factors, and reduce inflammatory cell infiltration and thus reduce pulmonary water production. Interestingly, in our previous study, we found that ATP1A1 interacts with P62 through Co-IP and western blot verification (24). It is thought-provoking that P62 may act as a key regulatory mediator in this, so we conjecture that insulin most likely regulates ATP1A1 and P62 expression through inhibition of autophagy and thereby plays some key role in the accumulation of alveolar epithelial fluid.

Inflammatory cytokines are involved in the control of autophagy and known to play a key role in the development of ARDS. In turn,

10.3389/fimmu.2023.1162159

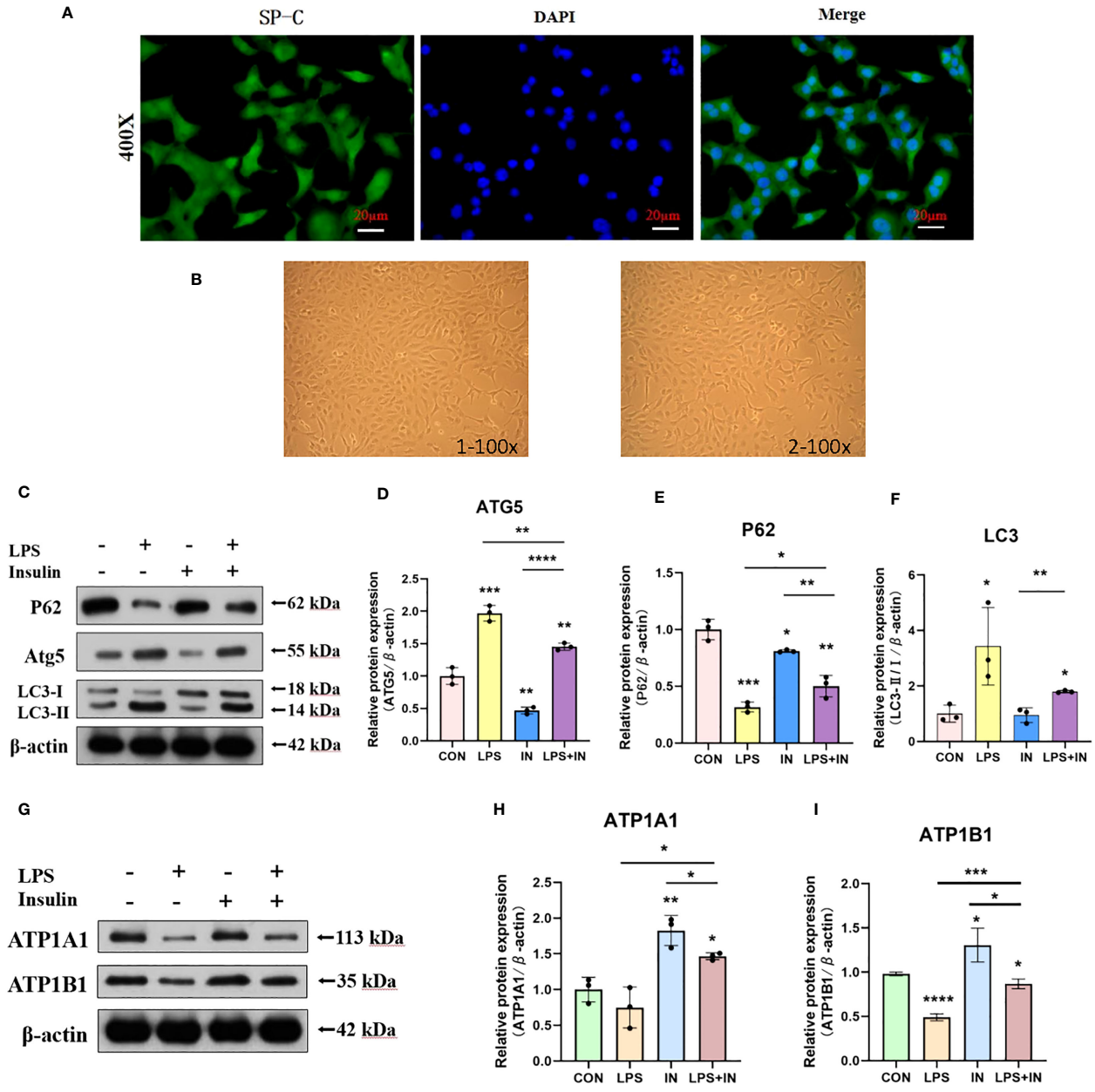

FIGURE 13
Effects of LPS and insulin on Na, K-ATPase expression and cellular activity in AT II cells. **(A)** Immunofluorescence detection of pulmonary surfactant protein SP-C, the scale bar is 20 μm, the positive signal is SP-C (green fluorescence), and the blue is the nuclear staining signal. **(B)** AT II cells were observed with an inverted phase-contrast microscope. the scale bar is 1×100 and 2×100, respectively. **(C, G)** Representative western blotting detected the levels of LC3-II/I, ATG5, P62 and ATP1A1 in AT II cells. **(D–F, H, I)** Quantitative analysis of LC3-II/I, ATG5, P62 and ATP1A1 were shown in bar graphs, respectively. The data are presented as mean ± SD. n = 3, the horizontal line represented the comparison between each two groups, *p<0.05. **p < 0.01. ***P < 0.001. ****P < 0.0001.

autophagy regulates inflammatory factors. TNF-α is the earliest endogenous mediator and amplifies the inflammatory response and the production of IL-1β leads to lung epithelial injury (26). Insulin inhibits the release of pro-inflammatory factors such as TNFα and IL-1β, and increases the production of anti-inflammatory factors such as IL-10 (27). Autophagy reduces IL-1β secretion by inhibiting inflammasome activation (28). Activation of autophagy inhibits TNF-α secretion (29). Yang S et al. found that decreased hepatocyte autophagy promotes IL-1β/TNF-induced necrosis from impaired energy homeostasis and lysosomal permeabilization and inflammation through the secretion of exosomal damage-associated molecular patterns (30). It is dependent on the PI3K/AKT/mTOR signalling pathway to promote autophagy and suppresses inflammation in TNF-α-treated keratinocytes and psoriatic mice (31). Based on these reports and our previous results, the specific mechanisms of insulin in inhibitng autophagy and inflammation deserve further exploration.

Nevertheless, there are some conflicting limitations to our study. In formal clinical care, some clinical observations and experimental animal studies suggest that it is uncertain whether insulin prevents

the development of ARDS, and studies have shown that in diabetes with systemic inflammatory, insulin exacerbates the production of pro-inflammatory mediators and inhibits cardiac function (32). There are much debates as to whether insulin is harmful or beneficial in ARDS. What is certain, however, is that the benefits of the right dose of insulin are more pronounced in patients with ARDS. In addition, it is known that autophagy has a dual roles in different models. The exact mechanism needs to be further investigated.

Zhang et al. reported that chloroquine, a chemical inhibitor of autophagy, and silencing of Atg7 attenuated LPS-induced autophagosome formation in human pulmonary microvascular endothelial cells, reduced cell viability, and aggravated LPS-induced monolayer permeability (11). This is contrary to our conclusion. It has also been reported that neutrophil autophagy is increased in LPS-induced mice, which leading to increased release of granule contents. Knockdown of the autophagy gene Atg5 abolishes the promotion of MPO by LPS and the chemokine fMLP, which limits the release of granule contents and thereby alleviates ARDS (33). Thus, autophagy appears to contribute to endothelial barrier disruption caused by edema-inducing agents and also plays an important role in acute lung injury, and inhibition of autophagy can protect against endothelial barrier function caused by ARDS. To address these phenomena, it is necessary to further investigate the effects of endothelial cell-specific genetic alterations in ARDS.

5 Conclusion

In summary, Our experiments were conducted in LPS-induced ARDS, with a view to investigating the impairment of AFC in ARDS. We first used the vivo experiments to confirm the effect of insulin inhibition of autophagy on alveolar epithelial damage and AFC under LPS-induced conditions. This was followed by functional reversion experiments, which were further confirmed in LPS-induced ARDS A459 cells and ATII cells. The aim is to elucidate the possible mechanisms by which insulin regulates Na, K-ATPase α1 and inflammatory response through inhibiting autophagy, thereby reverses the impaired AFC in LPS-induced ARDS. However, our studies are only preliminary, revealing the effects of insulin on Na, K-ATPase α1 and autophagy proteins expression and inflammatory responses. This work will provide a partial theoretical and experimental basis for the course and clinical treatment of ARDS by elucidating the biological functions of insulin and relevant autophagic markers in the field of lung protection in ARDS.

Data availability statement

The datasets presented in this study can be found in online repositories. The names of the repository/repositories and accession number(s) can be found below: PXD040288 (ProteomeXchange).

Ethics statement

All experimental animal treatment procedures were approved by the Department of Laboratory Animals of Xiangya School of Medicine, Central South University, and are carried out under the Guide for the Use of Laboratory Animals by the National Institutes of Health.

Author contributions

Q-QW designed the study, X-PW and Q-QW conducted the data analysis, and wrote the manuscript. X-PW and Q-QW participated in and contributed to the experiments of this study. X-PW, ML, R-QZ participated in manuscript revision. All authors read and approved the final manuscript.

Funding

This work was support by the Key project of Hunan Provincial Health Commission, China (grant numbers 202217012851).

Acknowledgments

The authors thank KangChen Bio-Tech, Shanghai, China, for their technical support for the proteomic works.

Conflict of interest

The authors declare that the research was conducted in the absence of any commercial or financial relationships that could be construed as a potential conflict of interest.

Publisher's note

Supplementary material

The Supplementary Material for this article can be found online at: https://www.frontiersin.org/articles/10.3389/fimmu.2023.1162159/full#supplementary-material

References

1. Griffiths MJD, Mcauley DF, Perkins GD, Barrett N, Blackwood B, Boyle A, et al. Guidelines on the management of acute respiratory distress syndrome. *BMJ Open Respir Res* (2019) 6(1):e000420. doi: 10.1136/bmjresp-2019-000420

2. Fan E, Brodie D, Slutsky AS. Acute respiratory distress syndrome: advances in diagnosis and treatment. *JAMA* (2018) 319(7):698–710. doi: 10.1001/jama.2017.21907

3. Matthay MA, Mcauley DF, Ware LB. Clinical trials in acute respiratory distress syndrome: challenges and opportunities. *Lancet Respir Med* (2017) 5(6):524–34. doi: 10.1016/S2213-2600(17)30188-1

4. Levitt JE, Calfee CS, Goldstein BA, Vojnik R, Matthay MA. Early acute lung injury: criteria for identifying lung injury prior to the need for positive pressure ventilation*. *Crit Care Med* (2013) 41(8):1929–37. doi: 10.1097/CCM.0b013e31828a3d99

5. Matthay MA, Zemans RL. The acute respiratory distress syndrome: pathogenesis and treatment. *Annu Rev Pathol* (2011) 6:147–63. doi: 10.1146/annurev-pathol-011110-130158

6. Laffey JG, Matthay MA. Fifty years of research in ARDS. Cell-based therapy for acute respiratory distress syndrome. Biology and potential therapeutic value. *Am J Respir Crit Care Med* (2017) 196(3):266–73. doi: 10.1164/rccm.201701-0107CP

7. Zhang JL, Zhuo XJ, Lin J, Luo LC, Ying WY, Xie X, et al. Maresin1 stimulates alveolar fluid clearance through the alveolar epithelial sodium channel Na,K-ATPase via the ALX/PI3K/Nedd4-2 pathway. *Lab Invest* (2017) 97(5):543–54. doi: 10.1038/labinvest.2016.150

8. Cui X, Xie Z. Protein interaction and na/K-ATPase-mediated signal transduction. *Molecules* (2017) 22(6):990. doi: 10.3390/molecules22060990

9. Suhail M. Na, K-ATPase: ubiquitous multifunctional transmembrane protein and its relevance to various pathophysiological conditions. *J Clin Med Res* (2010) 2(1):1–17. doi: 10.4021/jocmr2010.02.263w

10. Liu Y, Shoji-Kawata S, Sumpter RM Jr., Wei Y, Ginet V, Zhang L, et al. Autosis is a Na+,K+-ATPase-regulated form of cell death triggered by autophagy-inducing peptides, starvation, and hypoxia-ischemia. *Proc Natl Acad Sci USA*. (2013) 110(51):20364–71. doi: 10.1073/pnas.1319661110

11. Zhang D, Zhou J, Ye LC, Li J, Wu Z, Li Y, et al. Autophagy maintains the integrity of endothelial barrier in LPS-induced lung injury. *J Cell Physiol* (2018) 233 (1):688–98. doi: 10.1002/jcp.25928

12. Li C, Liu H, Sun Y, Wang H, Guo F, Rao S, et al. PAMAM nanoparticles promote acute lung injury by inducing autophagic cell death through the Akt-TSC2-mTOR signaling pathway. *J Mol Cell Biol* (2009) 1(1):37–45. doi: 10.1093/jmcb/mjp002

13. Vishnupriya S, Priya Dharshini LC, Sakthivel KM, Rasmi RR. Autophagy markers as mediators of lung injury-implication for therapeutic intervention. *Life Sci* (2020) 260:118308. doi: 10.1016/j.lfs.2020.118308

14. Chen HI, Yeh DY, Liou HL, Kao SJ. Insulin attenuates endotoxin-induced acute lung injury in conscious rats. *Crit Care Med* (2006) 34(3):758–64. doi: 10.1097/01.CCM.0000201902.37115.22

15. He J, Qi D, Wang DX, Deng W, Ye Y, Feng LH, et al. Insulin upregulates the expression of epithelial sodium channel in *vitro* and in a mouse model of acute lung injury: role of mTORC2/SGK1 pathway. *Exp Cell Res* (2015) 331(1):164–75. doi: 10.1016/j.yexcr.2014.09.024

16. Smith KM, Mrozek JD, Simonton SC, Bing DR, Meyers PA, Connett JE, et al. Prolonged partial liquid ventilation using conventional and high-frequency ventilatory techniques: gas exchange and lung pathology in an animal model of respiratory distress syndrome. *Crit Care Med* (1997) 25(11):1888–97. doi: 10.1097/00003246-199711000-00030

17. Messier EM, Mason RJ, Kosmider B. Efficient and rapid isolation and purification of mouse alveolar type II epithelial cells. *Exp Lung Res* (2012) 38(7):363–73. doi: 10.3109/01902148.2012.713077

18. Zheng Y, Gu S, Li X, Tan J, Liu S, Jiang Y, et al. Berbamine postconditioning protects the heart from ischemia/reperfusion injury through modulation of autophagy. *Cell Death Dis* (2017) 8(2):e2577. doi: 10.1038/cddis.2017.7

19. Leligdowicz A, Chun LF, Jauregui A, Vessel K, Liu KD, Calfee CS, et al. Human pulmonary endothelial cell permeability after exposure to LPS-stimulated leukocyte supernatants derived from patients with early sepsis. *Am J Physiol Lung Cell Mol Physiol* (2018) 315(5):L638–44. doi: 10.1152/ajplung.00286.2018

20. Clausen MV, Hilbers F, Poulsen H. The structure and function of the na,K-ATPase isoforms in health and disease. *Front Physiol* (2017) 8:371. doi: 10.3389/fphys.2017.00371

21. Yen YT, Yang HR, Lo HC, Hsieh YC, Tsai SC, Hong CW, et al. Enhancing autophagy with activated protein C and rapamycin protects against sepsis-induced acute lung injury. *Surgery* (2013) 153(5):689–98. doi: 10.1016/j.surg.2012.11.021

22. Felippe Goncalves-De-Albuquerque C, Ribeiro Silva A, Ignacio Da Silva C, Caire Castro-Faria-Neto H, Burth P. Na/K pump and beyond: Na/K-ATPase as a modulator of apoptosis and autophagy. *Molecules* (2017) 22(4):578. doi: 10.3390/molecules22040578

23. Zhu M, Cao L, Xiong S, Sun H, Wu Z, Bian JS. Na(+)/K(+)-ATPase-dependent autophagy protects brain against ischemic injury. *Signal Transduct Target Ther* (2020) 5(1):55. doi: 10.1038/s41392-020-0153-7

24. Wen XP, Long G, Zhang YZ, Huang H, Liu TH, Wan QQ. Identification of different proteins binding to Na, K-ATPase alpha1 in LPS-induced ARDS cell model by proteomic analysis. *Proteome Sci* (2022) 20(1):10. doi: 10.1186/s12953-022-00193-3

25. Kageyama S, Saito T, Obata M, Koide RH, Ichimura Y, Komatsu M. Negative regulation of the Keap1-Nrf2 pathway by a p62/sqstm1 splicing variant. *Mol Cell Biol* (2018) 38(7):e00642-17. doi: 10.1128/MCB.00642-17

26. Gouwy M, Struyf S, Proost P, Van Damme J. Synergy in cytokine and chemokine networks amplifies the inflammatory response. *Cytokine Growth Factor Rev* (2005) 16(6):561–80. doi: 10.1016/j.cytogfr.2005.03.005

27. Van Niekerk G, Christowitz C, Conradie D, Engelbrecht AM. Insulin as an immunomodulatory hormone. *Cytokine Growth Factor Rev* (2020) 52:34–44. doi: 10.1016/j.cytogfr.2019.11.006

28. Zhou R, Yazdi AS, Menu P, Tschopp J. A role for mitochondria in NLRP3 inflammasome activation. *Nature* (2011) 469(7329):221–5. doi: 10.1038/nature09663

29. Harris J, Hartman M, Roche C, Zeng SG, O'shea A, Sharp FA, et al. Autophagy controls IL-1beta secretion by targeting pro-IL-1beta for degradation. *J Biol Chem* (2011) 286(11):9587–97. doi: 10.1074/jbc.M110.202911

30. Shen Y, Malik SA, Amir M, Kumar P, Cingolani F, Wen J, et al. Decreased hepatocyte autophagy leads to synergistic IL-1beta and TNF mouse liver injury and inflammation. *Hepatology* (2020) 72(2):595–608. doi: 10.1002/hep.31209

31. Tang ZL, Zhang K, Lv SC, Xu GW, Zhang JF, Jia HY. LncRNA MEG3 suppresses PI3K/AKT/mTOR signalling pathway to enhance autophagy and inhibit inflammation in TNF-alpha-treated keratinocytes and psoriatic mice. *Cytokine* (2021) 148:155657. doi: 10.1016/j.cyto.2021.155657

32. Hagiwara S, Iwasaka H, Kudo K, Hasegawa A, Kusaka J, Uchida T, et al. Insulin treatment of diabetic rats reduces cardiac function in a lipopolysaccharide-induced systemic inflammation model. *J Surg Res* (2011) 171(1):251–8. doi: 10.1016/j.jss.2010.03.032

33. Zhu Q, Wang H, Wang H, Luo Y, Yu Y, Du Q, et al. Protective effects of ethyl pyruvate on lipopolysaccharide–induced acute lung injury through inhibition of autophagy in neutrophils. *Mol Med Rep* (2017) 15(3):1272–8. doi: 10.3892/mmr.2017.6118

frontiers | Frontiers in Immunology

TYPE Original Research
PUBLISHED 08 September 2023
DOI 10.3389/fimmu.2023.1238774

OPEN ACCESS

EDITED BY
Kai Wang,
Southwest Medical University, China

REVIEWED BY
Shen Shengnan,
China Academy of Chinese Medical Science, China
Xiaoli Yang,
The Affiliated Hospital of Southwest Medical University, China
Guo-wei Tu,
Fudan University, China

*CORRESPONDENCE
Cheng Li
chengli_2017@tongji.edu.cn
Hui Zhang
15077169795@163.com
Qidong Liu
qidongliu670@foxmail.com

†These authors have contributed equally to this work

RECEIVED 12 June 2023
ACCEPTED 10 August 2023
PUBLISHED 08 September 2023

CITATION
Cao S, Tang J, Fei M, Jing Q, Meng F, Zhang M, Liu Q, Zhang H and Li C (2023) Identification of potential hub genes linked to immune and metabolic alterations in postoperative systemic inflammatory dysregulation. *Front. Immunol.* 14:1238774. doi: 10.3389/fimmu.2023.1238774

Identification of potential hub genes linked to immune and metabolic alterations in postoperative systemic inflammatory dysregulation

Silu Cao[1†], Jinxuan Tang[1†], Miaomiao Fei[1†], Qi Jing[1], Fanbing Meng[1], Meixian Zhang[1], Qidong Liu[1,2*], Hui Zhang[1*] and Cheng Li[1*]

[1]Department of Anesthesiology and Perioperative medicine, Shanghai Key Laboratory of Anesthesiology and Brain Functional Modulation, Clinical Research Center for Anesthesiology and Perioperative Medicine, Translational Research Institute of Brain and Brain-Like Intelligence, Shanghai Fourth People's Hospital, School of Medicine, Tongji University, Shanghai, China, [2]Key Laboratory of Spine and Spinal Cord Injury Repair and Regeneration of Ministry of Education, Orthopedic Department of Tongji Hospital, Tongji University School of Medicine, Shanghai, China

Background: Postoperative systemic inflammatory dysregulation (PSID) is characterised by strongly interlinked immune and metabolic abnormalities. However, the hub genes responsible for the interconnections between these two systemic alterations remain to be identified.

Methods: We analysed differentially expressed genes (DEGs) of individual peripheral blood nucleated cells in patients with PSID (n = 21, CRP > 250 mg/L) and control patients (n = 25, CRP < 75 mg/L) following major abdominal surgery, along with their biological functions. Correlation analyses were conducted to explore the interconnections of immune-related DEGs (irDEGs) and metabolism-related DEGs (mrDEGs). Two methods were used to screen hub genes for irDEGs and mrDEGs: we screened for hub genes among DEGs via 12 algorithms using CytoHubba in Cytoscape, and also screened for hub immune-related and metabolic-related genes using weighted gene co-expression network analysis. The hub genes selected were involved in the interaction between changes in immunity and metabolism in PSID. Finally, we validated our results in mice with PSID to confirm the findings.

Results: We identified 512 upregulated and 254 downregulated DEGs in patients with PSID compared with controls. Gene enrichment analysis revealed that DEGs were significantly associated with immune- and metabolism-related biological processes and pathways. Correlation analyses revealed a close association between irDEGs and mrDEGs. Fourteen unique hub genes were identified via 12 screening algorithms using CytoHubba in Cytoscape and via weighted gene co-expression network analysis. Among these, *CD28*, *CD40LG*, *MAPK14*, and *S100A12* were identified as hub genes among both immune- and metabolism-related genes; these genes play a critical role in the interaction between alterations in immunity and metabolism in PSID. The experimental results also showed that the expression of these genes was significantly altered in PSID mice.

Conclusion: This study identified hub genes associated with immune and metabolic alterations in patients with PSID and hub genes that link these alterations. These findings provide novel insights into the mechanisms underlying immune and metabolic interactions and new targets for clinical treatment can be proposed on this basis.

KEYWORDS

postoperative systemic inflammatory dysregulation, hub genes, metabolism, C-reactive protein, surgery

1 Introduction

Postoperative systemic inflammatory dysregulation (PSID), a state of inflammation that may occur postoperatively, can be identified through postoperative phenotypic changes, such as elevated levels of C-reactive protein (CRP) and pro-inflammatory cytokines. PSID is an important feature of postoperative sepsis (1, 2). The Third International Consensus Definition for Sepsis indicates that underlying inflammation and metabolic abnormalities substantially increase the risk of mortality (3).

During surgical procedures, the body is exposed to innate pathogens and cellular debris that can activate the immune system (4), while severe tissue damage can result in higher levels of inflammatory mediators and cytokine release, ultimately driving immune, metabolic, and hormonal processes and leading to a stress response. Although the inflammatory immune response is essential for repairing damage and fighting harmful products, it can lead to PSID, which increases the risk of complications, prolongs hospital stays, and may cause death. PSID increases the risk of postoperative infection and induces inflammation-mediated complications and organ dysfunction (4–8). Metabolic alterations, including changes in energy and nitrogen balance, as well as the utilisation of substrates such as proteins, carbohydrates, and lipids, influence the occurrence of postoperative complications (9). These processes can alter glucose and protein catabolism and can cause hormonal dysregulation and other effects that impede recovery and increase morbidity (10).

The transition of immune responses from quiescent to activated states involves multiple metabolic pathways (11). Both innate and adaptive immune cells increase their metabolic flux upon stimulation, promoting energy production and biosynthesis while restoring metabolic pathways to support proliferation, effector molecule production, and cell differentiation (12–15). However, few studies have focused on the correlation between immunological and metabolic changes in patients following surgery, and even fewer have prospectively observed the early postoperative period before clinical signs become evident. CRP, an acute-phase protein, has a half-life of 19 h, and white cell count is a commonly used marker of postoperative inflammation and infection. Investigation and identification of the potential hub genes associated with immune and metabolic alterations in patients with PSID and linking these alterations should provide insights into the mechanisms underlying immune and metabolic interactions and new targets for clinical treatment (16).

In this study, we comprehensively analysed the public RNA-seq dataset GSE184039 to evaluate differential genetic characteristics and alterations to biological processes in patients with high and low levels of CPR after major abdominal surgery. We screened hub genes associated with both immune and metabolic changes in patients with PSID. Our results provide a new perspective on the diagnosis and treatment of PSID. The workflow of this study is illustrated in Figure 1.

2 Results

2.1 DEGs in PSID and function enrichment analysis

Significant alterations associated with immunity and metabolism were detected in patients with PSID. A total of 766 differentially expressed genes (DEGs), with absolute log2(fold change) ≥ 1 and adjusted P value < 0.05, were identified (512 upregulated and 254 downregulated in the PSID group). A heatmap of DEGs in the high- and low-CRP groups is presented in Figure 2A. In terms of biological process functions, the DEGs were significantly enriched in immune system processes (13.550%) and metabolic processes (12.647%) (Figure 2B). The top 10 biological processes related to the immune system process and the top 10 biological processes related to the metabolic process are shown in Figure 2C. These findings suggest significant differences between the groups in terms of the immune and metabolic processes involved in PSID. We performed Kyoto Encyclopedia of Genes and Genomes (KEGG) pathway enrichment analyses to investigate the potential pathways involved in immune and metabolic changes in PSID and found that 8 immune-related pathways and 10 metabolism-related pathways were significantly enriched (Figure 2D). The most prominent of these were the complement and coagulation cascades and arachidonic acid metabolism. The enriched DEGs for specific immune- and metabolic-related KEGG pathways were plotted using network plots (Supplementary Figures 2A, B). Most

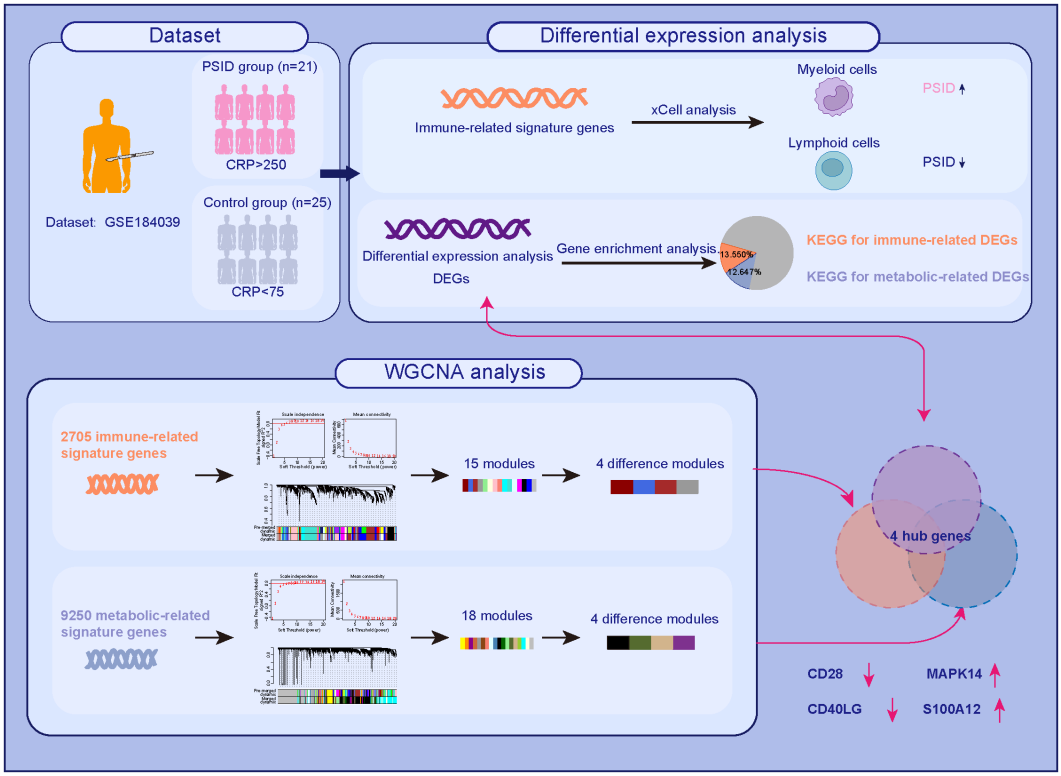

FIGURE 1
The workflow of this study.

DEGs were enriched in complement and coagulation cascades; theIL-7 signalling pathway; leukocyte transendothelial migration; neutrophil extracellular trap formation; arachidonic acid metabolism; glycerolipid metabolism; glycine, serine, and threonine metabolism; pantothenate and CoA biosynthesis; starch and sucrose metabolism. Additionally, 88 genes were identified in screening based on the top 20 genes selected according to the 12 different analysis methods via the CytoHubba tool, of which 31 genes detected using at least three different methods were considered to be hub genes among the DEGs (Table 1).

2.2 Analyses of immune scores

The immune scores of various cell types were determined using the xCell package according to the expression profile of immune cell signature genes; immune scores for 34 immune cells are shown in Figure 3A. In a comparison between the high- and low-CRP groups in terms of immune cell scores, B cells, CD4+ memory T-cells, TD4+ naïve T-cells, CD4+ T-cells, CD4+Tcm, CD4+Tem, TD8+ naïve T-cells, CD8+ T-cells, CD8+Tcm, CD8+Tem, cDC, class-switched memory B-cells, and naïve B-cells had lower scores in the PSID group ($P < 0.05$). In contrast, macrophages, macrophages M1, macrophages M2, monocytes, neutrophils, NKT cells, and Tg cells had higher scores. In a comparison between the groups in terms of immune cell scores for myeloid and lymphoid cells, scores for myeloid cells were elevated in the PSID group ($P < 0.05$); in contrast, lymphoid cells had lower scores (Figure 3B). The enriched DEGs for specific immune cells were plotted using net plots (Figure 2C and Supplementary Figure 3). Most DEGs enriched in macrophages, monocytes, and neutrophils were expressed more in the PSID group than in the Control group (Figure 3C), while most DEGs enriched in lymphoid cells were expressed less in the PSID group (Supplementary Figure 3A).

2.3 Correlation between immunity and metabolism in PSID

To elucidate the relevance of immune and metabolic alterations in patients with PSID, we first analysed the correlations between irDEGs and mrDEGs. The results showed a significant positive correlation between irDEGs and mrDEGs in the PSID group ($R^2 = 0.99$, Figure 4A). To further examine this correlation, we further analysed 41 downregulated and 76 upregulated immune-related genes (Figure 4B) among the 766 DEGs. The results showed that upregulated irDEGs were positively correlated with mrDEGs ($R^2 = 0.99$, Figure 4C) in the PSID group. This correlation was weaker in the Control group ($R^2 = 0.86$, Figure 4D). Analysis of downregulated the irDEGs also showed that the immune–metabolic correlation was stronger in the PSID group ($R^2 = -0.75$, Figure 4E) than in the Control group ($R^2 = -0.36$, Figure 4F). These results suggest a close correlation between immunity and metabolism in patients with PSID.

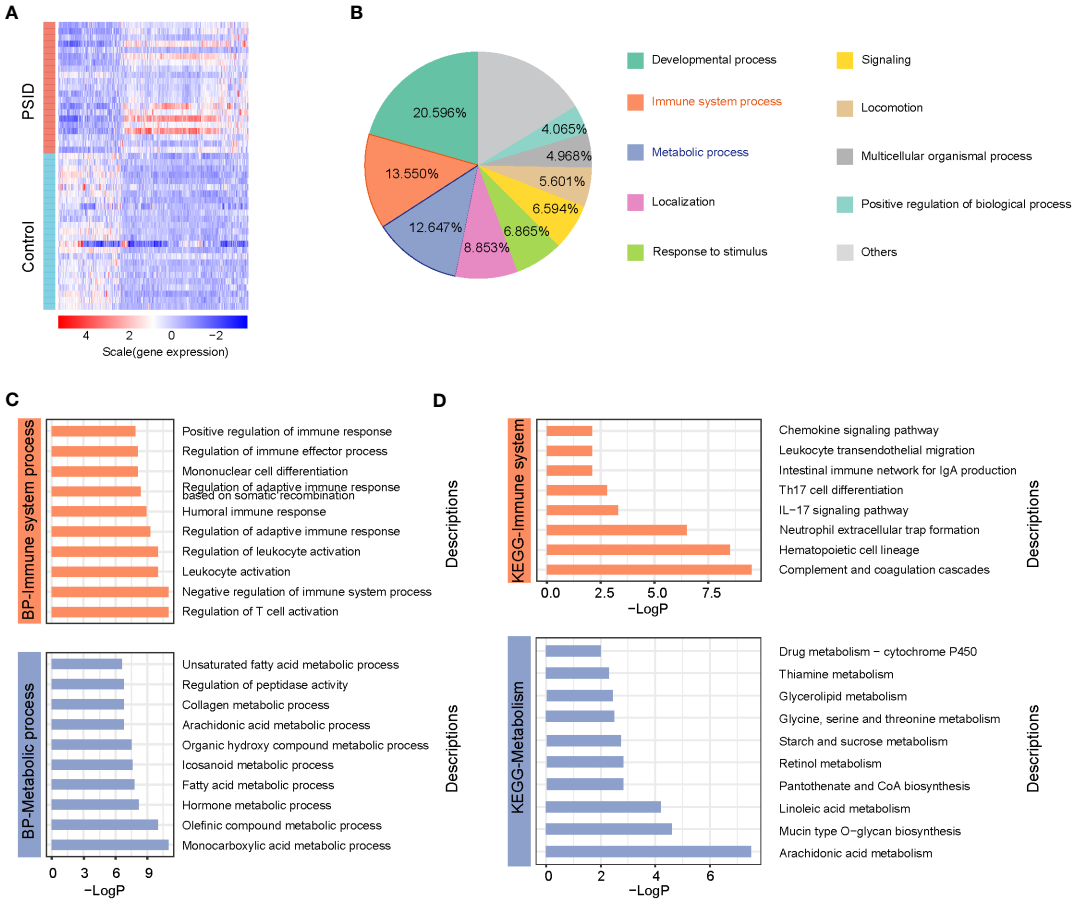

FIGURE 2
Widespread alterations to immune system and metabolic processes are associated with PSID. **(A)** Heatmap of 766 differentially expressed genes between the PISD and Control groups. DEGs were filtered on the criteria |log2 fold change (FC)|≥1 and adjusted p value < 0.05. **(B)** Biological functions of the biological processes associated with 766 DEGs, annotated based on Gene Ontology (GO) enrichment analysis. **(C)** Top 10 biological processes associated with immunology and metabolism enriched by 766 DEGs based on GO enrichment analysis. **(D)** 8 immune-related pathways and 10 metabolism-related pathways were significantly enriched by 766 DEGs based on KEGG enrichment analysis.

2.4 Hub genes involved in immune-related genes

To identify the hub genes associated with immune changes in PSID, we performed weighted gene co-expression network analysis (WGCNA) for 2,705 immune cell signature genes to construct gene expression networks. Samples were excluded based on standardised connectivity values < -5, and all 46 samples were included in the WGCNA. Furthermore, a soft-threshold value (β) of 7 is considered to be the optimal soft-threshold parameter for construction of a gene expression network. Using this parameter, we obtained 21 gene expression modules for immune cell signature genes (Supplementary Figures 4A, B). The modules were merged according to a correlation coefficient of > 0.75, resulting in 15 modules. The correspondences between the 15 modules and age, sex, and CRP group were identified to detect the correlations between them (Supplementary Figure 4C). Using the criteria of absolute value of the correlation coefficient > 0.5 and P < 0.05, the brown, grey60, black, and blue modules were found to be closely associated with the high-CRP group, and gene significance was closely associated with module membership (MM) in these modules (Figure 5A). There were significant differences in gene expression between the high- and low-expression groups in these four modules (Figure 5B). Absolute gene significance in the modules is shown in Figure 5C. A total of 171 hub genes among the immune cell signature genes were identified through screening with the criteria of absolute gene significance > 0.6 and MM > 0.8. Finally, five intersecting genes (*CD163*, *MAPK14*, *S100A12*, *CD40LG*, and CD28) were obtained after merging hub genes among the DEGs and hub genes among immune cell signature genes (Figure 5D). These were identified as immune-related hub genes for PSID. Compared with the low-CRP group, *CD163*, *MAPK14*, and *S100A12* were increased, while *CD40LG* and *CD28* were decreased in the PSID group (Figure 5E).

2.5 Hub genes involved in metabolism-related genes

The same method was used to identify hub genes associated with metabolic changes in PSID. We used $\beta = 17$ to construct gene expression networks (Supplementary Figure 5A). Ultimately, 37 gene co-expression modules were identified (Supplementary

TABLE 1 Number of identifications (*n*) of the top 20 hub genes selected using 12 algorithms via the CytoHubba tool in Cytoscape.

Gene	*n*	Genes	*n*	Gene	*n*	Gene	*n*	Gene	*n*
ALB	10	CD28	4	FLT3LG	2	CYP4F3	1	MAGED4	1
IL6	10	CEBPB	4	HIST1H2AI	2	F12	1	MAGED4B	1
PPARG	10	CTGF	4	HIST1H2BC	2	FBLN5	1	MAL	1
IL10	9	CXCL9	4	HIST2H2AB	2	FFAR3	1	MS4A4A	1
ITGAM	9	IL7R	4	NR3C2	2	HBM	1	OSM	1
MMP9	9	ALOX5	3	PRL	2	HIST1H1C	1	PLIN5	1
CCL2	8	ARG1	3	SOCS3	2	HIST1H1E	1	RHOU	1
MMP2	8	COL5A1	3	SYN1	2	HIST1H3J	1	SFTPD	1
BMP4	7	GPR29	3	CCL23	1	HIST1H4F	1	SLC22A31	1
CD163	6	KCNH7	3	CD207	1	HIST2H2AA	1	SLC39A8	1
MAPK14	6	LEF1	3	CD27	1	HIST2H3D	1	STX3	1
NT5E	6	NES	3	CEACAM3	1	HLF	1	TREML4	1
S100A12	6	SCN5A	3	CEP55	1	IL1R2	1	TRIB2	1
CCR7	5	ACE	2	CLDN9	1	IL22	1	TROAP	1
CD40LG	5	CD1B	2	COL8A2	1	IL23R	1		
HGF	5	CD1E	2	CTSD	1	IRAK3	1		
RETN	5	CD276	2	CYP2C9	1	LPL	1		
CD1C	4	CSF3R	2	CYP4F2	1	LRG1	1		

Figure 5B). The modules were merged according to a correlation coefficient of > 0.75, resulting in 18 modules. The correspondences of the 18 modules with age, sex, and CRP group were also identified in order to detect correlations between them (Supplementary Figure 5C). The dark olive green, tan, black, and dark magenta modules were associated with the PSID group, and gene significance was closely associated with MM in these modules (Figure 6A). There were significant differences in gene expression between the high- and low-expression groups in these four modules (Figure 6B). Absolute gene significance in the modules is shown in Figure 6C. A total of 559 hub genes among the metabolism-related genes were identified through screening with the criteria of absolute gene significance > 0.6 and MM > 0.8. Finally, 13 intersecting genes, namely *ALOX5*, *CEBPB*, *ITGAM*, *IL10*, *MAPK14*, *PPARG*, *S100A12*, *CCR7*, *CD28*, *CD40LG*, *IL7R*, *LEF1*, and *NT5E*, were obtained after merging hub genes among the DEGs and hub genes among the metabolism-related genes (Figure 6D, E). Compared with the Control, *ALOX5*, *CEBPB*, *ITGAM*, *IL10*, *MAPK14*, *PPARG*, *S100A12*, *CCR7*, *CD28*, and *CD40LG* were increased in the PSID group, while *L7R*, *LEF1*, and *NT5E* were decreased (Figure 5E).

2.6 Hub genes linked with immune and metabolism alterations in PSID

Fourteen unique hub genes were associated with immune and metabolic alterations in PSID. Four genes, namely *CD28*, *CD40LG*, *MAPK14*, and *S100A12*, fell into the area of overlap between hub genes among the immune cell signature genes and metabolic-related genes, defined as a gene set; these were extremely closely associated with linking of the immune and metabolic changes in PSID (Figure 7A). The close correlations between these four hub genes and the metabolic hub genes is shown in a heatmap in Figure 7B. *CD28* is a signature gene of CD8+ Tcm, CD4+ Tem, CD4+ Tcm, CD4+ T cells, naïve CD4 + T cells, and CD4+ memory T cells. S100A12 is a signature gene in neutrophils and monocytes. CD40LG is a signature gene of Tgd, CD4+ Tem, CD4+ Tcm, CD4+ T cells, CD4+ naïve T cells, and CD4+ memory T cells. Finally, MAPK14 was identified as the signature gene for monocytes (Figure 7C). This suggests that alterations in these cells are involved in the metabolic alterations occurring in PSID. Receiver Operating Characteristic (ROC) curves were used to validate the diagnostic value of the four hub genes in our cohort; *CD28*, *CD40LG*, *MAPK14*, and *S100A12* all had high diagnostic value, with area under the ROC curve (AUC) > 0.9 in all cases (Figure 7D).

2.7 Decreased CD28 and CD40LG expression in T cells of PSID mice

Most PBMCs are lymphocytes, including B and T cells, among which $CD3^{+}$T cells account for the majority. According to the results of the bioinformatics analysis, the expression of *CD28* and *CD40LG* in patients with PSID was significantly reduced. To further validate the results of the biological analysis, we examined the

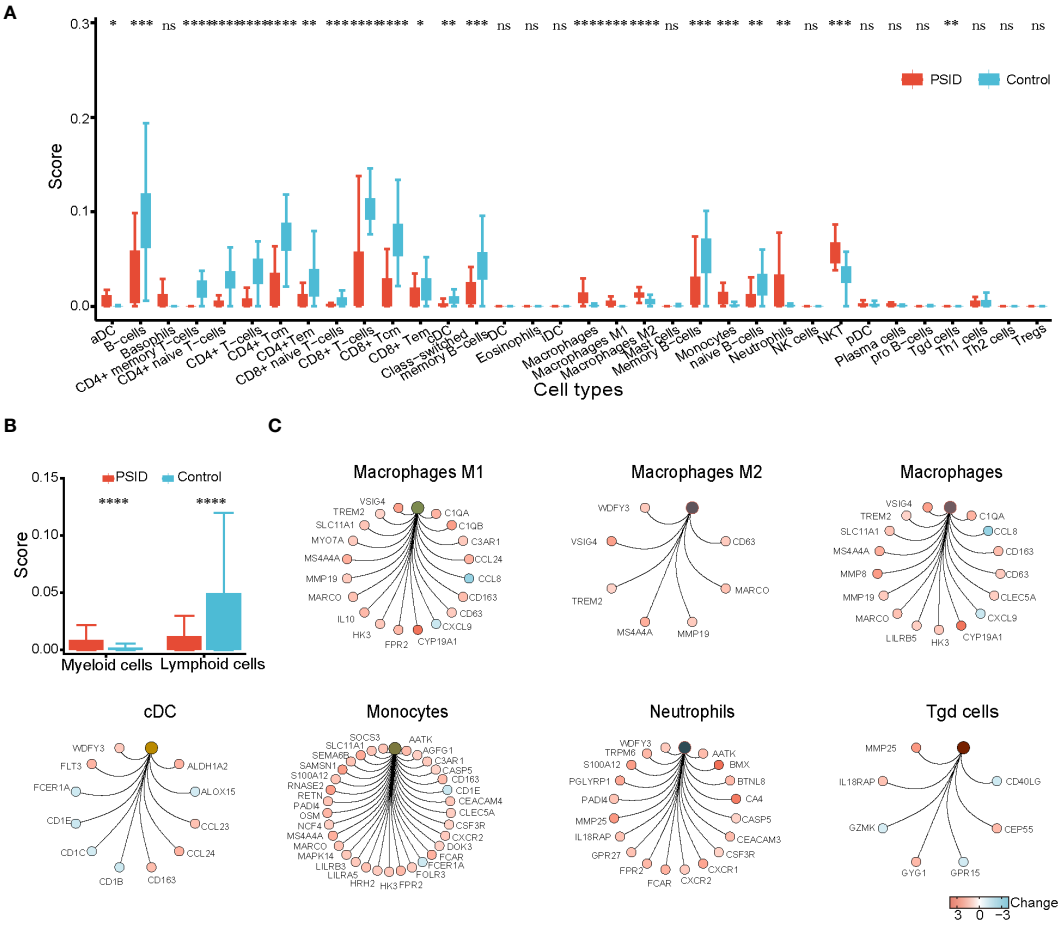

FIGURE 3
Enrichment of immune cells. **(A)** Differences in immune cell scores between the PSID group (n=21) and Control group (n=25) ($p < 0.05$). Asterisks indicate significant difference between the two groups: *P < 0.05, **P < 0.01, ***P < 0.001, ****P < 0.0001. **(B)** Differences in myeloid cells and lymphoid cell scores between the PSID group (n=21) and Control group (n=25). Asterisks indicate significant differences between the two groups: ****P < 0.0001. **(C)** Specific genes associated with these myeloid cells, based on cnetplot analysis. ns, P>0.05.

expression of *CD28* and *CD40LG* in modulating LPS-induced PSID. Flow cytometry was used to detect the expression of *CD28* and *CD40LG* in the $CD3^+$T cells of septic mice; this showed that *CD28* expression in the $CD3^+$T cells of the blood (Figures 8A, B) and spleen (Figures 8C, D) was significantly decreased. The results on *CD40LG* in blood (Figures 8E, F) and spleen (Figures 8G, H) were consistent with the results of the bioinformatics analysis. These data confirm the accuracy of our bioinformatics analysis and will help to facilitate subsequent research.

3 Methods

3.1 Data collection and processing

We downloaded the gene expression matrix data for GSE184039 from the Gene Expression Omnibus (GEO) database (https://www.ncbi.nlm.nih.gov/geo/query/acc.cgi?acc=GSE184039). The GEO database is an international public repository that archives and freely distributes high-throughput gene expression datasets and other functional genomics datasets (17). This mainly consists of gene sequencing data, including microarray and second- and third-generation sequencing data, which can be downloaded using the GEO query package in the R programming environment (version 4.2.2) (18). The dataset analysed in this study contains transcriptomic data from patients undergoing major abdominal surgery. Patients were divided into a PSID group (n = 21, CRP > 250 mg/L) and a Control group (n = 25, CRP < 75 mg/L) based on postoperative levels; clinical information on all patients is listed in Table 2. The GSE184039 matrix contains expression data for 60,662 genes. If there were two or more expression counts for the same gene name, the average value was determined. Ultimately, 60,583 non-duplicate gene expression counts were obtained for analysis of DEGs.

3.2 Function enrichment analysis of DEGs and identification of hub genes

Raw counts were normalised to the vst function using the DESeq2 package. DEGs between the PSID and Control groups were screened for based on cutoff criteria of absolute log2(fold change) ≥ 1 and adjusted P value < 0.05. Biological process (BP) and

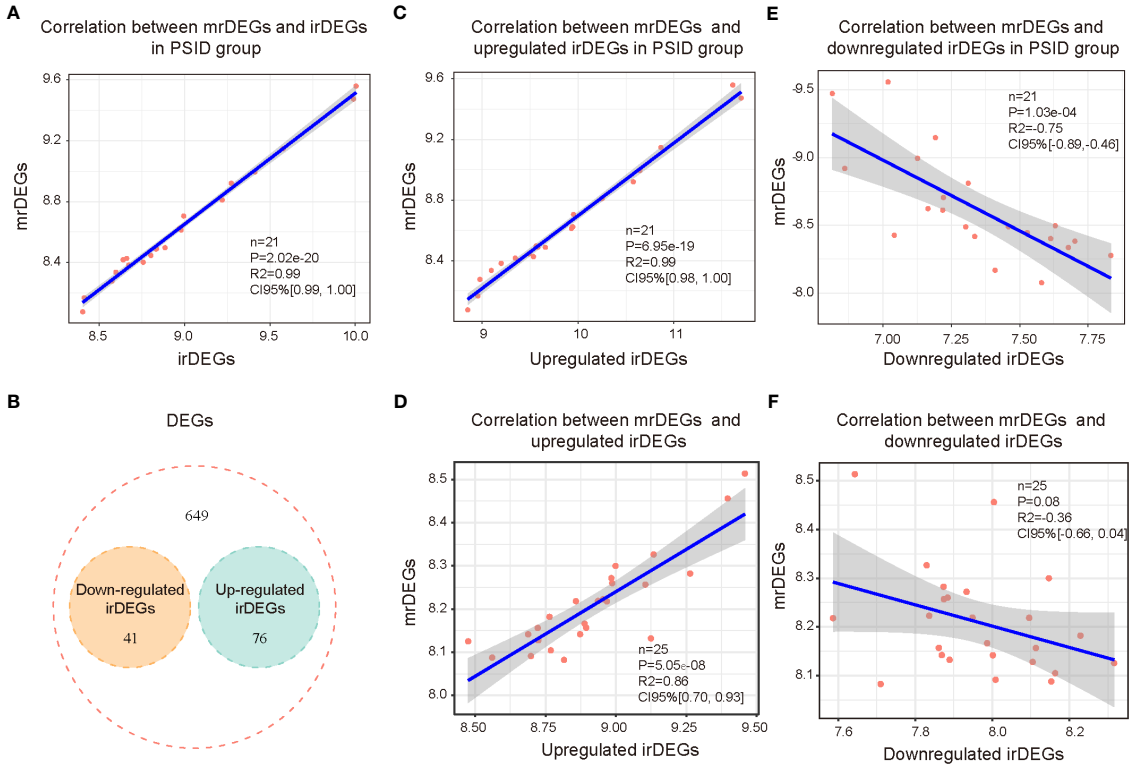

FIGURE 4
Correlation between immunity and metabolism in PSID. **(A)** Correlation analysis of all immune-related genes and metabolism-related genes after surgery. **(B)** Venn diagram displaying the intersections of the 766 DEGs with upregulated and downregulated irDEGs. **(C)** Correlation analysis of postoperatively upregulated irDEGs and mrDEGs in the PSID group. **(D)** Correlation analysis of postoperatively upregulated irDEGs and mrDEGs in the Control group. **(E)** Correlation analysis of mrDEGs and postoperatively downregulated irDEGs in the PSID group. **(F)** Correlation analysis of mrDEGs and postoperatively downregulated irDEGs in the Control group.

(KEGG) analyses for DEGs were performed using Metascape (https://metascape.org/gp/index.html) to predict the biological functions and pathways in which the DEGs were involved (19). The threshold for statistical significance was set at $P < 0.05$. The biological processes and pathways associated with immunity and metabolism were detected, and data on genes enriched in the immune- and metabolism-related pathways were visualised using the igraph, ggraph, and tidygraph packages.

Potential interactions between the DEGs were analysed using the STRING database. The network with a confidence score ≥ 0.4 in STRING was retained and then input to Cytoscape (version 3.7.1) for visualisation. The top 20 genes were selected via 12 different analysis methods using the CytoHubba tool; genes detected using at least 3 different methods were considered to be hub genes among the DEGs.

3.3 Comparison of immune scores between two groups

The xCell tool, which uses a set of 10,808 genes to calculate the scores of 64 immune and stromal cell types based on a novel gene signature-based method, was used to calculate scores for immune cell infiltration in the peripheral blood of each sample. According to cell gene markers, 34 immune cell types were scored using xCell. A total of 21 of the immune cells were identified as lymphoid cells. Differences in cell type scores between the PSID and Control groups were estimated using the Mann–Whitney *U* test, with a threshold for statistical significance of $P < 0.05$.

3.4 Hub genes among immune-related and metabolism-related genes

WGCNA is an algorithm used to identify co-expressed gene modules with high biological significance and explore relationships between gene networks and diseases. It can also be used as a data-exploratory tool or screening method to identify key gene modules using unsupervised clustering without a priori–defined gene sets. In our study, 2,705 immune-related genes (based on immune cell signatures) were used to explore the hub genes associated with immune alterations in PSID, and 9,250 metabolism-related genes (according to the MSigDB database, https://www.gsea-msigdb.org/gsea/msigdb/) were used to explore the hub genes associated with metabolic changes. Hub genes were screened using the WGCNA package with the following steps. First, the cutreeDynamic function was used for tree pruning of the gene hierarchical clustering dendrograms, resulting in co-expression modules; correlated modules ($r > 0.75$) were then merged. The dissimilarity of module eigengenes was calculated using the module eigengene function. The

10.3389/fimmu.2023.1238774

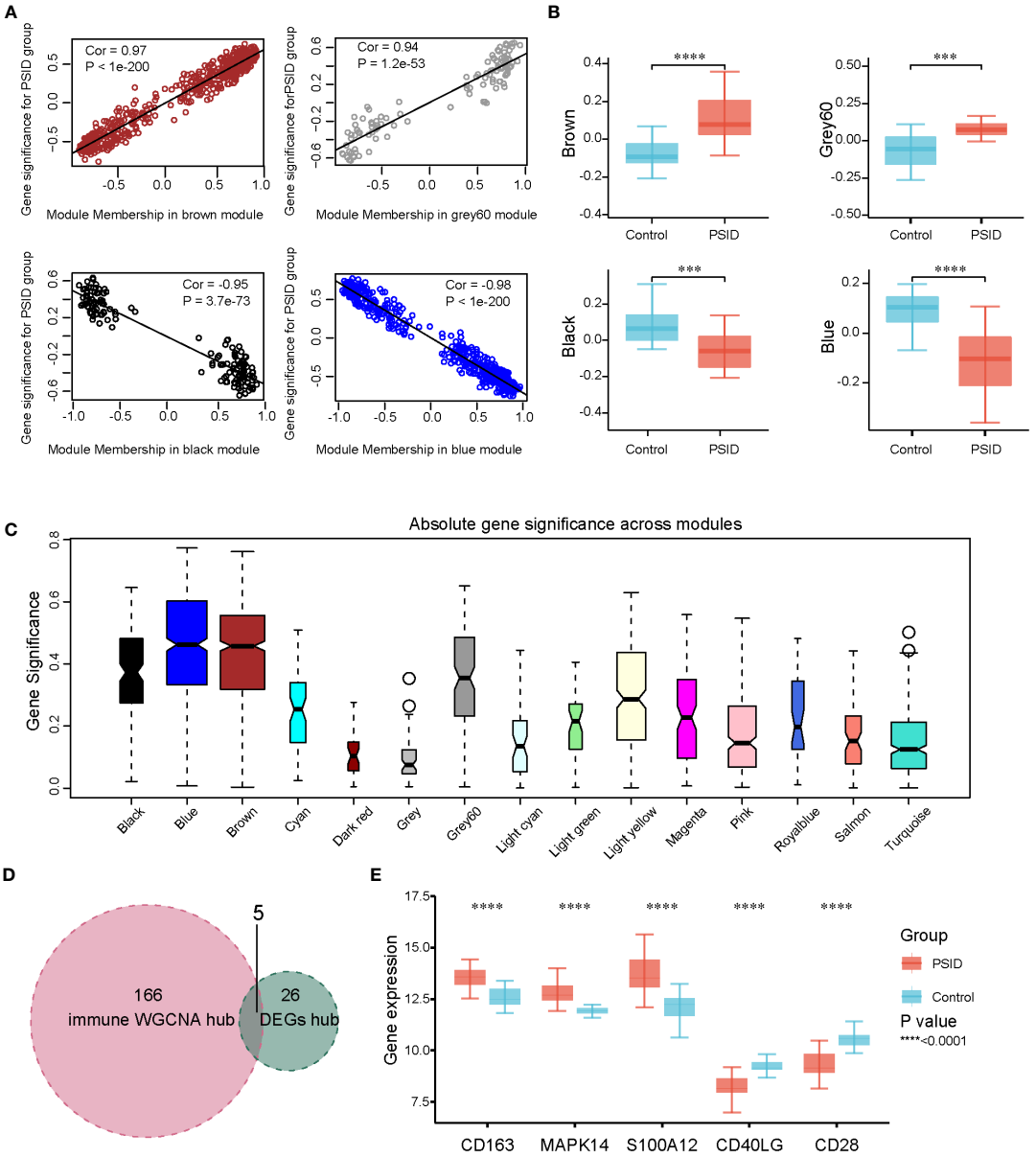

FIGURE 5
WGCNA and identification of significant modules among immune-related genes. **(A)** Scatterplots of gene significance against MM in the brown, grey60, black, and blue modules. **(B)** Comparison of immune cell signature genes in the four modules between the PSID group (n=21) and the Control group (n=25). Asterisks indicate significant difference between the two groups: ***P < 0.001, ****P < 0.0001. **(C)** Gene significance across 15 modules. **(D)** Venn diagram illustrating the intersection between the 171 immune hub genes identified using WGCNA method and the 31 immune hub genes based on cell signatures. The 5 genes at the intersection of these two groups are shown in panel **(E)**. **(E)** Differential expression analysis of five key genes for the PSID and Control groups. Asterisks indicate significant differences between the two groups: ****P < 0.0001.

associations between eigengene values and clinical traits were subsequently assessed using Pearson's correlation. Hub genes were screened using criteria of gene significance > 0.6 and MM > 0.8.

3.5 Hub genes linked with immune and metabolism alterations in PSID

Hub genes associated with immune changes in PSID were detected by merging the hub genes with DEGs and immune-related genes. Similarly, hub genes associated with metabolic changes in PSID were detected by merging hub genes among DEGs with metabolism-related genes. Hub genes detected in relation to both immune and metabolic changes were identified as playing a critical role in linking immune and metabolic alterations in PSID. We then explored the interactions between hub genes using the corrplot package. ROC curves and their AUC were examined using the pROC package to determine the predictive value of hub genes linked to immune and metabolic alterations in PSID.

10.3389/fimmu.2023.1238774

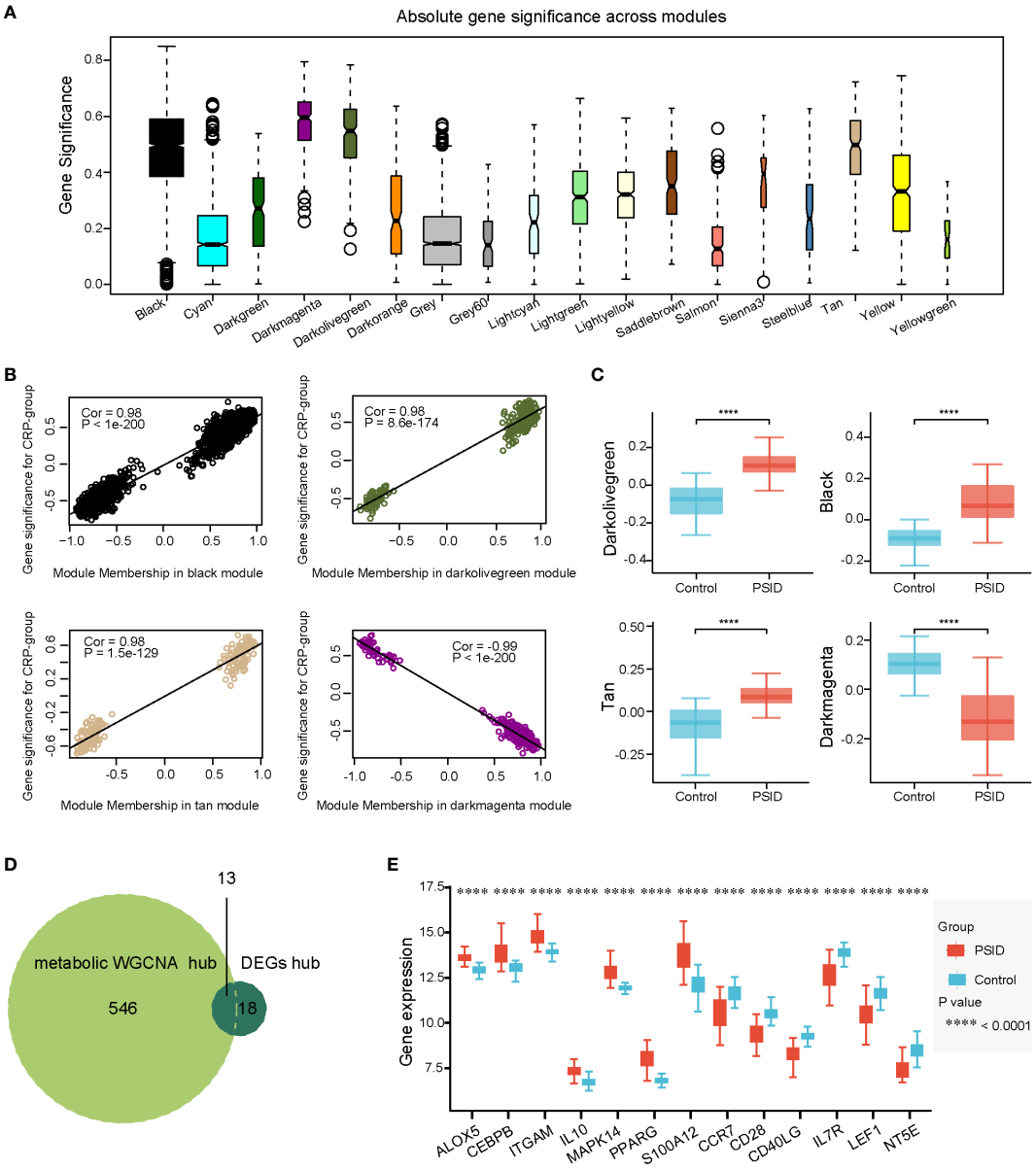

FIGURE 6
Selection of metabolic-related hub genes. **(A)** Gene significance across 18 modules. **(B)** Scatterplots of GS against MM in the dark olive green, tan, black, and dark magenta modules. **(C)** Comparison of metabolism-related genes in the four modules between the PSID group (n=21) and the Control group (n=25) ($p < 0.05$). Asterisks indicate significant differences between the two groups: ****$P < 0.0001$. **(D)** Venn diagram illustrating the intersection between the 559 metabolic hub genes identified using the WGCNA method and the 31 immune hub genes based on cell signatures. The 13 genes at the intersection of these two groups are shown in panel **(E)**. **(E)** Differential expression analysis of 13 key genes for the PSID and Control groups. Asterisks indicate significant difference between the two groups: ****$P < 0.0001$.

3.6 LPS model and flow cytometry

C57BL/6 mice were challenged via intraperitoneal injection with 10 mg/kg LPS (Sigma, Germany, L2630) or vehicle. Blood samples and spleen were collected 4 h after LPS injection. The spleen mucosa was filtered to prepare a 1ml single-cell suspension, after which 100µl peripheral blood and the spleen suspension were treated with red cell lysis solution (Biosharp, China). T cells were identified by labelling with anti-CD3-APC. For CD28 and CD40L expression, we stained samples with anti-CD28-FITC and anti-CD40L-FITC, respectively, in order to observe the changes in the CD28 and CD40L levels of T cells in the different groups. Antibodies for flow cytometry were purchased from BioLegend. Stained cells were analysed using a BD-LSRFortessa flow cytometer (BD Biosciences). Data were analysed using the FlowJo software package.

3.7 Statistical analysis

Transcriptomic data were analysed using R version 4.2.2. Partial packages were employed to analyse the data; these processes are

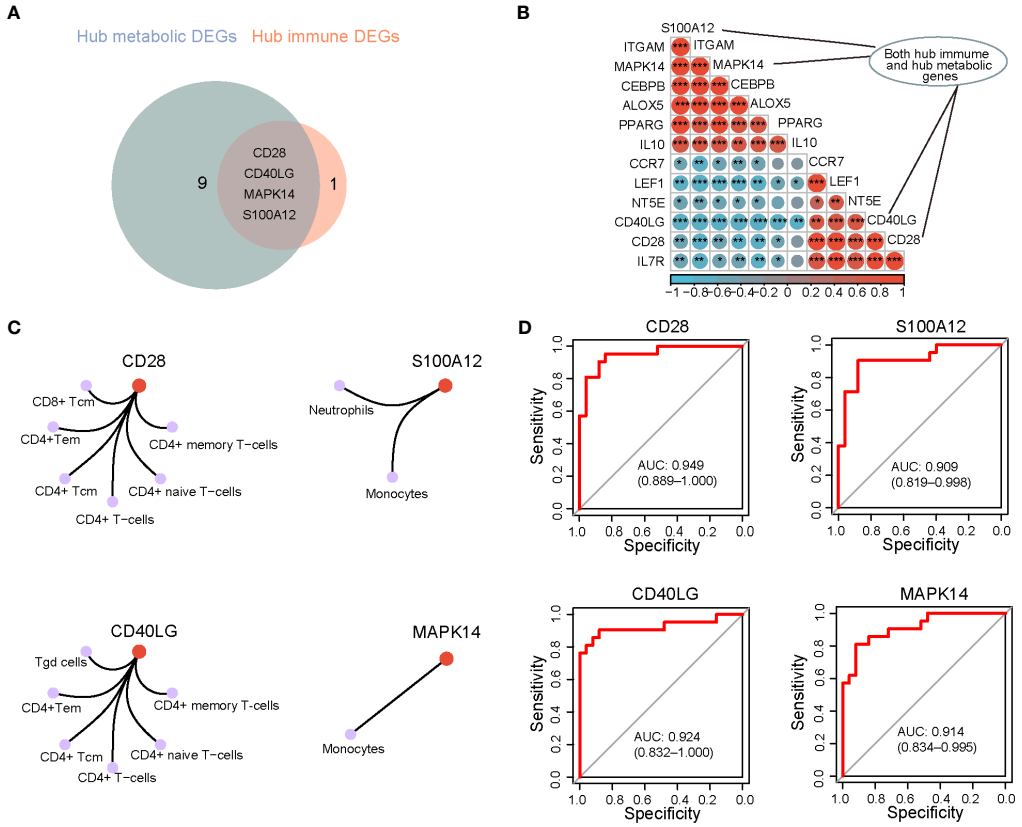

FIGURE 7
Identification of the key genes related to PSID. **(A)** Venn diagram illustrating the number of hub metabolic and hub immune genes. **(B)** Correlation analysis of metabolic-related hub genes and PSID hub genes. **(C)** The 4 hub genes associated with specific types of immune cell, based on cnetplot analysis. **(D)** Diagnostic value of hub genes. The higher the AUC, the greater the diagnostic value of the gene. *P < 0.05, **P < 0.01, ***P < 0.001.

described in the data collection and processing sections. In addition, the packages dplyr, reshape2, and tidyverse were employed for data conversion and analysis, and ggplot2, ggpubr, ggstatsplot, pheatmap, RColorBrewer, and VennDiagram were used to visualise the results of data analysis. For comparisons, normally distributed data were analysed using the Student's *t*-test or one-way analysis of variance (ANOVA), and the results are reported in the form mean ± standard deviation; $P < 0.05$ was considered to represent statistical significance. Statistical analyses of flow cytometry data were conducted using the GraphPad Prism software package (version 8.0; GraphPad Software, US).

4 Discussion

The inflammatory immune response to surgical injury can progress to a dysregulated state (20). Early intervention is essential to manage the systemic inflammatory state; therefore, predictive biomarkers for postoperative outcomes may positively affect outcomes. Many inflammatory mediators have been evaluated as potential biomarkers in patients with non-surgical sepsis, but only a small number of studies have focused on surgical patients, and even fewer have looked prospectively at blood samples taken early after surgery before clinical signs become evident. However, studies investigating the link between immunity and metabolism have provided new perspectives on the state of immune imbalance after surgery, thereby expanding our understanding of the immunological basis of postoperative complications, and identified prognostic biological signatures. In this study, we used plasma CRP levels to assess the extreme phenotypic state of PSID and conducted a comprehensive integrated analysis of immune- and metabolic-related gene expression in PSID. CRP level is a good indicator of infection status. CRP > 250 mg/L as PSID classification standard, the control for > 75mg/L. Postoperative CRP>150 mg/L (at 3–5 days postoperatively) is the most sensitive biochemical indicator of infection (21), and patients with CRP levels lower than 135mg/L on the 4th day after surgery are less likely to develop postoperative infectious complications (22). ROC analysis of cutoff points associated with AUC≥0.8 has identified relatively similar CRP levels (123 to 190 mg/l) as the optimal cutoff point for balancing sensitivity and specificity in the identification of surgical infection for various gastrointestinal cancers (23). Therefore, the criteria we selected are in good agreement with the critical values identified in the above studies.

We confirmed that immunity and metabolism were significantly and positively correlated during PSID, and that, at the PSID stage, the activation of myeloid cells and the suppression of lymphoid cells were significant. WGCNA hub genes were

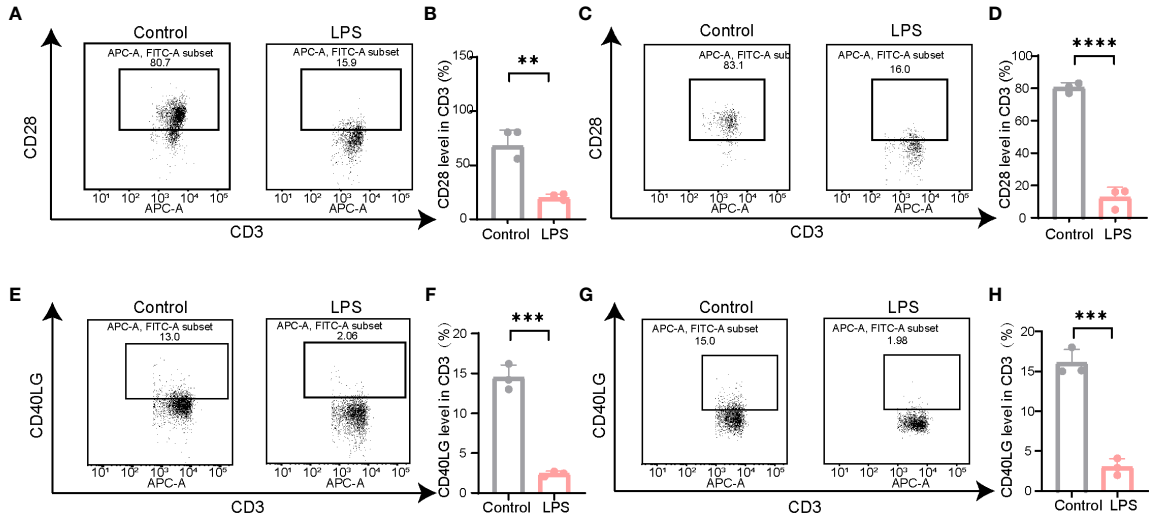

FIGURE 8
The expression of *CD28* and *CD40LG* decreased in LPS-induced mouse model. **(A)** Representative illustrations of flow cytometry gating strategy for identification of the level of *CD28* in the spleen in mice. **(B)** Statistical comparison of CD28 levels in the spleen between LPS and Control. For each group, n = 3. **P =0.0031, t = 6.384. **(C)** Representative illustrations of flow cytometry gating strategy for identification of the level of *CD28* in the blood in mice. **(D)** Statistical comparison of CD28 levels in the blood between LPS and Control. For each group, n = 3. ****P < 0.0001, t = 16.42. **(E)** Representative illustrations of flow cytometry gating strategy for identification of the level of *CD40LG* in the spleen in mice. **(F)** Statistical comparison of *CD40LG* levels in the spleen between LPS and Control. For each group, n = 3. ***P =0.0002, t = 12.65. **(G)** Representative illustrations of flow cytometry gating strategy for identification of the level of *CD40LG* in the blood in mice. **(H)** Statistical comparison of CD40LG levels in the blood between LPS and Control. For each group, n = 3. ***P =0.0004, t = 11.25. Statistical results: two-sided unpaired t-test. Values plotted are means ± SEM.

identified during PSID: these consisted of *CD28* and *CD40LG* downregulation and *MAPK14* and *S100A12* upregulation.

Inflammation is essential in reducing exposure to harmful cell debris and pathogens and in promoting healing. The immune response is balanced between the innate and adaptive immune systems through proinflammatory and anti-inflammatory processes (24). Disruption of this balance increases the risk of development of life-threatening inflammatory complications, including infections, systemic inflammatory response syndrome (SIRS), or sepsis. Myeloid-derived suppressor cells consist of immature myeloid cells, including progenitors or precursors of monocytes, neutrophils, and dendritic cells (25), and are characterised primarily by their inhibitory properties (to both innate and adaptive immunity) and their release in response to various inflammatory and/or infectious signals (26). The number of these cells is substantially increased in experimental models of sepsis (27–30). The development of severe lymphopenia in patients with sepsis is a major feature of adaptive immune sepsis (31). Retrospective studies have shown that persistent lymphatic disease is associated with an increased risk of death and nosocomial infections in patients with sepsis (32–34). Our results indicated that these characteristics are also present at the PSID stage; we also described the changes in the immune scores of myeloid and lymphoid cells, as well as in the genes enriched in these cells (Figure 2 and Supplementary Figure 2).

Key proinflammatory responses during sepsis include activation of the complement system, coagulation system, vascular endothelium, neutrophils, and platelets, whereas immune suppression is primarily caused by the reprogramming of antigen-presenting cells, apoptosis, and exhaustion of lymphocytes (2). Genes enriched for specific immune-related KEGG pathways were plotted using cNetplots (Supplementary Figure 1A). The results showed that complement and coagulation cascades were upregulated.

The interplay between the complement system and coagulation has clinical implications in inflammatory pathogenesis, in which complement–coagulation interactions contribute to the development of life-threatening complications (16–18). In addition, genes associated with the neutrophil extracellular trap (NET) formation pathway were upregulated in the entire population. NET is a regulated form of neutrophil cell death that contributes to host defence against pathogens and is linked to various diseases (19, 20).

TABLE 2 Characteristics of the patients who provided high-CRP and low-CRP postoperative samples in the GSE184039 dataset.

Characteristics	Control group (n = 25)	PSID (n = 21)
Age	55.88 ± 14.15	70.14 ± 10.49
Gender (male/female)	6/19	5/16
CPR (highest level)	48.48 ± 14.31	308.13 ± 54.09

CD28 functions as a co-stimulator of T-cell receptor-mediated antigen activation, while the interleukin-7 receptor is critical in mediating T-cell maturation and survival (35, 36). Downregulation of *CD28* during inflammatory dysregulation is associated with outcomes following major trauma and sepsis (35, 37). The similarity between the downstream signalling pathways of the insulin receptor and CD28 suggests that CD28 may regulate glucose utilisation in a manner similar to that of the insulin receptor, coordinating the control of T cell activation and metabolism (38). In non-diabetic patients, levels > 10 mmol/L may remain elevated for days following surgery. Increased serum glucose concentration and peripheral insulin resistance result in persistently elevated blood glucose levels (39). CD28 co-stimulation of human peripheral blood T cells enhances the expression of glucose transporters, glucose uptake, and glycolysis (38, 40), which suggests that CD28 expression is of great significance for the prediction and diagnosis of PSID.

CD40 is a membrane glycoprotein belonging to the tumour necrosis family receptor superfamily, and its ligand CD40LG is a glycoprotein belonging to the tumour necrosis factor family. CD40–CD40LG interactions are essential in immune responses and inflammation (41–43). Dendritic cells (DCs) activate CD4+ T cells, which in turn provide help to B cells for antibody production (44–46). Importantly, CD40LG is transiently expressed in T cells and other non-immune cells under inflammatory conditions (45, 47). This finding suggests its importance in predicting inflammation in the early stages. Expression of CD40LG on various vascular cells contributes to the pathogenesis of atherosclerosis, thrombosis, and inflammatory processes (48, 49). Previous studies have shown that CD40LG is also closely associated with insulin resistance (50–52).

Interestingly, PSID-related hub genes encoding S100 proteins were upregulated. S100 proteins are potent TLR4 ligands with the potential to stimulate monocytes and to amplify ongoing inflammation (53–55) and myeloid expansion (56). The human *S100A12* gene, located on chromosome 1q21 (57), plays a role in the innate immune response and is associated with certain autoimmune responses. Human S100A12 is significantly overexpressed in the inflammatory compartment, and elevated serum levels of S100A12 are observed in patients with various inflammatory, neurodegenerative, metabolic, and neoplastic diseases (58, 59). This evidence suggests the strong potential of S100A12 as a sensitive and specific diagnostic marker for PSID.

MAPK14 plays a direct and essential role in relieving inhibitory control by autophagy (60). In our study, the upregulation of *MAPK14* observed in the postoperative hyper-inflammatory state suggests this suppressed state. MAPK14-driven metabolic reprogramming sustains the production of NADPH, an important cofactor for several reduction reactions, and the maintenance of a proper intracellular redox environment, thereby reducing the levels of reactive oxygen species (61).

In this study, we used co-expression network analysis to explore the changes in immune-related hub genes and metabolic hub genes occurring in PSID and identified differences in myeloid and lymphoid cells between PSID and Control groups. Our findings provide novel insights into the pathogenesis of PSID.

Data availability statement

The original contributions presented in the study are included in the article/Supplementary Material. Further inquiries can be directed to the corresponding authors.

Ethics statement

The animal study was approved by Standing Committee on Animals at the Tongji University. The study was conducted in accordance with the local legislation and institutional requirements.

Author contributions

Project design and supervision: CL, HZ, and QL. Generation of critical concepts: SC and JT. Experimental work and data analysis: MF, QJ, MZ, and FM. Writing and revision of the manuscript: SC and JT.

Funding

We acknowledge the National Natural Science Foundation [grant number: 82271223], Shanghai Municipal Committee of Science and Technology [grant number: 23XD1422900], and Shanghai Fourth People's Hospital, School of Medicine, Tongji University [grant numbers: sykyqd01902 and SY-XKZT-2021-2001] for providing funding support for the current work.

Acknowledgments

The authors are grateful to the providers who submitted their data to public databases.

Conflict of interest

The authors declare that the research was conducted in the absence of any commercial or financial relationships that could be construed as a potential conflict of interest.

Publisher's note

Supplementary material

The Supplementary Material for this article can be found online at: https://www.frontiersin.org/articles/10.3389/fimmu.2023.1238774/full#supplementary-material

References

1. Lelubre C, Vincent J-L. Mechanisms and treatment of organ failure in sepsis. *Nat Rev Nephrol* (2018) 14(7):417–27. doi: 10.1038/s41581-018-0005-7

2. van der Poll T, van de Veerdonk FL, Scicluna BP, Netea MG. The immunopathology of sepsis and potential therapeutic targets. *Nat Rev Immunol* (2017) 17(7):407–20. doi: 10.1038/nri.2017.36

3. Cecconi M, Evans L, Levy M, Rhodes A. Sepsis and septic shock. *Lancet (London England)* (2018) 392(10141):75–87. doi: 10.1016/S0140-6736(18)30696-2

4. Bain CR, Myles PS, Taylor R, Trahair H, Lee YP, Croft L, et al. Methylomic and transcriptomic characterization of postoperative systemic inflammatory dysregulation. *Trans Res: J Lab Clin Med* (2022) 247:79–98. doi: 10.1016/j.trsl.2022.04.004

5. Lahiri R, Derwa Y, Bashir Z, Giles E, Torrance HDT, Owen HC, et al. Systemic inflammatory response syndrome after major abdominal surgery predicted by early upregulation of TLR4 and TLR5. *Ann Surg* (2016) 263(5):1028–37. doi: 10.1097/SLA.0000000000001248

6. Kaukonen K-M, Bailey M, Pilcher D, Cooper DJ, Bellomo R. Systemic inflammatory response syndrome criteria in defining severe sepsis. *New Engl J Med* (2015) 372(17):1629–38. doi: 10.1056/NEJMoa1415236

7. Gaieski DF, Edwards JM, Kallan MJ, Carr BG. Benchmarking the incidence and mortality of severe sepsis in the United States. *Crit Care Med* (2013) 41(5):1167–74. doi: 10.1097/CCM.0b013e31827c09f8

8. Singer M, Deutschman CS, Seymour CW, Shankar-Hari M, Annane D, Bauer M, et al. The third international consensus definitions for sepsis and septic shock (Sepsis-3). *JAMA* (2016) 315(8):801–10. doi: 10.1001/jama.2016.0287

9. Wilson J, Wilson GJ. Contemporary issues in protein requirements and consumption for resistance trained athletes. *J Int Soc Sports Nutr* (2006) 3(1):7–27. doi: 10.1186/1550-2783-3-1-7

10. Helander EM, Webb MP, Menard B, Prabhakar A, Helmstetter J, Cornett EM, et al. Metabolic and the surgical stress response considerations to improve postoperative recovery. *Curr Pain Headache Rep* (2019) 23(5):33. doi: 10.1007/s11916-019-0770-4

11. Pearce EL, Pearce EJ. Metabolic pathways in immune cell activation and quiescence. *Immunity* (2013) 38(4):633–43. doi: 10.1016/j.immuni.2013.04.005

12. O'Neill LAJ, Pearce EJ. Immunometabolism governs dendritic cell and macrophage function. *J Exp Med* (2016) 213(1):15–23. doi: 10.1084/jem.20151570

13. MacIver NJ, Michalek RD, Rathmell JC. Metabolic regulation of T lymphocytes. *Annu Rev Immunol* (2013) 31:259–83. doi: 10.1146/annurev-immunol-032712-095956

14. Kim JS, Sklarz T, Banks LB, Gohil M, Waickman AT, Skuli N, et al. Retraction: Natural and inducible TH17 cells are regulated differently by Akt and mTOR pathways. *Nat Immunol* (2013) 14(6):611–8. doi: 10.1038/ni.2607

15. Buck MD, O'Sullivan D, Pearce EL. T cell metabolism drives immunity. *J Exp Med* (2015) 212(9):1345–60. doi: 10.1084/jem.20151159

16. Varadhan KK, Constantin-Teodosiu D, Constantin D, Greenhaff PL, Lobo DN. Inflammation-mediated muscle metabolic dysregulation local and remote to the site of major abdominal surgery. *Clin Nutr (Edinburgh Scotland)* (2018) 37(6 Pt A):2178–85. doi: 10.1016/j.clnu.2017.10.020

17. Clough E, Barrett T. The gene expression omnibus database. *Methods Mol Biol (Clifton NJ)* (2016) 1418:93–110. doi: 10.1007/978-1-4939-3578-9_5

18. Davis S, Meltzer PS. GEOquery: a bridge between the Gene Expression Omnibus (GEO) and BioConductor. *Bioinf (Oxford England)* (2007) 23(14):1846–7. doi: 10.1093/bioinformatics/btm254

19. Hänzelmann S, Castelo R, Guinney J. GSVA: gene set variation analysis for microarray and RNA-seq data. *BMC Bioinf* (2013) 14:7. doi: 10.1186/1471-2105-14-7

20. Bain CR, Myles PS, Corcoran T, Dieleman JM. Postoperative systemic inflammatory dysregulation and corticosteroids: a narrative review. *Anaesthesia* (2023) 78(3):356–70. doi: 10.1111/anae.15896

21. McDermott FD, Heeney A, Kelly ME, Steele RJ, Carlson GL, Winter DC. Systematic review of preoperative, intraoperative and postoperative risk factors for colorectal anastomotic leaks. *Br J Surg* (2015) 102(5):462–79. doi: 10.1002/bjs.9697

22. Warschkow R, Beutner U, Steffen T, Müller SA, Schmied BM, Güller U, et al. Safe and early discharge after colorectal surgery due to C-reactive protein: a diagnostic meta-analysis of 1832 patients. *Ann Surg* (2012) 256(2):245–50. doi: 10.1097/SLA.0b013e31825b60f0

23. Shishido Y, Fujitani K, Yamamoto K, Hirao M, Tsujinaka T, Sekimoto M. C-reactive protein on postoperative day 3 as a predictor of infectious complications following gastric cancer resection. *Gastric Cancer: Off J Int Gastric Cancer Assoc Japanese Gastric Cancer Assoc* (2016) 19(1):293–301. doi: 10.1007/s10120-014-0455-y

24. Alazawi W, Pirmadjid N, Lahiri R, Bhattacharya S. Inflammatory and immune responses to surgery and their clinical impact. *Ann Surg* (2016) 264(1):73–80. doi: 10.1097/SLA.0000000000001691

25. Gabrilovich DI. Myeloid-derived suppressor cells. *Cancer Immunol Res* (2017) 5 (1):3–8. doi: 10.1158/2326-6066.CIR-16-0297

26. Ost M, Singh A, Peschel A, Mehling R, Rieber N, Hartl D. Myeloid-derived suppressor cells in bacterial infections. *Front Cell Infect Microbiol* (2016) 6:37. doi: 10.3389/fcimb.2016.00037

27. Delano MJ, Scumpia PO, Weinstein JS, Coco D, Nagaraj S, Kelly-Scumpia KM, et al. MyD88-dependent expansion of an immature GR-1(+)CD11b(+) population induces T cell suppression and Th2 polarization in sepsis. *J Exp Med* (2007) 204 (6):1463–74. doi: 10.1084/jem.20062602

28. Brudecki L, Ferguson DA, McCall CE, El Gazzar M. Myeloid-derived suppressor cells evolve during sepsis and can enhance or attenuate the systemic inflammatory response. *Infect Immun* (2012) 80(6):2026–34. doi: 10.1128/IAI.00239-12

29. Zhang W, Fang X, Gao C, Song C, He Y, Zhou T, et al. MDSCs in sepsis-induced immunosuppression and its potential therapeutic targets. *Cytokine Growth Factor Rev* (2023) 69:90–103. doi: 10.1016/j.cytogfr.2022.07.007

30. Vance JK, Rawson TW, Povroznik JM, Brundage KM, Robinson CM. Myeloid-derived suppressor cells gain suppressive function during neonatal bacterial sepsis. *Int J Mol Sci* (2021) 22(13):7047. doi: 10.3390/ijms22137047

31. Venet F, Davin F, Guignant C, Larue A, Cazalis M-A, Darbon R, et al. Early assessment of leukocyte alterations at diagnosis of septic shock. *Shock (Augusta Ga)* (2010) 34(4):358–63. doi: 10.1097/SHK.0b013e3181dc0977

32. Drewry AM, Samra N, Skrupky LP, Fuller BM, Compton SM, Hotchkiss RS. Persistent lymphopenia after diagnosis of sepsis predicts mortality. *Shock (Augusta Ga)* (2014) 42(5):383–91. doi: 10.1097/SHK.0000000000000234

33. Chung K-P, Chang H-T, Lo S-C, Chang L-Y, Lin S-Y, Cheng A, et al. Severe lymphopenia is associated with elevated plasma interleukin-15 levels and increased mortality during severe sepsis. *Shock (Augusta Ga)* (2015) 43(6):569–75. doi: 10.1097/SHK.0000000000000347

34. Adrie C, Lugosi M, Sonneville R, Souweine B, Ruckly S, Cartier J-C, et al. Persistent lymphopenia is a risk factor for ICU-acquired infections and for death in ICU patients with sustained hypotension at admission. *Ann Intensive Care* (2017) 7 (1):30. doi: 10.1186/s13613-017-0242-0

35. ElKassar N, Gress RE. An overview of IL-7 biology and its use in immunotherapy. *J Immunotoxicol* (2010) 7(1):1–7. doi: 10.3109/15476910903453296

36. Wang C, Kong L, Kim S, Lee S, Oh S, Jo S, et al. The role of IL-7 and IL-7R in cancer pathophysiology and immunotherapy. *Int J Mol Sci* (2022) 23(18):10412. doi: 10.3390/ijms231810412

37. Wong HR. Clinical review: sepsis and septic shock–the potential of gene arrays. *Crit Care (London England)* (2012) 16(1):204. doi: 10.1186/cc10537

38. Frauwirth KA, Riley JL, Harris MH, Parry RV, Rathmell JC, Plas DR, et al. The CD28 signaling pathway regulates glucose metabolism. *Immunity* (2002) 16(6):769–77. doi: 10.1016/S1074-7613(02)00323-0

39. Eberhart LHJ, Graf J, Morin AM, Stief T, Kalder M, Lattermann R, et al. Randomised controlled trial of the effect of oral premedication with dexamethasone on hyperglycaemic response to abdominal hysterectomy. *Eur J Anaesthesiol* (2011) 28 (3):195–201. doi: 10.1097/EJA.0b013e32834296b9

40. Revu S, Wu J, Henkel M, Rittenhouse N, Menk A, Delgoffe GM, et al. IL-23 and IL-1β Drive human Th17 cell differentiation and metabolic reprogramming in absence of CD28 costimulation. *Cell Rep* (2018) 22(10):2642–53. doi: 10.1016/j.celrep.2018.02.044

41. Freedman JE. CD40-CD40L and platelet function: beyond hemostasis. *Circ Res* (2003) 92(9):944–6. doi: 10.1161/01.RES.0000074030.98009.FF

42. Díaz Á., González-Alayón I, Pérez-Torrado V, Suárez-Martins M. CD40-CD154: A perspective from type 2 immunity. *Semin Immunol* (2021) 53:101528. doi: 10.1016/j.smim.2021.101528

43. Tang T, Cheng X, Truong B, Sun L, Yang X, Wang H. Molecular basis and therapeutic implications of CD40/CD40L immune checkpoint. *Pharmacol Ther* (2021) 219:107709. doi: 10.1016/j.pharmthera.2020.107709

44. Laman JD, Claassen E, Noelle RJ. Functions of CD40 and its ligand, gp39 (CD40L). *Crit Rev Immunol* (2017) 37(2-6):371–420. doi: 10.1615/CritRevImmunol.v37.i2-6.100

45. Elgueta R, Benson MJ, de Vries VC, Wasiuk A, Guo Y, Noelle RJ. Molecular mechanism and function of CD40/CD40L engagement in the immune system. *Immunol Rev* (2009) 229(1):152–72. doi: 10.1111/j.1600-065X.2009.00782.x

46. Yin X, Chen S, Eisenbarth SC. Dendritic cell regulation of T helper cells. *Annu Rev Immunol* (2021) 39:759–90. doi: 10.1146/annurev-immunol-101819-025146

47. Karnell JL, Rieder SA, Ettinger R, Kolbeck R. Targeting the CD40-CD40L pathway in autoimmune diseases: Humoral immunity and beyond. *Adv Drug Delivery Rev* (2019) 141:92–103. doi: 10.1016/j.addr.2018.12.005

48. Henn V, Slupsky JR, Gräfe M, Anagnostopoulos I, Förster R, Müller-Berghaus G, et al. CD40 ligand on activated platelets triggers an inflammatory reaction of endothelial cells. *Nature* (1998) 391(6667):591–4. doi: 10.1038/35393

49. Mach F, Schönbeck U, Sukhova GK, Atkinson E, Libby P. Reduction of atherosclerosis in mice by inhibition of CD40 signalling. *Nature* (1998) 394 (6689):200–3. doi: 10.1038/28204

50. Penno G, Pucci L, Dell'Omo G, Lucchesi D, Miccoli R, Del Prato S, et al. Soluble CD40 ligand levels in essential hypertensive men: evidence of a possible role of insulin resistance. *Am J Hypertension* (2009) 22(9):1007–13. doi: 10.1038/ajh.2009.121

51. Wright RJ, Newby DE, Stirling D, Ludlam CA, Macdonald IA, Frier BM. Effects of acute insulin-induced hypoglycemia on indices of inflammation: putative mechanism for aggravating vascular disease in diabetes. *Diabetes Care* (2010) 33 (7):1591–7. doi: 10.2337/dc10-0013

52. Guo C-A, Kogan S, Amano SU, Wang M, Dagdeviren S, Friedline RH, et al. CD40 deficiency in mice exacerbates obesity-induced adipose tissue inflammation, hepatic steatosis, and insulin resistance. American Journal of Physiology. *Endocrinol Metab* (2013) 304(9):E951–63. doi: 10.1152/ajpendo.00514.2012

53. Foell D, Wittkowski H, Kessel C, Lüken A, Weinhage T, Varga G, et al. Proinflammatory S100A12 can activate human monocytes via Toll-like receptor 4. *Am J Respir Crit Care Med* (2013) 187(12):1324–34. doi: 10.1164/rccm.201209-1602OC

54. Lira-Junior R, Holmström SB, Clark R, Zwicker S, Majster M, Johannsen G, et al. S100A12 expression is modulated during monocyte differentiation and reflects periodontitis severity. *Front Immunol* (2020) 11:86. doi: 10.3389/fimmu.2020.00086

55. Holzinger D, Tenbrock K, Roth J. Alarmins of the S100-family in juvenile autoimmune and auto-inflammatory diseases. *Front Immunol* (2019) 10:182. doi: 10.3389/fimmu.2019.00182

56. Uhel F, Azzaoui I, Grégoire M, Pangault C, Dulong J, Tadié J-M, et al. Early expansion of circulating granulocytic myeloid-derived suppressor cells predicts development of nosocomial infections in patients with sepsis. *Am J Respir Crit Care Med* (2017) 196(3):315–27. doi: 10.1164/rccm.201606-1143OC

57. Marenholz I, Heizmann CW, Fritz G. S100 proteins in mouse and man: from evolution to function and pathology (including an update of the nomenclature). *Biochem Biophys Res Commun* (2004) 322(4):1111–22. doi: 10.1016/j.bbrc.2004.07.096

58. Pietzsch J, Hoppmann S. Human S100A12: a novel key player in inflammation? *Amino Acids* (2009) 36(3):381–9. doi: 10.1007/s00726-008-0097-7

59. Li Y, He Y, Chen S, Wang Q, Yang Y, Shen D, et al. S100A12 as biomarker of disease severity and prognosis in patients with idiopathic pulmonary fibrosis. *Front Immunol* (2022) 13:810338. doi: 10.3389/fimmu.2022.810338

60. She H, He Y, Zhao Y, Mao Z. Release the autophage brake on inflammation: The MAPK14/p38α-ULK1 pedal. *Autophagy* (2018) 14(6):1097–8. doi: 10.1080/15548627.2018.1446626

61. Desideri E, Vegliante R, Cardaci S, Nepravishta R, Paci M, Ciriolo MR. MAPK14/p38α-dependent modulation of glucose metabolism affects ROS levels and autophagy during starvation. *Autophagy* (2014) 10(9):1652–65. doi: 10.4161/auto.29456

frontiers | Frontiers in Immunology

TYPE Review
PUBLISHED 11 September 2023
DOI 10.3389/fimmu.2023.1206452

OPEN ACCESS

EDITED BY
Anwen Shao,
Zhejiang University, China

REVIEWED BY
Zhongqi Cui,
Tongji University, China
Hai-Jian Sun,
National University of Singapore, Singapore

*CORRESPONDENCE
Qiang Fu
fuqiang@sztu.edu.cn
Bin Zeng
zengbin@sztu.edu.cn
Chao Yang
yc52028@hotmail.com

†These authors have contributed equally to this work

RECEIVED 15 April 2023
ACCEPTED 28 July 2023
PUBLISHED 11 September 2023

CITATION
Jiang Y, Song S, Liu J, Zhang L, Guo X, Lu J, Li L, Yang C, Fu Q and Zeng B (2023) Epigenetic regulation of programmed cell death in hypoxia-induced pulmonary arterial hypertension.
Front. Immunol. 14:1206452.
doi: 10.3389/fimmu.2023.1206452

Epigenetic regulation of programmed cell death in hypoxia-induced pulmonary arterial hypertension

Yuan Jiang[1†], Shasha Song[2†], Jingxin Liu[2†], Liyuan Zhang[3], Xiaofei Guo[4], Jiayao Lu[2], Lie Li[5,6], Chao Yang[4*], Qiang Fu[2*] and Bin Zeng[2*]

[1]College of Pharmacy, Harbin Medical University, Harbin, Heilongjiang, China, [2]College of Pharmacy, Shenzhen Technology University, Shenzhen, China, [3]Shanghai Baoxing Biological Equipment Engineering Co., Ltd, Shanghai, China, [4]National Engineering Research Center for Marine Aquaculture, Institute of Innovation & Application, Zhejiang Ocean University, Zhoushan, China, [5]Shenzhen Reyson Biotechnology Co., Ltd, Shenzhen, China, [6]Nanjing Evertop Electronics Ltd., Nanjing, China

Pulmonary arterial hypertension (PAH) is a severe progressive disease that may cause early right ventricular failure and eventual cardiac failure. The pathogenesis of PAH involves endothelial dysfunction, aberrant proliferation of pulmonary artery smooth muscle cells (PASMCs), and vascular fibrosis. Hypoxia has been shown to induce elevated secretion of vascular endothelial growth factor (VEGF), leading to the development of hypoxic PAH. However, the molecular mechanisms underlying hypoxic PAH remain incompletely understood. Programmed cell death (PCD) is a natural cell death and regulated by certain genes. Emerging evidence suggests that apoptotic resistance contributes to the development of PAH. Moreover, several novel types of PCD, such as autophagy, pyroptosis, and ferroptosis, have been reported to be involved in the development of PAH. Additionally, multiple diverse epigenetic mechanisms including RNA methylation, DNA methylation, histone modification, and the non-coding RNA molecule-mediated processes have been strongly linked to the development of PAH. These epigenetic modifications affect the expression of genes, which produce important changes in cellular biological processes, including PCD. Consequently, a better understanding of the PCD processes and epigenetic modification involved in PAH will provide novel, specific therapeutic strategies for diagnosis and treatment. In this review, we aim to discuss recent advances in epigenetic mechanisms and elucidate the role of epigenetic modifications in regulating PCD in hypoxia-induced PAH.

KEYWORDS

pulmonary arterial hypertension (PAH), apoptosis, autophagy, pyroptosis, ferroptosis, DNA methylation, histone modification, non-coding RNA (ncRNA)

1 Introduction

Pulmonary arterial hypertension (PAH) is a fatal cardiovascular disease, also known as malignancy of the cardiovascular system. PAH is characterized by a progressive increase in pulmonary vascular resistance (PVR) and pulmonary vascular remodeling, leading to right ventricular remodeling and ultimately death from right ventricular failure (1, 2). Pulmonary vascular remodeling is a common pathological feature of PAH and encompasses multiple cell types within the blood vessel wall, including endothelial cells (ECs), pulmonary artery smooth muscle cells (PASMCs), fibroblasts, pericytes, and circulating inflammatory cells (3). Although the pathological mechanism of PAH remains incompletely understood, the basic pathological processes are related to the interplay among diverse cellular types in the pulmonary vascular wall, such as abnormal cell energy metabolism, cell differentiation, apoptosis resistance, excessive cell proliferation, and extracellular matrix deposition (4). Therefore, further understanding of cellular processes and mechanisms involved in PAH will provide more efficient therapeutic strategies.

Cell death mechanisms are generally classified into two distinct types: programmed cell death (PCD) and necrotic cell death. PCD is required to control the balance of normal cell homeostasis (5). The canonical form of PCD is apoptosis. Additionally, many other types of programmed cell death, including autophagy, pyroptosis, and ferroptosis, have been characterized (6). Nevertheless, the molecular mechanisms in different types of PCD are complex and usually provoke through a variety of independent pathways. Therefore, the discovery of the underlying mechanisms of PCD is urgently needed.

Epigenetics is indispensable for regulating gene expression, protein transcription, and translation in many biological processes, including DNA methylation, histone modification, non-coding RNA molecules, and N^6-methyladenosine methylation (7). Epigenetics differs from classical genetics, which is independent of changes in genomic DNA base sequence (8). Epigenetic modifications can be added to molecules by transferases, also known as "writers" and removed by "erasers". Crucially, the molecular effects of epigenetics rely on the recognition by specific proteins, also known as "readers" (9). Previous studies have suggested an association between epigenetic modifications and various pathological processes (10). Recently, the underlying functional machinery of epigenetic modifications in PAH has also been attracting extensive attention.

In this review, we focus on the latest advances in epigenetic modifications, such as DNA methylation, histone modification, non-coding RNA molecules, and N^6-methyladenosine methylation related to PCD in hypoxia-induced PAH, thereby identifying the potential therapeutic strategy for PAH.

2 Programmed cell death in PAH

PAH is characterized by abnormal functioning of various cell types, including pulmonary arterial endothelial cells (PAECs), PASMCs, fibroblasts, and inflammatory cells (11). Studies have indicated that abnormal proliferation and anti-apoptotic phenotype of PAECs and PASMCs contribute to the occlusion of pulmonary arterioles, resulting in right heart hypertrophy and eventual cardiac failure. Additionally, fibroblasts isolated from the models of pulmonary hypertension exhibit a hyperproliferative, apoptosis-resistant, and proinflammatory phenotype (12). Chronic inflammation plays an essential role in PAH. Pulmonary vasculopathy has been identified with the presence of immune cell infiltrates, consisting of macrophages, lymphocytes, and mast cells. Autophagy plays an essential role in inflammasome activity. However, whether autophagy-mediated inhibition of inflammasome activity is involved in regulating the progression of PAH remains unclear (13). Furthermore, the presence of interleukin (IL)-1β, IL-18, and pyroptosis, which are end products of inflammasome activation, serves as a pivotal biomarker for PAH (14). These observed changes suggest a connection between programmed cell death mechanisms, including apoptosis, autophagy, pyroptosis, and even ferroptosis in the key cells associated with PAH.

2.1 Apoptosis

Apoptosis, the first identified form of programmed cell death, is a crucial process by which cells autonomously regulate their own death under physiological or pathological conditions (15). The initiation of apoptosis is dependent on morphological changes in cell structure and the activation of cysteine and aspartic protease processes (16). Mechanically, apoptosis is mainly activated by two pathways: the intrinsic pathway (the mitochondrial pathway of apoptosis) and the extrinsic pathway of apoptosis (the death receptor pathway of apoptosis) (17). The intrinsic apoptosis is dependent on factors released from the mitochondria and can be triggered by a series of external stimuli such as hypoxia, reactive oxygen species, and viruses. Conversely, extrinsic apoptosis is initiated by the specific death ligands binding to the death receptors (18).

Multiple studies have suggested that apoptosis is associated with pulmonary vascular remodeling in PAH. Under physiological conditions, apoptosis plays a crucial role in maintaining organ and tissue integrity by regulating the balance between cell proliferation and programmed cell death (19). Nevertheless, the underlying molecular mechanisms of apoptosis in PAH remain to be explored. In a study by Chowdhury et al., it was discovered that dysfunctional bone morphogenetic protein receptor II (BMPRII) impairs apoptosis *via* the BMPRII-ALK1-Bcl-xL pathway in PAH (20). Wang et al. demonstrated that mutations in the bone morphogenetic protein 9 (BMP9) contribute to the etiology of PAH by impairing the anti-apoptotic abilities of PAECs (21). Additionally, Cao et al. reported that prohibitin 1 (PHB1) contributes to PAH by balancing PASMC proliferation and apoptosis, which involves AKT phosphorylation (22). In Jiang's study, prostaglandin E1 (PGE1) modulates the apoptotic properties of mesenchymal stem cells (MSCs) by regulating the HIF pathway, thereby enhancing the therapeutic potential of the MSCs in PAH (23). He et al. conducted studies that revealed the inhibition of apoptosis in distal pulmonary artery smooth muscle cells

(dPASMCs) by PRDC, which was able to reverse the effects of BMP2/4 on the upregulation of apoptosis-associated proteins such as caspase 3, caspase 9, and Bax while downregulating the expression of Bcl-2 (24). Novoyatleva et al. found that deficiency of Axl aggravated PAH and abrogated bone morphogenetic protein receptor 2 (BMPR2) signaling, thereby increasing pulmonary endothelial cell apoptosis (25). Recently, Ruffenach et al. reported that the RNA-binding protein HNRNPA2B1 (heterogeneous nuclear ribonucleoprotein A2B1; A2B1) silencing in PASMCs led to a decrease in proliferation and resistance to apoptosis, which is expected to become a therapeutic target for PAH (26) (Figure 1).

2.2 Autophagy

Autophagy, a form of programmed cell death, plays a pivotal role in the self-renewal process of eukaryotic cells (27). It involves the degradation of cytoplasmic proteins and damaged organelles through the action of lysosomes and is regulated by a set of autophagy-related genes (Atgs). Autophagy can be classified into three forms—macroautophagy, microautophagy, and chaperone-mediated autophagy (CMA)—among which macroautophagy is the most widely studied (28). The process of autophagy can be broken down into several successive steps: initiation and nucleation of autophagosome → elongation and formation of autophagosome → fusion with lysosomes (29).

Autophagy can be induced by cellular stress responses such as hypoxia and nutrient deficiency. Studies have confirmed that the level of autophagy is upregulated during the PAH, which plays an important role in vascular remodeling. Studies by Zhai et al. discovered that activation of AMPK prevents PAH by suppression of NF-κB-mediated autophagy activation (30). In another study, Chang et al. proposed Aldehyde Dehydrogenase 2 (ALDH2) protected against hypoxia-induced PASMC proliferation *via* inhibition of ERK1/2-mediated autophagy (31). Ning et al. found that β-arrestin1 inhibits hypoxia-induced autophagy *via* the Akt/mTOR signaling pathway (32). Moreover, Gomez-Puerto et al. observed an increase in levels of microtubule-associated protein 1 light chain 3 beta (MAP1LC3B) in PAH, while pulmonary microvascular endothelial cells (MVECs) from PAH patients exhibited heightened autophagic flux (33). Feng et al. further elucidated the promotion of PASMC proliferation and pulmonary vascular remodeling by high mobility group box-1 (HMGB1) through the activation of the ERK1/2/Drp1/Autophagy/BMPR2/Id1 axis (34). Jin et al. demonstrated that farnesyl diphosphate synthase (FDPS) contributes to active small G protein-induced autophagy during PAH (35). In a separate investigation, it was found that glucagon-like peptide-1 (GLP-1) receptor agonist, liraglutide, can suppress the proliferation of PASMCs by inhibiting cellular Drp1/nicotinamide adenine dinucleotide phosphate (NADPH) oxidase (NOX) pathways and Atg-5/Atg-7/Beclin-1/LC3β-dependent pathways of autophagy in PAH (36). He et al. conducted a study showing that quercetin enhances hypoxia-induced autophagy through the FOXO1-SENS3-mTOR-dependent pathway in PASMCs (37). In a systematic study, Yamanaka et al. showed that TP53-induced glycolysis and apoptosis

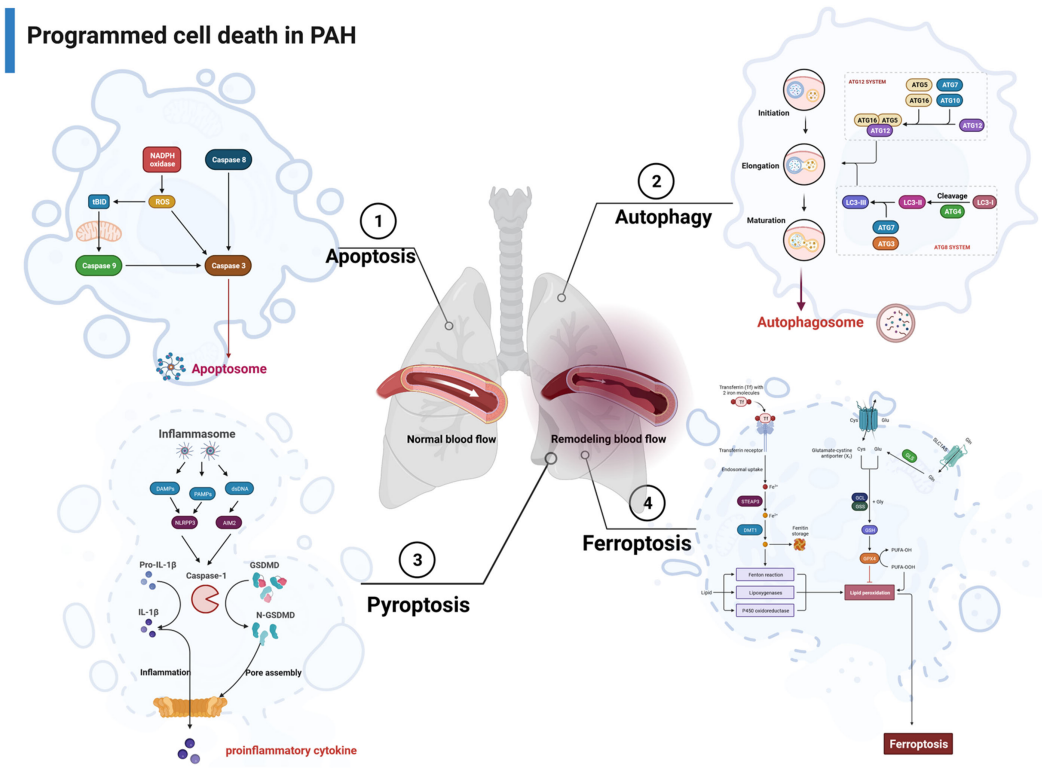

FIGURE 1
The major pathways associated with apoptosis, autophagy, pyroptosis, and ferroptosis in PAH. PAH, pulmonary arterial hypertension.

regulator (TIGAR) regulates PASMC proliferation and migration by inhibiting autophagy and improving hypoxia-induced PAH (38) (Figure 1).

2.3 Pyroptosis

PCD encompasses various forms of cell death, namely, apoptosis, autophagy, and pyroptosis, which are regulated by unique host proteins. In contrast to apoptosis, pyroptosis is a necrotic and inflammatory programmed cell death induced by inflammasome-associated caspases, such as caspase 1, caspase 4, caspase 5, and caspase 11 (mouse), whereas some apoptotic caspases, such as caspase 3 and caspase 8, also play a role in the occurrence of pyroptosis (39). Pyroptosis can be initiated through two main pathways: the typical inflammasome activation pathway (caspase 1-dependent pathway) and the atypical inflammasome activation pathway (caspase 1-independent pathway) (Figure 1). Traditionally, apoptosis-related caspases, such as caspase 3 and caspase 8, were not associated with pyroptosis. However, recent studies have unveiled that caspase 3 can catalyze the cleavage of GSDME, leading to the production of N-GSDME termini and consequent pyroptosis in tumor cells. In addition, caspase 8 has been found to promote the cleavage of GSDMD in mouse macrophages, which further enhances our comprehension of pyroptosis (40).

Pyroptosis may act as a crucial part of the pathogenesis of hypoxia-induced PAH, thus offering insights into potential therapeutic strategies. In the study of Wu et al., caspase 4/11 plays a key role in regulating pulmonary vascular dysfunction and accelerating the progression of PAH (41). Studies from Hu et al. demonstrated disulfiram (DSF) attenuated vascular remodeling and hypoxia-induced PAH by inhibiting GSDMD cleavage and pyroptosis in human pulmonary artery smooth muscle cells (hPASMCs) (42). Additionally, Zhang et al. found that signal transducer and activator of transcription 1 (STAT1) promoted programmed death-ligand 1 (PD-L1) upregulation and activation of caspase 1-dependent pyroptosis, thereby accelerating the progression of PAH (43). Along similar lines, He et al. identified that GLI1 affected the progression of PAH by promoting PASMC pyroptosis through the apoptosis-associated speck-like protein containing a caspase recruitment domain (ASC) pathway (44). Furthermore, a separate study revealed that G-protein coupled receptor 146 (GPR146) induced PAEC pyroptosis through the NLRP3/caspase 1 signaling axis, resulting in the promotion of endothelial injury and PAH progression (45). Wu et al. also demonstrated that KIF23 regulated the expression of caspase 3, NLRP3, and HMGB1 by inhibiting the pyroptosis and proliferation of PASMCs (46) (Figure 1).

2.4 Ferroptosis

Ferroptosis is an intracellular iron-dependent form of cell death that is distinct from apoptosis, autophagy, and pyroptosis. The characteristic morphological features of ferroptosis are mitochondrial changes, including reduction or disappearance of mitochondrial cristae, rupture of the mitochondrial outer membrane, and concentration of mitochondrial membrane (47). The process of ferroptosis is closely related to the System Xc-/GPX4 signaling pathway, iron homeostasis, and lipid oxidative metabolism (48).

Accumulating evidence supports the hypothesis that ferroptosis is involved in the progression of lung diseases. However, only a few studies have investigated the role of ferroptosis in PAH. In a recent systematic investigation conducted by Zhang et al., they revealed a substantial upregulation in the expression of all ferroptosis-associated genes in individuals with PAH. In addition, all 10 ferroptosis-associated genes exhibited positively correlated expression patterns, suggesting that PAH initiated ferroptosis (49). Another study discovered that peroxiredoxin 6 (PRDX6) facilitates ferroptosis in PAECs and instigates pulmonary vascular remodeling. This process is mediated by the release of HMGB1 and subsequent activation of the TLR4/NLRP3 pathway, thereby leading to the pathogenesis of PAH (50). Xie et al. indicated that PAEC ferroptosis stimulates the NLRP3 inflammatory response *via* the HMGB1/TLR4 pathway and participated in the progression of PAH (51). However, Hu et al. demonstrated that SLC7A11 inhibits ferroptosis and promoted proliferation in PAH, thus restoring the balance between cell death and proliferation in PASMCs (52). In fact, further studies on the role of ferroptosis in PAH are still required (Figure 1).

3 Epigenetic regulation in programmed cell death in PAH

3.1 RNA methylation

3.1.1 Overview of RNA methylation

Epigenetics is the study that modulates heritable gene expression without DNA sequence changes, including DNA and RNA methylation, histone modification, and non-coding RNA regulation (53). m^6A methylation is the most prevalent epigenetic modification of RNA nucleotides. Moreover, m^6A methylation modification plays a crucial role in governing the process of RNA splicing, gene expression, transcription, translation, and nuclear export. The modification of m^6A is reversible and mediated by "writers", "erasers", and "readers" (54).

The m^6A process is mainly catalyzed by the m^6A methyltransferase complex, including methyltransferase like 3 (METTL3), METTL14, Wilms' tumor 1-associated protein (WTAP), RNA-binding motif protein 15 (RBM15), zinc finger CCCH-type containing 13 (ZC3H13), and KIAA1429 (55). The demethylases act as erasers in RNA molecules to remove the m^6A modifications. RNA demethylases mainly consist of fat mass and obesity-associated protein (FTO) and alpha-ketoglutarate-dependent homolog 5 (ALKBH5). Reader proteins play a crucial role in recognizing m^6A binding sites and interacting with them, each performing specific m^6A-dependent biological functions (56). The m^6A reader proteins containing the YTH domain include YTHDF1-3 and YTHDC1-2. YTHDF1 promotes mRNA

translation initiation, while YTHDF2 promotes mRNA degradation. YTHDF3 interacts with YTHDF1 to promote mRNA translation or with YTHDF2 to enhance mRNA degradation. Furthermore, YTHDC1 facilitates pre-mRNA splicing and nuclear export of mRNA. YTHDC2, however, enhances the translation efficiency of target mRNA (57). Another kind of reader protein, IGF2BP1-3, promotes mRNA stability and translation in an m^{6}A-dependent manner. In addition, the eukaryotic initiation factor 3 (eIF3) promotes mRNA translation (58). Moreover, the nuclear m^{6}A reader HNRNPA2B1 is involved in promoting miRNA processing and mRNA splicing (59) (Figure 2).

3.1.2 RNA methylation in programmed cell death in PAH

In the latest systematic study, the m^{6}A methyltransferase METTL3 has been identified as a strong proponent of PAH development (60). Conversely, Xu et al. demonstrated that sustained low expression of METTL3 impacts the m^{6}A level of PAH-related genes, consequently facilitating PAH development (61). Meanwhile, the m^{6}A reading protein YTHDF1 promotes PAH by contributing to MAGED1 translation in an m^{6}A-dependent manner (62). Additionally, another investigation discovered that YTHDF1 recognizes and promotes Forkhead box M1 (Foxm1) protein translation efficiency, thereby enhancing the hypoxic PAH (63). Emerging evidence supports that m^{6}A is associated with PAH pathology; however, the effects of m^{6}A on PCD in PAH have been scarcely reported. Accumulating evidence suggests that hypoxic signaling plays a fundamental and pivotal role in the pathogenesis of PAH (64). Supporting this notion, it has been observed that the upregulation of FTO effectively suppresses hypoxia/reoxygenation (H/R)-treated cardiomyocyte apoptosis (65, 66). In line with this notion, the expression of m^{6}A reader YTHDF1 is significantly correlated with hypoxia-induced autophagy in patients with hepatocellular carcinoma (HCC) (67). Similarly, Lin et al. revealed a connection between METTL3-mediated m^{6}A modification, sorafenib resistance, and autophagy in HCC under hypoxic conditions (68). Furthermore, separate investigations have demonstrated that hypoxia leads to the suppression of METTL14, resulting in enhanced SLC7A11 mRNA degradation in an m^{6}A-dependent manner, which may serve as a potential therapeutic target for the ferroptosis of hepatocellular carcinoma (69). In the meanwhile, Yang et al. found that hypoxia induces long non-coding RNA (lncRNA)–CBSLR to recruit YTHDF2 protein and destabilizes CBS, and mRNA destabilizes through m^{6}A-YTHDF2-dependent modulation. This process ultimately contributes to ferroptosis resistance in gastric cancer (70). Based on the diverse regulatory roles of m^{6}A in hypoxic diseases, it is plausible that the m^{6}A epigenetic modifications regulate signaling pathways and targets associated with programmed cell death, thereby contributing to the occurrence of PAH. Consistent with the above reports, YTHDC1-mediated m^{6}A modification induces lncRNA FENDRR degradation, which subsequently promotes hypoxia-induced PAH by regulating DNA methylation of the promoter region of dynamin-related protein 1 (DRP1) (71).

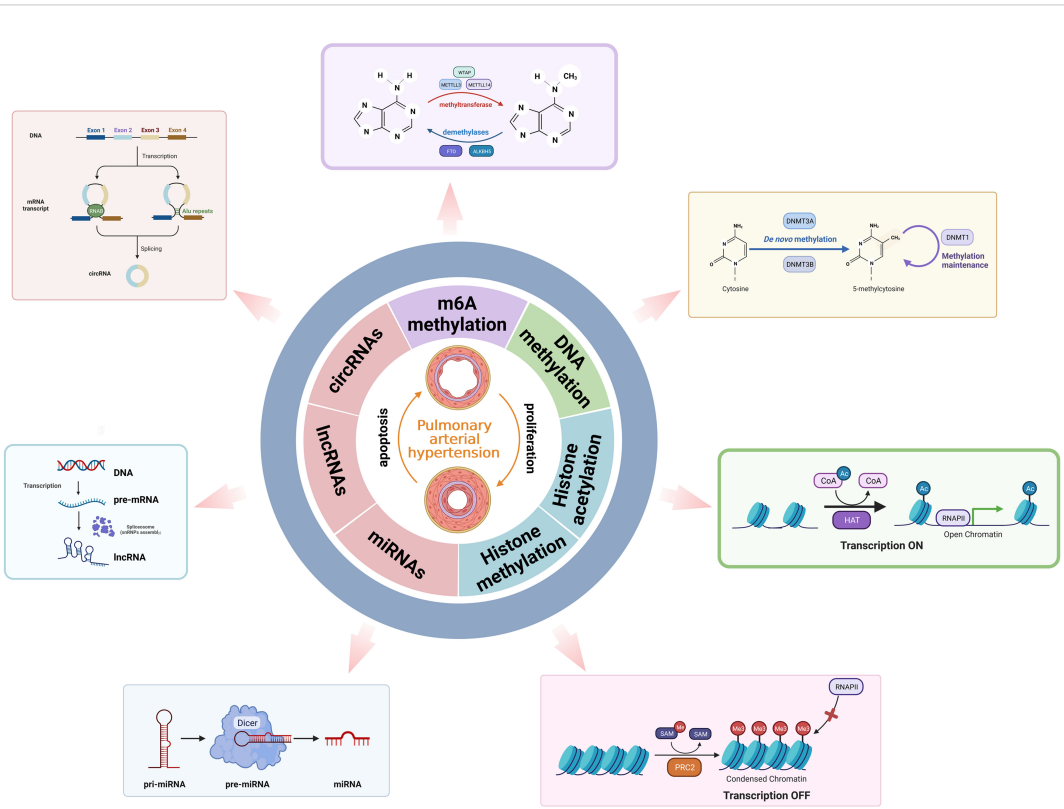

FIGURE 2
An overview of epigenetic remodeling.

3.2 DNA methylation

3.2.1 Overview of DNA methylation

DNA methylation is one of the major epigenetic modifications in cells, which is based on the transfer of a methyl group (CH_3^-) from an *S*-adenosylmethionine donor to the C-5 position of a cytosine ring of DNA to form 5-methylcytosine (5-mC) (72). DNA methylation is catalyzed by three DNA methyltransferases (DNMTs): DNMT1, DNMT3A, and DNMT3B (73). Of these, DNMT1 is able to copy CpG methylation patterns and add to the newly synthesized DNA strand, which plays a role in maintaining DNA methylation status during DNA replication. Conversely, DNMT3A and DNMT3B are categorized as *de novo* methyltransferases that reversibly methylate the unmethylated CpG dinucleotides and set the initial pattern of the methyl groups on the DNA sequence (74). DNMT3-like protein, also known as DNMT3-L, is the third member of the DNMT3 family, which can increase the DNA methylation of the whole genome by activating DNMT3A and DNMT3B, thereby affecting the transcription expression of related downstream genes (75). The DNA demethylation process is performed by TET family enzymes (TET1, TET2, and TET3), which oxidize 5-methylcytosines to 5-hydroxymethylcytosines and reverse the modification (76) (Figure 2).

3.2.2 DNA methylation in programmed cell death in PAH

Several studies have investigated that DNA methylation is associated with the vascular pathology of PAH. Specifically, studies have shown that 5-Aza-2′-deoxycytidine (5-Aza-dC), a DNA methyltransferase inhibitor, attenuates hypoxic PAH *via* demethylation of the PTEN promoter (77). Along this line, DNMT3B has been confirmed to be upregulated in both PAH patients and rat models. Overexpressing of DNMT3B in PASMCs has been shown to ameliorate hypoxia-mediated PAH (78). While the function of DNA methylation in PAH is well characterized, its understanding of the function in programmed cell death and the underlying functional machinery in PAH remain unexplored. Dysregulation of oxygen-sensing mechanisms is a common feature of both PAH and cancer, especially apoptosis resistance. Many of these abnormalities are regulated by epigenetic modifications (79). Therefore, we hypothesize that the DNA methylation mechanism in programmed cell death in PAH under hypoxic conditions may be similar to that in cancer. Supporting this hypothesis, Mamo et al. demonstrated that the demethylation of intron 18 of epidermal growth factor receptor (EGFR) restored the hypoxic regulation of EGFR, leading to apoptosis resistance and migration (80). In the study of Feng et al., it was found that hypermethylated gene ankyrin repeat and death domain-containing 1A (ANKDD1A) is a tumor suppressor in glioblastoma multiforme (GBM). The recovery of ANKDD1A expression results in reduced transactivation function and stability of HIF1α to inhibit autophagy and induce apoptosis in the hypoxic microenvironment (81). Recent research indicates that DNA methylation modifier lymphoid-specific helicase (LSH) interacts with WDR76 to impede ferroptosis. However, EGLN1 and c-Myc directly activate the expression of LSH by inhibiting HIF-1α (82). Due to the regulatory role in tumors, DNA methylation may regulate targets associated with programmed cell death in PAH. Indeed, DNA methylation in the promoter region of BMPR2 induces PAH by regulating BMP signaling pathways and increasing cell apoptosis (83). It is worth noting that more investigations are required to ascertain the involvement of DNA methylation in the processes of ferroptosis, autophagy, and pyroptosis in PAH.

3.3 Histone modification

3.3.1 Overview of histone modification

In eukaryotic cells, the nucleosome is the basic unit of chromatin, which is comprised of a histone octamer with one H2A–H2B tetramer and two H3–H4 dimers surrounded by 146–147 base pairs of double helix DNA (84). The N-terminal and C-terminal tails of histone can be modified for post-translational modification catalyzed by enzymes, directly affecting chromatin status and gene expression. Histone modification includes histone acetylation, histone methylation, and other modifications such as histone phosphorylation and histone ubiquitination (85). Acetylation of lysine residues reduces the positive charge, hindering the interaction between histone tails and negatively charged DNA. Consequently, chromatin structure is relaxed, enabling exposure of underlying DNA and facilitating transcriptional activation (86). Histone acetylation at lysine residues is catalyzed by histone acetyltransferases (HATs) to induce transcriptional activation. Histone deacetylation is regulated by histone deacetylases (HDACs), leading to transcriptional inhibition (87). Histone methylation is an extensively researched post-translational modification of histones. Histone methylation usually occurs at the arginine, lysine, and histidine residues of histone H1, H2A, H2B, H3, and H4 by adding methyl groups. The arginine residue methylation can be mono-(me) and di-(me2) methylated, while lysine residues can be mono-(me), di-(me2), and tri-(me3) methylated (88). The process of histone methylation is catalyzed by the histone methyltransferase (HMT), which transfers methyl groups to lysine, arginine, or histidine residues of histones by using *S*-adenosine methionine (SAM). Additionally, most histone modifications are reversible. Methyl groups are removed from lysine, arginine, or histidine residues by histone demethylases (HDMs) (89). Lysine-specific demethylase 1 (LSD1) is the first demethylase to remove the methylation at H3K4 and H3K9. Histone phosphorylation occurs on residues of serine, threonine, and tyrosine. Histone phosphorylation and histone dephosphorylation are regulated by protein kinase (PK) and protein phosphatase (PP) in a state of homeostasis (90). The methylation sites H3K9 and H3K27 share the same serine residue and can be phosphorylated. Based on the different histones and modification sites, histone phosphorylation is associated with chromosome condensation, gene transcription, and the DNA damage repair process. Furthermore, other modifications such as histone ubiquitination and histone ADP-ribosylation regulate gene transcription in various directions (91) (Figure 2).

3.3.2 Histone modification in programmed cell death in PAH

Recently, an expanding body of evidence has highlighted that histone modification is a promising strategy for the treatment of PAH. In a systematic study, Qi et al. reveal a pivotal role of the

histone modifier SUV4-20H1. Inactivation of Suv4-20h1 increased expression of the secreted superoxide dismutase 3 (Sod3), resulting in an imbalance of reactive oxygen species (ROS) in the alveolar and pulmonary vascular ventricles, ultimately leading to PAH (92). Bisserier et al. found that SIN3a regulates BMPR2 expression and pulmonary vascular remodeling by a dual mechanism. On the one hand, SIN3a inhibits EZH2 expression and decreases the levels of H3K27me3 in the promoter region of BMPR2. On the other hand, the methylation level of the BMPR2 promoter is decreased by upregulating TET1 and inhibiting DNMT1 activity (93). However, it remains unclear whether histone modification regulates PAH by targeting PCD. Shedding light on this aspect, studies have demonstrated that the acetylation of vestigial-like family member 4 (VGLL4) inhibits PASMC apoptosis and pulmonary arterial remodeling through signal transducer and activator of transcription 3 (STAT3) signaling (94). Moreover, RVX208, a clinically available BET inhibitor, has the potential to modulate anti-apoptotic and proinflammatory pathways through interactions with FoxM1 and PLK1. This discovery supports the establishment of a clinical trial of RVX208 in patients with PAH (95). Another study has revealed the detrimental effects of HDAC inhibitor trichostatin A (TSA) on RV remodeling under pressure overload may be achieved through antiangiogenic or proapoptotic effects (96). Based on these findings, histone modification is significant in PASMC apoptosis during the PAH process; however, knowledge of the contribution of histone modification in regulating other types of PCD in PAH remains fairly limited so far.

3.4 Non-coding RNA molecules

Non-coding RNAs (ncRNAs) can be divided into two types based on their length: small ncRNAs (sncRNAs), which consist of fewer than 200 nucleotides, including microRNAs (miRNAs), and lncRNAs, which are longer than 200 nucleotides (97). The three major types of ncRNAs (miRNAs, lncRNAs, and circRNAs) are involved in the disease onset and progression of PAH (Figure 2).

3.4.1 MicroRNAs

MiRNAs are the most extensively studied endogenous RNAs of approximately 22 nucleotides (98). The biological functions of miRNAs depend on complementary targeting to the 3′-untranslated region (UTR) of mRNAs and then negatively regulate the expression of target genes at the post-transcriptional level (99). In a study conducted by Russomanno et al., miR-150 was shown to reduce the expression of inflammation-, apoptosis-, and fibrosis-related genes in the pathology of PAH and enhance mitochondrial metabolic potential *via* increased expression of PTEN-like mitochondrial phosphatase (PTPMT1) (100). Chen et al. found that MiD expression is epigenetically upregulated by the decreased levels of miR-34a-3p. This upregulation promoted mitotic fission, leading to pathological proliferation and resistance to apoptosis (101). In the prospective study, the secretion of miR-195-5p by anti-apoptotic endothelial cells was found to promote the proliferation and migration of PASMCs in PAH (102). Furthermore, miR-244-5p promotes apoptosis of PASMCs under hypoxia *via* DEGS1/PI3K/Akt signaling pathway (103). In addition, miR-15a-5p was shown to induce PASMC apoptosis in an animal model of PAH through the vascular endothelial growth factor (VEGF)/p38/MMP-2 signaling pathway (104). The modulation of the miR-143/145 cluster in PASMCs, as demonstrated by Deng et al., significantly altered cell migration and apoptosis (105). MiR-760, a microRNA, plays a regulatory role in hypoxia-induced hPASMC proliferation, migration, and apoptosis by targeting toll-like receptor 4 (TLR4) (106). In the study of Cai et al., miR-125a-5p ameliorates PAHs by directly targeting STAT3 to regulate PASMC proliferation and apoptosis and has a negative feedback regulation with TGF-β1 and IL-6 (107). Zhu et al. indicated that miR−371b−5p inhibits endothelial cell apoptosis in PAH *via* PTEN/PI3K/Akt signaling pathways (108). Another study further found the MFF-SIRT1/3 axis, regulated by miR-340-5p, improved mitochondrial homeostasis and proliferation–apoptosis imbalance of hypoxia-treated PAMSCs (109). Moreover, miR-874-5p was found to regulate autophagy and proliferation in PASMCs by targeting Sirtuin3 (110). In addition, miR-204 was shown to attenuate endothelial–mesenchymal transition by enhancing autophagy in hypoxia-induced PAH (111). Ou et al. reported that miR-let−7d alleviates PAH by inhibiting the autophagy of PAECs and suppressing endothelin synthesis through negative regulation of autophagy−related 16−like 1 (ATG16L1) (112). In conclusion, numerous studies have provided clear demonstrations of miRNAs with programmed cell death in hypoxia-induced PAH; however, other ncRNAs still need to be further studied in the same manner.

3.4.2 Long non-coding RNAs

LncRNAs are a class of ncRNAs greater than 200 bp in length, with low expression levels and wide tissue specificity. LncRNAs have a complex regulatory mechanism in the nucleus and cytoplasm by directly binding to DNA, RNA, and proteins to regulate gene expression (113). Recently, several studies have investigated the impact of lncRNAs on the pathogenesis of PAH. For instance, one study showed that silencing of lncRNA SOX2-OT attenuates hypoxia-induced hPASMC proliferation, migration, anti-apoptosis, and inflammation by modulating the miR-455-3p/SUMO1 axis (114). In the meanwhile, Li et al. identified that lncRNA HOXA-AS3 suppresses hPASMC apoptosis *via* regulation of miR-675-3p/PDE5 axis (115). Additionally, overexpression of lncRNA Ang362 decreases apoptosis of hPASMCs by regulating miR-221 and miR-222 (116). Notably, studies have indicated that lncRNA TCONS_00034812 regulates PASMC proliferation and apoptosis and participates in vascular remodeling during PAH (117). Furthermore, lncRNA PVT1 was found to promote the mRNA and protein expression of serum response factor (Srf) and CTGF by suppressing miR-26b and miR-186, leading to deregulation of autophagy and abnormal proliferation of PASMCs (118). Another study reported that the lncRNA−GAS5/miR−382−3p axis inhibits pulmonary artery remodeling and promoted autophagy in PAH (119). Along this line, studies by Li et al. pointed to lnc-Rps4l inhibiting hypoxia-

induced PASMC pyroptosis through the encoded peptide RPS4XL (120).

3.4.3 Circular RNAs

Circular RNAs are a unique class of lncRNAs that are directly produced by back-spliced exons and introns, thus establishing a covalent closed-loop structure. Circular RNAs regulate gene expression through transcriptional or post-transcriptional mechanisms, such as regulating miRNA target genes, regulating RBP-dependent functions, recruiting proteins, and even producing unique peptides (121). Due to the functional diversity of circRNAs, several articles have reported that circRNAs regulate signaling pathways and targets relevant to PAH. For instance, data from Jiang et al. found that circ-Calm4 functions as a competitive endogenous RNA to regulate the expression of miR-124-3p and exacerbate hypoxia-induced PASMC pyroptosis (122). Concordant with this scenario, circ-Calm4 was also confirmed to regulate hypoxia-induced PASMC autophagy by binding Purb (123). Similarly, circ-Sirtuin1 has been shown to mitigate PAH by improving PASMC proliferation, migration, and autophagy by targeting miR-145-5p/protein kinase-B3 axis under hypoxic environments (124). Interestingly, Jin et al. analyzed circRNA profiles in whole-blood samples and found that circ-NFXL1_009 attenuates hypoxia-induced proliferation, apoptotic resistance, and migration of PASMCs (125). Furthermore, circ_0016070 has been implicated in reducing hypoxia-induced apoptosis in PAHs by interacting with miR-340-5p/TCF4/β-catenin/TWIST1 signaling pathway (126). Collectively, the prevailing mechanism of action for most circRNAs in PAH involves functioning as miRNA sponges. However, the other roles and molecular mechanisms of circRNAs have not been fully elucidated (Table 1).

4 Conclusion and prospects

PAH is a complex progressive disease, which involves multiple cellular processes. The hyperproliferation and anti-apoptosis of

TABLE 1 NcRNAs and their function in hypoxia-induced PAH.

NcRNAs	Expression	Functional role (PCD)	Molecular targets	References
miR-150	Down	Apoptosis	PTPMT1	100
miR-34a-3p	Down	Apoptosis	MiD	101
miR-195-5p	Up	Apoptosis	Smad7	102
miR-244-5p	Up	Apoptosis	DEGS1	103
miR-15a-5p	Up	Apoptosis	VEGF/p38/MMP−2	104
miR-143/145	Up	Apoptosis	–	105
miR-760	Down	Apoptosis	TLR4	106
miR-125a-5p	Down	Apoptosis	STAT3	107
miR−371b−5p	Down	Apoptosis	PTEN/pI3K/Akt	108
miR-340-5p	Down	Apoptosis	IL-1β and IL-6	109
miR-874-5p	Up	Autophagy	Sirt 3	110
miR-204	Down	Autophagy	ATG7	111
miR-let−7d	Down	Autophagy	ATG16L1	112
LncRNA SOX2-OT	Up	Apoptosis	miR-455-3p	114
LncRNA HOXA-AS3	Up	Apoptosis	miR−675−3p	115
LncRNA Ang362	Up	Apoptosis	miR-221/miR-222	116
LncRNA TCONS_00034812	Down	Apoptosis	Stox1	117
LncRNA PVT1	Up	Autophagy	miR-26b/miR-186	118
LncRNA GAS5	Down	Autophagy	miR−382−3p	119
LncRNA Rps4l	Up	Pyroptosis	ILF3	120
Circ-Calm4	Up	Pyroptosis	miR-124-3p	122
Circ-Calm4	Up	Autophagy	Purb	123
Circ-SIRT1	Up	Autophagy	miR-145-5p	124
Circ-NFXL1_009	Down	Apoptosis	hsa-miR-29b-2-5p	125
Circ-0016070	Up	Autophagy	miR-340-5p	125

ncRNAs, non-coding RNAs; PAH, pulmonary arterial hypertension; PCD, programmed cell death; VEGF, vascular endothelial growth factor.

PASMCs are the basic pathophysiological processes of PAH. Based on the studies presented in our review, other forms of programmed cell death, such as autophagy, pyroptosis, and ferroptosis, have been shown to be involved in the development of PAH. Therefore, a better understanding of the processes and mechanisms of programmed cell death involved in PAH will provide novel therapeutic strategies. Research studies have found that epigenetic modification plays a crucial role in the pathological process of PAH; therefore, exploring the epigenetic modification of PAH may be a new treatment strategy (127). Epigenetic modifications are involved in programmed cell death processes at different levels. Multiple lines of evidence indicate that epigenetic alterations, including regulation mediated by ncRNAs, play a significant role in apoptosis, autophagy, and pyroptosis in PAH (128). Although current evidence provides epigenetic modifications that regulate signaling pathways associated with programmed cell death, a significant proportion of research studies have focused on ncRNAs. Other epigenetic modifications such as methylation and acetylation as well as phosphorylation should be further studied, as they may be important contributors to the pathogenesis of PAH. In particular, there is substantial evidence that HDAC inhibitors may be effective anti-cancer agents, especially when used in combination with conventional chemotherapy drugs. As such, regulating these HDACs may also have therapeutic potential for PAH (129). Despite this progress, the relationship between histone modification and programmed cell death in hypoxia-induced PAH remains largely unexplored. Furthermore, DNA methylation has been associated with gene silencing and has been shown to regulate apoptosis in the pathogenesis of PAH (11). However, our current understanding of this intricate process is still very limited. In addition, direct evidence on other DNA methylation-mediated types of programmed cell death in PAH remains lacking. Therefore, more studies are still needed to reveal the complex mechanisms of connecting epigenetic modification factors and different modes of programmed cell death during hypoxia-induced PAH.

Author contributions

YJ, SS, and JXL designed and wrote the manuscript. XG and JYL collected documents. CY, QF, and BZ revised and edited the manuscript. All authors read and approved the final version of the manuscript.

Funding

This work was supported by the National Natural Science Foundation of China (contract grant nos. 82000226 and 81700056), Innovation Foundation of Harbin Medical University (No. 31041220054), and Research Founding of post-doctor who came to Shenzhen (grant no. 20211063010052).

Conflict of interest

Author LZ was employed by company Shanghai Baoxing Biological Equipment Engineering Co., Ltd. Author LL was employed by companies Shenzhen Reyson Biotechnology Co., Ltd. and Nanjing Evertop Electronics Ltd.

The remaining authors declare that the research was conducted in the absence of any commercial or financial relationships that could be construed as a potential conflict of interest.

Publisher's note

References

1. Naeije R, Richter MJ, Rubin LJ. The physiological basis of pulmonary arterial hypertension. *Eur Respir J* (2022) 59(6):2102334. doi: 10.1183/13993003.02334-2021

2. Hassoun PM. Pulmonary arterial hypertension. *N Engl J Med* (2021) 385 (25):2361–76. doi: 10.1056/NEJMra2000348

3. Ruopp NF, Cockrill BA. Diagnosis and treatment of pulmonary arterial hypertension: A review. *Jama* (2022) 327(14):1379–91. doi: 10.1001/jama.2022.4402

4. Huston JH, Shah SJ. Understanding the pathobiology of pulmonary hypertension due to left heart disease. *Circ Res* (2022) 130(9):1382–403. doi: 10.1161/circresaha.122.319967

5. Kesavardhana S, Malireddi RKS, Kanneganti TD. Caspases in cell death, inflammation, and pyroptosis. *Annu Rev Immunol* (2020) 38:567–95. doi: 10.1146/annurev-immunol-073119-095439

6. Bertheloot D, Latz E, Franklin BS. Necroptosis, pyroptosis and apoptosis: an intricate game of cell death. *Cell Mol Immunol* (2021) 18(5):1106–21. doi: 10.1038/s41423-020-00630-3

7. Nakamura M, Sadoshima J. Mechanisms of physiological and pathological cardiac hypertrophy. *Nat Rev Cardiol* (2018) 15(7):387–407. doi: 10.1038/s41569-018-0007-y

8. Shao J, Liu J, Zuo S. Roles of epigenetics in cardiac fibroblast activation and fibrosis. *Cells* (2022) 11(15):2347. doi: 10.3390/cells11152347

9. Zhao LY, Song J, Liu Y, Song CX, Yi C. Mapping the epigenetic modifications of DNA and RNA. *Protein Cell* (2020) 11(11):792–808. doi: 10.1007/s13238-020-00733-7

10. Zhang L, Lu Q, Chang C. Epigenetics in health and disease. *Adv Exp Med Biol* (2020) 1253:3–55. doi: 10.1007/978-981-15-3449-2_1

11. Thenappan T, Ormiston ML, Ryan JJ, Archer SL. Pulmonary arterial hypertension: pathogenesis and clinical management. *Bmj* (2018) 360:j5492. doi: 10.1136/bmj.j5492

12. Evans CE, Cober ND, Dai Z, Stewart DJ, Zhao YY. Endothelial cells in the pathogenesis of pulmonary arterial hypertension. *Eur Respir J* (2021) 58(3):2003957. doi: 10.1183/13993003.03957-2020

13. Racanelli AC, Kikkers SA, Choi AMK, Cloonan SM. Autophagy and inflammation in chronic respiratory disease. *Autophagy* (2018) 14(2):221–32. doi: 10.1080/15548627.2017.1389823

14. Foley A, Steinberg BE, Goldenberg NM. Inflammasome activation in pulmonary arterial hypertension. *Front Med (Lausanne)* (2021) 8:826557. doi: 10.3389/fmed.2021.826557

15. Ketelut-Carneiro N, Fitzgerald KA. Apoptosis, pyroptosis, and necroptosis-oh my! The many ways a cell can die. *J Mol Biol* (2022) 434(4):167378. doi: 10.1016/j.jmb.2021.167378

16. D'Arcy MS. Cell death: a review of the major forms of apoptosis, necrosis and autophagy. *Cell Biol Int* (2019) 43(6):582–92. doi: 10.1002/cbin.11137

17. Lin X, Ouyang S, Zhi C, Li P, Tan X, Ma W, et al. Focus on ferroptosis, pyroptosis, apoptosis and autophagy of vascular endothelial cells to the strategic targets for the treatment of atherosclerosis. *Arch Biochem Biophys* (2022) 715:109098. doi: 10.1016/j.abb.2021.109098

18. Galluzzi L, Vitale I, Aaronson SA, Abrams JM, Adam D, Agostinis P, et al. Molecular mechanisms of cell death: recommendations of the Nomenclature Committee on Cell Death 2018. *Cell Death Differ* (2018) 25(3):486–541. doi: 10.1038/s41418-017-0012-4

19. Kocken JMM, da Costa Martins PA. Epigenetic regulation of pulmonary arterial hypertension-induced vascular and right ventricular remodeling: new opportunities? *Int J Mol Sci* (2020) 21(23):8901. doi: 10.3390/ijms21238901

20. Chowdhury HM, Sharmin N, Yuzbasioglu Baran M, Long L, Morrell NW, Trembath RC, et al. BMPRII deficiency impairs apoptosis *via* the BMPRII-ALK1-BclX-mediated pathway in pulmonary arterial hypertension. *Hum Mol Genet* (2019) 28 (13):2161–73. doi: 10.1093/hmg/ddz047

21. Wang XJ, Lian TY, Jiang X, Liu SF, Li SQ, Jiang R, et al. Germline BMP9 mutation causes idiopathic pulmonary arterial hypertension. *Eur Respir J* (2019) 53 (3):1801609. doi: 10.1183/13993003.01609-2018

22. Cao YY, Ba HX, Li Y, Tang SY, Luo ZQ, Li XH. Regulatory effects of Prohibitin 1 on proliferation and apoptosis of pulmonary arterial smooth muscle cells in monocrotaline-induced PAH rats. *Life Sci* (2020) 250:117548. doi: 10.1016/j.lfs.2020.117548

23. Jiang DT, Tuo L, Bai X, Bing WD, Qu QX, Zhao X, et al. Prostaglandin E1 reduces apoptosis and improves the homing of mesenchymal stem cells in pulmonary arterial hypertension by regulating hypoxia-inducible factor 1 alpha. *Stem Cell Res Ther* (2022) 13(1):316. doi: 10.1186/s13287-022-03011-x

24. He T, Zhang J, Qiao T, Zhang Z, Han H, Yang C, et al. Compensatory roles of Protein Related to DAN and Cerberus (PRDC) decrease in pulmonary arterial hypertension. *Int J Biol Sci* (2022) 18(6):2372–91. doi: 10.7150/ijbs.70247

25. Novoyatleva T, Rai N, Kojonazarov B, Veeroju S, Ben-Batalla I, Caruso P, et al. Deficiency of Axl aggravates pulmonary arterial hypertension *via* BMPR2. *Commun Biol* (2021) 4(1):1002. doi: 10.1038/s42003-021-02531-1

26. Ruffenach G, Medzikovic L, Aryan L, Li M, Eghbali M. HNRNPA2B1: RNA-binding protein that orchestrates smooth muscle cell phenotype in pulmonary arterial hypertension. *Circulation* (2022) 146(16):1243–58. doi: 10.1161/circulationaha.122.059591

27. Levy JMM, Towers CG, Thorburn A. Targeting autophagy in cancer. *Nat Rev Cancer* (2017) 17(9):528–42. doi: 10.1038/nrc.2017.53

28. Wu X, Liu Z, Yu XY, Xu S, Luo J. Autophagy and cardiac diseases: Therapeutic potential of natural products. *Med Res Rev* (2021) 41(1):314–41. doi: 10.1002/med.21733

29. Sciarretta S, Maejima Y, Zablocki D, Sadoshima J. The role of autophagy in the heart. *Annu Rev Physiol* (2018) 80:1–26. doi: 10.1146/annurev-physiol-021317-121427

30. Zhai C, Shi W, Feng W, Zhu Y, Wang J, Li S, et al. Activation of AMPK prevents monocrotaline-induced pulmonary arterial hypertension by suppression of NF-κB-mediated autophagy activation. *Life Sci* (2018) 208:87–95. doi: 10.1016/j.lfs.2018.07.018

31. Chang S, Wu J, Jin J, Shi H, Gao R, Li X, et al. Aldehyde Dehydrogenase 2 (ALDH2) Elicits Protection against Pulmonary Hypertension *via* Inhibition of ERK1/2-Mediated Autophagy. *Oxid Med Cell Longev* (2022) 2022:2555476. doi: 10.1155/2022/2555476

32. Ning H, Deng J, Chen F, Liu Y, Kong D, Shan L, et al. β-arrestin1 inhibits hypoxic injury-induced autophagy in human pulmonary artery endothelial cells *via* the Akt/mTOR signaling pathway. *Int J Biochem Cell Biol* (2020) 125:105791. doi: 10.1016/j.biocel.2020.105791

33. Gomez-Puerto MC, van Zuijen I, Huang CJ, Szulcek R, Pan X, van Dinther MA, et al. Autophagy contributes to BMP type 2 receptor degradation and development of pulmonary arterial hypertension. *J Pathol* (2019) 249(3):356–67. doi: 10.1002/path.5322

34. Feng W, Wang J, Yan X, Zhang Q, Chai L, Wang Q, et al. ERK/Drp1-dependent mitochondrial fission contributes to HMGB1-induced autophagy in pulmonary arterial hypertension. *Cell Prolif* (2021) 54(6):e13048. doi: 10.1111/cpr.13048

35. Jin T, Lu J, Lv Q, Gong Y, Feng Z, Ying H, et al. Farnesyl diphosphate synthase regulated endothelial proliferation and autophagy during rat pulmonary arterial hypertension induced by monocrotaline. *Mol Med* (2022) 28(1):94. doi: 10.1186/s10020-022-00511-7

36. Wu YC, Wang WT, Lee SS, Kuo YR, Wang YC, Yen SJ, et al. Glucagon-like peptide-1 receptor agonist attenuates autophagy to ameliorate pulmonary arterial hypertension through drp1/NOX- and atg-5/atg-7/beclin-1/LC3β Pathways. *Int J Mol Sci* (2019) 20(14):3435. doi: 10.3390/ijms20143435

37. He Y, Cao X, Guo P, Li X, Shang H, Liu J, et al. Quercetin induces autophagy *via* FOXO1-dependent pathways and autophagy suppression enhances quercetin-induced apoptosis in PASMCs in hypoxia. *Free Radic Biol Med* (2017) 103:165–76. doi: 10.1016/j.freeradbiomed.2016.12.016

38. Yamanaka R, Hoshino A, Fukai K, Urata R, Minami Y, Honda S, et al. TIGAR reduces smooth muscle cell autophagy to prevent pulmonary hypertension. *Am J Physiol Heart Circ Physiol* (2020) 319(5):H1087–h1096. doi: 10.1152/ajpheart.00314.2020

39. Yu P, Zhang X, Liu N, Tang L, Peng C, Chen X. Pyroptosis: mechanisms and diseases. *Signal Transduct Target Ther* (2021) 6(1):128. doi: 10.1038/s41392-021-00507-5

40. Fritsch M, Günther SD, Schwarzer R, Albert MC, Schorn F, Werthenbach JP, et al. Caspase-8 is the molecular switch for apoptosis, necroptosis and pyroptosis. *Nature* (2019) 575(7784):683–7. doi: 10.1038/s41586-019-1770-6

41. Wu Y, Pan B, Zhang Z, Li X, Leng Y, Ji Y, et al. Caspase-4/11-mediated pulmonary artery endothelial cell pyroptosis contributes to pulmonary arterial hypertension. *Hypertension* (2022) 79(3):536–48. doi: 10.1161/hypertensionaha.121.17868

42. Hu S, Wang L, Xu Y, Li F, Wang T. Disulfiram attenuates hypoxia-induced pulmonary hypertension by inhibiting GSDMD cleavage and pyroptosis in HPASMCs. *Respir Res* (2022) 23(1):353. doi: 10.1186/s12931-022-02279-0

43. Zhang M, Xin W, Yu Y, Yang X, Ma C, Zhang H, et al. Programmed death-ligand 1 triggers PASMCs pyroptosis and pulmonary vascular fibrosis in pulmonary hypertension. *J Mol Cell Cardiol* (2020) 138:23–33. doi: 10.1016/j.yjmcc.2019.10.008

44. He S, Ma C, Zhang L, Bai J, Wang X, Zheng X, et al. GLI1-mediated pulmonary artery smooth muscle cell pyroptosis contributes to hypoxia-induced pulmonary hypertension. *Am J Physiol Lung Cell Mol Physiol* (2020) 318(3):L472–l482. doi: 10.1152/ajplung.00405.2019

45. Jiang Y, Huang J, Xia Y, Sun Z, Hu P, Wang D, et al. Hypoxia activates GPR146 which participates in pulmonary vascular remodeling by promoting pyroptosis of pulmonary artery endothelial cells. *Eur J Pharmacol* (2023) 941:175502. doi: 10.1016/j.ejphar.2023.175502

46. Wu Z, Zhou G, Wang H, Yao P. Inhibition of KIF23 alleviates IPAH by targeting pyroptosis and proliferation of PASMCs. *Int J Mol Sci* (2022) 23(8):4436. doi: 10.3390/ijms23084436

47. Stockwell BR, Jiang X, Gu W. Emerging mechanisms and disease relevance of ferroptosis. *Trends Cell Biol* (2020) 30(6):478–90. doi: 10.1016/j.tcb.2020.02.009

48. Mou Y, Wang J, Wu J, He D, Zhang C, Duan C, et al. Ferroptosis, a new form of cell death: opportunities and challenges in cancer. *J Hematol Oncol* (2019) 12(1):34. doi: 10.1186/s13045-019-0720-y

49. Zhang F, Liu H. Identification of ferroptosis-associated genes exhibiting altered expression in pulmonary arterial hypertension. *Math Biosci Eng* (2021) 18(6):7619–30. doi: 10.3934/mbe.2021377

50. Liao J, Xie SS, Deng Y, Wu DD, Meng H, Lan WF, et al. PRDX6-mediated pulmonary artery endothelial cell ferroptosis contributes to monocrotaline-induced pulmonary hypertension. *Microvasc Res* (2023) 146:104471. doi: 10.1016/j.mvr.2022.104471

51. Xie SS, Deng Y, Guo SL, Li JQ, Zhou YC, Liao J, et al. Endothelial cell ferroptosis mediates monocrotaline-induced pulmonary hypertension in rats by modulating NLRP3 inflammasome activation. *Sci Rep* (2022) 12(1):3056. doi: 10.1038/s41598-022-06848-7

52. Hu P, Xu Y, Jiang Y, Huang J, Liu Y, Wang D, et al. The mechanism of the imbalance between proliferation and ferroptosis in pulmonary artery smooth muscle cells based on the activation of SLC7A11. *Eur J Pharmacol* (2022) 928:175093. doi: 10.1016/j.ejphar.2022.175093

53. Xu Z, Lv B, Qin Y, Zhang B. Emerging roles and mechanism of m6A methylation in cardiometabolic diseases. *Cells* (2022) 11(7):1101. doi: 10.3390/cells11071101

54. Jiang X, Liu B, Nie Z, Duan L, Xiong Q, Jin Z, et al. The role of m6A modification in the biological functions and diseases. *Signal Transduct Target Ther* (2021) 6(1):74. doi: 10.1038/s41392-020-00450-x

55. An Y, Duan H. The role of m6A RNA methylation in cancer metabolism. *Mol Cancer* (2022) 21(1):14. doi: 10.1186/s12943-022-01500-4

56. Sendinc E, Shi Y. RNA m6A methylation across the transcriptome. *Mol Cell* (2023) 83(3):428–41. doi: 10.1016/j.molcel.2023.01.006

57. Chen XY, Zhang J, Zhu JS. The role of m(6)A RNA methylation in human cancer. *Mol Cancer* (2019) 18(1):103. doi: 10.1186/s12943-019-1033-z

58. Lan Q, Liu PY, Bell JL, Wang JY, Hüttelmaier S, Zhang XD, et al. The emerging roles of RNA m(6)A methylation and demethylation as critical regulators of tumorigenesis, drug sensitivity, and resistance. *Cancer Res* (2021) 81(13):3431–40. doi: 10.1158/0008-5472.Can-20-4107

59. Fabbiano F, Corsi J, Gurrieri E, Trevisan C, Notarangelo M, D'Agostino VG. RNA packaging into extracellular vesicles: An orchestra of RNA-binding proteins? *J Extracell Vesicles* (2020) 10(2):e12043. doi: 10.1002/jev2.12043

60. Qin Y, Qiao Y, Li L, Luo E, Wang D, Yao Y, et al. The m(6)A methyltransferase METTL3 promotes hypoxic pulmonary arterial hypertension. *Life Sci* (2021) 274:119366. doi: 10.1016/j.lfs.2021.119366

61. Xu S, Xu X, Zhang Z, Yan L, Zhang L, Du L. The role of RNA m(6)A methylation in the regulation of postnatal hypoxia-induced pulmonary hypertension. *Respir Res* (2021) 22(1):121. doi: 10.1186/s12931-021-01728-6

62. Hu L, Wang J, Huang H, Yu Y, Ding J, Yu Y, et al. YTHDF1 regulates pulmonary hypertension through translational control of MAGED1. *Am J Respir Crit Care Med* (2021) 203(9):1158–72. doi: 10.1164/rccm.202009-3419OC

63. Kang T, Liu L, Tan F, Zhang D, Yu L, Jiang H, et al. Inhibition of YTHDF1 prevents hypoxia-induced pulmonary artery smooth muscle cell proliferation by regulating Foxm1 translation in an m6A-dependent manner. *Exp Cell Res* (2023) 424 (2):113505. doi: 10.1016/j.yexcr.2023.113505

64. Pullamsetti SS, Mamazhakypov A, Weissmann N, Seeger W, Savai R. Hypoxia-inducible factor signaling in pulmonary hypertension. *J Clin Invest* (2020) 130 (11):5638–51. doi: 10.1172/jci137558

65. Shen W, Li H, Su H, Chen K, Yan J. FTO overexpression inhibits apoptosis of hypoxia/reoxygenation-treated myocardial cells by regulating m6A modification of Mhrt. *Mol Cell Biochem* (2021) 476(5):2171–9. doi: 10.1007/s11010-021-04069-6

66. Ke WL, Huang ZW, Peng CL, Ke YP. m(6)A demethylase FTO regulates the apoptosis and inflammation of cardiomyocytes *via* YAP1 in ischemia-reperfusion injury. *Bioengineered* (2022) 13(3):5443–52. doi: 10.1080/21655979.2022.2030572

67. Li Q, Ni Y, Zhang L, Jiang R, Xu J, Yang H, et al. HIF-1α-induced expression of m6A reader YTHDF1 drives hypoxia-induced autophagy and Malignancy of hepatocellular carcinoma by promoting ATG2A and ATG14 translation. *Signal Transduct Target Ther* (2021) 6(1):76. doi: 10.1038/s41392-020-00453-8

68. Lin Z, Niu Y, Wan A, Chen D, Liang H, Chen X, et al. RNA m(6) A methylation regulates sorafenib resistance in liver cancer through FOXO3-mediated autophagy. *EMBO J* (2020) 39(12):e103181. doi: 10.15252/embj.2019103181

69. Fan Z, Yang G, Zhang W, Liu Q, Liu G, Liu P, et al. Hypoxia blocks ferroptosis of hepatocellular carcinoma *via* suppression of METTL14 triggered YTHDF2-dependent silencing of SLC7A11. *J Cell Mol Med* (2021) 25(21):10197–212. doi: 10.1111/jcmm.16957

70. Yang H, Hu Y, Weng M, Liu X, Wan P, Hu Y, et al. Hypoxia inducible lncRNA-CBSLR modulates ferroptosis through m6A-YTHDF2-dependent modulation of CBS in gastric cancer. *J Adv Res* (2022) 37:91–106. doi: 10.1016/j.jare.2021.10.001

71. Wang X, Li Q, He S, Bai J, Ma C, Zhang L, et al. LncRNA FENDRR with m6A RNA methylation regulates hypoxia-induced pulmonary artery endothelial cell pyroptosis by mediating DRP1 DNA methylation. *Mol Med* (2022) 28(1):126. doi: 10.1186/s10020-022-00551-z

72. Horvath S, Raj K. DNA methylation-based biomarkers and the epigenetic clock theory of ageing. *Nat Rev Genet* (2018) 19(6):371–84. doi: 10.1038/s41576-018-0004-3

73. Edwards JR, Yarychkivska O, Boulard M, Bestor TH. DNA methylation and DNA methyltransferases. *Epigenet Chromatin* (2017) 10:23. doi: 10.1186/s13072-017-0130-8

74. He S, Feng X. DNA methylation dynamics during germline development. *J Integr Plant Biol* (2022) 64(12):2240–51. doi: 10.1111/jipb.13422

75. Martisova A, Holcakova J, Izadi N, Sebuyoya R, Hrstka R, Bartosik M. DNA methylation in solid tumors: functions and methods of detection. *Int J Mol Sci* (2021) 22(8):4247. doi: 10.3390/ijms22084247

76. Köhler F, Rodríguez-Paredes M. DNA methylation in epidermal differentiation, aging, and cancer. *J Invest Dermatol* (2020) 140(1):38–47. doi: 10.1016/j.jid.2019.05.011

77. Xing XQ, Li B, Xu SL, Zhang CF, Liu J, Deng YS, et al. 5-Aza-2'-deoxycytidine, a DNA methylation inhibitor, attenuates hypoxic pulmonary hypertension *via* demethylation of the PTEN promoter. *Eur J Pharmacol* (2019) 855:227–34. doi: 10.1016/j.ejphar.2019.05.021

78. Yan Y, He YY, Jiang X, Wang Y, Chen JW, Zhao JH, et al. DNA methyltransferase 3B deficiency unveils a new pathological mechanism of pulmonary hypertension. *Sci Adv* (2020) 6(50):eaba2470. doi: 10.1126/sciadv.aba2470

79. Wu D, Dasgupta A, Read AD, Bentley RET, Motamed M, Chen KH, et al. Oxygen sensing, mitochondrial biology and experimental therapeutics for pulmonary hypertension and cancer. *Free Radic Biol Med* (2021) 170:150–78. doi: 10.1016/j.freeradbiomed.2020.12.452

80. Mamo M, Ye IC, DiGiacomo JW, Park JY, Downs B, Gilkes DM. Hypoxia alters the response to anti-EGFR therapy by regulating EGFR expression and downstream signaling in a DNA methylation-specific and HIF-dependent manner. *Cancer Res* (2020) 80(22):4998–5010. doi: 10.1158/0008-5472.Can-20-1232

81. Feng J, Zhang Y, She X, Sun Y, Fan L, Ren X, et al. Hypermethylated gene ANKDD1A is a candidate tumor suppressor that interacts with FIH1 and decreases HIF1α stability to inhibit cell autophagy in the glioblastoma multiforme hypoxia microenvironment. *Oncogene* (2019) 38(1):103–19. doi: 10.1038/s41388-018-0423-9

82. Jiang Y, Mao C, Yang R, Yan B, Shi Y, Liu X, et al. EGLN1/c-myc induced lymphoid-specific helicase inhibits ferroptosis through lipid metabolic gene expression changes. *Theranostics* (2017) 7(13):3293–305. doi: 10.7150/thno.19988

83. Li N, Zhu L, Zhu C, Zhou H, Zheng D, Xu G, et al. BMPR2 promoter methylation and its expression in valvular heart disease complicated with pulmonary artery hypertension. *Aging (Albany NY)* (2021) 13(22):24580–604. doi: 10.18632/aging.203690

84. Xue T, Qiu X, Liu H, Gan C, Tan Z, Xie Y, et al. Epigenetic regulation in fibrosis progress. *Pharmacol Res* (2021) 173:105910. doi: 10.1016/j.phrs.2021.105910

85. Wang S, Zhang X, Wang Q, Wang R. Histone modification in podocyte injury of diabetic nephropathy. *J Mol Med (Berl)* (2022) 100(10):1373–86. doi: 10.1007/s00109-022-02247-7

86. Zhang Y, Sun Z, Jia J, Du T, Zhang N, Tang Y, et al. Overview of histone modification. *Adv Exp Med Biol* (2021) 1283:1–16. doi: 10.1007/978-981-15-8104-5_1

87. Chelladurai P, Boucherat O, Stenmark K, Kracht M, Seeger W, Bauer UM, et al. Targeting histone acetylation in pulmonary hypertension and right ventricular hypertrophy. *Br J Pharmacol* (2021) 178(1):54–71. doi: 10.1111/bph.14932

88. Khouly I, Braun RS, Ordway M, Aouizerat BE, Ghassib I, Larsson L, et al. The role of DNA methylation and histone modification in periodontal disease: A systematic review. *Int J Mol Sci* (2020) 21(17):6217. doi: 10.3390/ijms21176217

89. Du J, Johnson LM, Jacobsen SE, Patel DJ. DNA methylation pathways and their crosstalk with histone methylation. *Nat Rev Mol Cell Biol* (2015) 16(9):519–32. doi: 10.1038/nrm4043

90. Zhu D, Zhang Y, Wang S. Histone citrullination: a new target for tumors. *Mol Cancer* (2021) 20(1):90. doi: 10.1186/s12943-021-01373-z

91. El-Hashash AHK. Histone H3K27M mutation in brain tumors. *Adv Exp Med Biol* (2021) 1283:43–52. doi: 10.1007/978-981-15-8104-5_3

92. Qi H, Liu H, Pullamsetti SS, Günther S, Kuenne C, Atzberger A, et al. Epigenetic regulation by suv4-20h1 in cardiopulmonary progenitor cells is required to prevent pulmonary hypertension and chronic obstructive pulmonary disease. *Circulation* (2021) 144(13):1042–58. doi: 10.1161/circulationaha.120.051680

93. Bisserier M, Mathiyalagan P, Zhang S, Elmastour F, Dorfmüller P, Humbert M, et al. Regulation of the methylation and expression levels of the BMPR2 gene by SIN3a as a novel therapeutic mechanism in pulmonary arterial hypertension. *Circulation* (2021) 144(1):52–73. doi: 10.1161/circulationaha.120.047978

94. Tian Q, Fan X, Ma J, Li D, Han Y, Yin X, et al. Critical role of VGLL4 in the regulation of chronic normobaric hypoxia-induced pulmonary hypertension in mice. *FASEB J* (2021) 35(8):e21822. doi: 10.1096/fj.202002650RR

95. Van der Feen DE, Kurakula K, Tremblay E, Boucherat O, Bossers GPL, Szulcek R, et al. Multicenter preclinical validation of BET inhibition for the treatment of pulmonary arterial hypertension. *Am J Respir Crit Care Med* (2019) 200(7):910–20. doi: 10.1164/rccm.201812-2275OC

96. Bogaard HJ, Mizuno S, Hussaini AA, Toldo S, Abbate A, Kraskauskas D, et al. Suppression of histone deacetylases worsens right ventricular dysfunction after pulmonary artery banding in rats. *Am J Respir Crit Care Med* (2011) 183(10):1402–10. doi: 10.1164/rccm.201007-1106OC

97. Verhoeff TJ, Holloway AF, Dickinson JL. Non-coding RNA regulation of integrins and their potential as therapeutic targets in cancer. *Cell Oncol (Dordr)* (2023) 46(2):239–50. doi: 10.1007/s13402-022-00752-y

98. Marinescu MC, Lazar AL, Marta MM, Cozma A, Catana CS. Non-coding RNAs: prevention, diagnosis, and treatment in myocardial ischemia-reperfusion injury. *Int J Mol Sci* (2022) 23(5):2728. doi: 10.3390/ijms23052728

99. Braga L, Ali H, Secco I, Giacca M. Non-coding RNA therapeutics for cardiac regeneration. *Cardiovasc Res* (2021) 117(3):674–93. doi: 10.1093/cvr/cvaa071

100. RussOmanno G, Jo KB, Abdul-Salam VB, Morgan C, Endruschat J, Schaeper U, et al. miR-150-PTPMT1-cardiolipin signaling in pulmonary arterial hypertension. *Mol Ther Nucleic Acids* (2021) 23:142–53. doi: 10.1016/j.omtn.2020.10.042

101. Chen KH, Dasgupta A, Lin J, Potus F, Bonnet S, Iremonger J, et al. Epigenetic dysregulation of the dynamin-related protein 1 binding partners miD49 and miD51 increases mitotic mitochondrial fission and promotes pulmonary arterial hypertension: mechanistic and therapeutic implications. *Circulation* (2018) 138(3):287–304. doi: 10.1161/circulationaha.117.031258

102. Zeng Z, Yao J, Li Y, Xue Y, Zou Y, Shu Z, et al. Anti-apoptosis endothelial cell-secreted microRNA-195-5p promotes pulmonary arterial smooth muscle cell proliferation and migration in pulmonary arterial hypertension. *J Cell Biochem* (2018) 119(2):2144–55. doi: 10.1002/jcb.26376

103. Yi L, Liu J, Deng M, Zuo H, Li M. Emodin inhibits viability, proliferation and promotes apoptosis of hypoxic human pulmonary artery smooth muscle cells *via* targeting miR-244-5p/DEGS1 axis. *BMC Pulm Med* (2021) 21(1):252. doi: 10.1186/s12890-021-01616-1

104. Zhang W, Li Y, Xi X, Zhu G, Wang S, Liu Y, et al. MicroRNA−15a−5p induces pulmonary artery smooth muscle cell apoptosis in a pulmonary arterial hypertension model *via* the VEGF/p38/MMP−2 signaling pathway. *Int J Mol Med* (2020) 45(2):461–74. doi: 10.3892/ijmm.2019.4434

105. Deng L, Blanco FJ, Stevens H, Lu R, Caudrillier A, McBride M, et al. MicroRNA-143 activation regulates smooth muscle and endothelial cell crosstalk in pulmonary arterial hypertension. *Circ Res* (2015) 117(10):870–83. doi: 10.1161/circresaha.115.306806

106. Yang YZ, Zhang YF, Yang L, Xu J, Mo XM, Peng W. miR−760 mediates hypoxia-induced proliferation and apoptosis of human pulmonary artery smooth muscle cells *via* targeting TLR4. *Int J Mol Med* (2018) 42(5):2437–46. doi: 10.3892/ijmm.2018.3862

107. Cai Z, Li J, Zhuang Q, Zhang X, Yuan A, Shen L, et al. MiR-125a-5p ameliorates monocrotaline-induced pulmonary arterial hypertension by targeting the TGF-β1 and IL-6/STAT3 signaling pathways. *Exp Mol Med* (2018) 50(4):1–11. doi: 10.1038/s12276-018-0068-3

108. Zhu G, Zhang W, Liu Y, Wang S. miR−371b−5p inhibits endothelial cell apoptosis in monocrotaline−induced pulmonary arterial hypertension *via* PTEN/PI3K/Akt signaling pathways. *Mol Med Rep* (2018) 18(6):5489–501. doi: 10.3892/mmr.2018.9614

109. Huang CX, Jiang ZX, Du DY, Zhang ZM, Liu Y, Li YT. The MFF-SIRT1/3 axis, regulated by miR-340-5p, restores mitochondrial homeostasis of hypoxia-induced pulmonary artery smooth muscle cells. *Lab Invest* (2022) 102(5):515–23. doi: 10.1038/s41374-022-00730-w

110. Zhang L, Ma C, Wang X, Bai J, He S, Zhang J, et al. MicroRNA-874-5p regulates autophagy and proliferation in pulmonary artery smooth muscle cells by targeting Sirtuin 3. *Eur J Pharmacol* (2020) 888:173485. doi: 10.1016/j.ejphar.2020.173485

111. Liu T, Zou XZ, Huang N, Ge XY, Yao MZ, Liu H, et al. Down-regulation of miR-204 attenuates endothelial-mesenchymal transition by enhancing autophagy in

hypoxia-induced pulmonary hypertension. *Eur J Pharmacol* (2019) 863:172673. doi: 10.1016/j.ejphar.2019.172673

112. Ou M, Li X, Cui S, Zhao S, Tu J. Emerging roles of let–7d in attenuating pulmonary arterial hypertension *via* suppression of pulmonary artery endothelial cell autophagy and endothelin synthesis through ATG16L1 downregulation. *Int J Mol Med* (2020) 46(1):83–96. doi: 10.3892/ijmm.2020.4567

113. Toden S, Zumwalt TJ, Goel A. Non-coding RNAs and potential therapeutic targeting in cancer. *Biochim Biophys Acta Rev Cancer* (2021) 1875(1):188491. doi: 10.1016/j.bbcan.2020.188491

114. Jiang Y, Hei B, Hao W, Lin S, Wang Y, Liu X, et al. Clinical value of lncRNA SOX2-OT in pulmonary arterial hypertension and its role in pulmonary artery smooth muscle cell proliferation, migration, apoptosis, and inflammatory. *Heart Lung* (2022) 55:16–23. doi: 10.1016/j.hrtlng.2022.04.002

115. Li ZK, Gao LF, Zhu XA, Xiang DK. LncRNA HOXA-AS3 Promotes the Progression of Pulmonary Arterial Hypertension through Mediation of miR-675-3p/PDE5A Axis. *Biochem Genet* (2021) 59(5):1158–72. doi: 10.1007/s10528-021-10053-y

116. Wang H, Qin R, Cheng Y. LncRNA-Ang362 Promotes Pulmonary Arterial Hypertension by Regulating miR-221 and miR-222. *Shock* (2020) 53(6):723–9. doi: 10.1097/shk.0000000000001410

117. Liu Y, Sun Z, Zhu J, Xiao B, Dong J, Li X. LncRNA-TCONS_00034812 in cell proliferation and apoptosis of pulmonary artery smooth muscle cells and its mechanism. *J Cell Physiol* (2018) 233(6):4801–14. doi: 10.1002/jcp.26279

118. Xia X, Huang L, Zhou S, Han R, Li P, Wang E, et al. Hypoxia-induced long non-coding RNA plasmacytoma variant translocation 1 upregulation aggravates pulmonary arterial smooth muscle cell proliferation by regulating autophagy *via* miR-186/Srf/Ctgf and miR-26b/Ctgf signaling pathways. *Int J Cardiol* (2023) 370:368–77. doi: 10.1016/j.ijcard.2022.09.060

119. Feng X, Wang K, Yang T, Liu Y, Wang X. LncRNA-GAS5/miR-382-3p axis inhibits pulmonary artery remodeling and promotes autophagy in chronic thromboembolic pulmonary hypertension. *Genes Genomics* (2022) 44(4):395–404. doi: 10.1007/s13258-021-01202-z

120. Li Y, Zhang J, Sun H, Yu X, Chen Y, Ma C, et al. RPS4XL encoded by lnc-Rps4l inhibits hypoxia-induced pyroptosis by binding HSC70 glycosylation site. *Mol Ther Nucleic Acids* (2022) 28:920–34. doi: 10.1016/j.omtn.2022.05.033

121. Kristensen LS, Jakobsen T, Hager H, Kjems J. The emerging roles of circRNAs in cancer and oncology. *Nat Rev Clin Oncol* (2022) 19(3):188–206. doi: 10.1038/s41571-021-00585-y

122. Jiang Y, Liu H, Yu H, Zhou Y, Zhang J, Xin W, et al. Circular RNA calm4 regulates hypoxia-induced pulmonary arterial smooth muscle cells pyroptosis *via* the circ-calm4/miR-124-3p/PDCD6 axis. *Arterioscler Thromb Vasc Biol* (2021) 41 (5):1675–93. doi: 10.1161/atvbaha.120.315525

123. Zhang J, Li Y, Chen Y, Yu X, Wang S, Sun H, et al. Circ-calm4 regulates hypoxia-induced pulmonary artery smooth muscle autophagy by binding Purb. *J Mol Cell Cardiol* (2023) 176:41–54. doi: 10.1016/j.yjmcc.2023.01.009

124. Jing X, Wu S, Liu Y, Wang H, Huang Q. Circular RNA Sirtuin1 represses pulmonary artery smooth muscle cell proliferation, migration and autophagy to ameliorate pulmonary hypertension *via* targeting microRNA-145-5p/protein kinase-B3 axis. *Bioengineered* (2022) 13(4):8759–71. doi: 10.1080/21655979.2022.2036302

125. Jin X, Xu Y, Guo M, Sun Y, Ding J, Li L, et al. hsa_circNFXL1_009 modulates apoptosis, proliferation, migration, and potassium channel activation in pulmonary hypertension. *Mol Ther Nucleic Acids* (2021) 23:1007–19. doi: 10.1016/j.omtn.2020.09.029

126. Huang CX, Jiang ZX, Du DY, Zhang ZM, Liu Y, Li YT. Hsa_circ_0016070/micro-340-5p axis accelerates pulmonary arterial hypertension progression by upregulating TWIST1 transcription *via* TCF4/β-catenin complex. *J Am Heart Assoc* (2022) 11(14):e024147. doi: 10.1161/jaha.121.024147

127. Benincasa G, DeMeo DL, Glass K, Silverman EK, Napoli C. Epigenetics and pulmonary diseases in the horizon of precision medicine: a review. *Eur Respir J* (2021) 57(6):2003406. doi: 10.1183/13993003.03406-2020

128. Zhang JR, Sun HJ. MiRNAs, lncRNAs, and circular RNAs as mediators in hypertension-related vascular smooth muscle cell dysfunction. *Hypertens Res* (2021) 44 (2):129–46. doi: 10.1038/s41440-020-00553-6

129. Chelladurai P, Seeger W, Pullamsetti SS. Epigenetic mechanisms in pulmonary arterial hypertension: the need for global perspectives. *Eur Respir Rev* (2016) 25 (140):135–40. doi: 10.1183/16000617.0036-2016

frontiers | Frontiers in Immunology

TYPE Original Research
PUBLISHED 24 November 2023
DOI 10.3389/fimmu.2023.1250920

OPEN ACCESS

EDITED BY
Bailong Tao,
The First Affiliated Hospital of Chongqing Medical University, China

REVIEWED BY
Tianyi Zhang,
Emory University, United States
Minghan Yang,
New York University, United States
Tian-Yu Song,
Broad Institute, United States
Ke Wu,
Wuhan University, China

*CORRESPONDENCE
Bo Cheng
efzchengbo@163.com
Yu Tian
tianyu930314@126.com

RECEIVED 30 June 2023
ACCEPTED 24 October 2023
PUBLISHED 24 November 2023

CITATION
Wang R, Ma X, Zhang X, Jiang D, Mao H, Li Z, Tian Y and Cheng B (2023) Autophagy-mediated NKG2D internalization impairs NK cell function and exacerbates radiation pneumonitis. *Front. Immunol.* 14:1250920. doi: 10.3389/fimmu.2023.1250920

Autophagy-mediated NKG2D internalization impairs NK cell function and exacerbates radiation pneumonitis

Ruiqing Wang, Xinyue Ma, Xinyu Zhang, Dizhi Jiang, Hongyuan Mao, Zerun Li, Yu Tian* and Bo Cheng*

Qilu Hospital of Shandong University, Cheeloo College of Medicine, Shandong University, Jinan, China

Introduction: Radiation pneumonitis is a critical complication that constrains the use of radiation therapy for thoracic malignancies, leading to substantial morbidity via respiratory distress and lung function impairment. The role of Natural killer (NK) cells in inflammatory diseases is well-documented; however, their involvement in radiation pneumonitis is not fully understood.

Methods: To explore the involvement of NK cells in radiation pneumonitis, we analyzed tissue samples for NK cell presence and function. The study utilized immunofluorescence staining, western blotting, and immunoprecipitation to investigate CXCL10 and ROS levels, autophagy activity, and NKG2D receptor dynamics in NK cells derived from patients and animal models subjected to radiation.

Result: In this study, we observed an augmented infiltration of NK cells in tissues affected by radiation pneumonitis, although their function was markedly diminished. In animal models, enhancing NK cell activity appeared to decelerate the disease progression. Concomitant with the disease course, there was a notable upsurge in CXCL10 and ROS levels. CXCL10 was found to facilitate NK cell migration through CXCR3 receptor activation. Furthermore, evidence of excessive autophagy in patient NK cells was linked to ROS accumulation, as indicated by immunofluorescence and Western blot analyses. The association between the NKG2D receptor and its adaptor proteins (AP2 subunits AP2A1 and AP2M1), LC3, and lysosomes was intensified after radiation exposure, as demonstrated by immunoprecipitation. This interaction led to NKG2D receptor endocytosis and subsequent lysosomal degradation.

Conclusion: Our findings delineate a mechanism by which radiation-induced lung injury may suppress NK cell function through an autophagy-dependent pathway. The dysregulation observed suggests potential therapeutic targets; hence, modulating autophagy and enhancing NK cell activity could represent novel strategies for mitigating radiation pneumonitis.

KEYWORDS

radiation pneumonitis, CXCL10/CXCR3, autophagy, NKG2D, NK cell

Introduction

Radiotherapy (RT) is pivotal in the treatment of malignant tumors. Nonetheless, radiation pneumonitis (RP) stands out as a frequent clinical side effect observed in thoracic radiotherapy patients. This condition significantly impacts the long-term survival rates and prognoses of cancer patients, constituting a primary impediment to the efficacy of radiotherapy (1, 2). Consequently, the suppression of RP-associated inflammatory infiltration and incidence reduction represent pressing clinical imperatives. Given the intricate nature of its progression mechanism, enhanced prognostic outcomes may hinge on innovative therapeutic approaches stemming from an improved comprehension of RP's progression mechanism.

The progression of radiation pneumonitis is influenced by various factors, including alterations in the tumor and inflammatory microenvironments (3, 4). Natural killer (NK) cells constitute a vital component of the inflammatory microenvironments and play a pivotal role in inflammatory responses. On one hand, they possess the capability to directly eliminate pathogen-infected cells, thereby preventing further dissemination. On the other hand, they can secrete an array of cytokines and chemical factors, such as tumor necrosis factor-alpha (TNF-α), interferon-gamma (IFN-γ), and interleukins (such as IL-10 and IL-13), to modulate the inflammatory response (5, 6). The equilibrium between signals from activating and inhibitory receptors governs the functional outcomes of NK cells. Unlike B and T cell antigen receptors, NK cell receptors are encoded in the germline and do not undergo somatic recombination, enabling them to mount rapid responses in inflammatory reactions (7, 8). NKG2D, serving as a primary activating receptor on the surface of NK cells, primarily recognizes and binds to specific ligands expressed by stressed, infected, or cancerous cells, which are typically absent on healthy cell surfaces. Upon binding to these ligands, NKG2D activates the NK cell, resulting in the destruction of the target cell (9–11). However, the role of NK cells in the progression of RP has not been investigated to date.

NK cell function is primarily regulated by chemotactic factors in inflammatory environments (12). During influenza virus infection, previous research by Wareing MD et al. found that CXCR2 plays a critical role in recruiting neutrophils to the lungs, leading to their accumulation in lung tissue. Interestingly, this accumulation does not significantly contribute to virus clearance, offering valuable insights into the varying impacts of chemokines on the quantity and functionality of immune cells (13). Recent studies suggest that inflammation can trigger the release of numerous chemokines, including IL-8, which attract neutrophils and result in the production of additional reactive oxygen and nitrogen species, consequently impairing neutrophil function (14). Our study revealed that CXCL10/CXCR3 activation in radiation pneumonitis leads to increased NK cell infiltration, while the accumulation of reactive oxygen species (ROS) causes excessive autophagy, thereby inhibiting NK cell function. Delving deeper into these specific mechanisms is crucial for gaining a better understanding of NK cells' role in lung injury.

Autophagy is an intracellular biological process responsible for degrading and recycling cellular components, frequently triggered by ROS (15). This self-regulating mechanism aids in preserving normal cellular functions when moderately engaged. However, if excessively stimulated, it can cause irreparable harm to the cells (16). The process of autophagy comprises several sequential steps. Initially, an autophagosome engulfs materials earmarked for degradation, such as damaged proteins or organelles. Subsequently, the autophagosome fuses with a lysosome inside the cell, leading to the degradation and recycling of the contents encapsulated within the autophagosome. Autophagy plays a pivotal role in various biological processes, such as defending against infections, delaying the aging process, responding to hunger, and managing stress reactions (17–19).

In this study, we observed an elevated count of NK cells concurrent with a decrease in their functionality during radiation pneumonia. Mechanistically, radiation-induced lung injury results in the release of CXCL10, which activates CXCR3 on the surface of NK cells, resulting in the intracellular accumulation of ROS. Elevated ROS levels constitute the primary cause of excessive autophagy in NK cells during radiation pneumonia. Subsequently, autophagy initiates the internalization of NKG2D and its degradation via the lysosomal pathway, leading to a deterioration in NK cell function and exacerbating the advancement of radiation pneumonia. Our findings, which confirm the involvement of NK cells in radiation pneumonia, may provide valuable insights for the clinical diagnosis and treatment of this condition.

Methods

Cell culture

NK92 cells (ATCC®, CRL-2407™) were maintained in MEM-α (#12571063, GIBCO, USA) supplemented with 10% FBS, 10% horse serum, 1% non-essential amino acid, 1% pen-strep, 1% sodium pyruvate, 0.1 mM 2-β-mercaptoethanol, 0.2 mM myo-inositol, and 2.5 μM folic acid. Cells were maintained at 37 °C at 5% CO2 levels. For conditioning, cells were cultured for approximately 2 months and were routinely checked for mycoplasma infection.

The mouse lung cancer cell line CMT167 was obtained from the European Collection of Authenticated Cell Cultures (ECACC) and cultured in Dulbecco's modified Eagle's medium (DMEM; Life Technologies, USA), containing 10% (v/v) fetal bovine serum (FBS; Life Technologies, USA).

Animal

Animal studies were approved by Institutional Animal Care and Use Committee of Qilu Hospital affiliated to Shandong University. The mice were bred in our air-conditioned animal facility and housed with a 12/12 hr light/dark cycle and with ad libitum access to food and water. In the survival study, the animals were observed daily. Animals displaying symptoms, such as severe hunchback posture, apathy, decreased motion, or activity, dragging legs, unkempt fur, or drastic loss of body weight were killed by cervical

dislocation. Excised tumor tissues were further examined through hemtoxylin and eosin, and immunofluorescence staining.

Luciferase-expressing CMT167 cell lines (5 x 10^5 cells in 40 μL PBS) were injected through the chest wall into the lung of C57BL/6 (5-week-old; SPF Biotechnology Co., Ltd, Beijing, China) female mice on day 0. Depleting antibodies were NK1.1 clone PK136 (#BE0036, BioXCell), and IgG2a isotype control (#BE0085, BioXCell). Tumor growth was examined at 5, 10, and 15 days after inoculation via bioluminescence imaging (IVIS spectrum *in vivo* imaging system, PerkinElmer, USA). On day 5, mice were randomly assigned to each treatment group.

Western blotting

The RIPA (#89901, Thermo Fisher Scientific, USA) buffer were used to lyse the harvested NK92 cells on ice about 30 min and centrifuged at 4 °C and 17,000g for 50 min. The BCA protein assay kit (#P0010, Beyotime Institute of Biotechnology, China) was used for the protein concentration measurement. Subjected the samples to SDS-PAGE electrophoretically, and then transferred to PVDF membranes. All membranes were blocked by Tween-Tris-buffered saline containing 5% non-fat milk for 2 h at room temperature and then incubated with primary antibodies as follows: GAPDH (#ab9485, Abcam), β-tublin (#ab179511, Abcam), AP2A1 (#ab189995, Abcam), AP2M1(#ab75995, Abcam), LAMP2 (#ab13524, Abcam), LC3 (#ab62721, Abcam), NKG2D (#ab36136, Abcam), CXCR3 (#ab288437, Abcam). At room temperature, all the membranes were washed by TBST three times, and then incubated with horseradish peroxidase II antibody (#ZB-2301, #ZB-2305, ZSGB-BIO, China) for 1 hour. The synergistic chemical imager (ECL) kit (#34096, Thermo Fisher Scientific, USA) was used for staining protein gels and then used the manufacturer's ChemImager 5500 V2.03 software scan.

Co-IP

Co-Immunoprecipitations were used to detected the interaction between proteins. Briefly, the RIPA (#89901, Thermo Fisher Scientific, USA) buffer were used to lyse the harvested cell on ice about 60 min and corresponding antibodies were incubated with the Protein A/G Magnetic beads for immunoprecipitation (#B23201, Bimake, USA) on ice for 30 min. Cell lysates were centrifuged, and the supernatants were added to and incubated with the protein A/G Magnetic beads (above incubated with corresponding antibodies) under rotation at 4°C overnight. After being washed three times with high-salt buffer. The beads were boiled for 7 min with 2 × SDS sample buffer, followed by Western blotting with corresponding antibodies.

PCR

Total RNA was extracted from cells using TRIzol reagent (#10296010CN, Invitrogen, USA) and reverse-transcribed using the Rever Tra Ace qPCR RT Kit (#FSQ-101, Toyobo, Japan). cDNA was amplified using SYBR Green on the Roche Light Cycler 480 for quantification. The relative expression levels of mRNA were normalized to glycer- aldehyde-3-phosphate dehydrogenase (GAPDH). Sequences of the primers used are shown in Supplementary Table 1.

HE staining

HE staining was performed using a HE Staining Kit (#G1120, Solarbio, China). Briefly, staining of brain sections was carried out using Mayers hematoxylin, followed by eosin. Following eosin staining for 50 s, and dehydration by ethanol (95, 100%), the sections were cleared by xylene and mounted. These images were obtained using Nikon's confocal microscope (Nikon, Japan). We then calculated the proportion of radiation pneumonium area in the total area of the lobes.

Multiplex immunofluorescence staining

For multiplex immunofluorescence staining, we followed the Opal protocol staining method for the following markers: NK1.1 (#ab234107, Abcam), LC3B (#ab192890, Abcam), LysoTracker (Invitrogen. #L12492), and NKG2D (Abcam, #ab302907). All sections were cover-slipped using Anti-Fade Fluorescence Mounting Medium (#ab104135, Abcam). Phenochart software was used to perform a 20X (0.5 μm/pixel) scan analysis of selected tissue areas after scanning by Vectra Polaris Automated Quantitative Pathology Imaging System.

Staining images were evaluated by two blinded pathologists, with the intensity of autophagy scored from 0 to 3, with 0 (no LC3 staining), 1 (weakly LC3 staining), 2 (moderately LC3 staining), and 3 (severely LC3 staining). The positive rate of LC3 in NK cells was also scored using a scale of 0-3: 0 (0-9%), 1 (10%-25%), 2 (26%-50%), 3 (51%-75%), and 4 (76%-100%). The autophagy intensity score and the positive cell rate score are then multiplied, and the product is used as the final autophagy score.

3D-SIM

In our study, we use 3D structured illumination microscopy (3D-SIM), a super-resolution imaging technique, to enhance our understanding of NK cells. To begin with, specimens were prepared following standard fixation and staining procedures suitable for 3D-SIM. Once prepared, the specimens were placed under the 3D-SIM microscope, equipped with a high-numerical-aperture lens. Subsequently, these raw images were processed through a reconstruction algorithm. Live, three-color, 3D-SIM imaging was performed on the OMX-Flex system (GE Healthcare).

Flow cytometry

To detect apoptosis, cells were rinsed with PBS, incubated with Annexin V-FITC and PI (#556547, BD Biosciences, USA) at room

temperature for 15 min. Apoptosis results were analyzed on a C6 flow cytometer (BD Biosciences, USA). Data were analyzed in Accuri 6C software analysis.

Intracellular ROS production was detected using MitoSOX™ Red (#M36009, MitoSox, Invitrogen). And cell staining of single-cell suspensions was performed using the following fluorophore-conjugated antibodies: CD45 (#157214, Biolegend, USA), NK1.1 (#156506, Biolegend, USA), IFN-γ (#505808, Biolegend, USA), TNF-α (#506306, Biolegend, USA), Granzyme B (#372208, Biolegend, USA), NKG2D (#115711, Biolegend, USA).

Statistical analysis

The unpaired two-tailed Student's t-test was used to compare differences between two groups. Multiple comparisons were performed with one-way ANOVA using Dunnett's multiple comparisons test. Survival curves were estimated by the Kaplan–Meier method and compared using the log-rank test. Statistical analysis was conducted using GraphPad Prism (Version 8.0). $P < 0.050$ was considered statistically significant for all the two-sided tests.

Results

Radiation pneumonia is accompanied by an accumulation of NK cells and a decline in their functionality

To investigate changes in NK cell quantity and function during radiation pneumonitis, we induced radiation pneumonitis in 6-8-week-old C57/BL6 mice by exposing them to a single 20 Gy dose of radiation. Following irradiation, we collected lung tissue samples and observed an increase in both lung volume and weight, consistent with the potential development of pulmonary edema observed in clinical patients after radiation exposure. This observation aligns with the potential development of pulmonary edema observed in clinical patients after radiation exposure. The increased lung volume and weight signify fluid accumulation in lung tissue, a characteristic feature of pulmonary edema. These results imply that the mice exhibited a physiological response to radiation-induced lung injury similar to that observed in humans (Supplementary Figure 1A).

Hematoxylin and eosin (HE) staining revealed significant inflammatory infiltration in the lungs on the 14th day after irradiation, confirming the successful model establishment. Building on this foundation, we euthanized the mice on the 14th day and isolated pulmonary mononuclear cells for quantifying and assessing NK cell function. The results revealed a significant increase in the proportion of NK cells in the lungs of the RP group compared to the control group (non-irradiated mice) (Figures 1A, B). Subsequently, we assessed the expression of IFN-γ and granzyme B in NK cells using flow cytometry. Surprisingly, despite the increase in NK cell numbers, the function of NK cells in the RP group's lungs was significantly diminished compared to the control group (Figure 1C).

To gain a clearer understanding of NK cell status, we isolated and cultured NK cells obtained from the lungs of radiation pneumonitis mice using magnetic bead separation. The extracellular apoptosis rate of NK cells in the lungs of the RP group was higher than that in the control group (Figure 1D). Additionally, CCK8 results demonstrated significantly reduced vitality of NK cells in mice with radiation pneumonia (Figure 1E). Subsequently, we cultured the isolated NK cells *in vitro* and assessed the levels of IFN-γ and granzyme B in the culture supernatant after 48 hours. The results revealed a substantial reduction in the RP group's lung NK cells' ability to secrete cytokines, indicating a significant functional difference compared to the control group (Figures 1F, G). These findings indicate inconsistent changes in the number and function of NK cells in radiation pneumonitis, marked by an increase in infiltration but functional exhaustion.

Lung injury promotes the recruitment of NK cells via the CXCL10/CXCR3 pathway

In our previous research, we identified substantial alterations in both the quantity and function of NK cells in radiation pneumonitis (RP). To explore the underlying mechanisms, PCR and ELISA were used to quantify the levels of NK cell-associated chemokines in mouse lung tissue and bronchoalveolar lavage fluid (BALF), respectively. In lung tissue, we noted a significant elevation in CXCL8 and CXCL10 levels in the RP group (Figure 2A). Conversely, in the BALF, CCL5 and CXCL10 exhibited a substantial increase in the RP group (Figure 2B). Additionally, we collected peripheral blood samples from patients undergoing the same radiation regimen and divided them into two groups based on the presence or absence of radiation pneumonitis development. ELISA results reveal a significant increase in CXCL10 levels in the peripheral blood supernatant of patients who developed radiation pneumonitis (Supplementary Figure 1B). Given that CXCL10 displayed significant changes in both groups, we hypothesized that CXCL10 may play an important role in radiation pneumonitis.

Next, we assessed the activation status of CXCR3, the receptor for CXCL10, in NK cells. PCR and Western blot findings indicated significant activation of CXCR3 at both the RNA and protein levels in NK cells from the lungs of RP group mice (Figures 2C, D). To further investigate the chemotactic capacity<city/> of NK cells induced by the activation of CXCL10/CXCR3 in radiation pneumonitis, we examined the expression of cell migration-related molecules MAPK, RhoA, and AKT. The results show that in radiation pneumonitis, the transcription and protein levels of MAPK and RhoA in NK cells have increased, but the changes in AKT are not significant (Figures 2E, F). Immunofluorescence and transwell assays indicate that the CXCR3 inhibitor AMG487 significantly reduces the migratory capacity<city/> of NK cells after radiation exposure, leading to a decrease in NK cell infiltration (Figures 2G, H and Supplementary Figures 1F, G). In summary, we hypothesize that the release of CXCL10 induced by radiation activates the CXCR3 receptors on the surfaces of NK cells, thereby promoting their infiltration into lung tissues.

10.3389/fimmu.2023.1250920

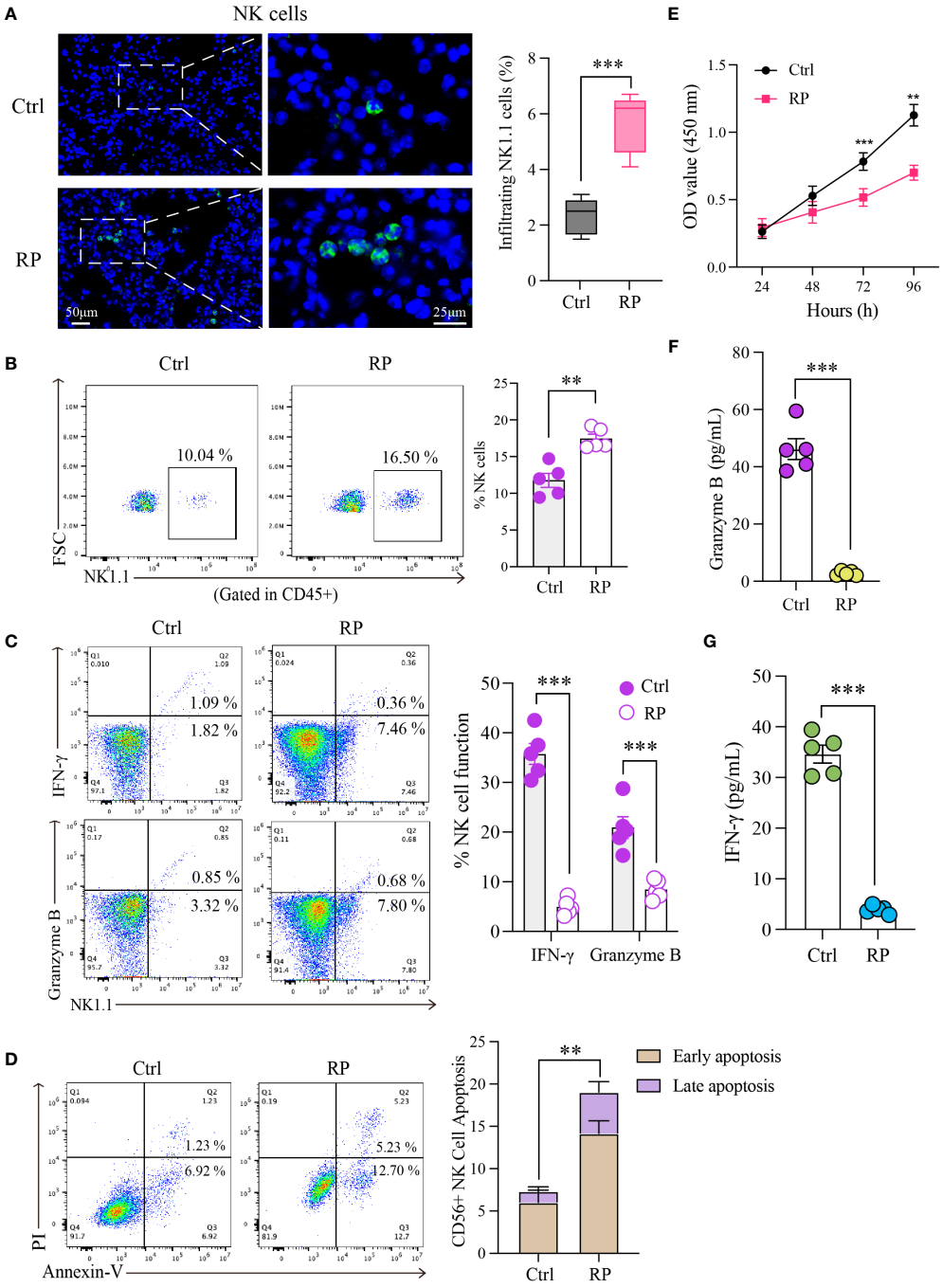

FIGURE 1
Radiation pneumonia is accompanied by an accumulation of NK cells and a decline in their functionality. Immunofluorescence staining **(A)** and flow cytometry analysis **(B)** for detecting the number of NK cells. Scale bar (left) = 50 μm, Scale bar (right) = 25 μm. **(C)** Flow cytometry analysis for the expression of functional indicators (IFN-γ and granzyme B) of lung tissue-infiltrating NK cells. **(D, E)** The apoptosis rate and CCK8 results indicated that the vitality of NK cells was significantly weaker when mice had a radiation pneumonia. **(F, G)** The levels of IFN-γ and granzyme B in the culture supernatant of NK cells. **(A–C, F, G)**: n = 5; **(D, E)**: n = 3. Each point represents an individual experiment. *, P < 0.050; **, P < 0.010; ***, P < 0.001. ***P = 0.0003 **(A)**, **P = 0.001 **(B)**, ***P < 0.0001 IFN-γ, ***P = 0.0008 Gran B **(C)**, **P = 0.0023 **(D)**, ***P = 0.0002 72h, **P = 0.0016 96h **(E)**, ***P < 0.001 **(F)**, ***P < 0.001 **(G)**.

Overactive autophagy in lung NK Cells induced by radiation

To better understand the mechanism of NK cell function suppression in radiation pneumonitis, we conducted RNA-seq analysis comparing NK cells from mice with radiation pneumonitis to those from healthy lungs. The results revealed significant transcriptomic differences between NK cells from the two groups of mice (Figures 3A, B). Subsequent enrichment analysis using the KEGG pathway indicated that the differentially expressed genes were predominantly associated with the autophagy pathway (Figure 3C).

10.3389/fimmu.2023.1250920

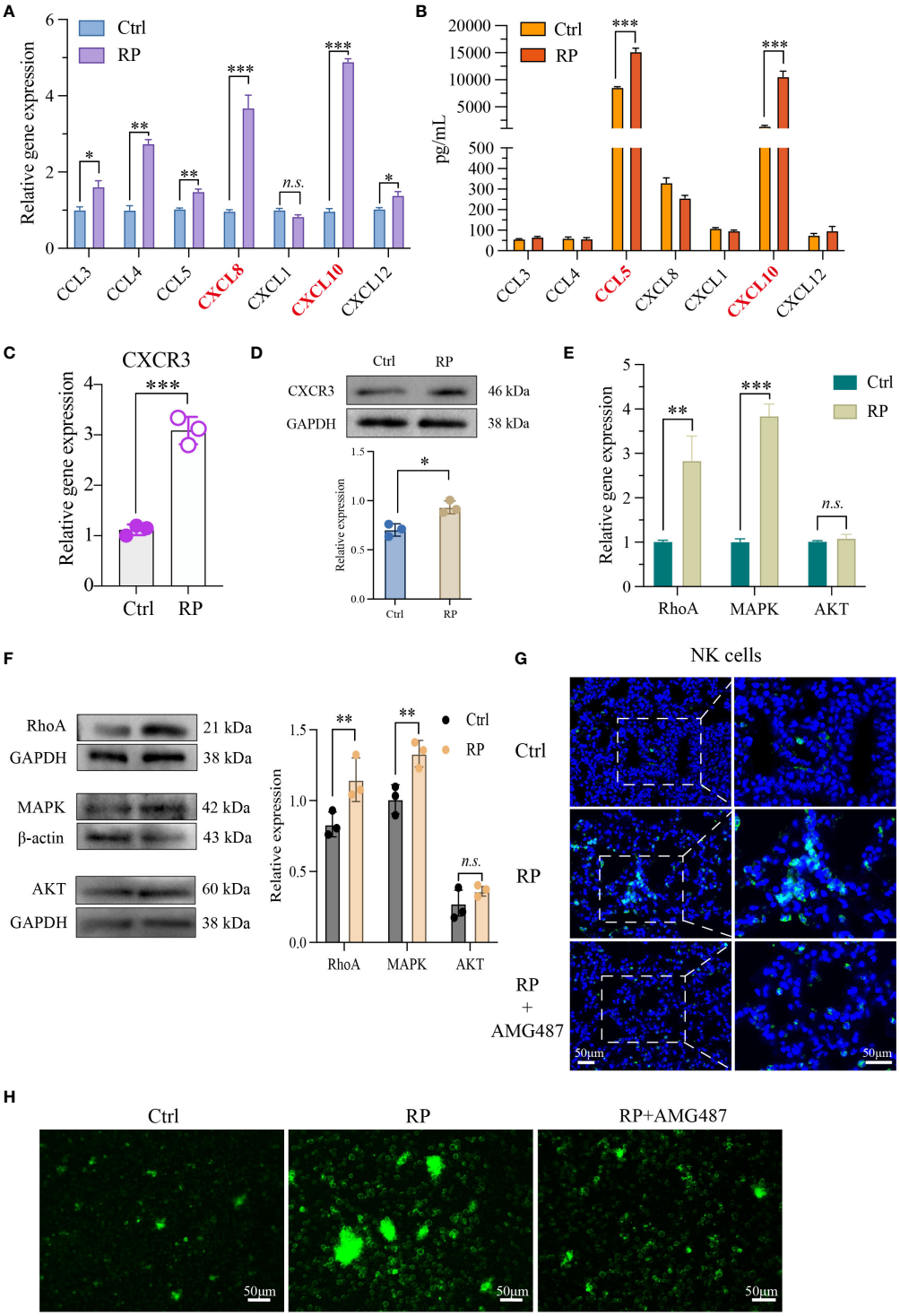

FIGURE 2
Lung injury promotes the recruitment of NK cells via the CXCL10/CXCR3 pathway. NK cell-associated chemokines in mouse lung tissue **(A)** and BALF **(B)** were detected respectively. PCR **(C, E)** as well as Western blotting analysis **(D, F)** revealed that NK cells from the lungs of RP group were markedly activated at both the RNA and protein levels. **(G)** Demonstration of AMG487 reversing radiotherapy-induced decline in NK cell count in mice. Scale bar (left) = 50 μm, Scale bar (right) = 50 μm. **(H)** Transwell assay depicting NK cell migration under control, radiotherapy, and radiotherapy with AMG487. Scale bar = 50 μm **(A-G)**: n = 3. Each point represents an individual experiment. *, P < 0.050; **, P < 0.010; ***, P < 0.001. *P = 0.0142 CCL3, **P = 0.0033 CCL4, **P = 0.0090 CCL5, ***P = 0.0002 CXCL8, ***P = 0.0005 CXCL10, *P = 0.0358 CXCL12 **(A)**, ***P < 0.0001 CCL5, ***P = 0.0001 CXCL10 **(B)**, ***P = 0.0003 **(C)**, *P = 0.0118 **(D)**, **P = 0.0048 RhoA, ***P< 0.0001 MAPK **(E)**, **P = 0.0044 RhoA, **P = 0.0038 MAPK **(F)**.

Immunofluorescence staining showed that the level of autophagy in lung NK cells was increased in the RP group compared with the control group (Figure 3D). RT-qPCR and Western blot results indicated elevated expression of autophagy-related proteins in lung NK cells from mice in the RP group (Figures 3E–G). These findings confirm that autophagy occurs in NK cells within the radiation pneumonia microenvironment, and further investigation is required to elucidate the downstream mechanism.

Restoration of NK cell function through inhibition of ROS accumulation or excessive autophagy

Numerous studies have shown that the buildup of reactive oxygen species (ROS) during inflammation is a major driver of excessive cellular autophagy. Consequently, we quantified ROS levels in lung tissues from mice with radiation pneumonitis and healthy mice. The results revealed a substantial increase in ROS accumulation in the radiation pneumonitis group (Figure 4A). ROS can accumulate through various mechanisms, and based on prior reports on other inflammatory conditions, CXCL10/CXCR3 activation can also contribute to ROS buildup. Accordingly, we conducted relevant experiments. However, in radiation pneumonitis, the primary source of ROS is radiation-induced cellular damage. These data are presented for reference purposes.

Our findings revealed an upward trend in mitochondrial ROS production in the CXCL10 treatment group compared to the control group (Supplementary Figure 1C). To confirm the essential role of CXCR3 in ROS accumulation, we used small interfering RNA (siRNA) to silence CXCR3 expression in the NK92 cell line, followed by CXCL10 stimulation. The results demonstrated significantly reduced ROS production in the si-CXCR3 group compared to the control (Supplementary Figures 1D, E). Following ROS suppression with NAC, there was a significant reduction in autophagy induced by ROS accumulation (Figure 4B).

Furthermore, we investigated the association between ROS levels and the severity of radiation pneumonitis using an animal model. As anticipated, the inhibition of ROS by NAC substantially ameliorated inflammatory lesions in lung tissues (Figure 4C and Supplementary Figure 2A).

To further investigate the direct regulatory impact of excessive autophagy on NK cell function, we performed the following experiments. First, we utilized a CCK-8 assay to evaluate the effect of autophagy on NK cell vitality. The results indicated that inhibiting radiation-induced excessive autophagy in NK cells with 3-MA led to a significant increase in their proliferation rate compared to the control group (Figure 4D). Subsequently, we evaluated alterations in NK cell function following the inhibition of radiation-induced excessive autophagy using flow cytometry. As anticipated, there was a significant recovery in NK cell function after autophagy inhibition (Figure 4E). To better illustrate the connection between NK cell function and autophagy, we simultaneously measured NK cell function and LC3 expression in the same samples and conducted a linear correlation analysis. The results demonstrated a significant negative correlation between the two variables (Figure 4F).

We further conducted *in vivo* experiments to confirm the influence of autophagy on NK cells. An experiment with two groups of mice (3-MA+RP vs RP) was designed. The results indicated that in the presence of 3-MA, there were no significant changes in the number of NK cells in mouse lungs (Figure 4G). This implies that autophagy may not directly control the quantity of NK cells, as the recruitment of NK cells induced by radiation is primarily governed by chemotactic factors. We then assessed the functionality of NK cells in the lungs of both groups of mice and observed that NK cell function in the RP+3-MA group significantly exceeded that in the RP-only group (Figure 4H). Targeting autophagy holds promise for restoring NK cell function impaired in radiation pneumonitis.

Excessive autophagy leads to the internalization of NKG2D

In our prior research, we confirmed the decline in NK cell function in radiation pneumonitis, although the precise mechanisms remain unknown. We employed RT-PCR to assess the RNA expression of key functional receptors on the NK cell surface, revealing a significant reduction in NKG2D receptor expression after radiotherapy compared to the control group (Figure 5A). The decreased NKG2D expression on NK cell surfaces after radiation was corroborated by western blot and flow cytometry, confirming the PCR findings (Figures 5B, C).

Next, we investigated the degradation mechanism of NKG2D. Immunoprecipitation studies showed enhanced interaction between NKG2D and the clathrin AP2 subunit after radiation therapy, which was blocked by 3-MA. AP2 is a crucial component in clathrin-mediated endocytosis, capable of binding to clathrin and membrane cargo proteins, thus playing a pivotal role in endocytosis. Conversely, LC3, a distinctive molecule in autophagosome formation, serves as a specific marker for autophagy. Moreover, LC3 lipidation can induce direct interaction with various autophagic components through cargo receptors. To ascertain the direct connection between NKG2D and autophagy, we further investigated the interaction between NKG2D and LC3, demonstrating an enhanced interaction between NKG2D and LC3 after radiation therapy. Furthermore, we noted a notable rise in the interaction between NKG2D and LAMP2 (a lysosomal marker protein) after radiation therapy, and the inhibition of autophagy similarly reduced their binding (Figures 5D, E).

To further explore the extent of autophagy in NK cells under different treatments, we utilized 3D-SIM (Structured Illumination Microscopy) technology to confirm autophagy at the organelle level. Our results indicated that after irradiation, there was an elevated binding of NKG2D (green) with lysosomes (red) compared to the control group, suggesting an increased co-localization. This effect was suppressed when irradiation was combined with the autophagy inhibitor 3-MA, providing a more direct and microscopic representation of the extent of autophagy within lysosomes (Figure 5F and Supplementary Figure 2B). These findings

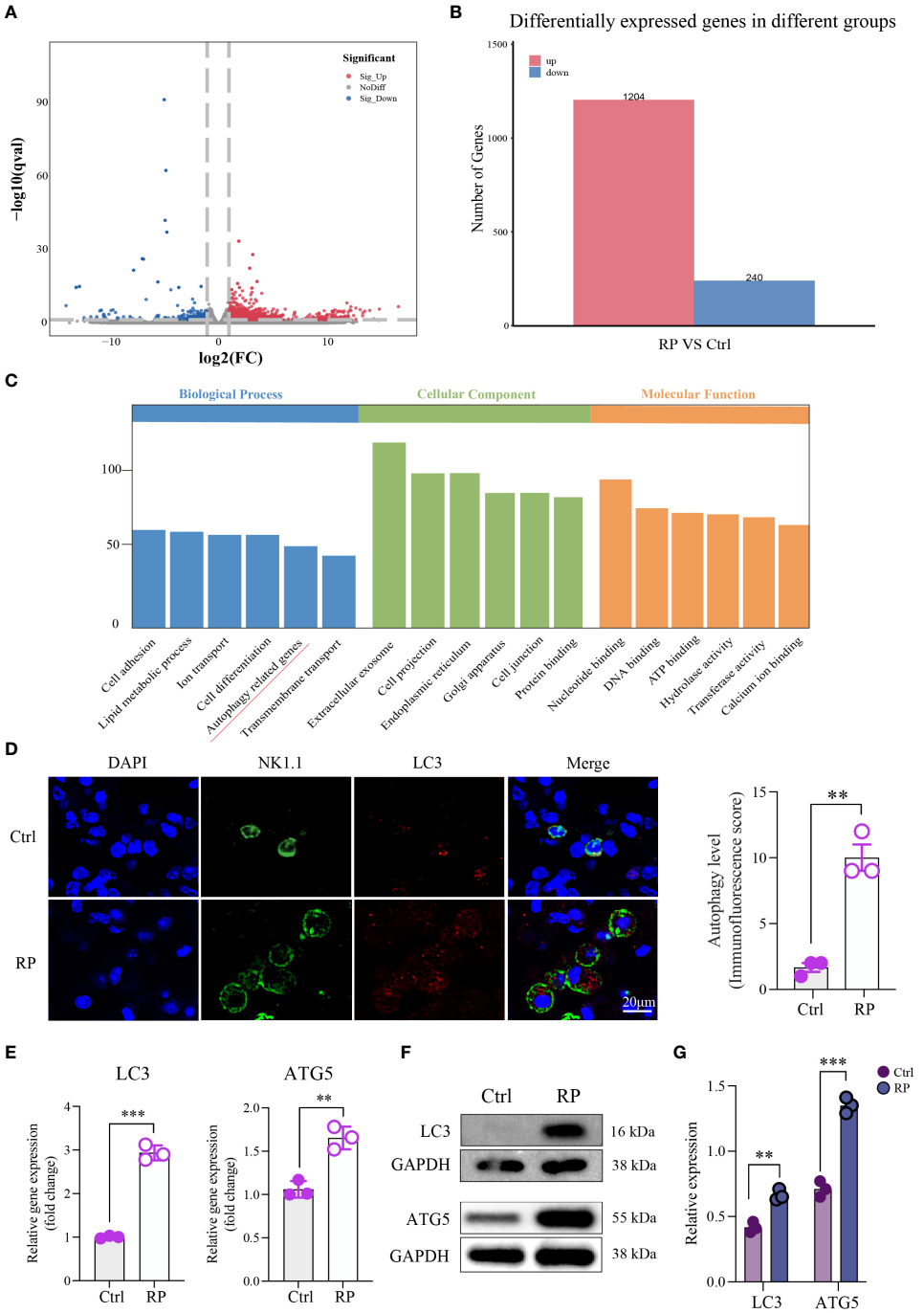

FIGURE 3
Overactive Autophagy in Lung NK Cells Induced by Radiation. **(A)** Volcano Plot of Differentially Expressed Genes: This plot shows the relationship between gene expression levels and statistical significance, highlighting genes that are differentially expressed between two conditions. The x-axis represents the log-transformed expression levels of genes, the y-axis represents the negative logarithm of statistical significance, and the scatter plot represents differentially expressed genes. Red dots indicate upregulated genes, blue dots indicate downregulated genes, and gray dots indicate genes with no significant difference. **(B)** Number of Differentially Expressed Genes: Comparison of the number of differentially expressed genes detected in RNA-seq analysis under different conditions. The numbers in the table represent the count of genes significantly upregulated or downregulated in each condition. **(C)** Pathway enrichment analysis of the differentially expressed gene set using the KEGG database. This plot shows the differentially expressed genes enriched KEGG pathways. **(D)** Compared to the control group, multiplex immunofluorescence staining showed that autophagy was excessively activated in the lung NK cells of the RP group mice. Scale bar = 20 μm. **(E–G)** RT-qPCR and Western blotting results indicated an increase in the expression of autophagy-related proteins in lung NK cells from the RP group mice. **(D–G)**: n = 3. Each point represents an individual experiment. *, P < 0.050; **, P < 0.010; ***, P < 0.001. **P = 0.0014 **(D)**, ***P < 0.001 LC3, **P = 0.0031 ATG5 **(E)**, **P = 0.0018 LC3, ***P = 0.0002 ATG5 **(G)**.

10.3389/fimmu.2023.1250920

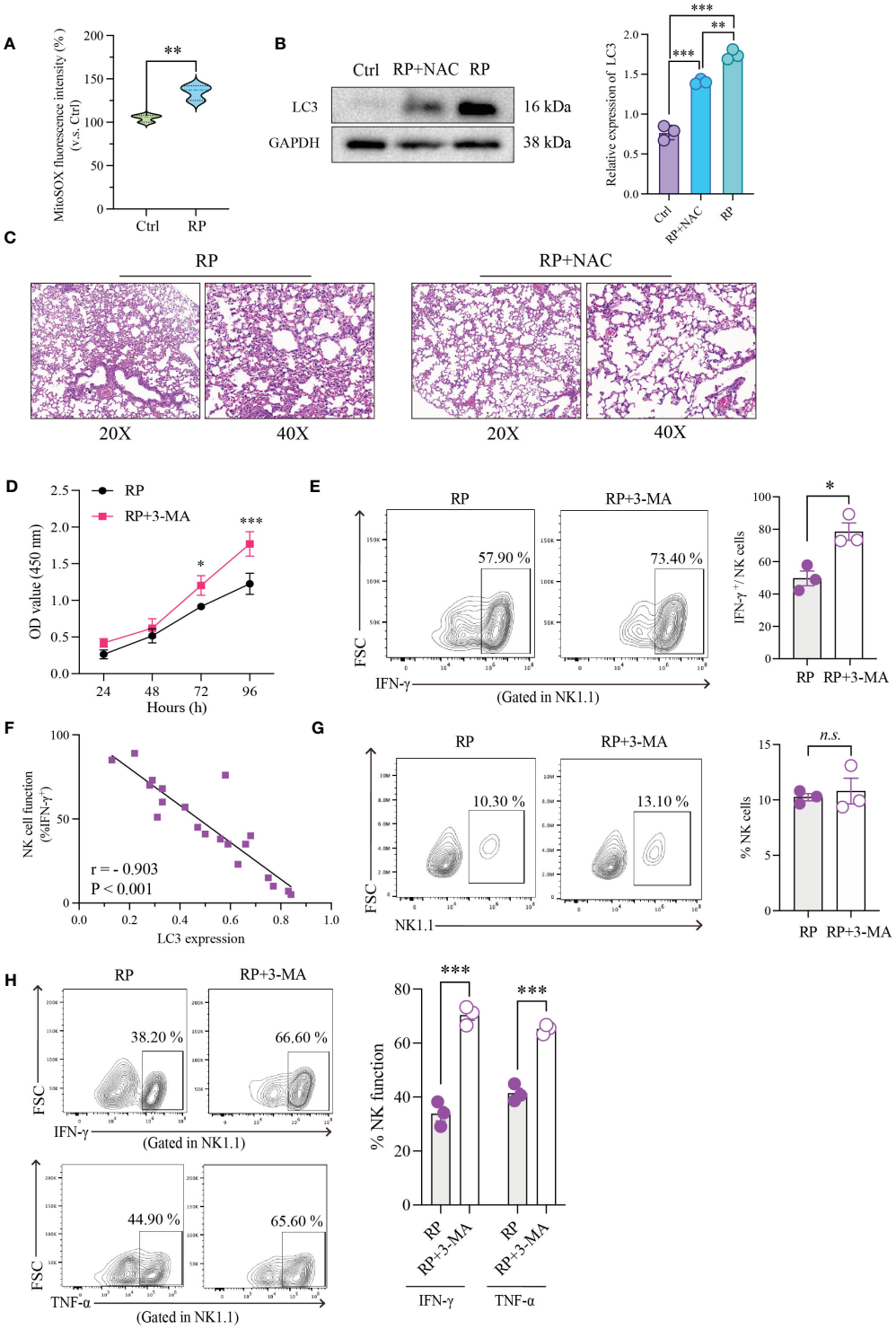

FIGURE 4
Restoration of NK Cell Function through Inhibition of ROS Accumulation or Excessive Autophagy. **(A)** Using mitochondrial ROS-specific fluorescent dye (MitoSOX red) to observe the distribution of mitochondrial ROS. **(B)** The effect of NAC on the expression of autophagy-related protein (LC3) in NK cells as demonstrated by Western blotting. **(C)** HE-staining of lung tissue from mice exposed to 20Gy irradiation with or without autophagy inhibitor treatment. Left: 20x magnification. Right: 40x magnification. ROS inhibition reduces radiation-induced lung damage. **(D)** As demonstrated by CCK8 assays, radiation-induced excessive autophagy of NK cells was inhibited by 3-MA, resulting in significantly higher proliferation rates than those in control group. **(E)** Flow cytometry showed that NK cell function was significantly restored after its autophagy was inhibited. **(F)** Linear correlation analysis confirmed that there was a significant negative correlation between NK cell function and LC3 expression level. **(G)** Flow cytometry showed that under the influence of 3-MA, the number of lung-infiltrating NK cells didn't show significant changes. **(H)** The RP+3-MA group significantly outperformed the RP-only group in terms of NK cell function. **(A–H)**: n = 3. Each point represents an individual experiment. *, P < 0.050; **, P < 0.010; ***, P < 0.001. **P = 0.0058 **(A)**, ***P < 0.0001 Ctrl vs RP+NAC, ***P < 0.0001 Ctrl vs RP, **P = 0.0019 RP vs RP+NAC **(B)**, *P = 0.0253 72h, ***P < 0.0001 96h **(D)**, *P = 0.0151 **(E)**, ***P = 0.0004 IFN-γ, ***P = 0.0003 TNF-α **(H)**.

10.3389/fimmu.2023.1250920

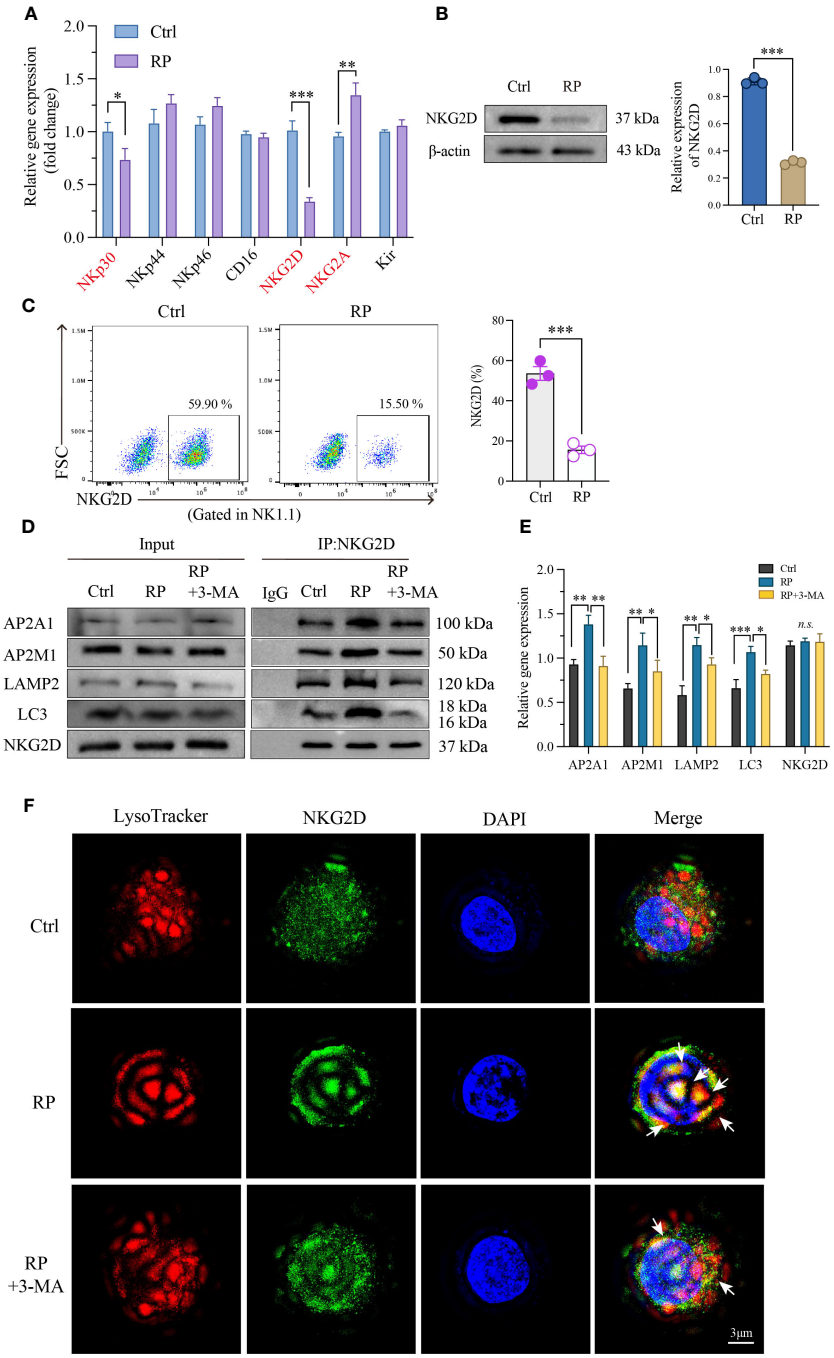

FIGURE 5
Excessive autophagy leads to the internalization of NKG2D. **(A)** Using RT-PCR technology to examine RNA expression of the main functional receptors on the NK cell surface. And the reduced NKG2D expression on the surface of NK cells was further confirmed by western blotting **(B)** and flow cytometry **(C)**. **(D, E)** Co-IP demonstrated a significant increase in the interaction between NKG2D and LAMP2 after radiation therapy, and inhibiting autophagy likewise attenuated their binding. **(F)** A reconstructed three-dimensional structured illumination microscopy (3D-SIM) image showing an NK cell. The cell surface is labeled with an antibody against NKG2D (green), and lysosomes are labeled with a specific lysosomal marker (red). The merged image demonstrates the co-localization of NKG2D and lysosomes (arrow) within the NK cell. Scale bar = 3 μm. A-E: n = 3. Each point represents an individual experiment. *, P < 0.050; **, P < 0.010; ***, P < 0.001. *P = 0.0236 NKp30, ***P = 0.0002 NKG2D, **P = 0.0044 NKG2A **(A)**, ***P < 0.0001 **(B)**, ***P = 0.0006 **(C)**, **P = 0.0021, **P = 0.0016, AP2A1; **P = 0.0039, *P = 0.0390, AP2M1; **P = 0.0060, *P = 0.0472, LAMP2; ***P = 0.0009, *P = 0.0116, LC3 **(E)**.

collectively indicate that radiation-induced excessive autophagy results in the degradation of the membrane protein NKG2D through a clathrin-lysosome-dependent pathway.

Autophagy-NK axis regulates radiation pneumonitis and tumor progression

As widely recognized, NK cells play a crucial role not only in inflammation but also in anti-cancer therapy. In clinical practice, patients undergoing thoracic radiotherapy often have concurrent tumors, and lung cancer is particularly closely linked to radiation pneumonitis. We combined the radiation pneumonitis model with a mouse model of *in situ* lung cancer to investigate the combined impact of targeting autophagy and NK cell function on inflammation and cancer (Figure 6A) . Firstly, we assessed the severity of radiation pneumonitis from two angles: HE staining and the number of neutrophils in bronchoalveolar lavage fluid. Results showed that 3-MA significantly inhibited the progression of pneumonitis, but this inhibitory effect was noticeably reduced when NK cells were depleted. Furthermore, pneumonitis significantly worsened when NK cells were independently depleted (Figures 6B, C). Next, we employed live animal imaging and survival time detection to assess how autophagy and NK cells influence tumor progression during radiotherapy. Results demonstrated that the progression of tumors mirrored the severity of inflammation (Figures 6D, E). In addition, we also assessed the cytotoxicity<city/> of NK cells against tumor cells in an *in vitro* experiment under the backdrop of radiation pneumonitis. The results showed that compared to the control group, NK cells from the lungs of radiation pneumonitis mice exhibited significantly reduced cytotoxicity<city/> against the mouse lung cancer cell line CMT167 (Supplementary Figures 2C, D). This suggests that targeting autophagy and NK cells has a significant effect in slowing the progression of radiation pneumonitis, as well as in inhibiting tumor growth.

Discussion

As a common early complication of chest radiation therapy, Radiation Pneumonitis (RP) can lead to treatment interruption, and even respiratory failure, significantly impacting patient prognosis and survival (2). Unfortunately, there is currently no effective medication for treating or preventing RP, and the specific pathogenesis of RP remains unclear, necessitating further investigation (20). NK cells, as integral components of the immune system, have a complex impact on inflammation. On one hand, NK cells, when in balanced quantities and functioning normally, can alleviate excessive inflammatory responses within the body; on the other hand, the excessive accumulation of NK cells can secrete a substantial amount of pro-inflammatory cytokines, intensifying the inflammatory response (21). NK cells also influence other immune cells in complex ways. For instance, NK cells regulate and enhance T cell immune responses by producing IFN-γ. Additionally, NK cells impact the maturation of macrophages by secreting IL-10 (5, 22).

Importantly, the role of NK cells in radiation pneumonitis remains unclear. In this context, our *in vivo* experiments revealed significant alterations in the quantity and function of NK cells within RP. These alterations are characterized by an increase in NK cell numbers and a loss of function. To delve into the role and specific mechanism of NK cells in radiation pneumonitis, we employed techniques such as Elisa and Western blot. We discovered that radiation-induced lung damage releases a substantial amount of CXCL10, which rapidly activates the primary chemotactic receptor, CXCR3, on the surface of NK cells, leading to a significant infiltration of NK cells into lung tissue. In contrast to the increase in quantity, radiation therapy results in an excessive accumulation of Reactive Oxygen Species (ROS) within the cells, causing overactive autophagy in NK cells. Mechanistically, we confirmed through techniques like co-immunoprecipitation (CO-IP) that autophagy mediates the endocytosis of the membrane-bound NKG2D via the adaptor protein 2 (AP2), resulting in a decrease in NKG2D expression in NK cells and, consequently, NK cell dysfunction. Our data also indicated a significant correlation between the expression of the active receptor NKG2D on the surface of NK cells and the level of autophagy. In summary, we observed alterations in the quantity and function of NK cells in RP and, regarding the mechanism, we discerned that the activation of the CXCL10/CXCR3 axis recruits a substantial number of NK cells and, to a certain extent, promotes the accumulation of intracellular ROS. A noteworthy point is that the ROS generated by the activation of the CXCL10/CXCR3 axis is limited, but it plays a significant role in the enrichment of NK cells. It is the accumulation of ROS due to cellular radiative damage that serves as the primary factor for excessive autophagy (Figure 7). Therefore, interventions targeting CXCR3 still require more in-depth research to support their clinical applications, while measures intervening in autophagy and NK cells are effective preventive strategies for RP, offering critical theoretical support for the early clinical intervention and treatment of RP.

The infiltration and functional abnormalities of Natural Killer (NK) cells represent typical characteristics of inflammatory diseases (23, 24). However, research on NK cells lags behind that of other immune cells, and reports on NK cells in radiation pneumonitis are particularly scarce. In our study, we observed impaired NK cell function due to radiation therapy. The activation of the CXCL10/CXCR3 axis exacerbated radiation pneumonitis by inducing excessive autophagy, thereby hindering NK cells from clearing damaged tissue cells and hyper-reactive inflammatory cells. One distinctive feature of NK cells lies in their rapid activation and direct functional exertion via receptor-ligand binding on their membrane surface. The balance between activating and inhibitory receptors ultimately dictates NK cell functional phenotypes. In this context, we primarily focused on NKG2D (an activating receptor) without delving into alterations in other receptors and their interplay with NKG2D. Furthermore, numerous studies have documented NKG2D downregulation following repeated ligand binding (25–

10.3389/fimmu.2023.1250920

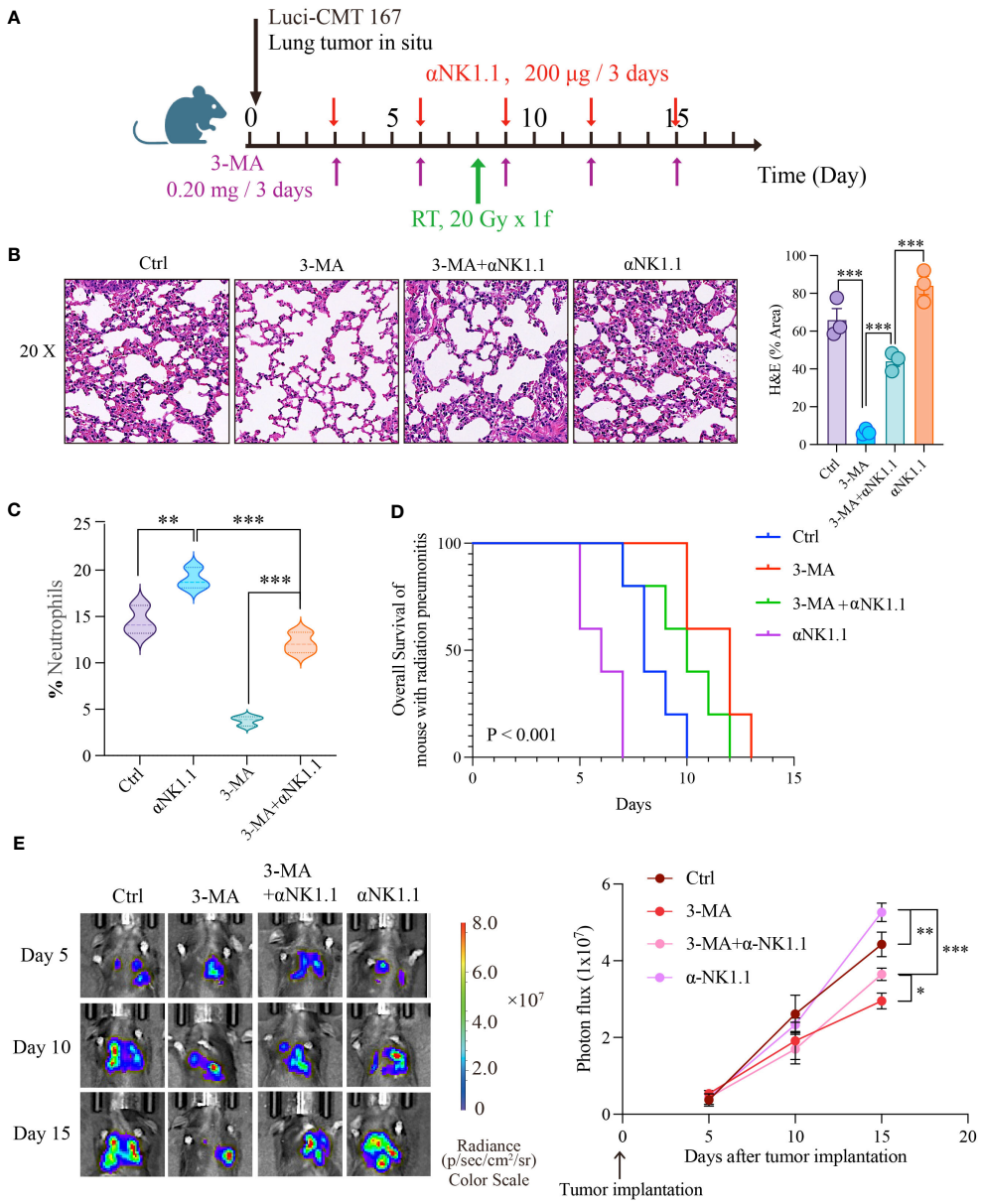

FIGURE 6
Autophagy-NK axis regulates radiation pneumonitis and tumor progression. **(A)** Animal model diagram. Evaluate the severity of radiation pneumonitis from three perspectives: HE of pulmonary tissue **(B)**, and the number of neutrophils in bronchoalveolar lavage fluid **(C)**. Then we examined the effect of autophagy and NK cells on tumor progression during radiotherapy using live animal imaging and survival time detection **(D, E)**. **(B, C)**: n = 3; **(D, E)**: n = 5. Each point represents an individual experiment. *, P < 0.050; **, P < 0.010; ***, P < 0.001. *** P < 0.0001 Ctrl vs 3-MA, ***P = 0.0008 3-MA vs 3-MA+αNK1.1, ***P = 0.0005 3-MA+αNK1.1 vs αNK1.1 **(B)**, **P = 0.0053 Ctrl vs αNK1.1, ***P = 0.0003 αNK1.1 vs 3-MA+αNK1.1, ***P < 0.0001 3-MA vs 3-MA+αNK1.1 **(C)**, **P = 0.0065 Ctrl vs αNK1.1, ***P < 0.0001 αNK1.1 vs 3-MA+αNK1.1, *P = 0.0242, 3-MA+αNK1.1 vs 3-MA **(E)**.

27), leading to what is termed NKG2D exhaustion. Investigating how this phenomenon impacts NK cell function in radiation pneumonitis merits our thorough examination.

Numerous reports have shown that tissue damage can trigger an increase in the release of inflammatory factors and chemokines, recruiting immune cells to infiltrate the site of inflammation (28, 29). In our study, we observed that CXCL10/CXCR3 accelerated NK cell infiltration into lung tissue, leading to intracellular ROS accumulation. While various studies have confirmed the impact of different chemokines on ROS release, research specifically focused on CXCR3's role in promoting ROS release remains limited, necessitating further investigation into the underlying mechanism. Research conducted by Victorelli S and colleagues demonstrated that senescent melanocytes' SASP induces telomere dysfunction in a paracrine manner, thereby limiting the proliferation of neighboring cells through CXCR3-dependent mitochondrial ROS. Conversely, Li MX et al. reported that knocking down CXCR3 in murine paw cells significantly inhibited high glucose-induced decreases in cell viability, cell cycle arrest, and intracellular ROS production. These related studies underscore the evident connection between CXCR3 and ROS, making the investigation of their interplay in radiation pneumonitis a key focus of our ongoing research.

10.3389/fimmu.2023.1250920

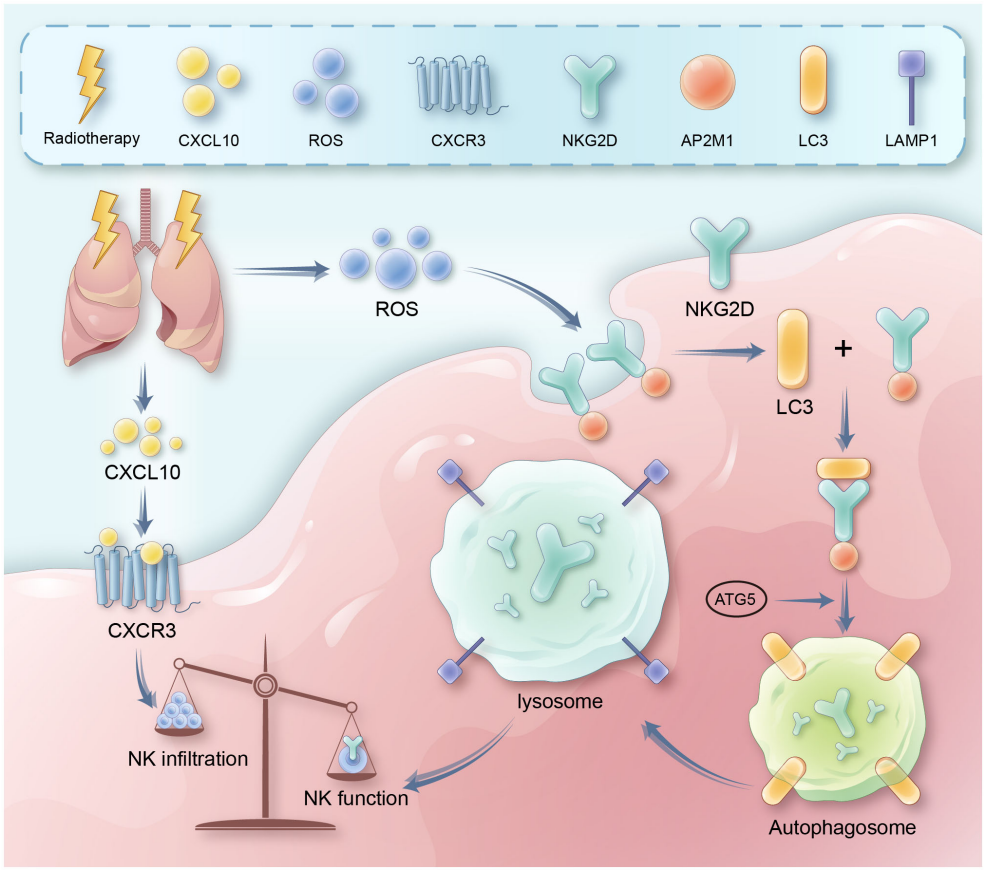

FIGURE 7
It presents a schematic diagram outlining the proposed mechanism. Key reactions, interactions, and resultant effects are represented with arrows. Radiation therapy induces DNA damage and cell death in lung tissue, leading to release of inflammatory cytokines like CXCL10. CXCL10 binds to and activates the CXCR3 receptor on natural killer (NK) cells, triggering signaling cascades involving RhoA and MAPK. This leads to recruitment and infiltration of more NK cells from circulation into the damaged lung tissue. Meanwhile, radiation also causes accumulation of reactive oxygen species (ROS) in lung tissue and NK cells. Excessive ROS induces overactivation of autophagy pathways in NK cells. This involves increased expression of autophagy proteins like LC3. Through adaptor proteins like AP2, LC3 binds to and internalizes the NKG2D activating receptor on NK cells, routing it for degradation in lysosomes. Loss of surface NKG2D impairs NK cell cytotoxicity<city/> and cytokine production, preventing efficient clearance of damaged cells and resolution of inflammation. Therefore, the CXCL10-CXCR3 axis and ROS-induced autophagy combine to both increase total NK cells yet suppress their functions in radiation pneumonitis.

As widely recognized, ROS is a well-established trigger for autophagy (30), as confirmed in our research on radiation pneumonitis (RP). Given that radiotherapy modulates NK cell function by activating autophagy, we investigated the deeper relationship and specific interaction between autophagy and NKG2D. Through co-immunoprecipitation, we verified that autophagy induces NKG2D internalization and degradation. Additionally, we observed that radiation enhances NKG2D binding with clathrin, adaptor protein 2 (AP2A1 and AP2M1 subunits), LC3, and lysosomes. This implies that clathrin-mediated endocytosis plays a pivotal role in autophagy-induced NKG2D degradation. Other studies also suggest that adaptor proteins can link autophagic lysosomes to membrane-surface Claudin-2, promoting its internalization and degradation, thereby reinforcing intestinal barrier tight junctions, aligning with our findings (31). Autophagy in Alzheimer's disease has been shown to target membrane-bound amyloid precursor protein (APP, the precursor of β-amyloid) for degradation (32), providing substantial support for autophagy-mediated degradation of membrane proteins via adaptor proteins. In conclusion, autophagy plays a crucial role in our research, and inhibiting autophagy is likely to be beneficial for radiation pneumonitis. 3-MA, as a common autophagy inhibitor, has demonstrated efficacy in reversing radiation-induced lung injury in our studies. However, in tumor cells, the use of 3-MA often inhibits tumor proliferation and increases their drug sensitivity (33, 34). Of course, there are many kinds of drugs that inhibit autophagy; phospho-chloroquine is also a commonly used autophagy inhibitor. Whether it can play a role in radiation pneumonitis remains to be further studied by us.

In summary, our research provides new insights into how radiation therapy regulates NK cell function through autophagy-mediated degradation of NKG2D. It's worth noting that in clinical treatments, the dosage and duration of radiation therapy vary widely, and different doses and durations produce different effects. In terms of mechanisms, apart from autophagy, the inflammatory environment in radiation pneumonitis exerts complex effects on the quantity and function of NK cells. Other mechanisms still require further in-depth exploration. Future studies will further elucidate

the fine-tuning of this mechanism, including CXCL10/CXCR3-mediated ROS release, its precise role in NKG2D endocytosis and autophagic degradation, as well as the interactive role of autophagy and endocytic pathways in regulating NK cell function and repairing lung injury.

Data availability statement

The data presented in the study are deposited in the NCBI repository, accession number PRJNA1035231.

Ethics statement

Ethical approval was not required for the studies on humans in accordance with the local legislation and institutional requirements because only commercially available established cell lines were used. The animal study was approved by the Institutional Animal Care and Use Committee of Qilu Hospital affiliated to Shandong University. The study was conducted in accordance with the local legislation and institutional requirements.

Author contributions

Conception and design: RW, BC, and YT. Acquisition of data: XM, XZ, and DJ. Analysis and interpretation of data: HM and ZL. Writing and review of the manuscript: RW, BC, XM, XZ, and DJ. Revision of the manuscript and study supervision: BC and YT. All authors contributed to the article and approved the submitted version.

Funding

This study was funded by National Key Research and Development Program (2021YFC2500904, 2021YFC2500905), Young Taishan Scholars Program of Shandong Province (tsqnz20221167), Shandong Provincial Natural Science Foundation (ZR2022QH380, ZR2021LSW006), National Natural Science Foundation of China (82300193, 82303700), and China Postdoctoral Science Foundation (2022M721956, 2023TQ0200).

Conflict of interest

The authors declare that the research was conducted in the absence of any commercial or financial relationships that could be construed as a potential conflict of interest.

Publisher's note

Supplementary material

The Supplementary Material for this article can be found online at: https://www.frontiersin.org/articles/10.3389/fimmu.2023.1250920/full#supplementary-material

References

1. Mehta V. Radiation pneumonitis and pulmonary fibrosis in non-small-cell lung cancer: pulmonary function, prediction, and prevention. *Int J Radiat Oncol Biol Phys* (2005) 63(1):5. doi: 10.1016/j.ijrobp.2005.03.047

2. Hanania AN, Mainwaring W, Ghebre YT, Hanania NA, Ludwig M. Radiation-induced lung injury: assessment and management. *Chest* (2019) 156(1):150. doi: 10.1016/j.chest.2019.03.033

3. Graves PR, Siddiqui F, Anscher MS, Movsas B. Radiation pulmonary toxicity: from mechanisms to management. *Semin Radiat Oncol* (2010) 20(3):201. doi: 10.1016/j.semradonc.2010.01.010

4. Zhang M, Qian J, Xing X, Kong FM, Zhao L, Chen M, et al. Inhibition of the tumor necrosis factor-alpha pathway is radioprotective for the lung. *Clin Cancer Res* (2008) 14(6):1868. doi: 10.1158/1078-0432.Ccr-07-1894

5. Vivier E, Tomasello E, Baratin M, Walzer T, Ugolini S. Functions of natural killer cells. *Nat Immunol* (2008) 9(5):503. doi: 10.1038/ni1582

6. Cooper MA, Fehniger TA, Caligiuri MA. The biology of human natural killer-cell subsets. *Trends Immunol* (2001) 22(11):633. doi: 10.1016/s1471-4906(01)02060-9

7. Long EO. Regulation of immune responses through inhibitory receptors. *Annu Rev Immunol* (1999) 17:875. doi: 10.1146/annurev.immunol.17.1.875

8. Moretta A, Bottino C, Vitale M, Pende D, Cantoni C, Mingari MC, et al. Activating receptors and coreceptors involved in human natural killer cell-mediated cytolysis. *Annu Rev Immunol* (2001) 19:197. doi: 10.1146/annurev.immunol.19.1.197

9. Moretta A, Bottino C, Vitale M, Pende D, Biassoni R, Mingari MC, et al. Receptors for HLA class-I molecules in human natural killer cells. *Annu Rev Immunol* (1996) 14:619. doi: 10.1146/annurev.immunol.14.1.619

10. Vilches C, Parham P. KIR: diverse, rapidly evolving receptors of innate and adaptive immunity. *Annu Rev Immunol* (2002) 20:217. doi: 10.1146/annurev.immunol.20.092501.134942

11. Stewart CA, Vivier E, Colonna M. Strategies of natural killer cell recognition and signaling. *Curr Top Microbiol Immunol* (2006) 298:1. doi: 10.1007/3-540-27743-9_1

12. Yang Q, Li J, Hu Y, Tang X, Yu L, Dong L, et al. MiR-218-5p suppresses the killing effect of natural killer cell to lung adenocarcinoma by targeting SHMT1. *Yonsei Med J* (2019) 60(6):500. doi: 10.3349/ymj.2019.60.6.500

13. Wareing MD, Shea AL, Inglis CA, Dias PB, Sarawar SR. CXCR2 is required for neutrophil recruitment to the lung during influenza virus infection, but is not essential for viral clearance. *Viral Immunol* (2007) 20(3):369. doi: 10.1089/vim.2006.0101

14. Azad N, Rojanasakul Y, Vallyathan V. Inflammation and lung cancer: roles of reactive oxygen/nitrogen species. *J Toxicol Environ Health B Crit Rev* (2008) 11(1):1. doi: 10.1080/10937400701436460

15. Li L, Tan J, Miao Y, Lei P, Zhang Q. ROS and autophagy: interactions and molecular regulatory mechanisms. *Cell Mol Neurobiol* (2015) 35(5):615. doi: 10.1007/s10571-015-0166-x

16. Li YJ, Lei YH, Yao N, Wang CR, Hu N, Ye WC, et al. Autophagy and multidrug resistance in cancer. *Chin J Cancer* (2017) 36(1):52. doi: 10.1186/s40880-017-0219-2

17. Kim KH, Lee MS. Autophagy–a key player in cellular and body metabolism. *Nat Rev Endocrinol* (2014) 10(6):322. doi: 10.1038/nrendo.2014.35

18. Klionsky DJ, Petroni G, Amaravadi RK, Baehrecke EH, Ballabio A, Boya P, et al. Autophagy in major human diseases. *EMBO J* (2021) 40(19):e108863. doi: 10.15252/embj.2021108863

19. Li W, He P, Huang Y, Li YF, Lu J, Li M, et al. Selective autophagy of intracellular organelles: recent research advances. *Theranostics* (2021) 11(1):222. doi: 10.7150/thno.49860

20. Bledsoe TJ, Nath SK, Decker RH. Radiation pneumonitis. *Clin Chest Med* (2017) 38(2):201. doi: 10.1016/j.ccm.2016.12.004

21. Wang Y, Li M, Chen L, Bian H, Chen X, Zheng H, et al. Natural killer cell-derived exosomal miR-1249-3p attenuates insulin resistance and inflammation in mouse models of type 2 diabetes. *Signal Transduct Target Ther* (2021) 6(1):409. doi: 10.1038/s41392-021-00805-y

22. Caligiuri MA. Human natural killer cells. *Blood* (2008) 112(3):461. doi: 10.1182/blood-2007-09-077438

23. Lünemann A, Lünemann JD, Münz C. Regulatory NK-cell functions in inflammation and autoimmunity. *Mol Med* (2009) 15(9-10):352. doi: 10.2119/molmed.2009.00035

24. Bozzano F, Perrone C, Moretta L, De Maria A. NK cell precursors in human bone marrow in health and inflammation. *Front Immunol* (2019) 10:2045. doi: 10.3389/fimmu.2019.02045

25. Roda-Navarro P, Reyburn HT. The traffic of the NKG2D/Dap10 receptor complex during natural killer (NK) cell activation. *J Biol Chem* (2009) 284 (24):16463. doi: 10.1074/jbc.M808561200

26. Molfetta R, Quatrini L, Capuano C, Gasparrini F, Zitti B, Zingoni A, et al. c-Cbl regulates MICA- but not ULBP2-induced NKG2D down-modulation in human NK cells. *Eur J Immunol* (2014) 44(9):2761. doi: 10.1002/eji.201444512

27. Oppenheim DE, Roberts SJ, Clarke SL, Filler R, Lewis JM, Tigelaar RE, et al. Sustained localized expression of ligand for the activating NKG2D receptor impairs natural cytotoxicity*in vivo* and reduces tumor immunosurveillance. *Nat Immunol* (2005) 6(9):928. doi: 10.1038/ni1239

28. Nguyen HX, Lusis AJ, Tidball JG. Null mutation of myeloperoxidase in mice prevents mechanical activation of neutrophil lysis of muscle cell membranes in *vitro* and in *vivo*. *J Physiol* (2005) 565(Pt 2):403. doi: 10.1113/jphysiol.2005.085506

29. Park SH, Park-Min KH, Chen J, Hu X, Ivashkiv LB. Tumor necrosis factor induces GSK3 kinase-mediated cross-tolerance to endotoxin in macrophages. *Nat Immunol* (2011) 12(7):607. doi: 10.1038/ni.2043

30. Liu H, He Z, Simon HU. Targeting autophagy as a potential therapeutic approach for melanoma therapy. *Semin Cancer Biol* (2013) 23(5):352. doi: 10.1016/j.semcancer.2013.06.008

31. Ganapathy AS, Saha K, Suchanec E, Singh V, Verma A, Yochum G, et al. AP2M1 mediates autophagy-induced CLDN2 (claudin 2) degradation through endocytosis and interaction with LC3 and reduces intestinal epithelial tight junction permeability. *Autophagy* (2022) 18(9):2086. doi: 10.1080/15548627.2021.2016233

32. Tian Y, Chang JC, Fan EY, Flajolet M, Greengard P. Adaptor complex AP2/PICALM, through interaction with LC3, targets Alzheimer's APP-CTF for terminal degradation via autophagy. *Proc Natl Acad Sci USA* (2013) 110(42):17071. doi: 10.1073/pnas.1315110110

33. Dong Y, Wu Y, Zhao GL, Ye ZY, Xing CG, Yang XD. Inhibition of autophagy by 3-MA promotes hypoxia-induced apoptosis in human colorectal cancer cells. *Eur Rev Med Pharmacol Sci* (2019) 23(3):1047. doi: 10.26355/eurrev_201902_16992

34. Shin D, Kim EH, Lee J, Roh JL. RITA plus 3-MA overcomes chemoresistance of head and neck cancer cells via dual inhibition of autophagy and antioxidant systems. *Redox Biol* (2017) 13:219. doi: 10.1016/j.redox.2017.05.025

frontiers | Frontiers in Immunology

TYPE Original Research
PUBLISHED 27 November 2023
DOI 10.3389/fimmu.2023.1263988

OPEN ACCESS

EDITED BY
Chao Yang,
Zhejiang Ocean University, China

REVIEWED BY
Abhishek Mishra,
Houston Methodist Research Institute, United States
Pavel Loskot,
The Zhejiang University-University of Illinois at Urbana-Champaign Institute, United States

*CORRESPONDENCE
Ni-Han Lan
lannihan@163.com
Jin-Min Zhao
zhaojinmin@126.com

†These authors have contributed equally to this work and share first authorship

RECEIVED 20 July 2023
ACCEPTED 08 November 2023
PUBLISHED 27 November 2023

CITATION
Qin J, Zhang J, Wu JJ, Ru X, Zhong QL, Zhao JM and Lan NH (2023) Identification of autophagy-related genes in osteoarthritis articular cartilage and their roles in immune infiltration. *Front. Immunol.* 14:1263988. doi: 10.3389/fimmu.2023.1263988

Identification of autophagy-related genes in osteoarthritis articular cartilage and their roles in immune infiltration

Jun Qin[1,2,3†], Jin Zhang[4†], Jian-Jun Wu[5], Xiao Ru[1,2], Qiu-Ling Zhong[1,2], Jin-Min Zhao[1,2,4,6*] and Ni-Han Lan[1,2*]

[1]Guangxi Engineering Center in Biomedical Materials for Tissue and Organ Regeneration, The First Affiliated Hospital of Guangxi Medical University, Nanning, China, [2]Guangxi Clinical Medical Research Center for Orthopedic Disease, The First Affiliated Hospital of Guangxi Medical University, Nanning, China, [3]Department of Medical Cosmetology, The First Affiliated Hospital of Guangxi Medical University, Nanning, China, [4]Department of Orthopaedics Trauma and Hand Surgery, The First Affiliated Hospital of Guangxi Medical University, Nanning, China, [5]Department of Orthopedics, Zhanjiang Central Hospital, Guangdong Medical University, Zhanjiang, China, [6]Research Centre for Regenerative Medicine, Department of Orthopedics, The First Affiliated Hospital of Guangxi Medical University, Nanning, China

Background: Autophagy plays a critical role in the progression of osteoarthritis (OA), mainly by regulating inflammatory and immune responses. However, the underlying mechanisms remain unclear. This study aimed to investigate the potential relevance of autophagy-related genes (ARGs) associated with infiltrating immune cells in OA.

Methods: GSE114007, GSE169077, and ARGs were obtained from the Gene Expression Omnibus (GEO) database and the Human Autophagy database. R software was used to identify the differentially expressed autophagy-related genes (DEARGs) in OA. Functional enrichment and protein–protein interaction (PPI) analyses were performed to explore the role of DEARGs in OA cartilage, and then Cytoscape was utilized to screen hub ARGs. Single-sample gene set enrichment analysis (ssGSEA) was used to conduct immune infiltration analysis and evaluate the potential correlation of key ARGs and immune cell infiltration. Then, the expression levels of hub ARGs in OA were further verified by the GSE169077 and qRT-PCR. Finally, Western blotting and immunohistochemistry were used to validate the final hub ARGs.

Results: A total of 24 downregulated genes and five upregulated genes were identified, and these genes were enriched in autophagy, mitophagy, and inflammation-related pathways. The intersection results identified nine hub genes, namely, CDKN1A, DDIT3, FOS, VEGFA, RELA, MAP1LC3B, MYC, HSPA5, and HSPA8. GSE169077 and qRT-PCR validation results showed that only four genes, CDKN1A, DDT3, MAP1LC3B, and MYC, were consistent with the bioinformatics analysis results. Western blotting and immunohistochemical (IHC) showed that the expression of these four genes was significantly downregulated in the OA group, which is consistent with the qPCR results. Immune infiltration correlation analysis indicated that DDIT3 was negatively correlated with immature dendritic cells in OA, and FOS was positively correlated with eosinophils.

Conclusion: CDKN1A, DDIT3, MAP1LC3B, and MYC were identified as ARGs that were closely associated with immune infiltration in OA cartilage. Among them, DDIT3 showed a strong negative correlation with immature dendritic cells. This study found that the interaction between ARGs and immune cell infiltration may play a crucial role in the pathogenesis of OA; however, the specific interaction mechanism needs further research to be clarified. This study provides new insights to further understand the molecular mechanisms of immunity involved in the process of OA by autophagy.

KEYWORDS

osteoarthritis, cartilage, autophagy, immune cell infiltration, bioinformatics analysis

1 Introduction

Osteoarthritis (OA) is a common chronic inflammatory disease in clinical practice, and its development is related to many factors including age, joint damage, and obesity (1). The development is characterized by inflammation, cartilage degeneration, narrowing of the joint space, formation of osteophytes, and sclerosis of the subchondral bone (2). Currently, there is no effective treatment to alleviate the disease. While non-steroidal anti-inflammatory drug (NSAID) interventions mainly address pain and inflammation, OA cannot be prevented. Joint replacement surgery is often a solution for end-stage patients but imposes a significant financial burden (3, 4). Therefore, understanding the molecular mechanisms of OA pathogenesis will provide new ideas for the treatment of OA. The process of OA has been reported to be associated with aging, inflammation, apoptosis, and autophagy (1, 5, 6). Previous studies have shown that the dysfunction of autophagy is a major factor in OA (7). Therefore, identifying novel molecular biological targets is crucial for the in-depth study of the underlying molecular mechanisms by which autophagy regulates the pathogenesis of OA.

Autophagy is an intracellular biological degradation system with highly evolutionary conservative features that slow down the OA process by restoring cellular dysfunction in cartilage (8). Autophagy has great clinical prospects as a potential therapeutic target for OA; however, the specific pathogenesis of OA exacerbated by dysregulated autophagy has not been elucidated. Previous research has indicated that mTOR, LC3-II, Beclin-1, and p62 were associated with OA progression and provide promising therapeutic targets for OA (9, 10). As an important key regulator, mTOR affects autophagic activity and is a key target for the autophagic pathway (8). Microtubule-associated proteins 1A/1B light chain 3B (LC3) are involved in the biosynthesis of autophagosomes. In OA, increased chondrocyte apoptosis was associated with the decrease of LC3 (11). The levels of autophagy-related markers, such as ATG5, LC3-II, and Beclin-1 gene expression, were significantly increased in chondrocytes in the early stage of OA. With the aggravation of the disease, oxidative stress-induced damage increased gradually while decreasing autophagy, resulting in chondrocyte hypertrophy (12). These research data demonstrate that autophagy plays a key role in OA. However, autophagy-related genes (ARGs) in OA development are still largely unknown. Therefore, in-depth exploration of autophagy-related markers in OA through bioinformatics could help identify new potential biomarkers for the treatment of osteoarthritis. In addition, studies have indicated that immune regulation may also play a key role in the pathogenesis of OA (13, 14). Autophagy is an important process in regulating immune responses, which not only eliminates infectious agents and modulates inflammatory responses but also selects antigen presentation and regulates T-cell homeostasis and activation (15, 16). Huang et al. showed that autophagy and immune regulation played different roles in OA and RA, but both are significantly correlated (17). However, few reports have comprehensively investigated the relationship between ARG expression and cartilage immune infiltration in OA and the role of ARGs' biological functions in cartilage immune infiltration. Therefore, we hypothesized that ARGs were differentially expressed in OA and normal cartilage tissues, and the change of autophagy level may related to immune cell infiltration.

In this study, we identified ARGs associated with OA based on OA-related data in the Gene Expression Omnibus (GEO) database. We found the association of the hub genes including *CDKN1A*, *DDIT3*, *MAP1LC3B*, and *MYC* with immune cell infiltration in OA, which was further verified using qRT-PCR, Western blotting, and immunohistochemical staining. Our study hopes to identify ARGs in OA cartilage tissue and then determine whether they regulate OA by modulating immune cell infiltration, which will provide a novel perspective for OA pathogenesis.

2 Materials and methods

2.1 Acquisition of raw data and pre-processing

Two independent human knee articular cartilage tissue mRNA expression profile datasets were downloaded from the GEO database (https://www.ncbi.nlm.nih.gov/geo/). The GSE114007

RNA-seq dataset included 20 OA samples and 18 normal samples from two different platforms, GPL18573 and GPL11154 (18). GSE169077 microarray dataset (GPL96 platform) included six OA samples and five normal samples, which served as a validation dataset for verifying hub genes. Detailed information on the datasets is shown in Table S1. In addition, 222 ARGs were obtained from the HADb database (http://www.autophagy.lu). The workflow of this research is shown in Figure 1.

2.2 Identification of differentially expressed autophagy-related genes

The GSE114007 gene expression of profile was quality assessed using the "factoextra" package (https://cloud.r-project.org/package=factoextra/) in R software before analyzing differentially expressed genes (DEGs) in OA, and sample clustering results suggested that there were large differences between two different platforms (Supplementary Figure S1); therefore, only data from the GPL18573 platform, which included 10 OA samples and 10 normal samples, were taken for subsequent analysis. The counts' data were standardized by the transcripts per kilobase per million mapped reads (TPM), and then the DEGs between OA and normal knee cartilage tissue were screened using the R package "DESeq2" with the threshold set as |log2FoldChange| > 1 and *p*-value <0.05 (19). Subsequently, differentially expressed ARGs (DEARGs) were obtained by intersecting genes between DEGs and ARGs. The Venn diagram drawn through the "VennDiagram" package displayed the number of DEARGs (https://CRAN.R-project.org/package=VennDiagram). Heatmap, volcano plot, and boxplot were drawn through the "pheatmap", "ggplot2", and "ggpubr" packages of R software, respectively.

2.3 Functional enrichment analysis of DEARGs

The Gene Ontology (GO) analysis and Kyoto Encyclopedia of Genes and Genomes (KEGG) pathway enrichment of DEARGs were conducted in the R package "clusterProfiler" (20), and gene IDs were converted using Perl scripts. Molecular function (MF), biological process (BP), and cellular component (CC) constitute the GO annotation. Under the conditions of $p < 0.05$ and $q < 0.05$, GO terms and signaling pathways with significant differences were screened, and then the R software packages "enrichment plot", "ggplot2", and "GOplot" (21) were used to present the results, respectively.

2.4 Correlation analysis and PPI network analysis of DEARGs

The correlation between DEARG was investigated using Spearman's correlation in the "Corrplot" package. The STRING online database (http://string-db.org/) was used to perform the protein–protein interaction (PPI) network analysis and investigate the underlying relationships between DEARGs with an interaction score >0.4, and then Cytoscape (version 3.8.1) was used to analyze and

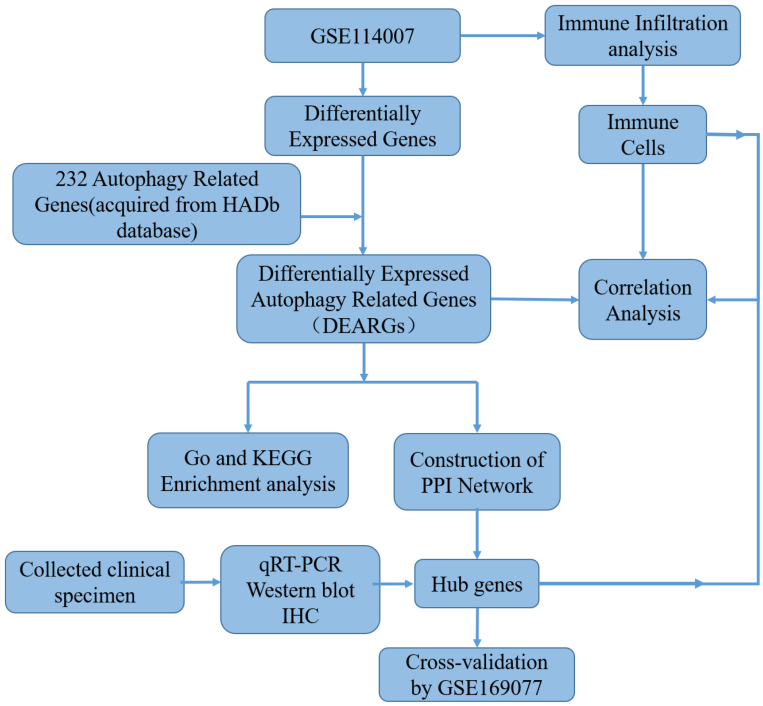

FIGURE 1
The workflow chart of this study.

visualize the screened networks. MCODE and CytoHubba, two plug-ins of Cytoscape, use different algorithms to obtain autophagy-related hub genes. CytoHubba was used to calculate hub genes based on four different algorithms: maximal clique centrality (MCC), degree, closeness, and maximum neighborhood component (MNC). The top 10 genes were screened out of each algorithm as autophagy-related hub genes. Finally, the hub genes of DEARGs were defined as the overlapped genes obtained by five algorithms, and these genes were screened by drawing an UpSet diagram through the R package "UpSetR".

2.5 Immune cell infiltration and correlation analysis

Single-sample gene set enrichment analysis (ssGSEA) was used to analyze the abundance of immune cell infiltration in OA and normal cartilage tissues and identify 28 types of immune cell infiltration (22). Immune cell infiltration between OA and normal samples was compared using the Wilcoxon test, and the results were then visualized by violin diagrams drawn through the "ggplots" package. The correlation analysis of 28 kinds of infiltrating immune cells was performed, and then the results were visualized using the "ggcorrplot" package. Finally, Spearman's correlation analysis was used to analyze the correlation between hub ARGs and the infiltration degree of different immune cells, and the results were visualized using the "ggcorrplot" and "ggstatsplot" packages. Furthermore, CIBERSORT algorithm was also adopted to investigate the immune cell infiltration.(As shown in Supplementary Figure S2).

2.6 Validation of hub gene expression with other osteoarthritis datasets

To understand the expression of these hub ARGs in cartilage, validation was performed on the GSE169077 OA dataset using the "limma" package in R software. The heatmaps and boxplots were performed using the "pheatmap" and "ggplot2" packages in R language.

2.7 Clinical specimen collection and chondrocyte isolation and culture

To confirm the hub ARGs, knee cartilage tissue samples from five cases of OA and five cases of traumatic amputation were collected after obtaining written informed consent from all patients. The study was approved by the Ethics Committee of the First Affiliated Hospital of Guangxi Medical University (Nanning, China) and complied with the tenets of the Declaration of Helsinki.

The fresh cartilage tissues were rinsed with sterile phosphate-buffered saline (PBS) three times and then cut into the size of approximately 0.3–0.5-mm^3 pieces. The tissues were first treated with trypsin/ethylenediaminetetraacetic acid (EDTA) (Solarbio, Beijing, China) at a concentration of 0.25% for 30 min and then digested with collagenase II (Solarbio, Beijing, China) at a concentration of 2 mg/mL for 4 h at 37°C. Dulbecco's Modified Eagle Medium (DMEM; Gibco, Shanghai, China) was used to culture chondrocytes after isolation, which consisted of 10% (v/v) fetal bovine serum (FBS; Tianhang, Zhejiang, China) and 1% (v/v) antibiotics (penicillin 10,000 U/ml and streptomycin 10,000 μg/ml, Solarbio, Beijing, China), cultured at an incubator with 5% CO_2 at 37°C. Passages 2–3 of chondrocytes were used for further experiments. Chondrocytes were divided into two groups: the control group (cultured with normal DMEM) and the treatment group (OA group). Chondrocytes treated with 10 ng/mL IL-1β (Solarbio, Beijing, China) for 24 hours were considered as the OA group. Then, total cellular RNA and protein were collected for further analysis.

2.8 RNA extraction and qRT-PCR

According to the instructions of HiPure Total RNA Mini Kit (Magen, Guangzhou, China), total RNA was extracted from normal and OA group chondrocytes, and then reverse transcription with a Reverse Transcription kit (Takara, Dalian, China) was performed after checking the RNA concentration by a micro-spectrophotometer (Thermo Fisher Scientific, Waltham, MA, USA). The mRNA expression levels of the DNA damage-inducible transcript 3 (*DDIT3*), cyclin-dependent kinase inhibitor 1A (*CDKN1A*), fos proto-oncogene (*FOS*), vascular endothelial growth factor A (*VEGFA*), rela proto-oncogene (*RELA*), heat shock protein family A member 5 (*HSPA5*), microtubule-associated protein 1 light chain 3 beta (*MAP1LC3B*), MYC proto-oncogene (*MYC*), and heat shock protein family A member 8 (*HSPA8*) were analyzed by qRT-PCR. Table 1 shows the primer sequences for the main qRT-PCR used in this study. qRT-PCR was performed as previously reported (23).

2.9 Protein extraction and Western blotting

According to the instructions of RIPA Lysis Buffer (Beyotime, Shanghai, China), total protein was extracted from normal and OA chondrocytes, and then the concentration of the extracted protein was determined by bicinchoninic acid (BCA) protein detection kit (Beyotime, Shanghai, China). The protein samples (40 μg/lane) were then separated by 10% sodium dodecyl sulfate (SDS)–polyacrylamide gels, and the blots were incubated overnight using antibodies against CDKN1A (1:1,000; Beyotime), DDIT3 (1:1,000; Beyotime), MAP1LC3B (1:1,000; Proteintech, Chicago, IL, USA), MYC (1:2,000; Proteintech), and GAPDH (1:5,000; Sangon Biotech, Shanghai, China) at 4°C. After washing with TBST, the membranes were incubated with goat anti-rabbit horseradish peroxidase (HRP)-conjugated secondary antibody (1:5,000; Sangon Biotech) at room temperature for 1 hour. The protein blots were detected with an enhanced chemiluminescence (ECL) system (Beyotime, Shanghai, China), and images were acquired with the Amersham Imager (Cytiva, Uppsala, Sweden). The intensity of these blots was quantified using ImageJ software (NIH, Bethesda, MD, USA).

TABLE 1 Primer sequences used in the qRT-PCR experiments.

Gene	Forward primer (5′–3′)	Reverse primer (3′–5′)
GAPDH	GTCAAGGCTGAGAACGGGAA	AAATGAGCCCCAGCCTTCTC
CDKN1A	CCCGTGAGCGATGGAACT	CCCGTGGGAAGGTAGAGC
DDIT3	ACCAGGAAACGGAAACAG	ACCATTCGGTCAATCAGA
FOS	ACCAGGAAACGGAAACAG	ACCATTCGGTCAATCAGA
RELA	AGAGCAGCGTGGGGACTA	ATGGGATGAGAAAGGACAGG
MAP1LC3B	CAGCATCCAACCAAAATC	CTGTAAGCGCCTTCTAAT
MYC	ATCCTGTCCGTCCAAGCA	CGCACAAGAGTTCCGTAG
HSPA5	TTGCCGTTCAAGGTGGTT	AGCGGTTTCTTTCATTTTAG
HSPA8	GACAACCGAATGGTCAAC	GTACGGAGGCGTCTTACA

2.10 Immunohistochemical analysis

Immunohistochemical (IHC) staining was conducted using a universal two-step detection kit (PV-9000; ZSGB-BIO, Beijing, China) following the manufacturer's instructions. After being dewaxed, the knee articular cartilage tissue slices were placed in EDTA antigen repair solution at 95°C for 15 min for antigen repair. Endogenous peroxidase's activity was blocked with peroxidase blocking reagent for 10 min at room temperature (RT). An appropriate amount of rabbit anti-CDKN1A (1:200; Beyotime), rabbit anti-DDIT3 (1:200; Beyotime), rabbit anti-MAP1LC3B (1:200, Proteintech), and rabbit anti-MYC (1:200, Proteintech) primary antibody working solution was added dropwise on the tissue slices and then incubated in a wet box overnight at 4°C. After rinsing with PBS, the appropriate amount of goat anti-mouse/rabbit IgG polymer labeled with enhanced enzyme was added dropwise on tissue slices and incubated at 37°C for 20 min. Subsequently, the tissue slices were visualized with DAB staining, and then counterstaining was achieved with hematoxylin.

2.11 Statistical analysis

Data are expressed as mean ± standard deviation (SD). Gene expression or protein levels in the two groups of chondrocytes were compared by unpaired Student's t-test or Wilcoxon test. R software (version 4.1.3) and GraphPad Prism 8.0 (San Diego, CA, USA) were used for statistical analysis and plots. All correlation analyses were performed using Spearman's method. Statistical significance required $p < 0.05$ (two-sided).

3 Results

3.1 Differential expression of ARGs in osteoarthritis cartilage

Through differential expression analysis of GPL18573 platform-derived data in the GSE114007 dataset, 2,567 genes were significantly expressed in OA compared with control cartilage tissue based on |log2Fold Change| > 1 with $p < 0.05$. Twenty-nine DEARGs were obtained from 222 ARGs, which intersected with 2,567 DEGs, and five upregulated genes and 24 downregulated genes were screened (Figure 2A, Table 2). Volcano plot and heatmap were used to visualize the expressions of the 29 DEARGs (Figures 2B, C). Furthermore, the boxplot showed 29 DEARG expression patterns in OA compared to control cartilage tissues (Figure 3).

3.2 GO and KEGG enrichment analyses of DEARGs

GO and KEGG pathway enrichment analyses were performed on these DEARGs using R software to explore their potential biological functions and pathways. The results of GO functional analysis revealed that the most significant items of GO enrichment included response to nutrient levels, cellular response to external stimulus, cellular response to extracellular stimulus, and regulation of autophagy (biological process); autophagosome, mitochondrial outer membrane, organelle outer membrane, and outer membrane (cellular component); chaperone binding, ubiquitin-protein ligase binding, ubiquitin-like protein ligase binding, and heat shock protein binding (molecular function) (Figures 4A, B). The results of KEGG pathway enrichment analysis showed that DEARGs were mainly enriched in autophagy, mitophagy, and inflammation-related pathways (Figures 4C, D).

3.3 Correlation analysis and PPI network analysis of DEARGs

Spearman's correlation analysis was used to explore the correlation of these DEARGs in OA. The results of the study indicated an interaction between 29 DEARGs (Figure 5A). A PPI network analysis was performed to determine the interactions between these DEARGs. PPI networks showed that DEARGs were involved in 26 nodes and 77 edges (Figure 5B) and the top 20 interactive genes (Figure 5C). According to the MCODE plug-ins of Cytoscape software, two clusters can be obtained (Figure 5D).

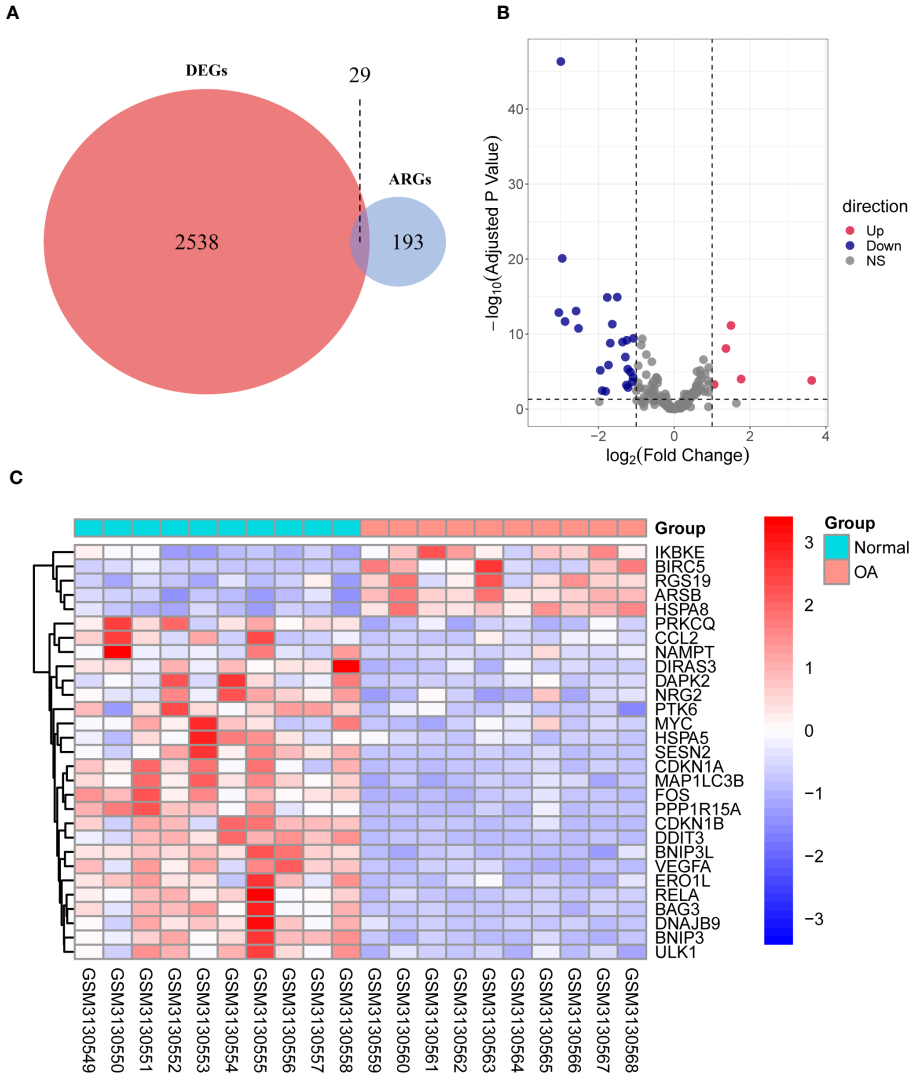

FIGURE 2
Identification of DEARGs. **(A)** Veen diagram showing the DEARGs. **(B)** Volcano plot displaying significantly differentially expressed ARGs. Red dots represent the upregulated genes, and dark purple dots denote the downregulated genes, with thresholds of |log2FoldChange| ≥ 1 and adjusted *p*-value <0.05. **(C)** The expressions of 29 DEARGs in OA are displayed in the heatmap. Red signifies significantly upregulated ARGs, and purple indicates significantly downregulated ARGs in the samples. DEARGs, differentially expressed autophagy-related genes; ARGs, autophagy-related genes; OA, osteoarthritis.

The first cluster consists of 11 genes (FOS, CDKN1A, VEGFA, RELA, DDIT3, PPP1R15A, ERO1L, CDKN1B, DNAJB9, HSPA8, and CCL2), whereas the second cluster involves six genes (BNIP3, MYC, HSPA5, ULK1, BNIP3L, and MAP1LC3B).

Subsequently, the CytoHubba plug-in was used to calculate the PPI network constructed by the 26 DEARGs using four algorithms (MCC, MNC, Degree, and Closeness) and selected the top 10 genes as hub genes (Figures 6A–D). Finally, hub genes obtained by the CytoHubba algorithm were intersected with those calculated using the MCODE algorithm, and nine common hub genes were obtained, which included CDKN1A, DDIT3, FOS, VEGFA, RELA, MAP1LC3B, MYC, HSPA5, and HSPA8 (Figure 6E).

3.4 Validation of the hub DEARGs by microarray dataset

The expression pattern of hub genes was validated based on the GSE169077 dataset. The heatmap showed the expression levels of nine hub genes (Figure 7A). Additionally, as displayed in Figures 7B–J, the expression levels of CDKN1A, DDIT3, VEGFA, RELA, MAP1LC3B, MYC, and HSPA5 in OA cartilage were significantly lower than those in control samples, whereas HSPA8 was significantly upregulated ($p < 0.05$), which was in agreement with bioinformatics analysis of GSE114007 dataset. However, no significant difference was found in FOS expression.

10.3389/fimmu.2023.1263988

TABLE 2 The 29 DEARGs in OA cartilage tissues compared to healthy control.

Gene symbol	log2FC	*p*-Value	Adj.*p*-value	Regulation
CDKN1A	−3.04249	1.18E−15	1.38E−13	Down
DDIT3	−2.99043	5.31E−51	4.64E−47	Down
SESN2	−2.95254	1.92E−23	8.17E−21	Down
FOS	−2.87791	2.31E−14	2.12E−12	Down
PPP1R15A	−2.58655	6.77E−16	8.51E−14	Down
VEGFA	−2.52378	2.48E−13	1.76E−11	Down
DAPK2	−1.94863	5.07E−07	6.87E−06	Down
NAMPT	−1.89816	0.000754	0.003466	Down
CCL2	−1.80804	0.000996	0.004336	Down
BNIP3	−1.76472	7.53E−18	1.31E−15	Down
DIRAS3	−1.73374	8.05E−08	1.37E−06	Down
DNAJB9	−1.68479	4.00E−11	1.64E−09	Down
BAG3	−1.63198	5.76E−14	4.79E−12	Down
CDKN1B	−1.50153	6.82E−18	1.20E−15	Down
RELA	−1.3636	2.77E−11	1.18E−09	Down
ULK1	−1.28682	4.83E−09	1.16E−07	Down
NRG2	−1.26045	0.000102	0.000644	Down
MAP1LC3B	−1.2514	1.44E−11	6.73E−10	Down
ERO1L	−1.22436	3.31E−07	4.75E−06	Down
MYC	−1.21702	0.000244	0.001345	Down
PRKCQ	−1.15477	8.88E−07	1.13E−05	Down
HSPA5	−1.10649	3.21E−05	0.000239	Down
PTK6	−1.08306	5.67E−06	5.50E−05	Down
BNIP3L	−1.07546	7.52E−12	3.74E−10	Down
IKBKE	1.053959	8.04E−05	0.000529	Up
ARSB	1.365099	2.56E−10	8.44E−09	Up
HSPA8	1.498921	9.21E−14	7.24E−12	Up
RGS19	1.765791	1.14E−05	9.97E−05	Up
BIRC5	3.62659	1.86E−05	0.000152	Up

DEARGs, differentially expressed autophagy-related genes; OA, osteoarthritis.

3.5 Assessment of immune cell infiltration and correlation analysis of hub DEARGs and infiltrating immune cells

ssGSEA was applied to explore immune cell infiltration in the OA cartilage. The results are shown in Figure 8A; the proportions of regulatory T cells, activated dendritic cells, central memory CD4 T cells, T follicular helper cell, type 2 helper cell, macrophage, central memory CD8 T cells, gamma delta T cells, and immature dendritic cell were higher in the OA group and lower in the control group. In contrast, the proportions of activated CD56 bright nature killer cells, mast cells, type 17 T helper cells, B cells, eosinophil, and effector memory CD8 T cells were relatively low in the OA group compared to the control group. Subsequently, the correlation of 28 subpopulations of immune cell infiltrate was further analyzed. As shown in Figure 8B, except for immature B cells, a significant correlation was found among infiltrating immune cells. Finally, to explore the relationship between hub DEARGs and infiltrating immune cells, Spearman's correlation analysis was performed (Figure 8C). The results suggest that the most positively correlated autophagy–immunocyte gene pair is FOS–Eosinophil, while the most negatively correlated autophagy–immunocyte gene pair is DDIT3–Immature dendritic cell (Figures 8D, E).

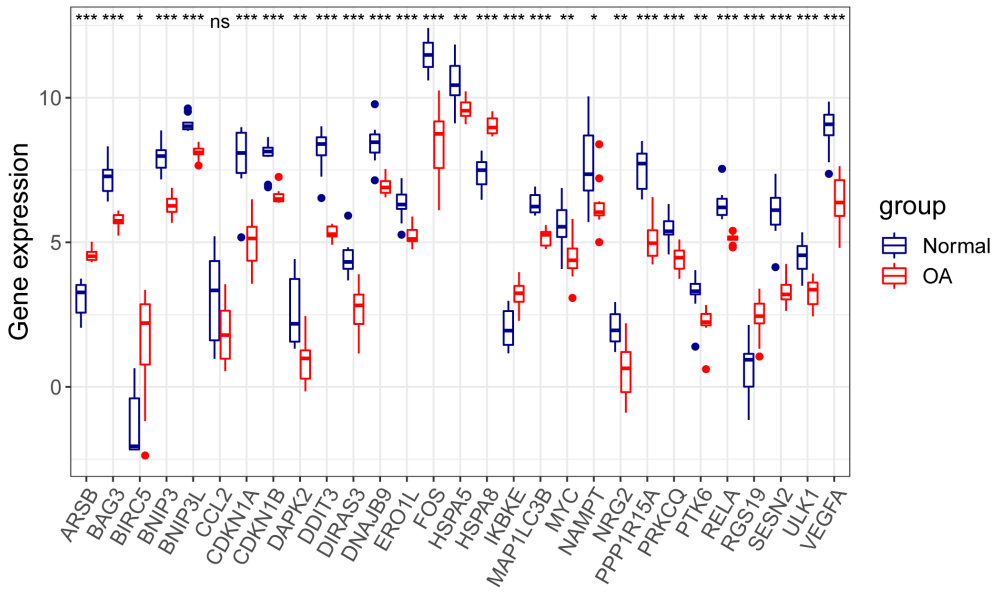

FIGURE 3
Boxplot displaying differential expressed of 29 autophagy-related genes in OA and normal cartilage samples. *p*-Values were calculated using Wilcoxon test. **p* < 0.05; ***p* < 0.01; ****p* < 0.01. ns, not significant; OA, osteoarthritis.

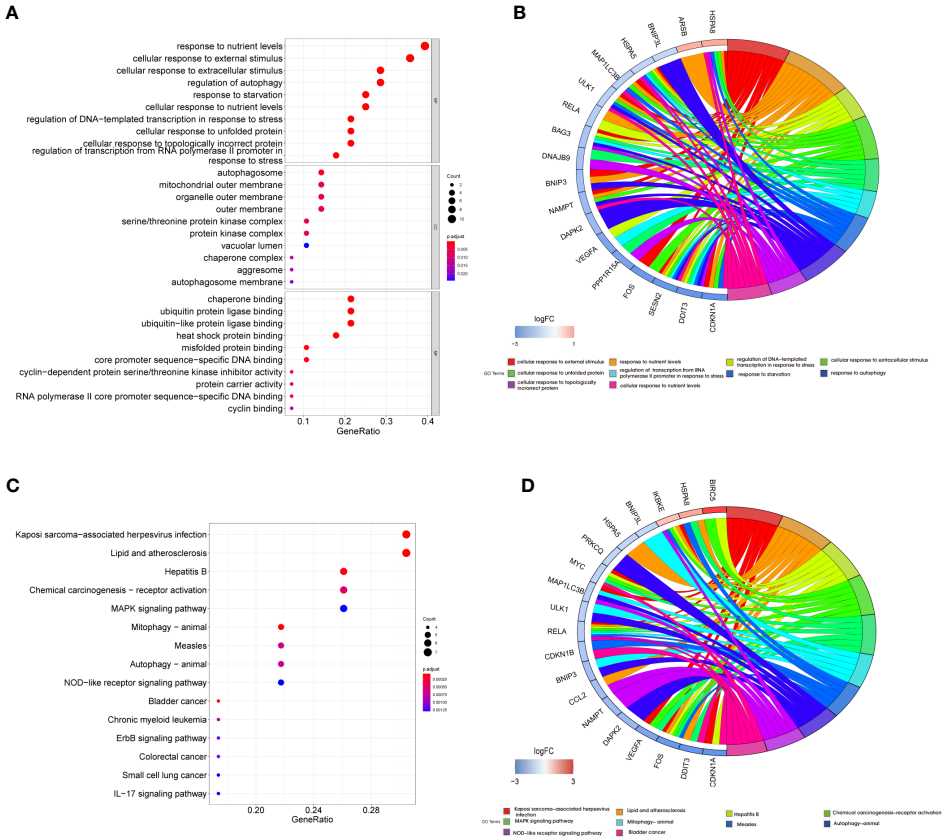

FIGURE 4
Functional enrichment analysis of differentially expressed autophagy-related genes. Bubble plot **(A)** and Circor chart **(B)** of Gene Ontology (GO) enrichment analysis results of 29 DEARGs in biological process (BP), cellular component (CC), and molecular function (MF). Bubble plot **(C)** and Circor chart **(D)** of KEGG pathway enrichment analysis by DEARGs. DEARGs, differentially expressed autophagy-related genes; KEGG, Kyoto Encyclopedia of Genes and Genomes.

10.3389/fimmu.2023.1263988

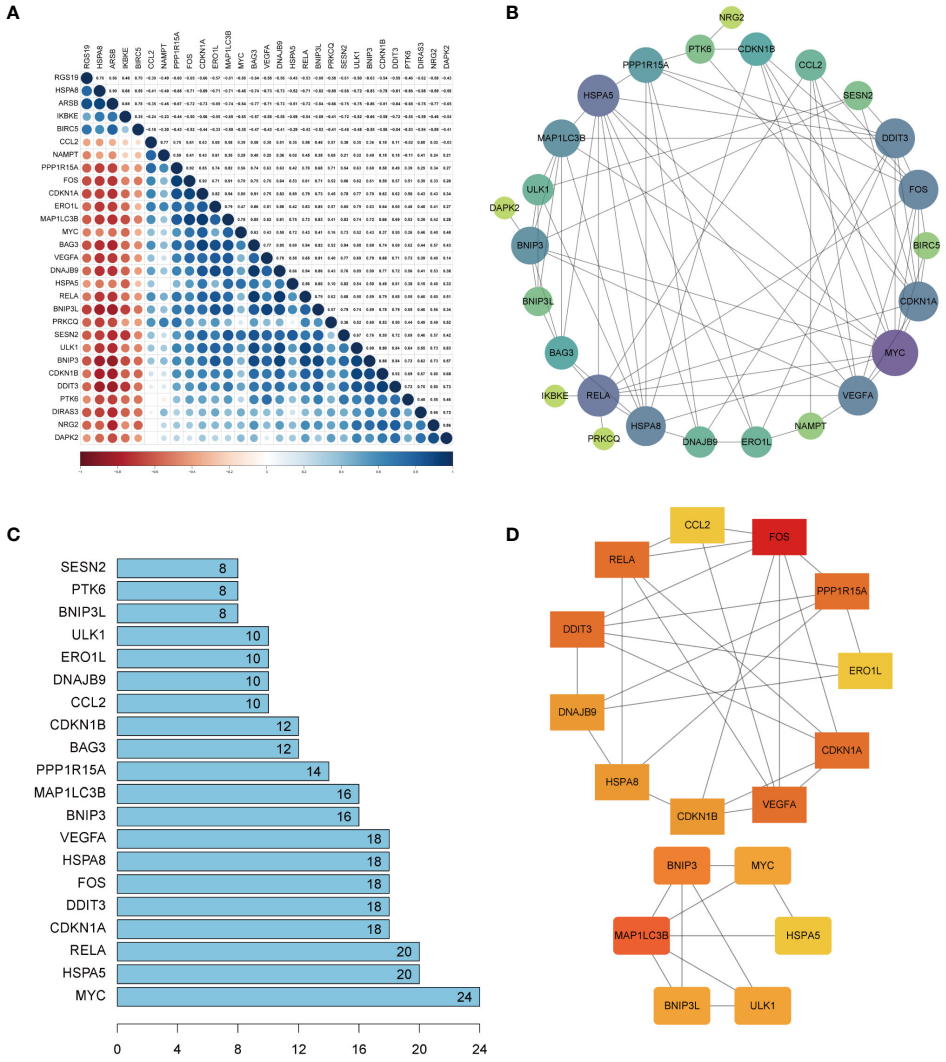

FIGURE 5
Correction analysis and protein–protein interaction (PPI) analysis of the 29 differentially expressed autophagy-related genes. **(A)** Spearman's correction analysis of the 29 differentially expressed autophagy-related genes. **(B)** PPI network of DEARGs; three disconnected nodes were removed. Circle size represents the node degree. **(C)** The interaction number of the top 20 DEARGs. **(D)** Two DEARG clusters were obtained using the MCODE plug-ins. DEARGs, differentially expressed autophagy-related genes.

3.6 Validation of hub DEARGs using an *in vitro* OA cell model

To verify the expression of hub DEARGs in OA chondrocytes, we further performed qRT-PCR and Western blotting. qRT-PCR results showed that the mRNA expressions of *CDKN1A*, *DDIT3*, *FOS*, *MAP1LC3B*, *MYC*, and *HSPA8* were significantly low in the OA group; *HSPA5* and *VEGFA* were significantly highly expressed ($p < 0.05$); and RELA gene expression was not significantly changed compared to normal controls (Figure 9A). Moreover, Western blotting results showed that the expression levels of CDKN1A, DDIT3, MAP1LC3B, and MYC were significantly decreased in the OA group (Figure 9B). Further, the IHC staining showed that compared with the normal group, expressions of CDKN1A, DDIT3, MAP1LC3B, and MYC were low in the OA articular cartilage tissue (Figure 9C).

4 Discussion

OA is the most common chronic degenerative joint disease with limited treatment options, as its etiology has not been fully elucidated (4). Many studies in recent years have demonstrated that autophagy defects contribute to OA and age-related diseases; in contrast, autophagy activation could promote cell survival and reduce the severity of experimental OA (24, 25). However, the relationship between autophagy and OA is currently not fully understood. In addition, ARGs in OA cartilage have not been well explored using bioinformatics analysis. Therefore, we conducted this study to explore whether the expression of ARGs in OA cartilage tissue was significantly different from that in healthy controls. Additionally, we investigated the correlation between ARGs and immune infiltration, which can help understand the

10.3389/fimmu.2023.1263988

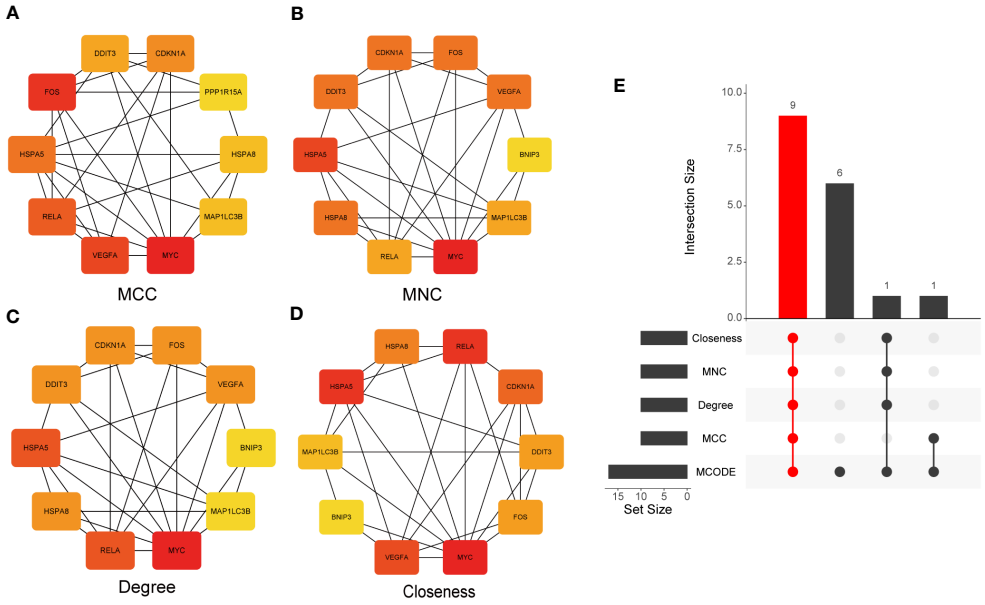

FIGURE 6
Identification of hub genes. **(A–D)** The PPI network constructed by 26 DEARGs was calculated using four algorithms, namely, MCC, MNC, Degree, and Closeness, and the top 10 genes were selected as hub genes. **(E)** UpSet diagram displays the intersection of five different algorithms, resulting in nine shared hub genes. PPI, protein–protein interaction; DEARGs, differentially expressed autophagy-related genes.

potential immune mechanisms of ARGs in cartilage and identify potential molecular targets in OA therapy.

In this study, bioinformatics analysis tools were used to identify ARGs and 29 potential DEARGs associated with OA. Among them, five genes were found to be upregulated in expression and 24 genes were downregulated in expression, as shown in Table 2. After construction using the PPI network, nine key ARGs (*CDKN1A*, *DDIT3*, *FOS*, *VEGFA*, *RELA*, *MAP1LC3B*, *MYC*, *HSPA5*, and *HSPA8*) were differentially expressed in OA cartilage. To understand the potential molecular biological function of DEARGs between OA and normal cartilage, we performed enrichment analysis using GO and KEGG. The enrichment results suggested that these DEARGs play important roles in various biological functions, including autophagy, mitochondrial autophagy, and inflammation-related pathways. In this case, we collected clinical samples to validate the expression of these nine genes. *In vitro*, cellular experiments showed that the expression of four genes, *CDKN1A*, *DDIT3*, *MAP1LC3B*, and *MYC*, were significantly consistent ($p < 0.05$) in bioinformatics analysis. Some ARGs have been previously studied in OA. *CDKN1A* is also known as protein p21. It was shown that *CDKN1A* expression was decreased in OA by inhibiting chondrocyte proliferation (26). Moreover, Huang et al. revealed that in cardiomyocytes, autophagy was inhibited when the expression level of p21 was decreased and that p21 regulates autophagy by interacting with *MAP1LC3B(LC3B)* (27). Yang et al. showed that *DDIT3* knockdown suppressed the autophagy of chondrocytes *in vitro* and *in vivo*, causing a decrease in *LC3B* and *Beclin1* gene expression; however, overexpression of *DDIT3* significantly promoted autophagy *in vitro* (28). In microglia, DEX promotes NLRP3 inflammasome degradation via the autophagy-ubiquitin pathway and reduces *MAP1LC3B* expression, thereby reducing hippocampal inflammation (29). Anti-Dlx5 slows the progression of OA by downregulating the chondrocyte apoptosis-related gene *MYC* (30). These results are consistent with our bioinformatics analysis and experimental results. Moreover, four genes, namely, *CDKN1A*, *DDIT3*, *MAP1LC3B*, and *MYC*, may determine the progression of OA. The specific mechanisms need to be further investigated.

Many publications have reported that the infiltration of immune cells is a key factor in promoting the development of OA (31). For example, immune cells such as neutrophils, M1 macrophages, CD4+ T cells, and mast cells have a significant infiltration in OA synovium, suggesting that immune infiltration is a key target for the treatment of osteoarthritis (31–33). Many immune infiltration studies have been performed in OA synovial tissue, and relatively few immune infiltration studies have been performed in cartilage tissue. Therefore, we comprehensively evaluated the types of immune infiltration cells in OA cartilage tissues using ssGSEA, hoping to explore in-depth the potential mechanisms of immune infiltration in OA cartilage. We performed a correlation analysis of immune cell subsets in normal cartilage tissue and OA samples. It was found that the proportions of the 28 immune cell subpopulations differed significantly between healthy cartilage and OA cartilage samples. The proportion of regulatory T cells, activated dendritic cells, central memory CD4 T cells, T follicular helper cells, type 2 helper cells, macrophage, central memory CD8 T cells, gamma delta T cells, and immature dendritic cells were present in a higher proportion of OA samples compared with healthy controls. In contrast, the fraction of activated CD56 bright nature killer cells, mast cells, type 17 T helper cells, B cells, eosinophils, and effector memory CD8 T cells was lower in OA. Han et al. performed analysis using ssGSEA, MCPcounter, and ESTIMATE software and found that immune scores were significantly lower in normal control samples than in OA samples (34). The discrepancy could be caused by the difference in the methods of analysis and sample

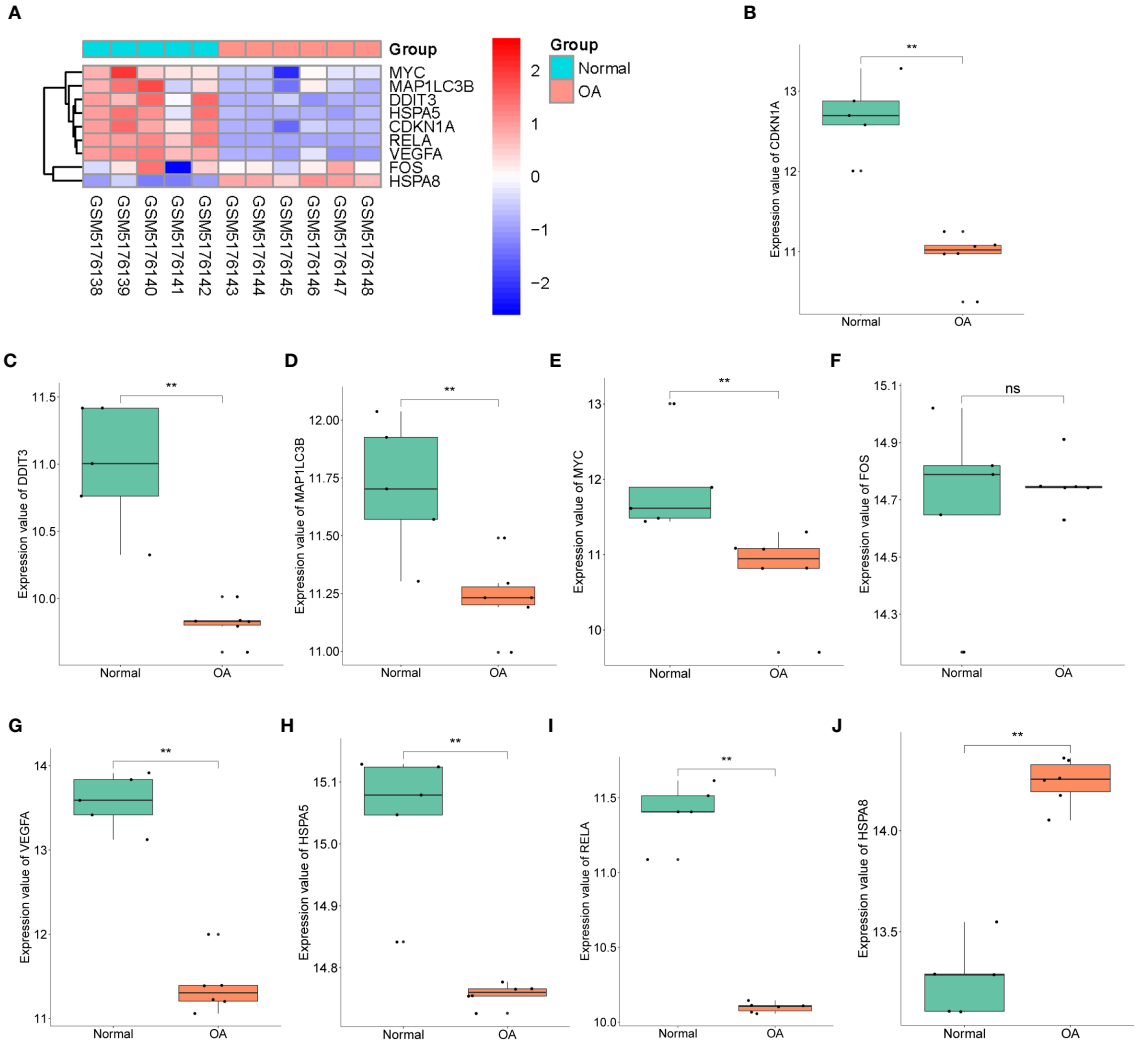

FIGURE 7
Cross-validation of hub genes. **(A)** The expression levels of *CDKN1A*, *DDIT3*, *FOS*, *VEGFA*, *RELA*, *MAP1LC3B*, *MYC*, *HSPA5*, and *HSPA8* were verified by GSE169077 dataset, the results of which are presented as heatmap. **(B–J)** Detailed expression of nine hub genes. $^{**}p < 0.001$. ns, not significant.

numbers. Previous studies have illustrated that the immune system is associated with autophagic pathways, including innate and adaptive immunity, and when autophagy is disturbed, it contributes to the implications of inflammatory diseases (35–37). However, few studies have shown the relationships between ARGs and immune cell infiltration in OA cartilage.

This study also analyzed the potential link between nine key ARGs and infiltrating immune cell subpopulations, contributing to an in-depth understanding of the regulatory role of the ARGs in OA cartilage and also providing new insights into the pathogenesis of OA. Our study showed that *DDIT3* and *FOS* genes were significantly correlated with immune cells, with *FOS* expression being positively associated with eosinophils and *DDIT3* expression being positively associated with immature dendritic cells. It has been reported that *FOS* may treat dermatomyositis by regulating the infiltration of immune cells (38). Deng et al. found that infiltration of eosinophils may be associated with OA progression (32). Dendritic cells (DCs) present a prominent immunomodulatory capacity in innate and adaptive immune responses and are specialized antigen-presenting cells. DCs in OA patients have been reported to secrete large amounts of inflammatory cytokines that exacerbate the inflammatory response (39). However, no report proved the role of eosinophils in OA; in addition, the pairs *FOS*–Eosinophil and *DDIT3*–Immature dendritic cell have also not been investigated in OA. These findings suggest that there may be an interaction between autophagy and the immune response in OA. All of these studies suggest that autophagy and immune infiltration may have a reciprocal regulatory role in OA cartilage. However, more experimental studies may be needed to elucidate in-depth the mechanisms of these ARG–immune cell interactions for validation.

However, this study still has some inevitable limitations. First, we re-mined and analyzed previously published datasets. Second, not multiple datasets but only one dataset was used for cross-validation, and datasets and clinical samples were insufficient in our study, which may lead to deviations in the results. Thus, larger sample sizes are required to confirm our findings. Finally, we simply verified the expression levels of hub DEARGs by qRT-PCR, Western blotting, and IHC staining *in vitro* by collecting clinical samples without in-depth exploration of the underlying

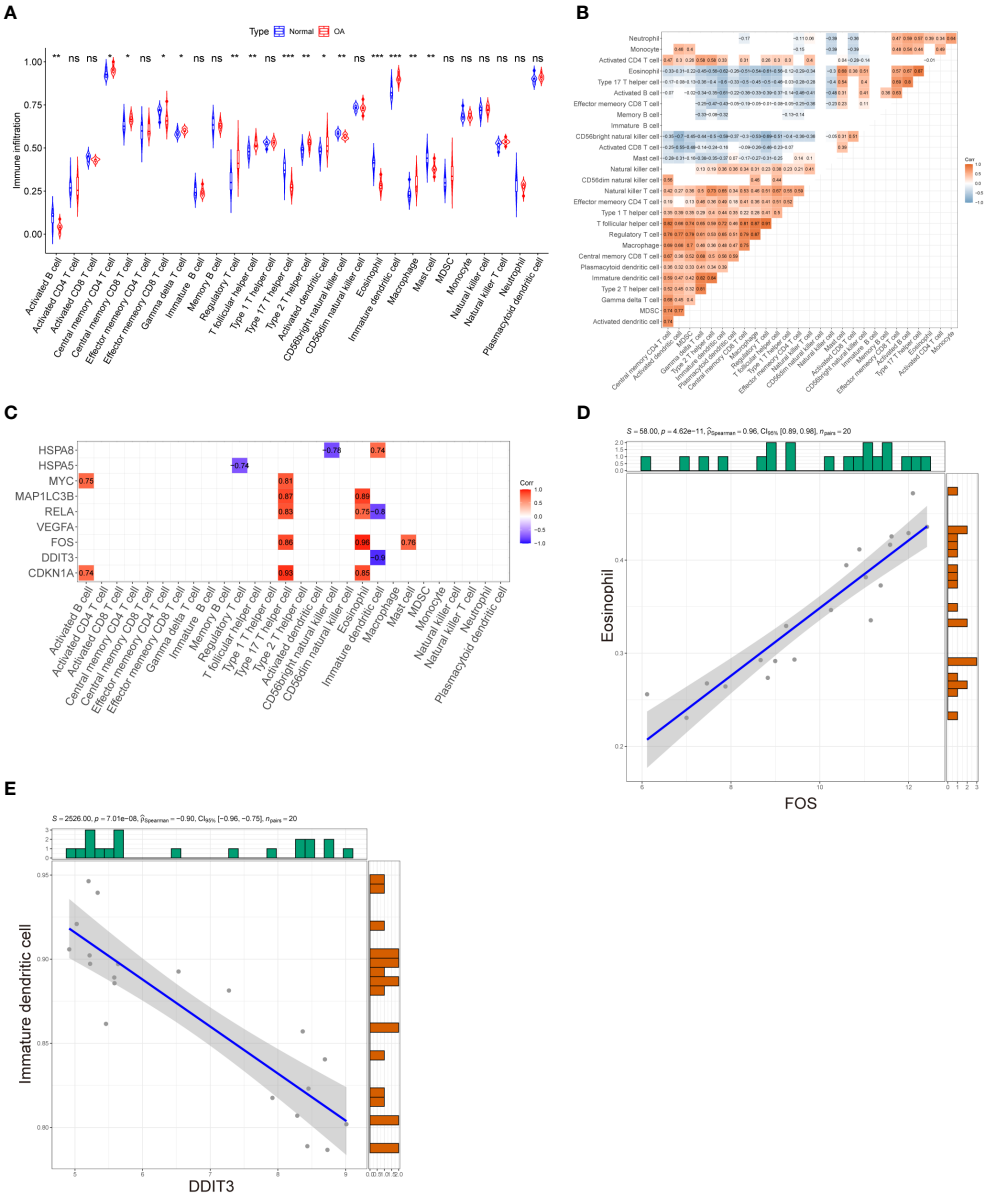

FIGURE 8
Evaluation of immune cell infiltration and correlation analysis between hub genes and immune cell infiltration. **(A)** Violin plot of differential infiltrating fractions of all 28 immune cells between OA and normal samples. **(B)** Spearman's correlation heatmap demonstrates the correlation of all 28 immune cells. The blank squares in the upper left corner represent *p*-values >0.05, red presents a positive correlation, and blue denotes a negative correlation. **(C)** Correlation heatmap displaying the correlations between nine hub genes and 28 infiltrating immune cells. The red and purple squares indicate that the hub genes have a significant correlation with infiltrating immune cells, and the blank squares represent *p*-values >0.05 for the association of hub genes with infiltrating immune cells. **(D)** The most positively correlated autophagy–immunocyte gene pair is FOS–Eosinophil. **(E)** The most negatively correlated autophagy–immunocyte gene pair is DDIT3–Immature dendritic cell. *p*-Values were calculated using the Wilcoxon test. ***$p < 0.001$; **$p < 0.01$; *$p < 0.05$. ns, not significant.

mechanism. Therefore, further studies need to be conducted to reveal the underlying molecular mechanisms.

5 Conclusions

In conclusion, we identified nine key ARGs, namely, CDKN1A, DDIT3, FOS, VEGFA, RELA, MAP1LC3B, MYC, HSPA5, and HSPA8, in OA cartilage tissue by informatics analysis. Verified results confirm that CDKN1A, DDIT3, MAP1LC3B, and MYC could serve as potential biomarkers for OA cartilage tissue. Additionally, the correlation analysis between hub ARGs and immune infiltration in OA cartilage suggested that the interaction between ARGs and immune cell infiltration may be involved in regulating the pathogenesis of OA. Among them, the expression level of DDIT3 showed a strong negative correlation with immature

10.3389/fimmu.2023.1263988

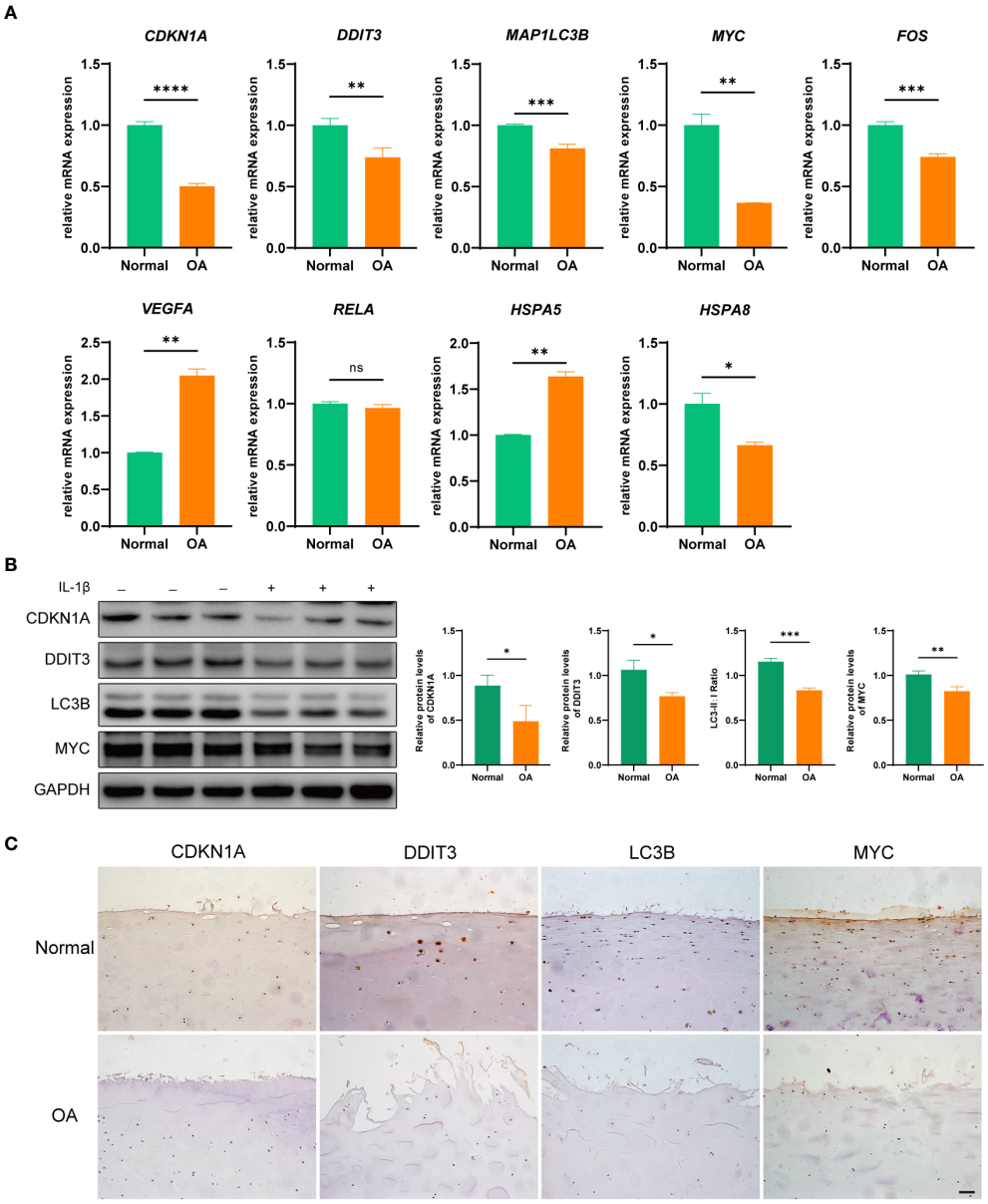

FIGURE 9
Validation of hub DEARGs using an *in vitro* OA cell model. **(A)** Boxplots show mRNA expression levels of nine hub genes that were measured by qRT-PCR in OA and normal chondrocytes. **(B)** The expression levels of CDKN1A, DDIT3, MAPLC3B, and MYC were detected by Western blotting. **(C)** The expression levels of CDKN1A, DDIT3, MAPLC3B, and MYC were detected by IHC. *$p < 0.05$, **$p < 0.01$, ***$p < 0.001$, and ****$p < 0.0001$. ns, not significant; DEARGs, differentially expressed autophagy-related genes; OA, osteoarthritis; IHC, immunohistochemistry. Scale bar, 50 μm.

dendritic cells. The present study revealed that autophagy may regulate the progression of OA by regulating immune infiltration, providing new insights into the molecular immune mechanisms of treating OA.

Data availability statement

The original contributions presented in the study are included in the article/Supplementary Material, further inquiries can be directed to the corresponding author/s.

Ethics statement

The studies involving humans were approved by The Ethics Committee of Guangxi Medical University (NO. 2019-SB-058, 7 Mar. 2019). The studies were conducted in accordance with the local legislation and institutional requirements. Written informed consent for participation in this study was provided by the participants' legal guardians/next of kin.

Author contributions

JQ: Conceptualization, Data curation, Formal Analysis, Methodology, Resources, Software, Validation, Visualization,

Writing – original draft, Writing – review & editing. JZ: Conceptualization, Data curation, Methodology, Resources, Validation, Writing – original draft. J-JW: Conceptualization, Data curation, Software, Validation, Visualization, Writing – review & editing. XR: Data curation, Investigation, Writing – original draft. Q-LZ: Investigation, Writing – original draft. J-MZ: Funding acquisition, Project administration, Supervision, Writing – review & editing. N-HL: Funding acquisition, Project administration, Supervision, Writing – review & editing.

Funding

The author(s) declare financial support was received for the research, authorship, and/or publication of this article. This research was funded by the Guangxi Science and Technology Base and Talent Special Project, grant number GuikeAD19254003; the Guangxi Natural Science Foundation, grant number 2023GXNSFBA026032; the National Natural Science Foundation of China, grant number 81972120; and the Youth Science Foundation of Guangxi Medical University, grant number GXMUYSF202111.

Conflict of interest

The authors declare that the research was conducted in the absence of any commercial or financial relationships that could be construed as a potential conflict of interest.

Publisher's note

Supplementary material

The Supplementary Material for this article can be found online at: https://www.frontiersin.org/articles/10.3389/fimmu.2023.1263988/full#supplementary-material

References

1. Loeser RF, Collins JA, Diekman BO. Ageing and the pathogenesis of osteoarthritis. *Nat Rev Rheumatol* (2016) 12(7):412–20. doi: 10.1038/nrrheum.2016.65

2. Choi WS, Lee G, Song WH, Koh JT, Yang J, Kwak JS, et al. The ch25h-cyp7b1-roralpha axis of cholesterol metabolism regulates osteoarthritis. *Nature* (2019) 566 (7743):254–8. doi: 10.1038/s41586-019-0920-1

3. Gregori D, Giacovelli G, Minto C, Barbetta B, Gualtieri F, Azzolina D, et al. Association of pharmacological treatments with long-term pain control in patients with knee osteoarthritis: A systematic review and meta-analysis. *JAMA* (2018) 320 (24):2564–79. doi: 10.1001/jama.2018.19319

4. Hunter DJ, Bierma-Zeinstra S. Osteoarthritis. *Lancet* (2019) 393(10182):1745–59. doi: 10.1016/s0140-6736(19)30417-9

5. Robinson WH, Lepus CM, Wang Q, Raghu H, Mao R, Lindstrom TM, et al. Low-grade inflammation as a key mediator of the pathogenesis of osteoarthritis. *Nat Rev Rheumatol* (2016) 12(10):580–92. doi: 10.1038/nrrheum.2016.136

6. Castrogiovanni P, Ravalli S, Musumeci G. Apoptosis and autophagy in the pathogenesis of osteoarthritis. *J Invest Surg* (2020) 33(9):874–5. doi: 10.1080/08941939.2019.1576811

7. Giuliani C. The flavonoid quercetin induces ap-1 activation in frtl-5 thyroid cells. *Antioxidants (Basel)* (2019) 8(5):112. doi: 10.3390/antiox8050112

8. Duan R, Xie H, Liu ZZ. The role of autophagy in osteoarthritis. *Front Cell Dev Biol* (2020) 8:608388. doi: 10.3389/fcell.2020.608388

9. Liu J, Fu Q, Liu S. Transcriptional regulation based on network of autophagy identifies key genes and potential mechanisms in human osteoarthritis. *Cartilage* (2021) 13(2_suppl):1431S–41S. doi: 10.1177/1947603520951632

10. Meng Z, Shen B, Gu Y, Wu Z, Yao J, Bian Y, et al. Diazoxide ameliorates severity of experimental osteoarthritis by activating autophagy via modulation of the osteoarthritis-related biomarkers. *J Cell Biochem* (2018) 119(11):8922–36. doi: 10.1002/jcb.27145

11. Carames B, Taniguchi N, Otsuki S, Blanco FJ, Lotz M. Autophagy is a protective mechanism in normal cartilage, and its aging-related loss is linked with cell death and osteoarthritis. *Arthritis Rheum* (2010) 62(3):791–801. doi: 10.1002/art.27305

12. Yue J, Aobulikasimu A, Sun W, Liu S, Xie W, Sun W. Targeted regulation of foxo1 in chondrocytes prevents age-related osteoarthritis via autophagy mechanism. *J Cell Mol Med* (2022) 26(11):3075–82. doi: 10.1111/jcmm.17319

13. Rollin R, Marco F, Jover JA, Garcia-Asenjo JA, Rodriguez L, Lopez-Duran L, et al. Early lymphocyte activation in the synovial microenvironment in patients with osteoarthritis: comparison with rheumatoid arthritis patients and healthy controls. *Rheumatol Int* (2008) 28(8):757–64. doi: 10.1007/s00296-008-0518-7

14. Martel-Pelletier J, Barr AJ, Cicuttini FM, Conaghan PG, Cooper C, Goldring MB, et al. Osteoarthritis. *Nat Rev Dis Primers* (2016) 2(1):16072. doi: 10.1038/nrdp.2016.72

15. Germic N, Frangez Z, Yousefi S, Simon HU. Regulation of the innate immune system by autophagy: monocytes, macrophages, dendritic cells and antigen presentation. *Cell Death Differ* (2019) 26(4):715–27. doi: 10.1038/s41418-019-0297-6

16. Valdor R, Macian F. Autophagy and the regulation of the immune response. *Pharmacol Res* (2012) 66(6):475–83. doi: 10.1016/j.phrs.2012.10.003

17. Huang RZ, Zheng J, Liu FL, Li QL, Huang WH, Zhang DM, et al. A novel autophagy-related marker for improved differential diagnosis of rheumatoid arthritis and osteoarthritis. *Front Genet* (2021) 12:743560. doi: 10.3389/fgene.2021.743560

18. Fisch KM, Gamini R, Alvarez-Garcia O, Akagi R, Saito M, Muramatsu Y, et al. Identification of transcription factors responsible for dysregulated networks in human osteoarthritis cartilage by global gene expression analysis. *Osteoarthritis Cartilage* (2018) 26(11):1531–8. doi: 10.1016/j.joca.2018.07.012

19. Love MI, Huber W, Anders S. Moderated estimation of fold change and dispersion for rna-seq data with deseq2. *Genome Biol* (2014) 15(12):550. doi: 10.1186/s13059-014-0550-8

20. Wu T, Hu E, Xu S, Chen M, Guo P, Dai Z, et al. Clusterprofiler 4.0: A universal enrichment tool for interpreting omics data. *Innovation (N Y)* (2021) 2(3):100141. doi: 10.1016/j.xinn.2021.100141

21. Walter W, Sanchez-Cabo F, Ricote M. Goplot: an R package for visually combining expression data with functional analysis. *Bioinformatics* (2015) 31 (17):2912–4. doi: 10.1093/bioinformatics/btv300

22. Charoentong P, Finotello F, Angelova M, Mayer C, Efremova M, Rieder D, et al. Pan-cancer immunogenomic analyses reveal genotype-immunophenotype relationships and predictors of response to checkpoint blockade. *Cell Rep* (2017) 18 (1):248–62. doi: 10.1016/j.celrep.2016.12.019

23. Lu Z, Lei D, Jiang T, Yang L, Zheng L, Zhao J. Nerve growth factor from chinese cobra venom stimulates chondrogenic differentiation of mesenchymal stem cells. *Cell Death Dis* (2017) 8(5):e2801. doi: 10.1038/cddis.2017.208

24. Carames B, Hasegawa A, Taniguchi N, Miyaki S, Blanco FJ, Lotz M. Autophagy activation by rapamycin reduces severity of experimental osteoarthritis. *Ann Rheum Dis* (2012) 71(4):575–81. doi: 10.1136/annrheumdis-2011-200557

25. Lopez de Figueroa P, Lotz MK, Blanco FJ, Carames B. Autophagy activation and protection from mitochondrial dysfunction in human chondrocytes. *Arthritis Rheumatol* (2015) 67(4):966–76. doi: 10.1002/art.39025

26. Gang X, Xu H, Si L, Zhu X, Yu T, Jiang Z, et al. Treatment effect of cdkn1a on rheumatoid arthritis by mediating proliferation and invasion of fibroblast-like synoviocytes cells. *Clin Exp Immunol* (2018) 194(2):220–30. doi: 10.1111/cei.13161

27. Huang S, Xu M, Liu L, Yang J, Wang H, Wan C, et al. Autophagy is involved in the protective effect of P21 on lps-induced cardiac dysfunction. *Cell Death Dis* (2020) 11(7):554. doi: 10.1038/s41419-020-02765-7

28. Yang C, Xu X, Dong X, Yang B, Dong W, Luo Y, et al. Ddit3/chop promotes autophagy in chondrocytes via sirt1-akt pathway. *Biochim Biophys Acta Mol Cell Res* (2021) 1868(9):119074. doi: 10.1016/j.bbamcr.2021.119074

29. Zhang L, Xiao F, Zhang J, Wang X, Ying J, Wei G, et al. Dexmedetomidine mitigated nlrp3-mediated neuroinflammation via the ubiquitin-autophagy pathway to improve perioperative neurocognitive disorder in mice. *Front Pharmacol* (2021) 12:646265. doi: 10.3389/fphar.2021.646265

30. Lu Y, Zhang C, Jiang S, Yuan F. Anti-dlx5 retards the progression of osteoarthritis through inhibiting chondrocyte hypertrophy and apoptosis. *Evid Based Complement Alternat Med* (2022) 2022:5019920. doi: 10.1155/2022/5019920

31. Yuan WH, Xie QQ, Wang KP, Shen W, Feng XF, Liu Z, et al. Screening of osteoarthritis diagnostic markers based on immune-related genes and immune infiltration. *Sci Rep* (2021) 11(1):7032. doi: 10.1038/s41598-021-86319-7

32. Deng YJ, Ren EH, Yuan WH, Zhang GZ, Wu ZL, Xie QQ. Grb10 and E2f3 as diagnostic markers of osteoarthritis and their correlation with immune infiltration. *Diagnostics (Basel)* (2020) 10(3):171. doi: 10.3390/diagnostics10030171

33. Cai W, Li H, Zhang Y, Han G. Identification of key biomarkers and immune infiltration in the synovial tissue of osteoarthritis by bioinformatics analysis. *PeerJ* (2020) 8:e8390. doi: 10.7717/peerj.8390

34. Han Y, Wu J, Gong Z, Zhou Y, Li H, Wang B, et al. Identification and development of a novel 5-gene diagnostic model based on immune infiltration analysis of osteoarthritis. *J Transl Med* (2021) 19(1):522. doi: 10.1186/s12967-021-03183-9

35. Deretic V. Autophagy in inflammation, infection, and immunometabolism. *Immunity* (2021) 54(3):437–53. doi: 10.1016/j.immuni.2021.01.018

36. Deretic V, Levine B. Autophagy balances inflammation in innate immunity. *Autophagy* (2018) 14(2):243–51. doi: 10.1080/15548627.2017.1402992

37. Levine B, Mizushima N, Virgin HW. Autophagy in immunity and inflammation. *Nature* (2011) 469(7330):323–35. doi: 10.1038/nature09782

38. Wang L, Fang D, Liu Y. Autophagy-related genes are potential diagnostic biomarkers for dermatomyositis. *Ann Transl Med* (2022) 10(4):228. doi: 10.21037/atm-22-70

39. Alahdal M, Zhang H, Huang R, Sun W, Deng Z, Duan L, et al. Potential efficacy of dendritic cell immunomodulation in the treatment of osteoarthritis. *Rheumatol (Oxford)* (2021) 60(2):507–17. doi: 10.1093/rheumatology/keaa745

frontiers | Frontiers in Immunology

TYPE Original Research
PUBLISHED 06 February 2024
DOI 10.3389/fimmu.2024.1297454

OPEN ACCESS

EDITED BY
Chao Yang,
Zhejiang Ocean University, China

REVIEWED BY
Wuu-Tsun Perng,
National Pingtung University of Science and Technology, Taiwan
Jiarui Cui,
Shanghai University of Traditional Chinese Medicine, China

*CORRESPONDENCE
Hongfeng Sheng
hongfeng_sheng@hotmail.com

†These authors have contributed equally to this work and share first authorship

RECEIVED 20 September 2023
ACCEPTED 23 January 2024
PUBLISHED 06 February 2024

CITATION
Lu Y, Lu D, Zhang H, Li H, Yu B, Zhang Y, Hu H and Sheng H (2024) Causality between Ankylosing Spondylitis and osteoarthritis in European ancestry: a bidirectional Mendelian randomization study.
Front. Immunol. 15:1297454.
doi: 10.3389/fimmu.2024.1297454

Causality between Ankylosing Spondylitis and osteoarthritis in European ancestry: a bidirectional Mendelian randomization study

Yangguang Lu[1†], Di Lu[2†], Hongzhi Zhang[1], Haoyang Li[1], Bohuai Yu[1], Yige Zhang[1], Hantao Hu[1] and Hongfeng Sheng[2*]

[1]The First School of Medicine, School of Information and Engineering, Wenzhou Medical University, Wenzhou, China, [2]Department of Orthopedics, Tongde Hospital of Zhejiang Province, Hangzhou, China

Objective: To explore the bidirectional causal relationship between Ankylosing Spondylitis (AS) and Osteoarthritis (OA) at the genetic level within the European ancestry.

Methods: We implemented a series of quality control steps to select instrumental variables (IVs) related to the exposure. We conducted two-sample Mendelian randomization (MR) using the inverse-variance weighted method as the primary approach. We adjusted significance levels using Bonferroni correction, assessed heterogeneity using Cochrane's Q test. Sensitivity analysis was conducted through leave-one-out method. Additionally, external datasets and relaxed IV selection criteria were employed, and multivariate MR analyses were performed for validation purposes. Finally, Bayesian colocalization (COLOC) analysis identified common genes, validating the MR results.

Results: The investigation focused on the correlation between OA and AS in knee, hip, and hand joints. MR results revealed that individuals with AS exhibit a decreased risk of knee OA (OR = 0.9882, 95% CI: 0.9804-0.9962) but no significant increase in the risk of hip OA (OR = 0.9901, 95% CI: 0.9786-1.0018). Conversely, AS emerged as a risk factor for hand OA (OR = 1.0026, 95% CI: 1.0015-1.0036). In reverse-direction MR analysis, OA did not significantly influence the occurrence of AS. Importantly, minimal heterogeneity was observed in our MR analysis results ($p > 0.05$), and the robustness of these findings was confirmed through sensitivity analysis and multivariate MR analysis. COLOC analysis identified four colocalized variants for AS and hand OA (rs74707996, rs75240935, rs181468789, and rs748670681).

Conclusion: In European population, individuals with AS have a relatively lower risk of knee OA, whereas AS serves as a risk factor for hand OA. However, no significant causal relationship was found between AS and hip OA. Additionally, it offers novel insights into genetic research on AS and OA.

KEYWORDS

Ankylosing Spondylitis, osteoarthritis, Mendelian randomization, genetic analyses, orthopedics, inflammation

1 Introduction

Osteoarthritis (OA) is a prevalent chronic degenerative joint disease with an unclear etiology, exerting a substantial global impact (1, 2), and serving as a significant contributor to disability (3). It predominantly affects the hip and knee joints, characterized by progressive deterioration of articular cartilage, subchondral bone remodeling, chondrocyte hypertrophy, and synovial inflammation (4, 5). This condition imposes a considerable burden on healthcare resources, affecting over 500 million people worldwide, which is approximately 7% of the world's population (6). The incidence of OA is rising due to aging demographics and the prevalence of obesity (7). Additionally, the financial burden on OA patients is increasing (8), particularly in Western nations, where it accounts for an estimated 1% to 2.5% of the gross domestic product (9). For individuals with mild to moderate OA, conservative treatments are available, but their specific efficacy remains contentious (10). In advanced cases, total joint replacement surgery is a mature option, yet not all patients are suitable candidates, and post-operative complications can occur (11). OA is a complex condition influenced by multiple factors, including trauma, metabolism, biological stress, and genetic susceptibility (12, 13). Despite ongoing research, the precise mechanisms underlying OA pathogenesis remain incompletely elucidated. Therefore, a better understanding of its etiology and early prevention and treatment strategies is crucial.

Ankylosing spondylitis (AS) is an immune-mediated inflammatory arthritis characterized by a strong genetic predisposition, primarily affecting the axial skeleton, leading to sacroiliac joint damage, fusion, vertebral ankylosis, and the classic bamboo spine appearance, along with functional impairment and a reduced quality of life (14–16). AS predominantly affects young males, with about three-quarters of patients experiencing initial symptoms before the age of 30 (17). Research indicates that the highest risk of AS diagnosis occurs between the ages of 30 and 40, with common symptoms manifesting as non-specific back pain in the lower back and buttocks (18). Moreover, AS can also induce peripheral symptoms in the knees, hands, and feet, resembling rheumatoid arthritis (16). This can lead to misdiagnosis and delayed appropriate treatment, resulting in a frequently delayed diagnosis by 5 to 10 years (18).

Previous research has indicated that inflammation in AS may accumulate, potentially increasing the risk of secondary OA (19). Notably, the hip and knee joints, being the largest weight-bearing joints in the human body, are commonly affected by AS among peripheral joint. A cohort study conducted in Taiwan found a notably higher incidence of OA in male AS patients, who also showed a higher frequency of undergoing total hip replacement surgery (THRS) and total knee replacement surgery (TKRS) (19). A possible explanation for this phenomenon is that peripheral joint inflammation in AS results from the migration of HLA-B27 positive immune cells into the joints, triggering a local inflammatory response (20). Understanding the intricate relationship between AS and OA could pave the way for more precise prevention and treatment strategies. Nevertheless, the exact association between AS and OA remains unclear, necessitating further evidence for substantiation.

Mendelian randomization (MR) studies make use of genetic variations, such as single nucleotide polymorphisms (SNPs), which naturally occur during meiosis. This approach minimizes confounding factors and reverse causation bias in epidemiological research, as genetic variations precede disease onset (21). Consequently, MR studies enable the exploration of bidirectional causal relationships between OA and AS. In light of this, we conducted a bidirectional two-sample MR study to investigate the potential causal link between AS and OA at different anatomical sites.

2 Materials and methods

2.1 Study design

This study adhered to the Strengthening the Reporting of Observational Studies in Epidemiology Using Mendelian Randomization (STROBE-MR) guidelines (21). We utilized summary data from genome-wide association studies (GWAS) on AS and OA to select suitable NPs as instrumental variables (IVs) for MR analysis. Our objective was to investigate bidirectional causal relationships between AS and OA. The application of IVs in MR analysis relies on satisfying three critical assumptions: (i) the chosen IVs exhibit a robust association with the exposure of interest, (ii) there is no confounding of the IVs with factors influencing the outcome apart from the exposure, and (iii) the selected IVs solely influence the outcome through the exposure (22). Since all data were derived from previously published studies and public databases, no additional ethical approval was required.

2.2 GWAS summary data for AS

Genetic data for AS were obtained from the FinnGen consortium (https://r9.finngen.fi/, last accessed on September 2, 2023). The study cohort consisted of individuals of European descent who provided informed consent. The FinnGen research project integrated genetic data related to disease endpoints from the Finnish Biobank and Finnish Health Registry, encompassing a total of 2,860 AS patients and 270,964 healthy controls. Case identification was based on codes from the Tenth Revision of the International Classification of Diseases (ICD-10). Detailed information regarding participant characteristics, genotyping, imputation, and quality control can be found on the FinnGen website (https://finngen.gitbook).

To address potential population-specific limitations in the AS data from the FinnGen consortium and further validate our findings, we conducted a replication analysis using summary data from a genome-wide association study for AS published by the International Genetics of Ankylosing Spondylitis (IGAS) consortium (23) in 2013. This dataset consisted of European population cohorts, including 9,069 AS cases and 13,578 healthy controls, all of whom provided informed consent. Case definitions were based on ICD-10 codes. A comprehensive description of the study procedures is available in previously published research (23).

2.3 GWAS summary data for OA

We obtained summary genetic data for OA from the largest sample GWAS meta-analysis of OA, conducted by Dr. Cindy G. Boer et al. (24) in 2021. This extensive study incorporated data from 13 international OA cohorts. Our focus was on extracting relevant GWAS information related to knee OA, hip OA, and hand OA. The dataset included 62,497 cases and 333,557 healthy controls for knee OA, 36,445 cases and 316,943 healthy controls for hip OA, and 20,901 cases and 282,881 healthy controls for hand OA. The majority of participants were of European descent and provided informed consent. Case definitions were based on ICD-10 codes. Comprehensive research procedure details are available in the published study (24). Importantly, there was no overlap in populations between our study and the two cohorts related to AS.

2.4 Instrumental variable selection

To ensure the robustness and reliability of our MR analysis, we implemented a rigorous selection process for instrumental variables (IVs). Firstly, we identified SNPs closely associated with the exposure ($p < 5 \times 10^{-8}$). Secondly, we eliminated linkage disequilibrium (LD) between SNPs, as strong LD can introduce bias ($r^2 < 0.001$, clumping distance = 10,000 kb). In cases of LD genetic variants, we chose the variant with the lowest p-value associated with the exposure. Subsequently, we filtered out SNPs with an $F > 10$ to ensure a strong correlation between IVs and the exposure, excluding weak instrumental variables. Finally, we manually screened and removed SNPs associated with confounding factors and OA outcomes using the PhenoScanner database (http://www.phenoscanner.medschl.cam.ac.uk/, accessed on September 3, 2023). If multiple SNPs were missing in GWAS results, we searched for proxies using the LDlink online platform (https://ldlink.nci.nih.gov/, accessed on September 3, 2023). Any replaced SNPs were excluded from the final MR analysis.

We identified 10 SNPs associated with AS in the FinnGen consortium dataset. One SNP (rs181316459) was excluded due to its status as a proxy SNP, and no other SNPs were proxied (Table 1). To enhance the sensitivity of positive results, a sensitivity analysis was conducted on this dataset by relaxing the instrumental variables (IVs) selection criteria ($p < 1 \times 10^{-6}$, $r^2 < 0.001$, $F > 10$). This analysis identified 41 additional SNPs. In the IGBS consortium dataset, we identified 24 SNPs associated with AS (23). One SNP (rs130075) lacked the necessary information for MR testing, and one SNP (rs2517655) was missing from the results. Since the SNP missing rate fell within an acceptable range and to maintain population stability, proxy SNPs were not sought. Furthermore, in the dataset from Dr. Boer et al. (24), we identified 24 SNPs associated with knee OA, 33 SNPs with Hip OA, and 8 SNPs with hand OA. None of these were proxied.

2.5 Mendelian Randomization analysis

Our primary analytical method for assessing the correlation between exposure and outcomes was Inverse Variance Weighting (IVW). This method provides accurate estimates when all IVs are valid (25). In addition, we employed MR-Egger regression and the weighted median as supplementary analytical methods. MR-Egger regression is capable of detecting and adjusting for pleiotropy, although it tends to produce estimates with lower precision (22). The weighted median approach provides accurate estimates, assuming that at least 50% of IVs are valid (26). We presented our results in the form of odds ratios (ORs) and 95% confidence intervals (CIs). To gauge heterogeneity, we utilized Cochrane's Q test and quantified it with I^2. Heterogeneity was considered absent when I^2 was below 25% and mild when it was below 50%. We assessed potential horizontal pleiotropy through the intercept of MR-Egger regression and MR pleiotropy residual sum and outlier (MR-PRESSO) (22, 27). To ensure the robustness of our results, we conducted a sensitivity analysis using the leave-one-out method to identify SNPs that might exert potential influence. We also assessed the robustness of positive findings by either relaxing the IV selection criteria ($p < 1 \times 10^{-6}$, $r^2 < 0.001$, $F > 10$) to obtain more IVs or

TABLE 1 Extraction of instrumental SNPs for Mendelian randomization analysis from the GWAS study of ankylosing spondylitis.

SNP	Position	A1	A2	EAF	Beta	SE	*p*-value
rs10456271	6:23108189	T	C	0.0118	0.4553	0.0676	1.61E-11
rs10807943	7:5301033	C	T	0.1028	-0.3737	0.0494	3.77E-14
rs114799031	6:28185504	T	A	0.9747	1.2742	0.0364	8.28E-269
rs13192159	6:25583940	T	C	0.1809	0.5337	0.0315	2.50E-64
rs142695953	7:5804237	A	C	0.1391	0.2147	0.0323	7.38E-11
rs2032890	5:96785448	C	A	0.6996	-0.2432	0.0312	6.97E-15
rs6759003	2:62332070	C	T	0.3609	-0.1880	0.0277	1.12E-11
rs72749142	1:200982179	A	G	0.1677	-0.2353	0.0411	1.04E-08
rs78724843	6:35948243	A	C	0.0334	0.6199	0.0537	9.54E-31
rs9461388	6:27522650	C	T	0.9705	-0.5790	0.0957	1.44E-09

A1, Effect allele; A2, Other allele; EAF, Effect allele frequency; SE, Standard error.

performing MR analysis using another GWAS cohort for result validation (Figure 1). Moreover, given previous research highlighting the genetic correlation between OA occurrence and body mass index (BMI) (28), we conducted an additional multivariate MR analysis using summary data from the FinnGen R9, where BMI served as the exposure variable. This supplementary analysis was undertaken to disentangle the potential influence of BMI, providing a more comprehensive understanding of its impact on the observed associations.

Considering that our analyses encompassed three different OA sites, we took a conservative approach to address multiple testing. Specifically, we applied Bonferroni correction to the significance level, setting a threshold at 0.05 divided by 3 (i.e., 0.0167). Consequently, *p*-values less than 0.05 but above the Bonferroni-corrected significance threshold were deemed as potential evidence of association (29). For all other tests, *p*-values less than 0.05 were considered statistically significant. We conducted the statistical analyses using R version 4.3.2 and the "TwoSampleMR" package.

2.6 Colocalization analysis

To further validate the results of MR and explore the genetic connections between AS and OA, we conducted Bayesian colocalization (COLOC) analysis based on GWAS summary statistics of AS and OA. The data were sourced from FinnGen R9 and the study conducted by Dr. Boer et al. (24). COLOC analysis, a statistical method rooted in GWAS data, employs single-variant summary statistics to assess whether two independently associated genetically correlated traits share a common genetic locus. In this analysis, we assigned a prior probability of 1×10^{-6} to the random variable having a causal relationship with both GWAS datasets. This value indicates a sufficiently high posterior probability (PP4 > 0.8) for a single shared variant between AS and OA (30). We conducted this statistical analyses using R version 4.3.2 and the "coloc" package.

3 Results

3.1 MR analysis

Our analysis using the random-effects IVW model yielded insightful findings. Individuals with AS exhibited a relatively lower risk of knee OA (OR = 0.9883, 95% CI: 0.9804-0.9962, p = 0.0040). However, AS did not significantly affect the occurrence of hip OA (OR = 0.9901, 95% CI: 0.9786-1.0018, p = 0.0965). In contrast, AS was identified as a risk factor for Hand OA (OR = 1.0026, 95% CI: 1.0015-1.0036, p < 0.0001) (Figure 2). When assessing the impact of AS on knee OA, both IVW and Weighted Median models provided consistent results. Although MR-Egger regression did not indicate significant outcomes, a persistent trend toward a lower risk of knee OA in individuals with AS was observed (Figure 3A). For the evaluation of AS on hip OA, all three test models yielded similar results (Figure 3B). In the assessment of AS on hand OA, the IVW and Weighted Median models produced consistent outcomes, while MR-Egger resulted in nonsignificant results (Figure 3C).

The results of Cochrane's Q test demonstrated no heterogeneity in the MR analysis between AS and knee OA (Figure 3D) (p = 0.2620, I^2= 19.67%). For hip OA (Figure 3E), there was only mild heterogeneity (p = 0.1180, I^2 = 36.27%). However, a moderate level of heterogeneity was observed in the MR analysis between AS and hand OA (Figure 3F) (p = 0.0007, I^2 = 68.90%). Importantly, both MR Egger intercept tests and MR-PRESSO distortion tests indicated the absence of horizontal pleiotropy between AS and OA at all three sites (p > 0.05) (Table 2).

3.2 Reverse-direction MR analysis

In the reverse-direction MR analysis, the random-effects IVW model revealed that knee OA (OR = 0.8561, 95% CI: 0.6682-1.0968, p = 0.2191), hip OA (OR = 0.9431, 95% CI: 0.8078-1.1011, p = 0.4586), and hand OA (OR = 0.9335, 95% CI: 0.7112-1.2251, p = 0.6196) did not significantly influence the occurrence of AS. In fact, across all MR

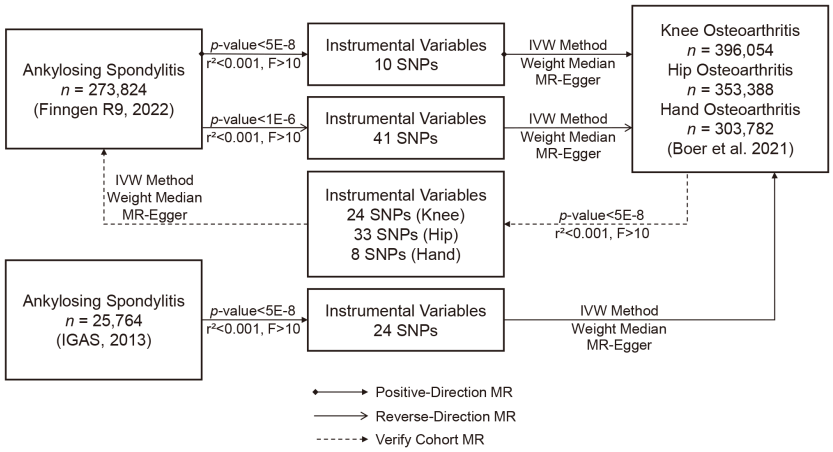

FIGURE 1
Flowchart of the study design overview.

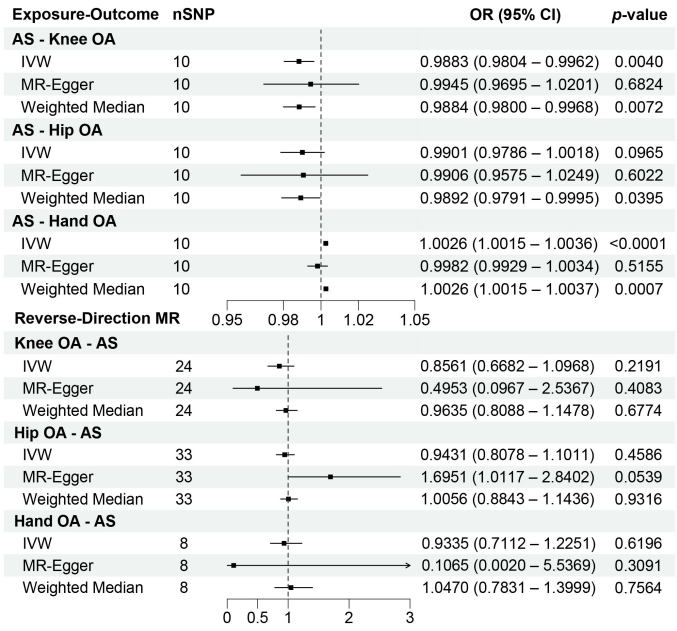

FIGURE 2
Forest plots of the results on two-sample bidirectional Mendelian randomization analysis. OR, Odds ratio.

models, the results consistently yielded nonsignificant statistical outcomes ($p > 0.0167$) (Figure 2).

Cochrane's Q test results indicated the absence of heterogeneity in the MR analysis between OA and AS (knee OA: $p = 0.3042$, $I^2 = 11.30\%$; hip OA: $p = 0.4230$, $I^2 = 12.86\%$; hand OA: $p = 0.4595$, $I^2 = 4.30\%$). While the MR Egger intercept tests showed the absence of horizontal pleiotropy between knee OA, hand OA, and AS ($p > 0.05$), some level of horizontal pleiotropy was observed between Hip OA and AS ($p = 0.0264$) (Table 2). Nevertheless, despite this observation, the models continued to yield negative combined results. Additionally, MR-PRESSO distortion tests indicated the absence of outliers related to OA instrumental variables.

3.3 Sensitive analysis

The leave-one-out sensitivity analysis demonstrated the robustness of the combined results from the IVW model in all MR

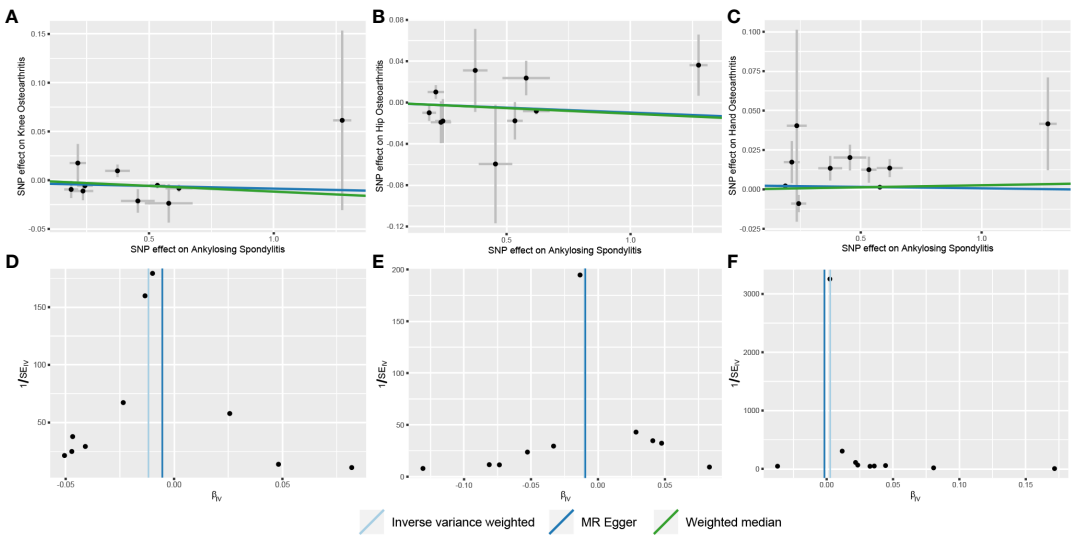

FIGURE 3
Scatter and funnel plots of the results of Mendelian randomization with AS as an exposure factor. **(A)** Scatterplot with knee OA as the outcome; **(B)** Scatterplot with hip OA as the outcome; **(C)** Scatterplot with hand OA as the outcome; **(D)** Funnel plot with knee OA as the outcome; **(E)** Funnel plot with hip OA as the outcome; **(F)** Funnel plot with hand OA as the outcome.

TABLE 2 Heterogeneity and horizontal pleiotropy analyses between ankylosing spondylitis and osteoarthritis.

Exposure	Outcome	Heterogeneity				Horizontal Pleiotropy		
		Q	Q df	I^2	*p*-value	Egger intercept	SE	*p*-value
AS	Knee OA	11.20	9	19.67	0.2620	-0.0031	0.0061	0.6225
AS	Hip OA	14.12	9	36.27	0.1180	-0.0003	0.0094	0.9751
AS	Hand OA	28.94	9	68.90	0.0007	0.0025	0.0015	0.1358
Knee OA	AS	25.93	23	11.30	0.3042	0.0284	0.0427	0.5133
Hip OA	AS	32.91	32	2.76	0.4224	-0.0453	0.0195	0.0264
Hand OA	AS	6.71	7	4.30	0.4595	0.1710	0.1583	0.3218

SE, Standard error.

analyses. No significant changes were observed upon excluding individual SNPs. For statistically significant findings, we conducted further verification (Table 3). We also expanded our analysis using instrumental variables obtained from the relaxed selection criteria, selecting a total of 41 instrumental variables related to AS. The influence of AS on knee OA (OR = 0.9982, 95% CI: 0.9976-0.9987, $p < 0.0001$) and hand OA (OR = 1.0026, 95% CI: 1.0015-1.0038, $p < 0.0001$) remained largely consistent with the previous results. In the validation MR analysis using an alternative cohort to investigate the relationship between AS and knee OA and hand OA, the results confirmed a lower risk of knee OA in individuals with AS (OR = 0.9959, 95% CI: 0.9946-0.9972, $p < 0.0001$). However, the significant association between AS and hand OA disappeared in the validation MR analysis (OR = 1.0102, 95% CI: 0.9998-1.0208, $p = 0.0556$). Considering the differentiated outcomes from the two datasets, we employed a meta-analysis approach to consolidate the corresponding OR values, which consistently indicated that AS serves as a risk factor for hand OA (OR = 1.0027, 95% CI: 1.0016-1.0037, $p < 0.0001$). In the context of the multivariate MR analysis accounting for BMI, we still observed at the genetic level that individuals with AS have a relatively lower risk of knee OA (OR = 0.9954, 95% CI: 0.9919-0.9988, $p = 0.0082$), while concurrently exhibiting an increased risk of hand OA (OR = 1.0028, 95% CI: 1.0020-1.0036, $p < 0.0001$).

3.4 Colocalization between AS and OA

In the pairwise GWAS of AS and hand OA, four loci, namely rs74707996 (PP4 = 0.9999), rs75240935 (PP4 = 0.9999), rs181468789 (PP4 = 0.9484), and rs748670681 (PP4 = 1), were classified as colocalized through COLOC analysis. Notably, except for rs748670681 located on chromosome 7, the remaining three loci are situated on chromosome 6. Furthermore, the nearest genes to rs74707996, rs75240935 and rs181468789 are *NRSN1*, *SLC17A3* and *OR2B6*, but all are at distances more than 100bp, while rs748670681 is located on the gene region of *TNRC18*.

4 Discussion

This study marks the pioneering exploration of the bidirectional relationship between AS and OA through Mendelian randomization analysis. Despite our research indicating only a modest genetic association between AS and knee OA as well as hand OA, the observed correlations carry significant *p*-values. Additionally, the COLOC analysis highlights four loci classified as colocalized with AS and hand OA, emphasizing the relevance of these subtle genetic effects. Therefore, the modest genetic associations uncovered at the genetic level should not be overlooked. Our conclusions based on the genetic level that differ from past perceptions also require new attention.

The intricate interplay between AS and OA has long confounded researchers, with limited existing literature and no definitive consensus. Notably, the pathogenesis and pathology of AS and OA are distinct; AS constitutes an autoimmune disease (15), whereas OA involves degenerative cartilage alterations (4). Our research findings significantly deviate from conventional clinical wisdom, particularly the discovery of a relatively lower risk of knee OA in patients with AS. One plausible mechanism could be attributed to individuals with ankylosing spondylitis often exhibiting elevated levels of serum bone

TABLE 3 Results of analyses using instrumental variables screened with low constraints, external validation cohorts, or multivariate MR analyses combined with BMI variables.

Outcome	Model 1		Model 2		Model 3	
	OR	*p*-value	OR	*p*-value	OR	*p*-value
Knee OA	0.9982 (0.9976-0.9987)	<0.0001	0.9959 (0.9946-0.9972)	<0.0001	0.9954 (0.9919-0.9988)	0.0082
Hand OA	1.0026 (1.0015-1.0038)	<0.0001	1.0102 (0.9998-1.0208)	0.0556	1.0028 (1.0020-1.0036)	<0.0001

OR, Odds ratio; Model 1, Relaxation of screening conditions for instrumental variables to $p < 1 \times 10^{-6}$, $r^2 < 0.001$, $F > 10$; Model 2, MR analysis using an external AS validation queue; Model 3, Multivariate MR analysis conducted using BMI as an adjustment variable.

formation markers like bone alkaline phosphatase, osteocalcin, and bone-specific alkaline phosphatase (31). These markers reflect the body's bone metabolism activity and may also correlate with cartilage metabolism (32), with knee joint cartilage metabolism being particularly sensitive to them. Alternatively, from a pharmacological standpoint, AS patients frequently require prolonged usage of non-steroidal anti-inflammatory drugs (NSAIDs) to manage symptoms and impede structural progression (33). NSAIDs not only inhibit prostaglandin E2 (PGE2) synthesis, thus mitigating inflammatory responses, but also obstruct osteoblast differentiation, curtailing new bone formation (34, 35). PGE2 serves as a pivotal mediator that incites degenerative changes in cartilage, prompting chondrocytes to release matrix metalloproteinases (MMPs), ultimately leading to cartilage matrix degradation (36, 37). Consequently, NSAID utilization might contribute to shielding knee joint cartilage from PGE2-induced harm.

It is worth noting that hip joint involvement frequently manifests in AS patients, with clinical hip joint involvement rates ranging from 24% to 36% and radiographic hip joint arthritis rates spanning 9% to 22% (38). Prior investigations have elucidated potential underlying mechanisms, revealing 193 differentially expressed proteins (DEPs) predominantly enriched in functional pathways like the phagosome pathway in ligament-like hip joint samples of AS patients. These pathways might represent pivotal pathogenic routes influencing hip joint engagement in AS patients. Notably, Myeloperoxidase (MPO), a pivotal protein in the phagosome pathway, registers upregulation in the AS group. MPO may potentially spur autoimmune inflammation in hip joints via the phagosome pathway, culminating in hip joint lesions (39). However, our study did not confirm a significant direct genetic association between AS and hip OA. One plausible explanation is that the effect of reducing the risk of developing knee OA in patients with AS may also extend to the hip joint, mitigating the impact of AS on hip joint involvement. Similarly, AS's risk factor impact on hand OA might originate from analogous mechanisms but exert heightened sensitivity when influencing the hand. Furthermore, the migration of HLA-B27-positive immune cells induced by AS to the hand joints via the bloodstream could potentially incite an inflammatory response (20).

When validating our MR analysis results using data from the IGAS alliance (23) in 2013, a trend of AS causing hand OA persists, but the statistical significance has disappeared. This phenomenon can be attributed to several factors. Innovative treatment strategies and drugs for AS, such as the IL-12/23 inhibitor ustekinumab, the pan-Janus kinase inhibitor tofacitinib, and the anti-IL-17A antibody secukinumab, have emerged. These advancements enable more effective control of inflammation and slowing down of ossification, ultimately enhancing patients' quality of life and prognosis (40). Moreover, diagnostic techniques have advanced, enabling earlier detection of AS and better disease management (41). Lastly, changes in people's lifestyles and work habits over the past decade have led to alterations in the spectrum of diseases related to OA and AS. These changes may influence the bidirectional relationship between OA and AS. To further substantiate the reliability of our obtained results, we conducted a meta-analysis using a fixed-effects model, merging the outcomes of two datasets. The meta-analysis results endorse the initial conclusion from the MR analysis, affirming that AS functions as a risk factor for hand OA. The choice of a fixed-effects model was based on the absence of significant heterogeneity between the two results (42). As future research endeavors expand, there is a necessity to undertake further systematic reviews and meta-analyses to comprehensively evaluate and consolidate the evolving body of evidence in this domain.

Additionally, among the IVs extracted from GWAS data of AS from the FinnGen consortium, rs10807943 showed some correlation with both knee OA ($p = 0.0419$) and hip OA ($p = 0.0407$) outcomes. Although these p-values remained above the Bonferroni-corrected thresholds, we retained this IV to comprehensively assess the impact of each SNP. Leave-one-out sensitivity analysis indicated that excluding this SNP did not affect the outcomes, and the MR-PRESSO test did not detect horizontal pleiotropy. Notably, while no significant correlation was observed between the selected IVs and AS, the reverse MR analysis using hip OA as the exposure factor suggested the presence of horizontal pleiotropy. Despite negative results from all three models, including MR-Egger regression, which can adjust for pleiotropy, further evaluation of the direct correlation between hip OA and AS is warranted, in conjunction with clinical data.

The results of COLOC suggest that the *TNRC18* gene, located on chromosome 7, may be a pleiotropic gene associated with both AS and hand OA. *TNRC18* specifically recognizes histone H3K9me3 modification, mediating the silencing of endogenous retrotransposons (ERVs) to uphold the integrity and stability of the genome (43). Genetic factors play a crucial role in the pathogenesis of both AS and OA (23, 24). In this context, TNRC18 may influence the expression or regulation of homologous frame genes, thereby impacting the risk of developing AS and hand OA. Furthermore, COLOC analysis identified three loci on chromosome 6 with a colocalized relationship with both AS and hand OA. Hence, the relationship between AS and hand OA may involve intricate gene-gene interactions, and further exploration of specific mechanisms is warranted by subsequent researchers. Additionally, given that both AS and OA are complex multifactorial diseases, gene-environment interactions may influence the potential relationship between AS and OA. For example, previous MR studies have suggested a correlation between an increased BMI and a higher risk of OA (28). Therefore, the relationship between genetic variations related to AS and the risk of hand OA may be modulated by BMI, with a more pronounced susceptibility to OA genes evident when BMI is higher. Although our study did not yield significantly altered MR results upon incorporating BMI as an adjusting variable, it is essential for future research endeavors to delve further into the exploration of gene-environment interactions.

Our study possesses several strengths. Firstly, we systematically investigated the bidirectional relationship between AS and OA using the Mendelian randomization method, a topic relatively underexplored in previous research. Unlike traditional observational studies, MR studies leveraging genetic variation from the genome are less susceptible to confounding factors (44). Secondly, we rigorously applied Bonferroni correction for significance levels, ensuring that the p-values for positive results were all below the adjusted significance threshold. Furthermore, robust results were indicated by

leave-one-out sensitivity analysis, reducing the risk of false positives. Lastly, we conducted our MR analysis meticulously, utilizing large-sample GWAS data from populations of European ancestry, with no overlap between exposure and outcome populations. In addition, we validated positive results by expanding the criteria for selecting IV and incorporating GWAS data from another cohort. By relaxing the IV selection criteria from a p-value of $< 5 \times 10^{-8}$ to $< 1 \times 10^{-6}$, we were able to identify more instrumental variables. This adjustment facilitated a more optimal balance between individual SNPs and the potential impact of horizontal pleiotropy on the results. Consequently, the amalgamation of SNP effects could be more precisely determined.

However, it's crucial to acknowledge certain research limitations. Firstly, our study focused exclusively on individuals of European descent, and the incidence of AS varies across different ethnicities (45). Therefore, caution should be exercised when applying our findings to other racial groups. Furthermore, constrained by the methods employed in MR studies, complete resolution of potential confounding factors such as population heterogeneity and factors like age, gender, and dietary habits may not be achievable. Additionally, the influence of time in the onset process is overlooked. Moreover, the potential presence of horizontal pleiotropy in MR analysis could impact result accuracy. To mitigate this, we conducted comprehensive sensitivity analyses and validation processes. Lastly, our study is solely an observational study based on MR methods. While MR provides a relatively high level of evidence, it cannot establish a genuine causal relationship between ankylosing spondylitis and osteoarthritis. More experiments and clinical evidence are required to either support or validate these results.

Our study carries significant clinical implications. Firstly, our findings can assist clinicians in better understanding the heterogeneity between osteoarthritis in different joint sites and ankylosing spondylitis, along with potential variations in pathogenic mechanisms and influencing factors. Based on this information, we recommend that clinicians perform regular screening for osteoarthritis in ankylosing spondylitis patients, especially for hand joints, using appropriate radiographic or ultrasonographic methods, as well as assess the clinical symptoms and functional status of these patients. Moreover, we suggest that clinicians provide preventive measures for osteoarthritis in ankylosing spondylitis patients, such as physical therapy, exercise, weight control, and anti-inflammatory drugs, as well as individualized treatment options for hand joint osteoarthritis, such as analgesics, corticosteroid injections, or surgery, depending on the severity and progression of the disease. Furthermore, while our research suggests that there is no significant causal relationship between OA and AS at the genetic level, it remains crucial to consider the possibility of AS being misdiagnosed as OA (18). We advise that clinicians consider the possibility of ankylosing spondylitis in osteoarthritis patients, especially those with axial involvement, and perform appropriate diagnostic tests, such as HLA-B27 typing, sacroiliac joint imaging, or inflammatory markers, to confirm or exclude the diagnosis of ankylosing spondylitis.

Future researchers can draw upon the genetic-level correlation we have established between AS and OA to delve deeper into the causal mechanisms governing their relationship. Conducting clinical cohort studies or cross-sectional epidemiological observations using follow-up data from AS and OA patients, while meticulously accounting for potential confounding factors, can unveil the dynamic changes and influences between AS and OA. Moreover, the application of network meta-analysis could offer insights into the differential correlations between various types of OA and AS. This approach would not only validate the genetic-level correlation in broader populations but also contribute novel evidence to the field. Additionally, considering the potential correlation of AS and OA with patients' lifestyles, future studies could use our preliminary research as a reference, collecting more detailed participant information such as dietary habits, physical activity levels, and other lifestyle factors. This would help further elucidate the role of these factors in the relationship between AS and OA.

5 Conclusions

Our MR analysis reveals that, among individuals of European ancestry, those with AS exhibit a lower risk of developing knee OA, while AS serves as a risk factor for hand OA. Furthermore, no significant correlation was found between AS and hip OA. However. reverse MR analysis suggests that OA does not significantly influence AS. COLOC analysis based on GWAS data from European populations identified four loci colocalized with AS and hand OA. This genetic-level insight challenges previous assumptions about the association between AS and the predilection for hip and knee involvement. Therefore, more experiment, epidemiological studies and clinical evidence is needed to support or validate our results and further elucidate the underlying mechanisms. Additionally, our study results offer new insights for genetic research on OA and AS.

Data availability statement

The original contributions presented in the study are included in the article/Supplementary Material. Further inquiries can be directed to the corresponding authors.

Ethics statement

Since all data were derived from previously published studies and public databases, no additional ethical approval was required. The studies were conducted in accordance with the local legislation and institutional requirements. The participants provided their written informed consent to participate in this study.

Author contributions

YL: Conceptualization, Data curation, Formal Analysis, Investigation, Methodology, Project administration, Resources,

Validation, Visualization, Writing – original draft, Writing – review & editing. DL: Data curation, Formal Analysis, Investigation, Methodology, Validation, Visualization, Writing – review & editing. HZ: Data curation, Formal Analysis, Writing – review & editing. HL: Data curation, Formal Analysis, Writing – review & editing. BY: Data curation, Writing – review & editing. YZ: Data curation, Writing – review & editing. HH: Data curation, Writing – review & editing. HS: Conceptualization, Investigation, Project administration, Resources, Supervision, Writing – review & editing.

Funding

The author(s) declare financial support was received for the research, authorship, and/or publication of this article. This study was supported by Student Research Project Funding Program of Wenzhou Medical University (No. wyx2023101112).

Acknowledgments

We thank the FinnGen consortium, the International Genetics of Ankylosing Spondylitis (IGAS) consortium and Dr. Boer and colleagues for providing the GWAS summary data that enabled this Mendelian randomization study. We acknowledge their valuable contributions to the advancement of genetic research on complex diseases.

Conflict of interest

The authors declare that the research was conducted in the absence of any commercial or financial relationships that could be construed as a potential conflict of interest.

Publisher's note

Supplementary material

The Supplementary Material for this article can be found online at: https://www.frontiersin.org/articles/10.3389/fimmu.2024.1297454/full#supplementary-material

SUPPLEMENTARY FIGURE 1
Leave-one-out sensitivity analysis. **(A)** AS on knee OA; **(B)** AS on hip OA; **(C)** AS on hand OA; **(D)** Knee OA on AS; **(E)** Hip OA on AS; **(F)** Hand OA on AS.

SUPPLEMENTARY FIGURE 2
Forest plot of the correlations between AS hand OA with different GWAS data sources.

References

1. Man GS, Mologhianu G. Osteoarthritis pathogenesis - a complex process that involves the entire joint. *J Med Life* (2014) 7(1):37–41.

2. Litwic A, Edwards MH, Dennison EM, Cooper C. Epidemiology and burden of osteoarthritis. *Br Med Bull* (2013) 105:185–99. doi: 10.1093/bmb/lds038

3. Trachana V, Ntoumou E, Anastasopoulou L, Tsezou A. Studying micrornas in osteoarthritis: critical overview of different analytical approaches. *Mech Ageing Dev* (2018) 171:15–23. doi: 10.1016/j.mad.2018.02.006

4. Hunter DJ, Bierma-Zeinstra S. Osteoarthritis. *Lancet* (2019) 393(10182):1745–59. doi: 10.1016/s0140-6736(19)30417-9

5. Neogi T, Zhang Y. Epidemiology of osteoarthritis. *Rheum Dis Clin North Am* (2013) 39(1):1–19. doi: 10.1016/j.rdc.2012.10.004

6. Hunter DJ, March L, Chew M. Osteoarthritis in 2020 and beyond: A lancet commission. *Lancet* (2020) 396(10264):1711–2. doi: 10.1016/s0140-6736(20)32230-3

7. Mandl LA. Osteoarthritis year in review 2018: clinical. *Osteoarthritis Cartilage* (2019) 27(3):359–64. doi: 10.1016/j.joca.2018.11.001

8. Fransen M, Bridgett L, March L, Hoy D, Penserga E, Brooks P. The epidemiology of osteoarthritis in asia. *Int J Rheum Dis* (2011) 14(2):113–21. doi: 10.1111/j.1756-185X.2011.01608.x

9. March LM, Bachmeier CJ. Economics of osteoarthritis: A global perspective. *Baillieres Clin Rheumatol* (1997) 11(4):817–34. doi: 10.1016/s0950-3579(97)80011-8

10. DeRogatis M, Anis HK, Sodhi N, Ehiorobo JO, Chughtai M, Bhave A, et al. Non-operative treatment options for knee osteoarthritis. *Ann Transl Med* (2019) 7(Suppl 7): S245. doi: 10.21037/atm.2019.06.68

11. Sodhi N, Piuzzi NS, Dalton SE, George J, Ng M, Khlopas A, et al. What influence does the time of year have on postoperative complications following total knee arthroplasty? *J Arthroplasty* (2018) 33(6):1908–13. doi: 10.1016/j.arth.2017.12.020

12. Cai C, Hu W, Chu T. Interplay between iron overload and osteoarthritis: clinical significance and cellular mechanisms. *Front Cell Dev Biol* (2021) 9:817104. doi: 10.3389/fcell.2021.817104

13. García-Ibarbia C, Neila S, Garcés C, Alonso MA, Zarrabeitia MT, Valero C, et al. Non-synonymous wnt16 polymorphisms alleles are associated with different osteoarthritis phenotypes. *Rheumatol Int* (2017) 37(10):1667–72. doi: 10.1007/s00296-017-3783-5

14. Voruganti A, Bowness P. New developments in our understanding of ankylosing spondylitis pathogenesis. *Immunology* (2020) 161(2):94–102. doi: 10.1111/imm.13242

15. Braun J, Sieper J. Ankylosing spondylitis. *Lancet* (2007) 369(9570):1379–90. doi: 10.1016/s0140-6736(07)60635-7

16. Bond D. Ankylosing spondylitis: diagnosis and management. *Nurs Stand* (2013) 28(16-18):52–9; quiz 60. doi: 10.7748/ns2013.12.28.16.52.e7807

17. Feldtkeller E, Khan MA, van der Heijde D, van der Linden S, Braun J. Age at disease onset and diagnosis delay in hla-B27 negative vs. Positive patients with ankylosing spondylitis. *Rheumatol Int* (2003) 23(2):61–6. doi: 10.1007/s00296-002-0237-4

18. Maksymowych WP. Biomarkers for diagnosis of axial spondyloarthritis, disease activity, prognosis, and prediction of response to therapy. *Front Immunol* (2019) 10:305. doi: 10.3389/fimmu.2019.00305

19. Lu MC, Tung CH, Yang CC, Wang CL, Huang KY, Koo M, et al. Incident osteoarthritis and osteoarthritis-related joint replacement surgery in patients with ankylosing spondylitis: A secondary cohort analysis of a nationwide, population-based health claims database. *PloS One* (2017) 12(11):e0187594. doi: 10.1371/journal.pone.0187594

20. Chen B, Li J, He C, Li D, Tong W, Zou Y, et al. Role of hla-B27 in the pathogenesis of ankylosing spondylitis (Review). *Mol Med Rep* (2017) 15(4):1943–51. doi: 10.3892/mmr.2017.6248

21. Skrivankova VW, Richmond RC, Woolf BAR, Yarmolinsky J, Davies NM, Swanson SA, et al. Strengthening the reporting of observational studies in epidemiology using mendelian randomization: the strobe-mr statement. *Jama* (2021) 326(16):1614–21. doi: 10.1001/jama.2021.18236

22. Burgess S, Thompson SG. Interpreting findings from mendelian randomization using the mr-egger method. *Eur J Epidemiol* (2017) 32(5):377–89. doi: 10.1007/s10654-017-0255-x

23. Cortes A, Hadler J, Pointon JP, Robinson PC, Karaderi T, Leo P, et al. Identification of multiple risk variants for ankylosing spondylitis through high-density genotyping of immune-related loci. *Nat Genet* (2013) 45(7):730–8. doi: 10.1038/ng.2667

24. Boer CG, Hatzikotoulas K, Southam L, Stefánsdóttir L, Zhang Y, Coutinho de Almeida R, et al. Deciphering osteoarthritis genetics across 826,690 individuals from 9 populations. *Cell* (2021) 184(18):4784–818.e17. doi: 10.1016/j.cell.2021.07.038

25. Lin Z, Deng Y, Pan W. Combining the strengths of inverse-variance weighting and egger regression in mendelian randomization using a mixture of regressions model. *PloS Genet* (2021) 17(11):e1009922. doi: 10.1371/journal.pgen.1009922

26. Bowden J, Davey Smith G, Haycock PC, Burgess S. Consistent estimation in mendelian randomization with some invalid instruments using a weighted median estimator. *Genet Epidemiol* (2016) 40(4):304–14. doi: 10.1002/gepi.21965

27. Burgess S, Bowden J, Fall T, Ingelsson E, Thompson SG. Sensitivity analyses for robust causal inference from mendelian randomization analyses with multiple genetic variants. *Epidemiology* (2017) 28(1):30–42. doi: 10.1097/ede.0000000000000559

28. Karlsson T, Hadizadeh F, Rask-Andersen M, Johansson Å, Ek WE. Body mass index and the risk of rheumatic disease: linear and nonlinear mendelian randomization analyses. *Arthritis Rheumatol* (2023) 75(11):2027–35. doi: 10.1002/art.42613

29. Curtin F, Schulz P. Multiple correlations and bonferroni's correction. *Biol Psychiatry* (1998) 44(8):775–7. doi: 10.1016/s0006-3223(98)00043-2

30. Giambartolomei C, Vukcevic D, SChadt EE, Franke L, Hingorani AD, Wallace C, et al. Bayesian test for colocalisation between pairs of genetic association studies using summary statistics. *PloS Genet* (2014) 10(5):e1004383. doi: 10.1371/journal.pgen.1004383

31. Arends S, Spoorenberg A, Bruyn GA, Houtman PM, Leijsma MK, Kallenberg CG, et al. The relation between bone mineral density, bone turnover markers, and vitamin D status in ankylosing spondylitis patients with active disease: A cross-sectional analysis. *Osteoporos Int* (2011) 22(5):1431–9. doi: 10.1007/s00198-010-1338-7

32. Christenson RH. Biochemical markers of bone metabolism: an overview. *Clin Biochem* (1997) 30(8):573–93. doi: 10.1016/s0009-9120(97)00113-6

33. Maksymowych WP. Update on the treatment of ankylosing spondylitis. *Ther Clin Risk Manag* (2007) 3(6):1125–33.

34. Lisowska B, Kosson D, Domaracka K. Lights and shadows of nsaids in bone healing: the role of prostaglandins in bone metabolism. *Drug Des Devel Ther* (2018) 12:1753–8. doi: 10.2147/dddt.S164562

35. Li M, Thompson DD, Paralkar VM. Prostaglandin E(2) receptors in bone formation. *Int Orthop* (2007) 31(6):767–72. doi: 10.1007/s00264-007-0406-x

36. Gosset M, Berenbaum F, Levy A, Pigenet A, Thirion S, Cavadias S, et al. Mechanical stress and prostaglandin E2 synthesis in cartilage. *Biorheology* (2008) 45(3-4):301–20. doi: 10.3233/BIR-2008-0494

37. Sun Q, Zhang Y, Ding Y, Xie W, Li H, Li S, et al. Inhibition of PGE2 in subchondral bone attenuates osteoarthritis. *Cells* (2022) 11(17):2760. doi: 10.3390/cells11172760

38. Jeong H, Eun YH, Kim IY, Kim H, Lee J, Koh EM, et al. Characteristics of hip involvement in patients with ankylosing spondylitis in Korea. *Korean J Intern Med* (2017) 32(1):158–64. doi: 10.3904/kjim.2015.229

39. Yu C, Zhan X, Liang T, Chen L, Zhang Z, Jiang J, et al. Mechanism of hip arthropathy in ankylosing spondylitis: abnormal myeloperoxidase and phagosome. *Front Immunol* (2021) 12:572592. doi: 10.3389/fimmu.2021.572592

40. Tahir H. Therapies in ankylosing spondylitis-from clinical trials to clinical practice. *Rheumatol (Oxford)* (2018) 57(suppl_6):vi23–vi8. doi: 10.1093/rheumatology/key152

41. Moon KH, Kim YT. Medical treatment of ankylosing spondylitis. *Hip Pelvis* (2014) 26(3):129–35. doi: 10.5371/hp.2014.26.3.129

42. Tufanaru C, Munn Z, Stephenson M, Aromataris E. Fixed or random effects meta-analysis? Common methodological issues in systematic reviews of effectiveness. *Int J Evid Based Healthc* (2015) 13(3):196–207. doi: 10.1097/xeb.0000000000000065

43. Zhao S, Lu J, Pan B, Fan H, Byrum SD, Xu C, et al. Tnrc18 engages H3k9me3 to mediate silencing of endogenous retrotransposons. *Nature* (2023) 623(7987):633–42. doi: 10.1038/s41586-023-06688-z

44. Lee K, Lim CY. Mendelian randomization analysis in observational epidemiology. *J Lipid Atheroscler* (2019) 8(2):67–77. doi: 10.12997/jla.2019.8.2.67

45. Jamalyaria F, Ward MM, Assassi S, Learch TJ, Lee M, Gensler LS, et al. Ethnicity and disease severity in ankylosing spondylitis a cross-sectional analysis of three ethnic groups. *Clin Rheumatol* (2017) 36(10):2359–64. doi: 10.1007/s10067-017-3767-6

Frontiers in Immunology

Explores novel approaches and diagnoses to treat immune disorders.

The official journal of the International Union of Immunological Societies (IUIS) and the most cited in its field, leading the way for research across basic, translational and clinical immunology.

Discover the latest Research Topics

See more →

Frontiers

Avenue du Tribunal-Fédéral 34
1005 Lausanne, Switzerland
frontiersin.org

Contact us

+41 (0)21 510 17 00
frontiersin.org/about/contact